Development of Chelators for Enhancing Radiometal-based Radiopharmaceuticals

A Thesis Submitted to the

College of Graduate and Postdoctoral Studies

In Partial Fulfillment of the Requirements

for the Degree of Doctor of Philosophy

in the Department of Chemistry

University of Saskatchewan

Saskatoon

By

Akam Kareem Salih

PERMISSION TO USE

In presenting this dissertation in partial fulfillment of the requirements for a Postgraduate degree from the University of Saskatchewan, I agree that the Libraries of the University may make it freely available for inspection. I further agree that permission for copying of this dissertation in any manner, in whole or in part, for scholarly purposes may be granted by Dr. Eric W. Price who supervised my dissertation work or, in their absence, by the Head of the Department or the Dean of the College in which my thesis work was done. It is understood that any copying or publication or use of this dissertation or parts thereof for financial gain shall not be allowed without my written permission. It is also understood that due recognition shall be given to me and to the University of Saskatchewan in any scholarly use which may be made of any material in my dissertation.

Requests for permission to copy or to make other uses of material in this dissertation in whole or part should be addressed to:

Head of the Chemistry Department
165-110 Science Place
University of Saskatchewan
Saskatoon, Saskatchewan S7N 5C9
Canada

OR

Dean
College of Graduate and Postdoctoral Studies
University of Saskatchewan
116 Thorvaldson Building, 110 Science Place
Saskatoon, Saskatchewan S7N 5C9
Canada

ABSTRACT

Zirconium-89 is one of the few radionuclides among positron emitters which have a relatively long physical half-life compatible with the biological half-life of most antibodies. Zirconium-89's low positron energy, well studied and established production and purification protocols, cost effective and wide availability illustrates it as the best currently available radionuclide for immuno-positron emission tomography (immuno-PET). To employ zirconium-89 in monoclonal antibody-based radiotracers a bifunctional chelator is required to attach the radiometal securely to the antibody and assure site specific delivery of the radiometal. Desferrioxamine (DFO) has been used as the "gold standard" chelator for zirconium-89 labeled monoclonal antibodies preclinically and clinically. However, the hexadentate nature of DFO is insufficient to saturate the coordination sphere of $[^{89}Zr]Zr^{4+}$, thus *in vivo* sub-optimal stability of it has been reported in various studies. The released oxophilic and osteophilic zirconium (IV) ion accumulates in healthy tissue particularly in bone. Furthermore, DFO, apart from binding to diagnostic radiometal like zirconium-89, it is not known to stably bind to any therapeutic radiometals which means it has little theranostic potential. Thus, the development of optimized chelators for zirconium-89 is ongoing and demands for new bifunctional chelators which can stably bind the radiometal and conjugate to targeting vectors such as antibodies has grown considerably in the last decade. This thesis describes the design, synthesis and evaluation of novel high denticity (8-12) desferrioxamine based ligands/chelators for zirconium-89 and potentially other high valent therapeutic radiometals. Following the synthesis and characterization of the new chelators with standard chemical characterization methods, the radiolabeling properties and *in vitro*/*in vivo* stability of unconjugated "bare" chelators and antibody conjugates were evaluated by using various radiochemical assays and animal studies. Two families of chelators are the highlights of this thesis: the DFO2 family

with 12 possible coordination sites, and an amino acid-based chelator family with 8-coordination sites. Each of the families consist of two chelators, for which their stabilities with zirconium-89 have been found to surpass the "gold standard" chelator DFO, and their higher denticities compared to DFO might offer the potential for utilizing other high valent and oxophilic radiometal ions such as thorium-227 or actinium-225 for theranostic applications.

ACKNOWLEDGEMENTS

TABLE OF CONTENTS

LIST OF FIGURES

Figure 2-1. Chemical structures of a selection of recently published bifunctional chelators based on desferrioxamine (DFO) for zirconium-89, including *p*-SCN-Ph-DFO, DFO*, oxoDFO*, DFO squate ester (H$_3$DFOSqOEt), DFO-cyclo*, and DFO2. ……………………………………42

Figure 2-2. Energy-minimized and geometry-optimization molecular structures calculating using DFT (Materials Studio, DMol^3 /PBE, solvent as water with COSMO) showing (a) the Zr(DFO2) complex, and (b) the close-up of Zr(IV) ion's geometry in Zr(DFO2) complex. Hydrogen atoms are removed from figure for visual clarity but are included for calculation. ……………………47

Figure 2-3. Results from *in vitro* stability assays (n=3) comparing the stability of zirconium-89 complexes of the new chelator DFO2 to the gold standard chelator DFO, with **A)** competition against human blood serum over a 7-day duration and evaluated via radio-iTLC, and **B)** the same blood serum stability assay evaluated by precipitating proteins (cold acetonitrile) and decanting supernatant via centrifugation. …………………………………………………………………..52

correction, the activies in the images are maximized to best visualize and compare bone uptake for

LIST OF SCHEMES

LIST OF EQUATIONS

LSIT OF TABLES

LIST OF ABBREVIATIONS

PET	positron emission tomography
TAT	targeted alpha therapy
$t_{1/2}$	half-life
h	hour

E	energy
keV	kilo electronvolt
EC	electron capture
SPECT	single photon emission computed chromatography
n	neutron
p	proton
d	day
BFC	bifunctional chelator
HSAB	Pearson hard-soft acid-base
CN	coordination number
DFO	desferrioxamine
HA	hydroxamic acid
iTLC	instant thin layer chromatography
HPLC	high performance liquid chromatography
K_{ML}	formation constant
EDTA	Ethylenediaminetetraacetic acid
DTPA	diethylenetriaminepentaacetic acid
mAb	monoclonal antibody
AAZTA	1,4-bis(carboxymethyl)-6-[bis(carboxymethyl)]amino-6-methylperhydro-1,4-diazepine
DOTA	1,4,7-Triazacyclononane-1,4,7-triacetic acid
NOTA	1,4,7-Triazacyclononane-1,4,7-triacetic acid
rt	room temperature
M	molar
TOC	octreotide
MG	minigastrin
cRGDfK	cycloArg-Gly-Asp-Dphe-Lys
MRI	magnetic resonance imaging
CyAAZYA	trans-3-amino-3-methyldecahydro-1H-1,5-benzodiaze-pine-N,N',N'',N''' tetraacetic acid

PIDAZTA	4-amino-4-methylperhydro-pyrido[1,2-a][1,4]diazepin- *N,N′,N″*-triacetic acid
CT	computed tomography
RCY	radiochemical yield
PA	picolinic acid
min	minute
PSMA	prostate-specific membrane antigen
RPS-070	PSMA/albumin dual-targeting agent
%ID/g	percentage of injected radioactive dose per gram of tissue
-NCS	isothiocyanate
$R_{\text{ave}}\,\beta^+$	average range of positron
Ci	Curie
mol	mole
RGD	Arginylglycylaspartic acid
TAFC	Triacetylfusarinine C
succ	succinyl
FSC	fusarinine C
p-	*para-*
Phe	phenyl
HPG	hyperbranched polyglycerol
DMF	Dimethyl formamide
DMSO	Dimethyl sulfoxide
DCM	dichloromethane
RP	Reverse phase
HEPES	4-(2-hydroxyethyl)-1-piperazineethanesulfonic acid
HTP	Hydroxyapatite
-Bn	Benzyl-
-Z	Benzyloxycarbonyl-

Chapter 1. Introduction

This chapter is adapted from the manuscript that is currently under preparation (Salih, A. K.; Price E. W., Matching chelators to radiometals for radiopharmaceuticals: part 2. (Manuscript under preparation)

1.1. Background

Radiometals are the radioactive isotopes (radionuclides) of metallic elements whose atomic nuclei contain an unstable combination of neutrons and protons. These radionuclides are unstable, but over time they can achieve stability through release of substantial energy in a process called radioactive decay, which can be harnessed for clinical applications such as nuclear imaging and cancer therapy.[1–3] Nuclear medicine leverages the use of radionuclides and their notable emissions upon decay, such as particles (α, β^-, β^+ and Auger electron) and photons (γ-ray) or combinations of these decay emissions (**Table 1-1**). The radionuclide's decay emission properties therefore indicate its suitability for nuclear imaging or therapy, or combinations of imaging and therapy (theranostics).[4] For instance, a positron emitter such as zirconium-89 is used in positron emission tomography (PET) whereas an alpha emitter such as Actinium-225 is utilized in targeted alpha therapy (TAT) for cancer treatment.[5,6] Another important parameter is the duration of the decay of a radionuclide measured in "half-life", which is a crucial consideration in the development of radiopharmaceuticals , which are radionuclide labeled small-molecule drugs or bioactive molecules (biovectors). While short half-life radiometals (Gallium-68 $t_{1/2}$ = 68 min) are used for labeling fast pharmacokinetic biovectors (peptides), slow pharmacokinetic biovectors such as antibodies require long half-life radiometals such zirconium-89 ($t_{1/2}$ = 78.5 h).[7]

Table 1-1. A selection of some common radiometals and their physical decay characteristics such as half-life ($t_{1/2}$), decay mode, average particle emission energy (mean values) and most noticeable gamma emissions.[8–15]

Radionuclide	$t_{1/2}$ (h)	Application	Decay mode	E (keV)	Production method
$[^{213}Bi]Bi^{3+}$	0.76	Therapy: α and β-	α (2%) β- (98%)	γ, 440 α, 8350 β-, 435	$[^{228}Th/^{212}Pb$ generator]
$[^{212}Bi]Bi^{3+}$	1.0	Therapy: α and β-	α (36%) β- (64%)	α, 6210 β-, 771	$[^{228}Th/^{212}Pb/^{212}Bi$ generator]
$[^{68}Ga]Ga^{3+}$	1.1	PET	β+ (89%) EC (11%)	γ, 1077 β+, 836	$[^{68}Ge/^{68}Ga$ generator] $^{68}Zn(p,n)^{68}Ga$
$[^{44}Sc]Sc^{3+}$	4.04	PET	β+ (94%) EC (6%)	γ, 1157 β+, 632	$[^{44}Ti/^{44}Sc$ generator] $^{44}Ca(p,n)^{44}Sc$
$[^{212}Pb]Pb^{2+}$ (daughter is $[^{212}Bi]Bi^{3+}$)	10.6	Therapy: β- (daughters emit α/β-)	β- (100%)	β-, 570	$[^{224}Ra/^{212}Pb$ generator]
$[^{64}Cu]Cu^{2+}$	12.7	PET	β+ (19%) EC (41%) β- (40%)	γ, 1346 β+, 278 β-, 579	Cyclotron $^{64}Ni(p,n)^{64}Cu$
$[^{86}Y]Y^{3+}$	14.7	PET	β+ (33%) EC (66%)	γ, 443-1920 (9) β+, 535, 681, 883 (664 avg)	Cyclotron $^{86}Sr(p,n)^{86}Y$
$[^{67}Cu]Cu^{2+}$	61.8 (2.6 d)	SPECT Therapy: β-	β- (100%)	γ, 91, 93, 184 β-, 141	$^{67}Zn(n,p)^{67}Cu$ $^{68}Zn(γ,p)^{67}Cu$
$[^{90}Y]Y^{3+}$	64.1 (2.7 d)	Therapy: β-	β- (100%)	β-, 934	$^{90}Zr(n,p)^{90}Y$ $[^{90}Sr/^{90}Y$ generator]
$[^{89}Zr]Zr^{4+}$	78.5 (3.3 d)	PET	β+ (23%) EC (77%)	γ, 909 β+, 396	Cyclotron $^{89}Y(p,n)^{89}Zr$
$[^{47}Sc]Sc^{3+}$	80.4 (3.4 d)	SPECT Therapy: β-	β- (100%)	γ, 159 β-, 162	$^{47}Ti(n,p)^{47}Sc$ $^{46}Ca(n,γ)^{47}Ca→^{47}Sc$
$[^{177}Lu]Lu^{3+}$	159.4 (6.6 d)	SPECT Therapy: β-	β- (100%)	γ, 112, 208 β-, 134	$^{176}Lu(n,γ)^{177}Lu$
$[^{225}Ac]Ac^{3+}$	238 (9.9 d)	Therapy: α (daughters emit α/β-)	α (100%)	α, 5800-8400 MeV	$^{226}Ra(p,2n)^{225}Ac$ $^{232}Th(p,2p6n)^{225}Ac$ $[^{229}Th → ^{225}Ac$ generator]
$[^{227}Th]Th^{4+}$	449 (18.7 d)	Therapy: α (daughters emit α/β-)	α (100%)	α, 5900	$^{226}Ra(n,γ)^{227}Ra$ ($t_{1/2}$ = 42 m) → ^{227}Ac $[^{227}Ac$ ($t_{1/2}$ = 21.8 y) → ^{227}Th generator]

While the development of radiopharmaceuticals closely follows that of traditional drug development, there are several key considerations in metal-based radiopharmaceutical synthesis. To apply the radiometals to specific biovectors to form an active radiopharmaceutical, chelators

(ligands) are used to tightly bind the radiometal ion and prevent non-specific tissue uptake and irradiation of healthy tissue. Furthermore, to provide site specific delivery of the radiometal, the chelator is covalently linked with the biovector. Thus, the chelator that is coordinated to the radiometal is a key factor in determining radiometal-based radiopharmaceutical stability and applicability for medical applications. In other words, the success and efficacy of a radiometal-based radiopharmaceutical is completely tied to the stability of the radiometal-chelate complex and therefore the selected chelator. There are many other factors in addition to the chelator, including the stability of the conjugation linkage, the stability and biological distribution of the biovector (e.g. peptide, antibody), and the overall formulation and dosing of the completed radiopharmaceutical. [2–4,7] In this introduction and thesis the focus will be on the chelators.

1.2. Chelators in Clinical Applications

Chelators/ligands are metal sequestering agents that bind metals (Lewis acids) via coordination bonding of their donor atoms/groups (Lewis bases) to metal ions to form metal-chelate complexes. The chelators used for radiometals are specialized, and for clinical applications they are designed to form highly stable complexes and generally have an additional reactive functional group for biovector conjugation, hence they are called bifunctional chelators (BFC).[1] These molecules are either synthesized specifically for the metal ions based on chemical requirements of the metal or they are obtained from natural products and modified for chelation to different metal ions. Chelators are considered central to radiopharmaceuticals since stable coordination with the radiometal ion prevents any radiometal loss from the radiopharmaceutical and non-specific accumulation *in vivo*, effectively supplying a site-specifically delivered radioactive source *in vivo* for imaging or therapy when radiopharmaceuticals are injected into a

patient. An ideal biovector guides the delivery of the chelated and conjugated radiometal ion exclusively to the targeted tissue, although in reality the distribution and pharmacokinetics are never perfect.[16]

Design and synthesis of new chelators, or selection of existing chelators for radiometals is a rational process and there are several important properties to be considered in the process which can affect the stability of the metal-chelate complex. According to the Pearson hard-soft acid-base (HSAB) concept, hard metals (e.g. Zr^{4+}) require chelators with hard donor groups (e.g. oxygen) to form stable complexes whereas soft metals (e.g. Ag^{1+}, $Cu^{1+/2+}$) form stable coordination with chelators containing soft donor groups (e.g. thiol/thiolate)[17]. Complexes where the ligand is bound to the metal ion through more than one bond (also referred to as multidentate ligands or chelators) are more kinetically inert and resistant to transchelation/demetallation due a phenomenon called the chelate effect which is explained by the enthalpy and entropy change when a multidentate ligand binds to a metal ion compared to a set of equivalent monodentate ligands.[18] Generally, chelators that saturate the maximum preferred coordination sphere of a metal ion (metal coordination number, CN) can maximize stability and resist transchelation by endogenous ligands *in vivo*.[19] Macrocyclic chelators generally provide greater kinetic inertness and overall stability than acyclic chelators at cost of slower radiolabeling kinetics. This is due the fact that a pre-organized macrocyclic chelator requires significantly less rearrangement and hence loss of entropy to coordinate with a metal ion, and this phenomenon is known as the macrocycle effect.[20]

The size of the chelate rings formed when two donor groups in a multidentate chelator coordinate with a metal ion are also known to have an effect on the complex stability, with larger metal ions preferring five-membered chelate rings and smaller metal ions preferring six-membered rings. However, chelate rings larger than six atoms result in decreased complex stability regardless

4

of the metal ion size.[21] This trend does appear to be broken in chelators with very large spacing between chelating moieties such as desferrioxamine (DFO), which forms 5-member chelate rings between hydroxamate (HA) moieties and Zr^{4+}, but also contains two different 14-member chelate rings between the three HA groups. Another consideration is that highly acidic radiometals such as gallium-68 require acidic conditions for labeling as they have a tendency to form insoluble hydroxide species under non-acidic aqueous solutions, therefore they undergo better complexation with lower basicity ligand donor groups.[4]

Although the labor of developing a chelator is difficult considering all the above key points in addition to notoriously difficult synthetic chemistry and purifications, one successfully developed radiometal-chelate complex could technically be conjugated to any compatible vectors for imaging (diagnostic radiopharmaceutical) or treatment of different targets (therapeutic radiopharmaceutical) making them very versatile chemical tools. In particular, theranostic radiopharmaceuticals which contain a chelator that can form highly stable complexes with several different radiometals to enable both nuclear imaging and targeted radionuclide therapy are in hot demand. Using this approach, a bifunctional chelator that can effectively bind a PET radionuclide such as zirconium-89 and a targeted radionuclide therapy radionuclide such as thorium-227 could be conjugated to peptides, antibodies, nanoparticles, or other vectors to create effective new theranostic agents. [1–3]

1.3. Selection and Evaluation of Chelators for Radiometals

When choosing a chelator for a particular radiometal for clinical applications, several important parameters are considered such as rate of complexation (radiolabeling kinetics), thermodynamic stability (e.g. formation constant, log K_{ML}), and kinetic inertness (rate of

transchelation/demetallation). Rate of complexation, known as complexation kinetics, is directly related to the radiolabeling properties of the chelators with a specific radiometal ion. The desired radiolabeling properties of a chelator include fast and high yielding complexation under mild conditions. Ideally, a quantitative conversion is obtained in 15 mins or less at ambient temperature. A subtle point is the buffer and pH, as near-neutral pH are preferred to minimize deleterious effects on the conjugated vector (e.g. peptide, antibody). Chelators which require long reaction times to provide high yields are not suitable for short half-life radionuclides. Although the reaction time can be reduced at elevated temperatures, most of the biovectors such as antibodies are heat sensitive molecules. Generally speaking, acyclic chelators possess much faster radiolabeling kinetics than do macrocycles. The radiolabeling properties are simply determined by radiolabeling experiments where the complexation reaction is monitored overtime by radio-iTLC or analytical radio-HPLC. [7,16, 18] Macrocyclic chelators such as DOTA require high temperatures (>80 °C) for fast radiolabeling with most radionuclides, but its exceptional *in vivo* stability and its commercial availability with many bifunctional derivatives for different bioconjugation chemistries overpower the non-ideal labeling properties.[1,7,16] Thermodynamic stability (formation constants, log K_{ML}) can be evaluated with stability constants determined experimentally by potentiometric or spectrometric titrations to probe metal complex formation under equilibrium conditions. This parameter depends mainly on the metal-ligand bond enthalpy and entropy, and it is strongly affected by hard/soft nature of the metal/chelator, chelator effect, and macrocyclic effect. Larger thermodynamic constant means higher tendency of the forward reaction (complex formation) than the reverse reactions (dissociation). However, it alone does not offer adequate prediction to *in vivo* stability as it does not account for the physiological conditions.[9,22] A derivative of the log K_{ML} formation constant is "pM", which is a measure of the amount of "free" metal ion present in solution in a

specific mixture of chelate and metal ion. A recent study by Holland et al has present a computational method to estimate thermodynamic formation constants, which is potentially of great utility due to the experimental complexity of traditional wet methods.[23]

Kinetic inertness of a radiometal complex is considered the most important parameter for predicting radiometal complex stability *in vivo* because it deals with the rate of dissociation or transchelation of the radiometal ion from the radiometal-chelate complex by other competing endogenous metal ions (e.g. calcium, magnesium), ligands (e.g. hydroxide, chloride), metal binding proteins (e.g. transferrin, albumin), and enzymes (e.g. superoxide dismutase). [1,4,16,19,23] Various *in vitro* experiments are performed to determine the relative kinetic inertness of radiometal complexes such as metal-exchange competition against physiological related mixtures such as blood serum, hydroxyapatite, *apo*-transferrin, or albumin, or competition against a large molar excess (100-1000×) of another chelator (e.g. EDTA, DTPA).[1,7,16,19] Generally, in the *in vitro* assays the radiometal complex is challenged by high molar excess of the biological reagents and often the results are compared to "gold standard" chelator(s) for that specific radiometal to gain an insight into the kinetic inertness and predict the *in vivo* stability of the metal-chelate complex. The ultimate *in vivo* stability of radiometallated chelators (unconjugated complex) and radiopharmaceuticals (in conjugation with vectors) are determined by animal studies such as PET imaging (*in vivo*) and biodistribution (*ex vivo*). Animal studies of the unconjugated radiometal-chelate complexes by PET imaging and biodistribution in healthy mice provides an important insight on their *in vivo* behavior, such as clearance and organ distribution, which could be clinically relevant if the metal-chelate complex is cleaved from the biovector and released into blood circulation.

Finally, the chelate complexes are typically conjugated to biovectors such as antibodies (mAb), peptides, or nanoparticles for functional *in vivo* evaluation. Conjugated radiometal complexes have slower pharmacokinetics and clearance than unconjugated complexes, which provides a great *in vivo* stability challenge, and a longer time period to monitor their stability. For example, most hydrophilic radiometal-chelate complexes clear through the renal system into the urine and are almost entirely excreted with a couple of hours, assuming the complex is stable. This does not present a serious *in vivo* stability challenge due to the short residence time in the body. A radiometal-chelate complex conjugated to a monoclonal antibody (mAb) can circulate in the body for weeks, thus providing a substantial stability challenge. Serial-PET imaging can be performed to monitor the pharmacokinetics and biodistribution over time, and *ex vivo* biodistributions can be performed on cohorts of mice at various timepoints to obtain more quantitative data. Using zirconium-89 as an example, it is a very oxophilic and osteophilic radiometal when not stably chelated *in vivo*, therefore a more stable [^{89}Zr]Zr-chelate should have lower bone uptake over extended periods of time. [5,12,16,19]

1.4. A Selection of Chelators Developed for Radiometals in the Last Decade

A list of recently developed radiometal chelators is shown below (**Table 1-2 – 1-8**) with the radiometals they have been evaluated with and their compatibility is discussed based on their available published data including radiolabeling performance, *in vitro* and *in vivo* stability, and other characterization methods. This discussion focuses on new chelators from the last ~10 years, as the chelators prior to this have already been extensively reviewed and are less relevant to the focus of this thesis.[1] A color-coding scheme has been assigned for the relative suitability of matching between each chelator and radiometal(s) based on my judgment from the information

obtained from literature: good (green), fair (orange) and poor (red). The chelators shown in the list are evaluated in different stages such as *in vitro*, *in vivo*, or clinical trials. Assigning of green may suggest the chelator is either currently the "gold standard" for the selected radiometal or it is a new chelator with promising results with a specific radiometal at the level of evaluation available in literature. An orange color assignment may mean the chelator is not the best choice for the radiometal, or it needs more study to determine its performance relative to "gold standard" chelators. An assignment of orange might also indicate a lack of broad utility (e.g. suboptimal stability), but some useful properties for certain applications. An assignment of red indicates that the chelator is not suitable for use with a specific radiometal due to substantial stability or radiolabeling issues.
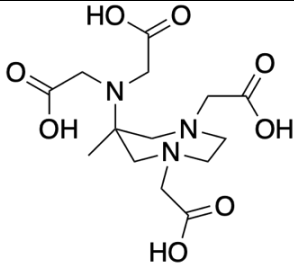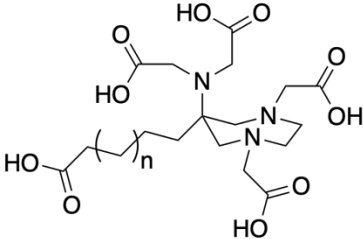
1.4.1. AAZTA, CyAAZTA and PIDAZTA-L2
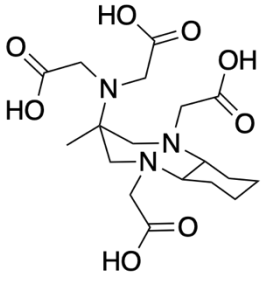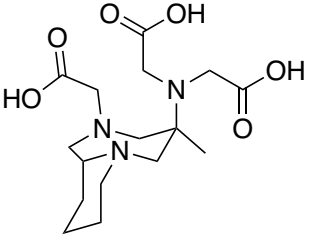
This family are derivatives of AAZTA chelator (**Table 1-2**), which originally was synthesized for Gd(III). It has a core of diazepane heterocyclic ring and 4 pendant carboxylic acid arms. This heptadentate ligand has shown to have high binding affinity for many transition metals.[24,25] It has excellent radiolabeling properties for [^{68}Ga]Ga, [^{44}Sc]Sc , [^{177}Lu]Lu, [^{111}In]In, superior to DOTA and NOTA at milder conditions (<5 mins, room temperature (rt), pH 4 - 5.5, 10 nM). Even though it's *in vitro* and *in vivo* stability with gallium is not optimum the bifunctional versions AAZTA have been conjugated to different vectors/biomolecules such as octreotide (TOC)[26], minigastrin (MG)[27], cycloArg-Gly-Asp-Dphe-Lys (cRGDfK)[28] and antibody[29].

AAZTA-TOC was radiolabeled with each of gallium, lutetium, indium, and scandium. [^{68}Ga]Ga-AAZTA^5-TOC showed >99% stability in each of EDTA and DTPA challenges and 95% serum stability after 2 h. [^{44}Sc]Sc-AAZTA^5-TOC and [^{177}Lu]Lu-AAZTA^5-TOC showed >99%

resistance to DTPA and EDTA challenge for 24 h with serum stability of 94% and 91% respectively.[24,26,30] Additionally, AAZTA-bevacizumab was successfully labelled with [^{177}Lu]Lu (90 mins, 37 C, pH 7).[29] Similar results were obtained for minigastrin conjugated versions of AAZTA; [^{68}Ga]Ga-AAZTA-MG, [^{44}Sc]Sc-AAZTA-MG, [^{111}In]In-AAZTA-MG and [^{177}Lu]Lu-AAZTA-MG.[27] Moreover, biodistribution and PET/MRI image of Sc-CNAAZTA-c(RGDfK) showed excellent in vivo stability of Sc-AAZTA complex and high tumor to background ratio of 25.[28] Most recent derivatives of AAZTA are the two less flexible chelators; CyAAZTA, PIDAZTA-L2, with integrated cyclohexane to the diazepane ring (**Table 1-2**). CyAAZTA has similar radiolabeling kinetics with even lower stability to the parent AAZTA.[31] However, PIDAZTA-L2 has a rapid Gallium labeling kinetics even at physiological conditions (5 mins, rt, pH 7.5, 10 µM) which is favoured for most biomolecule conjugations. Moreover, it showed improved *in vitro* stability over AAZTA.[24]

Table 1-2. AAZTA and its derivatives, highlighting paired radiometal ions, radiolabeling conditions, thermodynamic stability constant (log K_{ML}), level of evaluation, and color-coded ranking

Chelator and Common Bifunctional Derivatives	Radiometal Ion	a	Radiolabeling Conditions	Log K_{ML} (Log β)	b	Ref.
1,4-bis (carboxymethyl)-6-[bis (carboxymethyl)]amino-6-methylperhydro-1,4-diazepine), **AAZTA**, N$_3$O$_3$ or N$_3$O$_4$, CN = 6 - 7	[^{67}Ga]Ga^{3+}/ [^{68}Ga]Ga^{3+}	~	25 °C, < 5 min, pH 4 - 5.5 (>95%)	22.18	**In vivo**	25
	[^{177}Lu]Lu^{3+}	~	25 °C, < 5 min, pH 4 - 5.5 (>95%)	-	**In vivo**	27
	[^{47}Sc]Sc^{3+}/ [^{44}Sc]Sc^{3+}	✓	25 °C, < 5 min, pH 4 - 5.5 (>95%)	27.69	**In vivo**	25,30
	[^{111}In]In^{3+}	~	25 °C, < 5 min, pH 4 - 5.5 (>95%)	29.58	**In vivo**	25

	Bifunctional AAZTA chelators-**AAZTA5**[29,30] (n=1) and **CNAAZTA**[28] (n=6)						
trans-3-amino-3-methyldecahydro-1H-1,5-benzodiaze- pine-F*N,N',N'',N''* tetraacetic acid, **Cy-AAZTA,** N_3O_3 or N_3O_4, CN = 6 - 7	$[^{67}Ga]Ga^{3+}/$ $[^{68}Ga]Ga^{3+}$	~	25 °C, < 15 min, pH 3.8 (>80%)	21.92	**In vitro**	31
4-amino-4-methylperhydro-pyrido[1,2-a][1,4]diazepin-*N,N',N'*-triacetic acid, **PIDAZTA-L2**, N_3O_3, CN = 6	$[^{67}Ga]Ga^{3+}/$ $[^{68}Ga]Ga^{3+}$	~	25 °C, 5 min, pH 7-8 (93.5%)	21.70	**In vitro**	24
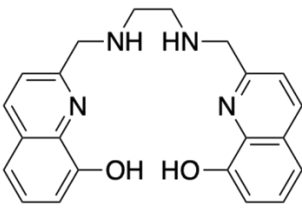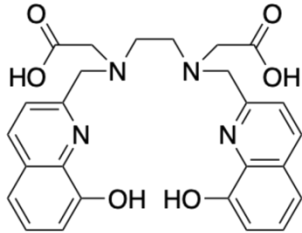
[a] My personal assessment of radiometal-chelator match based on available data cited in this work, and [b] the level of evaluation of the radiometal-chelator complex available in literature.
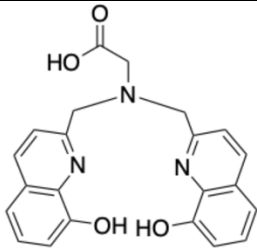
1.4.2. H₂hox, H₄octox and H₃glyox

These chelators generally contain 2 oxine groups on a single or di-amine backbone which are known to have easy synthesis pathways (**Table 1-3**). H_2hox, a hexadentate member of this family (**Table 1-3**), has fast radiolabeling kinetics with $[^{68}Ga]Ga^{3+}$ as quantitative radiolabeling was obtained in 5 mins at rt in nM concentrations. This non-bifunctional chelator showed >99% stability in mouse plasma for 60 minute. Moreover, PET/CT image and biodistribution in healthy mice fast clearance through kidney and liver was observed with no bone and muscle uptake.[32] H_4octox is another chelator from this family with two carboxylic acid arms (**Table 1-3**). This octadentate chelator was studied with $[^{111}In]In^{3+}$ and displayed great radiolabeling properties (~

98% RCY, at rt and nM concentrations). Furthermore, [^{111}In]In-octox was highly resistant to transchelation and transmetallation (transferrin 98% intact for 5 d, Fe^{3+} >97 % intact for 2 d). SPECT image after 1 h in healthy mice exhibited lipophilic character as it was observed to be excreted more through liver and gastrointestinal tract than kidney and bladder.[33] Another oxine based chelator is H$_3$glyox which consists of 2 oxine groups on a glycine backbone (**Table 1-3**). This hexadentate chelator showed excellent radiolabeling for each of [^{68}Ga]Ga^{3+}, [^{111}In]In^{3+}, and [^{44}Sc]Sc^{3+} (>95% RCY, at rt and μM). It was found to form most stable complex with indium with highest conditional stability constant (pM value) of 34 and had >99% stability in 7 d serum stability challenge. [^{68}Ga]Ga-glyox was also 98% intact in 60 minute transferrin challenge.[4] One advantage of oxine based chelators is that their fluorescence can be activated by coordination to some metals such as gallium, indium ytterbium and scandium, and can be potentially used as dual imaging modality. [4,32,33]

Table 1-3. oxine based chelators, highlighting paired radiometal ions, radiolabeling conditions, thermodynamic stability constant (log K_{ML}), level of evaluation, and color-coded ranking

Chelator and Common Bifunctional Derivatives	Radiometal Ion	a	Radiolabeling Conditions	Log K_{ML} (Log β)	b	Ref.
 H$_2$hox, N$_4$O$_2$, CN = 6	[^{67}Ga]Ga^{3+}/ [^{68}Ga]Ga^{3+}	~	25 °C, 5 min, pH 8.5	34.4	**In vivo**	32
 H$_4$octox, N$_4$O$_4$, CN = 8	[^{111}In]In^{3+}	✓	25 °C, 15 min, pH 5.5 (98%)	31.38	**In vivo**	33
	[^{86}Y]Y^{3+}/ [^{90}Y]Y^{3+}	~	-	23.78	**In vitro**	33

H2glyox, N₃O₃, CN = 6	[¹¹¹In]In³⁺	✓	25 °C, 5 min, pH 7.4	38.78	**In vitro**	4
	[⁶⁷Ga]Ga³⁺/ [⁶⁸Ga]Ga³⁺	~	25 °C, 5 min, pH 7.4 (95%)	29.82	**In vitro**	4
	[⁴⁷Sc]Sc³⁺/ [⁴⁴Sc]Sc³⁺	~	25 °C, 5 min, pH 7.4	30.9	**In vitro**	4

[a] My personal assessment of radiometal-chelator match based on available data cited in this work, and [b] the level of evaluation of the radiometal-chelator complex available in literature.

1.4.3. H₂CHXdedpa and H₄CHXoctapa
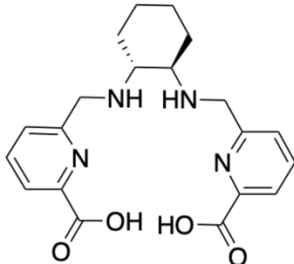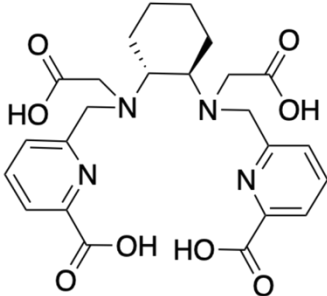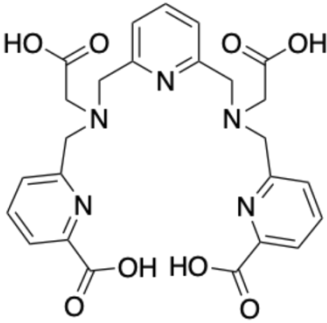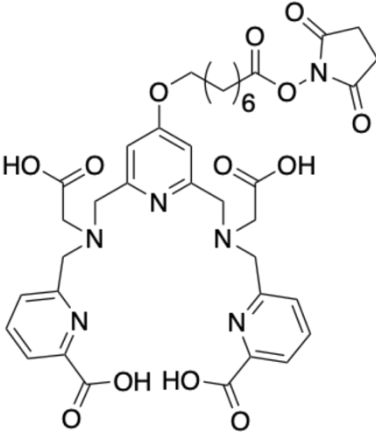
This group of chelators have picolinic acid arms (PA) on polyamine backbones (**Table 1-4**). they are derivatives of H₂dedpa and H₄octapa, two parent acyclic chelators which have superior radiolabeling kinetics to many radiometals over gold standard chelators DOTA and NOTA, in mild conditions. However, they are not as stable *in vitro* and *in vivo*.[34,35] H₂*CHX*dedpa and H₄*CHX*octapa are two new derivatives which their structures are rigidified by integration of a chiral cyclohexane (**Table 1-4**) for the purpose of improvement in *in vitro* and *in vivo* stability. H₂*CHX*dedpa has the same labeling properties as H₂dedpa (>99% RCY, at rt and µM) with [⁶⁷Ga]Ga³⁺. Unlike H₂dedpa, the radiolabeling yield decreases at lower concentrations (nM). As it was expected, its serum stability in 120 mins surpassed H₂dedpa and even DOTA (90.5%, 77.8 %and 80% respectively).[34] In coordination with [⁶⁴Cu]Cu²⁺, H₂*CHX*dedpa recorded even better labeling characteristics and serum stability (>99% RCY, rt, 10 min, µM and only 2% demetallation in 24 h incubation in serum, demetallation from H₂dedpa was 28%).[35] The octadentate H₄*CHX*octapa with two extra carboxylic acid arms (**Table 1-4**) had excellent radiolabeling properties (quantitative in 10 mins, at rt and µM) with [¹¹¹In]In³⁺, and its serum stability was 91% in 5 d slightly less than H₄octapa. H₄*CHX*octapa was also labeled with [²⁵⁵Ac]Ac³⁺ with high radiochemical yield at mild conditions (94% at rt, 60 mins in µM) and it was highly stable (95% intact for 7 d) in human serum superior to gold standard chelator DOTA. [36]
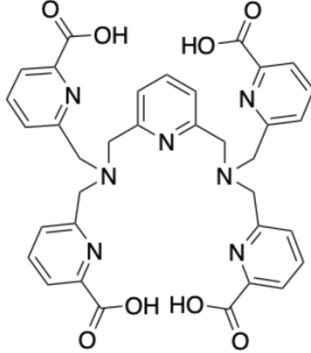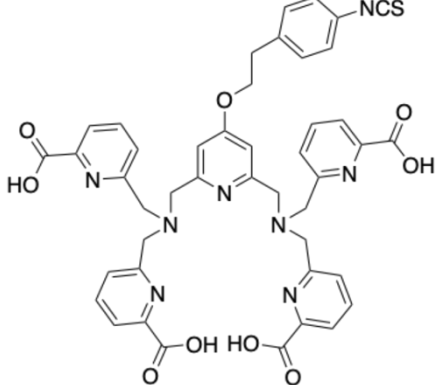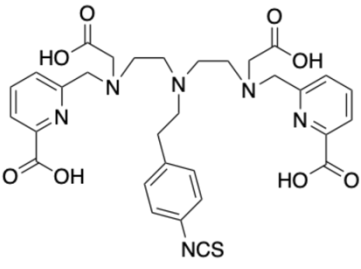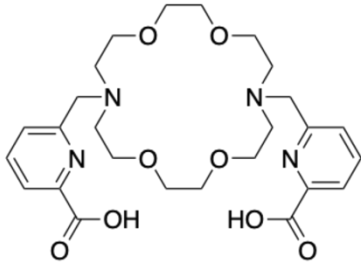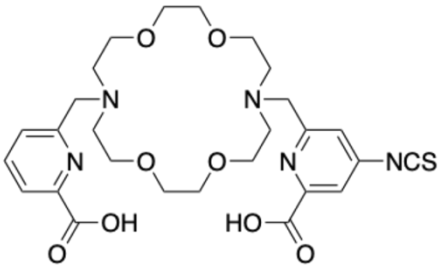
Another new picolinic acid-based chelator is nonadentate H$_4$pypa which has a pyridine backbone offering a semi-rigid structure (**Table 1-4**). It has excellent radiolabeling properties for [^{111}In]In^{3+} (SPECT radionuclide) and [^{177}Lu]Lu^{3+} (therapy) (>98% RCY at rt, 10 min, μM) with exceptional serum stabilities of >99% in 7 d for [^{177}Lu]Lupypa$^-$ and 5 d for [^{111}In]Inpypa$^-$. The PSMA conjugated version of pypa was also injected to tumor bearing mice and showed fast clearance in most organs except for kidney. The tumor to kidney ratio was ~ 7 after 24 h post injection for [^{177}Lu]Lupypa-C7-PSMA617 while it was much lower for [^{111}In]Inpypa-C7-PSMA617 (~ 0.25).[37] H$_4$pa4pa is an undecadentate derivative of pypa with 4 picolinic acid arms (**Table 1-4**). This large chelator was found to have great labeling kinetics with [^{225}Ac]Ac^{3+} (>99% RCY, rt, 30 min, μM) and high serum stability (>99% intact in 9 d). A bifunctional derivative of H$_4$pa4pa was conjugated to trastuzumab which was found to have clearance, stability and tumor uptake comparable to [^{225}Ac]AcDOTA-Trastuzumab in tumor bearing mice.[38]

Another nonadentate chelator is H$_4$neunpa with a diethylenetriamine backbone (**Table 1-4**) that displayed an excellent labeling kinetics and serum stability for [^{111}In]In^{3+}. However, its trastuzumab conjugate in tumor bearing mice showed decreased tumor accumulation and stability compared to [^{111}In]InCHX-A"-DTPA.[39] Macropa which has a slightly different structure (**Table 1-4**), with two picolinic acid groups on a diaza-crown ether (diaza-18-crown-6), is reported to have high affinity to large lanthanide metals.[40,41] Recently, macropa was tested for [^{225}Ac]Ac^{3+} and quantitative labeling was obtained in 10 mins at ambient temperature. Moreover, it was completely resistance to demetallation in 7 d serum challenge and only 2% demetallation was observed when incubated with 50 equivalents of La^{3+}. Its bifunctional derivative was successfully conjugated to trastuzumab and remained intact for 7 d in human serum. *In vivo* stability in tumor bearing mice, was assessed for [^{225}Ac]Ac-macropa in conjugation with RPS-070 (A PSMA/albumin dual-

targeting agent) and it was found to be stable up to 96 h. Although tumor accumulation reached 13%ID/g in the first 4 h, the activity decreased afterwards.[42]

Table 1-4. picolinic acid-based chelator, highlighting paired radiometal ions, radiolabeling conditions, thermodynamic stability constant (log K_{ML}), level of evaluation, and color-coded ranking

Chelator and Common Bifunctional Derivatives	Radiometal Ion	a	Radiolabeling Conditions	Log K_{ML} (Log β) b		Ref.
H₂CHXdedpa, N₄O₂, CN = 6	[^{64}Cu] Cu^{2+}	✓	25 °C, 10 min pH 5.5	-	In vitro	35
	[^{67}Ga]Ga^{3+}/ [^{68}Ga]Ga^{3+}	✓	25 °C, 10 min pH 4	27.61 pM = 26.7	In vitro	34
H₄CHXoctapa, N₄O₂, CN = 8	[^{67}Ga]Ga^{3+}/ [^{68}Ga]Ga^{3+}	~	25 °C, 10 min pH 4	22.32 pM = 21.4	In vitro	34,43
	[^{111}In]In^{3+}	✓	25 °C, 10 min pH 4	27.16 pM = 26.3	In vitro	34
	[^{225}Ac]Ac^{3+}	✓	25 °C, 60 min pH 5.5 (94%)	-	In vitro	36
H4pypa, N₅O₄, CN = 8 – 9	[^{111}In]In^{3+}	✓	25 °C, 10 min pH 7	30.5	In vivo	37
	[^{177}Lu]Lu^{3+}	✓	25 °C, 10 min pH 7	22.2	In vivo	37
	[^{225}Ac]Ac^{3+}	✓	25 °C, 30 min pH 7	-	In vivo	38

H4pypa-C7-NHS[37], bifunctional derivative of **H4pypa**

H4pa4pa, N_7O_4, CN = 11

H4pa4pa-NCS, bifunctional derivative of **H4pa4pa**

$[^{111}In]In^{3+}$	~	25 °C, 10 min pH 4	**28.17** pM = 23.6	In vivo		[39]
$[^{225}Ac]Ac^{3+}$	X	40 °C, 60 min pH 5.5 (87%)	-	-		[36]
$[^{177}Lu]Lu^{3+}$	X	25 °C, 10 min pH 4	-	-		[39]
$[^{212}Bi]Bi^{3+}/$ $[^{213}Bi]Bi^{3+}$	~	-	**28.76** pM = 27	-		[39]
$[^{225}Ac]Ac^{3+}$	✓	25 °C, 10 min, pH 5	-	In vivo		[41,42]

p-SCN-Bn-H4neunpa, N_5O_4

Macropa, N_4O_6, CN = 6 -10

Macropa-NCS, bifunctional derivative of Macropa

[a] My personal assessment of radiometal-chelator match based on available data cited in this work, and [b] the level of evaluation of the radiometal-chelator complex available in literature.

1.5. Zirconium-89 in PET Imaging

Zirconium-89 has quickly become an attractive radionuclide in nuclear medicine for its application in antibody-based positron emission tomography (immune-PET) due to its relatively long half-life that matches the biological half-life of intact antibodies, favorable decay properties, and well established and affordable production and purification.[44–47] Monoclonal antibodies

(mAbs) are macromolecules with high specificity and affinity for receptors and other pathological factors which made them valuable targets for constructing imaging agents. They generally demonstrate slow pharmacokinetics, and their biological half-life may extend weeks. Therefore, employing mAbs in nuclear imaging require a radionuclide with half-life long enough to allow the radiolabeled antibody to accumulate in the targeted tissue (~1-3 d) before imaging and zirconium-89 with a physical half-life of ~3.3 d is considered the most suitable radionuclide for that purpose.[48–50] Furthermore, [^{89}Zr]Zr(IV) decays to stable [^{89}Y]Y (III) through a short lived intermediate [^{89m}Y]Y ($t_{1/2}$ = 15.7 s) via positron emission (22.3%) with a relatively low average positron energy (395.5 keV), which produces high resolution PET images (R_{ave} β^+= 1.18 mm).[46,47] [^{89}Zr]Zr(IV) is produced by proton bombardment of commercially available, 100% natural abundance [^{89}Y]Y-foil target ^{89}Y(p,n)^{89}Zr, in high specific activity (470-1195 Ci/mmol) and radionuclidic and radiochemical purity (>99.99%).[7,51]

1.6. Chemistry of Zr-89

Zirconium is a transition metal from group IVB and exists predominantly in 4+ oxidation state in aqueous solution and its most stable compounds. The highly charged and relatively small size zirconium ion is a 'hard' oxophilic cation, usually prefers hard doner atoms especially oxygen in its coordination complexes.[19] Utilizing zirconium-89 for clinical application is strongly reliant on accessibility of a suitable chelator that forms kinetically inert complex *in vivo*. Previous studies have shown that, zirconium forms more stable complexes with chelators that saturate its coordination number (7-8).[52,53] Many chelators have been studied for [^{89}Zr]Zr(IV) coordination, Deferoxamine B (DFO) is the chelator most commonly used for synthesizing biomolecular conjugates when radiolabeling with [^{89}Zr]Zr^{+4}.[1] DFO is produced by bacteria with the specialized
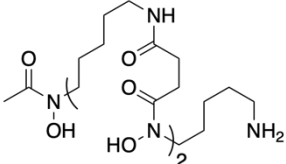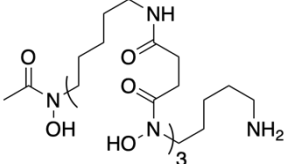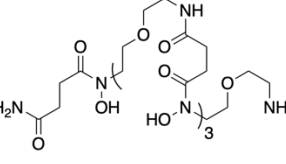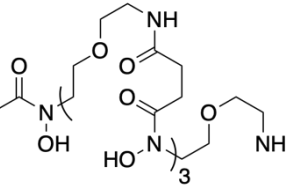
purpose of sequestering Fe(III) from the environment.[54] Fortuitously, DFO also quickly forms a stable complex with $[^{89}Zr]Zr^{+4}$ and is widely considered the golden standard chelator for $[^{89}Zr]Zr^{+4}$, having been used in most of its preclinical and clinical imaging applications to date.[1,55,56] It binds to the Zr^{+4} ion through three hydroxamic acid/hydroxamate groups, offering a hexadentate environment and a coordination number (CN) of 6. Despite the excellent radiolabeling properties, *in vitro* and *in vivo* studies have revealed the $[^{89}Zr]Zr$-DFO complex is not completely resistant to demetallation.[55,57,58] The Zr^{+4} ion is known to prefer a CN of seven or eight, which cannot be fulfilled by DFO alone. The two vacant coordination sites are thought to be filled with aqua ligands, which combined with its strong solvent activation effects (low metal pK_a) could be a reason behind some of the observed lability of the ^{89}Zr-DFO complex. Murine studies have shown part of the injected activity is accumulated in bones, likely due to the oxophilic and hard character of $[^{89}Zr]Zr^{4+}$ matching well with the bone's phosphate rich structure.[58,59] For that reason, the amount of activity taken up in mouse bones is considered a measure of *in vivo* stability of Zr^{4+} complexes in the body. It is important to note that PET imaging studies in humans using ^{89}Zr-immunoconjugates have not reported abnormally high bone uptake.[45,55,60–62] Prevention of unwanted irradiation of healthy tissues such as bone marrow by "free" $[^{89}Zr]Zr^{+4}$ has been the driving force behind numerous studies towards development of better chelators for $[^{89}Zr]Zr^{+4}$.

Increasing the denticity of DFO from a CN of 6 to 8 would hypothetically saturate the coordination sphere of Zr^{4+}, hence producing chelators with improved stability. For that reason, DFO* — the first octadentate derivative of DFO — was synthesized and examined (**Table 1-5**). With an extra hydroxamic acid group, bombesin conjugated DFO*, which labeled in high RCY yields (>95, rt, 2-16 h, 3 μM) showed total resistance to demetallation when competed against 300 molar equivalents of excess DFO for 24 h, and more than 90% was intact even against 3000 molar
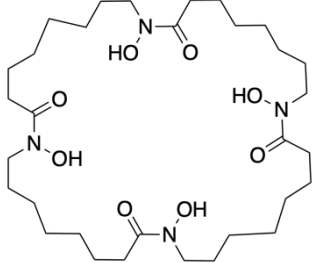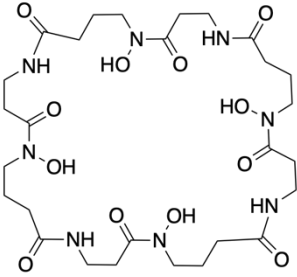
equivalents of DFO.[63] *In vivo* studies of [^{89}Zr]Zr-DFO*-trastuzumab showed the same superiority of DFO* over DFO in sequestering [^{89}Zr]Zr^{4+} as a biologically inert complex, demonstrated by a reduction in radioactivity accumulated in healthy tissue. Most notably, 7 d post injection in N87 tumor-bearing mouse bone uptake was reduced more than 3 folds compared to DFO.[52] Unsurprisingly, DFO* exhibits poor water solubility, which is undesired especially when antibody and peptide conjugation reactions are performed in water and mild temperatures. In order to improve solubility of DFO*, two ether-containing chelators; DFO-O$_3$-PBH-O$_1$ and oxoDFO* were synthesized (**Table 1-5**).[54,64] These octadentate derivatives of DFO possess 4 oxygen atoms as ether groups in the backbone of DFO*, which increased the log $D_{7.4}$ from ~ -0.44 (DFO*) to -1.5.[64] Although both of the chelators showed improved water solubility, detailed radiolabeling, *in vitro*, and *in vivo* studies are yet to be published.

A study by Guérard et al., showed that number of carbon atoms between hydroxamate groups effects the radiolabeling performance and stability of zirconium-89 chelators. Their study revealed that 7 carbons between consecutive hydroxamic acid moieties in a tetrahydroxamate chelator forms the right cavity size for Zr^{4+}. The chelators C7 (cyclic) and L7 (acyclic, **Table 1-5**) had faster radiolabeling kinetics (> 99% RCY, in 120 mins, at 20 °C and 160 µM) than chelators with smaller inter-hydroxamate atomic spacing. It is worth noting that DFO can quantitatively coordinate zirconium-89 in 15-30 mins at ambient temperature; however, this is concentration dependant.[65] Both C7 and L7 chelators showed better *in vitro* stability than DFO in each stability assay of blood serum, phosphate buffer (pH 7.4 and 6.5), and EDTA challenge.[66] Seibold et al. synthesized CTH36 — a macrocyclic chelator similar to C7 with an extra amide group between the successive hydroxamate groups (**Table 1-5**). High (> 96%) radiolabeling was obtained (in 60 min, at 25 ºC and ~125 nM concentrations). Moreover, it showed more than 95% stability after a

32 h EDTA challenge. A bifunctional version of CTH36 was conjugated to an RGD peptide analogue.[67] However, no *in vivo* studies of both chelators have been published to date.

Table 1-5. A selected group of $[^{89}Zr]Zr(IV)$ chelators, highlighting $[^{89}Zr]Zr(IV)$ and other paired radiometal ions, radiolabeling conditions, thermodynamic stability constant (log K_{ML}), level of evaluation, and color-coded ranking

Chelator and Common Bifunctional Derivatives	Radiometal Ion	a	Radiolabeling Conditions	Log K_{ML} (Log β)	b	Ref.
Desferrioxamine B (**DFO**), O_6, CN = 6	$[^{89}Zr]Zr^{4+}$	✓	25 °C, 60 min, pH 7-7.3	**40.04**	Clinical trial	65,67–69
	$[^{67}Ga]Ga^{3+}/$ $[^{68}Ga]Ga^{3+}$	~	25 °C, 30 min, pH 3.5	**28.6**	**In vivo**	1,70
DFO*, O_8, CN = 8	$[^{89}Zr]Zr^{4+}$	✓	25 °C, 2-16 h, pH 7-7.3 (>95%)	-	**In vivo**	52,63
oxoDFO*, O_8, CN = 8	$[^{89}Zr]Zr^{4+}$	~	-	-	-	64
DFO-O₃-PBH-O₁, O_8, CN = 8	$[^{89}Zr]Zr^{4+}$	~	-	-	-	54
	$[^{89}Zr]Zr^{4+}$	~	25 °C, 120 min, pH 7 (>99%)	-	**In vitro**	66

C7, O_8, CN = 8						
CTH36, O_8, CN = 8	$[^{89}Zr]Zr^{4+}$	✓	25 °C, 60 min, pH 7-9 (>96%)	-	**In vitro**	67
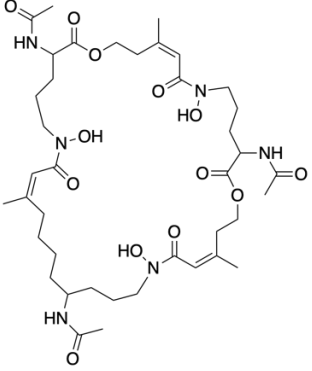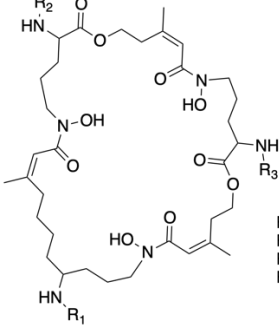
[a] *My personal assessment of radiometal-chelator match based on available data cited in this work, and* [b] *the level of evaluation of the radiometal-chelator complex available in literature.*

Triacetylfusarinine C (**TAFC**) is another siderophore, produced by fungi to enable it to sequester and utilize Fe^{3+} (**Table 1-6**).[71] TAFC is analogous to a cyclic version of DFO, where it is a hydroxamate-based, hexadentate, and macrocyclic chelator. Its *N*-deacetylated derivative, Fusarinine C has three primary amines, which are used to make bifunctional version of the chelator for bioconjugation. Fusarinine C derivatives have high radiolabeling performance and quantitative radiolabeling yields were obtained at room temperature in 1.5 h (0.3 μM concentrations).[72] *In vitro* stability was by far superior to DFO, when challenged to EDTA less than 3% demetallation was observed in 7 d, while DFO demetallation exceeded 50%.[72] Serum stability was comparable to DFO and both remained >90% intact. Its RGD conjugate showed fast renal excretion in $\alpha_v\beta_3$ integrin positive M21 tumor-bearing mice. Biodistribution results at 4 h post injection showed low bone uptake (0.71-0.79 % ID/g); however, DFO was not used as a control/comparison in this study, therefore any improvement in stability in mice cannot be confirmed.[72,73]

FSC(succ)$_2$AA, FSC(succ)$_2$ and FSC(succ)$_3$ are 3 FSC-based octadentate chelators with pendant carboxylic acid groups (**Table 1-6**). FSC(succ)$_2$ and FSC(succ)$_3$ have a free primary amine and a carboxylic acid group which can be used as chemical handles for bioconjugation reactions.[74] To my knowledge, they are the only octadentate chelators for Zr^{4+} with higher hydrophilicity than DFO (Log D for DFO, FSC(succ)$_2$AA and FSC(succ)$_3$ are -3.0 ± 0.1, -3.3 ± 0.1, and -3.5 ± 0.4, respectively). They have great radiolabeling kinetics and yields in mild conditions similar to TAFC (>97% RCY, 30-90 mins, rt, ~50 µM). *In vitro* stability assays with these chelators — EDTA challenge at various pHs, serum stability, and excess competing chelator (DFO) challenge up to 7 d — all showed better stability performance than DFO for both FSC(succ)$_2$AA and FSC(succ)$_3$. Fast clearance of the unconjugated chelators in healthy mice was further evidence of hydrophilicity.[74] Still yet, antibody/vector conjugation and imaging/biodistribution at longer time points are required to assess *in vivo* stability of the chelators with [^{89}Zr]Zr^{4+}. TAFC and its derivatives have also been shown to have high radiolabeling kinetics with [^{68}Ga]Ga^{3+}, quantitative labeling was obtained in 30 mins at rt in µM concentrations. Moreover, TAFC and its RGD conjugates showed high stability in serum, EDTA and DTPA challenges (>99, >96 and >98% respectively for 4 h). *In vivo* studies in healthy mice and mice with A413-CCK2R tumor xenografts displayed fast clearance, low background and high tumor uptake.[73,75,76]

Table 1-6. triacetylfusarinine C and its derivatives, highlighting [^{89}Zr]Zr(IV) and other paired radiometal ions, radiolabeling conditions, thermodynamic stability constant (log K_{ML}), level of evaluation, and color-coded ranking

Chelator and Common Bifunctional Derivatives	Radiometal Ion	*a*	Radiolabeling Conditions	Log K_{ML} (Log β)	*b*	Ref.
	[^{89}Zr]Zr^{4+}	✓	25 °C, 90 min, pH 6.8-7.2	-	In vivo	72

Triacetylfusarinine C, **TAFC**, O_6, CN = 6	$[^{67}Ga]Ga^{3+}/$ $[^{68}Ga]Ga^{3+}$	~	25 °C, 30 min, pH 4.5	-	**In vivo** [73,75]

FSC: $R_1 = R_2 = R_3 = H$
FSC(succ)$_2$: $R_1 = R_2 = COCH_2CH_2COOH$, $R_3 = H$
FSC(succ)$_2$AA: $R_1 = R_2 = COCH_2CH_2COOH$, $R_3 = COCH_3$
FSC(succ)$_3$: $R_1 = R_2 = R_3 = COCH_2CH_2COOH$

FSC and its derivatives[76]

[a] My personal assessment of radiometal-chelator match based on available data cited in this work, and [b] the level of evaluation of the radiometal-chelator complex available in literature.

Besides the infamous hydroxamic acid/hydroxamate moiety, there are other metal-binding groups with hard donor atoms which are known to bind to metals similar to Zr^{4+}, such as hydroxypyridinone/hydroxypyridinonate and various catechols/catecholates. 3,4,3-(LI-1,2-HOPO) — also recognized as HOPO, (**Table 1-7**) — consists of 4 hydroxypyridinone groups on a spermine backbone and is a known chelator of Plutonium (IV).[77] Quantitative radiolabeling of HOPO with $[^{89}Zr]Zr^{+4}$ was obtained in 1-3 h (10 µM at rt). All *in vitro* studies for non-bifunctional HOPO showed excellent stability, and even an excess metal challenge with Fe^{3+} showed $[^{89}Zr]Zr$-HOPO to be far more stable than $[^{89}Zr]Zr$-DFO.[78] Despite its *in vitro* prowess as a free chelator, its trastuzumab conjugate was slightly less stable *in vitro* after one week incubation in human serum (89.2%) than $[^{89}Zr]Zr$-DFO (94.7%). However, evaluation of its *in vivo* stability with animal studies proved higher stability of $[^{89}Zr]Zr$-HOPO-trastuzumab as bone uptake significantly decreased to only 2.4 ± 0.3 %ID/g compared to $[^{89}Zr]Zr$-DFO-trastuzumab (17.0 ± 4.1 %ID/g) in 14 d post injection. It is important to mention, surprisingly tumor uptake was significantly lower for mice was injected with $[^{89}Zr]Zr$-HOPO than mice was injected with $[^{89}Zr]Zr$-DFO.[79] This divergent tumor uptake could be related to inter-animal variability in tumor size and tumor-cell
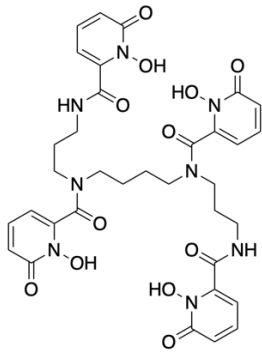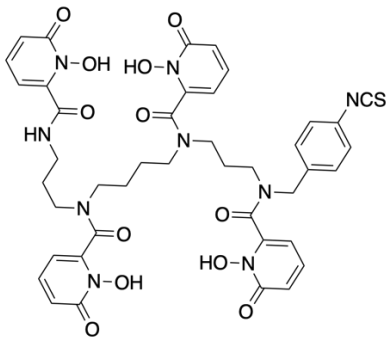
composition. This highlights the benefit of using a non-tumor bearing mouse models for these types of strict *in vivo* stability experiments, where the tumor variable is removed from the equation and pharmacokinetic (e.g. bone-uptake) can be observed without complication. A caveat to using healthy mice is that high tumor uptake could contribute to demetallation and/or metabolism of the radiometal-conjugate. For example, tumor-over-expressed or uniquely-expressed biological components such as proteases, or other tumor microenvironment factors such as lower pH or lower oxygen concentration would not be present in a healthy mouse model.
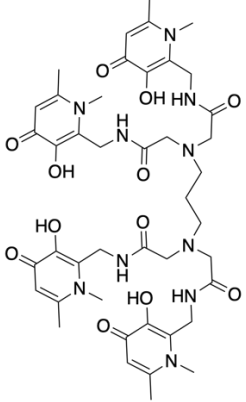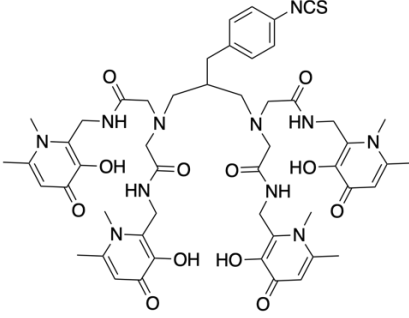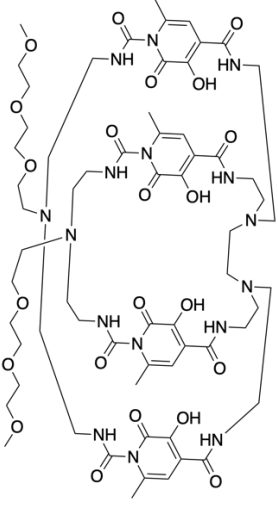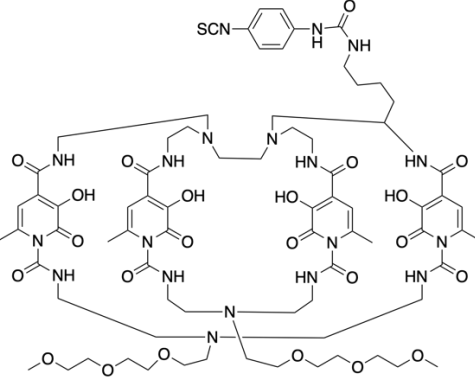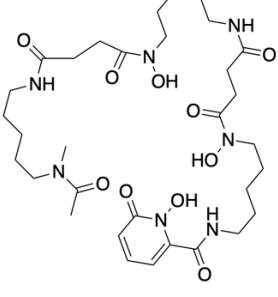
THPN is another chelator from the HOPO family, based on the core 3,4-HOPO group (**Table 1-7**). It has very rapid radiolabeling properties at μM scales ($\geq 16.7\ \mu$M) and quantitative yields were obtained in 10 to 30 mins at rt. It showed excellent *in vitro* stability in assays such as excess chelator competitions (DFO, EDTA, 100 times molar excess) and serum challenges, and appeared to be far superior to DFO in all assays.[80] The *in vitro* results were also supported by a high pM (pZr^{4+}) value of 42.8, the second highest reported to date for Zr^{4+} after HOPO, and the highest formation constant (log β = 50.3) among those measured and reported for Zr^{4+}. Its bifunctional version (p-SCN-Phe-THPN) was conjugated to hyperbranched polyglycerol (HPG) and injected to healthy mice, and in contrast to its exceptional *in vitro* stability results, biodistribution and PET imaging revealed inferior stability of THPN-HPG to both DFO-HPG and DFO*-HPG. The higher uptake in bones compared to DFO and DFO* conjugates was thought to be result of modification in the coordination system caused by the HPG conjugation.[81]

Another interesting HOPO derivative is BPDETLysH22-3,2-HOPO (**Table 1-7**), which is an octadentate dimacrocyclic chelator (two integrated macrocycles), that has rapid radiolabeling kinetics, (quantitative in 15 mins) in mild conditions. However, both *in vitro* and *in vivo* studies of

unconjugated and trastuzumab conjugated [^{89}Zr]Zr- BPDETLysH22-3, 2-HOPO revealed inferior

stability to DFO.[59] DFO-HOPO is a hybrid chelator of DFO and HOPO (**Table 1-7**), which has

been previously used for plutonium (IV) chelation. It showed similar DFO radiolabeling properties

for [^{89}Zr]Zr^{4+} (>99% RCY, in 60 min, at rt and low μM concentrations) with high resistance to

demetallation by excess DFO and by serum challenges (> 99%) up to 7 d. *In vivo* studies of the

non-bifunctional chelator in healthy mice showed rapid renal excretion and lower bone activity

accumulation compared to [^{89}Zr]Zr-DFO, which can be a good sign of high *in vivo* stability but in

this case is likely a result of the altered pharmacokinetics to faster urinary excretion.[53] Synthesis

of a bifunctional version and antibody conjugation studies of DFO-HOPO are not yet available for

review. A summary of the chelators I have developed in my PhD are shown in **table 1-8**.

Table 1-7. [^{89}Zr]Zr(IV) chelators with non-hydroxamic acid binding groups, highlighting radiolabeling conditions, thermodynamic stability constant (log K_{ML}), level of evaluation, and color-coded ranking

Chelator and Common Bifunctional Derivatives	Radiometal Ion	*a*	Radiolabeling Conditions	Log K_{ML} (Log β)	*b*	Ref.
	[^{89}Zr]Zr^{4+}	✓	25°C, 60-180 min, pH 7	**43.1**	**In vivo**	[78,79,82]
3,4,3-(LI-1,2-HOPO), **HOPO,** O$_8$, CN = 8 *p*-**SCN-Bn-HOPO**[79] a bifunctional version of **HOPO**						
	[^{89}Zr]Zr^{4+}	X	25°C, 10 min, pH 7.5	**50.3**		[80–82]

Structure	Ion		Conditions		Type	Ref
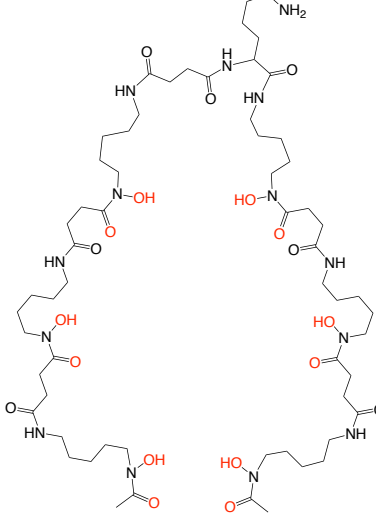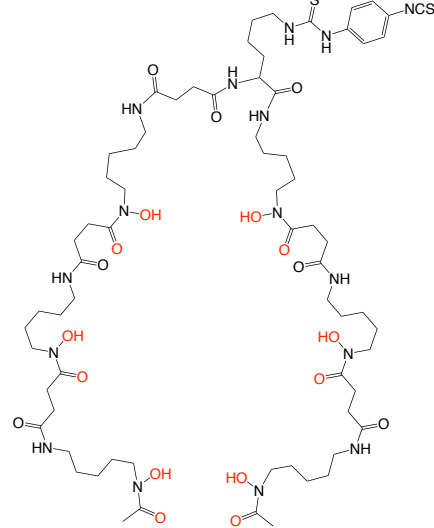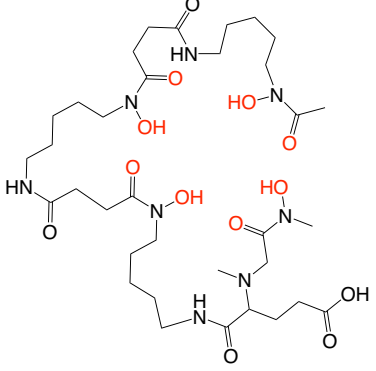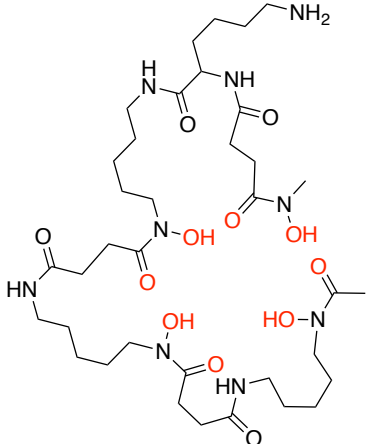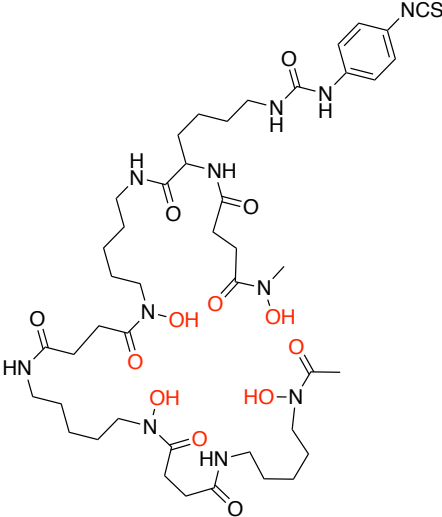
Tetrakis(3-hydroxy-4-pyridinone), **THPN**, O$_8$, CN = 8

***p*-Bn-NCS-THPN**[81]**,** bifunctional derivative of THPN

PDETLysH22-3, 2-HOPO, O$_8$, CN = 8

	[^{89}Zr]Zr^{4+}	X	25°C, 10 min, pH 7.5	-	**In vivo**	59

***p*-Bn- BPDETLysH22-3, 2-HOPO**[59]**,** bifunctional derivative of BPDETLysH22-3, 2-HOPO

DFO-HOPO, O$_8$, CN = 8

	[^{89}Zr]Zr^{4+}	~	25°C, 60 min, pH 7	-	**In vivo**	53
	[^{89}Zr]Zr^{4+}	✓	37 °C, 60 min, pH 7.4	-	**In vitro**	
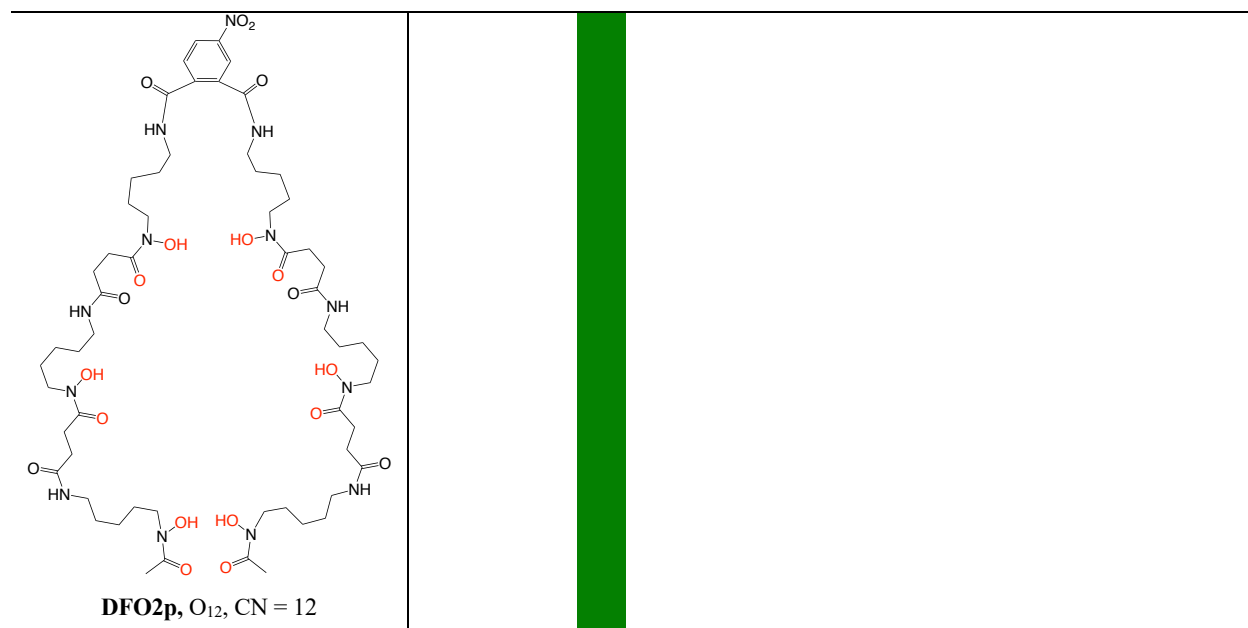
DFO2p, O_{12}, CN = 12

Table 1-8. Desferrioxamine-based [^{89}Zr]Zr(IV) chelators synthesized and evaluated in my PhD, highlighting radiolabeling conditions, level of evaluation, and color-coded ranking

Chelator and Common Bifunctional Derivatives	Radiometal Ion	a	Radiolabeling Conditions	Log K_{ML} (Log β)	b	Ref.
	[^{89}Zr]Zr^{4+}	✓	37 °C, 60 min, pH 7	-	**In vitro**	83
DFO2, O_{12}, CN = 12						
	[^{89}Zr]Zr^{4+}	✓	25°C, 5 min, pH 7	-	**In vivo**	-

DFO2K, O_{12}, CN = 12

p-SCN-Ph-DFO2K, bifunctional derivative of **DFO2K**

$[^{89}Zr]Zr^{4+}$	✓	25°C, 5 min, pH 7	-	**In vivo**	-

DFO-Em, O_8, CN = 8

$[^{89}Zr]Zr^{4+}$	✓	25 °C, 30 min, pH 7	-	**In vivo**	-

DFO-Km, O_8, CN = 8

28

	p-SCN-Ph-DFO-Km, bifunctional derivative of **DFO-Km**

1.7. Research Objectives

Increasing the denticity of DFO (from 6 to at least 8) has been shown to be an effective way to improve stability of zirconium-89 chelation both *in vitro* and *in vivo*. However, it is often accompanied by poor water solubility which makes aqueous bioconjugation chemistry complicated and limits their use with small vectors such as peptides and small molecules. Furthermore, the six coordination sites of DFO are not sufficient to stably coordinate any therapeutic radiometals, which are typically large and usually require 8+ coordinate chelators. This is a major shortcoming in the fields of radiochemistry and nuclear medicine because many people believe the future of cancer care lies in theranostic radiopharmaceuticals.[3] Zirconium-89 is perhaps the single best radionuclide available for PET imaging with excellent decay properties and a half-life (~3.3 d) long enough to match two of the most promising and highly potent therapeutic radionuclides — actinium-225 and thorium-227. Developing a chelator which can bind any therapeutic radiometal in addition to zirconium-89 can expand the utility of zirconium-89 into theranostic applications. To our knowledge, the only current theranostic application of zirconium-89 is with the chelator HOPO and the therapeutic radionuclide thorium-227 (in clinical trials, Bayer). The overarching objective of my Ph.D. was to develop new chelators that can form stable complexes with zirconium-89 that can survive *in vivo* and prevent release of radioactive zirconium into healthy tissue, possess suitable water solubility and conjugation efficiency, and have potential to bind therapeutic radiometals thus unlocking theranostic applications.

The process of developing new chelators passes through structure design, sourcing starting materials and planning a synthesis route, multi-step synthesis and purification, and then evaluation of metal ion binding and radiochemical stability. This process is iterative and often followed by structure modification, re-design, re-synthesis, and re-evaluation cycles, requiring multi-years long research. Chelators have notoriously challenging synthesis and difficult purification as these chelators usually contain many oxygen- and nitrogen-rich functional groups with high hydrogen-bonding potential. This means we must utilize extensive protecting group chemistry and many different purification techniques. Considering these synthetic challenges, we sought to devise a rapid and modular synthesis platform to enable fast evaluation of a variety of chelator derivatives, and to enable rapid synthetic iteration of the lead ligand scaffolds to optimize their properties for different metal ions or bioconjugation chemistries. The modular design allowed us to easily change the linker group, add different chelating moieties, change the bifunctional conjugation chemistry, and tune properties such as solubility as required. To peruse these objectives, we started by tethering two commercially available DFO molecules using a propylenediamine linker which contains a *p*-nitro-phenyl group for bifunctionalization and vector conjugation. This way we increased the denticity from 6 (DFO) to 12 and this novel molecule we called our first dodecadentate chelator DFO2 (**Chapter 2**) which was synthesized in 5 synthetic steps. Furthermore, to determine the most relevant *in vitro* stability assays for effective evaluation of our newly made chelators we performed many different types of *in vitro* stability assays.

Following the synthesis and evaluation of DFO2, our next objective was improving the poor water solubility which arise with increasing size/denticity in hydroxamic acid-based zirconium-89 chelators including DFO2. The strategy for that was to incorporate polar/highly water-soluble groups in our chelators. This was achieved by replacing the hydrophobic phenyl-based linker of

DFO2 by more water-soluble amino acid linkers in our next derivatives of DFO2. In our second project we introduced lysine as the linker in DFO2K (**Chapter 3**) which has a similar metal binding core structure with a significant improvement in stability and solubility. The name DFO2K was chosen because K is the single letter abbreviation for the amino acid lysine.

Another objective of my Ph.D. study was to utilize this new amino acid-based modular chelate platform to create a new octadentate DFO-based chelator which can saturate the coordination sphere of zirconium and has the potential to bind other oxophilic radiometals. This would also allow us to compare the stability and performance of an octadentate derivative of our dodecadentate chelators DFO2 and DFO2K. Octadentate chelators do not have the extra binding sites of DFO2 or DFO2K which could be important for large radiometals such as actinium-225 and thorium-227, yet they have sufficient binding groups to saturate the 8-coordination number of zirconium and similar radiometals. Reducing the size of the chelators results in further improvement in water solubility. This objective was achieved by combining a DFO molecule with an in-house synthesized hydroxamic acid monomer (m) via a glutamic acid linker (single letter abbreviation E), therefore we named this chelator DFO-Em (**Chapter 4**). DFO-Em presents a free carboxylic acid for conjugation chemistry which has limitations, and so to further improvement on DFO-Em was my final Ph.D. project. With the objective of introducing lysine (K) as a linker which is applicable for bifunctionalization compatible with hydroxamic acid-based chelators, and addition of extra length in the monomer to increase the coordinative/geometric flexibility of the chelator to form the lowest energy geometries with zirconium-89 and hence the most stable complex. This was accomplished by tethering a modified hydroxamic acid monomer (m) with a DFO molecule by using lysine (K) as linker in our octadentate DFO-Km chelator (**Chapter 5**).

This thesis presents the design, synthesis, characterization, and *in vitro*/*in vivo* (healthy

mice) validation of these chelators as excellent for zirconium-89 applications. Future work in the

Price lab following my Ph.D. projects will include further evaluation of these chelators especially

DFO2K and DFO-Km in tumor mouse models and assessment of the chelators with therapeutic

radiometals such as actinium-225 and throrium-227 for theranostic applications.

1.8. References

(1)   Price, E. W.; Orvig, C. Matching Chelators to Radiometals for Radiopharmaceuticals. *Chem. Soc. Rev.* **2014**, *43* (1), 260−290.

(2)   Kostelnik, T. I.; Orvig, C. Radioactive Main Group and Rare Earth Metals for Imaging and Therapy. *Chem. Rev.* **2019**, *119* (2), 902−956.

(3)   Notni, J.; Wester, H.-J. Re-Thinking the Role of Radiometal Isotopes: Towards a Future Concept for Theranostic Radiopharmaceuticals. *J. Labelled Comp. Radiopharm.* **2018**, *61* (3), 141−153.

(4)   Choudhary, N.; Guadalupe Jaraquemada-Peláez, M. de; Zarschler, K.; Wang, X.; Radchenko, V.; Kubeil, M.; Stephan, H.; Orvig, C. Chelation in One Fell Swoop: Optimizing Ligands for Smaller Radiometal Ions. *Inorg. Chem.* **2020**, *59* (8), 5728−5741.

(5)   Yoon, J.-K.; Park, B.-N.; Ryu, E.-K.; An, Y.-S.; Lee, S.-J. Current Perspectives on 89Zr-PET Imaging. *Int. J. Mol. Sci.* **2020**, *21* (12), 4309.

(6)   Guerra Liberal, F. D. C.; O'Sullivan, J. M.; McMahon, S. J.; Prise, K. M. Targeted Alpha Therapy: Current Clinical Applications. *Cancer Biother. Radiopharm.* **2020**, *35* (6), 404−417.

(7)   Zeglis, B. M.; Lewis, J. S. A Practical Guide to the Construction of Radiometallated Bioconjugates for Positron Emission Tomography. *Dalton Trans.* **2011**, *40* (23), 6168−6195.

(8)   Lederer, C. M.; Shirley, V. S. *Table of Isotopes*, 7th ed.; John Wiley & Sons: New York, 1978.

(9)   Holland, J. P.; Williamson, M. J.; Lewis, J. S. Unconventional Nuclides for Radiopharmaceuticals. *Mol. Imaging* **2010**, *9* (1), 1−20.

(10)   Qaim, S. M. Decay Data and Production Yields of Some Non-Standard Positron Emitters Used in PET. *Q. J. Nucl. Med. Mol. Imaging* **2008**, *52*, 111−120.

(11)   Kostelnik, T. I.; Orvig, C. Radioactive Main Group and Rare Earth Metals for Imaging and Therapy. *Chem. Rev.* **2019**, *119* (2), 902−956.

(12)   Wadas, T. J.; Wong, E. H.; Weisman, G. R.; Anderson, C. J. Coordinating Radiometals of Copper, Gallium, Indium, Yttrium, and Zirconium for PET and SPECT Imaging of Disease. *Chem. Rev.* **2010**, *110* (5), 2858−2902.

(13)   Chu, S. Y. F.; Ekström, L. P.; Firestone, R. B. *WWW table of radioactive isotopes, database version 2/28/1999, from http://nucleardata.nuclear.lu.se/nucleardata/toi/* **1999**.

(14)   Conti, M.; Eriksson, L. Physics of Pure and Non-Pure Positron Emitters for PET: A Review and a Discussion. *EJNMMI Phys.* **2016**, *3* (1), 8.

(15) Seidl, C. Radioimmunotherapy with α-Particle-Emitting Radionuclides. *Immunotherapy* **2014**, *6* (4), 431–458.

(16) Price, E. W.; Orvig, C. The Chemistry of Inorganic Nuclides (86Y, 68Ga, 64Cu, 89Zr, 124I). In *The Chemistry of Molecular Imaging*; John Wiley & Sons, Ltd, 2014; pp 105–135.

(17) Pearson, R. G. Hard and Soft Acids and Bases. *J. Am. Chem. Soc.* **1963**, *85* (22), 3533–3539.

(18) Martell, A. E. The Chelate Effect. In *Werner Centennial*; Advances in Chemistry; American Chemical Society, 1967; Vol. 62, pp 272–294.

(19) Summers, K. L.; Sarbisheh, E. K.; Zimmerling, A.; Cotelesage, J. J. H.; Pickering, I. J.; George, G. N.; Price, E. W. Structural Characterization of the Solution Chemistry of Zirconium(IV) Desferrioxamine: A Coordination Sphere Completed by Hydroxides. *Inorg. Chem.* **2020**, *59* (23), 17443–17452.

(20) Cabbiness, D. K.; Margerum, D. W. Macrocyclic Effect on the Stability of Copper(II) Tetramine Complexes. *J. Am. Chem. Soc.* **1969**, *91* (23), 6540–6541.

(21) Hancock, R. D.; Ngwenya, M. P. The Effect of Increase in Chelate Ring Size beyond Six-Membered on the Metal Ion Size Selectivity Patterns of Tetra-Aza Macrocycles. *J. Chem. Soc., Dalton Trans.* **1987**, No. 12, 2911–2915.

(22) Smith, R. M.; Martell, A. E. Critical Stability Constants, Enthalpies and Entropies for the Formation of Metal Complexes of Aminopolycarboxylic Acids and Carboxylic Acids. *Sci. Total Environ.***1987**, *64*, 125–147.

(23) Holland, J. P. Predicting the Thermodynamic Stability of Zirconium Radiotracers. *Inorg. Chem.* **2020**, *59* (3), 2070–2082.

(24) Farkas, E.; Vágner, A.; Negri, R.; Lattuada, L.; Tóth, I.; Colombo, V.; Esteban-Gómez, D.; Platas-Iglesias, C.; Notni, J.; Baranyai, Z.; Giovenzana, G. B. PIDAZTA: Structurally Constrained Chelators for the Efficient Formation of Stable Gallium-68 Complexes at Physiological PH. *Chemistry* **2019**, *25* (45), 10698–10709.

(25) Baranyai, Z.; Uggeri, F.; Maiocchi, A.; Giovenzana, G. B.; Cavallotti, C.; Takács, A.; Tóth, I.; Bányai, I.; Bényei, A.; Brucher, E.; Aime, S. Equilibrium, Kinetic and Structural Studies of AAZTA Complexes with Ga3+, In3+ and Cu2+. *Eur. J. Inorg. Chem.* **2013**, *2013* (1), 147–162.

(26) Sinnes, J.-P.; Nagel, J.; Rösch, F. AAZTA5/AAZTA5-TOC: Synthesis and Radiochemical Evaluation with 68Ga, 44Sc and 177Lu. *EJNMMI Radiopharm. Chem.* **2019**, *4* (1), 18.

(27) Pfister, J.; Summer, D.; Rangger, C.; Petrik, M.; von Guggenberg, E.; Minazzi, P.; Giovenzana, G. B.; Aloj, L.; Decristoforo, C. Influence of a Novel, Versatile Bifunctional Chelator on Theranostic Properties of a Minigastrin Analogue. *EJNMMI Res.* **2015**, *5* (1), 74.

(28) Nagy, G.; Szikra, D.; Trencsényi, G.; Fekete, A.; Garai, I.; Giani, A. M.; Negri, R.; Masciocchi, N.; Maiocchi, A.; Uggeri, F.; Tóth, I.; Aime, S.; Giovenzana, G. B.; Baranyai, Z. AAZTA: An Ideal Chelating Agent for the Development of 44 Sc PET Imaging Agents. *Angew. Chem. Int. Ed. Engl.* **2017**, *56* (8), 2118–2122.

(29) Klasen, B. Moon, E. Rösch F. AAZTA[5]-squaramide ester competing with DOTA-, DTPA- and CHX-A″-DTPA-analogues: Promising tool for ^{177}Lu-labeling of monoclonal antibodies under mild conditions. *Nucl. Med. Biol*. **2021**. 96-97

(30) Orteca, G.; Sinnes, J.-P.; Rubagotti, S.; Iori, M.; Capponi, P. C.; Piel, M.; Rösch, F.; Ferrari, E.; Asti, M. Gallium-68 and Scandium-44 Labelled Radiotracers Based on Curcumin Structure Linked to Bifunctional Chelators: Synthesis and Characterization of Potential PET Radiotracers. *J. Inorg. Biochem.* **2020**, *204*, 110954.

(31) Vágner, A.; D'Alessandria, C.; Gambino, G.; Schwaiger, M.; Aime, S.; Maiocchi, A.; Tóth, I.; Baranyai, Z.; Tei, L. A Rigidified AAZTA-like Ligand as Efficient Chelator for 68Ga Radiopharmaceuticals. *ChemistrySelect* **2016**, *1* (2), 163−171.

(32) Wang, X.; Jaraquemada-Peláez, M. de G.; Cao, Y.; Pan, J.; Lin, K.-S.; Patrick, B. O.; Orvig, C. H2hox: Dual-Channel Oxine-Derived Acyclic Chelating Ligand for 68Ga Radiopharmaceuticals. *Inorg. Chem.* **2019**, *58* (4), 2275−2285.

(33) Wang, X.; Jaraquemada-Pelaez, M.; Rodríguez-Rodríguez, C.; Cao, Y.; Buchwalder, C.; Choudhary, N.; Jermilova, U.; Ramogida, C.; Saatchi, K.; Häfeli, U.; Patrick, B.; Orvig, C. H4octox: Versatile Bimodal Octadentate Acyclic Chelating Ligand for Medicinal Inorganic Chemistry. *J. Am. Chem. Soc.* **2018**, *140*, 15487−15500.

(34) Ramogida, C. F.; Cawthray, J. F.; Boros, E.; Ferreira, C. L.; Patrick, B. O.; Adam, M. J.; Orvig, C. H2CHXdedpa and H4CHXoctapa—Chiral Acyclic Chelating Ligands for 67/68Ga and 111In Radiopharmaceuticals. *Inorg. Chem.* **2015**, *54* (4), 2017−2031.

(35) Ramogida, C. F.; Boros, E.; Patrick, B. O.; Zeisler, S. K.; Kumlin, J.; Adam, M. J.; Schaffer, P.; Orvig, C. Evaluation of H2CHXdedpa, H2dedpa- and H2CHXdedpa-N,N′-Propyl-2-NI Ligands for 64Cu(II) Radiopharmaceuticals. *Dalton Trans.* **2016**, *45* (33), 13082−13090.

(36) Ramogida, C. F.; Robertson, A. K. H.; Jermilova, U.; Zhang, C.; Yang, H.; Kunz, P.; Lassen, J.; Bratanovic, I.; Brown, V.; Southcott, L.; Rodríguez-Rodríguez, C.; Radchenko, V.; Bénard, F.; Orvig, C.; Schaffer, P. Evaluation of Polydentate Picolinic Acid Chelating Ligands and an α-Melanocyte-Stimulating Hormone Derivative for Targeted Alpha Therapy Using ISOL-Produced 225Ac. *EJNMMI Radiopharm. Chem.* **2019**, *4*.

(37) Li, L.; Jaraquemada-Peláez, M. de G.; Kuo, H.-T.; Merkens, H.; Choudhary, N.; Gitschtaler, K.; Jermilova, U.; Colpo, N.; Uribe-Munoz, C.; Radchenko, V.; Schaffer, P.; Lin, K.-S.; Bénard, F.; Orvig, C. Functionally Versatile and Highly Stable Chelator for 111In and 177Lu: Proof-of-Principle Prostate-Specific Membrane Antigen Targeting. *Bioconjug. Chem.* **2019**, *30* (5), 1539–1553.

(38) Li, L.; Rousseau, J.; Jaraquemada-Peláez, M. de G.; Wang, X.; Robertson, A.; Radchenko, V.; Schaffer, P.; Lin, K.-S.; Bénard, F.; Orvig, C. 225Ac-H4py4pa for Targeted Alpha Therapy. *Bioconjug. Chem.* **2021**, *32* (7), 1348–1363.

(39) Spreckelmeyer, S.; Ramogida, C. F.; Rousseau, J.; Arane, K.; Bratanovic, I.; Colpo, N.; Jermilova, U.; Dias, G. M.; Dude, I.; Jaraquemada-Peláez, M. de G.; Bénard, F.; Schaffer, P.; Orvig, C. P-NO2-Bn-H4neunpa and H4neunpa-Trastuzumab: Bifunctional Chelator for Radiometalpharmaceuticals and 111In Immuno-Single Photon Emission Computed Tomography Imaging. *Bioconjug. Chem.* **2017**, *28* (8), 2145–2159.

(40) Ferreirós-Martínez, R.; Esteban-Gómez, D.; Tóth, É.; de Blas, A.; Platas-Iglesias, C.; Rodríguez-Blas, T. Macrocyclic Receptor Showing Extremely High Sr(II)/Ca(II) and Pb(II)/Ca(II) Selectivities with Potential Application in Chelation Treatment of Metal Intoxication. *Inorg. Chem.* **2011**, *50* (8), 3772–3784.

(41) Roca-Sabio, A.; Mato-Iglesias, M.; Esteban-Gómez, D.; Tóth, É.; Blas, A. de; Platas-Iglesias, C.; Rodríguez-Blas, T. Macrocyclic Receptor Exhibiting Unprecedented Selectivity for Light Lanthanides. *J. Am. Chem. Soc.* **2009**, *131* (9), 3331–3341.

(42) Thiele, N. A.; Brown, V.; Kelly, J. M.; Amor-Coarasa, A.; Jermilova, U.; MacMillan, S. N.; Nikolopoulou, A.; Ponnala, S.; Ramogida, C. F.; Robertson, A. K. H.; Rodríguez-Rodríguez, C.; Schaffer, P.; Williams, C.; Babich, J. W.; Radchenko, V.; Wilson, J. J. An Eighteen-Membered Macrocyclic Ligand for Actinium-225 Targeted Alpha Therapy. *Angew. Chem. Int. Ed. Engl.* **2017**, *56* (46), 14712–14717.

(43) Ramogida, C. F.; Pan, J.; Ferreira, C. L.; Patrick, B. O.; Rebullar, K.; Yapp, D. T. T.; Lin, K.-S.; Adam, M. J.; Orvig, C. Nitroimidazole-Containing H2dedpa and H2CHXdedpa Derivatives as Potential PET Imaging Agents of Hypoxia with (68)Ga. *Inorg. Chem.* **2015**, *54* (10), 4953–4965.

(44) Zeglis, B. M.; Lewis, J. S. The Bioconjugation and Radiosynthesis of 89Zr-DFO-Labeled Antibodies. *J. Vis. Exp.* **2015**, No. 96, 52521.

(45) Jauw, Y. W. S.; Menke-van der Houven van Oordt, C. W.; Hoekstra, O. S.; Hendrikse, N. H.; Vugts, D. J.; Zijlstra, J. M.; Huisman, M. C.; van Dongen, G. A. M. S. Immuno-Positron Emission Tomography with Zirconium-89-Labeled Monoclonal Antibodies in Oncology: What Can We Learn from Initial Clinical Trials? *Front. Pharmacol.* **2016**, *7*, 131.

(46) Zhang, Y.; Hong, H.; Cai, W. PET Tracers Based on Zirconium-89. *Curr. Radiopharm.* **2011**, *4* (2), 131–139.

(47) van de Watering, F. C. J.; Rijpkema, M.; Perk, L.; Brinkmann, U.; Oyen, W. J. G.; Boerman, O. C. Zirconium-89 Labeled Antibodies: A New Tool for Molecular Imaging in Cancer Patients. *Biomed. Res. Int.* **2014**, *2014*, e203601.

(48) Wei, W.; Rosenkrans, Z. T.; Liu, J.; Huang, G.; Luo, Q.-Y.; Cai, W. ImmunoPET: Concept, Design, and Applications. *Chem. Rev.* **2020**, *120* (8), 3787–3851.

(49) Mestel, R. Cancer: Imaging with Antibodies. *Nature* **2017**, *543* (7647), 743–746.

(50) Knowles, S. M.; Wu, A. M. Advances in Immuno–Positron Emission Tomography: Antibodies for Molecular Imaging in Oncology. *J. Clin. Oncol.* **2012**, *30* (31), 3884–3892.

(51) Holland, J. P.; Sheh, Y.; Lewis, J. S. Standardized Methods for the Production of High Specific-Activity Zirconium-89. *Nucl. Med. Biol.* **2009**, *36* (7), 729–739.

(52) Vugts, D. J.; Klaver, C.; Sewing, C.; Poot, A. J.; Adamzek, K.; Huegli, S.; Mari, C.; Visser, G. W. M.; Valverde, I. E.; Gasser, G.; Mindt, T. L.; van Dongen, G. A. M. S. Comparison of the Octadentate Bifunctional Chelator DFO*-PPhe-NCS and the Clinically Used Hexadentate Bifunctional Chelator DFO-PPhe-NCS for 89Zr-Immuno-PET. *Eur. J. Nucl. Med. Mol. Imaging* **2017**, *44* (2), 286–295.

(53) Allott, L.; Da Pieve, C.; Meyers, J.; Spinks, T.; Ciobota, D. M.; Kramer-Marek, G.; Smith, G. Evaluation of DFO-HOPO as an Octadentate Chelator for Zirconium-89. *Chem. Commun. (Camb.)* **2017**, *53* (61), 8529–8532.

(54) Richardson-Sanchez, T.; Tieu, W.; Gotsbacher, M. P.; Telfer, T. J.; Codd, R. Exploiting the Biosynthetic Machinery of Streptomyces Pilosus to Engineer a Water-Soluble Zirconium(IV) Chelator. *Org. Biomol. Chem.* **2017**, *15* (27), 5719–5730.

(55) Ulaner, G. A.; Hyman, D. M.; Lyashchenko, S. K.; Lewis, J. S.; Carrasquillo, J. A. 89Zr-Trastuzumab PET/CT for Detection of HER2-Positive Metastases in Patients with HER2-Negative Primary Breast Cancer. *Clin. Nucl. Med.* **2017**, *42* (12), 912–917.

(56) Perk, L. R.; Visser, G. W. M.; Vosjan, M. J. W. D.; Walsum, M. S.; Tijink, B. M.; Leemans, C. R.; Dongen, G. A. M. S. van. 89Zr as a PET Surrogate Radioisotope for Scouting Biodistribution of the Therapeutic Radiometals 90Y and 177Lu in Tumor-Bearing Nude Mice After Coupling to the Internalizing Antibody Cetuximab. *J. Nucl. Med.* **2005**, *46* (11), 1898–1906.

(57) Raavé, R.; Sandker, G.; Adumeau, P.; Jacobsen, C. B.; Mangin, F.; Meyer, M.; Moreau, M.; Bernhard, C.; Da Costa, L.; Dubois, A.; Goncalves, V.; Gustafsson, M.; Rijpkema, M.; Boerman, O.; Chambron, J.-C.; Heskamp, S.; Denat, F. Direct Comparison of the in Vitro and in Vivo Stability of DFO, DFO* and DFOcyclo* for 89Zr-ImmunoPET. *Eur. J. Nucl. Med. Mol. Imaging* **2019**, *46* (9), 1966–1977.

(58) Abou, D. S.; Ku, T.; Smith-Jones, P. M. In Vivo Biodistribution and Accumulation of 89Zr in Mice. *Nucl. Med. Biol.* **2011**, *38* (5), 675−681.

(59) N Tinianow, J.; Pandya, D. N.; Pailloux, S. L.; Ogasawara, A.; Vanderbilt, A. N.; Gill, H. S.; Williams, S.-P.; Wadas, T. J.; Magda, D.; Marik, J. Evaluation of a 3-Hydroxypyridin-2-One (2,3-HOPO) Based Macrocyclic Chelator for (89)Zr(4+) and Its Use for ImmunoPET Imaging of HER2 Positive Model of Ovarian Carcinoma in Mice. *Theranostics* **2016**, *6* (4), 511−521.

(60) Pandit-Taskar, N.; O'Donoghue, J. A.; Durack, J. C.; Lyashchenko, S. K.; Cheal, S. M.; Beylergil, V.; Lefkowitz, R. A.; Carrasquillo, J. A.; Martinez, D. F.; Fung, A. M.; Solomon, S. B.; Gönen, M.; Heller, G.; Loda, M.; Nanus, D. M.; Tagawa, S. T.; Feldman, J. L.; Osborne, J. R.; Lewis, J. S.; Reuter, V. E.; Weber, W. A.; Bander, N. H.; Scher, H. I.; Larson, S. M.; Morris, M. J. A Phase I/II Study for Analytic Validation of 89Zr-J591 ImmunoPET as a Molecular Imaging Agent for Metastatic Prostate Cancer. *Clin. Cancer Res.* **2015**, *21* (23), 5277−5285.

(61) Pandit-Taskar, N.; O'Donoghue, J. A.; Ruan, S.; Lyashchenko, S. K.; Carrasquillo, J. A.; Heller, G.; Martinez, D. F.; Cheal, S. M.; Lewis, J. S.; Fleisher, M.; Keppler, J. S.; Reiter, R. E.; Wu, A. M.; Weber, W. A.; Scher, H. I.; Larson, S. M.; Morris, M. J. First-in-Human Imaging with 89Zr-Df-IAB2M Anti-PSMA Minibody in Patients with Metastatic Prostate Cancer: Pharmacokinetics, Biodistribution, Dosimetry, and Lesion Uptake. *J. Nucl. Med.* **2016**, *57* (12), 1858−1864.

(62) Jauw, Y. W. S.; O'Donoghue, J. A.; Zijlstra, J. M.; Hoekstra, O. S.; Oordt, C. W. M. der H. van; Morschhauser, F.; Carrasquillo, J. A.; Zweegman, S.; Pandit-Taskar, N.; Lammertsma, A. A.; Dongen, G. A. M. S. van; Boellaard, R.; Weber, W. A.; Huisman, M. C. 89Zr-Immuno-PET: Toward a Noninvasive Clinical Tool to Measure Target Engagement of Therapeutic Antibodies In Vivo. *J. Nucl. Med.* **2019**, *60* (12), 1825−1832.

(63) Patra, M.; Bauman, A.; Mari, C.; Fischer, C. A.; Blacque, O.; Häussinger, D.; Gasser, G.; Mindt, T. L. An Octadentate Bifunctional Chelating Agent for the Development of Stable Zirconium-89 Based Molecular Imaging Probes. *Chem. Commun.* **2014**, *50* (78), 11523−11525.

(64) Briand, M.; Aulsebrook, M. L.; Mindt, T. L.; Gasser, G. A Solid Phase-Assisted Approach for the Facile Synthesis of a Highly Water-Soluble Zirconium-89 Chelator for Radiopharmaceutical Development. *Dalton Trans.* **2017**, *46* (47), 16387−16389.

(65) Sharma, S. K.; Glaser, J. M.; Edwards, K. J.; Khozeimeh Sarbisheh, E.; Salih, A. K.; Lewis, J. S.; Price, E. W. A Systematic Evaluation of Antibody Modification and 89Zr-Radiolabeling for Optimized Immuno-PET. *Bioconjug. Chem.* **2020**.

(66) Guérard, F.; Lee, Y.-S.; Brechbiel, M. W. Rational Design, Synthesis, and Evaluation of Tetrahydroxamic Acid Chelators for Stable Complexation of Zirconium(IV). *Chem. Eur. J.* **2014**, *20* (19), 5584–5591.

(67) Seibold, U.; Wängler, B.; Wängler, C. Rational Design, Development, and Stability Assessment of a Macrocyclic Four-Hydroxamate-Bearing Bifunctional Chelating Agent for 89 Zr. *ChemMedChem* **2017**, *12* (18), 1555–1571.

(68) Savastano, M.; Bazzicalupi, C.; Ferraro, G.; Fratini, E.; Gratteri, P.; Bianchi, A. Tales of the Unexpected: The Case of Zirconium(IV) Complexes with Desferrioxamine. *Molecules* **2019**, *24* (11).

(69) Dijkers, E. C. F.; Kosterink, J. G. W.; Rademaker, A. P.; Perk, L. R.; Dongen, G. A. M. S. van; Bart, J.; Jong, J. R. de; Vries, E. G. E. de; Hooge, M. N. L. Development and Characterization of Clinical-Grade 89Zr-Trastuzumab for HER2/Neu ImmunoPET Imaging. *J. Nucl. Med.* **2009**, *50* (6), 974–981.

(70) Kojima, S.; Jay, M. Comparisons of Labeling Efficiency, Biological Activity and Biodistribution among 125I-, 67Ga-DTPA-and 67Ga-DFO-Lectins. *Eur. J. Nucl. Med.* **1987**, *13* (7), 366–370.

(71) Heymann, P.; Ernst, J. F.; Winkelmann, G. Identification of a Fungal Triacetylfusarinine C Siderophore Transport Gene (TAF1) in Saccharomyces Cerevisiae as a Member of the Major Facilitator Superfamily. *Biometals* **1999**, *12* (4), 301–306.

(72) Zhai, C.; Summer, D.; Rangger, C.; Franssen, G. M.; Laverman, P.; Haas, H.; Petrik, M.; Haubner, R.; Decristoforo, C. Novel Bifunctional Cyclic Chelator for (89)Zr Labeling-Radiolabeling and Targeting Properties of RGD Conjugates. *Mol. Pharm.* **2015**, *12* (6), 2142–2150.

(73) Summer, D.; Rangger, C.; Klingler, M.; Laverman, P.; Franssen, G. M.; Lechner, B. E.; Orasch, T.; Haas, H.; von Guggenberg, E.; Decristoforo, C. Exploiting the Concept of Multivalency with 68Ga- and 89Zr-Labelled Fusarinine C-Minigastrin Bioconjugates for Targeting CCK2R Expression. *Contrast Media Mol. Imaging* **2018**, *2018*, e3171794.

(74) Zhai, C.; He, S.; Ye, Y.; Rangger, C.; Kaeopookum, P.; Summer, D.; Haas, H.; Kremser, L.; Lindner, H.; Foster, J.; Sosabowski, J.; Decristoforo, C. Rational Design, Synthesis and Preliminary Evaluation of Novel Fusarinine C-Based Chelators for Radiolabeling with Zirconium-89. *Biomolecules* **2019**, *9* (3).

(75) Zhai, C.; Summer, D.; Rangger, C.; Haas, H.; Haubner, R.; Decristoforo, C. Fusarinine C, a Novel Siderophore-Based Bifunctional Chelator for Radiolabeling with Gallium-68. *J. Labelled Comp. Radiopharm.* **2015**, *58* (5), 209–214.

(76) Kaeopookum, P.; Summer, D.; Pfister, J.; Orasch, T.; Lechner, B. E.; Petrik, M.; Novy, Z.; Matuszczak, B.; Rangger, C.; Haas, H.; Decristoforo, C. Modifying the Siderophore Triacetylfusarinine C for Molecular Imaging of Fungal Infection. *Mol. Imaging Biol.* **2019**, *21* (6), 1097–1106.

(77) White, D. L.; Durbin, P. W.; Jeung, N.; Raymond, K. N. Specific Sequestering Agents for the Actinides. 16. Synthesis and Initial Biological Testing of Polydentate Oxohydroxypyridinecarboxylate Ligands. *J. Med. Chem.* **1988**, *31* (1), 11–18.

(78) Deri, M. A.; Ponnala, S.; Zeglis, B. M.; Pohl, G.; Dannenberg, J. J.; Lewis, J. S.; Francesconi, L. C. Alternative Chelator for 89Zr Radiopharmaceuticals: Radiolabeling and Evaluation of 3,4,3-(LI-1,2-HOPO). *J. Med. Chem.* **2014**, *57* (11), 4849–4860.

(79) Deri, M. A.; Ponnala, S.; Kozlowski, P.; Burton-Pye, B. P.; Cicek, H. T.; Hu, C.; Lewis, J. S.; Francesconi, L. C. P-SCN-Bn-HOPO: A Superior Bifunctional Chelator for 89Zr ImmunoPET. *Bioconjug. Chem.* **2015**, *26* (12), 2579–2591.

(80) Buchwalder, C.; Rodríguez-Rodríguez, C.; Schaffer, P.; Karagiozov, S. K.; Saatchi, K.; Häfeli, U. O. A New Tetrapodal 3-Hydroxy-4-Pyridinone Ligand for Complexation of 89zirconium for Positron Emission Tomography (PET) Imaging. *Dalton Trans.* **2017**, *46* (29), 9654–9663.

(81) Buchwalder, C.; Jaraquemada-Peláez, M. de G.; Rousseau, J.; Merkens, H.; Rodríguez-Rodríguez, C.; Orvig, C.; Bénard, F.; Schaffer, P.; Saatchi, K.; Häfeli, U. O. Evaluation of the Tetrakis(3-Hydroxy-4-Pyridinone) Ligand THPN with Zirconium(IV): Thermodynamic Solution Studies, Bifunctionalization, and in Vivo Assessment of Macromolecular 89Zr-THPN-Conjugates. *Inorg. Chem.* **2019**, *58* (21), 14667−14681.

(82) Sturzbecher-Hoehne, M.; Choi, T. A.; Abergel, R. J. Hydroxypyridinonate Complex Stability of Group (IV) Metals and Tetravalent f-Block Elements: The Key to the Next Generation of Chelating Agents for Radiopharmaceuticals. *Inorg. Chem.* **2015**, *54* (7), 3462−3468.

(83) Sarbisheh, E. K.; Salih, A. K.; Raheem, S. J.; Lewis, J. S.; Price, E. W. A High-Denticity Chelator Based on Desferrioxamine for Enhanced Coordination of Zirconium-89. *Inorg. Chem.* **2020**, *59* (16), 11715−11727.

Chapter 2: A High-Denticity Chelator Based on Desferrioxamine for Enhanced Coordination of Zirconium-89

This chapter is an adaptation of published work and is reproduced in part, with permission from Khozeimeh Sarbisheh, E.*; Salih A. K.*; Raheem, S. J.; Lewis, J. S.; and Price E. W. *Inorg. Chem*. **2020**, 59, 16, 11715-11727. Copyright © 2020 American Chemical Society (* These authors contributed equally to this work)

2.1. Author Contribution and Relation to the Research Objectives

This work was done in collaboration with Dr. Elaheh Khozeimeh Sarbisheh and Shvan J. Raheem (PhD candidate). I synthesized the propylenediamine linker (**3**) in three steps and performed a comprehensive characterization of each of **1, 2** and **3**. I assisted Dr. Khozeimeh Sarbisheh in synthesis and characterization of the modified DFO-COOH (**4**) and DFO2 (**5**). Dr. Khozeimeh Sarbisheh performed complexation and characterized Zr-DFO2 (**6**). I also assisted Dr. Khozeimeh Sarbisheh in performing radiolabeling studies of DFO2 with zirconium-89. Dr. Khozeimeh Sarbisheh executed all the stability assays for [^{89}Zr]Zr-DFO2 and DFT calculations for Zr-DFO2 complex. Shvan J. Raheem helped with the radiolabeling studies. I also contributed on preparation of the manuscript and compiling supporting information of the compounds I synthesized.

In this manuscript, we reported the design, synthesis and evaluation of a novel dodecadentate chelator, named DFO2, for zirconium-89 and potentially other larger oxophilic radiometals based on desferrioxamine. DFO2 is equipped with 6 hydroxamic acid metal binding groups and a p-NO$_2$-phenyl group for bifunctionalization and biomolecular conjugation. Moreover, DFO2 has a

modular design which facilitates exchanging the different parts of the chelator for fast synthetic iteration of the lead ligand scaffolds and tuning physical properties such as polarity/solubility as required. After synthesis and characterization of DFO2, it was evaluated radiolabeling with zirconium-89 and *in vitro* stability using numerous radiochemical assays. The results showed superior stability of DFO2 with zirconium-89 compared to the "gold standard" chelator DFO.

2.2. Abstract

Herein we report a new high-denticity chelator based on the iron siderophore desferrioxamine (DFO). Our new chelator– DFO2 –is acyclic and was designed and synthesized with the purpose of improving the coordination chemistry and radiolabeling performance with radioactive zirconium-89. The radionuclide zirconium-89 ($[^{89}Zr]$-Zr^{4+}) has found wide use for positron emission tomography (PET) imaging when it is coupled with proteins, antibodies, and nanoparticles. DFO2 has a potential coordination number of 12, which uniquely positions this chelator for binding large, high-valent, and oxophilic metal ions. Following synthesis of the DFO2 chelator and the ($[^{Nat}Zr]$-Zr-(DFO2) complex we performed density functional theory calculation to study its coordination sphere, followed by zirconium-89 radiolabeling experiments for comparisons with the "gold-standard" chelator DFO. DFO (CN 6) can coordinate with zirconium in a hexadentate fashion, leaving two open coordination sites where water is thought to coordinate (total CN 8). DFO2 (potential CN 12, dodecadentate) can saturate the coordination sphere of zirconium with four hydroxamate groups (CN 8) with no room left for water to directly coordinate, and only binds a single atom of zirconium per chelate. Following quantitative radiolabeling with zirconium-89, the performed $[^{89}Zr]Zr$-(DFO) and $[^{89}Zr]Zr$-(DFO2) radiometal-chelate complexes were subjected to a battery of *in vitro* stability challenges including human blood serum, *apo-*

transferrin, serum albumin, iron, hydroxyapatite, and EDTA. One objective of these stability challenges is to determine if the increased denticity of DFO2 over DFO imparted improved complex stability, and another was to determine which of these assays is most relevant to perform with future chelators. In all assays DFO2 showed superior stability with zirconium-89, except for the iron challenge where both DFO2 and DFO were identical. Substantial differences in stability were observed for human blood serum using a precipitation method of analysis, *apo*-transferrin, hydroxyapatite, and EDTA. These results suggest that DFO2 is a promising next-generation scaffold for zirconium-89 chelators and holds promise for radiochemistry with even larger radionuclides, which we anticipate will expand the utility of DFO2 into theranostic applications.

2.3. Introduction

The radionuclide zirconium-89 has gained popularity over the last decade due to its favorable decay characteristics ($[^{89}Zr]Zr^{4+}$, $t_{1/2}$ = 78.4 hr, β^+ ratio = 22.7%, $E_{\beta^+(mean)}$= 396 keV) for positron emission tomography (non-invasive nuclear imaging modality, PET).[1-3] The radiometal zirconium-89 has a half-life that is well matched with large and slowly distributing biological vectors such as antibodies and nanoparticles.[4-16] Previously, the only chelator capable of effectively coordinating with zirconium-89 (radiolabeling) and forming a complex with sufficient thermodynamic and kinetic stability *in vivo* was the iron siderophore desferrioxamine (DFO).[17-21] DFO is typically non-site-selectively conjugated to lysine residues (primary amine) on antibodies to form thiourea linkages, using the bifunctional chelator (BFC) *p*-SCN-Ph-DFO (commercially available), although amide linkages formed via DFO-activated esters are also used.[22, 23] Zirconium-89 is known to accumulate in bone when released from a chelate-complex *in vivo*, and experiments in mice have consistently shown a substantial amount of bone uptake (~5-10% ID/g after ~3-7 days).[2, 9, 24] Despite the apparent instability of the $[^{89}Zr]Zr$-(DFO) complex in mice, human

immuno-PET imaging studies using zirconium-89 do not appear to suffer from the same degree of high bone uptake.[6, 25-27] In recent years, a number of promising new chelators have been published which all aim to improve radiolabeling performance and *in vivo* stability with zirconium-89 (**Figure 2-1**).[3, 18, 28-44]
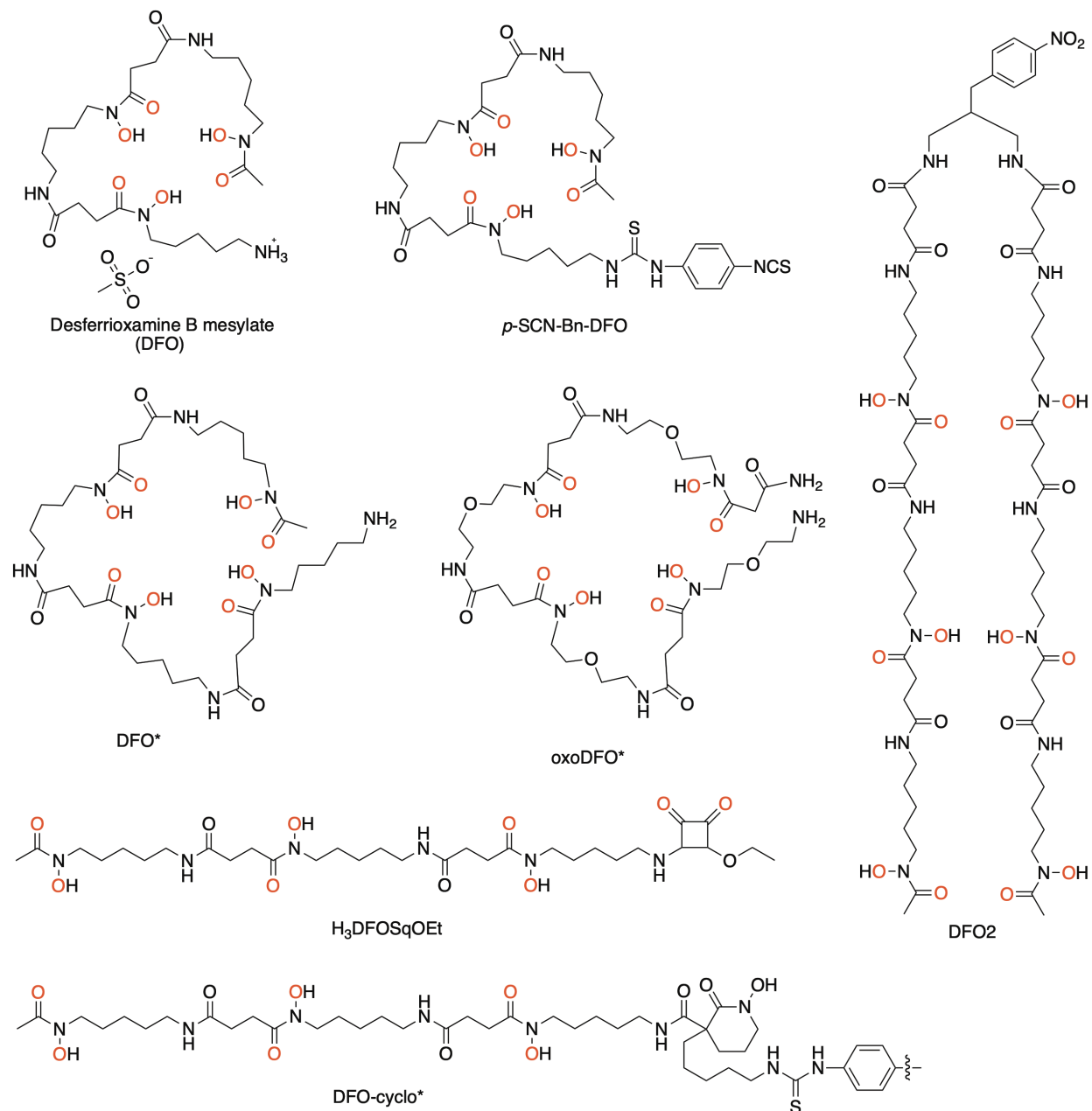
Figure 2-1. Chemical structures of a selection of recently published bifunctional chelators based on desferrioxamine (DFO) for zirconium-89, including *p*-SCN-Ph-DFO, DFO*, oxoDFO*, DFO squate ester (H₃DFOSqOEt), DFO-cyclo*, and DFO2.

42

Over the previous few years we have been working on the design, synthesis, and evaluation of a new family of DFO-based chelators. The first of these new chelators is presented herein and named DFO2, as it is comprised of two desferrioxamine molecules tethered together using a bifunctional linker. The resulting chelator is potentially 12-coordinate (six hydroxamic acid groups, CN=12), with an octadentate (CN=8) coordination sphere expected for Zr^{4+} with DFO2. One drawback of many new chelators is their cumbersome synthesis and difficult purification — typically a result of the intrinsic need of chelators to contain a large number of oxygen- and nitrogen-rich polar functional groups with high hydrogen bonding potential. We have achieved simple synthesis and purification by using commercial DFO as our major building block, although low water solubility of the unconjugated DFO2 was encountered.

The long-term goal of this new "DFO2" chelator family is a rapid and modular synthesis platform to enable fast evaluation of a variety of chelator derivatives, and then rapid synthetic iteration of the lead ligand scaffolds. The priorities of our chelate system are thus simple and fast synthesis, with the requirement to contain a modular design where we can easily change the linker group, add different chelating moieties, change the bifunctional conjugation chemistry, and tune physical properties such as polarity/solubility. The first example of this new chelator family, DFO2, has been synthesized, characterized, radiolabeled with zirconium-89, and evaluated via *in vitro* radiochemical stability assays. We have additionally evaluated the coordination sphere using density functional theory (DFT) calculations as we did not obtain diffractable crystals and therefore no X-ray crystallographic data. We have performed many different types of *in vitro* stability assays with the purpose of determining which assays are most relevant for probing ^{89}Zr-chelate stability. We hope that the results of these assays will make this process of screening

chelators more efficient in the future by identifying which *in vitro* assays best predict *in vivo* stability differences.

2.4. Results and Discussion

To expand the denticity of DFO from a potential coordination number of six (three hydroxamic acid groups), we chemically tethered two molecules of commercially available DFO together. To achieve this, we required a linker that could both tether two DFO molecules with suitable chemistry, but also provide orthogonal reactivity in the bifunctional component of the chelator. Synthesis of DFO2 revolved around a propylenediamine linker with a *p*-NO$_2$-phenyl group extending from the backbone. We synthesized this fragment in three steps starting from *p*-NO$_2$-benzylbromide and diethylmalonate (**Scheme 2-1**). An optimization was made to a previously published synthetic method for this linker fragment, where during step two of the synthesis to form compound **2** we used ammonium hydroxide as the source of amine instead of ammonia gas. This route does not require access to a compressed cylinder of ammonia gas, or the additional hazards of ammonia gas.[45] The functional linker moiety **3** was synthesized in three chemical steps with a cumulative yield of ~8%.
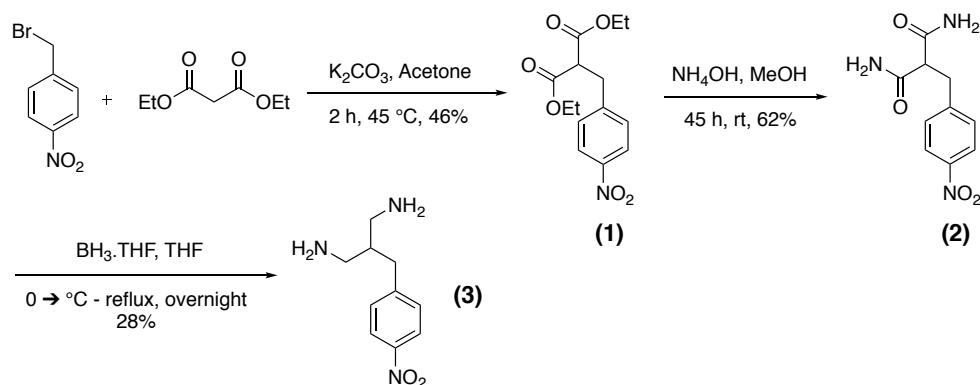
Scheme 2-1. Synthesis of the linker molecule **3**, which was used to tether two DFO molecules together to form DFO2.

To attach commercially available desferrioxamine B mesylate (**DFO**, **Scheme 2-2**) to our linker fragment (**3**), we had to modify DFO through a ring-opening reaction with succinic anhydride. This step formed DFO-COOH (**4**), which extended the length of the DFO chain by four atoms (from 31 to 35 atoms long), and also converted the terminal functional group from a primary amine to a carboxylic acid. The backbone linker **3** was then reacted with DFO-COOH (**4**) to form DFO2 (**5**) using standard peptide coupling conditions. As with the bifunctional chelators p-SCN-Ph-DFO or p-NO$_2$-Ph-DFO, the solubility of DFO2 is poor. During the synthetic step to produce DFO2 (**5**), the solvent DMF was required to achieve solubility and suitable reaction yields. The poor solubility of the resulting DFO2 (**5**) chelator enabled us to purify DFO2 by only precipitation and washing, where we tested a large number of solvent combinations and found cold ethyl acetate was most effective. Coordination of DFO2 with ZrCl$_4$ salt rapidly formed the coordinated Zr(DFO2) complex under mild ambient conditions. A small amount of strong polar solvent dimethylformamide (DMF) was required to solubilize DFO2 at the macro-scale and facilitate this non-radioactive coordination chemistry. At the low concentrations of chelator required for radiochemistry (µM-nM), sufficient solubility can be achieved by transferring a small volume of a DFO2 stock solution dissolved in DMF or DMSO into aqueous radiolabeling buffer. The non-radioactive Zr(DFO2) complex was characterized by standard techniques including ^{1}H/^{13}C-NMR spectroscopy and low- and high-resolution mass spectrometry. Despite the poor water solubility, we have not been able to grow X-ray crystallography quality crystals.

In lieu of crystallographic data, we performed density functional theory (DFT) calculations to evaluate the coordination sphere of the Zr(DFO2) complex (**Figure 2-2**). Calculations were performed using Materials Studio software with the DMol^3 functional and PBE basis set, with solvent effects modeled by COSMO. All the calculations were performed in solution with water

as the solvent. Due to the large structure of the Zr(DFO2) complex, it took substantial time to complete calculations. The DFO2 chelator with many polar hydroxamic acid and carbonyl groups was prone to getting stuck in local minima, potentially due to intramolecular hydrogen bonding between the two DFO chains. The calculated structure of the Zr(DFO2) complex at the global minimum energy suggests an octadentate structure with no bound water molecules (**Figure 2-2**).
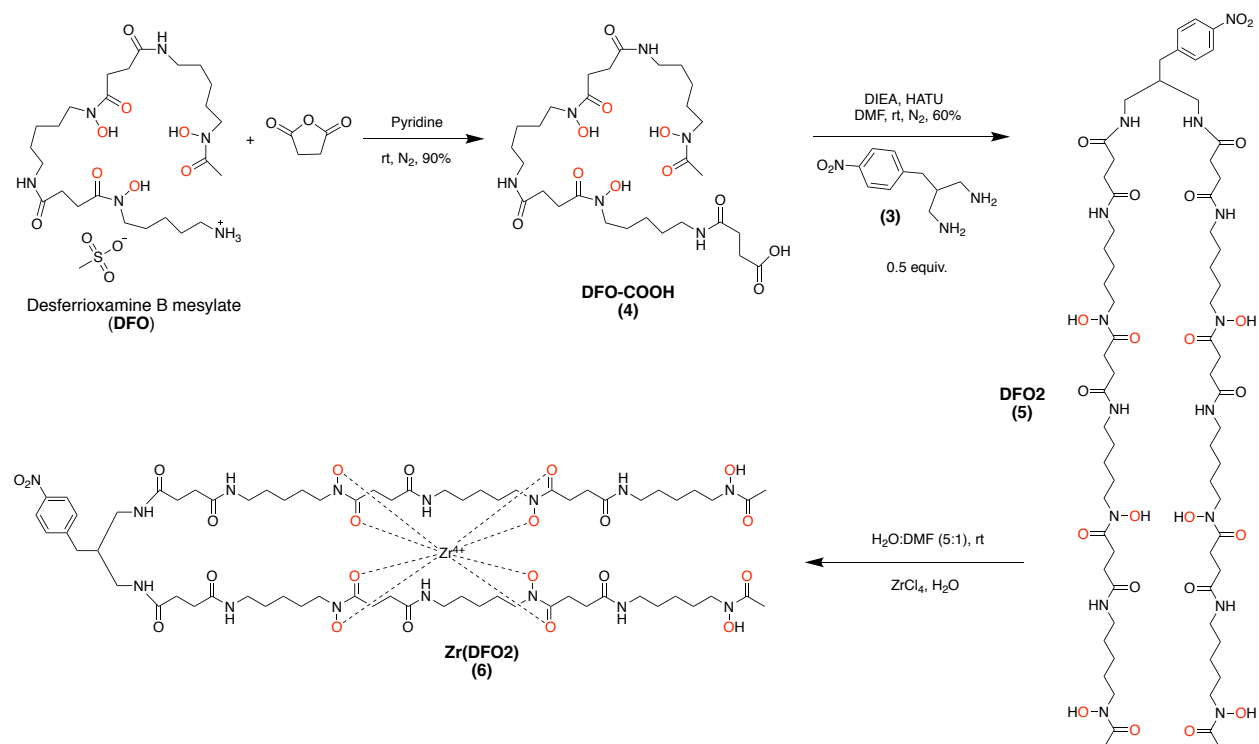
Scheme 2-2. Synthesis of **DFO2** from modified desferrioxamine B (**4**) and linker group (**3**), followed by non-radioactive Zr^{4+} coordination showing one possible conformational isomer (**6**).

Hydroxamic acid groups are known as being exceptionally well suited for binding Zr^{4+}, more so than endogenous biological ligands that would be available to compete (e.g. transferrin, albumin, chloride, phosphate). Brechbiel et al. in an investigation of the complexation of Zr^{4+} with hydroxamates showed that Zr^{4+} forms an eight coordinated complex with four bidentate hydroxamates.[46, 47] As ligands they used two hydroxamate derivatives, acetohydroxamic acid

(AHA) and *N*-methyl acetohydroxamic acid (Me-AHA). Single crystal X-ray diffraction studies of Zr(Me-AHA)$_4$ revealed the average bond length of 2.193 Å for the Zr-O bonds. Also, data obtained via DFT calculations for the Zr(Me-AHA)$_4$ complex suggested an average bond length of 2.248 Å for eight Zr-O bonds.
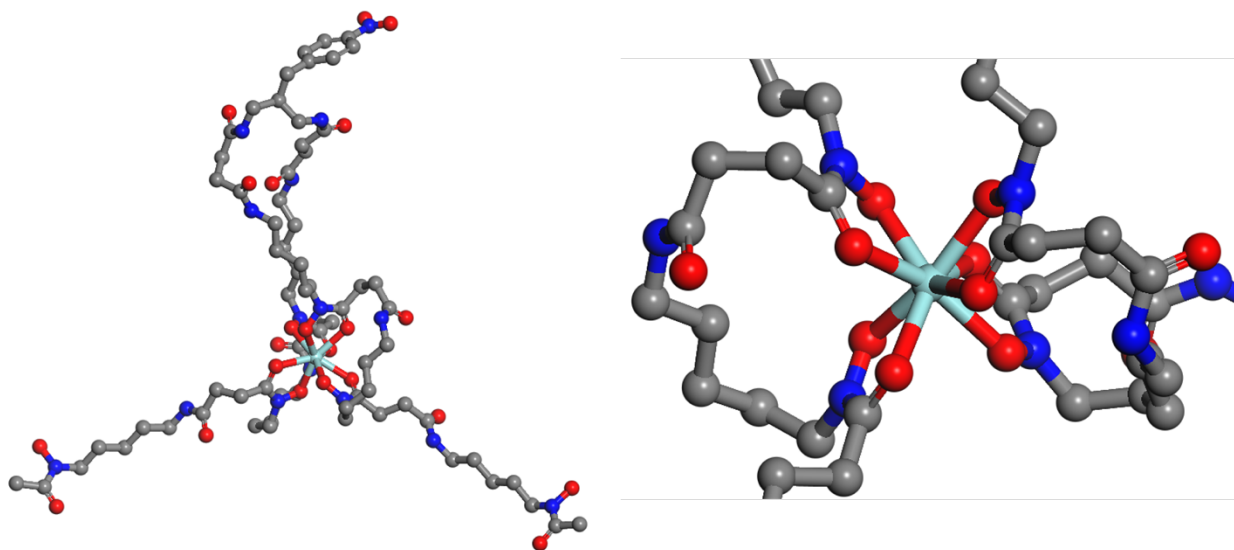
Figure 2-2. Energy-minimized and geometry-optimization molecular structures calculating using DFT (Materials Studio, DMol^3 /PBE, solvent as water with COSMO) showing (a) the Zr(DFO2) complex, and (b) the close-up of Zr(IV) ion's geometry in Zr(DFO2) complex. Hydrogen atoms are removed from figure for visual clarity but are included for calculation.

Table S1 (Supplementary I) shows our calculated bond lengths for the Zr(DFO2) complex. The calculated average bond length of 2.244 Å for Zr-O bonds in Zr(DFO2) complex is in agreement with those of the single crystal X-ray diffraction and DFT calculations of Zr(Me-AHA)$_4$ complex.[46, 47] The calculated structure of the Zr(DFO2) complex in **Figure 2-2** shows the bottom hydroxamic acid of each DFO tail in the DFO2 structure remaining un-bound. It is possible that other hydroxamates in DFO2 could bind instead of one or both of the bottom hydroxamate moieties and form alternative geometric isomers/conformers. It is also possible that these hydroxamates could switch during any reorganization of the coordination sphere, thereby forming an equilibrium between geometric isomers. More detailed DFT studies in combination with advanced

spectroscopy techniques will likely be required to better elucidate the precise details of the coordination sphere. At this stage of research, the *in vitro* and *in vivo* stability data is the most important as we are seeking a practical and functional improvement over existing chelators for use in molecular imaging and targeted radionuclide therapy.

It is possible that the two hydroxamate groups that are not strictly needed in the octadentate Zr(DFO2) complex could still improve the stability of the complex when compared with strictly octadentate chelators such as Zr(DFO*) through a process that could be roughly analogized to avidity. Although the resulting zirconium(IV) complexes for both DFO2 and DFO* are octadentate and should have comparable complex stability (both utilize hydroxamate groups), DFO2 could offer improved *in vivo* kinetic stability as a result of the two additional hydroxamic acid groups being covalently attached in close physical proximity to the coordination sphere, which should displace the position of the equilibrium toward Zr(DFO2) complex formation. This could hypothetically protect against *in vivo* competition from ligands such as water, chloride, phosphate, or proteins, and effectively increase stability. We radiolabeled both our new chelator DFO2 and the "gold standard" chelator DFO with zirconium-89 and have performed many *in vitro* stability assays. In the future it would be useful to obtain DFO* to serve as a comparison, and/or to synthesize an octadentate derivative of DFO2. DFO* was not commercially available at the time of performing these experiments. If the radiochemical stability of [^{89}Zr]Zr-DFO2 was compared with zirconium-89 complexes of structurally similar chelators (e.g. DFO*) with a denticity of only 8, and if [^{89}Zr]Zr-DFO2 demonstrated improved stability, it could hypothetically be attributed to the presence of the extra two hydroxamate groups.

Thermodynamic stability of metal-ligand complexes is an interesting and useful parameter that is often discussed for new chelators or new chelator-metal pairings. Although valuable

information, to date it doesn't appear that thermodynamic stability constants predict *in vivo* stability.[18] Despite a lack of predictive power for *in vivo* stability, formation constants can serve as a valuable tool for comparing overall thermodynamic stability of different ligands with a metal, therefore providing information about which types of metal-donor groups and which denticities are preferred. The high acidity (solvent activation and hydrolysis) of Zr^{4+} gives it the propensity to precipitate and form oxo/hydroxo-bridged species in aqueous solution (unless very acidic), making it challenging for physical chemistry studies. Recent studies have overcome these issues and determined formation constants for ligands with Zr^{4+} using potentiometric, UV/Vis spectroscopic, isothermal titration calorimetry, and mass spectrometry methods.[48-50] With a very high pM value of 32.2[50] for Zr(DFO) and logK_{ML} of 36.14[48], it is clear that any instability *in vivo* is not a result of insufficient thermodynamic stability. Now that these groups have overcome the solution chemistry challenges of determining stability constants with Zr^{4+}, it would be timely to obtain more values with new chelators. In addition, recent work has proposed a fascinating DFT-based method for predicting thermodynamic stability constants *in silico*, which is particularly useful for metal ions such as Zr^{4+} that are challenging to handle in aqueous solutions.[51]

Although it is possible that DFO2 could simply chelate two separate atoms of zirconium-89 at the same time with an expected coordination environment for each zirconium atom of three hydroxamate groups (CN = 6, with two H_2O total CN = 8), the huge molar excess of chelator over the radiometal used for radiolabeling experiments makes this very unlikely to occur. Even when performing coordination chemistry with DFO2 and ~0.9 molar equivalents of non-radioactive Zr^{4+} salt, there was no Zr_2-DFO2 observed via mass spectrometry. Radiolabeling experiments with zirconium-89 suggest the same result, where no appreciable difference in radiochemical yields (RCYs) or specific activity were observed when using 500 nmol, 50 nmol, 5 nmol, or 0.5 nmol of

DFO or DFO2 (**Table 2-1**). If each molar equivalent of DFO2 was binding two molar equivalents of zirconium-89, one would expect precisely two-times higher specific activity. The difference in polarity between [^{89}Zr]Zr(DFO) and [^{89}Zr]Zr(DFO2) was assessed by logD partition coefficients, determined using standard shake-flask methods with octanol and phosphate buffered saline (**Table 2-1**; pH=7.4). These results suggest that the [^{89}Zr]Zr(DFO) complex is more water soluble with a logD value of -2.70 ± 0.06; however, it is important to note that this DFO is not the bifunctional derivative containing a phenyl ring, but rather non-functionalized desferrioxamine B mesylate which is far more water soluble as it contains a protonated primary amine at physiological pH. The logD value obtained for the [^{89}Zr]Zr(DFO2) complex was -0.71 ± 0.01; however, this version contains a *p*-NO$_2$-Ph moiety which will substantially decrease water solubility relative to a protonated primary amine. Regardless, improved water solubility is a priority for future iterations of this new DFO2 family of chelators.

Table 2-1. Results from radiolabeling DFO and DFO2 with zirconium-89.*

Complex	Chelator (nmol)	[^{89}Zr]Zr-oxalate (μCi) / (MBq)	RCY 60 min (%)	SA (mCi•μmol^{-1}) / (MBq•μmol^{-1})	logD$_{PBS\ pH\ 7.4}$
[^{89}Zr]Zr- (DFO2)	500	459 / 17.0	99	0.9 / 33.6	-0.71 ± 01
	50	282 / 10.4	99	5.6 / 207	
	5	290 / 10.7	7.4	4.3 / 159	
	0.5	283 / 10.5	1	~	
[^{89}Zr]Zr-(DFO)	500	273 / 10.1	99	0.5 / 20.0	-2.70 ± 06
	50	276 / 10.2	99	5.5 / 202	
	5	269 / 10.0	2.3	~	
	0.5	282 / 10.4	1.4	~	

*At chelator concentrations of 500-0.5 nmol, radiochemical yields (RCY) determined via radio-iTLC (n=3), and logD octanol-buffer partition coefficient values (phosphate buffered saline pH=7.4) (n=5).

One of the most common *in vitro* stability assays performed for radiolabeled molecules is some form of a blood serum incubation/competition. For zirconium-89, DFO is known to form a stable

complex that is not appreciably transchelated by human or murine blood serum, even out beyond seven days incubation time. For zirconium-89 stability assays in blood serum, radio-iTLC is most commonly used to assess the degree of transchelation to serum proteins due to its simple and fast execution. Spotting the iTLC strips and eluting with mobile phase takes ~10-15 minutes, and many can be eluted simultaneously. Then using a standard radio-TLC reader (Bioscan/EZ AR2000) or even an automated gamma counter (cutting strips into pieces), these eluted radio-iTLC strips can be measured at a rate of about 1-3 mins each. When monitoring the radiolabeling of large proteins such as antibodies, size-exclusion HPLC chromatography provides more reliable information, including the detection of antibody aggregates, but it requires ~20-50 mins per HPLC run.

We radiolabeled both DFO and DFO2 with zirconium-89 quantitatively (>99% RCY) to form [^{89}Zr]Zr(DFO) and [^{89}Zr]Zr(DFO2) complexes (no free radiometal), and then without purification transferred aliquots of these complexes to human blood serum and assessed their stability for 7 days (**Figure 2-3**). We evaluated their serum stability using two versions of the same assay: standard radio-iTLC eluted with EDTA mobile phase (50 mM, pH=5-5.5) (**Figure 2-3A**), and by precipitating the serum proteins with cold acetonitrile, centrifugation to pellet the proteins, and decanting the water/acetonitrile which contained the intact [^{89}Zr]Zr(chelator). This was followed by rinsing the protein pellet with more ice-cold acetonitrile/water mix (~70:30) and measuring the radioactivity in each decanted fraction (**Figure 2-3B**). The results of both assays suggested superior stability of the [^{89}Zr]Zr(DFO2) radiometal complex by demonstrating less zirconium-89 associated with serum proteins. The precipitation method resulted in the largest difference in stability, with the percent intact radiometal complexes after 7 days incubation being 81% ± 4% for [^{89}Zr]Zr(DFO) complex and 87% ± 1% for [^{89}Zr]Zr(DFO2) complex.
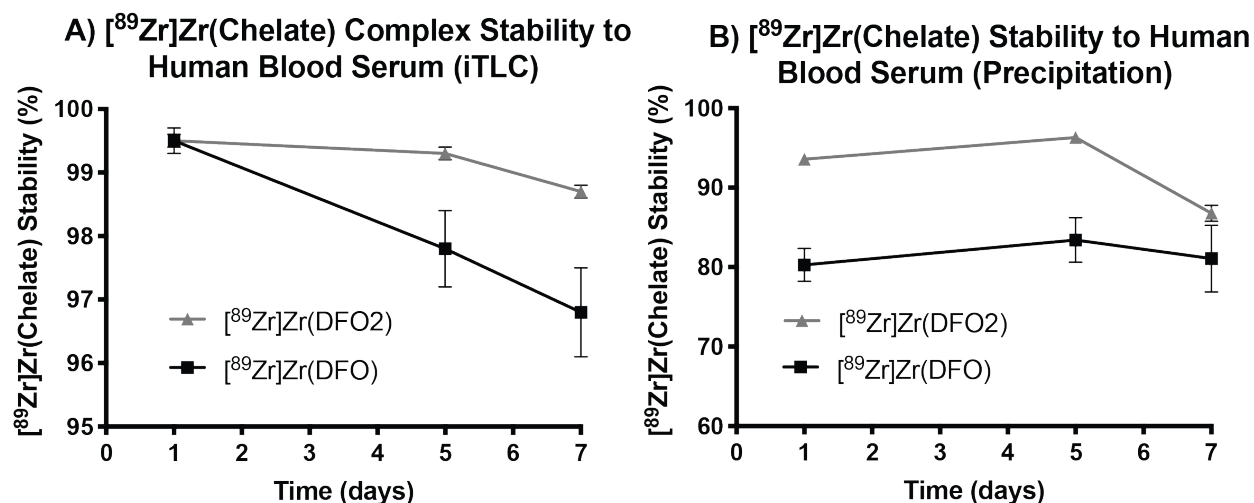
Figure 2-3. Results from *in vitro* stability assays (n=3) comparing the stability of zirconium-89 complexes of the new chelator DFO2 to the gold standard chelator DFO, with **A)** competition against human blood serum over a 7-day duration and evaluated via radio-iTLC, and **B)** the same blood serum stability assay evaluated by precipitating proteins (cold acetonitrile) and decanting supernatant via centrifugation.

The iron transport protein transferrin is the most obvious culprit for zirconium-89 transchelation due to the similarities in binding properties between Zr^{4+} and Fe^{3+}.[52-54] As such, we performed an *apo*-transferrin (*apo* = metal free, *holo* = metal bound) competition challenge, which should be more strict than blood serum for two reasons: 1) blood serum contains transferrin that is partially bound by iron (*holo*) and therefore not all binding sites are available, and 2) we used super-physiological concentrations of ~250 μM. For reference, human blood serum contains ~36 μM transferrin (~80 kDa), which is partially iron-bound (*holo*).[55] Another major blood protein that can bind to a variety of metal ions is serum albumin (~66.5 kDa), which is typically around 70 μM in the blood. For this assay we used human serum albumin (Aldrich, >96%) at a concentration of ~1.125 mM for a super-physiological quantity, but this was not the *apo*-form (**Figure 2-4B**). The results of these radiometal-chelator stability assays again suggest that the [^{89}Zr]Zr(DFO2) complex possesses superior stability to transchelation by blood serum proteins than the [^{89}Zr]Zr(DFO) complex (**Figure 2-4**). The difference in stability (percent intact radiometal-chelator complex) was

very small between both chelators (~1-3%), with the exception of the 9-day timepoint for the *apo*-transferrin challenge (**Figure 2-4A**). Only at this long timepoint did a substantial difference in stability manifest, with the percent intact radiometal complexes after 9 days incubation being 65% ± 11% for $[^{89}Zr]Zr(DFO)$ complex and 80% ± 1% for $[^{89}Zr]Zr(DFO2)$ complex. This curious and rapid drop in stability at 9-days incubation is perhaps explained by increasing baseline noise during radio-iTLC measurement as the remaining zirconium-89 had decayed to low levels. As such, the reliability of this 9-day data point is dubious.
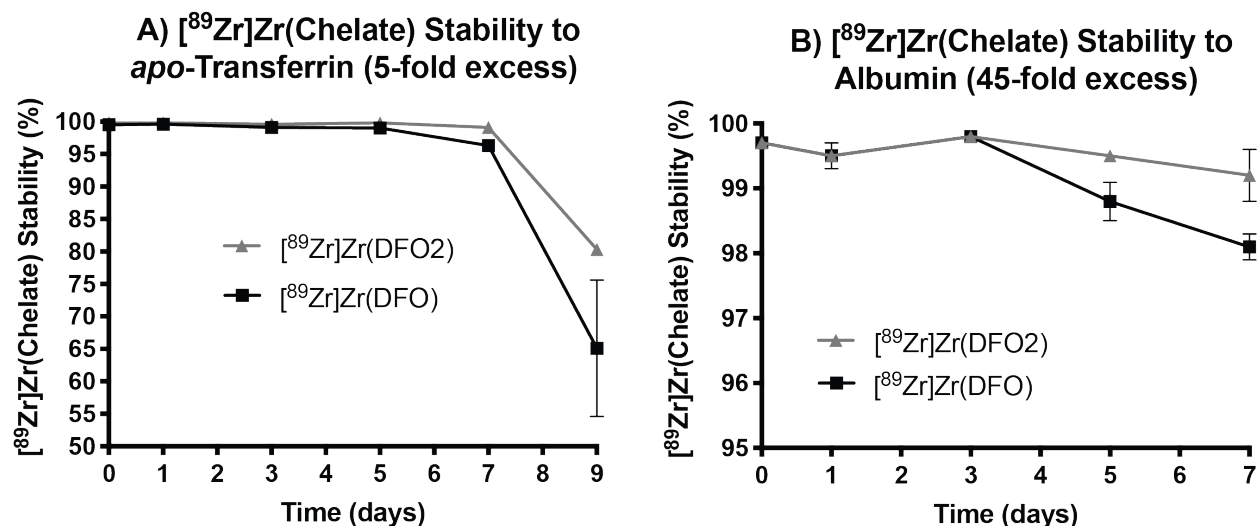
Figure 2-4. Results from *in vitro* stability assays comparing $[^{89}Zr]Zr(DFO)$ and $[^{89}Zr]Zr(DFO2)$ complexes. Both evaluated via radio-iTLC, with **A)** competition against the human iron transport protein *apo*-transferrin (5-fold molar excess), over a 9-day duration, and **B)** human serum albumin (45-fold molar excess) over a 7-day duration.

The chelator desferrioxamine is an iron siderophore produced by bacteria, and since our new chelator DFO2 is based on this siderophore, it is reasonable to assume that they will both have high selectivity and stable binding for Fe^{3+}.[56, 57] Following the methods of Deri et al,[32] we mixed the $[^{89}Zr]Zr(DFO)$ and $[^{89}Zr]Zr(DFO2)$ complexes with a 10-fold molar excess of ferric chloride ($FeCl_3$) and monitored stability via radio-iTLC for 11 days (**Figure 2-5A**). Within error, there appeared to be no difference in the ability of these two zirconium-89 chelate complexes to resist

transchelation with ferric iron. Because iron homeostasis is very tightly regulated in the body, there is essentially no "free" iron in the body and so we don't believe the lack of stability against transchelation by "free" iron is a practical issue for these hydroxamate-based zirconium-89 chelators.

High uptake of zirconium-89 is routinely observed in the bones of mice, and therefore stability of these complexes in the presence of hydroxyapatite is potentially very relevant. We mixed hydroxyapatite resin (BioRad biogel HTP) in TRIS/HCl buffer (50 mM, pH=7.4) with pre-complexed $[^{89}Zr]Zr(DFO)$ and $[^{89}Zr]Zr(DFO2)$ to determine the degree of transchelation and/or radiometal-chelate adsorption to the hydroxyapatite. After 24 hours incubation, competition mixtures were centrifuged to pellet the hydroxyapatite and the remaining solution was decanted via pipet. The hydroxyapatite pellet was re-suspended and then re-pelleted, and the solution decanted. The amount of radioactivity present in the pellet vs supernatant (plus rinse) was used to determine the percent stability, which was expressed as the percent of radiometal-chelate complex remaining in solution and not associated with the hydroxyapatite pellet. These results showed a substantial difference in stability, where the most stringent competition containing ~40 mg of hydroxyapatite revealed stability of 71% ± 1% for $[^{89}Zr]Zr(DFO)$ and 90% ± 1% for $[^{89}Zr]Zr(DFO2)$ (**Figure 2-5B**). A control of $[^{89}Zr]Zr$-oxalate (most zirconium-89 is delivered in 1 M oxalic acid, then neutralized to pH=7-7.4 for radiolabeling) was also added to ~40 mg of hydroxyapatite where only 1.4% ± 0.4% remained in solution and nearly all zirconium-89 was tightly associated with the hydroxyapatite.
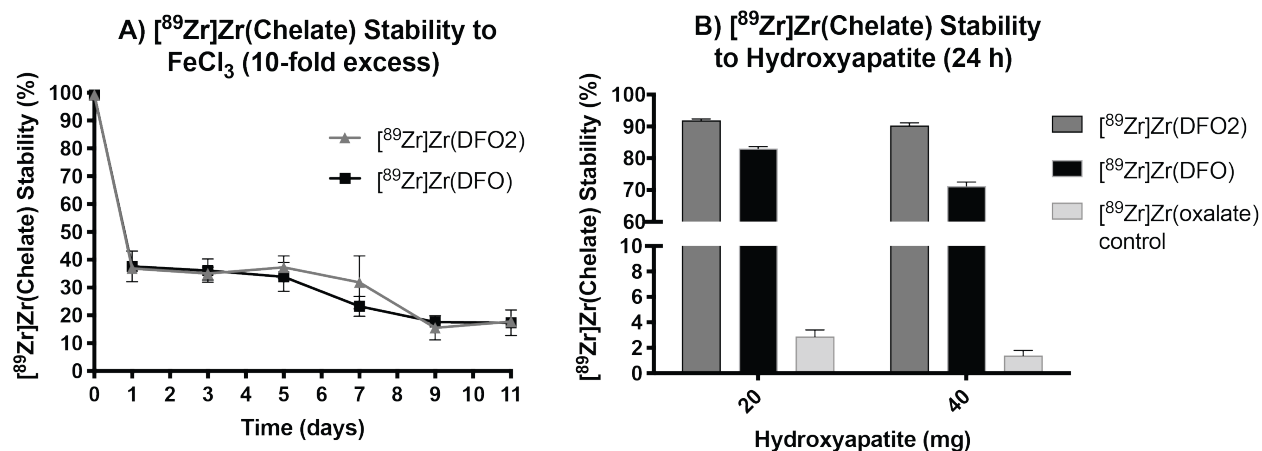
Figure 2-5. Results from *in vitro* stability assays comparing [^{89}Zr]Zr(DFO) complex and [^{89}Zr]Zr(DFO2) complex, with **A)** competition against free iron(III) chloride over an 11-day duration, evaluated via radio-iTLC, and **B)** hydroxyapatite (HTP, BioRad Bio-Gel®) competition over a 24 hour duration, evaluated via centrifugation and decanting supernatant from the HTP pellet.

As a final *in vitro* stability experiment we again followed a method by Deri et al,[32] where pre-formed radiometal-chelate complexes were mixed with a 100-fold molar excess of the chelator ethylenediaminetetraacetic acid (EDTA). Competition mixtures ranging from pH=5.0-8.0 (pH increments of 0.5) were incubated with shaking (as with all stability assays discussed) and monitored via radio-iTLC for 7 days (**Table 2-2**). This stability assay revealed a large difference in stability between [^{89}Zr]Zr(DFO) and the [^{89}Zr]Zr(DFO2) complex, particularly at physiologically relevant pH values of 6.5-7.5. After 7-days incubation and at pH 7.5, the [^{89}Zr]Zr(DFO) complex remained 23.7% ± 9.6% intact where the [^{89}Zr]Zr(DFO2) complex was 95.0% ± 0.5% intact.

Table 2-2. Results from *in vitro* EDTA transchelation stability assays.*

Starting complex	Ligand challenge	pH	% Intact starting species by incubation time						
			Initial	1 h	3 h	1 d	3 d	5 d	7 d
^{89}Zr(DFO2)	100 fold excess EDTA	8.0	100	100	100	99.9 ± 0.1	94.3 ± 2.2	88.6 ± 2.8	81.4 ± 1.4
		7.5	100	100	100	100	98.9 ± 1.0	97.6 ± 1.2	95.0 ± 0.5
		7.0	100	100	100	99.8 ± 0.1	98.7 ± 0.3	92.5 ± 6.4	85.3 ± 2.7
		6.5	100	100	99.5 ± 0.2	99.9 ± 0.2	98.0 ± 1.5	95.5 ± 1.9	90.4 ± 4.9
		6	100	98.6 ± 0.4	96.6 ± 0.7	77.6 ± 2.9	42.1 ± 8.0	27.1 ± 8.1	20.6 ± 5.9
		5.5	100	95.6 ± 1.0	90.2 ± 0.5	35.4 ± 1.1	7.0 ± 2.0	3.9 ± 1.8	1.5 ± 0.7
		5.0	100	74.3 ± 0.9	43.9 ± 3.0	1.6 ± 0.1	1.0 ± 0.4	1.0 ± 0.6	0.6 ± 0.2
^{89}Zr(DFO)	100 fold excess EDTA	8.0	98.1 ± 0.2	96.8 ± 1.3	97.5 ± 0.4	91.8 ± 1.3	75.9 ± 1.7	53.7 ± 1.4	33.6 ± 4.3
		7.5	97.3 ± 0.6	96.6 ± 0.3	95.8 ± 0.5	84.9 ± 2.1	59.7 ± 5.5	36.5 ± 11.2	23.7 ± 9.6
		7.0	96.2 ± 0.7	95.9 ± 0.7	95.5 ± 0.7	79.0 ± 1.6	50.2 ± 3.6	28.1 ± 8.1	16.1 ± 4.4
		6.5	95.5 ± 0.9	96.4 ± 2.2	92.7 ± 0.4	58.2 ± 3.6	21.6 ± 1.5	11.6 ± 0.7	8.5 ± 1.4
		6	99.3 ± 0.2	94.9 ± 0.2	84.6 ± 2.2	20.4 ± 1.5	4.5 ± 0.2	3.6 ± 0.5	3.4 ± 1.3
		5.5	99.1 ± 0.2	89.6 ± 0.7	69.9 ± 1.5	5.3 ± 0.8	2.4 ± 0.3	2.7 ± 0.3	1.9 ± 0.1
		5.0	97.0 ± 0.2	63.5 ± 1.3	27.3 ± 3.3	1.9 ± 0.7	1.1 ± 0.1	1.2 ± 0.1	1.1 ± 0.0

100-99%	98-90%	89-80%	≤ 79%

*Pre-radiolabeled [^{89}Zr]Zr(DFO) and [^{89}Zr]Zr(DFO2) complexes were mixed with a 100-fold molar excess of EDTA chelator at various pH values, and monitored by radio-iTLC for 7 days.

All together, these results suggest that our new chelator — DFO2 — offers a superior chelation environment for zirconium-89 when compared with DFO by offering a higher coordination number and improved stability to a wide variety of *in vitro* challenges. Although DFO2 having an abnormally high potential denticity of 12 might not improve its ability to complex zirconium, we believe it uniquely positions DFO2 to bind high valent metal ions such as lanthanides and actinides. We are working on next-generation DFO2 derivatives with further simplified synthesis, improved solubility, and different bifunctional linker groups with these goals in mind. For example, to obtain the *p*-NO$_2$-phenyl group in the backbone of DFO2 we performed a three synthetic steps, which has provided a challenge due to low yields and difficult purification. In the future we plan to optimize the design of DFO2 by exploring alternative linker options to the *p*-NO$_2$-phenyl propylenediamine linker that can help us achieve our goals of enhanced solubility and facile bioconjugation. New DFO2 derivatives will undergo bioconjugation with a model antibody, radiolabeling, and *in vivo* stability assessment in mice. Long-term, we hope to link *in*

vivo results back to this study and determine which of these *in vitro* stability assays were ultimately the most predictive of the chelators *in vivo* behavior.

2.5. Conclusion

The new chelator DFO2 presents a promising new modular and high-denticity chelator scaffold, which we will build upon using its modular synthesis scheme to produce highly stable and customizable bifunctional chelators for zirconium-89 and other interesting radiometals. With double the potential coordination number of the "gold standard" chelator for zirconium-89 — DFO (CN = 12 vs 6) — DFO2 appears to saturate the octadentate coordination sphere of zirconium and prevents the coordination of water. This conclusion is supported by high-resolution mass spectrometry of the non-radioactive Zr(DFO2) complex, density functional theory calculations, and radiolabeling results (specific activity). Following quantitative radiolabeling with zirconium-89, the [^{89}Zr]Zr(DFO) and [^{89}Zr]Zr(DFO2) complexes were compared using a large number of *in vitro* stability challenges including human blood serum, *apo*-transferrin, serum albumin, iron, hydroxyapatite, and EDTA. The results of these numerous stability assays demonstrated that our new chelator DFO2 formed a more stable zirconim-89 complex than DFO, except for the iron challenge where both chelators were identical. Substantial differences in stability were not observed for human blood serum using radio-iTLC, but when using a protein precipitation method of analysis, the stability values after 7 days deviated in favor of DFO2. To simulate transchelation/adsorption with bone we developed a hydroxyapatite resin challenge, and finally we performed a competition against a 100-fold molar excess of EDTA — where both assays revealed the superior stability of DFO2 with zirconium-89. Taken together, these suggest that our new DFO2 chelator is a promising next-generation scaffold for the elaboration of zirconium-89

chelators. We plan to use the modular synthesis of the DFO2 chelator to tune its polarity, conjugation chemistry, and coordination chemistry.

2.6. Experimental Section

Reagents. All solvents and reagents were purchased from commercial suppliers (Sigma Aldrich, St. Louis, MO; TCI America, Portland, OR; Fisher Scientific, Waltham, MA) and were used as received unless otherwise indicated. DMSO used for chelator stock solutions was of molecular biology grade (>99.9%: Sigma Aldrich). DFO.mesylate was purchased from Abcam. 1-[Bis(dimethylamino)methylene]-1H-1,2,3-triazolo[4,5-b]pyridinium 3-oxid hexafluorophosphate (HATU) was purchased from AK Scientific. *N,N*-diisopropylethylamine (DIEA), diethyl malonate, 4-nitrobenzyl bromide, and borane-tetrahydrofuran solution (BH$_3$.THF) were purchased from Sigma-Aldrich. ZrCl$_4$, potassium carbonate anhydrous, and ammonium hydroxide were purchased from Fisher Scientific. All the chemicals were used directly without purification.

Radiochemistry Instrumentation. ^{89}Zr was produced at Memorial Sloan Kettering Cancer Center using an EBCO TR19/9 variable-beam energy cyclotron (Ebco Industries Inc., British Columbia, Canada) via the ^{89}Y(p,n)^{89}Zr reaction. ^{89}Zr was purified in accordance with previously reported methods to create ^{89}Zr with a specific activity of 5.3 – 13.4 mCi/μg (195 – 497 MBq/μg).[2] Radiolabeling reactions were monitored using silica-gel impregnated glass-microfiber instant thin layer chromatography paper (iTLC-SG, iTLC-SA, Varian, Lake Forest, CA) and analyzed on a Bioscan AR-2000 radio-TLC plate reader using Winscan Radio-TLC software (Bioscan Inc., Washington, DC). All radiolabeling chemistry was performed with ultrapure water (>18.2 MΩ cm^{-1} at 25°C, Milli-Q, Millipore, Billerica, MA), and treatment of water or buffers with Chelex-

100 resin was performed as indicated (1.2 g/L, 24 h) (BioRad Laboratories, Hercules, CA). Radioactivity in samples was measured using a Capintec CRC-15R dose calibrator (Capintec, Ramsey, NJ). For [^{89}Zr]Zr^{4+} logD experiments, a Perkin-Elmer (Waltham, MA) Automated Wizard Gamma Counter was used for counting radioactivity.

Chemical Characterization Methods. ^{1}H and ^{13}C NMR spectra were recorded at the University of Saskatchewan on a 500 MHz Bruker Avance, and a 500 MHz Bruker Avance III HD NMR spectrometer at 25 °C in (CD$_3$)$_2$SO and CD$_3$OD. ^{1}H chemical shifts were referenced to the residual protons of the deuterated solvents (δ = 2.50 ppm for (CD$_3$)$_2$SO; δ = 3.31 ppm for CD$_3$OD); ^{13}C chemical shifts were referenced to the (CD$_3$)$_2$SO signal at δ = 39.52 ppm and the CD$_3$OD signal at δ = 49.00 ppm. Coupling constants are reported to the nearest 0.5 Hz (^{1}H NMR spectroscopy) or rounded to integer values in Hz (^{13}C NMR spectroscopy). Assignments were supported by additional NMR experiments, DEPT, HMQC, and COSY, for compounds **3**, **4**, **5**, and **6**. High resolution mass spectra were measured on a JEOL AccuTOF GCv 4G using field desorption ionization (FDI). For the isotopic pattern only the mass peak of the isotope with the highest natural abundance is given.

Density Functional Theory (DFT) Calculations. DFT geometry optimizations were carried out using DMol^3 and Biovia Materials Studio, version 2017 R2,[58, 59] using the generalized gradient approximation (GGA) employing the Perdew-Burke-Ernzerhof (PBE)[60] exchange-correlation functional both for the potential during the self-consistent field (SCF) procedure and for the energy.[61] All calculations employed double numerical plus d-function (DND) basis sets, using the 4.4 basis file, as implemented within the DMol^3 software, included polarization functions for all

atoms with all-electron core treatments. Quantum simulation of solvated molecules were modeled using the conductor-like screening model (COSMO) solvation model[62, 63] in DMol³, with a dielectric value representing water ($\varepsilon = 78.54$). Frequency optimizations were performed, and harmonic vibrational frequencies were positive, confirming that they were local minima. All graphical depictions of the structures were generated using CYLview software[64] using coordinates from the optimized log file.

Synthesis of diethyl-2-[(4-nitrophenyl)methyl]–propanedioate (1): This synthesis was adapted from Pandya et al.[65] Diethyl malonate (8.6 mL, 56.378 mmol) and potassium carbonate anhydrous (2.808 g, 20.318 mmol) were dissolved in acetone (8.0 mL). The mixture was stirred for 1 hour at room temperature. Then 4-nitrobenzyl bromide (2.213 g, 10.244 mmol) was added and stirred for 2 hours at 45°C. After cooling to room temperature, the yellow reaction mixture was filtered to remove the remaining potassium carbonate and was washed with acetone (20 mL). The filtrate was collected and the solvent was reduced by rotary evaporation *in vacuo*, ethanol was added (~10 mL), and then kept at -20 °C in the freezer overnight. Crystals formed and were separated by filtration and the filtrate was placed back in the freezer at -20 °C overnight to produce more crystals. This process was completed a total of three times. White crystals of (**1**) (1.393 g, 46.13%) was obtained from three rounds of precipitation and filtration. ¹H NMR (CDCl₃, 500 MHz) δ=1.22 [t, 6H, $J = 7.1$ Hz, CH₂C$\underline{H}$₃], 3.32 [d, 2H, $J = 7.8$ Hz, =CC$\underline{H}$₂CH], 3.66 [t, 1H, $J = 7.8$ Hz, =CCH₂C$\underline{H}$], 4.14 - 4.21 [m, 4H, OC$\underline{H}$₂CH₃], 7.39 [d, 2H, $J = 8.7$ Hz, C$\underline{H}$=CCH₂ Ar], 8.15 [d, 2H, $J = 8.7$ Hz, C$\underline{H}$=CNO₂ Ar].

Synthesis of 2-(4-nitrobenzyl) malonamide (2): This synthesis was adapted from Price et al.[45] Compound **1** (295 mg, 0.999 mmol) was dissolved in methanol (5 mL), followed by addition of ammonium hydroxide (5 mL). The reaction mixture was stirred for 45 hours at room temperature. A yellow precipitate was formed and isolated by filtration, and then washed with methanol and boiling acetonitrile. Solvent was removed by rotary evaporation *in vacuo*. Yellow crystals of compound (**2**) (180.78 mg, 61.7%) was obtained. ^{1}H NMR [(CD$_3$)$_2$SO, 500 MHz]: δ = 3.10 [d, 2H, J = 7.6 Hz, =CC$\underline{H}_2$CH], 3.38 [t, 1H, J = 7.7 Hz, =CCH$_2$C$\underline{H}$], 7.07 [s, 2H, CON$\underline{H}_2$], 7.27 [s, 2H, CON$\underline{H}_2$], 7.48 [d, 2H, J = 8.8 Hz, C$\underline{H}$=CCH$_2$ Ar], 8.14 [d, 2H, J = 8.8 Hz, C$\underline{H}$=CNO$_2$ Ar].

Synthesis of (2-(4-nitrobenzyl)-1,3-propylenediamine (3): This synthesis was adapted from Price et al.[45] A mixture of compound **2** (1.005 g, 4.237 mmol) in dry THF (15 mL) was cooled in an ice bath, followed by dropwise addition of a diborane (BH$_3$.THF) solution (8.14 mL, 1.0 M in THF) under nitrogen gas. After stirring for half an hour, the solution was left to warm up to room temperature, then it was heated to reflux under nitrogen gas overnight. Before HCl (12 M; 15 mL) was added, the reaction was cooled to room temperature. The reaction was then warmed to reflux with no inert gas for one hour. Then the solvent was evaporated by rotary evaporator and NaOH (6 M; 30 mL) was added to the residue, which was then extracted with dichloromethane (5 x 15 mL). The organic fractions were collected and dried with anhydrous Na$_2$SO$_4$. The solvent was then removed by rotary evaporation *in vacuo*, and ethanol (20 mL) was added followed by HCl (12 M; 4 mL). The solution was placed in the freezer at -20 °C overnight. A white solid formed, was filtered, and dried. Compound **3** (250 mg, 28.20%) was obtained. ^{1}H NMR (D$_2$O, 500 MHz): δ = 2.57 [sept, 1H, J = 6.9 Hz, CH$_2$C$\underline{H}$CH$_2$], 2.99 [d, 2H, J = 7.6 Hz, CC$\underline{H}_2$CH], 3.07 [dd, 2H, J = 6.7 Hz, J = 13.7 Hz, C$\underline{H}_2$NH$_2$], 3.19 [dd, 2H, J = 6.7 Hz, J = 13.7 Hz, C$\underline{H}_2$NH$_2$], 7.55 [d, 2H, J = 8.8,

NO$_2$CC$\underline{H}$], 8.28 [d, 2H, J =8.8, CC$\underline{H}$=CH]. ^{13}C NMR (D$_2$O, 500 MHz): δ 34.7, 36.5, 39.9, 124.0, 130.1, 145.2, 146.7. HRMS (ESI; m/z): [M+H]$^+$ calcd for C$_{10}$H$_{15}$N$_3$O$_2$: 210.1242; found: 210.1241.

Synthesis of DFOCOOH (4). Compound **4** (DFOCOOH) was prepared according to a published procedure.[66] To a solution of succinic anhydride (0.857 g, 8.56 mmol) in pyridine (4.0 mL), desferrioxamine (DFO) mesylate salt (0.250 g, 0.380 mmol) was added. It formed a white suspension. The reaction mixture was stirred at room temperature overnight. To this mixture was added an aqueous solution of sodium hydroxide (0.16 M; 45 mL) which was stirred for 5 hours and formed a clear solution. Hydrochloric acid (12 M; 6.0 mL) was added dropwise to this solution until the pH of the solution reached 2.0 (pH strip). The solution turned cloudy upon addition of hydrochloric acid. The mixture was left at 5 °C in the fridge for further precipitation. After vacuum filtration the precipitate was washed several times with a 0.01 M solution of hydrochloric acid, followed by lyophilization. Compound **4** was obtained as a white solid (0.232 g, 93%). ^{1}H NMR [(CD$_3$)$_2$SO, 500 MHz]: δ = 1.20 (m, 7H, C$\underline{H}$), 1.37 (m, 7H, C$\underline{H}$), 1.49 (m, 6H, C$\underline{H}$), 2.27 (m, 6H, C$\underline{H}$), 2.40 (t, 2H, C$\underline{H}$), 2.57 (t, 4H, C$\underline{H}$), 2.99 (q, 6H, C$\underline{H}$), 3.45 (t, 6H, C$\underline{H}$), 7.80 (m, 3H, N$\underline{H}$), 9.62 (s, 2H, N-O$\underline{H}$), 9.66 (s, 1H, N-O$\underline{H}$), 12.07 (m, 1H, COO$\underline{H}$) ppm; ^{13}C[^{1}H] NMR [(CD$_3$)$_2$SO, 126 MHz]: δ = 20.4, 23.5, 26.1, 27.6, 28.8, 29.2, 29.9, 30.0, 38.4, 46.8, 47.1 ($\underline{C}$H), 170.1, 170.7, 171.3, 172.0, 173.9 ($\underline{C}$O) ppm.

Synthesis of *p*-NO$_2$-Bn-DFO2 (5). Compound **4** (0.348 g, 0.527 mmol) is only sparingly soluble in DMF (10.5 mL) at room temperature and was dissolved at 80 °C. *N,N*-diisopropylethylamine (DIEA; 0.072 g, 0.557 mmol) was added to the solution of 1-[Bis(dimethylamino)methylene]-1H-1,2,3-triazolo[4,5-b]pyridinium 3-oxid hexafluorophosphate (HATU; 0.211 g, 0.555 mmol) in

DMF (11.0 mL) in a separate vial. This solution then was added to the solution of compound **4** in DMF followed by addition of a solution of compound **3** (0.052 g, 0.248 mmol) in DMF (5.3 mL). The reaction mixture was stirred at room temperature for 24 hours. Volatiles were evaporated to reduce the volume to ~1/6. The crude product was then precipitated by slow addition of ice-cold ultra-pure water (70.0 mL) into this residue. The product was separated by centrifugation, followed by two rounds of re-suspension in ice-cold ultra-pure water and centrifugation. Finally, product was dissolved in a minimum volume of DMF, followed by addition of ice-cold ethyl acetate to precipitate product, then centrifugation and decanting. The final powder was mixed with ultrapure water and lyophilized. The **p-NO₂-Bn-DFO2 (5)** product was obtained as a bone white powder (0.2216 g, 60%). ^{1}H NMR [$(CD_3)_2SO$, 500 MHz]: δ = 1.21 (m, 17H, C$\underline{H}$), 1.38 (m, 17H, C$\underline{H}$), 1.49 (m, 15H, C$\underline{H}$), 2.26 (m, 11H, C$\underline{H}$), 2.57 (m, 8H, C$\underline{H}$), 2.99 (m, 17H, C$\underline{H}$), 3.45 (m, 12H, C$\underline{H}$), 7.51 (d, 2H, J = 8.5 Hz, C$_6$$\underline{H}_4$), 7.76 (m, 6H, N$\underline{H}$), 7.82 (m, 2H, N$\underline{H}$), 8.14 (d, 2H, J = 8.1 Hz, C$_6$$\underline{H}_4$), 9.59 (s, 4H, N-O$\underline{H}$), 9.63 (s, 2H, N-O$\underline{H}$) ppm; ^{13}C[^{1}H] NMR [$(CD_3)_2SO$, 126 MHz]: δ = 20.3, 23.5, 26.0, 27.5, 28.0, 28.7, 28.8, 29.8, 29.9, 30.8, 30.9, 38.4, 46.8, 47.1 ($\underline{C}$H), 123.2, 130.3, 145.9, 149.0 ($\underline{C}_6$H$_4$), 170.0, 170.1, 171.1, 171.3, 171.7, 171.9, 177.7 ($\underline{C}$O) ppm; HRMS (TOF): m/z calcd for $C_{68}H_{115}N_{15}O_{22}$+H$^+$: 1494.8413 [$M$+H]$^+$; found: 1494.8565; calcd for $[C_{68}H_{115}N_{15}O_{22}+2H]^{2+}/2$: 747.9243 [$M$+2H]$^{2+}$/2; found: 747.9241.

Synthesis of Zr(DFO2) complex (6). Compound **5** (50.00 mg, 33.45 μmol) was dissolved in a solvent mixture of DMF:H$_2$O (1:5; 1.3 mL) at 80 °C. A solution of ZrCl$_4$ (7.64 mg, 32.78 μmol) in H$_2$O (0.7 mL) was slowly added to the resulting mixture. The reaction was stirred at room temperature for 24 hours. After removing all volatiles under high vacuum, the product was obtained as a thin yellow glassy film. ^{1}H NMR [$(CD_3)_2SO$, 500 MHz]: δ = 1.23, 1.27, 1.39, 1.49,

1.63, 1.96, 2.12, 2.26, 2.31, 2.58, 2.61, 2.99, 3.09, 3.45, 3.61 (m, C$\underline{H}$), 7.53 (m, C$_6$$\underline{H}$$_4$), 7.80, 7.88, 7.95 (m, N$\underline{H}$), 8.14 (d, 2H, J = 8.3 Hz, C$_6$$\underline{H}$$_4$), 9.73 (br, N-O$\underline{H}$) ppm; ^{13}C[^{1}H] NMR [(CD$_3$)$_2$SO, 126 MHz]: δ = 16.8, 20.4, 22.3, 22.5, 23.2, 23.5, 24.9, 25.7, 26.0, 26.6, 26.9, 27.7, 28.0, 28.8, 28.9, 29.2, 29.3, 30.0, 34.1, 38.4, 46.8, 47.1, 49.7, 50.0, 50.3, 50.6, 63.8 ($\underline{C}$H), 119.1, 123.2, 123.4, 127.5, 130.4, 145.9, 146.1, 148.0, 149.1 ($\underline{C}$$_6H_4$), 160.9, 161.0, 162.7, 162.8, 170.1, 170.4, 170.7, 170.8, 171.0, 171.17, 171.23, 171.3, 171.4, 171.8, 171.9, 173.6, 173.8, 173.9, 177.8 ($\underline{C}$O) ppm; HRMS (TOF): m/z calcd for C$_{68}$H$_{111}$N$_{15}$O$_{22}$Zr+H$^+$: 1580.7153 [M+H]$^+$; found: 1580.7109; calcd for [C$_{68}$H$_{111}$N$_{15}$O$_{22}$Zr+2H]$^{2+}$/2: 790.8610 [M+2H]$^{2+}$/2; found: 790.8643.

[^{89}Zr]Zr^{4+} Radiolabeling Studies. Zirconium-89 was received after target dissolution and purification as the [^{89}Zr]Zr(oxalate) complex in 1.0 M oxalic acid. Phosphate buffered saline (PBS, pH=7.4, pre-treated with Chelex resin) was used for radiolabeling buffer, sodium carbonate (1.0 M) was used to neutralize aliquots of zirconium-89 in oxalic acid to pH=6.8-7.2 (checked by pH strip), and an EDTA solution (50 mM, pH=5-5.5) was used as mobile phase for eluting radio-iTLC (Varian iTLC-SG) to check RCY and purity. For radio-iTLC analysis, intact [^{89}Zr]Zr(chelate) (chelate=DFO or DFO2) remained at the baseline, while the [^{89}Zr]Zr^{4+} that remained unbound or was transchelated to serum proteins eluted with the solvent front. Radio-iTLC were analyzed using a BioScan AR2000 and the integration of activity at the baseline and solvent front were used to calculate yields and degree of transchelation during stability assays. The commercially available chelator DFO mesylate (Macrocyclics) was used as a control alongside our new chelator DFO2. Stock solutions of both chelators were prepared in DMSO at a concentration of 17.0 mg/mL. Aliquots of these stock solution were transferred to radiolabeling buffer (Chelex treated PBS pH=7.4) to prepare separate solutions of DFO and DFO2 chelators at final volumes of 2.5 mL (100

μM). For each chelate solution, aliquots of 4-5 mCi (148-185 MBq) of [^{89}Zr]Zr(oxalate) was neutralized with sodium carbonate as described above, and diluted to a total volume of 2.5 mL in PBS. This solution was combined with the chelate solution to produce the final radiolabeling solution containing 5 mL total volume with 50 μM chelate and 4-5 mCi of zirconium-89. The radiolabeling reaction mixture was allowed to mix on an Eppendorf thermomixer (800 rpm, 60 minutes, 37 °C). Radiochemical yields via radio-iTLC for both DFO and DFO2 chelators were >99% after 60 minutes reaction time. These pre-formed [^{89}Zr]Zr(chelate) solutions were used without purification for stability assays. Radiolabeled complexes of DFO and DFO2 chelators with zirconium-89 were also prepared at 100 μM final concentration in the same manner as described above, and used for some of the stability assays described below.

In Vitro Stability Assays

Serum Stability Assay. [^{89}Zr]Zr(DFO) and [^{89}Zr]Zr(DFO2) complexes were prepared as described above, and 400 μL aliquots (100 μM) were transferred to microcentrifuge tubes (Eppendorf Low-Bind, 1.5 mL) containing 600 μL of previously frozen human blood serum (Sigma Aldrich). Samples were placed on Eppendorf Thermomixers at 37 °C and 800 rpm agitation. Assay progress was monitored by radio-iTLC at times of 1 day, 5 days, and 7 days. As with other assays performed for this study, zirconium-89 transchelated by blood serum components elutes to the solvent front in an EDTA mobile phase (50 mM, pH=5.0-5.5), where [^{89}Zr]Zr(chelate) remains at the baseline.

An alternative analysis method was performed, where aliquots (300 μL) of the [^{89}Zr]Zr(chelate)/human blood serum competition mixture was removed, mixed with ice-cold acetonitrile (700 μL) to precipitate proteins, and then centrifuged at 10,000 rpm for 10 minutes (4

°C). The supernatant was decanted via pipet and measured by dose calibrator, and the process was repeated with ice-cold water/acetonitrile mixture (30:70). The amount of zirconium-89 remaining stuck to the serum proteins in the original microcentrifuge tube was assumed to be transchelated, and the amount of radioactivity in the supernatant was assumed to be chelate-bound. This ratio was used to calculate the % stability of the [^{89}Zr]Zr(chelate) complexes. As a further control, 300 µL of only [^{89}Zr]Zr(chelate) complex with no blood serum was put through the same process (ice-cold acetonitrile, centrifugation) and it was found that for both [^{89}Zr]Zr(chelate) complexes ~10% of the activity in solution remained stuck in the microcentrifuge tubes after centrifugation and decanting twice. The stability values reported were not corrected for this sticking factor.

Apo-Transferrin Assay. [^{89}Zr]Zr(chelate) complexes were prepared as described above. For this assay, a 5-fold molar excess of *apo*-transferrin (Sigma Aldrich) was used relative to [^{89}Zr]Zr(chelate) complex, from a stock solution of *apo*-transferrin in PBS (Chelex treated, pH=7.4, 500 µM). The final competition solutions (n=3) for each of [^{89}Zr]Zr(DFO) complex and [^{89}Zr]Zr(DFO2) complex contained 200 µL total volume, 50 µM of [^{89}Zr]Zr(chelate) complex (PBS, 100 µL of 100 µM), and 250 µM of *apo*-transferrin (PBS, 100 µL at 500 µM). Samples were placed on Eppendorf Thermomixers at 37 °C and 800 rpm agitation. Assay progress was monitored by radio-iTLC at times of 0, 1 day, 3 days, 5 days, 7 days, and 9 days.

Serum Albumin Assay. [^{89}Zr]Zr(chelate) complexes were prepared as described above. Human serum albumin (Sigma Aldrich, >96%) was dissolved in PBS (chelex treated, pH=7.4) at a concentration of 100 mg/mL (~1.5 mM), and 150 µL aliquots were transferred to microcentrifuge tubes (n=3). [^{89}Zr]Zr(chelate) complex was then added (50 µL, 100 µM, ~50 µCi) to each tube for

a final concentration of 25 μM [^{89}Zr]Zr(chelate) complex and ~1.125 mM albumin (~45-fold molar excess). Samples were placed on Eppendorf Thermomixers at 37 °C and 800 rpm agitation. Assay progress was monitored by radio-iTLC at times of 0, 1 day, 3 days, 5 days, and 7 days.

EDTA Transchelation Assay. These transchelation challenges were setup following the methods of Deri et al.,[32] with a molar ratio of 100-fold molar excess of EDTA to pre-formed [^{89}Zr]Zr(DFO) complex or [^{89}Zr]Zr(DFO2) complex. The solutions prepared for this assay were: 1) 2.5 mL of [^{89}Zr]Zr(DFO) complex and [^{89}Zr]Zr(DFO2) complex (50 μM each) as described above, 2) EDTA stock solution (5 mM) split and then each sub-stock solution adjusted by pH meter to pH 5.0, 5.5, 6.0, 6.5, 7.0, 7.5, and 8.0, and 3) ammonium acetate buffer (500 mM) split and then each sub-stock solution adjusted by pH meter to pH 5.0, 5.5, 6.0, 6.5, 7.0, 7.5, and 8.0. These three stock solutions were combined in microcentrifuge tubes (1.5 mL tubes, n=3) for each chelator and pH range in ratios of [^{89}Zr]Zr(chelate) complex (200 μL, 50 μM), EDTA (200 μL, 5 mM), and ammonium acetate (100 μL, 500 mM), with the EDTA and ammonium acetate solutions matching pH (e.g. pH=7.0 each for the pH=7.0 challenge, n=3). The final EDTA transchelation assays solutions contained a total volume of 500 μL with [^{89}Zr]Zr(chelate) complex (20 μM, ~100 μCi, ~3.7 MBq) and EDTA solution (2 mM) for a 100-fold molar excess of EDTA challenge. Transchelation was monitored by radio-iTLC as described above (EDTA mobile phase, 50 mM, pH=5.0-5.5), where zirconium-89 associated with DFO or DFO2 chelators remained at the baseline and zirconium-89 transchelated to EDTA eluted with the solvent front. Samples were placed on Eppendorf Thermomixers at 37 °C and 800 rpm agitation. Assay progress was monitored at times 0, 1 hour, 3 hours, 1 day, 3 days, 5 days, and 7 days.

67

Iron(III) Competition Study. Radiolabeled $[^{89}Zr]Zr(DFO)$ complex and $[^{89}Zr]Zr(DFO2)$ complex were prepared as described above. The metal salt iron(III) chloride was prepared as a stock solution (1.0 mM, chelex-treated millipure water). Aliquots of $[^{89}Zr]Zr(chelate)$ complex (200 μL, 100 μM) were combined with iron(III) solution (200 μL, 1.0 mM) to yield final completion mixtures (n=3) containing 50 μM of $[^{89}Zr]Zr(chelate)$ complex and 500 μM of iron(III) solution (10-fold molar excess). Samples of $[^{89}Zr]Zr(chelate)$ complexes in competing iron solutions were placed on Eppendorf Thermomixers at 37 °C and 800 rpm agitation. Assay progress was monitored by radio-iTLC as described above at times 0, 1 day, 3 days, 5 days, 7 days, and 9 days.

Hydroxyapatite (HTP) Stability Challenge. Hydroxyapatite resin (HTP, BioRad Bio-Gel®) was weighed into microcentrifuge tubes (20 mg and 40 mg sets, n=3 per weight and per chelator/control). To each tube containing HTP, TRIS/HCl buffer was added (50 mM, 900 μL, pH=7.4). $[^{89}Zr]Zr(DFO)$ and $[^{89}Zr]Zr(DFO2)$ complexes were radiolabeled as described above, with the exception that TRIS/HCl buffer (50 mM, pH=7.4) was used. and aliquots were transferred to each tube (100 μM, 100 μL, ~100 μCi, ~3.7 MBq), as well as a set of unchelated but neutralized $[^{89}Zr]Zr(oxalate)$ complex as controls (~100 μCi, ~3.7 MBq, n=3). The final concentration of $[^{89}Zr]Zr(chelate)$ complex in each competition was 10 μM. HTP competition mixtures were placed on Eppendorf Thermomixers at 37 °C and 800 rpm agitation. After 24 hours, these samples were centrifuged (10,000 rpm, 10 minutes) to pellet the HTP, the supernatant decanted via pipet, and the pellet was washed with TRIS/HCl buffer (1.0 mL) twice, followed by centrifugation and decanting. The amount of zirconium-89 adsorbed/bound by the HTP and the amount remaining chelate-bound in the supernatant and washes was measured via dose calibrator. The percent

stability was determined from a ratio of the percent radioactivity in the supernatant/washes and the HTP pellet.

LogD Octanol/Buffer Partition Coefficient. Radiolabeled [^{89}Zr]Zr(DFO) and [^{89}Zr]Zr(DFO2) complexes were prepared as described above (100 µM). After radiolabeling, logD values were determined by transferring an aliquot of each radiolabeled chelator (~ 5 µCi, ~5-10 µL) to 3 mL of PBS (pH=7.4) in 15 mL falcon centrifuge tubes (n = 5). An equal volume of 1-octanol (3 mL) was then added, tubes were capped, and then vortex mixed for 60 seconds each. The tubes were then centrifuged for 10 minutes (3000 rpm) to aid in phase separation. Samples were removed from the centrifuge, allowed to sit for 10 minutes, and 1.0 mL aliquots of each phase were removed carefully via pipet and transferred to small microcentrifuge tubes (1.5 mL) and radioactivity measured on a gamma counter. The ratio of radioactivity (counts) in each phase was used to calculate the logD values (**equation 2-1**). The amount of radioactivity in the octanol phase was used in place of solute concentrations (ionized and un-ionized), and the amount in the PBS (pH=7.4) phase was used in place of solute concentration (ionized and un-ionized).

$$(2\text{-}1) \qquad \text{logD}_{octanol,PBS\ pH\ 7.4} = \log\left(\frac{[\text{solute}]_{octanol}^{ionized} + [\text{solute}]_{octanol}^{un-ionized}}{[\text{solute}]_{PBS\ pH\ 7.4}^{ionized} + [\text{solute}]_{PBS\ pH\ 7.4}^{un-ionized}}\right)$$

2.7. Associated Content

Supporting information

Supporting information for this article is available on the WWW under https://pubs.acs.org/doi/10.1021/acs.inorgchem.0c01629?goto=supporting-info. (*An electronic copy of the supporting information is provided at the end of this document as **Supplementary I***).

2.8.   References

(1)   Holland, J. P.; Williamson, M. J.; Lewis, J. S. Unconventional nuclides for radiopharmaceuticals. *Mol. Imaging* **2010,** *9* (1), 1-20.

(2)   Holland, J. P.; Sheh, Y.; Lewis, J. S. Standardized methods for the production of high specific-activity zirconium-89. *Nucl. Med. Biol.* **2009,** *36* (7), 729-739.

(3)   Bhatt, N. B.; Pandya, D. N.; Wadas, T. J. Recent Advances in Zirconium-89 Chelator Development. *Molecules* **2018,** *23 (*3), 638.

(4)   Escorcia, F. E.; Steckler, J. M.; Abdel-Atti, D.; Price, E. W.; Carlin, S. D.; Scholz, W. W.; Lewis, J. S.; Houghton, J. L. Tumor-Specific Zr-89 Immuno-PET Imaging in a Human Bladder Cancer Model. *Mol. Imaging Biol.* **2018,** (20), 808-815.

(5)   Price, E. W.; Carnazza, K. E.; Carlin, S. D.; Cho, A.; Edwards, K. J.; Sevak, K. K.; Glaser, J. M.; de Stanchina, E.; Janjigian, Y. Y.; Lewis, J. S. 89Zr-DFO-AMG102 Immuno-PET to Determine Local HGF Protein Levels in Tumors for Enhanced Patient Selection. *J. Nucl. Med.* **2017,** *58* (9), 1386-1394.

(6)   Ulaner, G. A.; Hyman, D. M.; Lyashchenko, S. K.; Lewis, J. S.; Carrasquillo, J. A. 89Zr-Trastuzumab PET/CT for Detection of Human Epidermal Growth Factor Receptor 2-Positive Metastases in Patients With Human Epidermal Growth Factor Receptor 2-Negative Primary Breast Cancer. *Clin. Nucl. Med.* **2017,** *42* (12), 912-917.

(7)   Price, E. W.; Orvig, C. In *The Chemistry of Molecular Imaging*; John Wiley & Sons, Inc: 2014; pp 105-135.

(8)   Zeglis, B. M.; Mohindra, P.; Weissmann, G. I.; Divilov, V.; Hilderbrand, S. A.; Weissleder, R.; Lewis, J. S. Modular Strategy for the Construction of Radiometalated Antibodies for Positron Emission Tomography Based on Inverse Electron Demand Diels-Alder Click Chemistry. *Bioconjug. Chem.* **2011,** *22* (10), 2048-2059.

(9)   Holland, J. P.; Divilov, V.; Bander, N. H.; Smith-Jones, P. M.; Larson, S. M.; Lewis, J. S. ^{89}Zr-DFO-J591 for ImmunoPET of Prostate-Specific Membrane Antigen Expression In Vivo. *J. Nucl. Med.* **2010,** *51* (8), 1293-1300.

(10) Dijkers, E. C.; Oude Munnink, T. H.; Kosterink, J. G.; Brouwers, A. H.; Jager, P. L.; de Jong, J. R.; van Dongen, G. A.; Schroder, C. P.; Lub-de Hooge, M. N.; de Vries, E. G. Biodistribution of 89Zr-trastuzumab and PET Imaging of HER2-Positive Lesions in Patients With Metastatic Breast Cancer. *Clin. Pharmacol. Ther.* **2010,** *87* (5), 586-592.

(11) Dijkers, E. C. F.; Kosterink, J. G. W.; Rademaker, A. P.; Perk, L. R.; van Dongen, G. A. M. S.; Bart, J.; de Jong, J. R.; de Vries, E. G. E.; Lub-de Hooge, M. N. Development and Characterization of Clinical-Grade ^{89}Zr-Trastuzumab for HER2/neu ImmunoPET Imaging. *J. Nucl. Med.* **2009,** *50* (6), 974-981.

(12) Perk, L.; Visser, O.; Stigter-van Walsum, M.; Vosjan, M.; Visser, G.; Zijlstra, J.; Huijgens, P.; van Dongen, G. Preparation and evaluation of ^{89}Zr-Zevalin for monitoring of ^{90}Y-Zevalin biodistribution with positron emission tomography. *Eur. J. Nucl. Med. Mol. Imaging* **2006,** *33* (11), 1337-1345.

(13) Börjesson, P. K. E.; Jauw, Y. W. S.; Boellaard, R.; de Bree, R.; Comans, E. F. I.; Roos, J. C.; Castelijns, J. A.; Vosjan, M. J. W. D.; Kummer, J. A.; Leemans, C. R.; Lammertsma, A. A.; van Dongen, G. A. M. S. Performance of Immuno–Positron Emission Tomography with

Zirconium-89-Labeled Chimeric Monoclonal Antibody U36 in the Detection of Lymph Node Metastases in Head and Neck Cancer Patients. *Clin. Cancer Res.* **2006,** *12* (7), 2133-2140.

(14) Perk, L. R.; Visser, O. J.; Stigter-van Walsum, M.; Vosjan, M. J. W. D.; Visser, G. W. M.; Zijlstra, J. M.; Huijgens, P. C.; Dongen, G. A. M. S. Preparation and evaluation of 89Zr-Zevalin for monitoring of 90Y-Zevalin biodistribution with positron emission tomography. *Eur. J. Nucl. Med. Mol. Imaging* **2006,** *33* (11), 1337-1345.

(15) Perk, L. R.; Visser, G. W. M.; Vosjan, M. J. W. D.; Stigter-van Walsum, M.; Tijink, B. M.; Leemans, C. R.; van Dongen, G. A. M. S. [89]Zr as a PET Surrogate Radioisotope for Scouting Biodistribution of the Therapeutic Radiometals ^{90}Y and ^{177}Lu in Tumor-Bearing Nude Mice After Coupling to the Internalizing Antibody Cetuximab. *J. Nucl. Med.* **2005,** *46* (11), 1898-1906.

(16) Verel, I.; Visser, G. W. M.; Boellaard, R.; Stigter-van Walsum, M.; Snow, G. B.; van Dongen, G. A. M. S. [89]Zr Immuno-PET: Comprehensive Procedures for the Production of [89]Zr-Labeled Monoclonal Antibodies. *J. Nucl. Med.* **2003,** *44* (8), 1271-1281.

(17) Poreddy, A. R.; Schall, O. F.; Osiek, T. A.; Wheatley, J. R.; Beusen, D. D.; Marshall, G. R.; Slomczynska, U. Hydroxamate-Based Iron Chelators: Combinatorial Syntheses of Desferrioxamine B Analogues and Evaluation of Binding Affinities. *J. Comb. Chem.* **2004,** *6* (2), 239-254.

(18) Price, E. W.; Orvig, C. Matching Chelators to Radiometals for Radiopharmaceuticals. *Chem. Soc. Rev.* **2014,** *43* (1), 260-290.

(19) Meijs, W. E.; Haisma, H. J.; Klok, R. P.; van Gog, F. B.; Kievit, E.; Pinedo, H. M.; Herscheid, J. D. M. Zirconium-Labeled Monoclonal Antibodies and Their Distribution in Tumor-Bearing Nude Mice. *J. Nucl. Med.* **1997,** *38* (1), 112-118.

(20) Meijs, W. E.; Haisma, H. J.; Van Der Schors, R.; Wijbrandts, R.; Van Den Oever, K.; Klok, R. P.; Pinedo, H. M.; Herscheid, J. D. M. A facile method for the labeling of proteins with zirconium isotopes. *Nucl. Med. Biol.* **1996,** *23* (4), 439-448.

(21) Meijs, W. E.; Herscheid, J. D. M.; Haisma, H. J.; Pinedo, H. M. Evaluation of desferal as a bifunctional chelating agent for labeling antibodies with Zr-89. *Int. J. Rad. Appl. Instrum. [A]* **1992,** *43* (12), 1443-1447.

(22) Perk, L.; Vosjan, M.; Visser, G.; Budde, M.; Jurek, P.; Kiefer, G.; van Dongen, G. p-Isothiocyanatobenzyl-desferrioxamine: a new bifunctional chelate for facile radiolabeling of monoclonal antibodies with zirconium-89 for immuno-PET imaging. *Eur. J. Nucl. Med. Mol. Imaging* **2010,** *37* (2), 250-259.

(23) Vosjan, M. J. W. D.; Perk, L. R.; Visser, G. W. M.; Budde, M.; Jurek, P.; Kiefer, G. E.; van Dongen, G. A. M. S. Conjugation and radiolabeling of monoclonal antibodies with zirconium-89 for PET imaging using the bifunctional chelate p-isothiocyanatobenzyl-desferrioxamine. *Nat. Protoc.* **2010,** *5* (4), 739-743.

(24) Price, E. W.; Zeglis, B. M.; Lewis, J. S.; Adam, M. J.; Orvig, C. H6phospa-Trastuzumab: Bifunctional Methylenephosphonate-based Chelator with 89Zr, 111In and 177Lu. *Dalton Trans.* **2014,** *43*, 119-131.

(25) Jauw, Y. W. S.; Menke-van der Houven van Oordt, C. W.; Hoekstra, O. S.; Hendrikse, N. H.; Vugts, D. J.; Zijlstra, J. M.; Huisman, M. C.; van Dongen, G. A. M. S. Immuno-Positron Emission Tomography with Zirconium-89-Labeled Monoclonal Antibodies in Oncology: What Can We Learn from Initial Clinical Trials? *Front. pharmacol.* **2016,** *7*, 131-131.

(26) Pandit-Taskar, N.; O'Donoghue, J. A.; Ruan, S.; Lyashchenko, S. K.; Carrasquillo, J. A.; Heller, G.; Martinez, D. F.; Cheal, S. M.; Lewis, J. S.; Fleisher, M.; Keppler, J. S.; Reiter, R. E.; Wu, A. M.; Weber, W. A.; Scher, H. I.; Larson, S. M.; Morris, M. J. First-in-Human Imaging with 89Zr-Df-IAB2M Anti-PSMA Minibody in Patients with Metastatic Prostate Cancer: Pharmacokinetics, Biodistribution, Dosimetry, and Lesion Uptake. *J. Nucl. Med.* **2016,** *57* (12), 1858-1864.

(27) Pandit-Taskar, N.; O'Donoghue, J. A.; Durack, J. C.; Lyashchenko, S. K.; Cheal, S. M.; Beylergil, V.; Lefkowitz, R. A.; Carrasquillo, J. A.; Martinez, D. F.; Fung, A. M.; Solomon, S. B.; Gönen, M.; Heller, G.; Loda, M.; Nanus, D. M.; Tagawa, S. T.; Feldman, J. L.; Osborne, J. R.; Lewis, J. S.; Reuter, V. E.; Weber, W. A.; Bander, N. H.; Scher, H. I.; Larson, S. M.; Morris, M. J. A Phase I/II Study for Analytic Validation of 89Zr-J591 ImmunoPET as a Molecular Imaging Agent for Metastatic Prostate Cancer. *Clin. Cancer Res.* **2015,** *21* (23), 5277-5285.

(28) Rousseau, J.; Zhang, Z.; Wang, X.; Zhang, C.; Lau, J.; Rousseau, E.; Čolović, M.; Hundal-Jabal, N.; Bénard, F.; Lin, K.-S. Synthesis and evaluation of bifunctional tetrahydroxamate chelators for labeling antibodies with 89Zr for imaging with positron emission tomography. *Bioorg. Med. Chem. Lett.* **2018,** *28* (5), 899-905.

(29) Briand, M.; Aulsebrook, M. L.; Mindt, T. L.; Gasser, G. A solid phase-assisted approach for the facile synthesis of a highly water-soluble zirconium-89 chelator for radiopharmaceutical development. *Dalton Trans.* **2017,** *46* (47), 16387-16389.

(30) Allott, L.; Da Pieve, C.; Meyers, J.; Spinks, T.; Ciobota, D. M.; Kramer-Marek, G.; Smith, G. Evaluation of DFO-HOPO as an octadentate chelator for zirconium-89. *Chem. Commun.* **2017,** *53* (61), 8529-8532.

(31) Pandya, D. N.; Bhatt, N.; Yuan, H.; Day, C. S.; Ehrmann, B. M.; Wright, M.; Bierbach, U.; Wadas, T. J. Zirconium tetraazamacrocycle complexes display extraordinary stability and provide a new strategy for zirconium-89-based radiopharmaceutical development. *Chem. Sci.* **2017,** *8* (3), 2309-2314.

(32) Deri, M. A.; Ponnala, S.; Zeglis, B. M.; Pohl, G.; Dannenberg, J. J.; Lewis, J. S.; Francesconi, L. C. Alternative Chelator for 89Zr Radiopharmaceuticals: Radiolabeling and Evaluation of 3,4,3-(LI-1,2-HOPO). *J. Med. Chem.* **2014,** *57* (11), 4849-4860.

(33) Patra, M.; Bauman, A.; Mari, C.; Fischer, C. A.; Blacque, O.; Haussinger, D.; Gasser, G.; Mindt, T. L. An octadentate bifunctional chelating agent for the development of stable zirconium-89 based molecular imaging probes. *Chem. Commun.* **2014,** *50* (78), 11523-11525.

(34) Adams, C. J.; Wilson, J. J.; Boros, E. Multifunctional Desferrichrome Analogues as Versatile 89Zr(IV) Chelators for ImmunoPET Probe Development. *Mol. Pharm.* **2017,** *14* (8), 2831-2842.

(35) Zhai, C.; Summer, D.; Rangger, C.; Franssen, G. M.; Laverman, P.; Haas, H.; Petrik, M.; Haubner, R.; Decristoforo, C. Novel Bifunctional Cyclic Chelator for 89Zr Labeling–Radiolabeling and Targeting Properties of RGD Conjugates. *Mol. Pharm.* **2015,** *12* (6), 2142-2150.

(36) Ma, M. T.; Meszaros, L. K.; Paterson, B. M.; Berry, D. J.; Cooper, M. S.; Ma, Y.; Hider, R. C.; Blower, P. J. Tripodal tris(hydroxypyridinone) ligands for immunoconjugate PET imaging with 89Zr4+: comparison with desferrioxamine-B. *Dalton Trans.* **2015,** *44* (11), 4884-4900.

(37) Pandya, D. N.; Pailloux, S.; Tatum, D.; Magda, D.; Wadas, T. J. Di-macrocyclic terephthalamide ligands as chelators for the PET radionuclide zirconium-89. *Chem. Commun.* **2015,** *51* (12), 2301-2303.

(38) Seibold, U.; Wängler, B.; Wängler, C. Rational Design, Development, and Stability Assessment of a Macrocyclic Four-Hydroxamate-Bearing Bifunctional Chelating Agent for 89Zr. *ChemMedChem* **2017,** *12* (18), 1555-1571.

(39) Boros, E.; Holland, J. P.; Kenton, N.; Rotile, N.; Caravan, P. Macrocycle-Based Hydroxamate Ligands for Complexation and Immunoconjugation of (89)Zirconium for Positron Emission Tomography (PET) Imaging. *ChemPlusChem* **2016,** *81* (3), 274-281.

(40) Tinianow, J. N.; Pandya, D. N.; Pailloux, S. L.; Ogasawara, A.; Vanderbilt, A. N.; Gill, H. S.; Williams, S.-P.; Wadas, T. J.; Magda, D.; Marik, J. Evaluation of a 3-hydroxypyridin-2-one (2, 3-HOPO) based macrocyclic chelator for 89Zr4+ and its use for immunoPET imaging of HER2 positive model of ovarian carcinoma in mice. *Theranostics* **2016,** 6 (4), 511-521.

(41) Tieu, W.; Lifa, T.; Katsifis, A.; Codd, R. Octadentate Zirconium(IV)-Loaded Macrocycles with Varied Stoichiometry Assembled From Hydroxamic Acid Monomers using Metal-Templated Synthesis. *Inorg. Chem.* **2017,** *56* (6), 3719-3728.

(42) Rudd, S. E.; Roselt, P.; Cullinane, C.; Hicks, R. J.; Donnelly, P. S. A desferrioxamine B squaramide ester for the incorporation of zirconium-89 into antibodies. *Chem. Commun.* **2016,** *52* (80), 11889-11892.

(43) Raave, R.; Sandker, G.; Adumeau, P.; Jacobsen, C. B.; Mangin, F.; Meyer, M.; Moreau, M.; Bernhard, C.; Da Costa, L.; Dubois, A.; Goncalves, V.; Gustafsson, M.; Rijpkema, M.; Boerman, O.; Chambron, J. C.; Heskamp, S.; Denat, F. Direct comparison of the in vitro and in vivo stability of DFO, DFO* and DFOcyclo* for (89)Zr-immunoPET. *Eur. J. Nucl. Med. Mol. Imaging* **2019,** *46* (9), 1966-1977.

(44) Patra, M.; Eichenberger, L. S.; Fischer, G.; Holland, J. P. Photochemical Conjugation and One-Pot Radiolabelling of Antibodies for Immuno-PET. *Angewandte Chemie International Edition* **2019,** *58* (7), 1928-1933.

(45) Price, E. W.; Zeglis, B. M.; Cawthray, J. F.; Lewis, J. S.; Adam, M. J.; Orvig, C. What a Difference a Carbon Makes: H$_4$octapa vs. H$_4$C3octapa, Ligands for In-111 and Lu-177 Radiochemistry. *Inorg. Chem.* **2014,** *53* (19), 10412-10431.

(46) Guérard, F.; Lee, Y.-S.; Brechbiel, M. W. Rational Design, Synthesis, and Evaluation of Tetrahydroxamic Acid Chelators for Stable Complexation of Zirconium(IV). *Eur. J. Chem.* **2014,** *20* (19), 5584-5591.

(47) Guérard, F.; Lee, Y.-S.; Tripier, R.; Szajek, L. P.; Deschamps, J. R.; Brechbiel, M. W. Investigation of Zr(IV) and 89Zr(IV) complexation with hydroxamates: progress towards designing a better chelator than desferrioxamine B for immuno-PET imaging. *Chem. commun.* **2013,** *49* (10), 1002-1004.

(48) Savastano, M.; Bazzicalupi, C.; Ferraro, G.; Fratini, E.; Gratteri, P.; Bianchi, A. Tales of the Unexpected: The Case of Zirconium(IV) Complexes with Desferrioxamine. *Molecules* **2019,** *24* (11), 2098.

(49) Buchwalder, C.; Jaraquemada-Peláez, M. d. G.; Rousseau, J.; Merkens, H.; Rodríguez-Rodríguez, C.; Orvig, C.; Bénard, F.; Schaffer, P.; Saatchi, K.; Häfeli, U. O. Evaluation of the Tetrakis(3-Hydroxy-4-Pyridinone) Ligand THPN with Zirconium(IV): Thermodynamic Solution Studies, Bifunctionalization, and in Vivo Assessment of Macromolecular 89Zr-THPN-Conjugates. *Inorg. Chem.* **2019,** *58* (21), 14667-14681.

(50) Toporivska, Y.; Gumienna-Kontecka, E. The solution thermodynamic stability of desferrioxamine B (DFO) with Zr(IV). *J. Inorg. Biochem.* **2019,** *198*, 110753.

(51) Holland, J. P. Predicting the Thermodynamic Stability of Zirconium Radiotracers. *Inorg. Chem.* **2020,** *59* (3), 2070-2082.

(52) Harris, W. R.; Yang, B.; Abdollahi, S.; Hamada, Y. Steric restrictions on the binding of large metal ions to serum transferrin. *J. Inorg. Biochem.* **1999,** *76* (3-4), 231-242.

(53) Sun, H.; Li, H.; Sadler, P. J. Transferrin as a Metal Ion Mediator. *Chem. Rev.* **1999,** *99* (9), 2817-2842.

(54) Harris, W. In *Less Common Metals in Proteins and Nucleic Acid Probes*; Clarke, M. J., Ed.; Springer-Verlag, Berlin Heidelberg: 1998; Vol. 92, pp 121-162.

(55) Tsung, S. H.; Rosenthal, W. A.; Milewski, K. A. Immunological Measurement of Transferrin Compared with Chemical Measurement of Total Iron-Binding Capacity. *Clin. Chem.* **1975,** *21* (8), 1063-1066.

(56) Hider, R. C.; Bickar, D.; Morrison, I. E. G.; Silver, J. Siderophore iron-release mechanisms. *J. Am. Chem. Soc.* **1984,** *106* (23), 6983-6987.

(57) Raymond, K. N.; Müller, G.; Matzanke, B. In *Top. Curr. Chem.*; Boschke, F. L., Ed.; Springer-Verlag, Berlin, Heidelberg: 1984; Vol. 123, pp 49-102.

(58) Delley, B. An all-electron numerical method for solving the local density functional for polyatomic molecules. *J Chem Phys* **1990,** *92* (1), 508-517.

(59) Delley, B. From molecules to solids with the DMol3 approach. *J. Chem. Phys.* **2000,** *113* (18), 7756-7764.

(60) Perdew, J. P.; Burke, K.; Ernzerhof, M. Generalized Gradient Approximation Made Simple. *Phys. Rev. Lett.* **1996,** *77* (18), 3865-3868.

(61) Peverati, R.; Truhlar, D. G. M11-L: A Local Density Functional That Provides Improved Accuracy for Electronic Structure Calculations in Chemistry and Physics. *The Journal of Phys. Rev. Lett.* **2011,** *3* (1), 117-124.

(62) Klamt, A.; Schuurmann, G. COSMO: A New Approach to Dielectric Screening in Solvents with Explicit Expressions for the Screening Energy and its Gradient. *J. Chem. Soc. Perkin. Trans.* **1993,** *2*, 799-805.

(63) Andzelm, J.; Ko¨lmel, C.; Klamt, A. Incorporation of solvent effects into density functional calculations of molecular energies and geometries. *J. Chem. Phys.* **1995,** *103* (21), 9312-9320.

(64) Legault, C. Y. CYLView, 1.0b; Université de Sherbrooke, Canada 2009-2012, http://www.cylview.org.

(65) Pandya, D. N.; Bhatt, N.; An, G. I.; Ha, Y. S.; Soni, N.; Lee, H.; Lee, Y. J.; Kim, J. Y.; Lee, W.; Ahn, H.; Yoo, J. Propylene Cross-Bridged Macrocyclic Bifunctional Chelator: A New Design for Facile Bioconjugation and Robust 64Cu Complex Stability. *J. Med. Chem.* **2014,** *57* (17), 7234-7243.

(66) Holland, J. P.; Caldas-Lopes, E.; Divilov, V.; Longo, V. A.; Taldone, T.; Zatorska, D.; Chiosis, G.; Lewis, J. S. Measuring the Pharmacodynamic Effects of a Novel Hsp90 Inhibitor on HER2/neu Expression in Mice Using [89]Zr-DFO-Trastuzumab. *PLoS One* **2010,** *5* (1), e8859.

Chapter 3: Synthesis and Evaluation of DFO2K: a Modular Chelator with Ideal Properties for Applications of Zirconium-89

The content of this chapter is adapted from the manuscript that is currently under preparation (Salih, A. K.; Khozeimeh Sarbisheh, E.; Raheem, S. J.; Dominguez-Garcia, M.; Mehlhorn, H.; Price, E. W. manuscript under preparation)

3.1. Author Contribution and Relation to the Research Objectives

This work was done in collaboration with Dr. Elaheh Khozeimeh Sarbisheh, Shvan J. Raheem (PhD candidate), Moralba Dominguez-Garcia (PhD candidate), and Hillary Mehlhorn (MSc candidate). Dr. Khozeimeh Sarbisheh assisted in the initial designing and synthesis attempts of the DFO2K chelator, while I followed her efforts and developed a successful synthesis of DFO2K in 6 steps (**7-10**). Furthermore, I prepared [^{Nat}Zr]Zr-DFO2K (**11**) and synthesized the bifunctional DFO2K-NCS (**12**). I also performed complete characterization of all the compounds (**7-12**). In addition, I accomplished the antibody purifications and conjugation reactions and MALDI sample preparation with the help of Dr. Price and Moralba Dominguez-Garcia. I carried out the radiolabeling studies, *in vitro* experiments, animal imaging, dissection and biodistribution studies with the help of Dr. Price, Moralba Dominguez-Garcia, Hillary Mehlhorn and Shvan J. Raheem. The animal injections were done by Dr. Price. Furthermore, I prepared the first draft of the manuscript and supporting information which was further edited by Dr. Price.

This chapter is a continuation from chapter 2 where we synthesized a dodecadentate chelator named DFO2 for the purpose of enhancing the stability of Zr-89 complex in immunoPET. The *in*

vitro stability assays showed significant improvement in zirconium-89 complex stability with DFO2 compared to DFO. However, the synthesis of the diamine linker was very low yielding, even with optimizations we achieved less than 10% overall yield. We speculated that the hydrophobic group in the linker is partially the reason behind the low solubility of the DFO2 chelator.

In this project, we designed and synthesized the third generation of DFO2, where we replaced the propylenediamine linker with a more hydrophilic lysine molecule. The second generation chelator was called DFO2p and was work completed by Dr. Elaheh Khozeimeh Sarbisheh. For DFO2K, since lysine (lys, K) has two amines and one carboxylic acid group, it serves as a linker for our new version of the chelator, named DFO2K. Lysine is commercially available, thus eliminates the difficulty and low yielding synthesis of the propylenediamine linker and concurrently, it improved solubility of the chelator. By overcoming the solubility issue and improving the stability with zirconium-89, DFO2K has a great potential to replace DFO in immunoPET imaging applications and has potential to chelate therapeutical radionuclides for theranostic purposes. After synthesis of DFO2K we examined its radiolabeling kinetics with zirconium-89 and evaluated its stability through various *in vitro* assays which was followed by *in vivo* and biodistribution studies of the stand-alone [^{89}Zr]Zr-DFO2K to understand the biodistribution of the unconjugated zirconium-89 chelate complex. I was encouraged by the results obtained, therefore I synthesized the bifunctional version of the chelator (*p*-SCN-Ph-DFO2K) and conjugated it with a non-specific human serum IgG antibody. I also conjugated bifunctional DFO to the same IgG for comparison in the following studies. Consequently, I radiolabeled the immunoconjugates with zirconium-89 and injected to healthy mice for *in vivo* and *ex vivo* stability assessment.

3.2. Abstract

Here we report the synthesis and evaluation of the newest generation of our DFO2 chelator family named DFO2K, which is designed to have improved water solubility, high denticity (potential CN 12) to enhance its stability in coordination with zirconium-89 and other large radiometals, improved pharmacokinetic profile, and improved aqueous bioconjugation chemistry. Zirconium-89 has emerged as the most suitable radionuclide to pair with large macromolecules such as antibodies (immunoPET) for molecular imaging applications. However, there are concerns related to its insufficient stability with desferoxamine B (DFO), the "gold standard" chelator in preclinical studies. Therefore, there is room to design and synthesize new chelators for zirconium-89. Additionally, we anticipate the dodecadentate DFO2K to have the potential to coordinate larger radiometals for theranostic applications as DFO is not suitable for binding any of the known therapeutic radiometals. Following the synthesis of DFO2K we assessed its radiolabeling efficiency with zirconium-89 and compared with DFO, which revealed rapid and nearly identical radiolabeling kinetics to DFO. The resultant [^{89}Zr]Zr-DFO2K complex showed superb stability over [^{89}Zr]Zr-DFO in different *in vitro* stability assays such as hydroxyapatite and 1000-fold molar excess EDTA challenges. Furthermore, biodistribution studies in healthy mice showed that [^{89}Zr]Zr-DFO2K had a similar distribution profile and clearance to [^{89}Zr]Zr-DFO. Overall, owing to its high denticity, good solubility, and excellent stability with zirconium-89, DFO2K has the potential to replace DFO in imaging tracers with zirconium-89 and might offer the potential to be used for high valent and oxophilic radiometal ions such as thorium-227 or actinium-225 for theranostic applications.

3.3. Introduction

Positron emission tomography (PET) is a type of functional molecular imaging which has bestowed us the power to non-invasively diagnose pathological conditions manifested in tissues such infection, inflammation, cancer, and other biochemical processes.[1–6] With the advent of monoclonal antibodies to target receptors or other pathological factors with high specificity, PET has been conjoined with mAbs to give rise to immunoPET, a technique in which mAbs are radiolabeled with PET radionuclides.[7,8] Radiolabeling of antibodies require radionuclides with decay property matching to mAb's pharmacokinetics. Most mAbs demonstrate slow pharmacokinetics with an average biological half-life of 1-3 weeks.[9] Zirconium-89 with a half-life of 3.3 days provides sufficient time for radiolabeled antibodies to accumulate in the targeted tissue (~1-3 days) before imaging, and has been used in numerous clinical and preclinical studies.[10–13] The most common chelator used for zirconium-89 is the bacterial siderophore desferrioxamine B (DFO). To chelate $[^{89}Zr]Zr^{4+}$ in a stable and inert form while simultaneously anchoring to a macromolecule such as a mAb, a bifunctional chelator is required. The bifunctional chelator p-SCN-Ph-desferrioxamine (p-SCN-Ph-DFO) is commercially available and contains the dual functionality of a metal/radiometal binding chelator moiety (DFO) and a reactive functional group (phenyl isothiocyanate) to facilitate bioconjugation to the mAb.

Although DFO and its bifunctional derivatives have proven effective, they are not without substantial shortcomings.[14] The incompatibility between hexadentate DFO and the optimum 8-coordinate binding environment for the zirconium (IV) ion has been identified in numerous rodent studies to be the likely reason for insufficient stability of the $[^{89}Zr]Zr$-DFO complex.[15–19] However, the same level of instability of $[^{89}Zr]Zr$-DFO is not reported in human studies, but the released radioactive zirconium is both oxophilic and osteophilic and therefore accumulates in bone.[20–22]

Moreover, non-specific uptake of zirconium-89 reduces the target-to-background signal ratio, deteriorating image quality, and increases radiation dose to bone marrow.[23] Thus, the development of optimized chelators for zirconium-89 is ongoing, with a particular importance placed on chelators that also effectively bind therapeutic radiometals for theranostic applications.

Emerging chelators such DFO*, oxoDFO*, DFO-Em, DFO-Km, DFO2, and DFO2p (**Figure 3-1**), with higher denticity than DFO (8 – 12 *vs* 6) are proven to effectively improve the *in vitro* and *in vivo* [^{89}Zr]Zr-chelate complex stability and kinetic inertness to transchelation/demetallation.[16,18,23–26] This discussion is focused on our dodecadentate chelate derivatives, and so the octadentate DFO-Em and DFO-Km will not be discussed. In our previous work we synthesized a modular dodecadentate chelator DFO2 to enhance the stability of the zirconium-89 complex, which was followed by an improved derivative DFO2p.[16] These 12-coordinate chelators (DFO2/DFO2p) were also designed with the purpose of coordinating both zirconium-89 and also larger radionuclides for theranostic applications. Results of numerous radiochemical (*in vitro*) stability assays showed that both DFO2 and DFO2p formed significantly more stable complexes with [^{89}Zr]Zr^{4+} than DFO. However, DFO2 exhibited poor water solubility in addition to the low yielding multi-step synthesis of the requisite propylenediamine linker.[16] The derivative DFO2p improved water solubility relative to DFO2 and drastically simplified the synthetic procedure down to a single reaction step; however, [^{89}Zr]Zr-DFO2p was slightly less stable than [^{89}Zr]Zr-DFO2. Aqueous solubility is an important property because the bifunctional chelators are typically conjugated to sensitive biomolecules such as antibodies and peptides in aqueous buffers under mild conditions.
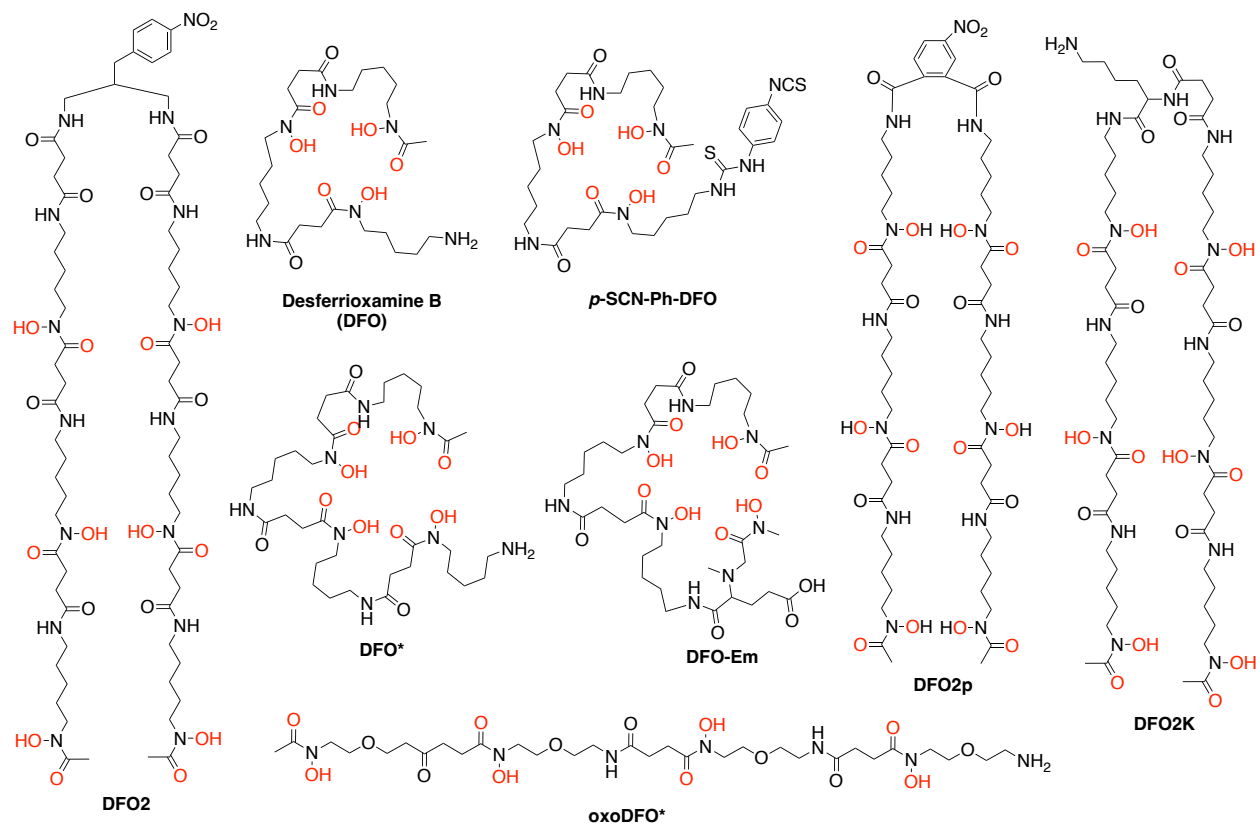
Figure 3-1. Chemical structures of a group of DFO-based zirconium-89 chelators including bifunctional forms of DFO (*p*-SCN-Ph-DFO), DFO*, oxoDFO*, DFO-Em, DFO2, DFO2p, and DFO2K.

Here we report the latest generation of the DFO2 family called DFO2K, which has a similar core structure to DFO2 and contains two DFO molecules tethered by a modular amino acid linker. As such, DFO2K has near-identical metal ion coordination properties to DFO2 and DFO2p with a total of 6 hydroxamate groups (CN 12), allowing it to form stable complexes with zirconium-89 and other radionuclides. Moreover, the *p*-NO$_2$-Ph-propylenediamine (DFO2) or *p*-NO$_2$-Ph-phthalic acid (DFO2p) linkers are replaced with the commercially available amino acid lysine, which eliminates the difficulty in synthesis of the DFO2 linker and is far more modular than the DFO2p linker. Importantly, the lysine linker improved the solubility of DFO2K relative to DFO2 and DFO2p, and this modular design allows for any natural or unnatural amino acid to be easily substituted to access a wide range of functionality. DFO2K has been designed so that switching the amino acid linker will preserve the identical coordination environment and therefore preserve

identical radiolabeling/stability properties. This means that a new DFO2K derivative which contains a different amino acid as linker (e.g. cysteine) would not require re-validation of radiolabeling and radiochemical stability properties, saving a lot of time and cost. For this proof-of-concept study, lysine was used to tether two molecules of DFO together and provide an extra primary amine functional group for bifunctionalization and conjugation with biomolecules/vectors. Following the synthesis and characterization of DFO2K, its radiolabeling kinetics were evaluated and its *in vitro* stability was assessed by using different radiochemical assays such as human serum stability, excess EDTA transchelation, and hydroxyapatite challenge. Furthermore, non-bifunctional chelate complexes of DFO and DFO2K with [^{89}Zr]Zr^{4+} were injected into healthy mice to compare their clearance and biodistribution.

3.4. Result and Discussion

Synthesis. One important feature of the DFO2 chelator family is they are designed with a modular synthesis platform, which has culminated in the design and synthesis of the amino acid-based DFO-Em, DFO-Km, and DFO2K. With DFO2K, its highly modular design is based around its chemically versatile amino acid-based linker, which allows us to easily change the different parts of the chelator including the amino acid, the chelating moieties, additional spacers, and the bioconjugation chemistry. Using a commercially available amino acid (lysine) as linker, we synthesized DFO2K in four steps with a cumulative yield of 27% (**Scheme 3-1**). First, DFO was connected to the commercially available diamino-protected lysine (Boc-Lys(Z)-OH) using the conventional coupling reagent HATU to form compound **7**. The *tert*-butyloxycarbonyl (Boc) group was then removed by using trifluoroacetic acid to produce compound **8**, which was reacted with a modified version of DFO (DFO-COOH, **4**, see scheme 2-2) to attach the second of two

DFO molecules and form the benzyloxycarbonyl protected version of DFO2K (**9**). Using HATU as a peptide coupling agent for the reaction of the first DFO molecule with the protected lysine to form compound **7** provided quantitative conversion. However, for addition of the second DFO molecule to form protected DFO2K the peptide coupling reaction (step 3) proceeded with poor yields when HATU was used, even at higher temperature (55 ºC). We speculate that the aggregation of DFO and its derivatives due to intermolecular and/or intramolecular hydrogen bonding could be a reason for poor solubility and low yields. An improved yield was achieved when EDC and oxyma was used as peptide coupling reagents, accompanied by one equivalent of sodium chloride and sonication to aid solubility. In both steps 1 and 2, a mixture of DMF and DMSO solvents with elevated temperature (up to 80 °C) was used to dissolve DFO and DFO-derivatives completely. The final step required removal of the benzyl protecting group using palladium on carbon to obtain the DFO2K chelator (**10**).

In this form, DFO2K is pre-bifunctional (unless reacted with an amine-reactive electrophile) as it will require chemical modification of the epsilon amino group to become bifunctional, such as attachment of a *p*-SCN-Ph, azide, maleimide, or another bioconjugation-ready moiety. Due to the poor solubility of DFO2K and DFO in organic solvents, reverse-phase (RP) chromatography was used to purify compounds **8** and **9**. Small amounts of ammonium hydroxide was required to dissolve the samples in water during sample loading in column chromatography or for mass spectrometry (MS) analysis. Finally, the pre-bifunctional chelator DFO2K (**10**) was purified with RP-HPLC before it was used for the radiolabeling and stability studies.
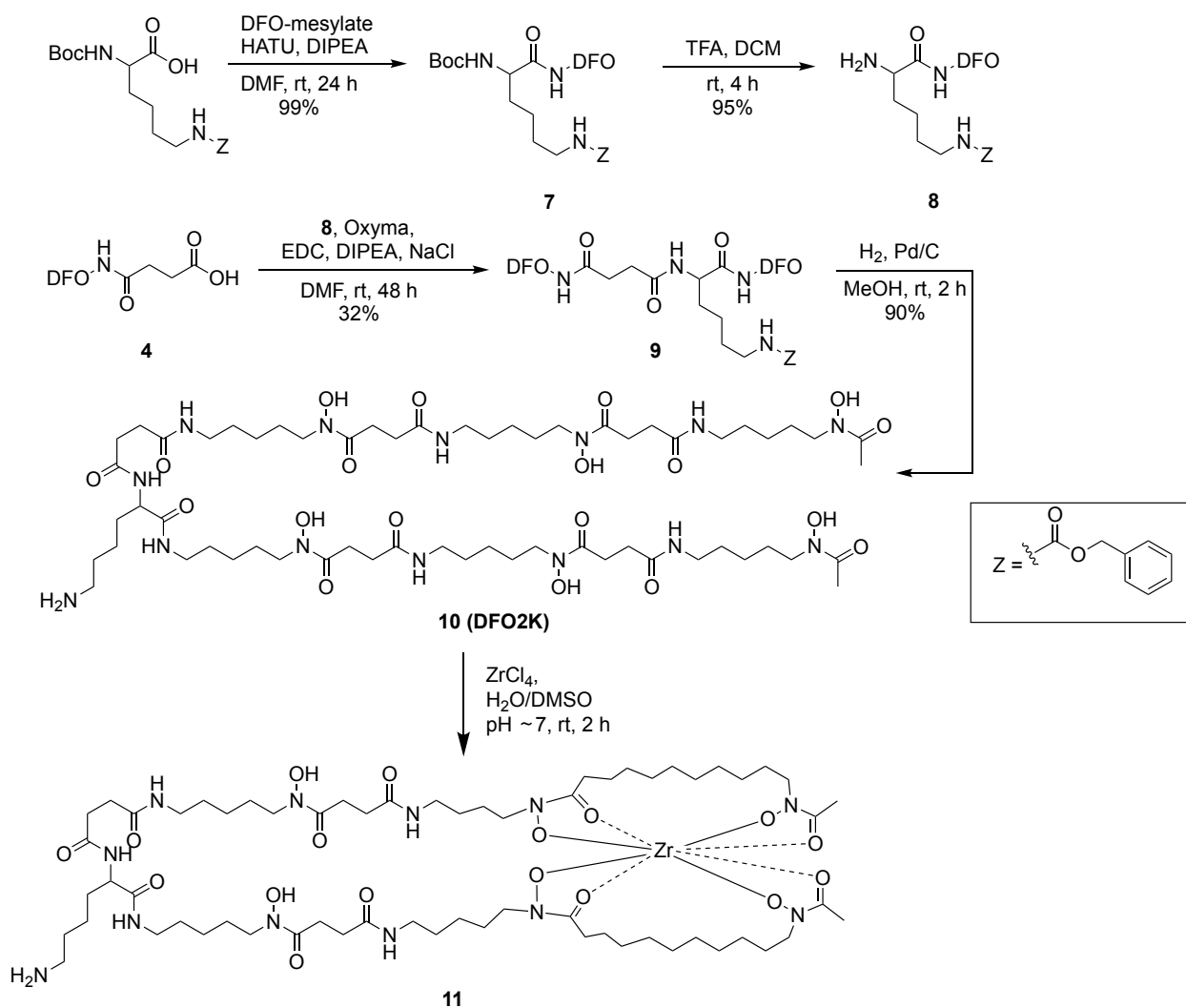
Scheme 3-1. Synthesis of DFO2K starting from reaction of a DFO mesylate molecule with a Boc-Lysine (Z) molecule (**7**) followed by Boc-deprotection reaction (**8**) and addition of a DFO-COOH molecule (**9**). The final compound (**10**) was obtained through hydrogenolysis using Pd/C as catalyst.

Density functional theory (DFT) modeling. Complexes of Zr(IV) and the large acyclic chelator DFO2K can form a large number of energetically similar geometric isomers in aqueous solution which can be a reason obtaining diffractable crystals for X-ray crystallography is rather difficult and has yet to be achieved for hydroxamate-based Zr(IV) chelators.[16,27] In lieu of crystallographic data, density functional theory (DFT) calculations have often been used to evaluate the coordination sphere of metal-chelate complexes. Metal-chelate structures derived from X-ray

crystallography represent their solid-state structures, but for radiometal-chelate complexes we are most interested in their behavior as water-solvated molecules. As such, DFT calculated structures are performed with solvent effects from water. Although detailed DFT calculations for all the possible isomers of DFO2 (over 500 possible isomers) has not been performed, previous studies have suggested that binding the two terminal hydroxamic acids of each DFO chain to the zirconium ion produces an ideal octadentate Zr(IV) coordination and is likely the most stable geometric isomer of Zr(IV)-DFO2 and Zr(IV)-DFO2p. To visualize and further evaluate the coordination sphere of the Zr(DFO2K) complex we implemented density functional theory (DFT) calculations to model its structure by using Materials Studio software (DMol^3) using water as solvent (**Figure 3-2**).
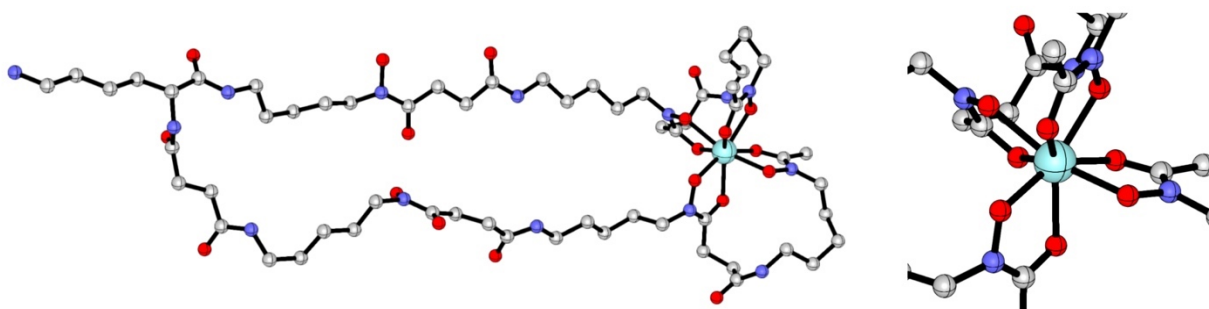
Figure 3-2. DFT calculated structure of Zr(DFO2K), geometry-optimized using Biovia Materials Studio, DMOL^3/ PBE, using water as solvent (COSMO) showing (left) the Zr-DFO2K complex and (right) a close up on the coordination sphere of the metal complex. Hydrogen atoms are omitted from the figure for clarity but are included for calculations.

Radiolabeling. DFO is an acyclic chelator and has excellent radiolabeling properties with zirconium-89 and provides fast binding kinetics, boasting quantitative radiolabeling under mild conditions (rt, pH 6.8 – 7.2) and under 15 mins. For a new zirconium-89 chelator to be considered "next-generation" and to be worthy of supplanting the existing industry "gold standard" chelator DFO, it must have properties that are as good or ideally much better. After synthesis and characterization of DFO2K we performed extensive zirconium-89 radiochemistry experiments in

direct competition with the "gold standard" chelator DFO. First we examined DFO2K's ability to form macroscale complexes with $[^{Nat}Zr]Zr^{4+}$ by reacting DFO2K with $ZrCl_4$ salt in the same mild conditions used for the radiolabeling of proteins (rt, pH 7) following a published procedure,[16] and rapid formation of $[^{Nat}Zr]Zr$-DFO2K complex was observed. Subsequently, the complex was characterized with HRMS and ^1H and ^{13}C NMR spectroscopy. This prompted us to proceed to radiolabel DFO2K with $[^{89}Zr]Zr^{4+}$ and study its labeling efficiency alongside DFO as a control (**Figure 3-3** and **3-4A**). Thus, we radiolabeled different concentrations of DFO2K with ~ 11 MBq of neutralized $[^{89}Zr]Zr$-oxalate. Similarly, we performed radiolabeling experiments with DFO mesylate under identical conditions to use it as a control in all experiments. With a quantity of 0.5 nmol (2 μM) chelate (DFO2K and DFO) and ~11 MBq of neutralized $[^{89}Zr]Zr$-oxalate in HEPEs buffer (0.5 M, pH 7.0), radiolabeling yields of 96.7 ± 2.5% (DFO2K) and 88.7 ± 2.2% (DFO) were achieved for both in just ~1 minute (radio-iTLC). Both chelators provide quantitative radiolabeling yields in 10-15 minutes. With 0.05 nmol (200 nM) of chelator and the same quantity of zirconium-89, a similar trend was noted where DFO2K showed slightly faster radiolabeling kinetics than DFO, but both required longer reaction times to achieve near-quantitative yields. With only 0.05 nmol of each chelator, DFO2K achieved 96.0 ± 0.1% after 60 minutes and DFO reached 91.7 ± 1.8%. Furthermore, at 0.005 nmol of chelator (20 nM), both chelators showed comparable labeling properties with maximum radiochemical conversion dropping below 20% even after 60-minute reaction time.
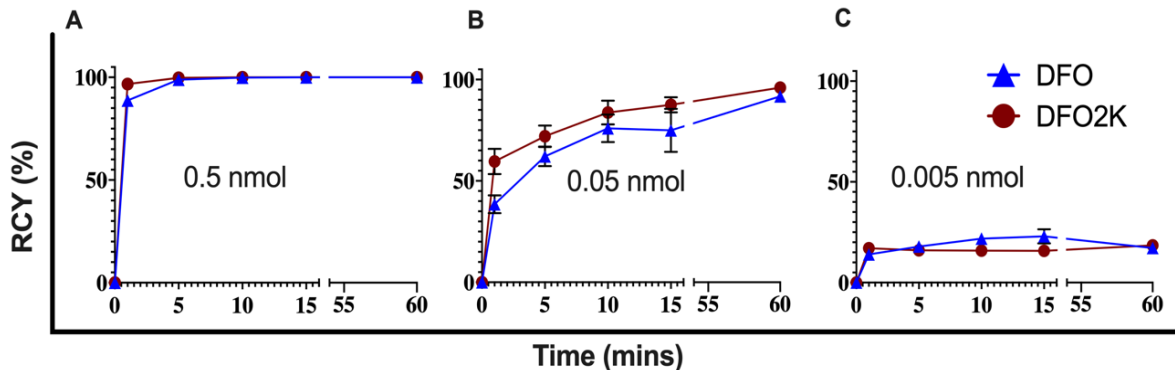
Figure 3.3. Time and concentration dependent radiolabeling study of each of DFO and DFO2K with ~11 MBq $[^{89}Zr]Zr^{4+}$ with (A) 0.5 nmol, (B) 0.05 nmol, and (C) 0.005 nmol of the chelators in HEPES buffer at pH 7.0 and ambient temperature (total volume of reactions were 250 μL, $n = 3$).

Polarity and water solubility. Our previous chelator DFO2 exhibited low aqueous solubility, an issue reported for many high denticity hydroxamate based chelators. Poor water solubility is undesirable, because it can complicate the aqueous conjugation chemistry between the bifunctional chelator and the biovectors such as monoclonal antibodies and peptides.[16,23,24] We assessed the hydrophilicity of $[^{89}Zr]Zr$-DFO2K by using a shake-flask method to determine log D partition coefficients of each of $[^{89}Zr]Zr$-DFO2K and $[^{89}Zr]Zr$-DFO complexes using octanol and phosphate buffer saline pH 7.4. The structures of both DFO and DFO2K contain a free primary amine and improve water solubility, because the $pK_a \sim 10$ means group will be a majority protonated at pH 7.4 to the quaternary ammonium ion (H-bonding, ion-ion interactions). The results reveal that $[^{89}Zr]Zr$-DFO2K has higher polarity and therefore higher aqueous solubility than $[^{89}Zr]Zr$-DFO (log D = -3.19 ± 0.01 and -3.04 ± 0.03, respectively). It is worth mentioning that using lysine as a linker in our new generation DFO2K resulted in a significant increase in hydrophilicity compared to $[^{89}Zr]Zr$-DFO2 (log D = -0.7 ± 0.1).

***In vitro* stability.** Although the "stability" of the Zr-DFO2K complex can be quantified by its thermodynamic stability (e.g. formation constants), it is generally more predictive of *in vivo* behavior to evaluate the "real-world" stability. This is often called "kinetic stability / kinetic inertness" and describes the general resistance and inertness of the radiometal-complex to all forms of demetallation/transchelation *in vivo*. In the radiochemistry labs we use a number of *in vitro* conditions and experiments to probe this inertness, and we've found several of these *in vitro* stability assays to do a good job predicting their relative stability and inertness *in vivo* in mice. To estimate the practical stability/inertness of our new chelators we perform a battery of *in vitro* stability assays, and we always include a relevant "gold standard' chelator such as DFO as a control. Assuming the *in vitro* stability of our new chelator is at least equal to the "gold standard", we follow with *in vivo* evaluation in mice.

To gain insight into the *in vitro* stability of [^{89}Zr]Zr-DFO2K compared to [^{89}Zr]Zr-DFO, we radiolabeled both DFO2K and DFO chelators quantitatively (>99% RCY) and used them for radiochemical stability assays without further purification. To determine the stability of [^{89}Zr]Zr-DFO2K in the presence of blood proteins, a human serum stability assay was used to test transchelation resistance against different blood proteins. We mixed aliquots of pre-labeled [^{89}Zr]Zr-DFO2K and [^{89}Zr]Zr-DFO with human blood serum and incubated with shaking at 37 °C, for a time period of 10 days (**Figure 3-4B**). The stability of the chelators was monitored by radio-iTLC using buffered EDTA (50 mM, pH 5.0-5.5) as developing solvent. The results indicated that [^{89}Zr]Zr-DFO2K was 99.5% ± 0.1% intact over 10 days, while [^{89}Zr]Zr-DFO stability dropped slightly to 96.4% ± 0.3%.
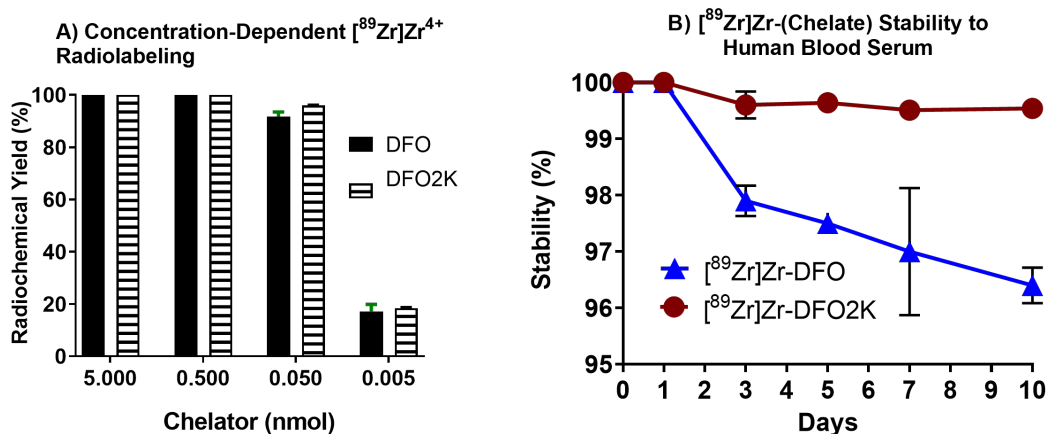
Figure 3-4. Results of radiolabeling and stability studies for [^{89}Zr]Zr-DFO and [^{89}Zr]Zr-DFO2K . (A) Concentration-dependent radiolabeling study of each of DFO and DFO2K with ~11 MBq [^{89}Zr]Zr^{4+} at ambient temperature, in HEPES buffer pH 7 (*n* = 3) after 60 minutes, and (B) stability challenge against human blood serum over 10 days determined by radio-iTLC (*n* = 3).

The superior stability of [^{89}Zr]Zr-DFO2K over [^{89}Zr]Zr-DFO was more dramatically revealed by hydroxyapatite (HTP) stability assay, which we previously designed in consideration of the oxophilic and osteophilic nature of [^{89}Zr]Zr^4. As such, we use HTP resin as a high surface area surrogate to simulate bone structure as hydroxyapatite is a major component of bone. For this assay, aliquots of [^{89}Zr]Zr-DFO2K and [^{89}Zr]Zr-DFO were mixed and shaken with (40 and 60 mg) hydroxyapatite resin (BioRad biogel HTP) in HEPES buffer (50 mM, pH 7.0) for 24 h. The stability percentage of the [^{89}Zr]Zr-chelators were determined following several rounds of centrifugation and rinsing of HTP pellets, where the ratio of activity in supernatant (intact [^{89}Zr]Zr-chelate complex) to activity in the HTP pellets was determined. The activity associated with the HTP pellets was considered "instability" and could either be from adsorbed [^{89}Zr]Zr-chelate or transchelated "free" [^{89}Zr]Zr^{4+}. The results reveal that the stability of [^{89}Zr]Zr-DFO2K was remarkably higher than [^{89}Zr]Zr-DFO, even when the highest quantity of 60 mg HTP was used (91.9% ± 1.4% vs 59.5% ± 0.4%, respectively, **Figure 3-5A**). As a control for this experiment, neutralized [^{89}Zr]Zr^{4+}-oxalate was also mixed with 40 and 60 mg of hydroxyapatite and it was

found that for both cases after 24 h more than 97% of the $[^{89}Zr]Zr^{4+}$ was associated with the HTP pellets (**Figure 3-5A**).
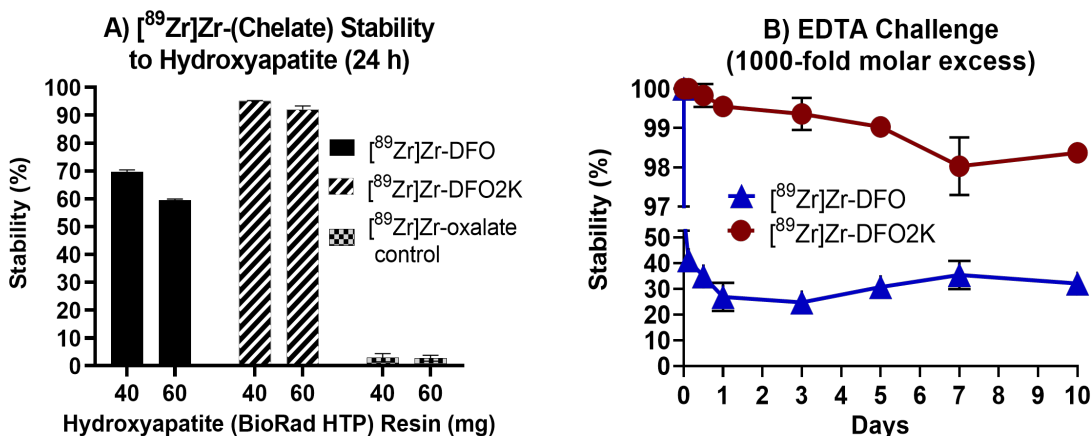
Figure 3-5. Results of *in vitro* stability assay for $[^{89}Zr]Zr$-DFO2K in comparison to $[^{89}Zr]Zr$-DFO ($n = 3$). (A) Against 40 and 60 mg hydroxyapatite (HTP, BioRad Bio-Gel, HEPES 0.5M, pH 7.0, 37 °C) after 24 h, and (B) against 1000-fold molar excess amount of EDTA over 10 days (ammonium acetate 0.25 M, pH 7.0, 37 °C). The stabilities are determined by using radio-iTLC.

Another method to examine the susceptibility of $[^{89}Zr]Zr$-DFO2K and $[^{89}Zr]Zr$-DFO to transchelation is challenging the metal-chelate complexes against a large molar excess of another chelator known to bind the zirconium(IV) ion. Ethylenediaminetetraacetic acid (EDTA) was chosen due to its low cost, ease of procurement, and most importantly the ease of resolving $[^{89}Zr]Zr$-EDTA from $[^{89}Zr]Zr$-DFO2K and $[^{89}Zr]Zr$-DFO via radio-iTLC. To make this stability assay more extreme than our previous studies, we challenged pre-formed $[^{89}Zr]Zr$-DFO2K and $[^{89}Zr]Zr$-DFO with 1000-fold molar excess of EDTA (in ammonium acetate buffer pH 7) instead of our previous 100-fold ratio. The results revealed that after a 10-day incubation period, $[^{89}Zr]Zr$-DFO was only 32.0% ± 4.0% stable, where $[^{89}Zr]Zr$-DFO2K remained 98.4% ± 0.2% intact (**Figure 3-4B**).

***In vivo* evaluation in healthy mice**. Conventionally, zirconium-89 chelate complexes are conjugated to biovectors such as antibodies (mAb), peptides, or other large macromolecular vectors such as nanoparticles or microparticles for preclinical and clinical applications. When testing a new chelator, conjugation to an antibody serves to provide slow pharmacokinetics and clearance, which provides a great "real-world" *in vivo* stability challenge as the radioimmunoconjugate can circulate and be measured for up to 2-3 weeks following injection. But first we must determine the pharmacokinetics of the unconjugated radiometal-chelate complex as a baseline. Animal studies of the unconjugated radiometal-chelate complexes by *ex vivo* biodistribution provides an important insight on their *in vivo* behavior, which could be clinically relevant if the [^{89}Zr]Zr-chelate complex is cleaved from the biovector and released into circulation.

To understand the pharmacokinetics and clearance of unconjugated and radiolabeled [^{89}Zr]Zr-DFO2K and compare it with [^{89}Zr]Zr-DFO, we intravenously injected ~4 MBq (200 µL, in 0.9% saline) of [^{89}Zr]Zr-DFO or [^{89}Zr]Zr-DFO2K into separate cohorts of healthy female CD-1 mice (n = 4). Mice were euthanized at 24 h post injection and *ex vivo* biodistribution revealed that both complexes cleared fast with minimal residual activity. Furthermore, [^{89}Zr]Zr-DFO2K and [^{89}Zr]Zr-DFO both appear to be cleared through renal excretion, which also confirms the hydrophilicity of DFO2K (**Figure 3-6**). Organ distribution was nearly identical between the two chelate-complexes, with the exception of slightly higher kidney retention of [^{89}Zr]Zr-DFO2K. Radiometallated peptides which are lysine-rich and cationic are known to accumulate in the kidneys, and the inclusion of lysine as the linker in DFO2K could explain this slightly higher kidney uptake than observed for DFO. We don't believe this is an issue because bifunctional DFO2K will not possess a free primary amine, as this amino group will be transformed into a bifunctional moiety such as a *p*-SCN-Ph group. This biodistribution data suggests no abnormal

organ uptake or tissue distribution of $[^{89}Zr]Zr\text{-}DFO2K$, making it an excellent prospect for future bifunctional chelate synthesis, biovector (e.g. mAb) conjugation, and longer-term *in vivo* stability studies.

Bifunctionalization of DFO2K and Antibody Conjugation. Zirconium-89 chelate complexes are generally used in conjugation with biovectors, which requires bifunctionalization of the chelator by adding a reactive group such as an activated ester or phenyl-isothiocyanate. These reactive functional groups can be reacted under aqueous mild conditions with a nucleophilic side chain of amino acids such as lysine (primary amine) or cysteine (thiol/thiolate) on antibodies and
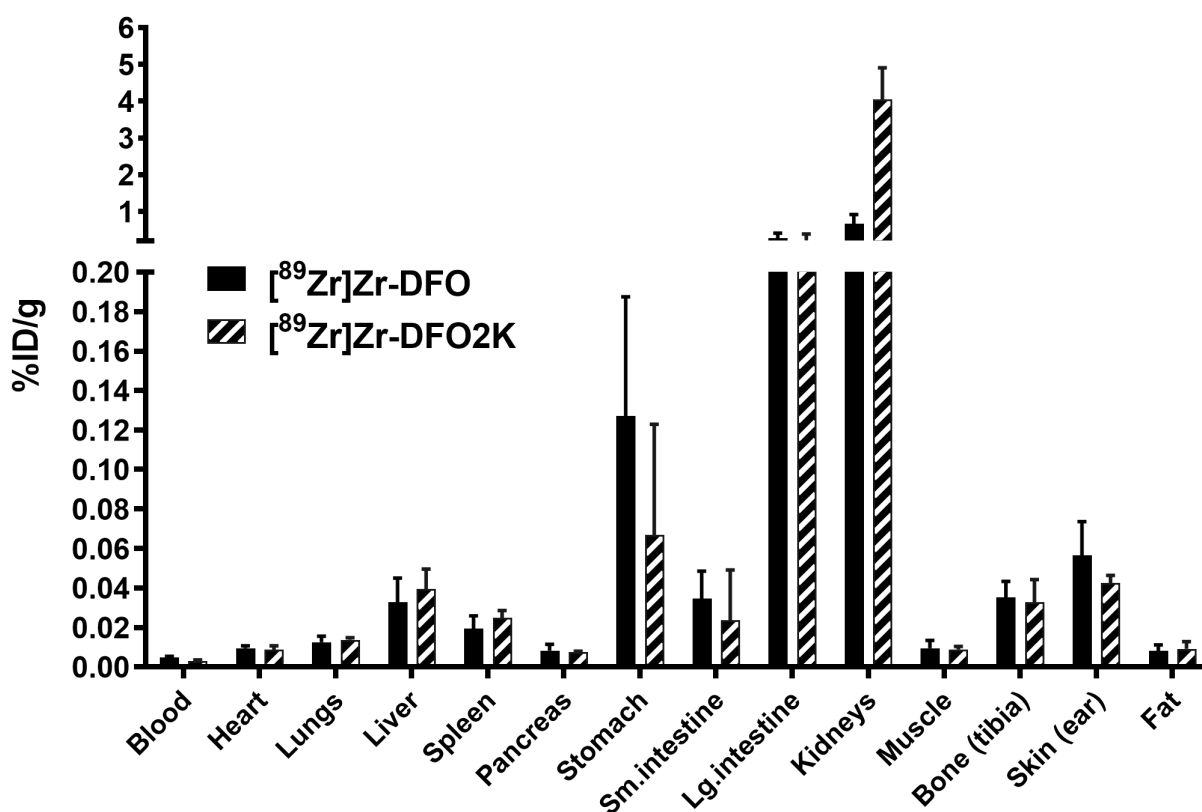
Figure 3-6. Results of biodistribution study 24 h post injection of unconjugated $[^{89}Zr]Zr\text{-}DFO$ and $[^{89}Zr]Zr\text{-}DFO2K$ in healthy female CD1 mice (*n* = 4). 4-5 MBq of zirconium-89 chelate complexes in 200 μL sterile saline were injected intravenously via tail vein catheter.

peptides. Bifunctionalization of DFO and its derivatives by using phenyl-isothiocyanate have

proven effective and compatible with unprotected hydroxamic acid (HA) groups, which constitute the metal ion coordinating moieties of DFO.[24,25,28] For this purpose, we synthesized the bifunctional version of DFO2K (*p*-SCN-Ph-DFO2K), which was synthesized through a thiourea linkage formed between the side chain amine of the lysine linker in DFO2K, and 1,4-phenylenediisocyanate. Phenyl-isothiocyanate reactive groups are typically conjugated to lysine side chains on antibodies under mildly basic and aqueous conditions (pH ~8-9) forming a stable thiourea linkage. To synthesize *p*-SCN-Ph-DFO2K, we instead used DMF as solvent and triethylamine as base together with DFO2K (free amine) and a large excess of 1,4-phenylenediisocyanate, and purified by RP-HPLC. The bifunctional *p*-SCN-Ph-DFO2K was then conjugated to a non-specific human serum IgG antibody (Sigma Aldrich), along with commercially available bifunctional DFO (*p*-SCN-Ph-DFO) to be used as a control for comparing *in vivo* stability (**Scheme 3-2**). The chelator antibody ratio for the DFO2K-IgG and DFO-IgG conjugates were determined by MALDI-TOF MS/MS mass spectrometry to be averages of 1.7 and 1.8 chelates per antibody, respectively (**Table 3-1**).
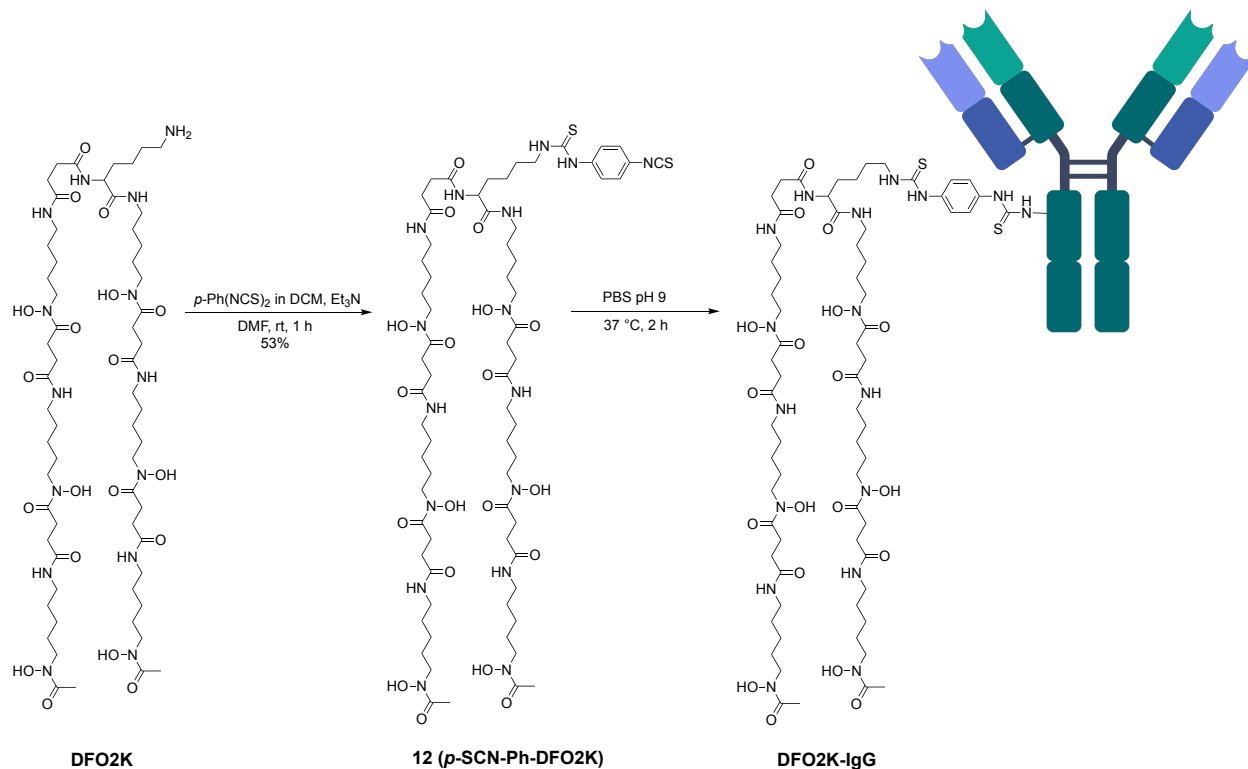
Scheme 3-2. Synthesis of bifunctional DFO2K (*p*-SCN-Ph-DFO2K) and conjugation to a non-specific human IgG antibody.

Table 3-1. Determination of chelator to antibody ratio (CAR) from results of MALDI-TOF MS/MS mass spectrometry analysis of unmodified IgG and the immunoconjugates.

Immunoconjugate	Molar equivalent of chelators	Measured average mass (Da)	Mass change (Da)	Mass of chelator (Da)	Chelator antibody ratio (CAR)
Unmodified IgG	-	148464.7	-	-	-
DFO-IgG	5.5	149795.0	1330.3	752.33	1.8
DFO2K-IgG	10	151105.9	2641.2	1522.8	1.7

Radiolabeling and *in vivo* Evaluation in Helathy Mice. The biological half-life of "free" radiometal-chelate complexes is typically very short with most activity excreted through the renal

system/urine within an hour, and therefore doesn't provide a useful measure of *in vivo* radiometal-chelate stability. This is exactly as we have observed with the zirconium-89 complexes of DFO, and DFO2K. When conjugated to an antibody, the radiometal-chelate-antibody radioimmunoconjugate can circulate in mice for weeks, therefore providing a clinically relevant challenge to assess true "real-world" *in vivo* stability for several weeks. Using this method, we can observe the distribution of zirconium-89 in mice after a period of ~ 2 weeks using highly sensitive PET-CT imaging and biodistribution studies. Zirconium-89 is known to be both oxophilic and osteophilic, and *in vivo* instability is known to manifest as increased bone uptake. Because we are using healthy mice and a non-specific antibody, there is no tumor to act as a sink for accumulating and retaining the [^{89}Zr]Zr-IgG's, and therefore we expect a gradual accumulation of the radiolabeled antibodies in the liver, and we anticipate greater stability and therefore lower bone uptake for DFO2K vs DFO.

Both conjugates were radiolabeled quantitatively in HEPES buffer (pH 7.0, 0.5 M) at 37 °C (>99% RCY confirmed by radio-iTLC) to be used to further assess the radiometal-chelate complex stability *in vivo* and compare the pharmacokinetics of the antibody conjugates in mice. Following purification of the radiolabeled immunoconjugates and solvent exchange by size-exclusion chromatography (PD-10 desalting columns) and eluting the compounds using sterile 0.9% saline solution, the [^{89}Zr]Zr-immunoconjugates (8.5-8.7 MBq, 200 µL, 0.9% saline) were administered to separate groups of healthy female CD-1 mice via tail-vein injection (n = 6 per cohort). After circulating in the living mice for 2 weeks, we set out to evaluate the difference in their biodistributions and therefore the difference in the chelate stabilities. Sets of 4 mice per compound were imaged by PET-CT at 14 d post injection followed by euthanizing the mice for *ex vivo* biodistribution study.

Both the PET-CT images and *ex vivo* (biodistribution) results showed similar pharmacokinetics and clearance for $[^{89}Zr]Zr$-DFO2K-IgG and $[^{89}Zr]Zr$-DFO-IgG. The major difference between the two compounds was that bone uptake was substantially lower in the mice injected with $[^{89}Zr]Zr$-DFO2K-IgG compared to $[^{89}Zr]Zr$-DFO-IgG (**Figures 3-7** and **3-8**). Although biodistribution results showed a statistically significantly lower uptake in bone for $[^{89}Zr]Zr$-DFO2K-IgG compared to $[^{89}Zr]Zr$-DFO-IgG (1.2 ± 0.4 %ID/g vs 1.9 ± 0.4 %ID/g, $p < 0.05$), these values reflect only the activity in the isolated bone (both tibia bones). Further, the joints are not obtained with the tibias, and in PET-CT imaging the highest uptake of free $[^{89}Zr]Zr^{4+}$ is always in the joints, jaw, and spine. Because the tibia is the only bone we can quickly and cleanly remove from the mice without attached tissue for *ex vivo* measurement, we are limited in this analysis and the biodistribution results do not properly reflect the true difference in bone uptake between these two chelators. Due to the high sensitivity of our Sofie GNEXT PET-CT scanner, we were able to obtain excellent images at 14 days post injection with only ~5-10 µCi (~185-370 kBq) of activity remaining in the mice. This enabled us to visualize the entire mouse and therefore the entire skeleton and see the true difference in bone uptake (**Figure 3-7**). The PET-CT images reveal a dramatic difference in skeletal uptake of zirconium-89, with $[^{89}Zr]Zr$-DFO2K-IgG having dramatically lower uptake than $[^{89}Zr]Zr$-DFO-IgG in the joints (e.g. joints, spine, jaw). These results are in agreement with the previous *in vitro* studies which showed DFO2K forms a much more stable complex with $[^{89}Zr]Zr^{4+}$ than DFO.

[⁸⁹Zr]Zr-DFO-IgG
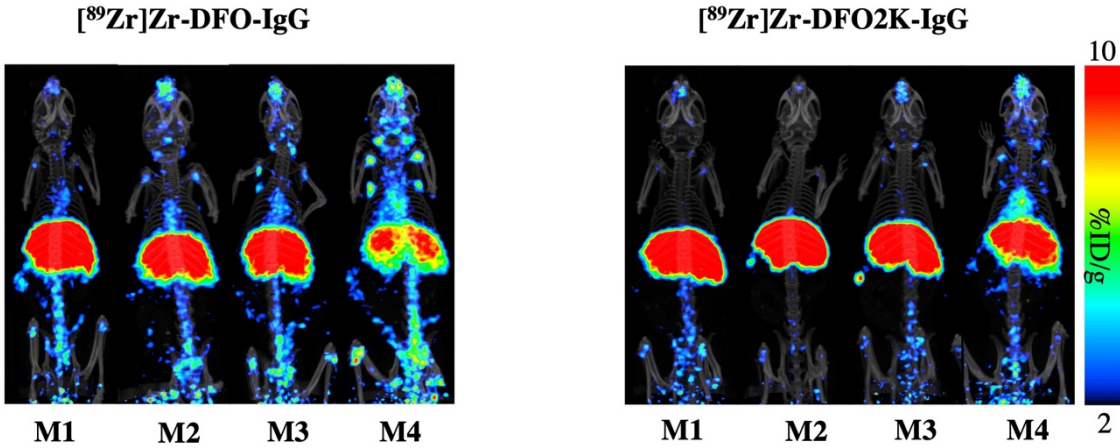
[⁸⁹Zr]Zr-DFO2K-IgG

Figure 3-7. PET-CT images (maximum intensity projections) of [^{89}Zr]Zr-DFO2K-IgG and [^{89}Zr]Zr-DFO-IgG (~8.7 MBq in 200 μL 0.9% saline per mouse) in healthy female CD-1 mice (4 mice of an n = 6 cohort imaged), 14 d post injection. After decay correction the activies in the images are maximized to visualize and compare bone uptake for both compounds.
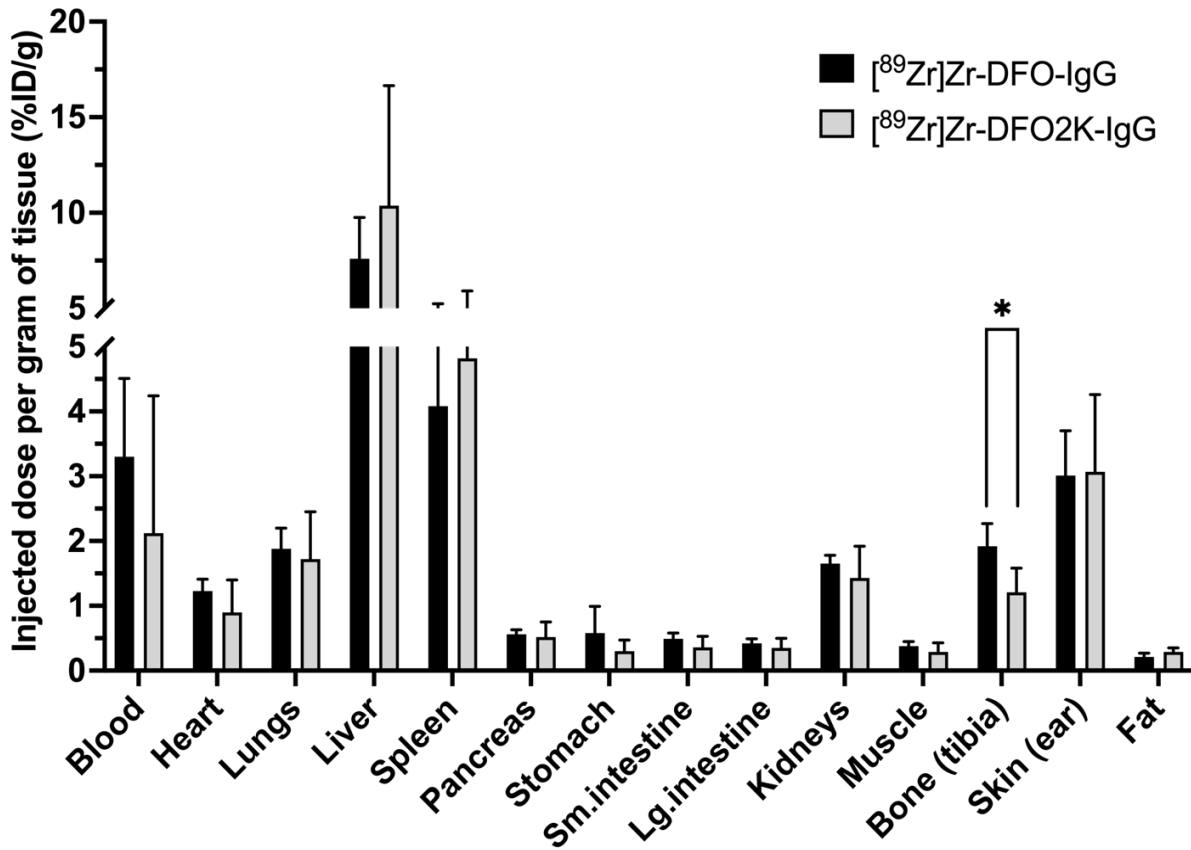
Figure 3-8. Results of biodistribution study of [^{89}Zr]Zr-DFO-IgG and ^{89}Zr]Zr-(DFO-Km)-IgG in female CD-1 mice 14 d post injection. ~8.7 MBq of either complex was injected in 200 μL, 0.9% saline, intravenously via tail vein injection ($n = 6$).

3.5. Conclusion

The new chelator DFO2K is a highly water soluble, dodecadentate (CN up to 12), amino acid-based derivative of our previously published chelators DFO2 and DFO2p, which has been designed for both zirconium-89 and other large oxophilic radiometals for theranostic applications. DFO2K was synthesized in 4 steps with an overall yield of ~27%, and its radiolabeling efficiency and *in vitro* stability with $[^{89}Zr]Zr^{4+}$ was evaluated. For ease of structural modification, DFO2K possesses a modular scaffold that can be tuned easily for different coordination numbers and conjugation chemistries. The modular design of DFO2K utilizes the amino acid lysine, but any natural or unnatural amino acid could be used while retaining identical metal-coordination properties and therefore identical radiolabeling and stability properties. The simplified synthesis and enhanced modularity of DFO2K make it more versatile and easy to derivatize, and its improved water solubility reduces the need for harsh organic solvents during bioconjugation reactions with sensitive biomolecules such as proteins and antibodies. The results of radiolabeling studies revealed that DFO2K has remarkably fast complexation kinetics with zirconium-89 under mild and desirable conditions, with crude radiochemical yields (radio-iTLC) at ambient temperature and neutral pH of >95% in only 1 minute (quantitative at 15 min). Furthermore, DFO2K was found to form a significantly more stable complex with $[^{89}Zr]Zr^{4+}$ than the "gold standard" chelator DFO when it was evaluated head-to-head by different *in vitro* stability challenges such as hydroxyapatite and 1000-fold molar excess EDTA. Biodistribution (*ex vivo*) studies of the non-bifunctional version in healthy mice showed that $[^{89}Zr]Zr$-DFO2K has a similar pharmacokinetic profile to $[^{89}Zr]Zr$-DFO with minimal residual organ activity at 24 h post injection. Furthermore, when $[^{89}Zr]Zr$-DFO2K-IgG was compared to $[^{89}Zr]Zr$-DFO-IgG in healthy mice, significant decrease in bone uptake was observed by PET/CT images and *ex vivo*

biodistribution studies 14 days post injection. Overall, these preliminary evaluations have indicated that DFO2K is superior to DFO for zirconium-89 coordination, and with the potential coordination number of up to 12 (vs 6 for DFO), DFO2K has the potential to be used with other large radiometals such as cerium-134, thorium-227, and actinium-225 for theranostic applications.

3.6. Experimental Section

Reagents. All reagents and solvents were purchased from commercial suppliers (Sigma-Aldrich, St. Louis, MO; TCI America, Portland, OR; Fisher Scientific, Waltham, MA) and were used without further purification unless otherwise indicated. Oxyma Pure and *N,N*-diisopropylethylamine (DIPEA) were purchased from Sigma-Aldrich. DFO mesylate was purchased from Abcam. 1-[Bis(dimethylamino)methylene]-1H-1,2,3-triazolo[4,5-b]pyridinium 3-oxid hexafluorophosphate (HATU) and Boc-Lys(Z)-OH were purchased from AK Scientific. $ZrCl_4$, EDTA, disodium salt dihydrate (Molecular biology grade), ammonium acetate, (Honeywell ≥ 99.99% trace metal basis), 1-ethyl-3-(3-dimethylaminopropyl)carbodiimide hydrochloride (EDC.HCl), and potassium carbonate anhydrous were purchased from Fisher Scientific.

Chemical Characterization Methods. ^{1}H and ^{13}C NMR spectra were recorded on a 500 MHz Bruker Avance III HD NMR spectrometer at the Saskatchewan Structural Science Centre at the University of Saskatchewan, at 25 ºC in D_2O, $CDCl_3$, or $(CD_3)_2SO$. Chemical shifts were referenced to the residual protons of the deuterated solvents for ^{1}H NMR (δ =4.79 ppm for D_2O; δ =7.26 ppm for $CDCl_3$ and δ = 2.50 ppm for $(CD_3)_2SO$. Similarly, ^{13}C chemical shifts were referenced to the $CDCl_3$ signal at 77.16 ppm and $(CD_3)_2SO$ signal at δ = 39.52 ppm. Coupling constants are reported to the nearest 0.5 Hz (^{1}H NMR spectroscopy) and for ^{13}C NMR spectroscopy

they are rounded to integer values in Hz. Field desorption ionization (FDI) was used on JEOL AccuTOF GCv 4G mass spectrometer to measure high resolution mass spectra and only the mass peak of the isotope with the highest natural abundance is recorded for the isotopic patterns. HPLC purifications were performed on Thermofisher Vanquish HPLC using C18 reversed-phase column (Inspire Semipreparative DIKMA; 5 μm, 21.2 × 250 mm), a VF-D40-A UV detector, two VF-P10-A pumps with Chromeleon 7 communication software. A flow rate of 6-8 mL/minute was used with a gradient of MeCN:H_2O (with 0.1% formic acid (FA) in both solvents). Low resolution mass spectrometry was performed on Advion Expression-L system (mass range <2000 amu). The Advion Expression-L was coupled with the Thermofisher Vanquish system to perform LC-MS.

Synthesis of DFO-Lys(Z)-Boc (7). Compound **7** was prepared according to a published procedure with modification.[16] A solution of Boc-Lys(z)-OH (264 mg, 0.69 mmol) in DMF (15 mL) was added to a stirring mixture of HATU (306 mg, 0.81 mmol) and DIPEA (0.14 mL, 0.81 mmol) in DMF (15 mL). DFO mesylate (501 mg, 0.76 mmol) was dissolved in DMF (17 mL) and DMSO (8 mL) at 65 °C. The clear solution of DFO was cooled to around 40 °C and then it was added to the above activated ester solution. The reaction was stirred at ambient temperature for 24 h and then the solvent was reduced to ~2 mL under reduced pressure. The residue was added dropwise to ethyl acetate and left in a spark proof -20 °C freezer for 30 minutes, to maximize precipitate formation. The precipitate was separated by centrifugation, washed with cold ethyl acetate 2 times, flash frozen in liquid nitrogen and then dried by freeze dryer. Compound **7** (632 mg, 99%) was used in the next step without further purification. ^{1}H NMR [(CD$_3$)$_2$SO, 500 MHz]: δ 1.21 (br s, 8H, CH$_2$), 1.34 – 1.39 (m, 17H, tBu and CH$_2$), 1.48-1.49 (m, 8H, CH$_2$), 1.96 (s, 3H, CH$_3$), 2.26 (t, J=7.3, 4H, CH$_2$), 2.57 (t, J = 7.2, 4H, CH$_2$), 2.94 – 3.01 (m, 8H, CH$_2$), 3.43 – 3.45 (m, 6H, CH$_2$),

3.80 – 3.81 (m, 1H, CH), 4.99 (s, 2H, CH$_2$), 7.23 (t, J = 5.5, 1H, NH), 7.29 – 7.37 (m, 5H, CH Ar), 7.75 (t, J = 5.4, 1H, NH), 7.79 (t, J = 5.0, 2H, NH). ^{13}C NMR [(CD$_3$)$_2$SO, 126 MHz]: δ 20.4, 22.9, 23.4, 23.5, 26.1, 27.6, 28.1, 28.2, 28.8, 28.9, 29.1, 29.9, 31.8, 38.3, 38.4, 46.8, 47.1, 54.4, 59.8, 65.1, 77.9, 127.8, 128.4, 137.3, 155.3, 156.1, 170.2, 171.3 and 172.0. HRMS: m/z Calcd for [C$_{44}$H$_{74}$N$_8$O$_{13}$Na + Na]$^+$: 945.5267; found: 945.5276.

Synthesis of DFO-Lys(Z)-NH$_2$ (8). This Boc-deprotection procedure was modified from a published procedure.[29] A mixture of trifluoroacetic acid (0.5 mL, 6.26 mmol) and dichloromethane (0.5 mL) was added to compound **7** (385.1 mg, 0.42 mmol). The reaction mixture was stirred for 4 h at ambient temperature. Then the solvent was evaporated via rotary evaporator, and the crude product was purified with reverse phase column chromatography (10 – 50% MeCN in water) to isolate compound **8** (327.1 mg, 95%) as a white powder. ^{1}H NMR [(CD$_3$)$_2$SO, 500 MHz]: δ 1.21 -1.63 (m, 26H, CH$_2$), 1.96 (s, 3H, CH$_3$), 2.26 (t, J = 7.2, 4H, CH$_2$), 2.57 (t, J= 7.1, 4H, CH$_2$), 2.95 – 3.03 (m, 6H, CH$_2$), 3.05 – 3.11 (m, 2H, CH$_2$), 3.44 -3.48 (m, 6H), 5.00 (s, 2H, CH$_2$), 7.23 (t, J=5.6 1H, NH), 7.31-7.38 (m, 5H, CH), 7.79 (t, J=5.3, 2H, NH), 8.20 (t, J=5.3, 1H, NH), 9.65 (br s, 3H, OH). ^{13}C NMR [(CD$_3$)$_2$SO, 126 MHz]: δ 20.4, 21.9, 23.5, 26.1, 27.6, 28.6, 28.9, 29.1,29.9, 32.8, 38.5, 46.8, 47.1, 53.0, 65.2, 127.8, 128.4, 156.1, 170.2, 170.3, 171.3 and172.0. HRMS: m/z Calcd for [C$_{39}$H$_{66}$N$_8$O$_{11}$ + Na]$^+$: 845.4743; found: 845.4741.

Synthesis of DFO2-Lys-Z (9). This procedure was adapted from a published literature procedure.[30] DFO-COOH (470 mg, 0.71 mmol) was dissolved in a mixture of DMF (10 mL) and DMSO (4 mL) with help of heating up to 75 °C. After the solution became clear, a mixture of oxyma (74.3 mg, 0.523 mmol) and EDC (103.3 mg, 0.665 mmol) in DMF (10 mL) was added.

The mixture was stirred for 30 minutes at ambient temperature. Then a solution of **8** (391 mg, 0.48 mmol) and NaCl (27.8 mg, 0.475 mmol) in DMF (10 mL) was added, and the mixture was sonicated for 5 minutes to ensure complete dissolution. The reaction was stirred for 48 h at ambient temperature then the solvent was reduced to ~1 mL. The residue was added dropwise to ethyl acetate and left in a spark proof -20 °C freezer for 30 minutes. The precipitate was separated with help of centrifugation and washed two times with cold ethyl acetate. The crude product was purified with reverse phase chromatography (10 – 50% MeCN in water) and the product (336 mg, 32%) was collected as a white powder. ^{1}H NMR [$(CD_3)_2SO$, 500 MHz]: δ 1.22 –1.63 (m, 46H, CH_2), 1.97 (s, 6H, CH_3), 2.26 – 2.37 (m, 12H, CH_2), 2.58 (t, J= 7.1, 8H, CH_2), 2.96 – 3.00 (m, 14H, CH_2), 3.44 – 3.47 (m, 12H, CH_2), 4.07 – 4.12 (m, 1H, CH), 5.00 (s, 2H, CH_2), 7.25 (t, J= 5.6, 1H, NH), 7.30 - 7.38 (m, 5H, CH-Ar), 7.82 (t, J= 5.3, 4 H, NH), 7.87 – 7.88 (m, 2H, NH), 8.0 (d, J= 8.0, 1H, NH). ^{13}C NMR [$(CD_3)_2SO$, 126 MHz]: δ 20.4, 22.9, 23.5, 26.1, 27.6, 28.7, 28.8, 29.2, 29.9, 30.7, 30.8, 31.5, 38.4, 46.8, 47.1, 52.7, 65.1, 127.7, 128.4, 137.3, 156.1, 170.1, 171.4, 171.6, 171.7 and 171.9. HRMS: m/z Calcd for $[C_{68}H_{116}N_{12}O_{21} + Na]^+$: 1487.8331; found: 1487.8366.

Synthesis of DFO2K (10). Compound **10** was prepared according to a published procedure with modification.[31] In a Schlenk flask, compound **9** (47.5 mg, 30 µmol) was dissolved in ethanol (30 mL) and 10% Pd/C (6.0 mg, 5 µmol) was added. The flask was sealed with a rubber septa and connected to an H_2 gas balloon fitted with a glass stopcock and a needle, and the flask was additionally connected to vacuum via Schlenk line. The flask was put under vacuum for 15 seconds and then the vacuum was closed, and the flask was purged with H_2 gas by slowly opening the glass stopcock valve. The vacuum and purging were repeated 4 times and finally the flask was left stirring under H_2 for 2 h. After reaction completion was confirmed with low resolution mass

spectrometry, the reaction mixture was filtered through celite to remove the Pd/C for safe disposal. The solvent was evaporated, and the crude product mixture was purified by semipreparative HPLC. HPLC conditions: C18 Inspire Semipreparative DIKMA; 5 µm, 21.2 × 250 mm; (20 – 30% acetonitrile in water (0.1% formic acid); flow rate, 4 mL/min, t_R = 18 min). Compound **10** (39.4 mg, 91%) was obtained as an off-white solid following rotary evaporation and then freeze drying of pooled HPLC fractions. ^{1}H NMR [D_2O, 500 MHz]: δ 1.24 – 1.81 (m, 44H, CH_2), 2.10 (s, 6H, CH_3), 2.44 – 2.53 (m, 12H, CH_2), 2.76 (t, J=7.0, 6H, CH_2), 2.96 (t, J=7.7, 2H, CH_2), 3.12 – 3.15 (m, 12H, CH_2), 3.56 – 3.62 (m, 12H, CH_2), 4.14 – 4.17 (m, 1H, CH). ^{13}C NMR D_2O, 126 MHz]: δ 19.2, 22.2, 23.0, 25.4, 26.2, 17.6, 27.9, 30.4, 30.8, 38.7, 39.1, 47.7, 47.8, 53.9, 173.5, 173.8, 174.3, 174.8, and 174.9. HRMS: m/z Calcd for $[C_{60}H_{110}N_{14}O_{19} + 2H]^{2+}$: 666.4109; found: 666.4123.

Synthesis of [^{Nat}Zr]Zr-DFO2K (11). DFO2K (10.5 mg, 7.89 µmol) was dissolved in a mixture of Chelex-treated Millipure water (1 mL) and DMSO (0.5 mL). Then a solution of $ZrCl_4$ (87.5 µL, 90.0 mM, 7.89 µmol, in Chelex-treated Millipure water) was added and the pH was adjusted to ~ 7 by adding sodium carbonate solution (1 M). The reaction mixture was shaken on a thermomixer (800 rpm) at ambient temperature for 2 h. Then the reaction mixture was flash frozen in liquid nitrogen and the solvent removed by lyophilization to obtain **[^{Nat}Zr]Zr-DFO2K** (8 mg, 71.5%) as a bone white powder. ^{1}H NMR [$(CD_3)_2SO$, 500 MHz]: δ 1.22-148 (m, 45H), 1.95-2.42 (m, 20H), 2.54-2.63 (m, 6H), 2.88-3.00 (m, 12H), 3.38-3.44 (m, 6H), 4.02-4.10 (m, 1H), 7.94-8.43 (m, 6H). ^{13}C NMR [$(CD_3)_2SO$, 126 MHz]: δ 16.9, 22.6, 22.9, 23.1, 23.7, 24.3, 25.4, 26.1, 26.6, 28.0, 28.7, 28.9, 29.0, 30.8, 31.3, 31.8, 32.8, 33.3, 34.1, 41.4, 50.8, 149.4, 150.2, 166.7, 171.5, 171.6, 172.9. HRMS: m/z Calcd for $[C_{60}H_{106}N_{14}O_{19}Zr + H]^+$: 1417.6884; found: 1417.6905.

Synthesis of DFO2K-*p*-Ph-NCS (12). A mixture of *p*-phenylene diisothiocyanate (28.9 mg, 15.0 μmol) and triethylamine (10.5 μL, 75.1 μmol) in dichloromethane (1 mL) was added to a solution of DFO2K (20 mg, 15.0 μmol) in DMF (2 mL). The reaction mixture was shaken on a thermomixer for 1 h at ambient temperature, and then it was added dropwise to diethyl ether (40 mL). The mixture was left in a spark proof -20 °C freezer for 30 minutes to precipitate the product. The crude product was separated by decantation after centrifugation followed by washing with cold diethyl ether two times. The crude was purified by semipreparative HPLC. HPLC conditions: C18 Inspire Semipreparative DIKMA; 5 μm, 21.2 × 250 mm; (30 – 60% acetonitrile in water (0.1% formic acid); flow rate, 4 mL/min, t_R = 34 min). Pure compound **12** (12 mg, 53%) was obtained as a white powder following rotary evaporation and then freeze drying of pooled HPLC fractions. ^{1}H NMR [(CD$_3$)$_2$SO, 500 MHz]: δ 1.20 - 1.49 (m, 46H, CH$_2$), 1.96 (s, 6H, CH$_3$), 2.24 – 2.32 (m, 12H, CH$_2$), 2.57 (t, J=7.1, 6H, CH$_2$), 2.99 (q, J=6.0, 12H, CH$_2$), 3.44 (t, J=6.8, 12H, CH$_2$), 4.02-4.16 (m, 1H, CH), 7.33 (d, J=8.8, 2H, CH$_2$), 7.69 (d, J=8.2, 1H, CH$_2$), 7.80 – 8.00 (m, 6H, CH, and NH), 8.07 (d, J=7.8, 1H, NH), 9.91 (s, 5H, OH). HRMS: m/z Calcd for [C$_{68}$H$_{114}$N$_{16}$O$_{19}$S$_2$ + H]$^+$: 1523.7966; found: 1523.7981.

Radiochemistry. [^{89}Zr]Zr-oxalate was received from Saskatchewan Centre for Cyclotron Sciences (SCCS) on the University of Saskatchewan campus, delivered as purified [^{89}Zr]Zr-oxalate in a minimum volume of 1.0 M oxalic acid. The apparent molar activity of the [^{89}Zr]Zr-oxalate produced routinely by the SCCS (as used for this study) was found to be in the range of 673-1161 MBq/μmol, by using a method adopted from Holland et al,[32,33] and radionuclidic purity was determined to be 99.99%.[34]

[⁸⁹Zr]Zr⁴⁺ Radiolabeling Studies. The [⁸⁹Zr]Zr-oxalate received from the Saskatchewan Centre for Cyclotron Sciences (in 1 M oxalic acid) was aliquoted and neutralized to pH 6.8-7.2 by using sodium carbonate (1.0 M), and radiolabeling reactions were performed in HEPES buffer (0.5 M, pH 7). Silica-gel impregnated glass-microfiber instant thin layer chromatography paper (iTLC-SG, Varian, Lake Forest, CA) was used for reaction progress monitoring and radiochemical yield determination. EDTA solution (50 mM, pH 5.5) was used to develop the iTLC strips, which eluted free ⁸⁹Zr]Zr⁴⁺ to the solvent front while radiolabeled (DFO and DFO2K bound to [⁸⁹Zr]Zr⁴⁺) remained at the baseline. The radio-iTLCs were analyzed on a Eckert & Ziegler AR-2000 radio-TLC plate reader and analyzed using the included Winscan Radio-TLC software. All solutions were prepared in Chelex-100 resin (BioRad Laboratories, Hercules, CA) treated (1.2 g/L water, 24 h) ultrapure water (>18.2 MΩ cm⁻¹ at 25°C, Milli-Q, Millipore, Billerica, MA). For activity measurements, either Perkin-Elmer (Waltham, MA) Automated Wizard Gamma Counter or Capintec CRC-15R dose calibrator (Capintec, Ramsey, NJ) was used and is indicated for each experiment. Radiolabeling of DFO2K chelator was performed following a published procedure.[28] Solutions of 1.00 nmol/μL of DFO2K and commercially available DFO mesylate were prepared in Chelex-100 resin treated water. After neutralization, aliquots of [⁸⁹Zr]Zr⁴⁺ (10-10.5 MBq) was mixed with different amounts of each chelator (0.005, 0.05, 0.5 and 5 nmol) in HEPES buffer pH 7 (0.5 M), the total volume of each reaction was completed to 250 μL, and the vials were mixed at 800 rpm at ambient temperature (*n* = 3). At time points 1, 5, 10, 15 and 60 minutes, 1 μL from each sample was spotted on an iTLC strip and the iTLCs were developed with EDTA (50 mM, pH 5.5) solution as mobile phase. Radiochemical yields were determined from integration of the activity at the baseline ([⁸⁹Zr]Zr-chelate complex) and solvent front (free/EDTA bound [⁸⁹Zr]Zr⁴⁺).

For stability assays, [^{89}Zr]Zr-chelate complex of each of DFO2K and DFO were prepared at the final concentration of 157 µM in the same way as described above and then aliquoted out to stability challenge vessels. The RCYs were determined by radio-iTLC to be >99% and they were used without further purification in radiochemical stability challenges.

Blood Serum Stability Assay. Solutions of [^{89}Zr]Zr-DFO2K or [^{89}Zr]Zr-DFO (63.6 µL, 157 µM) were mixed with 150 µL of freshly thawed human blood serum (Sigma-Aldrich) in microcentrifuge tubes ($n = 3$). The mixtures were shaken on a thermomixer at 800 rpm at 37 ºC for 10 days. Stability of the complexes was determined by radio-iTLC at 1h, 1, 3, 5, 7 and 10 days. Stable [^{89}Zr]Zr-DFO2K and [^{89}Zr]Zr-DFO remained at the baseline while transchelated [^{89}Zr]Zr^{4+} eluted to the solvent front.

EDTA Transchelation Assay (1000-fold molar excess). Aliquots of [^{89}Zr]Zr-DFO2K or [^{89}Zr]Zr-DFO (63.6 µL, 157 µM, ~2.1 MBq) were mixed with 400 µL of EDTA stock solution (25 mM prepared in ammonium acetate buffer pH 7, 0.25 M) microcentrifuge tubes. The final concentration of the EDTA and the chelate-complexes were 21.6 mM and 21.6 µM respectively in total volume of 463.6 µL ($n = 3$). The mixtures were shaken at 800 rpm at 37 ºC for 10 days. Stability of the complexes was determined by radio-iTLC at 1h, 3h, 13h, 1, 3, 5, 7 and 10 days.

Hydroxyapatite (HTP) Stability Challenge. Aliquots of [^{89}Zr]Zr-DFO2K or [^{89}Zr]Zr-DFO (63.6 µL, 157 µM, ~2.1 MBq) were mixed with 40 mg or 60 mg hydroxyapatite resin (HTP, BioRad Bio-Gel) and 900 µL HEPES buffer (0.5 M, pH 7) in microcentrifuge tubes ($n = 3$). As control, another set of tubes were prepared where only neutralized [^{89}Zr]Zr-Oxalate (~ 2.1 MBq) was

mixed with 40 mg or 60 mg hydroxyapatite resin instead of the zirconium complexes in HEPES buffer ($n = 3$). The mixtures were shaken on a thermomixer at 800 rpm and 37 ºC for 24 h. Then the mixtures were centrifuged for 10 minutes at 10000 rpm. The supernatant was carefully pipetted out into 5 mL tubes, and the pellet was washed (2 times) with 1 mL HEPES buffer, centrifuged to re-pellet the HTP resin, and the supernatants were pooled together. Activity of the pellets (transchelated [^{89}Zr]Zr^{4+}) and the pooled supernatants (intact [^{89}Zr]Zr-chelates) were measured via dose calibrator separately. Complex stability percentages were determined from percentage of activity in the supernatants relative to the total activity in both the pooled supernatants and the pelleted HTP resin.

Log*D* Octanol/Buffer Distribution Coefficient. 27 µL (~ 5 µCi) aliquots of [^{89}Zr]Zr-DFO or [^{89}Zr]Zr-DFO2 were mixed with 2.973 mL PBS buffer (pH 7.4, pre-saturated with octanol) and 3 mL 1-octanol, in 15 mL centrifuge tubes ($n = 3$). The mixtures were shaken aggressively by vortex mixer for 1 minute followed by 10 minutes of centrifugation at 3000 rpm. Carefully, 1 mL from each layer was pipetted out and transferred to a separate microcentrifuge tube to measure the activity on an automated gamma counter. Log*D* values were calculated from log of the ratio of activity (counts) in 1-octanol to activity in PBS buffer (pH 7.4) according to equation (**2-1,** see chapter 2), where ionized and un-ionized solute are indistinguishable and therefore total radioactive counts in octanol were used as numerator and total counts in PBS as denominator.

Biodistribution of Unconjugated [^{89}Zr]Zr-Chelator in Healthy Mice. [^{89}Zr]Zr-DFO2K and [^{89}Zr]Zr-DFO complexes were prepared in the same manner as explained above and >99% RCY was confirmed by radio-iTLC. Aliquots of ~4 MBq of the [^{89}Zr]Zr-chelator complexes were

injected to healthy female CD-1 mice (n = 6 per cohort), via tail vein catheter under anesthesia (2.5 % isoflurane in O_2, at a flow rate of 2-3 mL/min). The mice were euthanized (by anesthesia followed by cervical dislocation followed by cardiac puncture and blood draw) at 24 h post injection. Blood and specific organs were harvested, weighed, and residual activity in the organs were measured by using an automated gamma counter. The animals had access to cage enrichments and access to food and water ad-libitum. The experimental protocol was approved by the University of Saskatchewan Committee on Animal Care and procedures were performed in accordance with the guidelines of the Canadian Council on Animal Care and the Canadian Nuclear Safety Commission.

IgG conjugation. Following a standard procedure for antibody conjugation,[28] to 429 µL solution of purified IgG from human serum in PBS buffer pH 7 (1.5 mg mAb, 10.11 nmol, 1.52 mg/mL, Sigma), sodium carbonate (35 µL, 0.1 M) was added to adjust the pH to ~ 9. Followed by addition of 14 µL *p*-SCN-Ph-DFO2K solution (11.5 mg/ µL in DMSO) and the total volume was completed to 600 µL by adding PBS buffer pH 7. The reaction mixture was shaken on a thermomixer at 800 rpm, for 2 h at 37 °C. The resulting immunoconjugate was purified by using PD-10 desalting column and followed by Amicon® Ultra-4 Centrifugal Filter Ultracel-50K. Similarly, commercially available *p*-SCN-Ph-DFO was also conjugated to IgG and purified in the same manner explained for DFO2K-IgG. The concentration of the antibody and the immunoconjugates were determined on NanoDrop™ 2000c spectrophotometer and NanoDrop 8000 spectrophotometer (Thermo Scientific). Finally, samples of IgG conjugates along with unmodified IgG were prepared (10 µL, 1 mg/mL, in Chelex treated ultrapure water, *n* = 3) and analyzed by MALDI-TOF MS/MS to determine chelator to antibody ratio (CAR).

PET-CT imaging and biodistribution of [⁸⁹Zr]Zr-DFO2K-IgG in healthy mice. Radiolabeling of the immunoconjugates was performed according to an established procedure,[28] where 231 µL aliquots of neutralized [⁸⁹Zr]Zr⁴⁺ (~ 94 MBq) in HEPES buffer (0.5 M, pH 7) was added to solutions of the immunoconjugates in PBS buffer (340 µL, 1.47 mg/mL DFO2K-IgG; 365 µL, 1.37 mg/mL DFO-IgG). The reaction tubes were mixed on a thermomixer at ambient temperature for 60 minutes. The radiochemical yields were determined to be > 99% using radio-iTLC. To exchange the buffer from PBS/HEPES buffer to saline and for further purification the reaction solutions were passed through PD-10 desalting columns (preconditioned with sterile saline). The radiolabeled immunoconjugates were eluted by using sterile saline (0.9%). The animal studies were performed in healthy female CD-1 mice. For each immunoconjugate, groups of 6 mice per compound were injected with 8.5-8.8 MBq (200 µL) of radiolabeled antibody per mouse intravenously via tail vein. 4 animals from each group were imaged under anesthesia (2.5 % isoflurane in O_2, at a flow rate of 2 mL/min) at 14 d post injection on GNEXT PET-CT scanner (60 min scan time). The PET images were reconstructed with the Sofie GNEXT system and processed with VivoQuant® 2020 software (patch 1 64 bit, build vq-2020patch1-0-ga8255affc). All the animals were euthanized (by anesthesia followed by cervical dislocation followed by cardiac puncture and blood draw) at 14 d post injection following PET-CT imaging, where organs were harvested, weighed, and residual activity in each organ was measured using an automated gamma counter (Perkin-Elmer, Waltham, MA, USA) for biodistribution calculations.

Density Function Theory (DFT) Calculations. DFT geometry optimizations were carried out on DMOL³ and Biovia Materials Studio software, version 20.10.5 (2020)[35,36] on the PC (Windows

10) by using the generalized gradient approximation (GGA) employing the Perdew-Burke-Ernzerhof (PBE)[37] functional both for the potential during the self-consistent field (SCF) procedure and energy.[38] All calculations employed DMol^3 double numerical plus d-function (DND) basis set using 4.4 basis file included polarization functions for all atoms with all-electron core treatments. Conductor-like screening model (COSMO)[39,40] solvation model was used for quantum simulation of solvated molecules with a dielectric value of ((ε = 78.54) for water. CYLview software (CYLview, 1.0b; Legault, C. Y., Université de Sherbrooke, 2009, http://www.cylview.org) was used for graphical depiction of the structures from the log files of the optimized structures.

3.7. Associated Content

Supporting information

The supporting information for this chapter is summarized in Appendix-I

3.8. References

(1)   Iking, J.; Staniszewska, M.; Kessler, L.; Klose, J. M.; Lückerath, K.; Fendler, W. P.; Herrmann, K.; Rischpler, C. Imaging Inflammation with Positron Emission Tomography. *Biomedicines* **2021**, *9* (2), 212.
(2)   Kubota, K.; Ogawa, M.; Ji, B.; Watabe, T.; Zhang, M.-R.; Suzuki, H.; Sawada, M.; Nishi, K.; Kudo, T. Basic Science of PET Imaging for Inflammatory Diseases. In PET/CT for Inflammatory Diseases. Springer, Singapore, 2019, 1-42.
(3)   Bar-Shalom, R.; Valdivia, A. Y.; Blaufox, M. D. PET Imaging in Oncology. *Semin. Nucl. Med.* **2000**, *30* (3), 150–185.
(4)   Das, C. J.; Razik, A.; Sharma, S. Positron Emission Tomography in Prostate Cancer: An Update on State of the Art. *Indian J. Urol.* **2018**, *34* (3), 172–179.
(5)   Van de Wiele, C.; Ustmert, S.; De Spiegeleer, B.; De Jonghe, P.-J.; Sathekge, M.; Alex, M. Apoptosis Imaging in Oncology by Means of Positron Emission Tomography: A Review. *Int. J. Mol. Sci.* **2021**, *22* (5), 2753.
(6)   Cecchin, D.; Garibotto, V.; Law, I.; Goffin, K. PET Imaging in Neurodegeneration and Neuro-Oncology: Variants and Pitfalls. *Semin. Nucl. Med.* **2021**, *51* (5), 408–418.

(7)   Wei, W.; Rosenkrans, Z. T.; Liu, J.; Huang, G.; Luo, Q.-Y.; Cai, W. ImmunoPET: Concept, Design, and Applications. *Chem. Rev.* **2020**, *120* (8), 3787–3851.

(8)   Mestel, R. Cancer: Imaging with Antibodies. *Nature* **2017**, *543* (7647), 743–746.

(9)   Knowles, S. M.; Wu, A. M. Advances in Immuno–Positron Emission Tomography: Antibodies for Molecular Imaging in Oncology. *J. Clin. Oncol.* **2012**, *30* (31), 3884–3892.

(10)   Jauw, Y. W. S.; Menke-van der Houven van Oordt, C. W.; Hoekstra, O. S.; Hendrikse, N. H.; Vugts, D. J.; Zijlstra, J. M.; Huisman, M. C.; van Dongen, G. A. M. S. Immuno-Positron Emission Tomography with Zirconium-89-Labeled Monoclonal Antibodies in Oncology: What Can We Learn from Initial Clinical Trials? *Front. Pharmacol.* **2016**, *7*, 131.

(11)   Bhatt, N. B.; Pandya, D. N.; Wadas, T. J. Recent Advances in Zirconium-89 Chelator Development. *Molecules* **2018**, *23* (3), 638.

(12)   Zhang, Y.; Hong, H.; Cai, W. PET Tracers Based on Zirconium-89. *Curr. Radiopharm.* **2011**, *4* (2), 131–139.

(13)   Yoon, J.-K.; Park, B.-N.; Ryu, E.-K.; An, Y.-S.; Lee, S.-J. Current Perspectives on 89Zr-PET Imaging. *Int. J. Mol. Sci.* **2020**, *21* (12), 4309.

(14)   Price, E. W.; Orvig, C. Matching Chelators to Radiometals for Radiopharmaceuticals. *Chem. Soc. Rev.* **2014**, *43* (1), 260–290.

(15)   Feiner, I. V. J.; Brandt, M.; Cowell, J.; Demuth, T.; Vugts, D.; Gasser, G.; Mindt, T. L. The Race for Hydroxamate-Based Zirconium-89 Chelators. *Cancers* **2021**, *13* (17), 4466.

(16)   Sarbisheh, E. K.; Salih, A. K.; Raheem, S. J.; Lewis, J. S.; Price, E. W. A High-Denticity Chelator Based on Desferrioxamine for Enhanced Coordination of Zirconium-89. *Inorg. Chem.* **2020**, *59* (16), 11715–11727.

(17)   Patra, M.; Bauman, A.; Mari, C.; Fischer, C. A.; Blacque, O.; Häussinger, D.; Gasser, G.; Mindt, T. L. An Octadentate Bifunctional Chelating Agent for the Development of Stable Zirconium-89 Based Molecular Imaging Probes. *Chem. Commun.* **2014**, *50* (78), 11523–11525.

(18)   Deri, M. A.; Ponnala, S.; Zeglis, B. M.; Pohl, G.; Dannenberg, J. J.; Lewis, J. S.; Francesconi, L. C. Alternative Chelator for 89Zr Radiopharmaceuticals: Radiolabeling and Evaluation of 3,4,3-(LI-1,2-HOPO). *J. Med. Chem.* **2014**, *57* (11), 4849–4860.

(19)   Summers, K. L.; Sarbisheh, E. K.; Zimmerling, A.; Cotelesage, J. J. H.; Pickering, I. J.; George, G. N.; Price, E. W. Structural Characterization of the Solution Chemistry of Zirconium(IV) Desferrioxamine: A Coordination Sphere Completed by Hydroxides. *Inorg. Chem.* **2020**, *59* (23), 17443–17452.

(20)   Ulaner, G. A.; Hyman, D. M.; Lyashchenko, S. K.; Lewis, J. S.; Carrasquillo, J. A. 89Zr-Trastuzumab PET/CT for Detection of HER2-Positive Metastases in Patients with HER2-Negative Primary Breast Cancer. *Clin. Nucl. Med.* **2017**, *42* (12), 912–917.

(21)   Pandit-Taskar, N.; O'Donoghue, J. A.; Ruan, S.; Lyashchenko, S. K.; Carrasquillo, J. A.; Heller, G.; Martinez, D. F.; Cheal, S. M.; Lewis, J. S.; Fleisher, M.; Keppler, J. S.; Reiter, R. E.; Wu, A. M.; Weber, W. A.; Scher, H. I.; Larson, S. M.; Morris, M. J. First-in-Human Imaging with 89Zr-Df-IAB2M Anti-PSMA Minibody in Patients with Metastatic Prostate Cancer: Pharmacokinetics, Biodistribution, Dosimetry, and Lesion Uptake. *J. Nucl. Med.* **2016**, *57* (12), 1858–1864.

(22)   Pandit-Taskar, N.; O'Donoghue, J. A.; Durack, J. C.; Lyashchenko, S. K.; Cheal, S. M.; Beylergil, V.; Lefkowitz, R. A.; Carrasquillo, J. A.; Martinez, D. F.; Fung, A. M.; Solomon, S. B.; Gönen, M.; Heller, G.; Loda, M.; Nanus, D. M.; Tagawa, S. T.; Feldman,

J. L.; Osborne, J. R.; Lewis, J. S.; Reuter, V. E.; Weber, W. A.; Bander, N. H.; Scher, H. I.; Larson, S. M.; Morris, M. J. A Phase I/II Study for Analytic Validation of 89Zr-J591 ImmunoPET as a Molecular Imaging Agent for Metastatic Prostate Cancer. *Clin. Cancer Res.* **2015**, *21* (23), 5277–5285.

(23) Briand, M.; Aulsebrook, M. L.; Mindt, T. L.; Gasser, G. A Solid Phase-Assisted Approach for the Facile Synthesis of a Highly Water-Soluble Zirconium-89 Chelator for Radiopharmaceutical Development. *Dalton Trans.* **2017**, *46* (47), 16387–16389.

(24) Vugts, D. J.; Klaver, C.; Sewing, C.; Poot, A. J.; Adamzek, K.; Huegli, S.; Mari, C.; Visser, G. W. M.; Valverde, I. E.; Gasser, G.; Mindt, T. L.; van Dongen, G. A. M. S. Comparison of the Octadentate Bifunctional Chelator DFO*-PPhe-NCS and the Clinically Used Hexadentate Bifunctional Chelator DFO-PPhe-NCS for 89Zr-Immuno-PET. *Eur. J. Nucl. Med. Mol. Imaging* **2017**, *44* (2), 286–295.

(25) Deri, M. A.; Ponnala, S.; Kozlowski, P.; Burton-Pye, B. P.; Cicek, H. T.; Hu, C.; Lewis, J. S.; Francesconi, L. C. P-SCN-Bn-HOPO: A Superior Bifunctional Chelator for 89Zr ImmunoPET. *Bioconjug. Chem.* **2015**, *26* (12), 2579–2591.

(26) Sharma, S. K.; Glaser, J. M.; Edwards, K. J.; Khozeimeh Sarbisheh, E.; Salih, A. K.; Lewis, J. S.; Price, E. W. A Systematic Evaluation of Antibody Modification and 89Zr-Radiolabeling for Optimized Immuno-PET. *Bioconjug. Chem.* **2020**.

(27) Holland, J. P. Predicting the Thermodynamic Stability of Zirconium Radiotracers. *Inorg. Chem.* **2020**, *59* (3), 2070–2082.

(28) Vosjan, M. J. W. D.; Perk, L. R.; Visser, G. W. M.; Budde, M.; Jurek, P.; Kiefer, G. E.; van Dongen, G. A. M. S. Conjugation and Radiolabeling of Monoclonal Antibodies with Zirconium-89 for PET Imaging Using the Bifunctional Chelate p-Isothiocyanatobenzyl-Desferrioxamine. *Nat. Protoc.* **2010**, *5* (4), 739–743.

(29) Gudmundsdottir, A. V.; Paul, C. E.; Nitz, M. Stability Studies of Hydrazide and Hydroxylamine-Based Glycoconjugates in Aqueous Solution. *Carbohydr. Res.* **2009**, *344* (3), 278–284.

(30) Figueras, E.; Martins, A.; Borbély, A.; Le Joncour, V.; Cordella, P.; Perego, R.; Modena, D.; Pagani, P.; Esposito, S.; Auciello, G.; Frese, M.; Gallinari, P.; Laakkonen, P.; Steinkühler, C.; Sewald, N. Octreotide Conjugates for Tumor Targeting and Imaging. *Pharmaceutics* **2019**, *11* (5), 220.

(31) Summa, V.; Petrocchi, A.; Bonelli, F.; Crescenzi, B.; Donghi, M.; Ferrara, M.; Fiore, F.; Gardelli, C.; Gonzalez Paz, O.; Hazuda, D. J.; Jones, P.; Kinzel, O.; Laufer, R.; Monteagudo, E.; Muraglia, E.; Nizi, E.; Orvieto, F.; Pace, P.; Pescatore, G.; Scarpelli, R.; Stillmock, K.; Witmer, M. V.; Rowley, M. Discovery of Raltegravir, a Potent, Selective Orally Bioavailable HIV-Integrase Inhibitor for the Treatment of HIV-AIDS Infection. *J. Med. Chem.* **2008**, *51* (18), 5843–5855.

(32) Holland, J. P.; Sheh, Y.; Lewis, J. S. Standardized Methods for the Production of High Specific-Activity Zirconium-89. *Nucl. Med. Biol.* **2009**, *36* (7), 729–739.

(33) Alizadeh, E.; Behlol Ayaz Ahmed, K.; Raja Solomon, V.; Gaja, V.; Bernhard, W.; Makhlouf, A.; Gonzalez, C.; Barreto, K.; Casaco, A.; Geyer, C. R.; Fonge, H. 89Zr-Labeled Domain II-Specific ScFv-Fc ImmunoPET Probe for Imaging Epidermal Growth Factor Receptor In Vivo. *Cancers* **2021**, *13* (3), 560.

(34) Gaja, V.; Cawthray, J.; Geyer, C. R.; Fonge, H. Production and Semi-Automated Processing of 89Zr Using a Commercially Available TRASIS MiniAiO Module. *Molecules* **2020**, *25* (11), 2626.

(35)   Delley, B. From Molecules to Solids with the DMol3 Approach. *J. Chem. Phys.* **2000**, *113* (18), 7756–7764.

(36)   Delley, B. An All-electron Numerical Method for Solving the Local Density Functional for Polyatomic Molecules. *J. Chem. Phys.* **1990**, *92* (1), 508–517.

(37)   Perdew, null; Burke, null; Ernzerhof, null. Generalized Gradient Approximation Made Simple. *Phys. Rev. Lett.* **1996**, *77* (18), 3865–3868.

(38)   Peverati, R.; Truhlar, D. G. M11-L: A Local Density Functional That Provides Improved Accuracy for Electronic Structure Calculations in Chemistry and Physics. *J. Phys. Chem. Lett.* **2012**, *3* (1), 117–124.

(39)   Klamt, A.; Schüürmann, G. COSMO: A New Approach to Dielectric Screening in Solvents with Explicit Expressions for the Screening Energy and Its Gradient. *J. Chem. Soc., Perkin Trans. 2* **1993**, No. 5, 799–805.

(40)   Andzelm, J.; Kölmel, C.; Klamt, A. Incorporation of Solvent Effects into Density Functional Calculations of Molecular Energies and Geometries. *J. Chem. Phys.* **1995**, *103* (21), 9312–9320.

Chapter 4: Design, synthesis, and evaluation of DFO-Em: a highly soluble octadentate chelator for zirconium-89 radiochemistry

The content of chapter 4 is adapted from the manuscript that is currently under preparation (Salih, A. K.; Raheem, S. J.; Dominguez-Garcia, M.; Ahiahonu, W. K.; Price, E. W. manuscript under preparation)

4.1.   Author Contribution and Relation to the Research Objectives

This work was done in collaboration with Moralba Dominguez-Garcia (PhD candidate), Shvan J. Raheem (PhD candidate), William K. Ahiahonu (undergraduate student) and Dr. Price. I designed and synthesized the DFO-Em chelator in 9 steps (**13-21**) and performed the coordination reaction of DFO-Em with [^{Nat}Zr]Zr^{4+} (**22**). I also performed complete characterization of all the compounds (**13-22**). All the DFT calculations were done by Dr. Price, William K. Ahiahonu, and myself. I performed the radiolabeling studies, *in vitro* experiments, animal imaging and biodistribution studies with the help of Dr. Price, Moralba Dominguez-Garcia, and Shvan J. Raheem. Furthermore, I prepared the first draft of the manuscript and supporting information which was edited by Dr. Price.

In this project I designed an octadentate chelator (DFO-Em) to improve the stability of zirconium-89 complexes in their applications in immunoPET tracers. Although the DFO2 family offers a potential coordination number (CN) of up to 12 (dodecadentate), zirconium(IV) is known

to only utilize a maximum CN of 8 (octadentate). As such, we had interest in synthesizing an octadentate amino acid-based derivative of DFO2/DFO2K. A great focus in the design of this chelator was on increasing hydrophilicity of the chelator. Hydrophilicity in hydroxamate based chelators in general is greatly reduced by increasing denticity such as the example of original DFO (CN = 6) vs DFO* (CN = 8). Unfortunately, saturating the coordination sphere of metal ions is a proven way to maximize stability of their complexes with zirconium (IV), as demonstrated by the superior stability of DFO* over DFO. However, low water solubility (hydrophobicity) makes aqueous bioconjugation and radiolabeling procedures challenging. For this chelator I used a DFO molecule and a hydroxamate monomer with minimum number of carbon atoms. I combined the two molecules through the water-soluble amino acid glutamic acid, which is a modular design as used for DFO2K. After successful synthesis and characterization of DFO-Em, I assessed its complexation with zirconium by reacting it with ZrCl$_4$ (**22**) and characterization by HRMS and NMR spectroscopy.

For further evaluation of the chelator, I performed radiolabeling studies of DFO-Em with zirconium-89 and I used commercially available DFO as a reference in the study. Furthermore, I performed a series of *in vitro* stability experiments to obtain primary information on the stability of [^{89}Zr]Zr-DFO-Em. Finally, we carried out *in vivo* and *ex vivo* studies of the non-bifunctional DFO-Em and DFO in healthy mice to understand biodistribution of the intact zirconium-89 chelate complexes. The results revealed that our design in the new octadentate chelator was successful in improving the water solubility and stability in coordination with [^{89}Zr]Zr^{4+}.

4.2. Abstract

Zirconium-89 has quickly become a favorite radionuclide because it has a relatively long half-life that matches the biological half-life of most antibodies, suitable decay properties for positron emission tomography (PET), and efficient and affordable cyclotron production and purification. The "gold standard" chelator for $[^{89}Zr]Zr^{4+}$ is desferrioxamine B (DFO), and although it has been used both preclinically and clinically for immuno-PET with great success, it has revealed its sub-optimal stability *in vivo*. DFO can only bind to $[^{89}Zr]Zr^{4+}$ through its six available coordination sites made up by 3 hydroxamic acid (HA) moieties, which is not sufficient to saturate the coordination sphere (CN 7-8). In this study, we have designed, synthesized, and characterized a new octadentate chelator we have called DFO-Em, which is an improved derivative of our previously published dodecadentate chelator DFO2. This octadentate DFO-Em chelator is smaller than DFO2 but still satisfies the coordination sphere of zirconium-89 and forms a highly stable radiometal-chelator complex. DFO-Em was synthesized by tethering a hydroxamic acid monomer to commercially available DFO using glutamic acid as a linker, providing an octadentate chelator built on a modular amino acid-based synthesis platform. Radiolabeling performance and radiochemical stability of DFO-Em was assessed *in vitro* by serum stability, EDTA, and hydroxyapatite challenges. Furthermore, pharmacokinetics of $[^{89}Zr]Zr$-(DFO-Em) was measured *in vivo* by PET/CT imaging and *ex vivo* biodistribution and compared with $[^{89}Zr]Zr$-DFO. Additionally, the coordination of DFO-Em with Zr(IV) and its isomers were studied by using DFT calculations. The radiolabeling studies revealed DFO-Em has a comparable radiolabeling profile to the gold standard chelator DFO. The *in vitro* and *in vivo* stability evaluation showed that $[^{89}Zr]Zr$-(DFO-Em) was significantly more stable than $[^{89}Zr]Zr$-DFO and had improved pharmacokinetics in healthy mice with lower tissue retention. The DFT calculations also

confirmed that Zr-(DFO-Em) can adopt highly stable coordination geometries. We have synthesized and evaluated a new octadentate chelator and it's radiometal complex — DFO-Em and [^{89}Zr]Zr-(DFO-Em) — and have shown it to be a substantially improved chelator for zirconium-89 relative to DFO. Further, DFO-Em has potential to coordinate other large and oxophilic radiometals for other clinical applications including theranostics.

4.3. Introduction

The radionuclide zirconium-89 has gained significant attraction in the field of nuclear medicine for its applications in immuno-positron emission tomography (immunoPET) and radiolabeling nanomaterials. The synergy of highly target- specific antibodies with the high sensitivity of PET has led to a plethora of highly potent zirconium-89 labeled monoclonal antibodies used both preclinically and clinically [1–8]. Owing to zirconium-89's relatively long physical half-life ($t_{1/2}$ =3.3 days) which matches well with the biological half-life of most antibodies, zirconium-89 immunoconjugates can circulate and accumulate in targeted tissues such as tumors (1-4 days) while retaining sufficient radioactivity to produce useful PET images. Zirconium-89 also emits relatively low energy positrons ($E_{\beta^+(mean)}$ = 396 keV, E_{max} = 897 keV), allowing it to provide PET images with good spatial resolution [9,10]. Other desired properties of zirconium-89 include easy production and low cost [11]. However, the application of zirconium-89 in immunoPET tracers requires a bifunctional chelator to enable conjugation to the antibody, where the [^{89}Zr]Zr-chelate complex is covalently linked to the antibody. An unstable [^{89}Zr]Zr-chelate complex will result in zirconium-89 released into the body, which typically leads to undesired uptake in healthy tissues. This instability results in poor target-to-background ratios, poor contrast, and ultimately PET imaging of little to no diagnostic utility. The most used chelator

for zirconium-89- associated immunoPET tracers is Desferrioxamine B (DFO), which is not without some stability concerns [1].

DFO coordinates with zirconium-89 (metal) ions through 6 oxygen atoms from its 3 hydroxamic acid/hydroxamate bidentate groups, which is insufficient to satisfy the coordination sphere of the zirconium(IV) ion (CN 7-8) [12,13]. This unsaturated Zr(DFO) coordination sphere facilitates intrusion of endogenous ligands and ions such as chloride, phosphate, water (hydroxide), and proteins into the inner coordination sphere. We recently hypothesized that two hydroxide ligands complete the coordination sphere and form Zr-(DFO)(OH)$_2$ [12]. This phenomenon is speculated as the reason for the release of $[^{89}Zr]Zr^{+4}$ and bone uptake in preclinical $[^{89}Zr]Zr$-DFO-antibody studies in rodents [14,15]. Although the same level of bone uptake has not been reported when $[^{89}Zr]Zr$-immunoPET imaging is used in human studies [7,16–18], chelators with improved stability are desirable because non-specific accumulation of radioactive $[^{89}Zr]Zr^{+4}$ can damage healthy tissues and reduce the image contrast by increasing background activity.

To improve *in vivo* stability of zirconium-89 based radiopharmaceuticals, several new chelators such as DFO*, 4,3-(LI-1,2-HOPO), and DFO2 have been published in recent years with the potential of saturating the coordination sphere of zirconium-89 [15,19–25]. We have previously demonstrated that further expanding the coordination number to 12 donor oxygens in DFO2 also greatly improves zirconium-89 complex stability relative to DFO, even though Zr(IV) can only utilize 8 donor oxygen atoms at one time. Although the high denticity (dodecadentate) of DFO2 might uniquely position it to form highly stable complexes with larger radiometals such as lanthanides and actinides [15], there is a paucity of evidence showing whether they provide improved stability with zirconium-89 relative to octadentate chelators. Furthermore, DFO* and DFO2 which

have been shown to form more stable complexes than DFO (**Figure 4-1**) by the addition of more

hydroxamate groups to saturate the coordination sphere of zirconium-89, are found to be less water

soluble [15,20], thus making aqueous bioconjugation and radiolabeling procedures challenging.
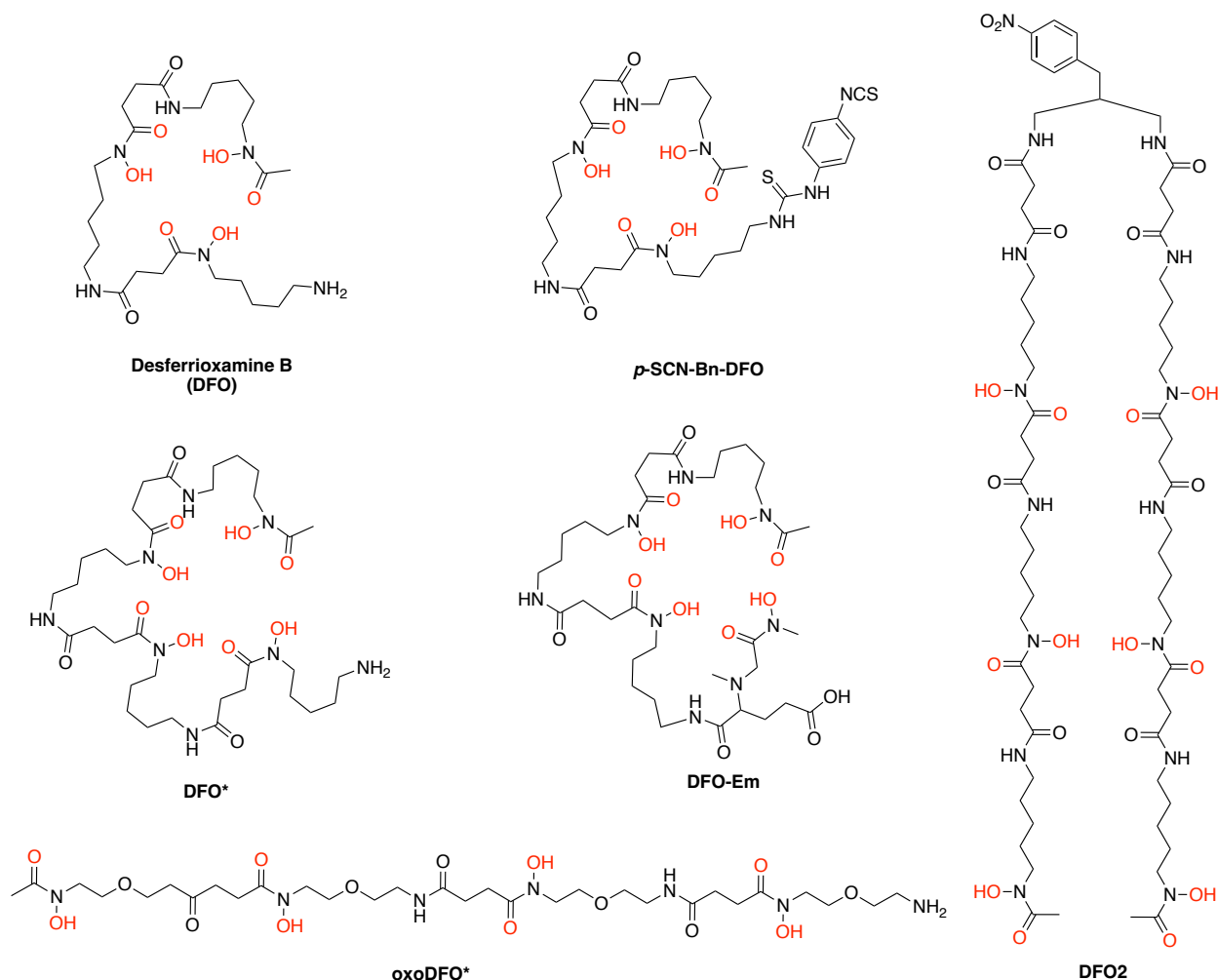
Figure 4-1. Chemical structures of a group of recently reported zirconium-89 desferrioxamine (DFO) based chelators, including *p*-SCN-Ph-DFO, DFO*, oxoDFO*, DFO2 and DFO-Em.

To overcome the limitations of existing chelators for zirconium-89, we have strategically

designed and synthesized a derivative of DFO that is inspired by DFO2 but is octadentate with

improved water solubility, which we have named DFO-Em (DFO-glutamic acid-monomer). Our

Improved chelator DFO-Em utilizes a single DFO molecule tethered to a hydroxamate monomer

by the amino acid glutamic acid. Additionally, glutamic acid serves as a pre-bifunctional linker

that can be later used for bifunctionalization and protein conjugation. Furthermore, glutamic acid can potentially be replaced by any other natural or unnatural amino acid to access different functional groups for bioconjugation while retaining an identical metal ion coordination sphere, making this chelator design modular and versatile.

In this chapter, we present the synthesis, radiolabelling, and *in vitro* stability evaluation of DFO-Em by using different radiochemical assays with zirconium-89. In addition, we implemented a detailed density functional theory (DFT) study of the different possible geometric isomers of Zr-(DFO-Em) in a similar manner to our recent study of Zr-DFO [12]. These calculations focus on the 16 possible lambda (Λ) geometric isomers that Zr^{4+} can form with the four hydroxamic acid moieties from DFO-Em. We believe that also calculating the 16 possible delta (Δ) isomers would have been largely redundant and taken a very long time to complete. We compared the relative total energies of these 16 Λ- geometric isomers to gain a better understanding of the inner coordination sphere and to gain a rough idea of the energy differences between them and what the most stable isomers could be. Finally, we performed dynamic PET/CT imaging in healthy mice, followed by *ex vivo* biodistribution to compare the *in vivo* behavior of [89Zr]Zr-DFO and [89Zr]Zr-(DFO-Em) as "free" unconjugated chelators.

4.4. Results and Discussion

It is well-known that expanding the coordination sphere of DFO from 6 donor oxygens (3 hydroxamates) to 8 donor oxygens (4 hydroxamates) and 12 donor oxygens (6 hydroxamates) is a successful strategy to saturate the coordination sphere and improve the stability of zirconium-89 complexes as seen in DFO* and DFO2 [15,20]. Concurrently, these larger hydroxamic acid-based chelators such as DFO* and DFO2 have decreased water solubility. We set out to synthesize an

octadentate derivative of DFO2 where one DFO chain is replaced by a hydroxamic acid (HA) monomer, and the hydrophobic phenyl-based linker is replaced by an amino acid (glutamic acid). We have called this chelator DFO-Em, as it is comprised of DFO, glutamic acid (E) as a linker, and an HA monomer (m).

Synthesis and characterization. This first required a synthetic route to a hydroxamic acid (HA) monomer with suitable chemistry to connect with glutamic acid or other amino acids. After attempting several possible routes, we found a robust synthesis to obtain a HA monomer in 4 steps with high overall yield, starting from O-benzyl protected hydroxyl amine (**Scheme 4-1**). A protecting group, *tert*-butyloxycarbonyl (Boc) group was then added to the amine to form compound **13**, before methylation by using iodomethane to form compound **14**. In the next step the Boc group was removed under acidic conditions to form **15**, which was reacted with bromoacetyl bromide to obtain the completed HA monomer **16** (**Scheme 4-1**). Following the synthesis of the monomer, it was reacted with the primary amine of a dicarboxylic acid protected glutamic acid to form **17**. Next, the secondary amine was methylated (**18**) to prevent interference with the following amide formation reactions. After removal of the *tert*-butyl protecting group from the C-terminus of glutamic acid using trifluoroacetic acid (TFA) to form compound **19**, it was coupled via amide bond with commercially available DFO mesylate . For this reaction, different activating agents were tested, such as HATU, HBTU and Oxyma/EDC. One equivalent each of Oxyma/EDC produced the highest yield for **20**. Finally, the benzyl protecting groups were removed by hydrogenolysis reaction using 10% palladium on carbon as a catalyst to obtain the final chelator DFO-Em in 8 synthetic steps with a cumulative yield of ~24% (**Scheme 4-1**).
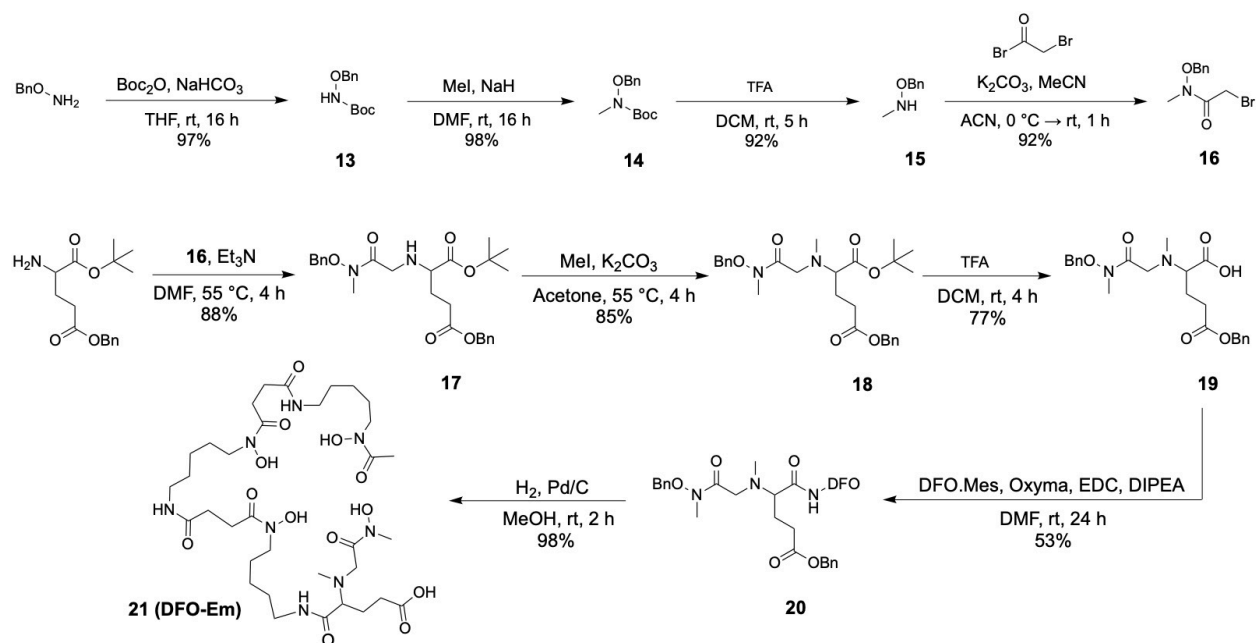
Scheme 4-1. Synthesis of DFO-Em (**21**) from hydroxamic acid monomer (**16**) and commercially available DFO, utilizing the amino acid glutamic acid as a modular and pre-bifunctional linker.

After synthesis and characterization of DFO-Em, its coordination with Zr^{4+} was examined with non-radioactive "cold" zirconium ($^{Nat}Zr^{4+}$). Following a previously published procedure [15], DFO-Em was reacted with $ZrCl_4$ at ambient temperature and neutral pH, in UltraPure water (18.2 mΩ, Millipore), without using any organic solvents such as DMSO or DMF. Formation of ^{Nat}Zr-(DFO-Em) was confirmed with high-resolution mass spectrometry and characterized with ^1H and ^{13}C NMR spectroscopy. It's worth mentioning that during the reverse-phase- (RP) -HPLC purification of DFO-Em, a small peak appear before the main DFO-Em peak at ~8 min (t_R= 8 min and 12 min, respectively). The LCMS shows a corresponding mass of 815.7 for the unknown peak compared to 791.4 for the mass of DFO-Em. The unknown peak could be due to complexation of DFO-Em with traces of ions such as Na^{+1} or Mg^{2+} in the elution solvents. However, when DFO-Em is reacted with $ZrCl_4$, the unknown peak disappeared completely, presumably displacing the

unknown coordinated ion, and only one RP-HPLC peak is observed (t_R = 10 min) which corresponds to the mass of Zr-(DFO-Em) of 877.3 amu.

Denisty functional theory modeling. X-ray crystallography has for a long time been the primary technique used to understand the coordination sphere of metal-ligand complexes, which is not only important to comprehend the shortcomings of the available chelators, but also useful to design and match new chelators for desireable metals. However, obtaining X-ray crystallography quality crystals is challenging especially for zirconium complexes with hydroxamate-based chelators. As an alternative to X-ray crystallography, density functional theory (DFT) calculations are frequently used as an *in silico* method for studying the coordination spheres of metal-chelate complexes. Many DFT calculation studies have been performed for Zr-chelator complexes such as Zr-DFO, Zr-DFO2, and Zr-DFO*, and Zr-O bond lengths have been estimated [12,15,20,26]. These DFT calculated Zr-O bond lengths are generally ~0.05 A longer than the average of previously reported crystal structures of 8-coordinated Zr(IV) [12,15,20,27]. Since DFO-Em possesses 8 oxygen donor groups similar to other HA-based octadendate chelators such as Zr-DFO*, we did not focus on the calculated Zr-O bond length from our DFT calculation but rather focused on total energy. DFT calculations can also assists in predicting the most stable geometric isomers of Zr-chelator complexes by comparing the total energies of each geometric isomer and finding the lowest possible energy configuration [12,15,28]. The total energy is related to the number of atoms in the structure, therefore each of the 16 calculated Zr-(DFO-Em) isomers contained identical numbers and types of atoms. One advantage of DFT over X-ray crystallography is that it can include solvent such as water in the calculation and provides assistance in modeling spatial orientation of the metal-chelator complexes in solution. This could help to recognize the most stable arrangements of the chelators around the metal ions *in vivo* (water), compared with the solid-state structures

obtained from X-ray crystallography. It is predicted that Zr-DFO can form 16 possible geometric and optical isomers [28]. However, there are no studies showing geometric and optical isomers for Zr-ocatdentate chelate complexes. Herein we have calculated 16 geometric isomers, which should account for all of the possible Λ- enantiomers of Zr-(DFO-Em). The lambda isomers are optically active, which means there are also 16 possible Δ-enantiomers (not calculated). All of the Λ-isomers have been calculated with Materials Studio (DMOL3) and their energies are compared to estimate the energy differences between isomers and suggest which are the most stable isomers (**Figure 4-2** and **4-3**). Given that these are very large and complicated structures with many possible orientations, the energy values must be considered approximate. Even if the arrangement of the four HA chelating moieties in DFO-Em are bound to Zr(IV) remain fixed, other parts of the chelate complex can move and change configuration, which could lead to multiple results for the same geometric isomer and different energy values. As such, we present these results as an interesting discussion but without firm conclusions, and we present a useful graphical depictions of each geometric isomer (**Figures 4-2** and **4-3**).

Previous studies of both the solid-state X-ray crystal structure and the DFT calculated structure of Zr-(MeAHA)$_4$ suggest the most stable arrangement of hydroxamic acid (HA) coordination is the cis, cis, trans, trans arrangement [13,27]. This compound contains 4 individual HA monomers (MeAHA) and therefore no serious steric barriers restricting its conformation; however, DFO and derivatives such as DFO-Em possess far greater restrictions in their binding because each HA moiety is covalently linked in a linear chain. The three lowest energy isomers calculated for Zr-(DFO-Em) were the Λ-C-trans, trans, cis isomer (**Figure 4-2**, **A**), followed closely by the Λ-C-cis, cis, cis (**B**) and Λ-C-trans, cis, trans (**C**) isomers which were only ~4-5 kJ/mol higher in energy. To explain our naming convention, these compounds can form both lambda and delta

isomers (left and right handed), and because the 4 HA moeities are linked together covalently and the molecule does not contain inherent symmetry, each HA is distinct. Therefore, we start our naming by defining HA-1 as the synthetic HA monomer and end with HA-4 as the terminal HA in the DFO molecule. As such, we assign HA-1 as having either the carbon (C-) or the nitrogen (N-) in the back, and assign each subsequent HA as either cis or trans relative to the first HA. Using this naming convention, the isomer most similar to the most stable Zr-(MeAHA)$_4$ isomer (cis-cis-trans-trans) is the Λ-*C*-trans, cis, trans (**C**) isomer. Following the 3 most stable isomers which are similar in energy, the next most stable isomer was the most stable of the *N*-isomers, Λ-*N*-trans, cis, trans (**Figure 4-3**, **I**), which was a little over 20 kJ/mol higher in energy than the most stable *C*-isomer. The highest energy isomer was nearly 70 kJ/mol higher than the most stable isomer. It is generally accepted that a calculated energy difference of ~20-30 kJ/mol is consider significant enough that interconversion is not likely at ambient temperature. There is a possibility that the 3 most stable isomers (**Figure 4-2**, **A/B/C**) could interconvert at ambient temperature because they are all within 5-6 kJ/mol; however, it might be that the exchange energy for first de-coordinating a HA moeity from Zr(V) is too high for interconversion to be possible for any isomers at ambiemt temperature. Interestingly, both Zr-(DFO-Em) isomers **A** and **C** contain two cis and two trans oriented HA groups, with isomer **A** having them positioned cis-trans-cis-trans, and isomer **C** having them positioned cis-cis-trans-trans, which is the same orientation found to be most stable for Zr-(MeAHA)$_4$ [13,27].
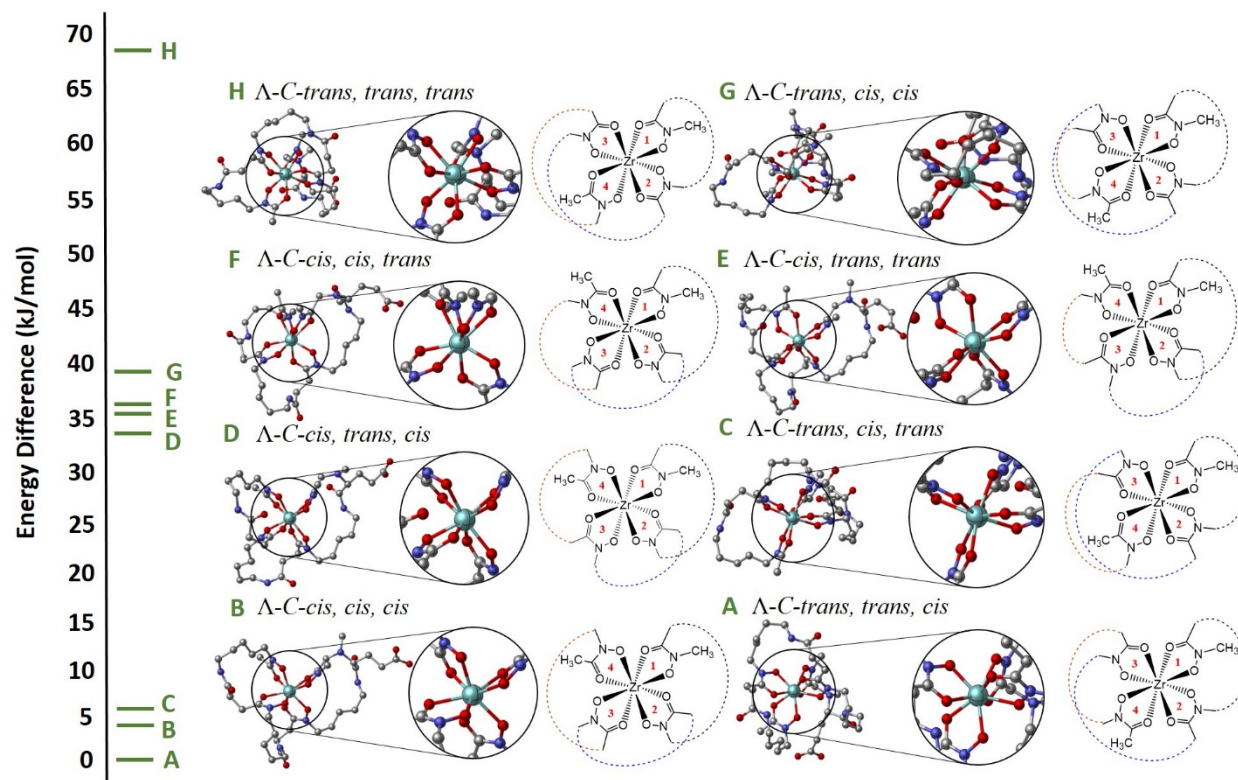
Figure 4-2. Optimized structures of geometric isomers of Zr-(DFO-Em), showing the 8 possible Λ-*C*-isomers of complexes with their relative energy differences, with the most stable geometric isomer of all 16 (C- and N-, **Figures 4-2** and **4-3**) set as a reference of 0 kJ/mol. Hydrogen atoms are present and included for calculation but excluded from the graphic for clarity.
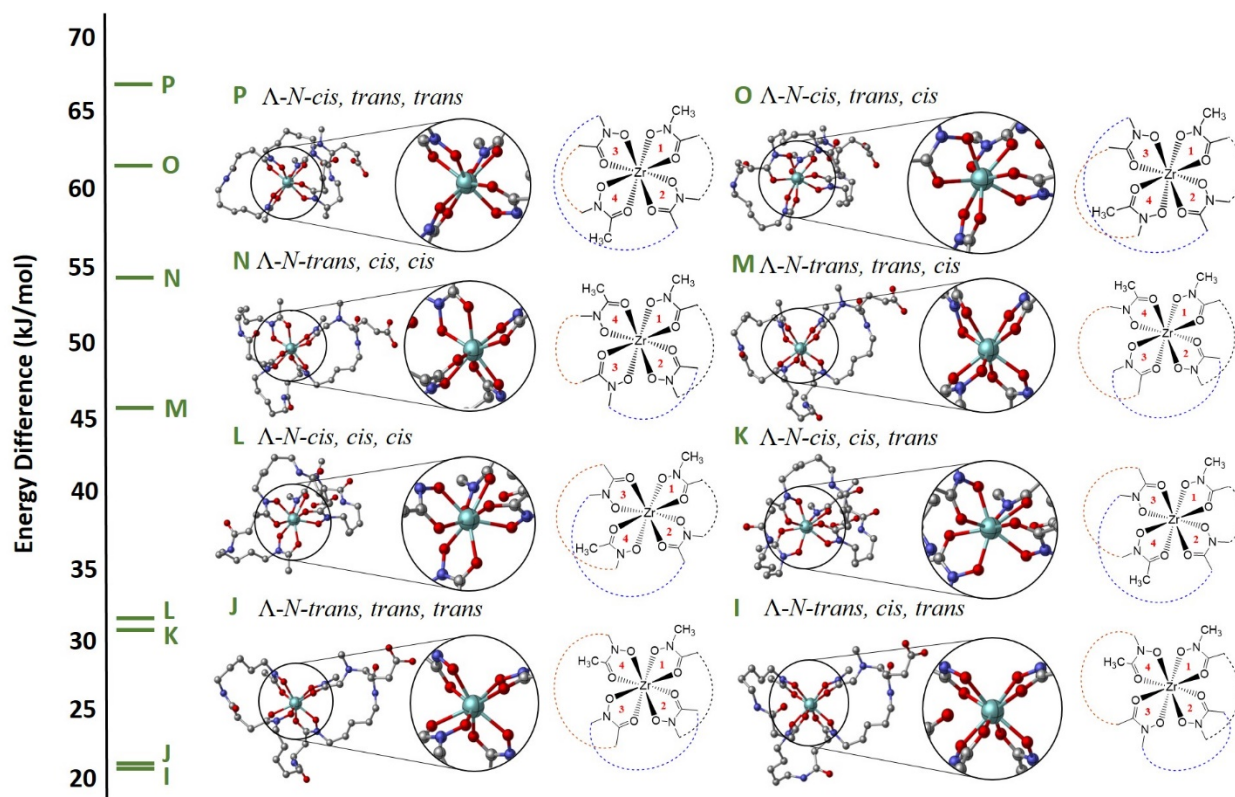
Figure 4-3. Optimized structures of geometric isomers of Zr-(DFO-Em), showing the 8 possible Λ-*N*-isomers of complexes with their relative energy differences, with the most stable geometric isomer of all 16 (C- and N-, **Figures 4-2** and **4-3**) set as a reference of 0 kJ/mol. Hydrogen atoms are present and included for calculation but excluded from the graphic for clarity.

Zirconium-89 radiochemistry. After synthesizing and characterizing DFO-Em and its $^{Nat}Zr^{4+}$ complex, we proceeded to determine its radiolabeling performance and radiochemical stability. Radiolabeling experiments revealed similar metal ion coordination kinetics of DFO-Em to DFO, where both quantitatively radiolabel with zirconium-89 under conditions of ~10 MBq $[^{89}Zr]Zr^{4+}$ and 0.5 nmol of chelator in only 5-10 minutes at ambient temperature (HEPES buffer, pH 7, **Figure 4-4**). However, radiolabeling yields started to drop when lower concentration of chelator (0.05 and 0.005 nmol) was used (**Figure 4-5A**). These experiments show that the addition of one more hydroxamate unit does not significantly affect the radiolabeling properties of the chelators, as the

same approximate radiolabeling kinetics and apparent molar activities were achieved. We observed similar results with zirconium-89 and the potentially dodecadentate chelator DFO2 [15].

Octanol-water partition coefficient (log$D$) experiments were performed with the zirconium-89 complexes, which revealed that [^{89}Zr]Zr-(DFO-Em) is more polar and has improved water solubility relative to [^{89}Zr]Zr-DFO (log$D$ = -3.29, -3.04 respectively). This was qualitatively observed during the stock solution preparations as DFO-Em was completely soluble in water without requiring heat, sonication, or organic solvents. Hydroxamate based chelators such as DFO and higher denticity derivatives often face low water solubility issues which could be partly because of intramolecular hydrogen bonding. During stock solution preparation of many zirconium chelators such as p-SCN-Ph-DFO, a small amount of organic solvent such DMF or DMSO is required, which is not desired during antibody/protein conjugations.
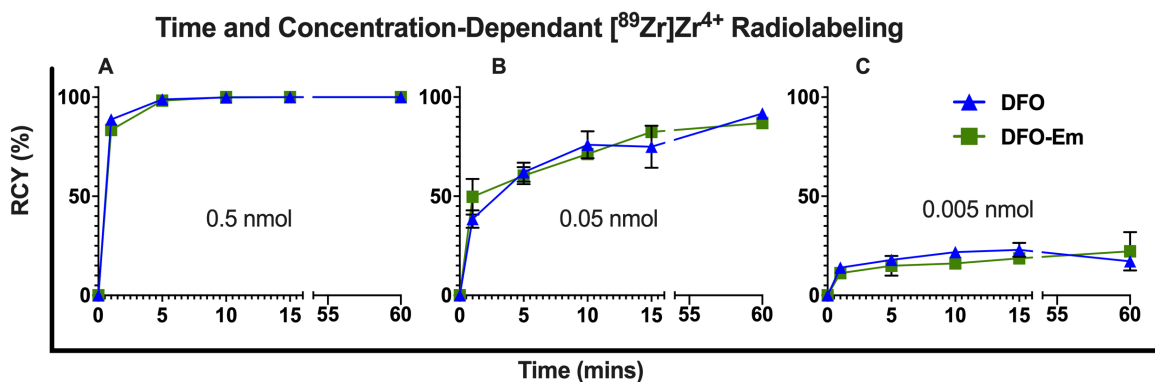
Figure 4-4. Time dependent radiolabeling study with ~10 MBq of [^{89}Zr]Zr^{4+} per reaction and DFO or DFO-Em with (A) 0.5 nmol, (B) 0.05 nmol, and (C) 0.005 nmol of the chelators in HEPES buffer at pH 7.0 and ambient temperature. The total volume of all reactions were 250 μL.

After determining the excellent radiolabeling properties of DFO-Em with zirconium-89, we performed a battery of *in vitro* radiochemical stability assays to compare the new [^{89}Zr]Zr-(DFO-Em) with the "gold-standard" [^{89}Zr]Zr-DFO. For stability assays, both DFO and DFO-Em were

radiolabeled quantitatively (>99% RCY) with $[^{89}Zr]Zr^{4+}$ and used without purification. Aliquots of $[^{89}Zr]Zr$-DFO and $[^{89}Zr]Zr$-(DFO-Em) were mixed with human blood serum and their stability was monitored over 10 days by radio-iTLC using EDTA (50 mM, pH 5.5) as mobile phase. Although human blood serum is known to have mild effects on the stability of zirconium-89 complexes, most radiopharmaceuticals are injected intravenously. As such, this assay is still commonly used to confirm blood stability of radiometal-chelates to assess their resistance to transchelation by blood proteins. Results for the human blood serum assay showed that $[^{89}Zr]Zr$-(DFO-Em) was 97.5% ± 1% stable after 10 days, effectively equivalent to $[^{89}Zr]Zr$-DFO (96.4%
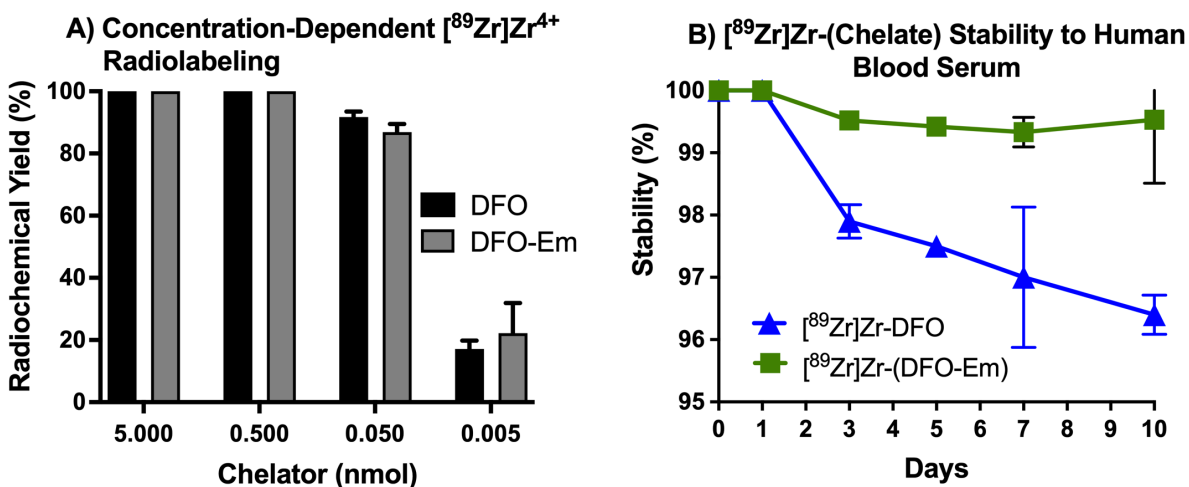
± 0.5%) (**Figure 4-5B**).

Figure 4-5. Results of radiolabeling and stability experiments for $[^{89}Zr]Zr$-DFO and $[^{89}Zr]Zr$-(DFO-Em). (A) Concentration-dependent radiolabeling study at ambient temperature and pH 7 (*n* = 3), and (B) stability challenge against human blood serum over 10 days evaluated by radio-iTLC (*n* = 3).

Studies in mice have shown that free $[^{89}Zr]Zr^{4+}$ tends to accumulate in bones and joints due to its osteophilic nature [14], and it is even possible that some intact radiometal-chelate complexes could adsorb to bone. We previously developed a hydroxyapatite (HTP) stability assay using a HTP resin (BioRad) as a high-surface area surrogate for bone, as HTP is the major component of bone structure [15]. For this stability challenge, aliquots of $[^{89}Zr]Zr$-DFO and $[^{89}Zr]Zr$-(DFO-Em)

were added to hydroxyapatite resin (BioRad biogel HTP) in HEPES buffer (0.5 M, pH 7.0). After incubation with shaking for 24 hours, the microcentrifuge tubes were centrifuged to pellet the HTP resin, and the supernatant was decanted via pipet (with rinsing steps). The ratio of zirconium-89 between the hydroxyapatite and the supernatant was measured, with the percentage remaining in the supernatant assumed to be intact [^{89}Zr]Zr-chelate. In this assay, two sets were run with different amounts of hydroxyapatite used (40 and 60 mg). The results show that even at 60 mg hydroxyapatite, after 24 hours the [^{89}Zr]Zr-(DFO-Em) was 92% ± 0.6% stable while [^{89}Zr]Zr-DFO was only 60% ± 1% (**Figure 4-6A**). Neutralized [^{89}Zr]Zr-oxalate was used as a control, and when incubated with 60 mg of hydroxyapatite, only ~ 3% remained in the supernatant (**Figure 4-6A**).

Challenging new radiometal-chelate complexes against a large molar excess of other known chelators is a common transchelation stability evaluation method. For this purpose, we chose EDTA, which is a hexadentate chelator that forms complexes with a wide range of metal ions. We previously have used 100-fold molar excess of EDTA, but increased to 1000-fold molar excess for this study [15,29]. We added aliquots of [^{89}Zr]Zr-DFO and [^{89}Zr]Zr-(DFO-Em) to 1000 molar excess of EDTA solution in ammonium acetate buffer (pH 7). The mixtures were incubated with shaking and the stability of the complexes were determined over 10 days by using radio-iTLC. The results showed a significant difference in stability between the two complexes. [^{89}Zr]Zr-DFO was only 32% ± 4% stable after 10 days, while [^{89}Zr]Zr-(DFO-Em) was 98% ± 0.3% intact (**Figure 4-6B**).
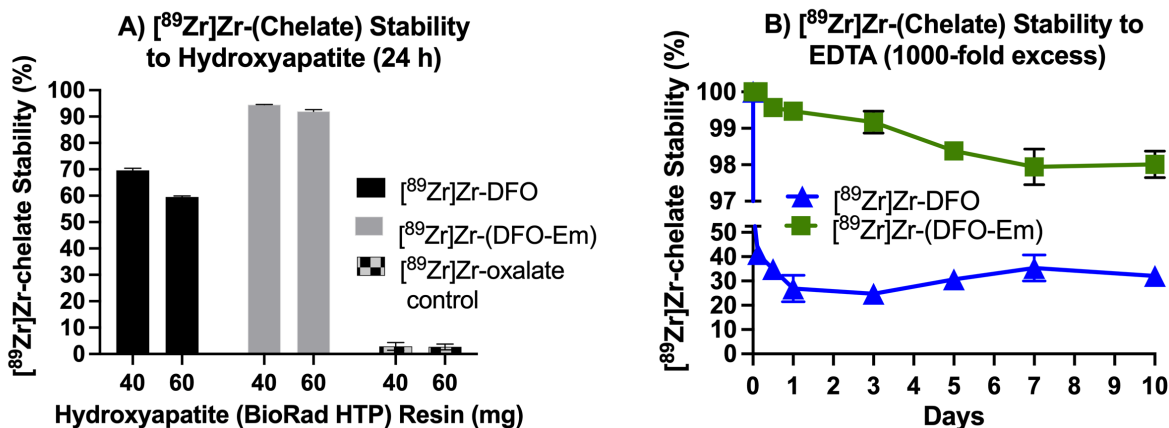
Figure 4-6. Results of *in vitro* stability assays (*n* = 3) comparing [⁸⁹Zr]Zr-DFO and [⁸⁹Zr]Zr-(DFO-Em) against (A) 40 mg and 60 mg hydroxyapatite (HTP, BioRad Bio-Gel, HEPES 0.5 M, pH 7, 37 C) after 24 h, and (B) against 1000–fold molar excess EDTA over 10 days (ammonium acetate 0.25 M, pH 7, 37 C), monitored by radio-iTLC.

Evaluation in healthy mice. Although zirconium-89 chelate complexes are typically used as conjugates with biovectors such as antibodies, the intact chelate complex could be cleaved from the biovector *in vivo*. Although it is known that "free" zirconium-89 (including neutralized [⁸⁹Zr]Zr-oxalate) localizes largely in the bones/joints and kidneys, it is also useful to understand the biodistribution of the intact zirconium-89 chelate complexes. To study the behavior of the DFO and DFO-Em complexes with zirconium-89, around 5 MBq (200 µL, in saline) was injected into healthy female BALB/c mice (*n* = 4 per cohort). Dynamic-PET/CT images were collected from time zero by injecting the four mice in the scanner, simultaneously, via tail vein catheter. The images show that in less than an hour the complexes are mostly cleared through the renal system and urine, with some activity remaining in the kidneys and bladder (**Figure 4-7**). Similarly, *ex vivo* biodistribution was performed 24 hr post injection and showed nearly complete clearance of the complexes with little residual activity. Moreover, [⁸⁹Zr]Zr-(DFO-Em) had the faster clearance compared to [⁸⁹Zr]Zr-DFO in all the organs except the digestive organs, which are not known to uptake these types of complexes. A reasonable explanation for the high uptake of [⁸⁹Zr]Zr-(DFO-Em) in digestive organs is that the mice quickly excreted the radioactivity in their cages following

imaging (urine), and the cage bedding was not changed to remove the contaminated bedding. Likely some of this activity was ingested by the mice through grooming and/or eating, resulting in digestive system uptake. Residual activity of $[^{89}Zr]Zr$-(DFO-Em) was notably lower than $[^{89}Zr]Zr$-DFO in the liver, spleen, kidneys, lungs, muscle, pancreas, skin, and fat. PET/CT images of $[^{89}Zr]Zr$-DFO are unfortunately not available due to a scanner error, but the more critical 24 hr biodistribution data were collected and are shown in **Figure 4-8**.
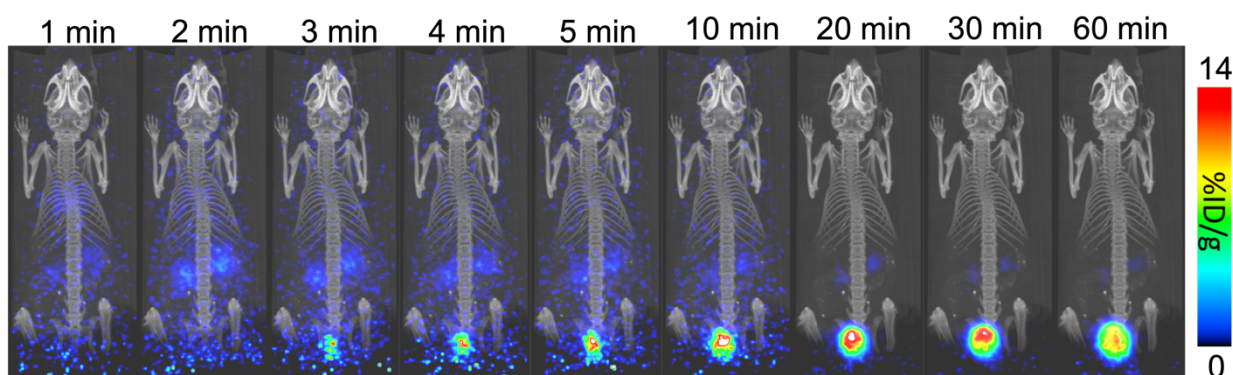
Figure 4-7. Results of 1 hour dynamic PET-CT imaging of $[^{89}Zr]Zr$-(DFO-Em), following injection of 5 MBq (200 μL, in saline) in healthy female BALB/c mice (n = 4), showing maximum intensity projection (MIP) views at a selection of timepoints.

Activated esters are commonly used for bifunctionalization of compounds with carboxylic acid functionality for bioconjugation through amide bond formation.[22] To synthesize the bifunctional version of DFO-Em (DFO-Em-NHS), I reacted DFO-Em with *N*-hydroxysuccinimide in presence of EDC and monitored the reaction using LC-MS. The LC-MS results showed that the major product was the intramolecular cyclization form reaction between the nucleophilic hydroxyl groups of the hydroxamic acids and highly electrophilic NHS ester to form the undesired cyclized product.
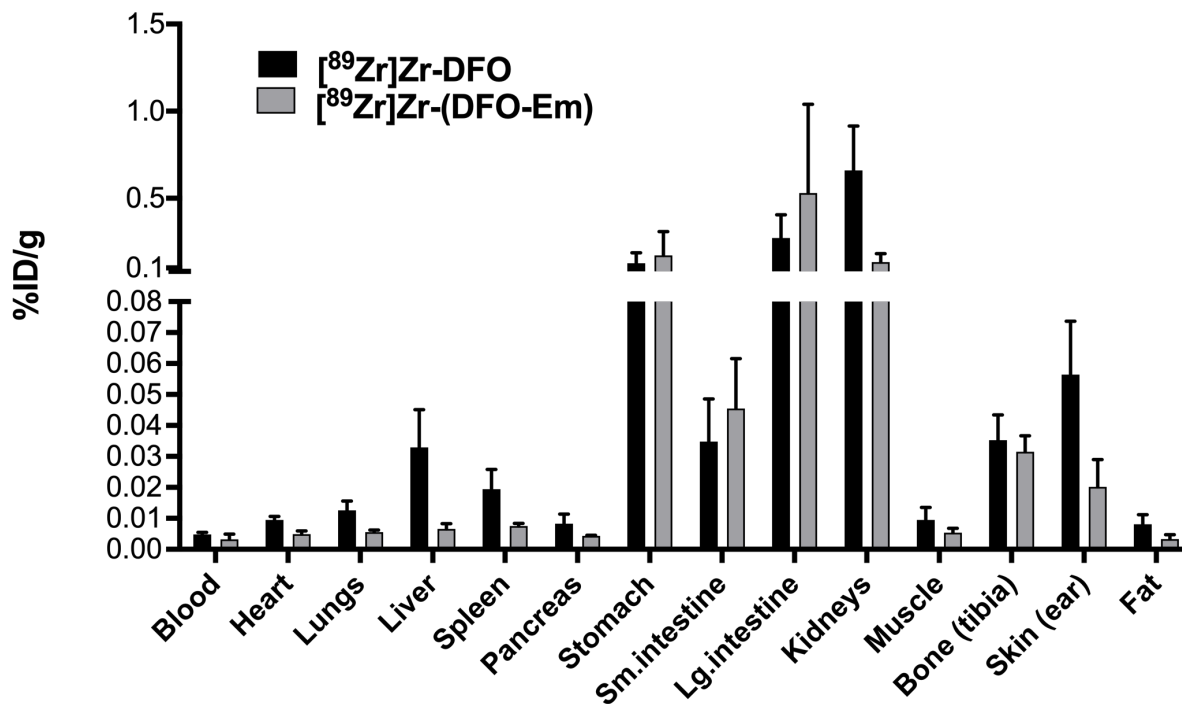
Figure 4-8. Results of *ex vivo* biodistribution study of $[^{89}Zr]Zr$-DFO and $[^{89}Zr]Zr$-DFO-Em in female BALB/c mice at 24 h post injection. 4-5 MBq of either complex was injected in 200 µL, 0.9% saline intravenously via tail vein catheter (*n* = 4).

4.5. Conclusions

Our new chelator DFO-Em is a derivative of our recently published chelator DFO2 and is a highly water soluble hydroxamate-based octadentate chelator designed for binding zirconium-89. DFO-Em was synthesized in 8 synthetic steps with a cumulative yield of ~24%, and its radiolabeling and *in vitro* stability with $[^{89}Zr]Zr^{4+}$ was evaluated. We completed detailed density functional theory calculations on 16 possible geometric isomers of Zr-(DFO-Em) to better understand the coordination sphere and discuss energy differences between isomers. Concentration-dependant radiolabeling experiments demonstrated that DFO-Em achieves nearly identical binding kinetics and apparent molar activity to the "gold standard" zirconium-89 chelator DFO. Although the increase in denticity of DFO-Em over DFO (CN = 8 vs 6) did not seem to

influence the basic radiolabeling properties of DFO-Em, it had a significant and positive effect on the stability of the resultant $[^{89}Zr]Zr^{4+}$ complex. Stability assays performed *in vitro* such as a hydroxyapatite challenge and a 1000-fold molar excess EDTA challenge revealed $[^{89}Zr]Zr$-(DFO-Em) to have remarkably higher stability than $[^{89}Zr]Zr$-DFO. Biodistribution and PET images in healthy mice revealed that $[^{89}Zr]Zr$-(DFO-Em) had faster blood and tissue clearance and substantially lower healthy tissue retention at 24 h post injection compared to $[^{89}Zr]Zr$-DFO. The higher denticity of DFO-Em over DFO grants it much greater stability with zirconium-89, and also potential for theranostic applications with large therapeutic radiometals.

4.6. Experimental Section

Radiochemistry. $[^{89}Zr]Zr$-oxalate was obtained from Saskatchewan Centre for Cyclotron Sciences (SCCS) on the University of Saskatchewan campus and was delivered purified in a minimum volume of 1M oxalic acid. The apparent molar activity of the $[^{89}Zr]Zr$-oxalate produced routinely in SCCS (as used for this study), was found to be in the range of 673-1161 MBq/μmol, by using a method adapted from Holland et al [30,31], and radionuclidic purity was determined to be 99.99% [32].

Chemical Characterization Methods. ^1H and ^{13}C NMR spectra were recorded at the Saskatchewan Structural Science Centre at the University of Saskatchewan on a 500 MHz Bruker Avance III HD NMR spectrometer, at 25 ºC in D_2O, $CDCl_3$ or $(CD_3)_2SO$. ^1H chemical shifts were referenced to the residual protons of the deuterated solvents (δ =4.79 ppm for D_2O; δ =7.26 ppm for $CDCl_3$ and δ = 2.50 ppm for $(CD_3)_2SO$). ^{13}C chemical shifts were referenced to the $CDCl_3$ signal at 77.16 ppm and $(CD_3)_2SO$ signal at δ = 39.52 ppm. Coupling constants are reported to the

nearest 0.5 Hz (^{1}H NMR spectroscopy) or rounded to integer values in Hz (^{13}C NMR spectroscopy). High resolution mass spectra were measured on a JEOL AccuTOF GCv 4G using field desorption ionization (FDI). For the isotopic pattern only the mass peak of the isotope with the highest natural abundance is given. HPLC purifications were performed on Thermofisher Vanquish HPLC using C18 reversed-phase column (Inspire Semipreparative DIKMA; 5 μm, 21.2 × 250 mm), a VF-D40-A UV detector, two VF-P10-A pumps with Chromeleon 7 communication software, and a DIONEX UltiMate 3000 fraction collector. A flow rate of 4 mL/ minute was used with a gradient of MeCN:H$_2$O (with 0.1% formic acid (FA) in both solvents) and the UV-Detector was set at 220 and 280 nm. Low resolution mass spectrometry was performed on Advion Expression-L system (mass range <2000 amu). The Advion Expression-L was coupled with the Thermofisher Vanquish system to perform liquid chromatography-mass spectrometry (LC-MS).

Reagents. All reagents and solvents were purchased from commercial suppliers and were used without further purification unless otherwise indicated. O-benzylhydroxylamine hydrochloride, sodium hydride, bromoacetyl bromide, Oxyma Pure and *N,N*-diisopropylethylamine (DIPEA) were purchased from Sigma-Aldrich. DFO.mesylate was purchased from Abcam. 1-[Bis(dimethylamino)methylene]-1H-1,2,3-triazolo[4,5-b]pyridinium 3-oxid hexafluorophosphate (HATU) and L-glutamic acid gamma-benzyl ester alpha-*tert*-butyl ester hydrochloride were purchased from AK Scientific. ZrCl$_4$, EDTA disodium salt dihydrate (Molecular biology grade), ammonium acetate (Honeywell ≥ 99.99% trace metal basis), 1-ethyl-3-(3-dimethylaminopropyl)carbodiimide hydrochloride (EDC.HCl), and potassium carbonate anhydrous were purchased from Fisher Scientific.

Synthesis of Compound (13). Compound **13** was prepared according to a published procedure with modification [33]. O-benzylhydroxylamine hydrochloride (1.00 g, 6.27 mmol) and di-tert-butyl dicarbonate (1.33 mL, 6.23 mmol) were dissolved in THF (7 mL). Then an aqueous solution of sodium hydrogen carbonate (1 M, 7 mL) was added slowly. The reaction was stirred at ambient temperature overnight. The organic solvent was removed by rotary evaporator, then the residue was diluted with water (20 mL) and extracted with dichloromethane (20 mL, 3 times). The organic layers were collected, dried over anhydrous sodium sulfate and then the solvent was removed by rotary evaporator to give the product as a white solid (1.27 g, 97%), no further purification was required. ^{1}H NMR [CDCl$_3$, 500 MHz]: δ 1.48 (s, 9H, CH$_3$), 4.86 (s, 2H, CH$_2$), 7.1 (s, 1H, NH), 7.3 -7.4 (m, 5H, CH). ^{13}C NMR [CDCl$_3$, 126 MHz]: δ 28.3, 78.5, 81.8, 128.6, 129.2, 135.82, 156.8. HRMS (TOF): m/z Calcd for $[C_{12}H_{17}NO_3 + Na]^+$: 246.1100; found: 246.1103.

Synthesis of Compound (14). This procedure was adapted from a published literature procedure [34]. Sodium hydride (90%, 197.07 mg, 7.39 mmol) was weighed carefully in a Schlenk flask under nitrogen gas and washed with hexane (4 mL) 3 times. Then anhydrous DMF (15 mL) was added and followed by slow addition of compound **13** (1.50 g, 6.72 mmol). After stirring the mixture for 30 minutes at ambient temperature, iodomethane (0.46 mL, 7.39 mmol) was added and the reaction was left to stir at ambient temperature overnight. The reaction was then quenched by careful addition of water (5 mL) and stirred for 10 minutes. The mixture was further diluted with 20 mL water and extracted with hexane (25 mL, 3 times). The organic layers were pooled, dried over anhydrous sodium sulfate and the solvent was removed by rotary evaporator to give compound **14** as a clear oil (1.54 g, 98%). ^{1}H NMR [CDCl$_3$, 500 MHz]: δ1.49 (s, 9H, CH$_3$), 3.04 (s, 3H, CH$_3$), 4.82 (s, 2H, CH$_2$), 7.31 – 7.41 (m, 5H, CH). ^{13}C NMR [CDCl$_3$, 126 MHz]: δ 28.3, 36.9, 76.6,

81.3, 128.5, 128.6, 129.5, 136.7 and 157.1. HRMS (TOF): m/z Calcd for $[C_{13}H_{19}NO_3 + H]^+$: 238.1437; found: 238.1432.

Synthesis of Compound (15). This Boc-deprotection procedure was modified from a published procedure [35]. To a mixture of compound **14** (1.49 g, 6.28 mmol) in dichloromethane (7.5 mL), trifluoroacetic acid (7.5 mL, 97.32 mmol) was added and stirred for 5 h at ambient temperature. A saturated sodium hydrogen carbonate solution (20 mL) was added and extracted with dichloromethane (20 mL, 3 times). The organic layers were collected and dried over anhydrous sodium sulfate. The solvent was evaporated via rotary evaporator, and the crude product mixture was purified with column chromatography (30% ethyl acetate in hexane). Compound **15** was obtained (0.79 g, 92%) as a clear oil. ^{1}H NMR [CDCl$_3$, 500 MHz]: δ 2.74 (s, 3H, CH3), 4.73 (2H, CH2), 5.56 (s, 1H, NH), 7.31 – 7.41 (m, 5H, CH). ^{13}C NMR [CDCl$_3$, 126 MHz]: δ 39.3, 75.6, 127.8, 128.3, 128.4, 138.0. HRMS (TOF): m/z Calcd for $[C_{18}H_{11}NO + H]^+$: 138.0913; found: 138.0908.

Synthesis of Compound (16). This procedure was modified from a published literature procedure [36]. Compound **15** (7.5 g, 54.6 mmol) was dissolved in acetonitrile (55 mL) and potassium carbonate (37.8 g, 273.4 mmol) was added. The solution was cooled in an acetone and ice bath and then bromoacetyl bromide (10.95 mL, 25.38 mmol) was added, and the reaction mixture was stirred for 1 hour in the ice bath then followed by 30 minutes at ambient temperature. After the reaction was complete, the solvent was evaporated via rotary evaporator. The residue was dissolved in water and extracted with dichloromethane. The organic layers were collected, dried over anhydrous sodium sulfate and then the solvent was removed via rotary evaporator. The crude product mixture

was purified by column chromatography (20% ethyl acetate in hexane). Compound **16** (12.92 g, 92%) was obtained as a pale-yellow oil. ^{1}H NMR [CDCl$_3$, 500 MHz]: δ 3.25 (s, 3H, CH$_3$), 3.90 (s, 2H, CH$_2$), 4.93 (s, 2H, CH$_2$), 7.40 (br s, 5H, CH). ^{13}C NMR [CDCl$_3$, 126 MHz]: δ 25.7, 33.9, 76.5, 128.9, 129.4, 133.92, 168.2. HRMS (TOF): m/z Calcd for [C$_{10}$H$_{13}$NO$_2$Br + H]$^+$: 258.0124; found: 258.0121.

Synthesis of Compound (17). This procedure was adapted from a published literature procedure [37]. H$_2$N-Glu(OBzl)-OtBu HCl (2.20 g, 6.67 mmol) was dissolved in DMF (10 mL), then triethylamine (1.01 mL, 67.28 mmol) was added and stirred for 30 minutes at ambient temperature. A precipitate formed, which was removed by filtration and discarded. Compound **16** (1.57 g, 6.07 mmol) and triethylamine (1.01 mL, 67.28 mmol) were added, and the reaction mixture was stirred for 4 hours at 55 °C. After completion, water (20 mL) was added and extracted with dichloromethane. The organic layers were dried over anhydrous sodium sulfate and the solvent was evaporated via rotary evaporator. The crude product mixture was purified by using column chromatography (50% ethyl acetate in hexane) to obtain the product **17** (2.51 g, 88%). ^{1}H NMR [DMSO-d$_6$, 500 MHz]: δ 1.38 (s, 9H, CH3), 1.69 – 1.86 (m, 2H, CH$_2$), 2.17 (s, 1H, NH), 2.36 – 2.46 (m, 2H, CH$_2$), 3.14 (s, 3H, CH$_3$), 3.28 (d, *J*=16.7, 1H), 3.42 (d, *J*=16.7, 1H), 4.86 (s, 2H, CH$_2$), 5.08 (s, 2H, CH$_2$), 7.31 – 7.43 (m, 10H, CH). ^{13}C NMR [DMSO-d$_6$, 126 MHz]: δ 27.93, 28.1, 30.4, 47.7, 60.2, 65.9, 75.8, 81.0, 128.4, 128.3, 128.4, 128.8, 128.9, 129.2, 130.0, 135.2, 136.7, 173.0, 173.5. HRMS (TOF): m/z Calcd for [C$_{26}$H$_{34}$N$_2$O$_6$ + H]$^+$: 471.2489; found: 471.2497.

Synthesis of Compound (18). This procedure was adapted from a published literature procedure [38]. Compound **17** (0.32 g, 0.68 mmol) was dissolved in acetone (5 mL), then potassium carbonate

(0.14 g, 1.02 mmol) was added and stirred for 20 minutes before iodomethane (63.5 µL, 1.02 mmol) was added. The reaction mixture was heated to reflux at 55 °C for 4 hours. After completion, the solvent was evaporated via rotary evaporator, then water (20 mL) was added to the residue and extracted with dichloromethane. The organic layers were pooled, dried over anhydrous sodium sulfate and the solvent was evaporated via rotary evaporator. The crude product mixture was purified by column chromatography (5%-50% ethyl acetate in hexane). The product **18** was obtained as oil (0.28 g, 85%). ^{1}H NMR [CDCl$_3$, 500 MHz]: δ 1.44 (s, 9H, CH$_3$), 1.86 – 2.02 (m, 2H, CH$_2$), 2.37 (s, 3H, CH$_3$), 2.46 – 2.50 (m, 2H, CH$_2$), 3.17 (s, 3H, CH3), 3.27 (t, J= 5.1, 1H, CH), 3.50 (s, 2H, CH$_2$), 4. 81 (s, 2H, CH$_2$), 5.09 (s, 2H, CH$_2$), 7.29 – 7.37 (m, 10H, CH).^{13}C NMR [CDCl$_3$, 126 MHz]: δ 24.9, 28.3, 30.8, 39.2, 54.3, 65.9, 66.1, 76.2, 81.2, 128.1, 128.2, 128.5, 128.7, 129.0, 129.4, 134.5, 136.1, 171.5, 172.7, 173.2. HRMS (TOF): m/z Calcd for [C$_{27}$H$_{36}$N$_2$O$_6$ + H]$^+$: 485.2646; found: 485.2652.

Synthesis of Compound (19). Compound **18** (0.97 g, 2.00 mmol) was dissolved in a (1:1) mixture of dichloromethane and trifluoroacetic acid (4 mL) and the reaction mixture was stirred at ambient temperature for 4 hours. Then the volatiles were evaporated via rotary evaporator, and the crude product mixture was purified by using column chromatography to isolate compound **19** (0.66 g, 77%) as a clear oil. ^{1}H NMR [CDCl$_3$, 500 MHz]: δ 1.81 – 2.05 (m, 2H, CH$_2$), 2.37 (br s, 3H, CH$_3$), 2.55 (br s, 2H, CH$_2$), 3.20 (s, 3H, CH$_3$), 3.41 (br s, 1H, CH), 3.65 (br s, 2H, CH$_2$), 4.81 (s, 2H, CH$_2$), 5.04 – 5.11 (m, 2H, CH$_2$), 7.31 – 7.40 (m, 10H, CH). ^{13}C NMR [CDCl$_3$, 126 MHz]: δ 31.1, 33.5, 37.9, 55.4, 65.9, 66.4, 76.1, 128.3, 128.6, 128.9, 129.5, 129.8, 133.8, 135.9, 173.2. HRMS (TOF): m/z Calcd for [C$_{23}$H$_{28}$N$_2$O$_6$ + H]$^+$: 429.2020; found: 429.2028.

Synthesis of compound (20). To solution of compound **19** (100 mg, 0.23 mmol) in DMF (3 mL), oxyma pure (43.12 mg, 0.30 mmol), 1-ethyl-3-(3-dimethylaminopropyl)carbodiimide hydrochloride (EDC, 47.10 mg, 0.30 mmol) and *N,N-* diisopropylethylamine (0.099 mL, 70.85 mmol) was added and stirred for 30 minutes at ambient temperature. In a different flask, desferrioxamine mesylate salt (199.27 mg, 0.30 mmol) was dissolved in DMF (3 mL) with help of heating up to 80 ºC. After cooling the desferrioxamine solution for few minutes (~ 50 ºC), it was added to the activated ester and the reaction was stirred overnight at ambient temperature. After completion, the DMF was reduced to ~1 mL under reduced pressure, the residue was added to ethyl acetate and left in a spark proof -20 ºC freezer for 30 minutes to obtain maximum precipitation. Then the precipitate was separated by centrifugation, and it was washed with cold ethyl acetate 2 times. The crude then was purified by using reverse phase column chromatography (0% - 60% acetonitrile in water). The acetonitrile was removed under reduced pressure via rotary evaporator and followed by addition of Chelex-treated Millipure water, flash freezing in liquid nitrogen, and freeze-drying to collect compound **20** (120 mg, 53%) as a white powder. ^{1}H NMR [DMSO-d_6, 500 MHz]: δ 1.21 – 1.49 (m, 19H, CH_2), 1.72 -1.85 (m, 2H, CH_2), 1.96 (s, 3H, CH_3), 2.18 (s, 3H, CH_3), 2.26 (t, *J*=7.2, 4H, CH_2), 2.34 – 2.28 (m, 2H, CH_2), 2.56 – 2.58 (m, 4H, CH_2), 2.99 – 3.11 m, 7H, CH & CH_2), 3.14 (s, 2H, CH_3), 3.33 (s, 3H, CH_3), 3.43 – 3.46 (m, 8H, CH_2), 4.86 (s, 2H, CH_2), 5.08 (s, 2H, CH_2), 7.31 – 7.44 (m, 10H, CH Ar), 7.76 -7.77 (m, 2H, NH), 8.06 (t, J = 5.5, 1H, NH), 9.62 (s, 3H, OH). ^{13}C NMR [DMSO-d_6, 126 MHz]: δ 17.8, 19.4, 19.5, 20.4, 205, 20.6, 21.9, 22.7, 30.4, 30.5, 30.8, 57.8, 58.1, 67.4, 119.7, 119.8, 120.1, 120.3, 120.7, 121.6, 128.2, 164.0, 165.0, 165.4. HRMS (TOF): m/z Calcd for $[C_{48}H_{74}N_8O_{13} + H]^+$: 971.5448; found: 971.5450.

Synthesis of Compound (21). In a Schlenk flask, compound **20** (100 mg, 0.10 mmol), was dissolved in ethanol (30 mL) and 10% Pd/C (16.44 mg, 0.015 mmol) was added. The flask was sealed with a rubber septa and connected to an H_2 gas balloon fitted with a glass stopcock and a needle, and the flask was additionally connected to vacuum via Schlenk line. The flask was put under vacuum for 15 seconds and then the vacuum was closed, and the flask was purged with H_2 gas by *slowly* opening the glass stopcock valve. The vacuum and purging were repeated 4 times and finally the flask was left stirring under H_2 for 2 hours, then the reaction mixture was filtered through celite to remove the Pd/C for safe disposal. The solvent was evaporated, and the crude product mixture was purified by semipreparative HPLC. HPLC conditions: C18 Inspire Semipreparative DIKMA; 5 μm, 21.2 × 250 mm; (15 – 35% acetonitrile in water (0.1% formic acid); flow rate, 4 mL/min, t_R = 10.25 min). Pure compound **21** (80 mg, 98%) was obtained as a white solid following rotary evaporation and then freeze drying of pooled HPLC fractions. ^{1}H NMR [D_2O, 500 MHz]: δ 1.54 – 1.69 (m, 19H, CH_2), 2.09 – 2.18 (m, 4H, CH_2), 2.11 (s, 3H, CH_3), 2.47 (t, J= 7.0, 4H, CH_2), 2.78 (t, J = 7.0, 4H, CH_2), 2.96 (s, 3H, CH_3), 3.13 – 3.27 (m, 6H, CH_2), 3.26 (s, 3H, CH_3), 3.59 (t, J = 6.9, 6H, CH_2), 3.99 (m, 1H, CH), 4.29 (q, J = 13.9, 2H, CH_2). ^{13}C NMR [D_2O, 126 MHz]: δ 19.2, 22.9, 23.0, 23.2, 23.7, 25.4, 26.1, 26.2, 27.6, 27.7, 27.8, 27.9, 28.0, 30.4, 31.9, 36.0, 39.2, 39.5, 40.6, 47.7, 47.8, 51.5, 54.0, 67.0, 165.0, 167.4, 169.7, 173.6, 173.8, 174.8 and 178.6. HRMS (TOF): m/z Calcd for $[C_{34}H_{62}N_8O_{13} + H]^+$: 791.4509; found: 791.4533.

Labeling of DFO-Em with ^{nat}Zr (22). Following a published procedure [15], to a solution of compound **9** (8.16 mg, 10.32 μmol) in ultrapure water (400 μL), a mixture of $ZrCl_4$ in Chelex-treated Millipure water (101.4 μL, 9.3 μmol) was added. The pH of the mixture was adjusted to ~ 7 by adding Na_2CO_3 solution (12 μL, 1 M) and another 486.6 μL ultrapure water was added to

adjust the total volume to 1 mL. The reaction mixture was left in a thermomixer to agitate at ambient temperature at 800 rpm overnight. The reaction mixture was flash frozen in liquid nitrogen and the solvent removed by lyophilization to obtain **^{nat}Zr-(DFO-Em)** (8.0 mg, 98%) as a white solid. ^{1}H NMR [D$_2$O, 500 MHz]: δ 1.23 – 1.70 (m, 19H, CH$_2$), 2.12 (s, 3H, CH$_3$), 2.16 – 2.29 (m, 2H, CH$_2$), 2.41 – 2.60 (m, 6H, CH$_2$), 2.74 – 2.75 (m, 4H, CH$_2$), 3.02 (s, 3H, CH$_3$), 3.17 – 3.28 (m, 6H, CH$_2$), 3.24 (, s, 3H, CH$_3$), 3.57 – 3.67 (m, 6H, CH$_2$), 4.10 (dd, J = 4.3, J = 10.1, 1H, CH), 4.30 – 4.40 (m, 2H, CH$_2$). ^{13}C NMR [D$_2$O, 126 MHz]: δ 16.28, 21.86, 22.12, 22.41, 23.12, 25.09, 25.18, 26.12, 26.31, 27.15, 27.22, 27.75, 29.41, 30.69, 30.89, 36.01, 38.39, 38.44, 39.55, 40.84, 50.24, 50.54, 51.08, 54.26, 66.53, 164.14, 164.27, 164.43, 164.90, 166.57, 174.02 and 174.20. HRMS (TOF): m/z Calcd for [C$_{34}$H$_{58}$N$_8$O$_{13}$Zr + H]$^+$: 877.3243; found: 877.3210.

[^{89}Zr]Zr^{4+} Radiolabeling Studies. [^{89}Zr]Zr-oxalate was received from the Saskatchewan Centre for Cyclotron Sciences in 1 M oxalic acid. Required amounts were aliquoted and neutralized to pH 6.8-7.2 by adding sodium carbonate (1.0 M), and radiolabeling reactions were performed in HEPES buffer (0.5 M, pH 7). Radiochemical yields were determined using silica-gel impregnated glass-microfiber instant thin layer chromatography paper (iTLC-SG, Varian, Lake Forest, CA), and EDTA solution (50 mM, pH 5.5) was used as mobile phase. Free [^{89}Zr]Zr^{4+} was eluted by mobile phase to the solvent front, while radiolabeled (DFO and DFO-Em bound) [^{89}Zr]Zr^{4+} remained at the baseline. The radio-iTLCs were analyzed on a Bioscan AR-2000 radio-TLC plate reader and analyzed using Winscan Radio-TLC software (Bioscan Inc., Washington, DC). All solutions were prepared in Chelex-100 resin (BioRad Laboratories, Hercules, CA) treated (1.2 g/L water, 24 h) Ultrapure water (>18.2 MΩ cm^{-1} at 25°C, Milli-Q, Millipore, Billerica, MA). For activity measurements, either Perkin-Elmer (Waltham, MA) Automated Wizard Gamma Counter

or Capintec CRC-15R dose calibrator (Capintec, Ramsey, NJ) was used and is indicated for each experiment. Stock solutions of DFO-Em and commercially available DFO mesylate (used as a control) were prepared in Chelex-100 resin treated water at concentrations of 1.00 nmol/μL. Different amounts of each chelator (0.005, 0.05, 0.5 and 5 nmol) were mixed with 10 -10.6 MBq neutralized $[^{89}Zr]Zr^{4+}$ solutions ($n = 3$) in HEPES buffer pH 7 (0.5 M), the total volume of each reaction was completed to 250 μL, and the vials were mixed at 800 rpm at ambient temperature. At time points 1, 5, 10, 15 and 60 minutes, 1 μL from each sample was spotted on an iTLC strip and the iTLCs were developed with EDTA (50 mM, pH 5.5) solution as mobile phase. Radiochemical yields were determined from integration of the activity at the baseline ($[^{89}Zr]Zr$-chelate complex) and solvent front (free/EDTA bound $[^{89}Zr]Zr^{4+}$). For stability assays, $[^{89}Zr]Zr$-chelate complex of each of DFO-Em and DFO were prepared at the final concentration of 157 μM in the same way as described above and then aliquoted out to stability challenge vessels. The RCYs were determined by radio-iTLC to be >99% and they were used without further purifications.

Serum Stability Assay. 63.6 μL aliquots of $[^{89}Zr]Zr$-(DFO-Em) or $[^{89}Zr]Zr$-DFO (157 μM) were added to 150 μL of freshly thawed human blood serum (Sigma-Aldrich) in microcentrifuge tubes ($n = 3$). The samples were mixed on a thermomixer at 800 rpm and 37 °C. Stability of the complexes was monitored by radio-iTLC at 1 h, 1, 3, 5, 7 and 10 days. Stable $[^{89}Zr]Zr$-(DFO-Em) and $[^{89}Zr]Zr$-DFO remained at the baseline while transchelated $[^{89}Zr]Zr^{4+}$ eluted to the solvent front.

EDTA Transchelation Assay (1000 fold molar excess EDTA). A stock solution of EDTA (25 mM) was prepared in ammonium acetate buffer pH 7 (0.25 M). 400 μL (10 mmol) aliquots from

the EDTA stock solution were added to 63.6 µL (~ 2.1 MBq) of $[^{89}Zr]$Zr-(DFO-Em) or $[^{89}Zr]$Zr-DFO (157 µM each) in microcentrifuge tubes (*n* = 3). The final concentration of the EDTA and the $[^{89}Zr]$Zr-chelator complexes were 21.6 mM and 21.6 µM (respectively) in the final volume of 463.6 µL. The samples were mixed on a thermomixer at 800 rpm and 37 ºC. The stability of the complexes was monitored by radio-iTLC at 1 h, 3 h, 13 h, 1, 3, 5, 7 and 10 days.

Hydroxyapatite (HTP) Stability Challenge. 63.6 µL (~ 2.1 MBq) aliquots of $[^{89}Zr]$Zr-(DFO-Em) or $[^{89}Zr]$Zr-DFO (157 µM each) were added to microcentrifuge tubes containing 40 mg or 60 mg hydroxyapatite resin (HTP, BioRad Bio-Gel) and 900 µL HEPES buffer (0.5 M, pH 7). Another set of tubes were prepared to be used as controls. In the controls, instead of $[^{89}Zr]$Zr-(DFO-Em) and $[^{89}Zr]$Zr-DFO, only neutralized $[^{89}Zr]$Zr-Oxalate (~ 2.1 MBq) was added for 40 mg and 60 mg (*n* = 3). The tubes were mixed on a thermomixer at 800 rpm and 37 ºC. After 24 hours, the tubes were centrifuged for 10 minutes at 10000 rpm. The supernatant was carefully pipetted out and transferred to 5 mL tubes. The pellet was washed (2 times) with 1 mL HEPES buffer, centrifuged to re-pellet the HTP resin, and the supernatants were pooled in the 5 mL tubes. Activity of the pellets (transchelated $[^{89}Zr]$Zr) and the pooled supernatants (intact $[^{89}Zr]$Zr-chelates) were measured via dose calibrator separately. The percentage of activity in the supernatants determines the stability of the $[^{89}Zr]$Zr-chelate complexes.

Log*D* Octanol/Buffer Distribution Coefficient. Following quantitative radiolabeling as described above, $[^{89}Zr]$Zr-DFO or $[^{89}Zr]$Zr-(DFO-Em) were added in aliquots of 27 µL (~ 5 µCi) to 2.973 mL PBS buffer (pH 7.4) and 3 mL 1-octanol, in 15 mL centrifuge tubes (n = 3). The mixtures were mixed aggressively via vortex mixer for 1 minute and then centrifuged for 10 minutes at 3000 rpm. 1 mL of each layer was carefully transferred to separate microcentrifuge

144

tubes to measure the activity on an automated γ-counter. Log$D$ values were calculated from log of the ratio of activity (counts) in 1-octanol to activity in PBS buffer (pH 7.4) according to equation (**2-1**, see chapter 2).

PET/CT and Biodistribution in Healthy Mice. [^{89}Zr]Zr-DFO and [^{89}Zr]Zr-(DFO-Em) complexes were prepared in the same manner as explained above and >99% RCY was confirmed by using radio-iTLC. Aliquots of 3.8-4.1 MBq of the [^{89}Zr]Zr-chelator complexes were injected to healthy female BALB/c mice (n = 4), via tail vein catheter while in the PET scanner with image acquisition started, under anesthesia (2.5 % isoflurane in O$_2$, at a flow rate of 2-3 mL/min). 60-minute dynamic images of all four mice were collected simultaneously on the Sofie GNEXT PET/CT small animal imaging system using the included 4-mouse heated bed. The PET/CT images were reconstructed with Sofie GNEXT software and processed with VivoQuant® 2020 software (patch 1 64 bit, build vq-2020patch1-0-ga8255affc). The mice were euthanized (by anesthesia followed by cervical dislocation followed by cardiac puncture and blood draw) at 24 h post injection. Blood and specific organs were harvested, weighed, and residual activity in the organs were measured by using an automated gamma counter. The animals had access to cage enrichments and access to food and water ad-libitum. The experimental protocol was approved by the University of Saskatchewan Committee on Animal Care and procedures were performed in accordance with the guidelines of the Canadian Council on Animal Care and the Canadian Nuclear Safety Commission.

Density Function Theory (DFT) Calculations. DFT geometry optimizations were performed using the PC (Windows 10) software DMOL^3 and Biovia Materials Studio, version 20.10.5 (2020)

[39,40] using the generalized gradient approximation (GGA) employing the Perdew-Burke-Ernzerhof (PBE) [41] exchange-correlation functional for energy and potential during the self-consistent field (SCF) procedure [42]. DMol^3's own basis set (4.4 basis file) was used to apply double-numerical plus d-function (DND) in the calculations, including polarization functions for core electrons of all the atoms. Conductor-like screening model (COSMO) solvation model [43,44] was used for modeling quantum simulations of solvated molecules with dielectric value of ($\varepsilon = 78.54$) for water. CYLview software (CYLview, 1.0b; Legault, C. Y., Université de Sherbrooke, 2009, http://www.cylview.org) was used for graphical depiction of the structures from the log files of the optimized structures.

4.7. Associated Content

Supporting information

The supporting information for this chapter is summarized in Appendix-II

4.8. References

(1)   Zeglis, B. M.; Lewis, J. S. The Bioconjugation and Radiosynthesis of 89Zr-DFO-Labeled Antibodies. *J Vis Exp* **2015**, No. 96.
(2)   Patra, M.; Bauman, A.; Mari, C.; Fischer, C. A.; Blacque, O.; Häussinger, D.; Gasser, G.; Mindt, T. L. An Octadentate Bifunctional Chelating Agent for the Development of Stable Zirconium-89 Based Molecular Imaging Probes. *Chem. Commun.* **2014**, *50* (78), 11523–11525.
(3)   Price, E. W.; Carnazza, K. E.; Carlin, S. D.; Cho, A.; Edwards, K. J.; Sevak, K. K.; Glaser, J. M.; de Stanchina, E.; Janjigian, Y. Y.; Lewis, J. S. 89Zr-DFO-AMG102 Immuno-PET to Determine Local HGF Protein Levels in Tumors for Enhanced Patient Selection. *J. Nucl. Med.* **2017**, *58* (9), 1386–1394.
(4)   Fung, K.; Vivier, D.; Keinänen, O.; Sarbisheh, E. K.; Price, E. W.; Zeglis, B. M. 89Zr-Labeled AR20.5: A MUC1-Targeting ImmunoPET Probe. *Molecules* **2020**, *25* (10), 2315.
(5)   Price, E. W.; Zeglis, B. M.; Lewis, J. S.; Adam, M. J.; Orvig, C. H6phospa-Trastuzumab: Bifunctional Methylenephosphonate-Based Chelator with 89Zr, 111In and 177Lu. *Dalton Trans.* **2014**, *43*, 119–131.

(6)   Meijs, W. E.; Haisma, H. J.; Van Der Schors, R.; Wijbrandts, R.; Van Den Oever, K.;
        Klok, R. P.; Pinedo, H. M.; Herscheid, J. D. M. A Facile Method for the Labeling of
        Proteins with Zirconium Isotopes. *Nucl. Med. Biol.* **1996**, *23* (4), 439–448.

(7)   Jauw, Y. W. S.; Menke-van der Houven van Oordt, C. W.; Hoekstra, O. S.; Hendrikse, N.
        H.; Vugts, D. J.; Zijlstra, J. M.; Huisman, M. C.; van Dongen, G. A. M. S. Immuno-
        Positron Emission Tomography with Zirconium-89-Labeled Monoclonal Antibodies in
        Oncology: What Can We Learn from Initial Clinical Trials? *Front. pharmacol.* **2016**, *7*,
        131–131.

(8)   Vosjan, M. J. W. D.; Perk, L. R.; Visser, G. W. M.; Budde, M.; Jurek, P.; Kiefer, G. E.;
        van Dongen, G. A. M. S. Conjugation and Radiolabeling of Monoclonal Antibodies with
        Zirconium-89 for PET Imaging Using the Bifunctional Chelate p-Isothiocyanatobenzyl-
        Desferrioxamine. *Nat. Protoc.* **2010**, *5* (4), 739–743.

(9)   van de Watering, F. C. J.; Rijpkema, M.; Perk, L.; Brinkmann, U.; Oyen, W. J. G.;
        Boerman, O. C. Zirconium-89 Labeled Antibodies: A New Tool for Molecular Imaging in
        Cancer Patients. *Biomed. Res. Int.* **2014**, *2014*, 203601.

(10)   Zhang, Y.; Hong, H.; Cai, W. PET Tracers Based on Zirconium-89. *Curr. Radiopharm.*
        2011, *4* (2), 131–139.

(11)   Yoon, J.-K.; Park, B.-N.; Ryu, E.-K.; An, Y.-S.; Lee, S.-J. Current Perspectives on 89Zr-
        PET Imaging. *Int. J. Mol. Sci.* **2020**, *21* (12), 4309.

(12)   Summers, K. L.; Sarbisheh, E. K.; Zimmerling, A.; Cotelesage, J. J. H.; Pickering, I. J.;
        George, G. N.; Price, E. W. Structural Characterization of the Solution Chemistry of
        Zirconium(IV) Desferrioxamine: A Coordination Sphere Completed by Hydroxides.
        Inorg. Chem. **2020**, *59* (23), 17443–17452.

(13)   Holland, J. P.; Vasdev, N. Charting the Mechanism and Reactivity of Zirconium Oxalate
        with Hydroxamate Ligands Using Density Functional Theory: Implications in New
        Chelate Design. *Dalton Trans.* **2014**, *43* (26), 9872–9884.

(14)   N Tinianow, J.; Pandya, D. N.; Pailloux, S. L.; Ogasawara, A.; Vanderbilt, A. N.; Gill, H.
        S.; Williams, S.-P.; Wadas, T. J.; Magda, D.; Marik, J. Evaluation of a 3-Hydroxypyridin-
        2-One (2,3-HOPO) Based Macrocyclic Chelator for (89)Zr(4+) and Its Use for
        ImmunoPET Imaging of HER2 Positive Model of Ovarian Carcinoma in Mice.
        Theranostics **2016**, *6* (4), 511–521.

(15)   Sarbisheh, E. K.; Salih, A. K.; Raheem, S. J.; Lewis, J. S.; Price, E. W. A High-Denticity
        Chelator Based on Desferrioxamine for Enhanced Coordination of Zirconium-89. *Inorg.
        Chem.* **2020**, *59* (16), 11715–11727.

(16)   Ulaner, G. A.; Hyman, D. M.; Lyashchenko, S. K.; Lewis, J. S.; Carrasquillo, J. A. 89Zr-
        Trastuzumab PET/CT for Detection of HER2-Positive Metastases in Patients with HER2-
        Negative Primary Breast Cancer. *Clin. Nucl. Med.* **2017**, *42* (12), 912–917.

(17)   Pandit-Taskar, N.; O'Donoghue, J. A.; Durack, J. C.; Lyashchenko, S. K.; Cheal, S. M.;
        Beylergil, V.; Lefkowitz, R. A.; Carrasquillo, J. A.; Martinez, D. F.; Fung, A. M.;
        Solomon, S. B.; Gönen, M.; Heller, G.; Loda, M.; Nanus, D. M.; Tagawa, S. T.; Feldman,
        J. L.; Osborne, J. R.; Lewis, J. S.; Reuter, V. E.; Weber, W. A.; Bander, N. H.; Scher, H.
        I.; Larson, S. M.; Morris, M. J. A Phase I/II Study for Analytic Validation of 89Zr-J591
        ImmunoPET as a Molecular Imaging Agent for Metastatic Prostate Cancer. *Clin. Cancer
        Res.* **2015**, *21* (23), 5277–5285.

(18)   Pandit-Taskar, N.; O'Donoghue, J. A.; Ruan, S.; Lyashchenko, S. K.; Carrasquillo, J. A.;
        Heller, G.; Martinez, D. F.; Cheal, S. M.; Lewis, J. S.; Fleisher, M.; Keppler, J. S.; Reiter,

R. E.; Wu, A. M.; Weber, W. A.; Scher, H. I.; Larson, S. M.; Morris, M. J. First-in-Human Imaging with 89Zr-Df-IAB2M Anti-PSMA Minibody in Patients with Metastatic Prostate Cancer: Pharmacokinetics, Biodistribution, Dosimetry, and Lesion Uptake. *J. Nucl. Med.* **2016**, *57* (12), 1858–1864.

(19) Deri, M. A.; Ponnala, S.; Kozlowski, P.; Burton-Pye, B. P.; Cicek, H. T.; Hu, C.; Lewis, J. S.; Francesconi, L. C. P-SCN-Bn-HOPO: A Superior Bifunctional Chelator for 89Zr ImmunoPET. *Bioconjug. Chem.* **2015**, *26* (12), 2579–2591.

(20) Vugts, D. J.; Klaver, C.; Sewing, C.; Poot, A. J.; Adamzek, K.; Huegli, S.; Mari, C.; Visser, G. W. M.; Valverde, I. E.; Gasser, G.; Mindt, T. L.; van Dongen, G. A. M. S. Comparison of the Octadentate Bifunctional Chelator DFO*-PPhe-NCS and the Clinically Used Hexadentate Bifunctional Chelator DFO-PPhe-NCS for 89Zr-Immuno-PET. *Eur. J. Nucl. Med. Mol. Imaging* **2017**, *44* (2), 286–295.

(21) Guérard, F.; Lee, Y.-S.; Brechbiel, M. W. Rational Design, Synthesis, and Evaluation of Tetrahydroxamic Acid Chelators for Stable Complexation of Zirconium(IV). *Chem. Eur. J.* **2014**, *20* (19), 5584–5591.

(22) Rudd, S. E.; Roselt, P.; Cullinane, C.; Hicks, R. J.; Donnelly, P. S. A Desferrioxamine B Squaramide Ester for the Incorporation of Zirconium-89 into Antibodies. *Chem. Commun.* **2016**, *52* (80), 11889–11892.

(23) Buchwalder, C.; Rodríguez-Rodríguez, C.; Schaffer, P.; Karagiozov, S. K.; Saatchi, K.; Häfeli, U. O. A New Tetrapodal 3-Hydroxy-4-Pyridinone Ligand for Complexation of 89zirconium for Positron Emission Tomography (PET) Imaging. *Dalton Trans.* **2017**, *46* (29), 9654–9663.

(24) Briand, M.; Aulsebrook, M. L.; Mindt, T. L.; Gasser, G. A Solid Phase-Assisted Approach for the Facile Synthesis of a Highly Water-Soluble Zirconium-89 Chelator for Radiopharmaceutical Development. *Dalton Trans.* **2017**, *46* (47), 16387–16389.

(25) Klasen, B.; Lemcke, D.; Mindt, T. L.; Gasser, G.; Rösch, F. Development and in Vitro Evaluation of New Bifunctional 89Zr-Chelators Based on the 6-Amino-1,4-Diazepane Scaffold for Immuno-PET Applications. *Nucl. Med. Biol.* **2021**, *102–103*, 12–23.

(26) Holland, J. P.; Divilov, V.; Bander, N. H.; Smith-Jones, P. M.; Larson, S. M.; Lewis, J. S. 89Zr-DFO-J591 for ImmunoPET of Prostate-Specific Membrane Antigen Expression In Vivo. *J. Nucl. Med.* **2010**, *51* (8), 1293–1300.

(27) Guérard, F.; Lee, Y.-S.; Tripier, R.; Szajek, L. P.; Deschamps, J. R.; Brechbiel, M. W. Investigation of Zr(IV) and 89Zr(IV) Complexation with Hydroxamates: Progress towards Designing a Better Chelator than Desferrioxamine B for Immuno-PET Imaging. *Chem. Commun. (Camb.)* **2013**, *49* (10), 1002–1004.

(28) Holland, J. P. Predicting the Thermodynamic Stability of Zirconium Radiotracers. *Inorg. Chem.* **2020**, *59* (3), 2070–2082.

(29) Deri, M. A.; Ponnala, S.; Zeglis, B. M.; Pohl, G.; Dannenberg, J. J.; Lewis, J. S.; Francesconi, L. C. Alternative Chelator for 89Zr Radiopharmaceuticals: Radiolabeling and Evaluation of 3,4,3-(LI-1,2-HOPO). *J. Med. Chem.* **2014**, *57* (11), 4849–4860.

(30) Holland, J. P.; Sheh, Y.; Lewis, J. S. Standardized Methods for the Production of High Specific-Activity Zirconium-89. *Nucl. Med. Biol.* **2009**, *36* (7), 729–739.

(31) Alizadeh, E.; Behlol Ayaz Ahmed, K.; Raja Solomon, V.; Gaja, V.; Bernhard, W.; Makhlouf, A.; Gonzalez, C.; Barreto, K.; Casaco, A.; Geyer, C. R.; Fonge, H. 89Zr-

Labeled Domain II-Specific ScFv-Fc ImmunoPET Probe for Imaging Epidermal Growth Factor Receptor In Vivo. *Cancers* **2021**, *13* (3), 560.

(32) Gaja, V.; Cawthray, J.; Geyer, C. R.; Fonge, H. Production and Semi-Automated Processing of 89Zr Using a Commercially Available TRASIS MiniAiO Module. *Molecules* **2020**, *25* (11), 2626.

(33) Bieliauskas, A. V.; Weerasinghe, S. V. W.; Negmeldin, A. T.; Pflum, M. K. H. Structural Requirements of Histone Deacetylase Inhibitors: SAHA Analogs Modified on the Hydroxamic Acid. *Arch. Pharm. (Weinheim, Ger.)* **2016**, *349* (5), 373–382.

(34) Olshvang, E.; Szebesczyk, A.; Kozłowski, H.; Hadar, Y.; Gumienna-Kontecka, E.; Shanzer, A. Biomimetic Ferrichrome: Structural Motifs for Switching between Narrow- and Broad-Spectrum Activities in P. Putida and E. Coli. *Dalton Trans.* **2015**, *44* (48), 20850–20858.

(35) Gudmundsdottir, A. V.; Paul, C. E.; Nitz, M. Stability Studies of Hydrazide and Hydroxylamine-Based Glycoconjugates in Aqueous Solution. *Carbohydr. Res.* **2009**, *344* (3), 278–284.

(36) J. Donohoe, T.; P. Fishlock, L.; A. Basutto, J.; F. Bower, J.; A. Procopiou, P.; L. Thompson, A. Synthesis of Substituted Pyridines and Pyridazines via Ring Closing Metathesis. *Chem. Commun.* **2009**, *0* (21), 3008–3010.

(37) Randolph, J. T.; Huang, P. P.; Flosi, W. J.; DeGoey, D.; Klein, L. L.; Yeung, C. M.; Flentge, C.; Sun, M.; Zhao, C.; Dekhtyar, T.; Mo, H.; Colletti, L.; Kati, W.; Marsh, K. C.; Molla, A.; Kempf, D. J. Synthesis, Antiviral Activity, and Pharmacokinetic Evaluation of P3 Pyridylmethyl Analogs of Oximinoarylsulfonyl HIV-1 Protease Inhibitors. *Bioorg. Med. Chem.* **2006**, *14* (12), 4035–4046.

(38) Harini, S. T.; Kumar, H. V.; Rangaswamy, J.; Naik, N. Synthesis of Thiazole-Based Substituted Piperidinone Oximes: Profiling of Antioxidant and Antimicrobial Activity. *Russ. J. Bioorg. Chem.* **2017**, *43* (2), 186–196.

(39) Delley, B. From Molecules to Solids with the DMol3 Approach. *J. Chem. Phys.* **2000**, *113* (18), 7756–7764.

(40) Delley, B. An All-electron Numerical Method for Solving the Local Density Functional for Polyatomic Molecules. *J. Chem. Phys.* **1990**, *92* (1), 508–517.

(41) Perdew, null; Burke, null; Ernzerhof, null. Generalized Gradient Approximation Made Simple. *Phys. Rev. Lett.* **1996**, *77* (18), 3865–3868.

(42) Peverati, R.; Truhlar, D. G. M11-L: A Local Density Functional That Provides Improved Accuracy for Electronic Structure Calculations in Chemistry and Physics. *J. Phys. Chem. Lett.* **2012**, *3* (1), 117–124.

(43) Andzelm, J.; Kölmel, C.; Klamt, A. Incorporation of Solvent Effects into Density Functional Calculations of Molecular Energies and Geometries. *J. Chem. Phys.* **1995**, *103* (21), 9312–9320.

(44) Klamt, A.; Schüürmann, G. COSMO: A New Approach to Dielectric Screening in Solvents with Explicit Expressions for the Screening Energy and Its Gradient. *J. Chem. Soc., Perkin Trans. 2* **1993**, No. 5, 799–805.

Chapter 5: DFO-Km: A modular chelator with an amino-acid based linker and ideal properties for the construction of zirconium-89 based radiopharmaceuticals

The content of chapter 5 is adapted from the manuscript that is currently under preparation (**Salih, A. K**.; Dominguez-Garcia, M.; Raheem, S. J.; Ahiahonu, W. K.; Price, E. W. manuscript under preparation)

5.1. Author Contribution and Relation to the Research Objectives

This work was done in collaboration with Shvan J. Raheem (PhD candidate), William K. Ahiahonu (undergraduate student), Moralba Dominguez-Garcia (PhD candidate), and Dr. Price. I synthesized the hydroxamic acid monomer (**23**) in 4 steps and I designed and synthesized the DFO-Km chelator in 4 steps (**24-27**). Furthermore, I prepared [^{Nat}Zr]Zr-DFO-Km (**28**) and synthesized the bifunctional *p*-SCN-Ph-DFO-Km (**29**). I also performed complete characterization of all the compounds (**23-29**). All the DFT calculations were done by Dr. Price, William K. Ahiahonu, and myself. Moralba Dominguez-Garcia and I performed the antibody purifications, antibody conjugation reactions and MALDI sample preparation. I performed the radiolabeling studies, *in vitro* experiments, animal imaging, dissection and biodistribution studies with assistance of Dr. Price, Moralba Dominguez-Garcia and Shvan J. Raheem. Furthermore, I prepared the first draft of the manuscript and supporting information which was further edited by Dr. Price.

This work is a continuation of the DFO-Em chelator, whose bifunctional version could not be synthesized for the purpose of biovector conjugation. Like DFO2K and DFO-Em, this new chelator DFO-Km was designed with a modular synthesis that utilizes an amino acid as the linker. Thus, I designed a DFO-Km based on lysine, with some additional modifications in the hydroxamic acid monomer. The new monomer has two extra atoms spacing and carboxylic acid functionality (**23**) instead of the bromo group in the hydroxamic acid monomer of DFO-Em (**16**). For this chelator, I changed the linker from glutamic acid to a lysine to avoid the intramolecular cyclization during the side chain carboxylic acid activation (NHS ester) to synthesize the bifunctional chelator. Following the successful synthesis of DFO-Km and its bifunctional version *p*-SCN-Ph-DFO-Km, it was successfully conjugated to a non-specific human serum IgG. The [^{89}Zr]Zr(IV) labeled immunoconjugate in comparison with its equivalent DFO based immunoconjugate was assessed in healthy mice with PET/CT imaging and *ex vivo* biodistribution studies. The results showed that the DFO-Km complex with zirconium-89 was significantly more stable than DFO. Interestingly, the *in vivo* and *ex vivo* results also suggest that DFO-Km (CN = 8) forms a more stable complex with zirconium-89 than does DFO2K (CN = 12) owing to its lower bone uptake.

5.2. Abstract

Zirconium-89 labeled monoclonal antibodies and other large macromolecules such as nanoparticles hold great promise as positron emission tomography imaging agents. As such, demand for new bifunctional chelators which both stably bind the radiometal and can conjugate to targeting vectors such as antibodies has grown considerably. The six coordination sites of the commonly used chelator desferrioxamine B (DFO) are insufficient to saturate the coordination

sphere of $[^{89}Zr]Zr^{4+}$ (CN 7-8), which results in sub-optimal stability and release of the radiometal *in vivo*. We recently published a promising and new octadentate chelator DFO-Em, which formed far more stable $[^{89}Zr]Zr^{4+}$ complexes than DFO and is a modular amino acid-based chelator comprised of DFO, glutamic acid (E), and a hydroxamic acid monomer (m). Building on the modular and efficient design of DFO-Em, herein we present the further improved derivative DFO-Km, which is instead based on lysine. DFO-Km presents a free primary amine for easy synthesis of bifunctional derivatives and offers improved stability and water solubility as a $[^{89}Zr]Zr^{4+}$ complex relative to DFO. DFO-Km includes a re-designed hydroxamic acid monomer that is 2 carbon atoms longer to provide greater flexibility for metal ion coordination. We utilized the incorporated lysine linker to synthesize the bifunctional derivative *p*-SCN-Ph-DFO-Km, which showed efficient and high-yielding conjugation to a non-specific human serum antibody (IgG). The stability of the radiolabeled immunoconjugate was studied in healthy mice and compared to radiolabeled DFO immunoconjugate as a "gold standard" control. PET/CT and biodistribution results revealed significantly higher stability of $[^{89}Zr]Zr$-(DFO-Km)-IgG *in vivo* over $[^{89}Zr]Zr$-DFO-IgG, proven by the significant reduction of activity in bone visualized by PET/CT at 14 days post injection. Moreover, a set of comprehensive DFT calculations were performed to model and evaluate 16 geometric isomers of Zr-(DFO-Km). All the results indicate that DFO-Km is an ideal chelator for $[^{89}Zr]Zr^{4+}$ applications and with its increased denticity relative to DFO, it has the potential to be used with larger therapeutic radiometals for theranostic applications. Our new bifunctional chelator *p*-SCN-Ph-DFO-Km shows strong potential as a new chemical tool for creating ideal bioconjugates with targeting vectors such as antibodies, peptides, and nanoparticles.

5.3. Introduction

Among the available positron emitting radionuclides with appropriate properties for positron emission tomography (PET) applications, zirconium-89 is still widely considered the best available radiometal for imaging large macromolecules such as antibodies (immunoPET) and has been used in numerous preclinical and clinical studies.[1–9] Its relatively long half-life (3.3 days) provides sufficient time for slow circulating targeting vectors such as radiolabeled macromolecules (e.g. antibodies, protein domains, nanoparticles) to reach optimal biodistribution and produce high target-to-background signal ratio for PET images with good contrast.[1,10] In addition to the powerful diagnostic potential of zirconium-89-based radioimmunoconjugates, it could avail new theranostic options if a suitable chelator is identified.[11] Moreover, its half-life makes it a suitable imaging companion for therapeutic radionuclides such as actinium-225 and thorium-227, which is critical for theranostic agents. Generally, when utilizing radiometals for imaging and targeted radionuclide therapy, one must have access to a suitable bifunctional chelator, which is a chelator that possess Lewis basic donor groups to bind and stabilize a cationic radiometal ion, in addition to a reactive functional group for biovector conjugation under mild conditions. Despite an abundance of knowledge about the coordination chemistry of zirconium-89, we believe there is still room to develop new chelators that can form stable complexes with zirconium-89 *in vivo* and prevent its release into healthy tissue, possess suitable water solubility and conjugation efficiency, and have potential to bind therapeutic radiometals thus unlocking theranostic applications.[12–14]

The most commonly used chelator for $[^{89}Zr]Zr(IV)$ — a bacterial siderophore called desferrioxamine B (DFO) — has in numerous animal studies shown to have sub-optimal *in vivo* stability, which results in non-specific uptake of the osteophilic and radioactive zirconium in healthy tissue and especially in bone.[12,13,15–19] Even though the same degree of bone uptake has

154

not been reported in human studies, better chelators with improved stability and more versatility are still desired.[4,7,20–23] This instability of [^{89}Zr]Zr-DFO complexes is suggested to be a result of the fact that the hexadentate DFO binds to zirconium ions (preferred coordination number 7-8) through 3 hydroxamic acid (HA) groups, with the coordination sphere completed by 1-2 more labile ligands such as H_2O or hydroxides. These two readily accessible sites in the coordination sphere of zirconium leave space for intrusion of endogenous biological ligands such as transferrin, albumin, chloride, and phosphate.[13] Most critically, DFO does not have value as a theranostic agent, because its limited hexadentate donor set is not sufficient for therapeutic radiometals, which are typically large and ideally form 8+ coordinate species. Other hydroxamic acid-based chelators such as DFO2, DFO2p, DFO2K, DFO-Em, and DFO* have been developed with higher numbers of hydroxamate groups (**Figure 5-1**).[13,17] These chelators are proven to form highly stable complexes with Zr(IV) by saturating its coordination number with 4 HAs in an octadentate fashion. Incorporation of the extra HA moieties often results in poor solubility in these chelators. An ideal radiometal chelator must have suitable water solubility, as radiolabeling reactions and bioconjugation to biomolecules such as antibodies and peptides are typically performed in aqueous buffer under mild conditions.

In our previous work, we reported the synthesis and evaluation of a glutamic acid based octadentate chelator we named DFO-Em (Chapter 4). We designed DFO-Em as an octadentate chelator to saturate the coordination sphere of zirconium(IV) and maximize stability, and to solve the issue of low aqueous solubility which is often reported for higher denticity DFO-based chelators such DFO2, DFO2p, and DFO*.[13,17] Following synthesis and characterization, we performed a series of radiochemical stability experiments that demonstrated DFO-Em has great potential to replace DFO for zirconium-89 chelation with efficient radiolabeling, high aqueous

solubility, excellent *in vitro* stability, and a favorable biodistribution profile in mice. Therefore, we tried to synthesize the bifunctional version of DFO-Em via *N*-hydroxysuccinimide (NHS) ester activation of the glutamic acid side chain carboxylic acid to enable biovector conjugation through amide linkage chemistry. However, this method was not successful due to intramolecular cyclization resulting from reaction of hydroxamate groups with the activated ester. One of the attractive features of DFO-Em (Chapter 4) and DFO2K (Chapter 3) is their modular amino acid linker system, which allows for modular synthesis of many derivatives by simply using a different natural or un-natural amino acid as a linker to connect different chelating moieties such as DFO and HA monomers.
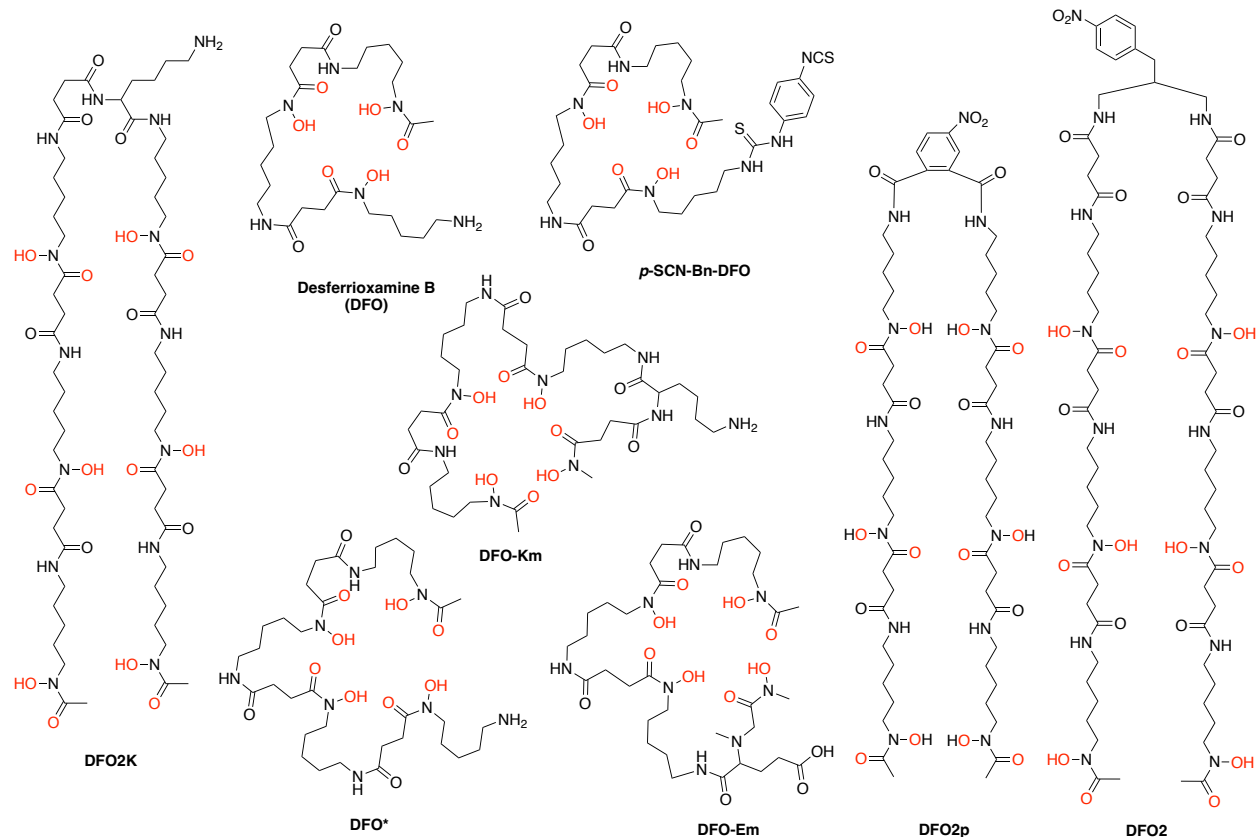
Figure 5-1: Chemical structures of the "gold standard" zirconium-89 chelator DFO, with its bifunctional isothiocyanates derivative, and recently developed DFO-based chelators including DFO2, DFO2p, DFO2K, DFO*, DFO-Em and the new DFO-Km. The binding donor groups are indicated in red.

As such, we switched the glutamic acid linker in DFO-Em (E = glutamic acid, m = HA monomer) for lysine, and also took this opportunity to redesign the monomer unit for ease of synthesis and to increase the length by two carbons to improve flexibility for metal ion coordination. Here we present the synthesis and evaluation of a lysine based bifunctional derivative of DFO-Em called DFO-Km (K = lysine, m = HA monomer). Simply switching the amino acid from glutamic acid to lysine will retain an identical coordination sphere, however the monomer structure was changed slightly for DFO-Km relative to DFO-Em. Despite this minor structural change, DFO-Km has a similar core structure to DFO-Em with 4 HA moieties (CN = 8), and we anticipate similar radiolabeling and *in vitro* stability properties. To attain a better insight on the possible arrangements of the hydroxamate groups in DFO-Km around the Zr(IV) ion we also performed a comprehensive density functional theory (DFT) study of all 16 possible Λ-enantiomers of Zr-(DFO-Km). We performed a similar DFT evaluation of geometric isomers for Zr-DFO-Em, which yielded similar results, suggesting nearly identical coordination spheres around Zr(IV). Following the synthesis and characterization, DFO-Km was successfully bifunctionalized by reacting the side chain primary amine (ε-amino group) of the lysine with *p*-phenylene diisothiocyanate to form its *p*-isothiocyanatophenyl-derivative (*p*-SCN-Ph-DFO-Km). This new bifunctional chelator and the "gold standard" *p*-SCN-Ph-DFO were conjugated to a non-specific human IgG antibody via thiourea linkage, a common strategy used for bioconjugation of chelators to antibodies.[24] Furthermore, the stability of the zirconium-89 labeled immunoconjugates were assessed *in vivo* by PET imaging and biodistribution studies.

157

5.4. Results and Discussion

Synthesis. We have previously shown with DFO-Em that a successful method to increase the coordination number of DFO for saturating the coordination sphere of $[^{89}Zr]Zr^{4+}$ and thus improving the stability of its complex, without curtailing its solubility, is to incorporate an amino acid such as glutamic acid or lysine. For DFO-Km we modified the HA monomer to have two extra carbon atoms compared to the monomer used in DFO-Em to increase the flexibility of HA groups in coordination with $[^{89}Zr]Zr^{4+}$ and enable it to reach the arrangement of cis, cis, trans, trans, which has been predicted to be most stable. The monomer in DFO-Em had only one carbon spacing, which could be why our DFT evaluation resulted in the lowest energy conformation being predicted as trans, cis, trans, cis. Thus, we chose compound **23** (**Scheme 5-1**) as the monomer for DFO-Km to provide extra flexibility.

We synthesized the monomer in four steps starting from commercially available O-benzyl protected hydroxyl amine adapted from a published procedure.[25] The amine of the hydroxyl amine was first protected with a *tert*-butyloxycarbonyl (Boc) group to form compound **13**, followed by reaction with iodomethane to obtain compound **14**. Then the Boc group was removed by using trifluoroacetic acid to form **15**, which was then reacted with succinic anhydride to produce the desired HA monomer **23**. The monomer was added to the α-amino group of the lysine linker to form **24** via amide bond formation reaction using HATU as coupling reagent. After the *tert*-butyl ester was hydrolyzed by using trifluoroacetic acid to form compound **25**, DFO was coupled to the free carboxilic acid of the lysine via amide bond formation to yield **26**. Subsequent deprotection of the *N*-benzyl protecting group via hydrogenolysis using hydrogen gas and paladium on carbon as catalyst resulted in formation of the "pre-bifunctional" DFO-Km chelator (**27**), which was purified with RP-HPLC before characterization. The pre-bifunctional chelator DFO-Km was

synthesized in 8 steps with a cumulative yield of ~11.4%. To test its complexation with the Zr(IV) ion the purified DFO-Km was reacted with [^{Nat}Zr]ZrCl$_4$ in Ultapure water at pH ~7 and at ambient temperature. The resultant complex **28** was characterized with ^{1}H, ^{13}C NMR spectroscopy, and high resolution mass spectrometry.
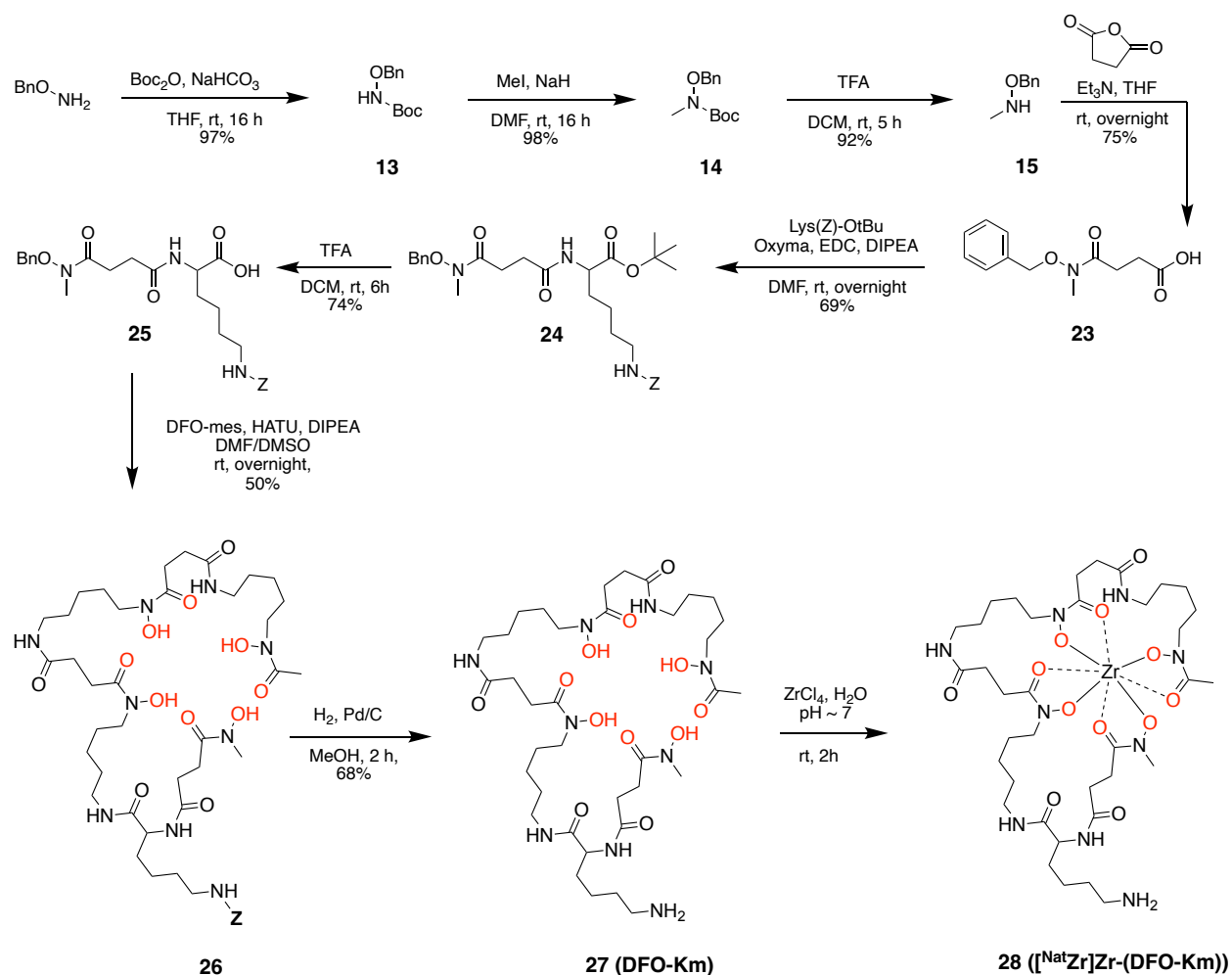
Scheme 5-1: Schematic depiction of synthesis pathway of DFO-Km (**26**) by coupling desferoxamine B and hydroxamic acid monomer (**23**) followed by complexation with non-radioactive Zr^{4+} (**28**)

Density functional theory (DFT) calculations. The real-world stability of radiometal-chelate complexes *in vivo* aren't accurately predicted by thermodynamic stability parameters such as formation constants. Instead, the practical "real-world" stability of radiometal-chelate complexes

is often referred to as their "kinetic inertness", which is a somewhat vague term used to describe their ability to resist transchelation/demetallation by a variety of *in vitro* stability assays, and ultimately *in vivo*. However, thermodynamic parameters can be useful metrics for comparing chelators of similar structures/denticities. For zirconium(IV) complexes with hydroxamic acid ligands, it has been previously deteremined by both X-ray crystal structure and DFT structure evaluation that the most thermodynamically stable conformation of four individual hydroxamic acid ligands (bidentate) in coordination with Zr(IV) ion as in Zr-(MeAHA)$_4$ to be cis-cis-trans-trans. However, when the hydroxamic acids are incorporated in a linear chelator such as DFO or DFO*, steric strain is introduced which limits the number of acessible geometric isomers and in most cases this thermodynamically prefered cis-cis-trans-trans arrangement is not accessible.

To assess whether Zr-(DFO-Km) can attain this prefered cic-cis-trans-trans octadentate Zr(IV) coordination geometry, we performed DFT calculation by using Materials Studio (DMOL3) to determine the energy of 16 possible geometric isomers (Λ- enantiomers) of Zr-(DFO-Km) (**Figures 5-2** and **5-3**). All calculations contained identical molecular formulas and the same number of atoms, and were calculated with water as solvent (COSMO). As with our DFT study of Zr-(DFO-Em), the large size and flexibility of Zr-(DFO-Km) makes it difficult to settle on a single most stable confirmation of each isomer. Even if the inner coordination sphere around Zr(IV) remains constant, the rest of the chelator is flexible and can hold many different orientations and thus different total energy values. As such, we cannot draw any firm conclusions from these results. Comparing the relative total energy of the isomers (the most stable set as 0 kJ/mol) we found that the most stable arrangment was Λ-C- trans, cis, trans (**Figure 5-2, A**) which is equivalent to the most stable geometry of Zr-(MeAHA)$_4$ (cis-cis-trans-trans isomer). We used the same naming convention as Holland,[26] where we chose the terminal HA monomer as the first

160

moiety and assigned as either the cabonyl (C) or the hydroxylamine (N) oriented towards the back, and then the sequential HA units being cis or trans relative to this first HA. Based on these DFT calculations we can suggest that DFO-Km has sufficient flexibility in the monomer unit to reach the same thermodynamically prefered orientation around the zirconium ion as Zr-(MeAHA)$_4$ (cis-cis-trans-trans isomer). Following the most stable isomer Λ-C- trans, cis, trans (**A**), the next most stable isomers was Λ-C- cis, cis, trans (**B**) with a non-trivial energy difference of ~30 kJ/mol higher. The highest energy isomer was Λ-C- trans, trans, cis (**H**) at ~100 kJ/mol higher than the most stable isomer. Considering the high energy difference between isomer (**A**) and the other isomers (>30 kJ/mol), it is likely that isomer (**A**) is the major isomer in aqueous solution under ambient conditions. In a DFT study on Zr-DFO2 and Zr-DFO2p, we calculated the exchange energy for a single HA bound to Zr(IV) of ~40-50 kJ/mol, suggesting a substantial energy barrier at ambient temperature. As such, regardless of whether isomer (**A**) is really the most stable and abudnant geometric isomer of Zr-(DFO-Km), interconversion between isomers is not likely without substantial heating. Note that each Λ- isomer has a Δ- enantiomer that makes up a total of 32 possible isomers, however for this study only the Λ- enantiomers are calculated for practical reasons due to the long calculation times for each structure.
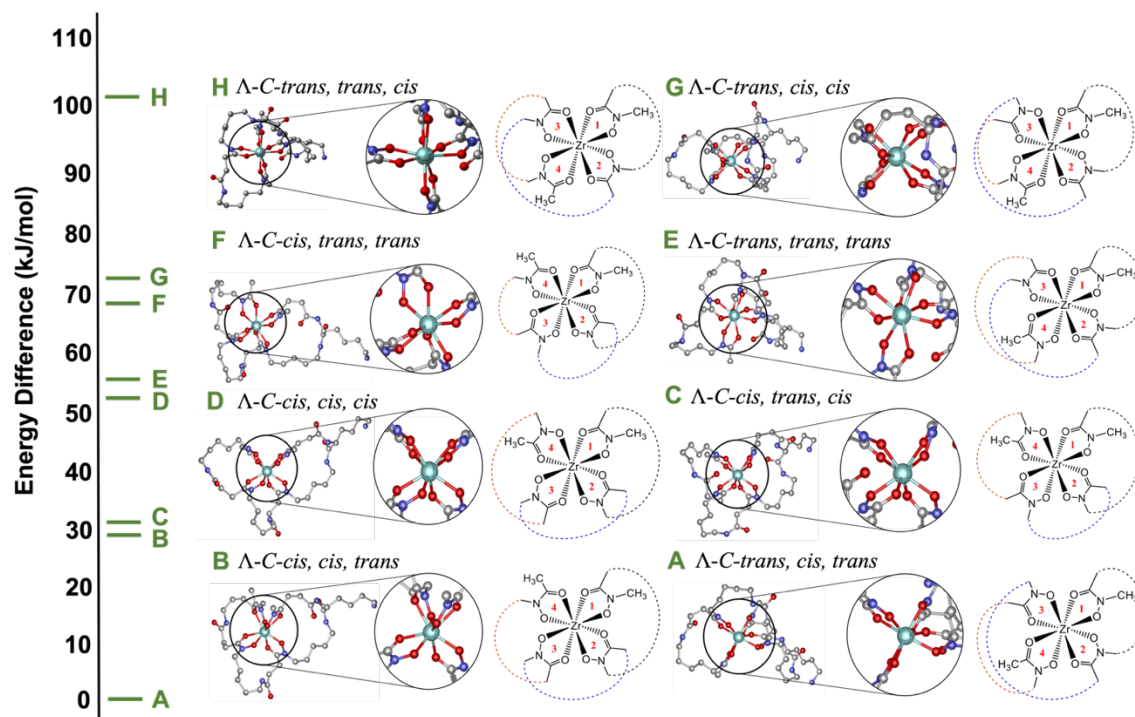
Figure 5-2. Optimized structures of geometric isomers of Zr-(DFO-Km), showing the 8 possible Λ-*C*-isomers of complexes with their relative energy differences, with the most stable geometric isomer of all 16 (C- and N-, **Figures 5-2** and **5-3**) set as a reference of 0 kJ/mol. Hydrogen atoms are present and included for calculation but excluded from the graphic for clarity.
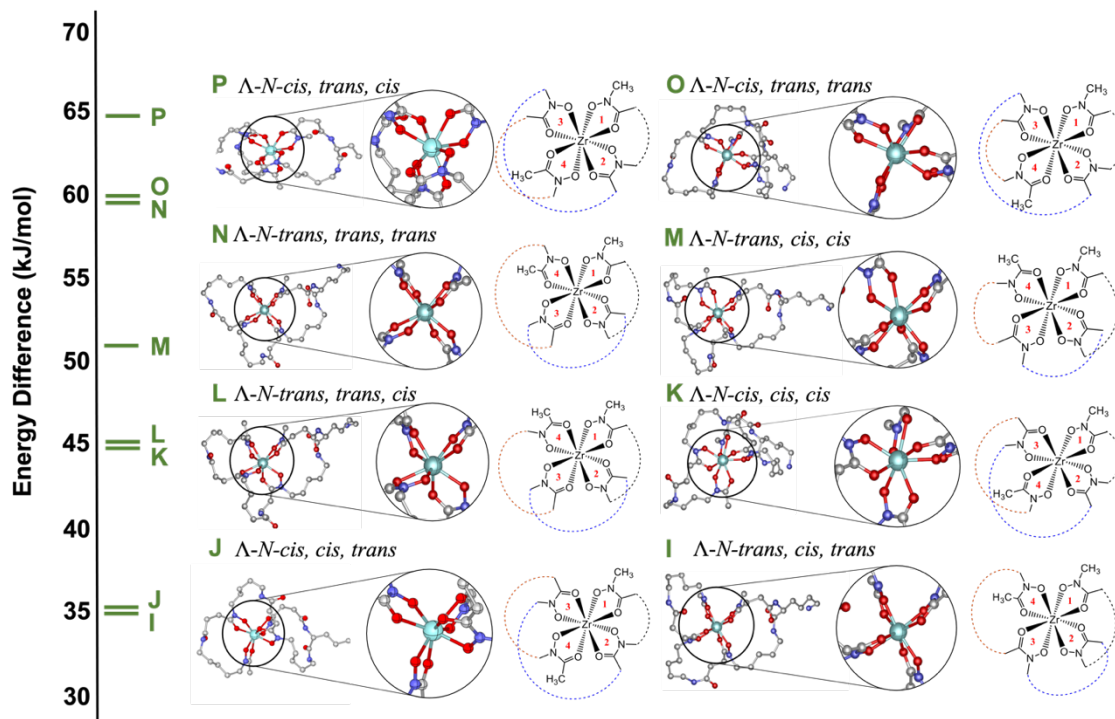
Figure 5-3. Optimized structures of geometric isomers of Zr-(DFO-Km), showing the 8 possible Λ-*N*-isomers of complexes with their relative energy differences, with the most stable geometric isomer of all 16 (C- and N-, **Figures 5-2** and **5-3**) set as a reference of 0 kJ/mol. Hydrogen atoms are present and included for calculation but excluded from the graphic for clarity.

Bifunctional DFO-Km synthesis and antibody conjugation. The bifunctional derivative of DFO-Km — *p*-SCN-Ph-DFO-Km (**29**) — was synthesized by coupling the free amino group of DFO-Km with an excess amount of *p*-phenylene diisocyanate via thiourea bond formation. Including previous steps, bifunctional *p*-SCN-Ph-DFO-Km was synthesized in 9 steps with a cumulative yield of ~4.2%. The bifuctional *p*-SCN-Ph-DFO-Km and commercially available *p*-SCN-Ph-DFO were subsequently conjugated to purified non-specific human IgG antibody (Sigma) (**Scheme 5-2**). It's know in antibody bioconjugation chemistry that the chelator to antibody ratio (CAR) affects the binding affinity and the pharmacokinetics of the immunoconjugate *in vivo*.[27] A high number of chelators on the antibody may result in reduction of immunoreactivity and binding affinity, change the receptor binding kinetics (on/off rates), decrease tumor uptake, and even result in immune system activation and macrophage uptake.[27] In general, for modification of antibodies with DFO, ~5 molar equivalents of bifunctional DFO is used to achieve a safe CAR of 1-2 chelates per antibody.[27] The conjugatoin efficiency of a chelator is highly effected by factors such as solubility and sterics, and so we tested a few ratios to determine optimized conditions. We used two different molar equivalents of *p*-SCN-Ph-DFO-Km (5.5 and 10.2) to evaluate conjugation efficiency with the IgG (PBS, pH 8-9). Following conjugation, the antibody was purified via PD10 (size exclusion) columns and centrifugal filtration (Amicon Ultra, 50 kDa), and we then deteremined the average chelate to antibody ratio (CAR) using MALDI-TOF mass spectrometry analysis (**Table 5-1**). We achieved CARs of 1.8, 1.4, and 3.1 for DFO-IgG (5 molar equivalents of chelator), (DFO-Km)-IgG (5.5 molar equivalents), and (DFO-Km)-IgG (10.2 molar equivalents), respectively. As such, we demonstrate equivalent bioconjugation efficient to *p*-SCN-Ph-DFO, and we pressed forward with the 5.5 molar equivalent conjugation conditions and the resulting 1.4 CAR (DFO-Km)-IgG bioconjugate for radiolabeling and *in vivo* study.
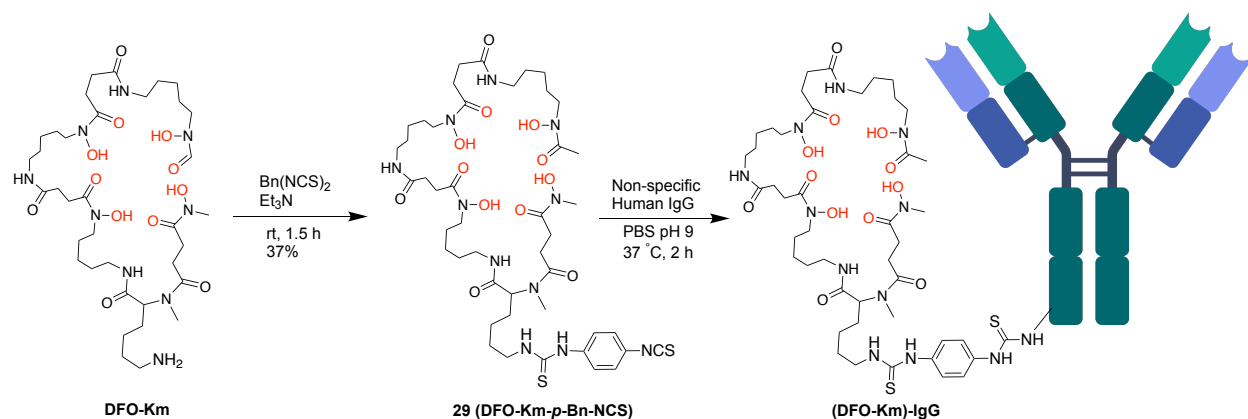
Scheme 5-2. Schematic depiction of bifunctional DFO-Km (*p*-SCN-Ph-DFO-Km, **29**) synthesis and its conjugation reaction with a non-specific human IgG antibody.

Table 5-1. Determination of chelator to antibody ratios (CAR) from results of MALDI-TOF MS/MS mass spectrometry analysis of unmodified IgG and the immunoconjugates.

Immunoconjugate	Molar equivalent of chelators	Measured average mass (Da)	Mass change (Da)	Mass of chelator (Da)	CAR
Unmodified IgG	-	148464.67	-	-	-
DFO-IgG	5.5	149795.00	1330.33	752.33	1.8
(DFO-Km)-IgG	5.5	149864.00	1399.33	1023.49	1.4
(DFO-Km)-IgG	10.2	151649.00	3184.33	1023.49	3.1

Radiolabeling and *in vivo* evaluation in healthy mice. To investigate the *in vivo* behaviour and pharmacokinetics of the [^{89}Zr]Zr-(DFO-Km)-IgG immunoconjugate in comparison with [^{89}Zr]Zr-DFO-IgG, the antibody conjugates DFO-IgG (1.8 CAR) and (DFO-Km)-IgG (1.4 CAR) were quantitatively radiolabeled with neutralized zirconium-89 in HEPES buffer (pH 7.0, 0.5 M) at 37 °C (>99% radiochemical conversion confirmed by radio-iTLC), followed by buffer exchange to saline (0.9%) by using PD-10 desalting columns. Subsequently, 9-10 MBq (50 µg, 200 µL sterile

saline) of the radiolabeled immunoconjugates were administered to 6 healthy female CD-1 mice intravenously via tail injection, the first 4 mice of each compound were imaged (4-mouse bed, serial PET/CT) over 14 days. The resulting images showed that the pharmacokinetics of the two radiolabeled immunoconjugates over time were similar, as expected since both immunoconjugates were based on the same antibody. As expected, due to the much greater stability previously observed for [^{89}Zr]Zr-(DFO-Em) vs [^{89}Zr]Zr-DFO, the bone uptake in the mice injected with [^{89}Zr]Zr-(DFO-Km)-IgG was reduced significantly (**Figures 4** and **5**), which confirms the outstanding stability of the [^{89}Zr]Zr-(DFO-Km) complex *in vivo*.
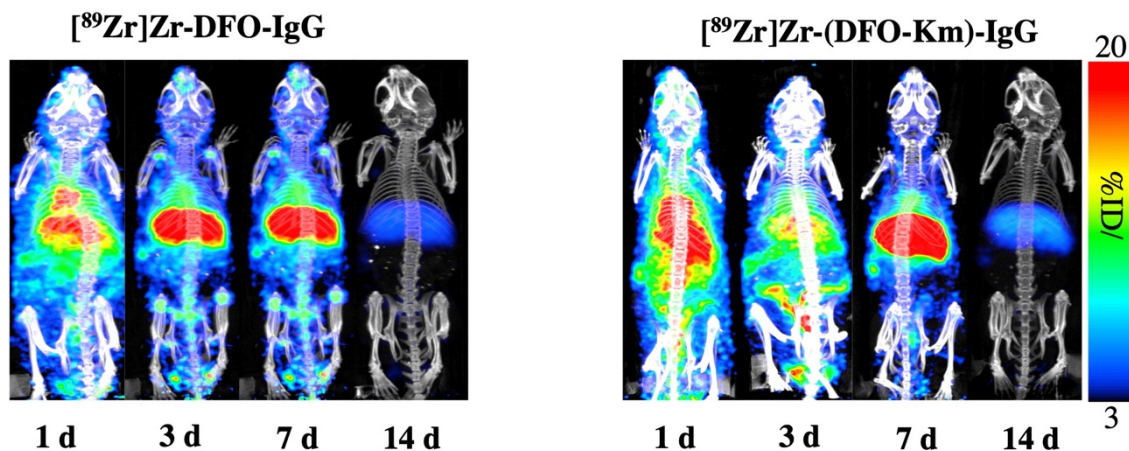
Figure 5-4. Representative PET/CT images (maximum intensity projections) of [^{89}Zr]Zr-(DFO-Km)-IgG and [^{89}Zr]Zr-DFO-IgG (9-10 MBq in 200 μL 0.9% saline) in healthy female CD-1 mice (n=4 per cohort), the images shown are for a single representative mouse from each cohort and are collected at four different time points over 14 days.
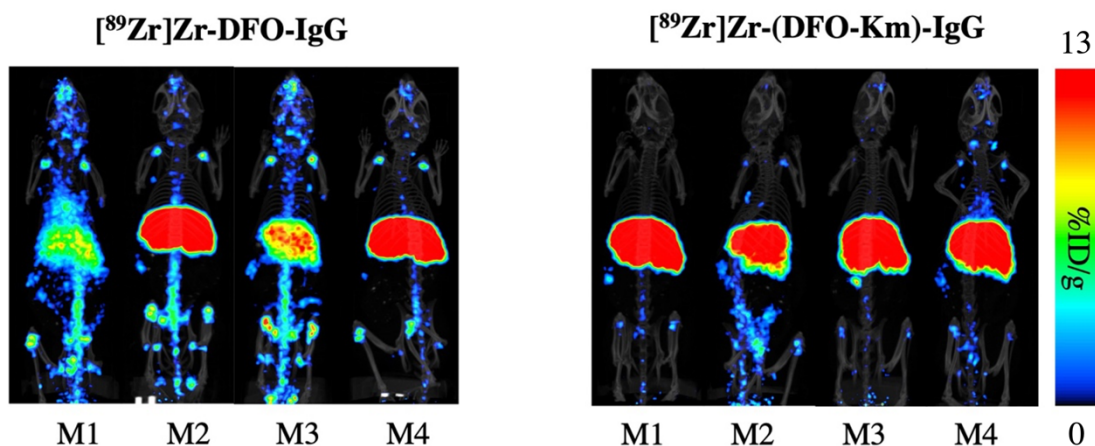
Figure 5-5. PET/CT images (maximum intensity projections) of [^{89}Zr]Zr-(DFO-Km)-IgG and [^{89}Zr]Zr-DFO-IgG (9-10 MBq in 200 μL 0.9% saline) in healthy female CD-1 mice (n = 4), with only the 14 days post injection time point shown for all mice in each cohort of 4. After decay correction, the activies in the images are maximized to best visualize and compare bone uptake for both compounds.

To further probe the organ uptake of the radiolabeled immunoconjugates, an *ex vivo* biodistribution study was performed at 14 days post injection (n = 6) immediately following the final PET/CT imaging. The results of the biodistribution corroborate the PET images with residual activity in the collected organs reported as the percentage of injected dose normalized per gram of tissue. Although in this study only two tibia bones were collected, which are not the best representation of the whole skeleton, the bone uptake was still statistically significantly lower for the [^{89}Zr]Zr-(DFO-Km)-IgG conjugate than [^{89}Zr]Zr-DFO-IgG (2.0 ± 0.6 %ID/g vs 3.7 ± 1.3 %ID/g, $p < 0.05$) (**Figure 5-6**). It is known that free zirconium-89 accumulates most significantly at sites of higher bone remodeling such as the joints (e.g. knees, hips, shoulders, elbows, spine, jaw). The tibia bones isolated for biodistribution do not include the joints, and it is the only bone we can cleanly remove (stripped of muscle) from the mice for biodistribution measurement. As such, the PET/CT images are a far better representation of the true difference in stability between DFO-Km and DFO, as the entire skeleton can be visualized (**Figures 5-5** and **5-6**). Further, the purpose of zirconium-89 PET radiotracers is to obtain useful images, and therefore the visually

striking difference in bone uptake between DFO-Km and DFO as seen in the PET images is a far more impressive and useful comparison than the relatively small difference in tibia uptake measured via *ex vivo* biodistribution.
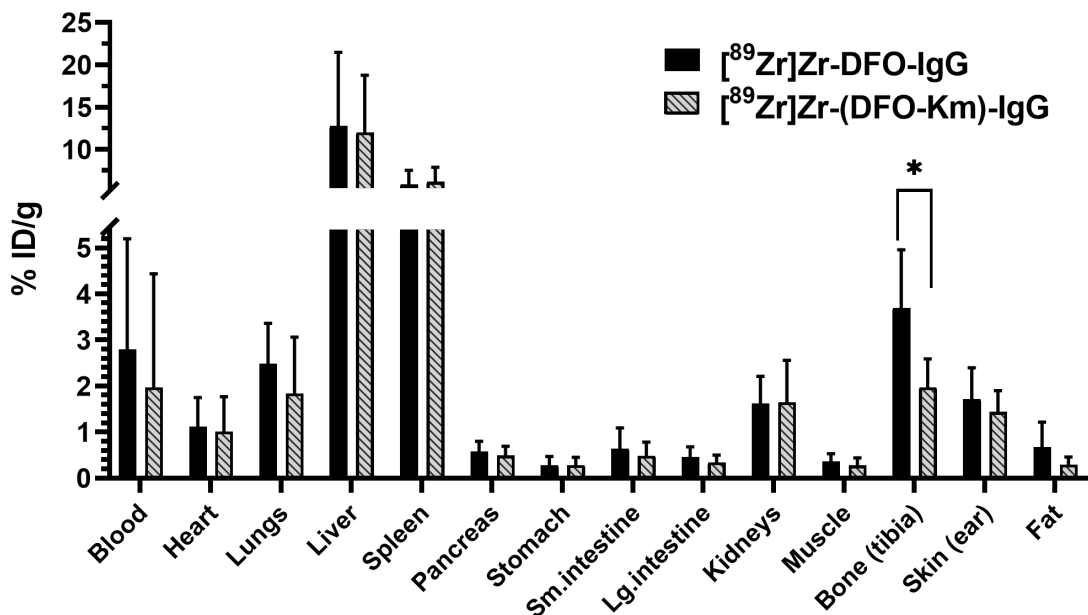
Figure 5-6. Results of biodistribution study of $[^{89}Zr]Zr$-DFO-IgG and $[^{89}Zr]Zr$-(DFO-Km)-IgG in healthy female CD-1 mice 14 d post injection. 9-10 MBq of either complex was injected in 200 µL of 0.9% saline, intravenously via tail vein catheter ($n = 6$). * = $p < 0.05$.

5.5. Conclusions

A hydrophilic tetrahydroxamate-based bifunctional chelator, DFO-Km (*p*-SCN-Ph-DFO-Km), was rationally designed to form extremely stable coordination complexes with $[^{89}Zr]Zr^{4+}$ and potentially other large and oxophilic radiometals for theranostic applications. Following the synthesis in 9 steps and complexation with non-radioactive zirconium(IV), *p*-SCN-Ph-DFO-Km was conjugated to a non-specific human serum antibody (IgG) along with *p*-SCN-Ph-DFO as a "gold standard" control. These immunoconjugates were radiolabeled with zirconium-89, purified, and their stability *in vivo* was investigated in healthy mice with a focus on bone uptake via PET/CT images and *ex vivo* biodistribution. The results showed that the IgG immunoconjugate with

[^{89}Zr]Zr-(DFO-Km) possessed significantly superior stability to [^{89}Zr]Zr-DFO as a notable reduction in bone uptake was observed. A statistically significant decrease in bone uptake was observed from the biodistribution data (14 days post injection), but more impressively the serial PET/CT images collected over a 14 day period revealed a visually striking difference with DFO-Km more effectively holding [^{89}Zr]Zr^{4+} than DFO and thus showing far lower skeletal uptake. Additionally, we performed a detailed study using DFT calculations and confirmed that DFO-Km has sufficient flexibility to reach an "ideal" coordination geometry with zirconium (IV). Improved water solubility makes DFO-Km accessible for conjugation of sensitive biomolecules in desirable and mild aqueous conditions, and its ability to form octadentate complexes could allow it to stably bind therapeutic radiometals such as actinium-225 or thorium-227 for theranostic applications.

5.6. Experimental Section

Reagents. All reagents and solvents were purchased from commercial suppliers (Sigma-Aldrich, St. Louis, MO; TCI America, Portland, OR; Fisher Scientific, Waltham, MA) and were used without further purification unless otherwise indicated. O-benzylhydroxylamine hydrochloride, Oxyma Pure and *N,N*-diisopropylethylamine (DIPEA), were purchased from Sigma-Aldrich. DFO mesylate was purchased from Abcam. 1-[Bis(dimethylamino)methylene]-1H-1,2,3-triazolo[4,5-b]pyridinium 3-oxid hexafluoroph-osphate (HATU) and H-Lys(Z)-OtBu were purchased from AK Scientific. ZrCl$_4$, EDTA, disodium salt, dihydrate (Molecular biology grade), ammonium acetate, succinic anhydride and 1-ethyl-3-(3-dimethylaminopropyl)carbodiimide hydrochloride (EDC. HCl) were purchased from Fisher Scientific.

Chemical Characterization Methods. ^{1}H and ^{13}C NMR spectra were recorded on a 500 MHz Bruker Avance III HD NMR spectrometer at the Saskatchewan Structural Science Centre at the University of Saskatchewan, at 25 ºC in D$_2$O, CDCl$_3$, or (CD$_3$)$_2$SO. Chemical shifts were referenced to the residual protons of the deuterated solvents for ^{1}H NMR (δ =4.79 ppm for D$_2$O; δ =7.26 ppm for CDCl$_3$ and δ = 2.50 ppm for (CD$_3$)$_2$SO. Similarly, ^{13}C chemical shifts were referenced to the CDCl$_3$ signal at 77.16 ppm and (CD$_3$)$_2$SO signal at δ = 39.52 ppm. Coupling constants are reported to the nearest 0.5 Hz (^{1}H NMR spectroscopy) and for ^{13}C NMR spectroscopy they are rounded to integer values in Hz. Field desorption ionization (FDI) was used on JEOL AccuTOF GCv 4G mass spectrometer to measure high resolution mass spectra and only the mass peak of the isotope with the highest natural abundance is recorded for the isotopic patterns. Antibody conjugates were analyzed on MALDI-TOF MS/MS using Bruker Ultraflex MALDI-TOF/TOF (Bruker Daltonic GmbH) (Alberta Proteomics and Mass spectrometry Facility, University of Alberta, Canada). HPLC purifications were performed on Thermofisher Vanquish HPLC using C18 reversed-phase column (Inspire Semipreparative DIKMA; 5 μm, 21.2 × 250 mm), a VF-D40-A UV detector, two VF-P10-A pumps, and Chromeleon 7 communication software. A flow rate of 4 mL/ minute was used with a gradient of MeCN:H$_2$O (with 0.1% formic acid (FA) in both solvents). Low resolution mass spectrometry was performed on Advion Expression-L system (mass range <2000 amu). The Advion Expression-L was coupled with the Thermofisher Vanquish system to perform LCMS. Concentration of antibody mixtures were determined using a Thermofisher NanoDrop UV/Vis instrument.

Synthesis of Compounds (13-15)

Synthetic procedures and characterization data for compounds **13-15** are detailed in chapter 4.

Synthesis of Compound (23). Compound **23** was synthesized according to a published procedure with modifications.[25] Succinic anhydride (2.19 g, 21.9 mmol) was added to a mixture of **15** (1.00 g, 7.29 mmol) and triethylamine (2.0 mL, 14.3 mmol) in THF (16 mL). The reaction mixture was stirred overnight at ambient temperature. After the reaction completion was confirmed with TLC (50% ethyl acetate in hexane, Rf = 0.28), the solvent was evaporated, and the residue was dissolved in aqueous sodium hydroxide (30 mL, 0.5 M). The solution was washed with diethyl ether (20 mL × 2). Then the solution was acidified to pH ~2 with hydrochloric acid and the product was extracted with dichloromethane (40 mL × 3). The organic layers were combined, dried over anhydrous sodium sulfate, and the solvent was removed by rotary evaporator to give compound **23** (1.29 g, 75%). ^{1}H NMR [CDCl$_3$, 500 MHz]: δ 2.62 (t, J=6.5 Hz, 2H, CH$_2$), 2.72 (t, J=6.4 Hz, 2H, CH$_2$), 3.19 (s, 3H, CH$_3$), 4.82 (s, 2H, CH$_2$), 7.32-737 (m, 5H, CH Ar), 10.93 (s, 1H, OH). ^{13}C NMR [CDCl$_3$, 126 MHz]: δ 27.0, 28.5, 76.1, 128.6, 129.2, 134.2, 173.5, 177.5. HRMS: m/z Calcd for [C$_{12}$H$_{15}$NO$_4$ + H]$^+$: 238.1074; found: 238.1082.

Synthesis of Compound (24). To solution of **23** (500.2 mg, 2.11 mmol) in DMF (15 mL), Oxyma (331.1 mg, 2.33 mmol), EDC (448.1 mg, 2.32 mmol), and *N,N*-diisopropylethylamine (1.1 mL, 6.32 mmol) were added. The mixture was stirred for 20 minutes at ambient temperature before H-Lys(Z)-OtBu HCl (851.4 mg, 2.28 mmol) was added, and the reaction was stirred overnight at ambient temperature. Then the reaction mixture was added to water (50 mL) and extracted with dichloromethane (30 mL × 4). The combined organic layers were collected and washed with water, dried with anhydrous sodium sulfate. The solvent was removed by using rotary evaporator and the obtained crude product mixture was purified with column chromatography (50% ethyl acetate in

hexane, Rf = 0.21) to give compound **24** (809.7 mg, 69%). ^{1}H NMR [CDCl$_3$, 500 MHz]: δ 1.36-1.40 (m, 2H, CH$_2$), 1.44 (s, 9H, CH$_3$), 1.50 (quint, J=7.0, 2H, CH$_2$), 1.58-1.86 (m, 2H, CH$_2$), 1.50 (quint, J=7.0 Hz, 2H, CH$_2$), 2.45-2.48 (m, 2H, CH$_2$), 2.67-2.84 (m, 2H, CH$_2$), 3.1 (s, 3H, CH$_3$), 3.14-3.22 (m, 2H, CH$_2$), 4.43, 4.48 (m, 1H, CH), 4.82 (s, 2H, CH$_2$), 5.06 (q, J=11. 4 Hz, 2H, CH$_2$), 5.31 (br s, 1H, NH), 6.45 (d, J=7.8 Hz, 1H, NH), 7.27-7.32 (m, 5H, CH), 7.36-7.38 (m, 5H, CH). ^{13}C NMR [CDCl$_3$, 126 MHz]: δ 22.0, 27.6, 28.0, 29.2, 30.5, 32.1, 40.5, 66.5, 76.3, 81.9, 128.0, 128.1, 128.5, 128.7, 129.0, 129.3, 156.6, 171.6, 171. 9. HRMS: m/z Calcd for [C$_{30}$H$_{41}$N$_3$O$_7$ + H]$^+$: 556.3017; found: 556.2992.

Synthesis of Compound (25). This procedure was modified from a published procedure.[28] Compound **24** (1.11 g, 2.00 mmol) was dissolved in a mixture of TFA (2.5 mL, 32.7 mmol) and dichloromethane (5 mL). The reaction was stirred for 6 hours at rt. Then the volatiles were removed by using rotary evaporator and the crude mixture was purified through column chromatography (10% methanol in ethyl acetate, Rf = 0.4) to give compound **25** (0.73 g, 74%). ^{1}H NMR [CDCl$_3$, 500 MHz]: δ 1.36-1.1.50 (m, 4H, CH$_2$), 1.66-1.92 (m, 2H, CH$_2$), 2.51 (br s, 2H, CH$_2$), 2.77 (br s, 2H, CH$_2$), 3.11 (s, 3H, CH$_3$), 3.15-3.19 (m, 2H, CH$_2$), 4.54 (q, J=6.7 Hz, 1H, CH), 4.82 (s, 2H, CH$_2$), 5.03-5.12 (m, 2H, CH$_2$). 7.03 (br s, 1H, NH), 7.28 – 7.36 (m, 10H, CH), 10.17 (br s, 1H, OH). ^{13}C NMR [CDCl$_3$, 126 MHz]: δ 22.3, 27.7, 29.3, 30.4, 31.4, 33.7, 40.6, 52.3, 66.7, 76.4, 128.1, 128.2, 128.6, 128.8, 129.1, 129.4, 134.3, 136.7, 156.9, 173.1, 174.2, 174.8. HRMS: m/z Calcd for [C$_{26}$H$_{33}$N$_3$O$_7$ + H]$^+$: 500.2391; found: 500.2410.

Synthesis of Compound (26). A solution of HATU (0.27 g, 0.71 mmol) and DIPEA (0.35 mL, 0.70 mmol) in 14 mL DMF was added to a solution of **25** (0.30 g, 0.60 mmol) in 13 mL DMF and

the mixture was stirred for 10 minutes at ambient temperature. DFO mesylate (0.44 g, 0.67 mmol) was dissolved in 10 mL DMF and 4 mL DMSO (at 80 °C). Once fully dissolved, the DFO mixture was allowed to cool for few minutes (~ 50 °C), it was then added to the above solution of the activated ester. The reaction was left to stir overnight at ambient temperature. Then the reaction mixture was condensed to ~2 mL by using rotary evaporator and the residue was added dropwise to ~70 mL ethyl acetate spread into 2 falcon tubes (50 mL size tubes). The tubes were kept in a spark proof -20 °C freezer until maximum amount of precipitate was formed (overnight). The precipitate was separated by decantation after centrifugation (4000 rpm, 15 minutes) and washed two times with cold ethyl acetate. The crude was then purified by using reverse phase column chromatography (Biotage Isolera) (10 -100% acetonitrile in water) to collect **26** (316 mg, 50%) as an off-white powder. ^{1}H NMR [(CD$_3$)$_2$SO, 500 MHz]: δ 1.19 – 1.67 (m, 28H, CH$_2$), 1.95 (s, 3H, CH$_3$), 2.26 (t, J= 7.3 Hz, 4H, CH$_2$), 2.31-2.38 (m, 2H, CH$_2$), 2.57 (t, J=6.9 Hz, 4H, CH$_2$), 2.65 (br s, 2H, CH$_2$), 2.9-3.00 (m, 8H, CH$_2$), 3.12 (s, 3H, CH$_3$), 3.44 (q, J=6.6 Hz, 6H, CH$_2$), 4.08-4.13 (m, 1H, CH), 4.90 (s, 2H, CH$_2$), 4.99 (s, 2H, CH$_2$), 7.22 (t, J=5.6 Hz, 1H, NH), 7.30-7.45 (m, 10H, CH), 7.76 (t, J=5.5 Hz, 1H, NH), 7.82 (br s, 2H, NH), 8.00 (br d, J=8, 1H, NH), 9.74 (br s, 3H, OH). ^{13}C NMR [(CD$_3$)$_2$SO, 126 MHz]: δ 22.8, 23.1, 23.5, 26.0, 27.1, 27.6, 28.7, 28.8, 29.1, 29.6, 30.0, 31.6, 38.4, 46.8, 47.1, 65.1, 127.7, 128.4, 128.5, 128.7, 129.4, 137.3, 156.1, 171.3, 171.6, 171.9. HRMS: m/z Calcd for [C$_{51}$H$_{79}$N$_9$O$_{14}$ + H]$^+$: 1042.5825; found: 1042.5819.

Synthesis of Compound (27) DFO-Km. In a Schlenk flask, 10% Palladium on carbon (25.0 mg, 23.5 μmol) was added to a solution of compound **26** (120.0 mg, 115 μmol) in 20 mL methanol. The flask was sealed with a rubber septa and connected to an H$_2$ gas balloon fitted with a glass stopcock and a needle, and the flask was additionally connected to vacuum via Schlenk line. The

flask was put under vacuum for 15 seconds and then the vacuum was closed, and the flask was purged with H_2 gas by slowly opening the glass stopcock valve. The vacuum and purging were repeated 4 times and finally the flask was left stirring under H_2 for 2 h, the reaction solution was filtered through celite to remove the Pd/C, and the solvent was evaporated by using rotary evaporator. The crude product mixture was purified by using semipreparative RP-HPLC. HPLC conditions: C18 Inspire Semipreparative DIKMA; 5 µm, 21.2 × 250 mm; (20 – 32% acetonitrile in water (0.1% formic acid); flow rate, 4 mL/min, t_R = 15 min) to give **27** (83.5 mg, 89%) as white powder. ^{1}H NMR [D_2O, 500 MHz]: δ 1.20-1.83 (m, 24H, CH_2), 2.09 (s, 3H, CH_3), 2.44-2.53 (m, 6H, CH_2), 2.62-2.81 (m, 6H, CH_2), 2.96 (t, J=7.6 Hz, 2H, CH_2), 3.12-3.16 (m, 6H, CH_2), 3.19 (s, 3H, CH_3), 3.55-3.62 (m, 6H, CH_2), 4.17 (q, J=4.8, 1H, CH). ^{13}C NMR [D_2O, 126 MHz]: δ 19.3, 22.1, 23.0, 25.4, 26.2, 27.1, 27.6, 27.8, 28.0, 29.8, 30.3, 30.4, 30.7, 35.8, 39.1, 47.6, 47.8, 51.0, 51.5, 53.8, 170.8, 173.5, 173.8, 173.9, 174.7, 175.4. HRMS: m/z Calcd for $[C_{36}H_{67}N_9O_{12} + H]^+$: 818.4982; found: 818.4942.

Synthesis of Compound (28) ^{Nat}Zr-(DFO-Km). Following a published procedure,[29] a solution of $ZrCl_4$ (200µL, 90.0 mM, 18.3 µmol, in Chelex-treated Millipure water) was added to a solution of **DFO-Km (27)** (15 mg, 18.3 µmol) in 0.9 mL of Chelex-treated Millipure water. The pH of the reaction mixture was adjusted to ~7 by adding sodium carbonate (1 M), and it was shaken on a thermomixer at 800 rpm, at ambient temperature for 2 hours. Then the solvent was lyophilized and compound **28 ^{nat}Zr(IV)-(DFO-Km)** (16 mg, 96%) was obtained as a white powder. ^{1}H NMR [D_2O, 500 MHz]: δ 1.21- 1.71 (m, 24H, CH_2), 2.09 (s, 3H, CH_3), 2.44-2.90 (m, 12H, CH_2), 2.92-3.04 (m, 4H, CH_2), 3.15-3.19 (m, 3H, CH_3), 3.28-3.86 (m, 10H, CH_2), 4.15-4.21 (m, 1H, CH). HRMS: m/z Calcd for $[C_{36}H_{63}N_9O_{12}Zr + Na]^+$: 926.3535; found: 926.3534.

Synthesis of Compound (29) *p*-SCN-Ph-DFO-Km. The bifunctionalization of DFO-Km was performed according to published procedure with modifications.[30] *p*-phenylene diisothiocyanate (70.5 mg, 0.37 mmol) in 1 mL DCM was added to solution of **DFO-Km (27)** (31.5 mg, 0.037 mmol) and triethylamine (26.0 µL, 0.19 mmol) in 2 mL DMF and the reaction mixture was stirred for 1.5 hour at ambient temperature. Then the mixture was added dropwise to 40 mL diethyl ether and left in a spark proof -20 °C freezer for 30 minutes. The formed precipitate was separated by using centrifugation and it was washed with more diethyl ether. The obtained precipitate was purified by using semipreparative RP-HPLC. HPLC conditions: C18 Inspire Semipreparative DIKMA; 5 µm, 21.2 × 250 mm; (40 – 65% acetonitrile in water (0.1% formic acid); flow rate, 4 mL/min, t_R = 25 min) to give **29** (14.3 mg, 37%) as an off-white powder. ^{1}H NMR [$(CD_3)_2SO$, 500 MHz]: δ 1.20-1.72 (m, 24H, CH_2), 1.96 (s, 3H, CH_3), 2.25-2.40 (m, 6H, CH_2), 2.54-2.60 (m, 8H, CH_2), 2.97-3.02 (m, 6H, CH_2), 3.07 (s, 3H, CH_3), 3.44 (q, J=6.6 Hz, 6H, CH_2), 4.10 (quint, 1H, CH), 7.4 (d, J=8.8, 2H, CH), 7.55 (d, J=8.8, 2H, CH), 7.78 (t, J=5.0, 3H, NH), 8.05 (d, J=8.0, 2H, NH), 9.64-9.88 (m, 4H, OH). ^{13}C NMR [$(CD_3)_2SO$, 126 MHz]: δ 20.4, 23.1, 23.5, 26.1, 27.5, 28.1, 28.7, 28.8, 29.8, 29.9, 31.5, 35.7, 46.8, 47.1, 52.7, 123.0, 126.2, 132.6, 139.5, 170.1, 171.3, 171.5, 171.8, 172.0. HRMS: m/z Calcd for $[C_{44}H_{71}N_{11}O_{12}S_2 + H]^+$: 1010.4803; found: 1010.4809.

IgG Conjugation. Following a standard procedure,[24] a 205 µL solution of nonspecific human serum IgG in PBS buffer pH 7 (1.5 mg mAb, 10.2 nmol, 7.4 mg/mL, purchased as lyophilized powder from Sigma) was diluted by addition of 250 µL PBS buffer pH 7, then sodium carbonate (35 µL, 0.1 M) was added to adjust the pH to ~ 8-9 (by pH strip). This was followed by addition of 7 µL *p*-SCN-Ph-DFO solution (5.5 molar equivalent, 8.25 mg/µL in DMSO) or 13 µL (10.2

molar equivalent). The reaction mixture was shaken on a thermomixer at 800 rpm, at 37 °C for 2 h. The resultant immunoconjugates were purified by using PD-10 desalting column and Amicon® Ultra-4 Centrifugal Filter Ultracel-50K (3500 rpm). Commercially available *p*-SCN-Ph-DFO was purchased from Macrocyclics and was also conjugated to IgG (using 5.5 molar equivalent) and purified in the same manner explained for (DFO-Km)-IgG. Finally, samples of IgG conjugates along with unmodified IgG were prepared (10 μL, 1.0 mg/mL, in Chelex treated ultrapure water, n = 3) and analyzed by MALDI-TOF MS/MS to determine the average chelator to antibody ratio (CAR).

Radiochemistry. [^{89}Zr]Zr-oxalate in 1.0 M oxalic acid was received from the Saskatchewan Centre for Cyclotron Sciences (SCCS) on the University of Saskatchewan campus. The apparent molar activity of the [^{89}Zr]Zr-oxalate produced routinely by the SCCS (as used for this study), was found to be in the range of 673-1161 MBq/μmol, by using a method from Holland et al.[31,32] Purity was determined to be 99.99%.[33] For radiolabeling of the immunoconjugates, the required amount of the [^{89}Zr]Zr^{4+} (in 1.0 M oxalic acid) was neutralized to pH 6.8-7.2 by using sodium carbonate (1.0 M) and the reactions were performed in HEPES buffer (0.5 M, pH 7). Silica-gel impregnated glass-microfiber instant thin layer chromatography paper (iTLC-SG, Varian, Lake Forest, CA) was used for reaction progress monitoring and radiochemical yield determination. EDTA solution (50 mM, pH 5.5) was used to develop the iTLCs, which in general elutes free [^{89}Zr]Zr^{4+} to the solvent front while radiolabeled immunoconjugates remained at the baseline. The radio-iTLCs were analyzed on a Eckert & Ziegler AR-2000 radio-TLC plate reader using Winscan Radio-TLC software. All solution were prepared in Chelex-100 resin (BioRad Laboratories, Hercules, CA) treated (1.2 g/L water, 24 h) Ultrapure water (>18.2 MΩ cm^{-1} at 25°C, Milli-Q, Millipore, Billerica,

MA). For activity measurements, either Perkin-Elmer (Waltham, MA) Automated Wizard Gamma Counter or Capintec CRC-15R dose calibrator (Capintec, Ramsey, NJ) was used and is indicated for each experiment. The concentration of the immunoconjugates were determined on NanoDrop^{TM} 2000c spectrophotometer (Thermo Scientific).

Radiolabeling of the Immunoconjugates. Radiolabeling of the immunoconjugates was performed according to established procedures,[24] 190 µL (112 MBq) aliquots of freshly neutralized [^{89}Zr]Zr^{4+} in HEPES buffer pH 7, was mixed with 500 µg solutions of either (DFO-Km)-IgG (329 µL, only immunoconjugate with 1.4 CAR was used) or DFO-IgG (303 µL). The reaction mixtures were further diluted to 500 µL final volume by adding more HEPES buffer pH 7 and then they were shaken on a thermomixer at 800 rpm, at 37 °C. Radio-iTLC confirmed >99% radiochemical yield of both radioimmunoconjugates after 30 minutes. To exchange the buffer from HEPES buffer to sterile saline and for further purification the reaction solutions were passed through PD-10 desalting columns, and they were eluted by 2.0 mL saline. The final concentration of the solutions was determined by using nanodrop spectrophotometer.

PET/CT Imaging and Biodistribution in Healthy Mice. [^{89}Zr]Zr-(DFO-Km)-IgG and [^{89}Zr]Zr-DFO-IgG immunoconjugates were prepared as described above and 99% RCY was confirmed by using radio-iTLC. Aliquots of ~10 MBq of radiolabeled immunoconjugates were injected intravenously into healthy female CD-1 mice (n = 6 per cohort). PET/CT imaging was performed using the first 4 mice from each cohort (4-mouse bed) and were collected at time points of 1, 3, 7 and 14 days post injection on the Sofie GNEXT PET/CT small animal imaging system using the included 4-mouse heated bed. The PET/CT images were reconstructed with Sofie GNEXT

software and processed with VivoQuant® 2020 software (patch 1 64 bit, build vq-2020patch1-0-ga8255affc). Following the final 14 day imaging timepoint, all the 12 mice (6 per compound) were euthanized by anesthesia followed by cervical dislocation followed by cardiac puncture and blood draw. Blood and specific organs were harvested, weighed, and residual activity in the organs were measured by using an automated gamma counter. The animals had access to cage enrichments and access to food and water ad-libitum. The experimental protocol was approved by the University of Saskatchewan Committee on Animal Care and procedures were performed in accordance with the guidelines of the Canadian Council on Animal Care and the Canadian Nuclear Safety Commission.

Density Function Theory (DFT) Calculations. DFT geometry optimizations were carried out on DMOL³ and Biovia Materials Studio software, version 20.10.5 (2020)[34,35] on the PC (Windows 10) by using the generalized gradient approximation (GGA) employing the Perdew-Burke-Ernzerhof (PBE)[36] functional both for the potential during the self-consistent field (SCF) procedure and energy.[37] All calculations employed DMol³ double numerical plus d-function (DND) basis set using 4.4 basis file included polarization functions for all atoms with all-electron core treatments. Conductor-like screening model (COSMO)[38,39] solvation model was used for quantum simulation of solvated molecules with a dielectric value of ($\varepsilon = 78.54$) for water. CYLview software (CYLview, 1.0b; Legault, C. Y., Université de Sherbrooke, 2009, http://www.cylview.org) was used for graphical depiction of the structures from the log files of the optimized structures.

5.7. Associated Content

Supporting information

The supporting information for this chapter is summarized in Appendix-III

5.8. References

(1)   Kasbollah, A.; Eu, P.; Cowell, S.; Deb, P. Review on Production of 89Zr in a Medical Cyclotron for PET Radiopharmaceuticals. *J. Nucl. Med. Technol.* **2013**, *41* (1), 35–41.

(2)   Zeglis, B. M.; Lewis, J. S. The Bioconjugation and Radiosynthesis of 89Zr-DFO-Labeled Antibodies. *J Vis Exp* **2015**, No. 96.

(3)   Price, E. W.; Carnazza, K. E.; Carlin, S. D.; Cho, A.; Edwards, K. J.; Sevak, K. K.; Glaser, J. M.; de Stanchina, E.; Janjigian, Y. Y.; Lewis, J. S. 89Zr-DFO-AMG102 Immuno-PET to Determine Local Hepatocyte Growth Factor Protein Levels in Tumors for Enhanced Patient Selection. *J. Nucl. Med.* **2017**, *58* (9), 1386–1394.

(4)   Jauw, Y. W. S.; O'Donoghue, J. A.; Zijlstra, J. M.; Hoekstra, O. S.; Oordt, C. W. M. der H. van; Morschhauser, F.; Carrasquillo, J. A.; Zweegman, S.; Pandit-Taskar, N.; Lammertsma, A. A.; Dongen, G. A. M. S. van; Boellaard, R.; Weber, W. A.; Huisman, M. C. 89Zr-Immuno-PET: Toward a Noninvasive Clinical Tool to Measure Target Engagement of Therapeutic Antibodies In Vivo. *J. Nucl. Med.* **2019**, *60* (12), 1825–1832.

(5)   van de Watering, F. C. J.; Rijpkema, M.; Perk, L.; Brinkmann, U.; Oyen, W. J. G.; Boerman, O. C. Zirconium-89 Labeled Antibodies: A New Tool for Molecular Imaging in Cancer Patients. *Biomed. Res. Int.* **2014**, *2014*, 203601.

(6)   Holland, J. P.; Divilov, V.; Bander, N. H.; Smith-Jones, P. M.; Larson, S. M.; Lewis, J. S. 89Zr-DFO-J591 for ImmunoPET of Prostate-Specific Membrane Antigen Expression In Vivo. *J. Nucl. Med.* **2010**, *51* (8), 1293–1300.

(7)   Jauw, Y. W. S.; Menke-van der Houven van Oordt, C. W.; Hoekstra, O. S.; Hendrikse, N. H.; Vugts, D. J.; Zijlstra, J. M.; Huisman, M. C.; van Dongen, G. A. M. S. Immuno-Positron Emission Tomography with Zirconium-89-Labeled Monoclonal Antibodies in Oncology: What Can We Learn from Initial Clinical Trials? *Front. Pharmacol.* **2016**, *7*, 131.

(8)   Yoon, J.-K.; Park, B.-N.; Ryu, E.-K.; An, Y.-S.; Lee, S.-J. Current Perspectives on 89Zr-PET Imaging. *Int. J. Mol. Sci.* **2020**, *21* (12), 4309.

(9)   McKnight, B. N.; Viola-Villegas, N. T. 89Zr-ImmunoPET Companion Diagnostics and Their Impact in Clinical Drug Development. *J. Labelled Comp. Radiopharm.* **2018**, *61* (9), 727–738.

(10)   N Tinianow, J.; Pandya, D. N.; Pailloux, S. L.; Ogasawara, A.; Vanderbilt, A. N.; Gill, H. S.; Williams, S.-P.; Wadas, T. J.; Magda, D.; Marik, J. Evaluation of a 3-Hydroxypyridin-2-One (2,3-HOPO) Based Macrocyclic Chelator for (89)Zr(4+) and Its Use for ImmunoPET Imaging of HER2 Positive Model of Ovarian Carcinoma in Mice. *Theranostics* **2016**, *6* (4), 511–521.

(11) Longtine, M.; Hoegger, M.; Abou, D.; Shim, K.; Thorek, D.; Wahl, R. Comparative Biodistribution of 89Zr-Ofatumumab and 225Ac-Ofatumumab for Lymphoma Radioimmunotherapy. *J. Nucl. Med.* **2020**, *61* (supplement 1), 381–381.

(12) Deri, M. A.; Ponnala, S.; Zeglis, B. M.; Pohl, G.; Dannenberg, J. J.; Lewis, J. S.; Francesconi, L. C. Alternative Chelator for 89Zr Radiopharmaceuticals: Radiolabeling and Evaluation of 3,4,3-(LI-1,2-HOPO). *J. Med. Chem.* **2014**, *57* (11), 4849–4860.

(13) Sarbisheh, E. K.; Salih, A. K.; Raheem, S. J.; Lewis, J. S.; Price, E. W. A High-Denticity Chelator Based on Desferrioxamine for Enhanced Coordination of Zirconium-89. *Inorg. Chem.* **2020**, *59* (16), 11715–11727.

(14) Price, E. W.; Orvig, C. Matching Chelators to Radiometals for Radiopharmaceuticals. *Chem. Soc. Rev.* **2014**, *43* (1), 260–290.

(15) Deri, M. A.; Ponnala, S.; Kozlowski, P.; Burton-Pye, B. P.; Cicek, H. T.; Hu, C.; Lewis, J. S.; Francesconi, L. C. P-SCN-Bn-HOPO: A Superior Bifunctional Chelator for 89Zr ImmunoPET. *Bioconjug. Chem.* **2015**, *26* (12), 2579–2591.

(16) Allott, L.; Da Pieve, C.; Meyers, J.; Spinks, T.; Ciobota, D. M.; Kramer-Marek, G.; Smith, G. Evaluation of DFO-HOPO as an Octadentate Chelator for Zirconium-89. *Chem. Commun. (Camb.)* **2017**, *53* (61), 8529–8532.

(17) Patra, M.; Bauman, A.; Mari, C.; Fischer, C. A.; Blacque, O.; Häussinger, D.; Gasser, G.; Mindt, T. L. An Octadentate Bifunctional Chelating Agent for the Development of Stable Zirconium-89 Based Molecular Imaging Probes. *Chem. Commun.* **2014**, *50* (78), 11523–11525.

(18) Seibold, U.; Wängler, B.; Wängler, C. Rational Design, Development, and Stability Assessment of a Macrocyclic Four-Hydroxamate-Bearing Bifunctional Chelating Agent for 89 Zr. *ChemMedChem* **2017**, *12* (18), 1555–1571.

(19) Klasen, B.; Lemcke, D.; Mindt, T. L.; Gasser, G.; Rösch, F. Development and in Vitro Evaluation of New Bifunctional 89Zr-Chelators Based on the 6-Amino-1,4-Diazepane Scaffold for Immuno-PET Applications. *Nucl. Med. Biol.* **2021**, *102–103*, 12–23.

(20) Pandit-Taskar, N.; O'Donoghue, J. A.; Ruan, S.; Lyashchenko, S. K.; Carrasquillo, J. A.; Heller, G.; Martinez, D. F.; Cheal, S. M.; Lewis, J. S.; Fleisher, M.; Keppler, J. S.; Reiter, R. E.; Wu, A. M.; Weber, W. A.; Scher, H. I.; Larson, S. M.; Morris, M. J. First-in-Human Imaging with 89Zr-Df-IAB2M Anti-PSMA Minibody in Patients with Metastatic Prostate Cancer: Pharmacokinetics, Biodistribution, Dosimetry, and Lesion Uptake. *J. Nucl. Med.* **2016**, *57* (12), 1858–1864.

(21) Ulaner, G. A.; Hyman, D. M.; Lyashchenko, S. K.; Lewis, J. S.; Carrasquillo, J. A. 89Zr-Trastuzumab PET/CT for Detection of HER2-Positive Metastases in Patients with HER2-Negative Primary Breast Cancer. *Clin. Nucl. Med.* **2017**, *42* (12), 912–917.

(22) Pandit-Taskar, N.; O'Donoghue, J. A.; Durack, J. C.; Lyashchenko, S. K.; Cheal, S. M.; Beylergil, V.; Lefkowitz, R. A.; Carrasquillo, J. A.; Martinez, D. F.; Fung, A. M.; Solomon, S. B.; Gönen, M.; Heller, G.; Loda, M.; Nanus, D. M.; Tagawa, S. T.; Feldman, J. L.; Osborne, J. R.; Lewis, J. S.; Reuter, V. E.; Weber, W. A.; Bander, N. H.; Scher, H. I.; Larson, S. M.; Morris, M. J. A Phase I/II Study for Analytic Validation of 89Zr-J591 ImmunoPET as a Molecular Imaging Agent for Metastatic Prostate Cancer. *Clin. Cancer Res.* **2015**, *21* (23), 5277–5285.

(23) Summers, K. L.; Sarbisheh, E. K.; Zimmerling, A.; Cotelesage, J. J. H.; Pickering, I. J.; George, G. N.; Price, E. W. Structural Characterization of the Solution Chemistry of

Zirconium(IV) Desferrioxamine: A Coordination Sphere Completed by Hydroxides. *Inorg. Chem.* **2020**, *59* (23), 17443–17452.

(24) Vosjan, M. J. W. D.; Perk, L. R.; Visser, G. W. M.; Budde, M.; Jurek, P.; Kiefer, G. E.; van Dongen, G. A. M. S. Conjugation and Radiolabeling of Monoclonal Antibodies with Zirconium-89 for PET Imaging Using the Bifunctional Chelate p-Isothiocyanatobenzyl-Desferrioxamine. *Nat. Protoc.* **2010**, *5* (4), 739–743.

(25) Olshvang, E.; Szebesczyk, A.; Kozłowski, H.; Hadar, Y.; Gumienna-Kontecka, E.; Shanzer, A. Biomimetic Ferrichrome: Structural Motifs for Switching between Narrow- and Broad-Spectrum Activities in P. Putida and E. Coli. *Dalton Trans.* **2015**, *44* (48), 20850–20858.

(26) Holland, J. P. Predicting the Thermodynamic Stability of Zirconium Radiotracers. *Inorg. Chem.* **2020**, *59* (3), 2070–2082.

(27) Sharma, S. K.; Glaser, J. M.; Edwards, K. J.; Khozeimeh Sarbisheh, E.; Salih, A. K.; Lewis, J. S.; Price, E. W. A Systematic Evaluation of Antibody Modification and 89Zr-Radiolabeling for Optimized Immuno-PET. *Bioconjug. Chem.* **2020**.

(28) Gudmundsdottir, A. V.; Paul, C. E.; Nitz, M. Stability Studies of Hydrazide and Hydroxylamine-Based Glycoconjugates in Aqueous Solution. *Carbohydr. Res.* **2009**, *344* (3), 278–284.

(29) Zhang, Y.; Hong, H.; Cai, W. PET Tracers Based on Zirconium-89. *Curr. Radiopharm.* **2011**, *4* (2), 131–139.

(30) Perk, L. R.; Vosjan, M. J. W. D.; Visser, G. W. M.; Budde, M.; Jurek, P.; Kiefer, G. E.; van Dongen, G. A. M. S. P-Isothiocyanatobenzyl-Desferrioxamine: A New Bifunctional Chelate for Facile Radiolabeling of Monoclonal Antibodies with Zirconium-89 for Immuno-PET Imaging. *Eur. J. Nucl. Med. Mol. Imaging* **2010**, *37* (2), 250–259.

(31) Holland, J. P.; Sheh, Y.; Lewis, J. S. Standardized Methods for the Production of High Specific-Activity Zirconium-89. *Nucl. Med. Biol.* **2009**, *36* (7), 729–739.

(32) Alizadeh, E.; Behlol Ayaz Ahmed, K.; Raja Solomon, V.; Gaja, V.; Bernhard, W.; Makhlouf, A.; Gonzalez, C.; Barreto, K.; Casaco, A.; Geyer, C. R.; Fonge, H. 89Zr-Labeled Domain II-Specific ScFv-Fc ImmunoPET Probe for Imaging Epidermal Growth Factor Receptor In Vivo. *Cancers* **2021**, *13* (3), 560.

(33) Gaja, V.; Cawthray, J.; Geyer, C. R.; Fonge, H. Production and Semi-Automated Processing of 89Zr Using a Commercially Available TRASIS MiniAiO Module. *Molecules* **2020**, *25* (11), 2626.

(34) Delley, B. From Molecules to Solids with the DMol3 Approach. *J. Chem. Phys.* **2000**, *113* (18), 7756–7764.

(35) Delley, B. An All-electron Numerical Method for Solving the Local Density Functional for Polyatomic Molecules. *J. Chem. Phys.* **1990**, *92* (1), 508–517.

(36) Perdew, null; Burke, null; Ernzerhof, null. Generalized Gradient Approximation Made Simple. *Phys. Rev. Lett.* **1996**, *77* (18), 3865–3868.

(37) Peverati, R.; Truhlar, D. G. M11-L: A Local Density Functional That Provides Improved Accuracy for Electronic Structure Calculations in Chemistry and Physics. *J. Phys. Chem. Lett.* **2012**, *3* (1), 117–124.

(38) Klamt, A.; Schüürmann, G. COSMO: A New Approach to Dielectric Screening in Solvents with Explicit Expressions for the Screening Energy and Its Gradient. *J. Chem. Soc., Perkin Trans. 2* **1993**, No. 5, 799–805.

(39) Andzelm, J.; Kölmel, C.; Klamt, A. Incorporation of Solvent Effects into Density Functional Calculations of Molecular Energies and Geometries. *J. Chem. Phys.* **1995**, *103* (21), 9312–9320.

Chapter 6. Conclusions and Future Work

6.1. Conclusions

DFO is the current gold standard chelator for zirconium-89 that lacks optimum stability as evident from mouse *in vivo* biodistribution studies. Although stable enough for successful clinical imaging, chelators with improved stability relative to DFO are still of value. Further, DFO cannot be used for true theranostic applications given its limited coordination number of six and inability to stably coordinate any therapeutic radiometal ions. The focus of my PhD work presented in this thesis was to develop new chelators for zirconium-89 with the objective of improving stability over DFO, and provide a high enough coordination number to bind larger radiometal ions. Zirconium-89 has the desired properties for immunoPET and has the potential to be used as an imaging companion with several interesting therapeutic radiometals such as actinium-225 and thorium-227. To achieve these goals, we had to develop chelators with not only improved stability, but with increased coordination potential to complex with therapeutic radiometals. DFO being a hexadentate, fails to meet even the 8-coordination number of zirconium-89. I reviewed the literature, studied, and developed chelators with higher denticity scaffolds (8-12) that have successfully improved stability with zirconium-89 relative to DFO and have the possibility of coordination with other oxophilic radiometals.

Several chelators for zirconium-89 have been developed over the past years such as DFO*, HOPO, and DFO-HOPO to tackle the stability concern of DFO. This has been done by increasing the denticities of these chelators from 6 to 8 to meet the coordination numbers of zirconium-89. Therefore, my goal was to develop a chelator which could saturate the coordination numbers of zirconium-89 to increase its stability but also to develop a modular platform for synthesizing a broad range of chelators which could be complexed with larger therapeutics radiometals such as

actinium-225 and thorium-227. For that purpose, I developed and evaluated DFO2, a dodecadentate chelator which was found to form highly stable coordination complexes with zirconium-89 (Chapter 2, **Figures 2-3** to **2-5**, **Table 2-2**).

A lingering problem exists in these previously published chelators with increased denticities, which is their low water solubility. DFO2 shared this common and undesirable trait amongst hydroxamic acid-based chelators of limited water solubility (see **Table 2-1**). Thus, I intended to synthesize a chelator overcoming the concern of water solubility in my second project (Chapter 3). The water solubility concern of DFO2 was resolved by developing DFO2K and DFO-Km, which are two derivatives of DFO2 where the propylenediamine linker was replaced by a lysine. DFO2K was designed to have a simpler and higher yielding synthesis and better overall *in vitro* stability compared to DFO and DFO2 (see **Figures 3-4** and **3-5**). The chelator DFO-Km had a more involved synthesis as it contains a single DFO chain along with a custom synthesized hydroxamic acid monomer unit (Chapter 5). The *in vivo* stability of the pre-bifunctional and then its bifunctional immunoconjugate revealed DFO2K to be an excellent chelator for zirconium-89 (see **Figures 3-6** to **3-8**). The expanded coordination sphere/number of DFO2K (CN up to 12) from its two extra hydroxamic acid groups might contribute towards expanding its usage for larger therapeutic radiometals for which DFO is not compatible, although the hard-soft acid base properties of the hydroxamic acid donor groups remains the same.

Given the concept existent in the field, that with increasing denticities, the stability increases but the solubility attenuates, I was interested to develop a chelator which can still have an octadentate coordination sphere which is matching zirconium(IV). This new chelator was designed to maintain optimal stability and employ the same modular amino acid linker as used for synthesizing DFO2K to improve the solubility. First, I synthesized and evaluated a novel glutamic

acid-based octadentate chelator DFO-Em (Chapter 4). This chelator showed a successful chelator design for zirconium-89 from the combination of DFO and a hydroxamate monomer. The *in vitro* studies (see **Figures 4-5** and **4-6**) showed that octadentate DFO-Em has comparable stability to dodecadentate DFO2K in coordination with zirconium (IV) with much higher hydrophilicity as measured by $LogD_{PBS}$ and observed qualitatively when dissolving in aqueous buffers.

Interestingly, DFO-Em studies led me to the recognition that hydroxamic acid-based chelators are incompatible with standard peptide-coupling chemistry required to insert bifunctionalization via activated esters. To this end, I have synthesized and demonstrated the properties of a lysine-based derivative of DFO-Em, called DFO-Km (Chapter 5). The dramatic decrease in bone uptake of zirconium-89 from murine studies of antibody conjugated DFO-Km showed that this chelator formed the most stable coordination among all the other chelators developed in this thesis, with all being substantially more stable than DFO (see **Figures 5-4** and **4-5**).

It is important to mention that the modular platform I developed during my PhD study can be transferred to develop chelators for different metals with different coordination requirements such as coordination number and donor ligands/groups, and various conjugation chemistry, as evident from the synthesis DFO-Em and DFO-Km by modifying the modular amino acid-based scaffold of DFO2K. This modularity can be used beyond zirconium-89 by replacing the hydroxamic acid groups with groups/moieties suitable for coordination of other radiometals for diagnostic or/and therapeutic applications. Overall, these chelators developed in this thesis not only improve the pool of chelators for zirconium-89 based PET diagnosis but also contribute to the theranostic approach by providing higher denticity chelators that form stable complexes with zirconium-89.

Some limitations of this work are immunoconjugation studies with non-specific IgG antibodies are used, which in the future can be followed-up with immuno-PET studies using clinically relevant monoclonal antibodies such as trastuzumab or nimotuzumab. Another drawback of my work is the animal studies are performed only in healthy mice and due to COVID restrictions and time permeability I could not leverage cancer models of mice to test these radiometal-chelators. This work is planned for the near future. Finally, we were not able to source other exotic radiometals such as actinium-225 or thorium-227 on time to test them with these new chelators.

6.2. Future work

The lead chelators *p*-SCN-Ph-DFO-Km and *p*-SCN-Ph-DFO2K will be conjugated to different functional antibodies and further *in vivo* studies will be carried out in cancer mouse models to compare tumor to healthy tissue uptake ratios, especially in liver and bone. Furthermore, these chelators are designed with higher denticity numbers compared to DFO with the purpose of increasing the possibility of binding to high valent and oxophilic radiometals. If therapeutic radiometal(s) can be found which the DFO2 family of chelators can bind quickly and stably, it will enable zirconium-89 to be paired with therapeutic radiometals for theranostic applications. The evaluation of these chelators especially DFO2K and DFO-Km with therapeutic radiometals such as actinium-225 and thorium-227 are future work.

Other derivatives of these chelators could be synthesized which are based on different amino acids, which will provide access to different conjugation chemistries. For example, conjugation to other amino acids including unnatural amino acids will provide different functional groups. This could include azido-lysine for access to click chemistry or cysteine for thiol conjugations. To access other clinically relevant radiometals with far different coordination

preferences to zirconium-89 such as copper-64, gallium-68, lutetium-177, yttrium-90, or indium-111, different donor groups than hydroxamic acids will likely be required. This would mean a substantial redesign of the chelators described in this thesis, but perhaps the modular amino acid backbone of the DFO2 family can be utilized.

Synthesis and Evaluation of DFO2K: a Modular Chelator with Ideal Properties for Theranostic Applications of Zirconium-89

DFO-Lys(Z)-Boc (7)
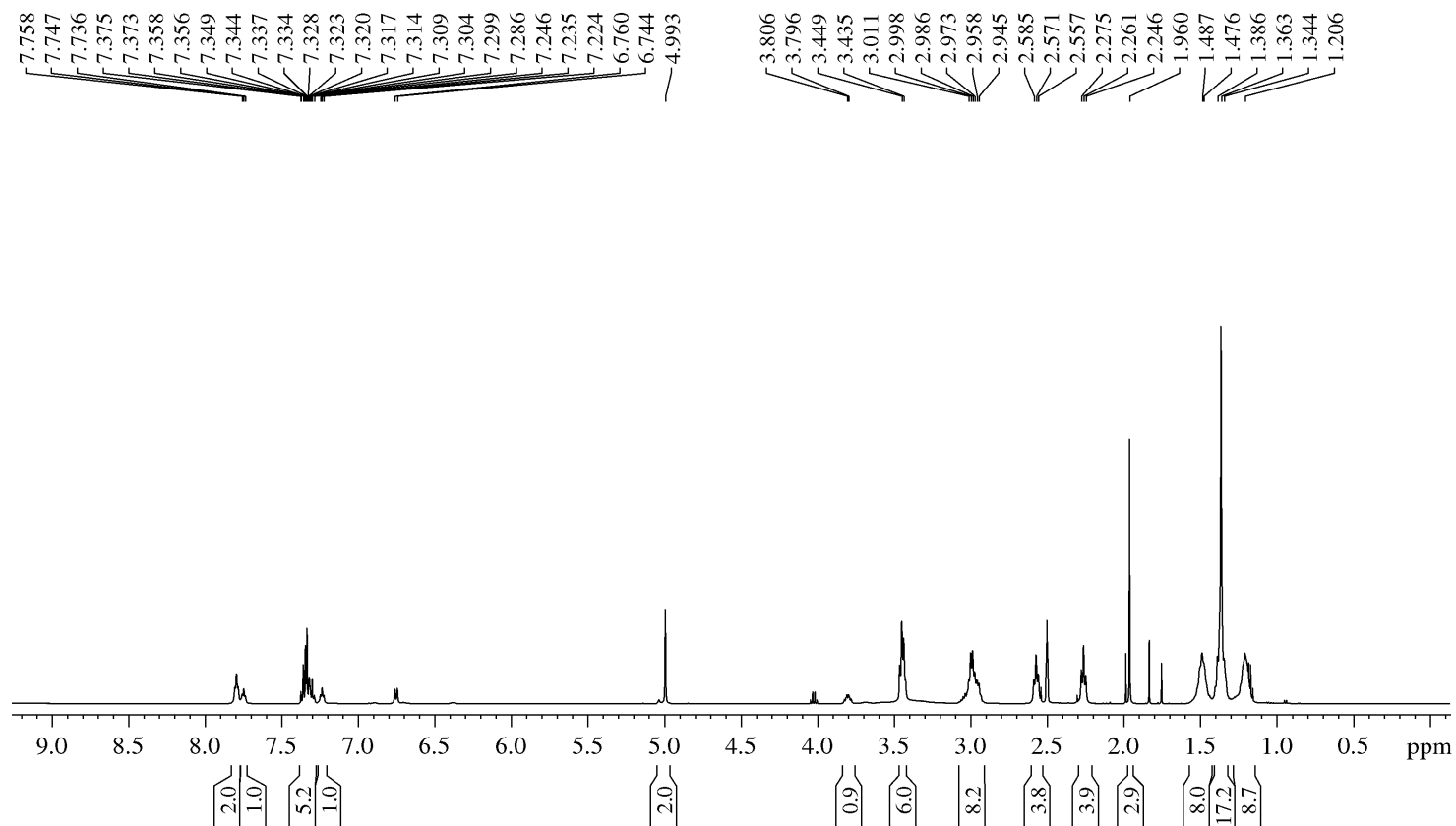
Figure S3-1. ^{1}H NMR spectrum of compound **7** in $(CD_3)_2SO$. The signals at 1.17, 1.99, 4.02 ppm are assigned to residual ethyl acetate and signal at 2.50 is assigned to residual DMSO in the NMR sample.

DFO-Lys(Z)-Boc (7)
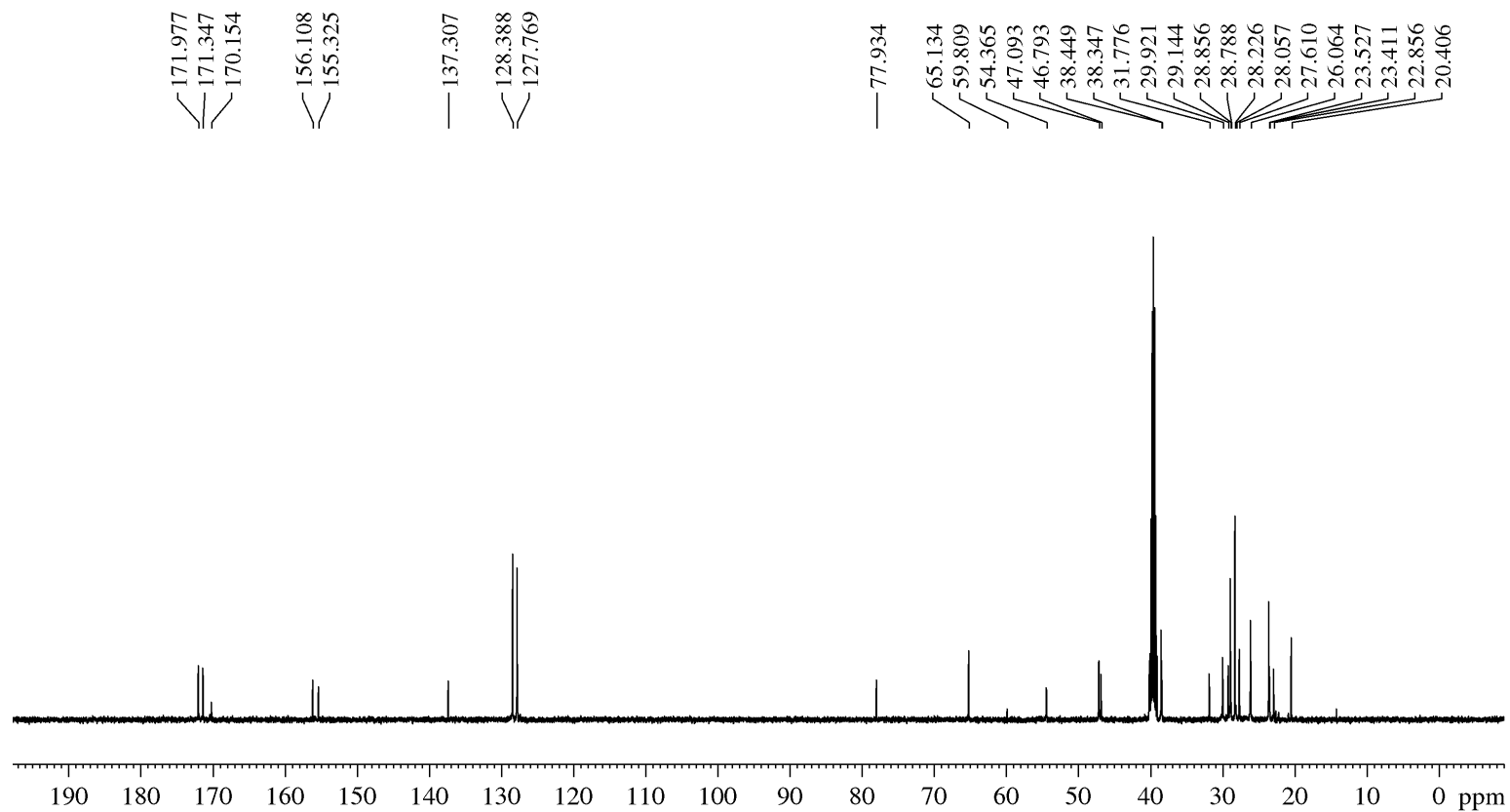
Figure S3-2. ^{13}C NMR spectrum of compound **7** in $(CD_3)_2SO$.

DFO-Lys(Z)-NH₂ (8)

8.196
8.185
7.796
7.785
7.774
7.377
7.362
7.353
7.348
7.336
7.322
7.311
7.306
7.241
7.230
7.218
4.996
3.484
3.464
3.450
3.436
3.086
3.073
3.060
3.012
2.999
2.987
2.974
2.962
2.948
2.586
2.572
2.558
2.277
2.262
2.248
1.961
1.616
1.604
1.577
1.561
1.547
1.502
1.490
1.433
1.418
1.404
1.390
1.375
1.361
1.346
1.274
1.257
1.221
1.208

2.5 | 1.0 | 2.0 | 5.0 | 1.0 | 2.0 | 6.1 | 2.0 | 6.2 | 3.9 | 4.0 | 3.0 | 26.0

10 9 8 7 6 5 4 3 2 1 ppm
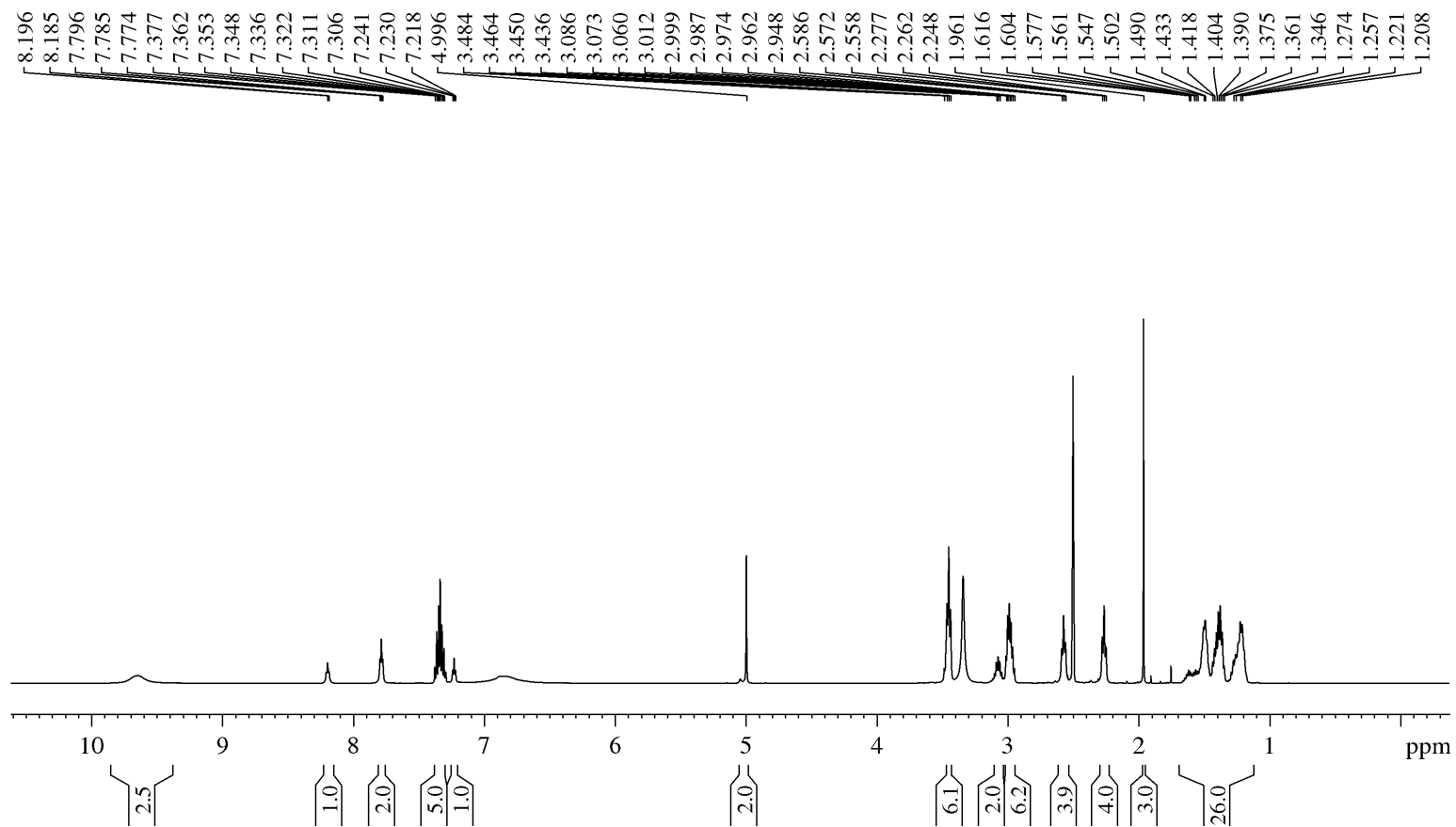
Figure S3-3. ¹H NMR spectrum of compound **8** in (CD₃)₂SO. The signal at 2.50 is assigned to residual DMSO in the NMR sample.

DFO-Lys(Z)-NH₂ (8)
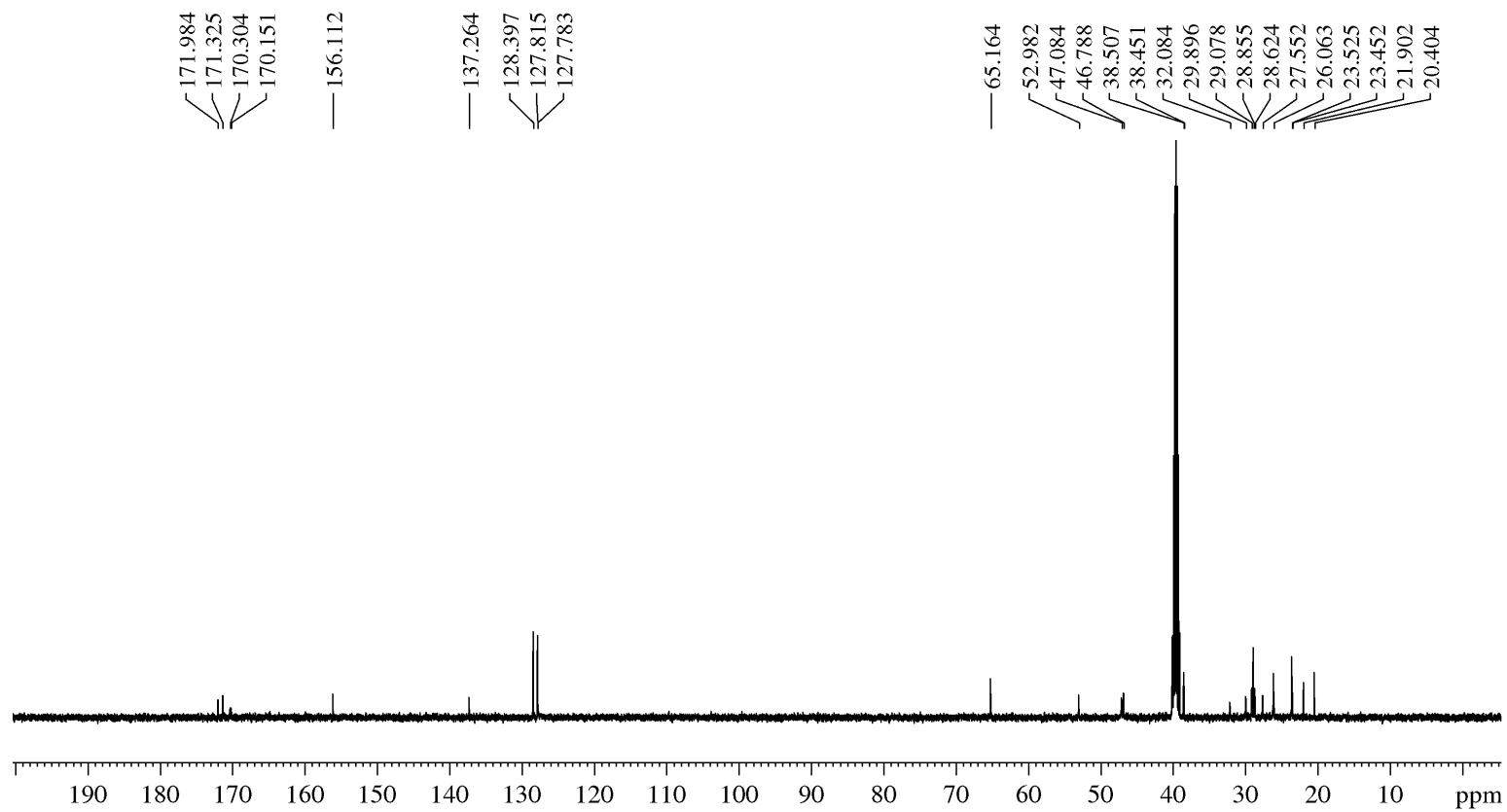
Figure S3-4. ^{13}C NMR spectrum of compound **8** in (CD₃)₂SO.

DFO2-Lys-Z (9)

8.005 7.989 7.879 7.873 7.831 7.821 7.810 7.383 7.368 7.354 7.344 7.331 7.327 7.309 7.296 7.259 7.247 7.236

5.003 4.118 4.101 4.092 4.075 3.472 3.458 3.445 3.010 2.997 2.985 2.956 2.596 2.582 2.568 2.365 2.345 2.333 2.324 2.310 2.286 2.272 2.257 1.970 1.637 1.498 1.396 1.382 1.368 1.217

9.5 9.0 8.5 8.0 7.5 7.0 6.5 6.0 5.5 5.0 4.5 4.0 3.5 3.0 2.5 2.0 1.5 1.0 0.5 ppm

1.0 2.0 4.0 5.5 1.0   2.0   1.0   12.4   14.4   7.9 12.2   6.0   46.0
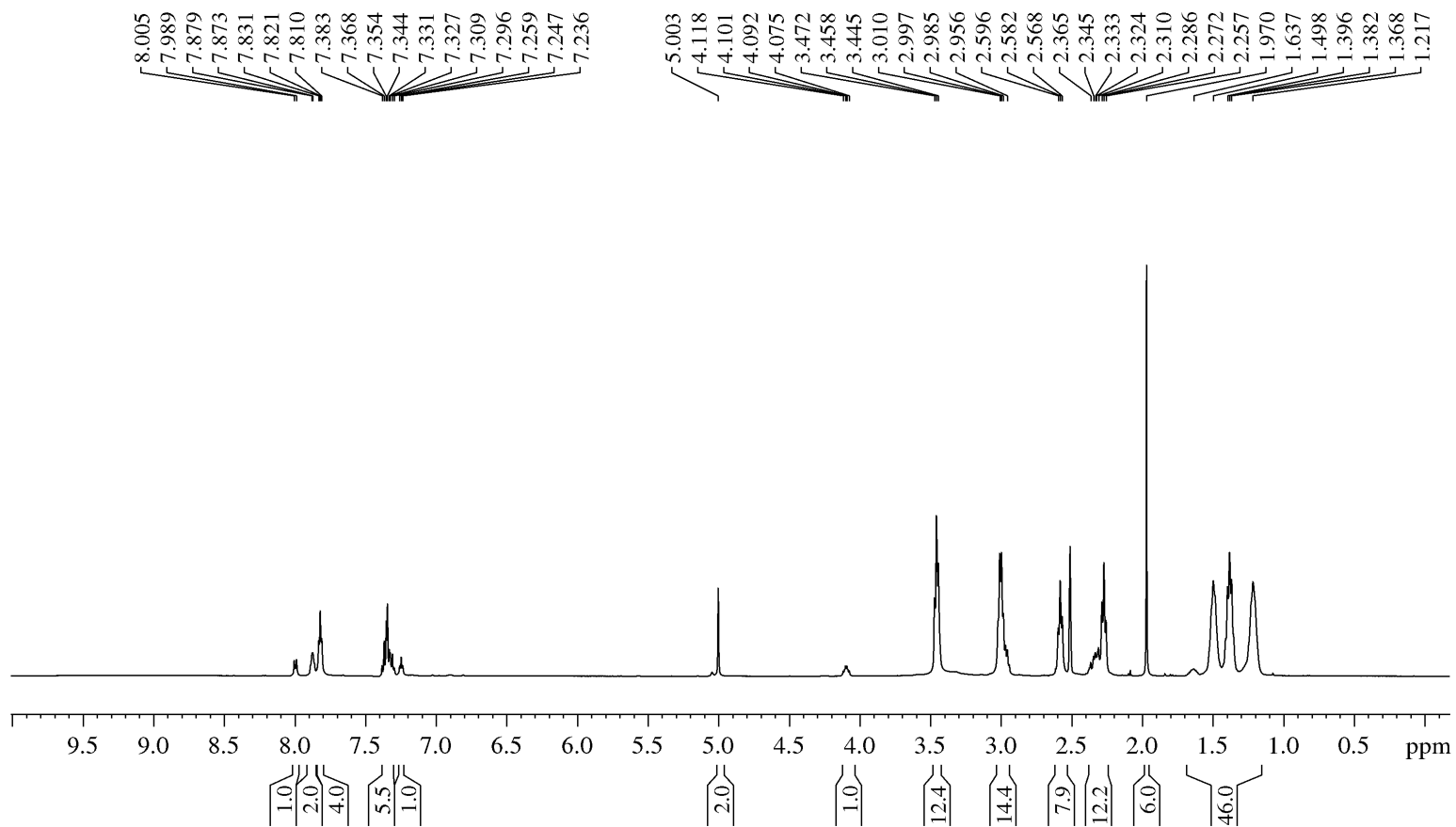
Figure S3-5. ^{1}H NMR spectrum of compound **9** in $(CD_3)_2SO$. The signal at 2.50 is assigned to residual DMSO in the NMR sample.

DFO2-Lys-Z (9)

171.944
171.689
171.555
171.432
171.358
170.137
156.100
137.311
128.386
127.769
65.135
52.666
47.085
46.785
38.442
38.425
31.548
30.772
30.731
29.945
29.153
28.842
28.688
27.624
26.054
23.517
22.855
20.404
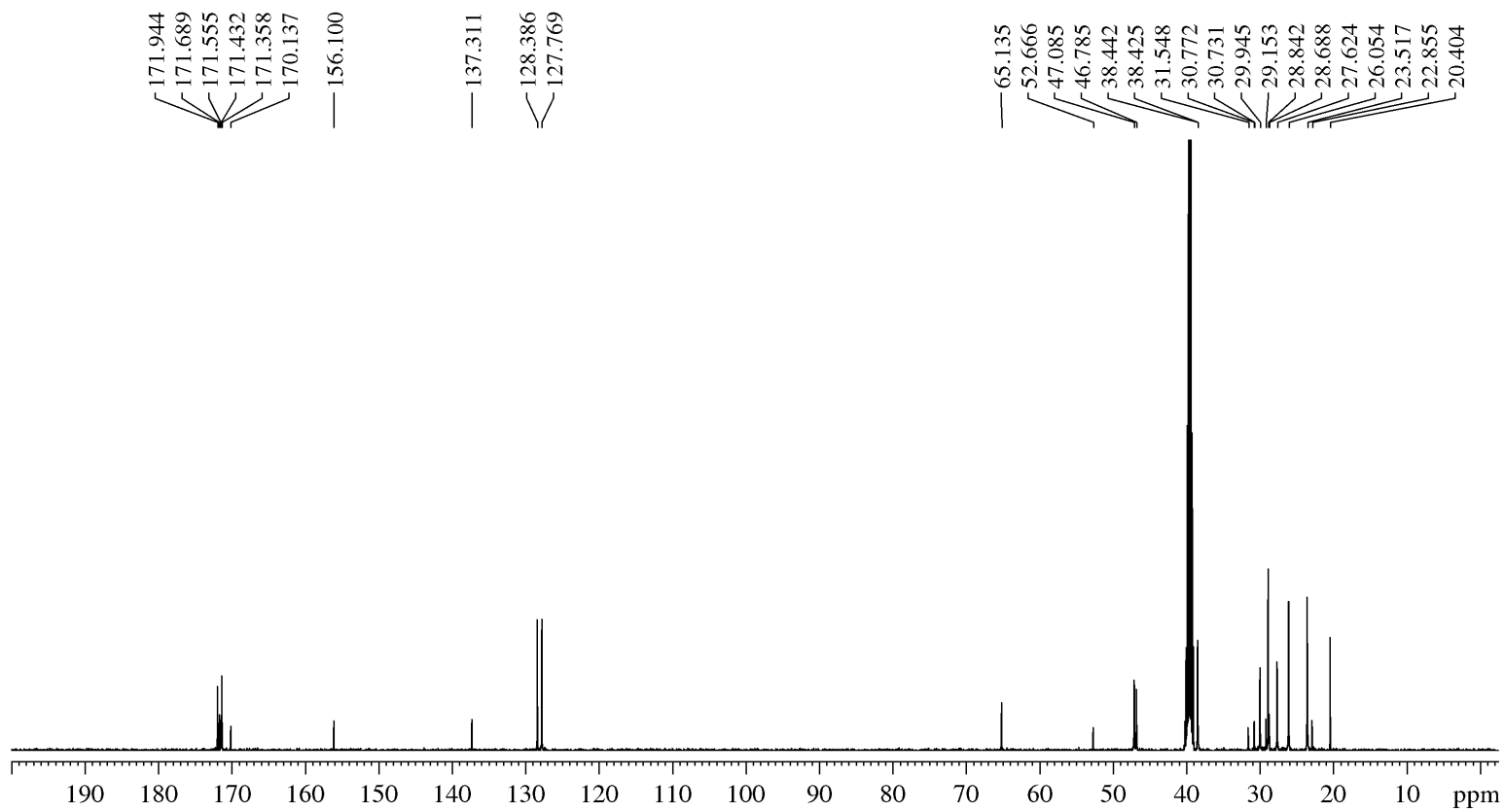
Figure S3-6. ^{13}C NMR spectrum of compound **9** in $(CD_3)_2SO$.
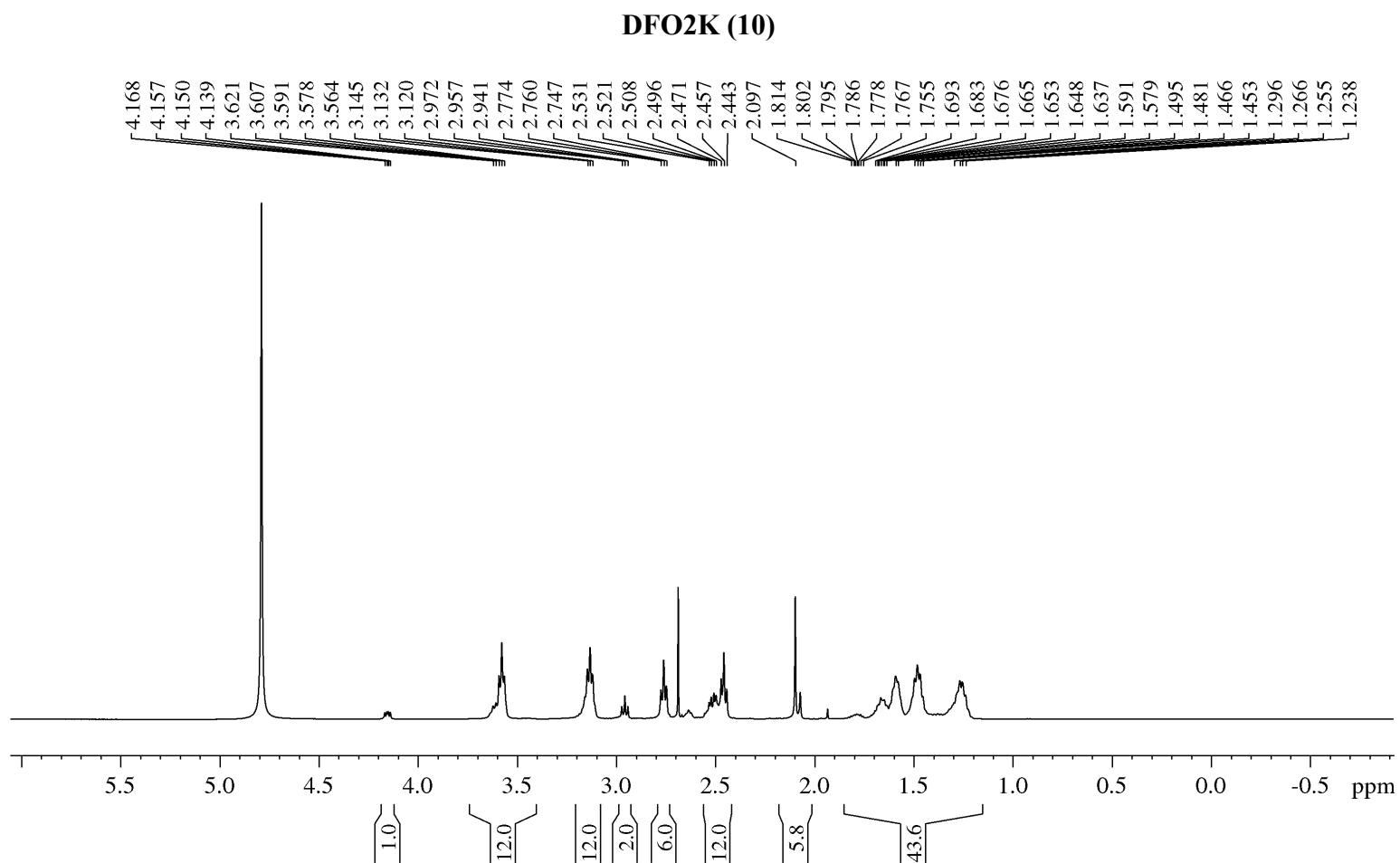
DFO2K (10)

Figure S3-7. ^{1}H NMR spectrum of compound **10** in D$_2$O. The signal at 4.79 is assigned to residual H$_2$O in the NMR sample.

DFO2K (10)

174.938
174.771
174.321
173.781
173.532

53.863
47.823
47.670
39.130
38.680
30.757
30.417
28.018
27.895
27.605
26.238
25.422
23.018
22.154
19.222

200 190 180 170 160 150 140 130 120 110 100 90 80 70 60 50 40 30 20 10 ppm
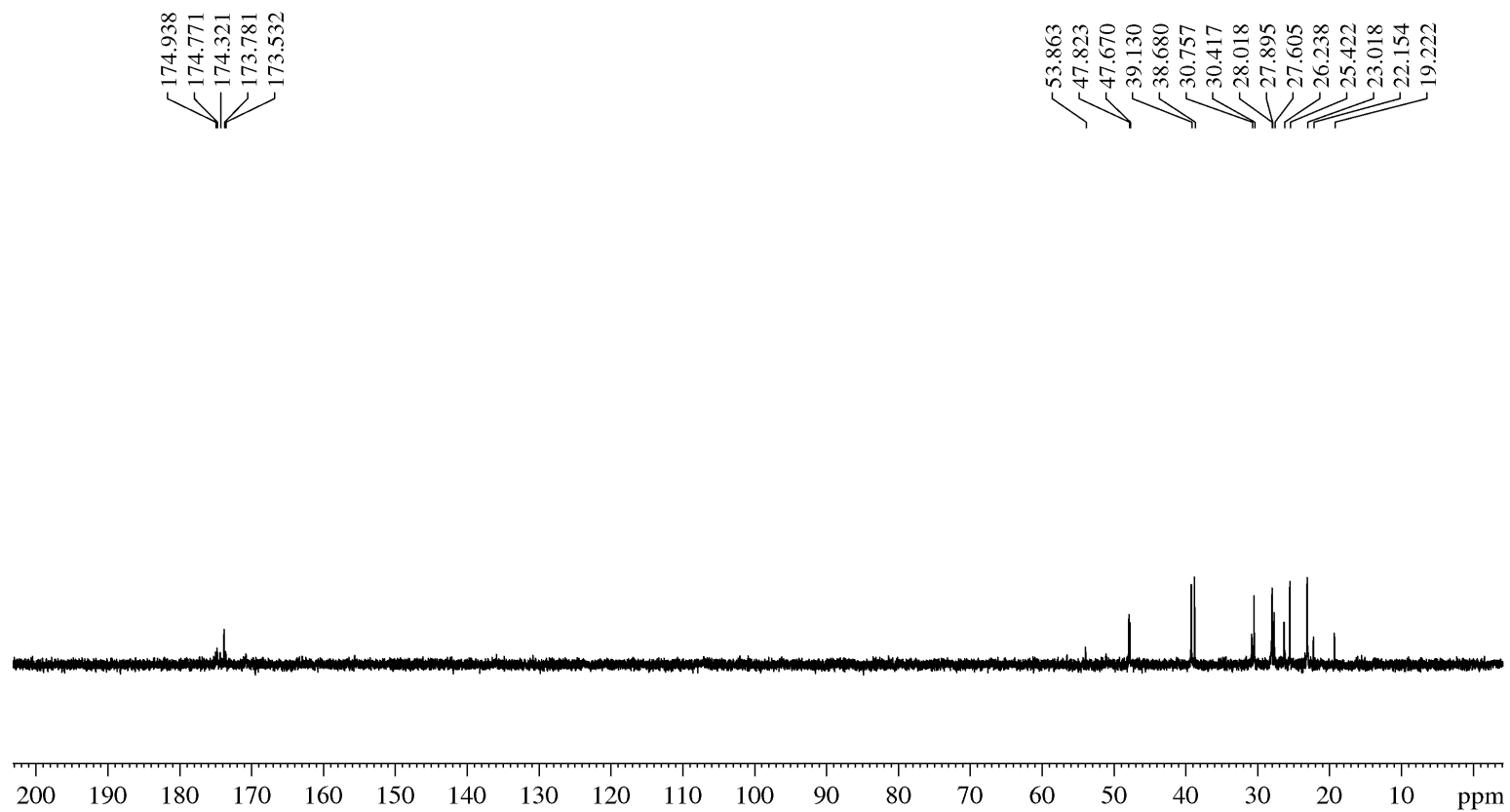
Figure S3-8. ^{13}C NMR spectrum of compound **10** in D$_2$O.
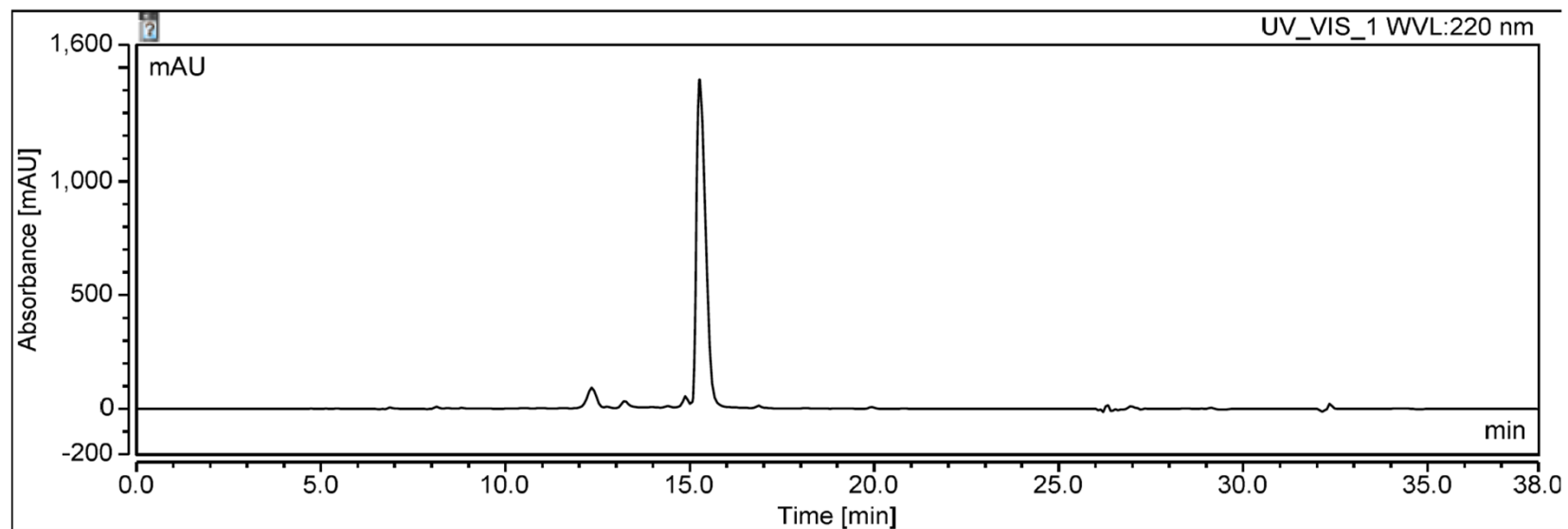
Figure S3-9. Analytical HPLC chromatogram for semi-pure DFO2K (**10**). HPLC conditions: C18 Inspire analytical DIKMA; 5 μm, 250 × 10.0 mm; (15 – 30% acetonitrile in water (0.1% formic acid); flow rate, 2 mL/min, t_R = 15.3 min)

[^{Nat}Zr]Zr-DFO2K (11)
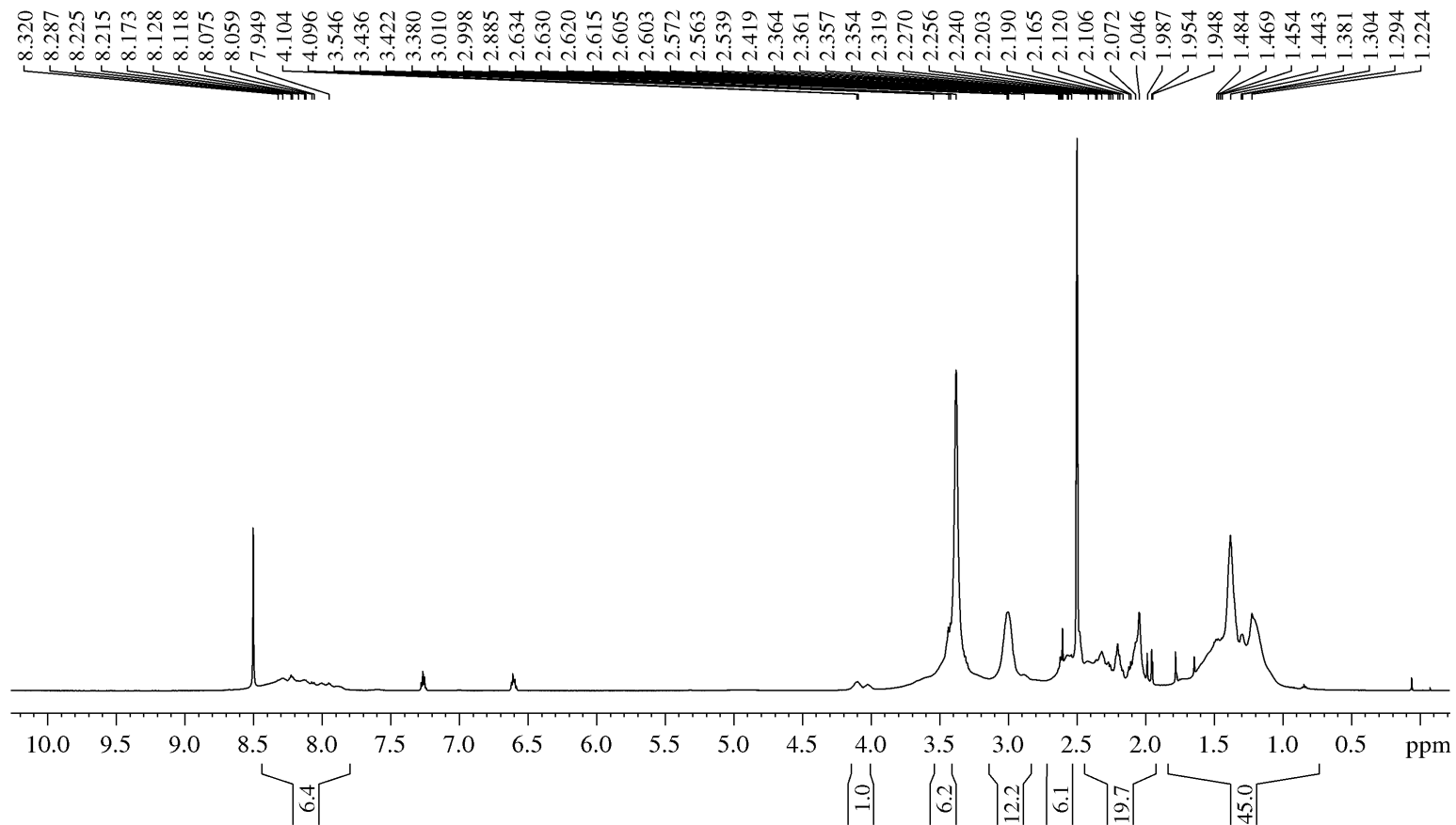
Figure S3-10. ¹H NMR spectrum of compound **11** in (CD₃)₂SO. The signal at 2.50 is assigned to residual DMSO and the signal at 3.33 pm is assigned to residual H₂O in the NMR sample.

[^{Nat}Zr]Zr-DFO2K (11)
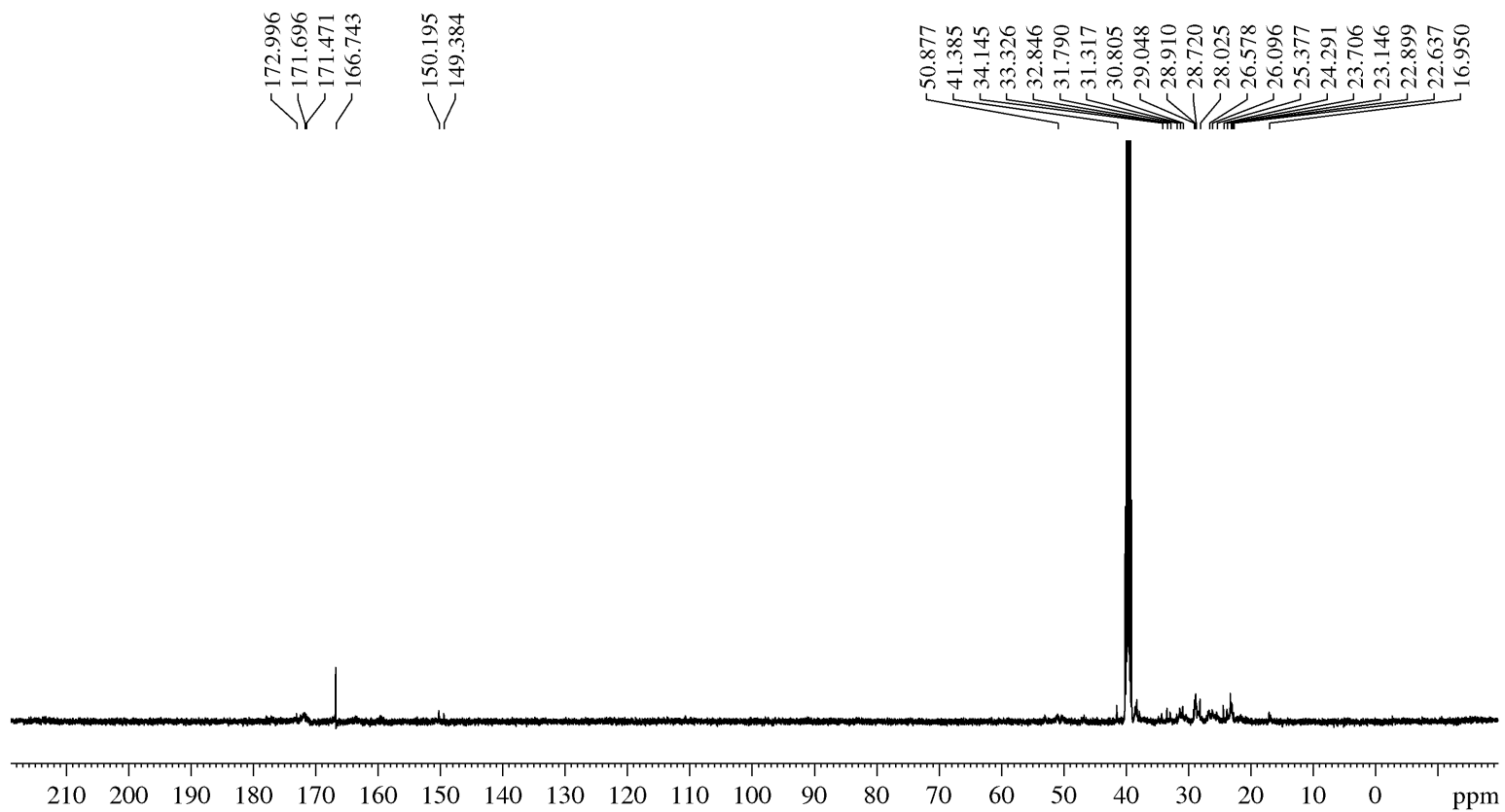
Figure S3-11. ^{13}C NMR spectrum of compound **11** in $(CD_3)_2SO$.

p-Ph-SCN-DFO2K (12)
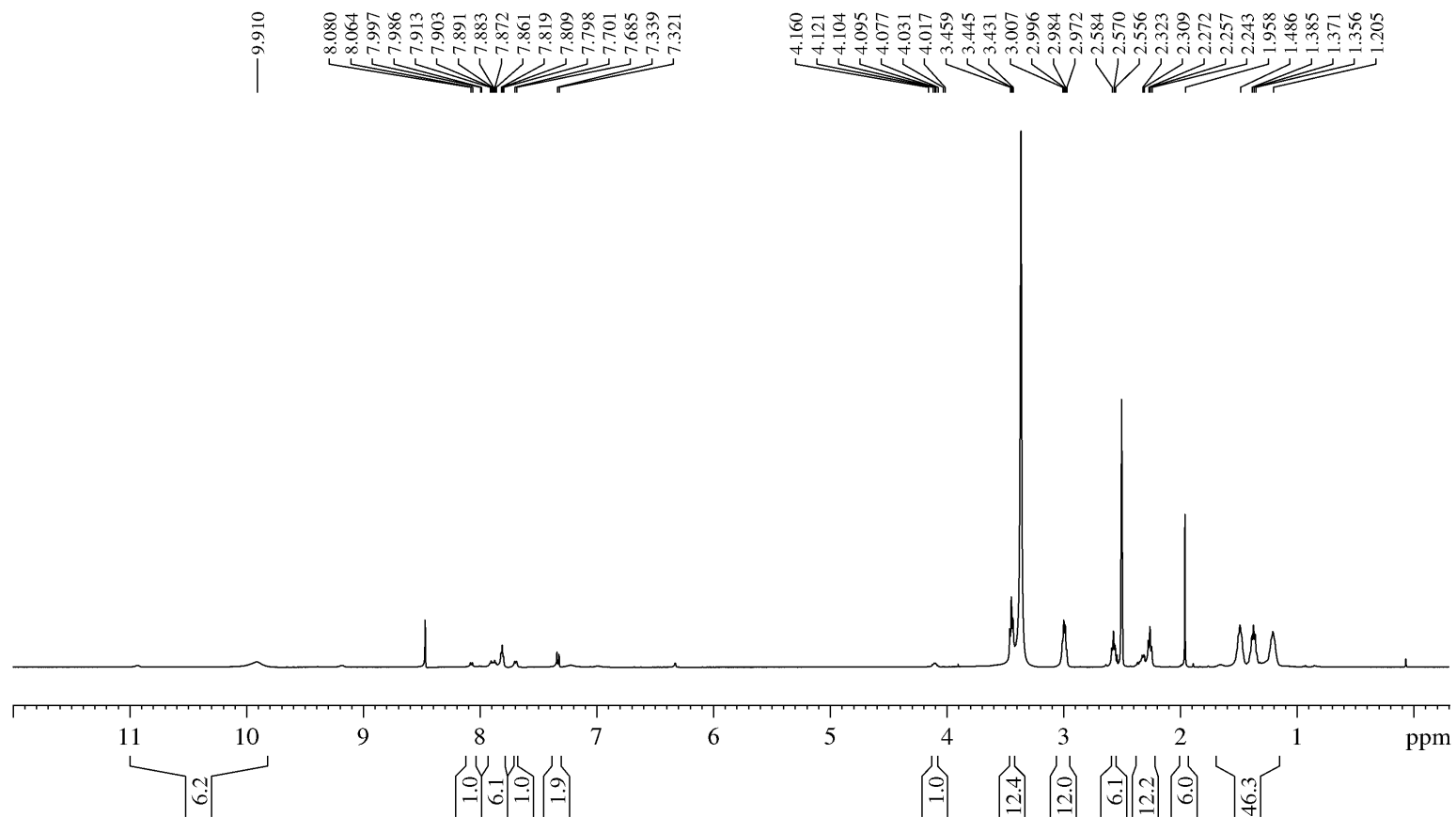
Figure S3-12. ^{1}H NMR spectrum of compound **12** in (CD$_3$)$_2$SO. The signal at 2.50 is assigned to residual DMSO and the signal at 3.33 pm is assigned to residual H$_2$O in the NMR sample.

p-Ph-SCN-DFO2K (12)
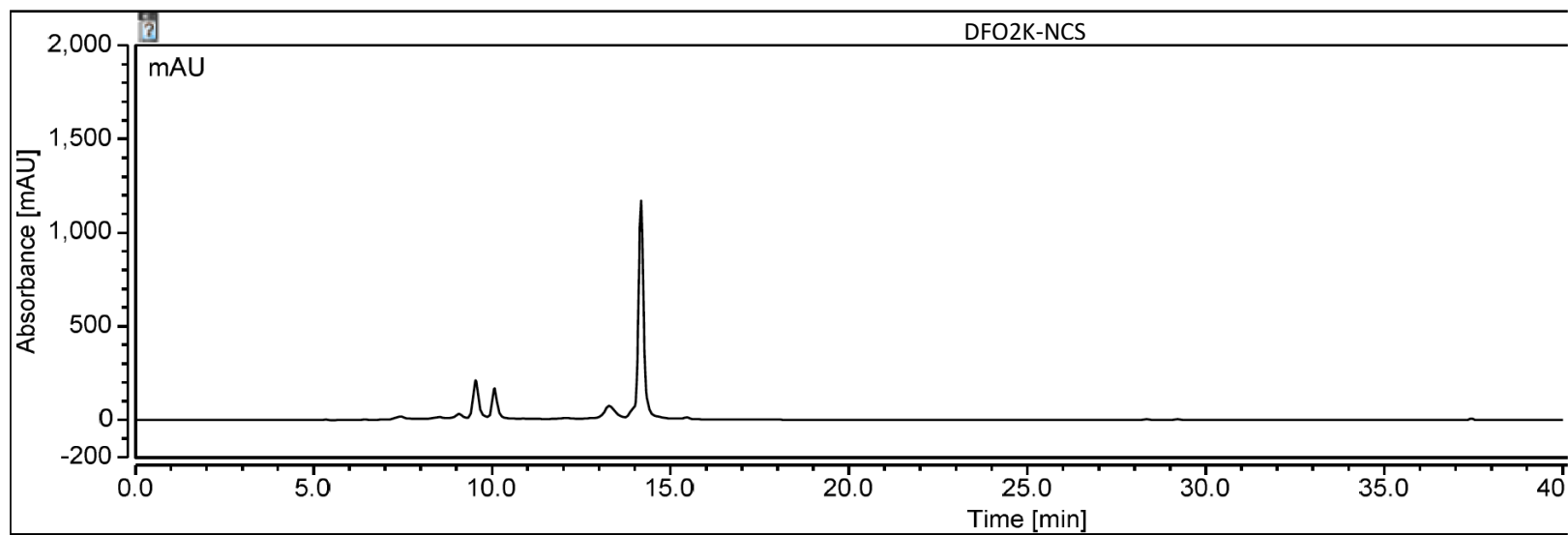
Figure S3-13. Analytical HPLC chromatogram for *p*-Ph-SCN-DFO2K (12). HPLC conditions: C18 Inspire analytical DIKMA; 5 μm, 250 × 10.0 mm; (30 – 60% acetonitrile in water (0.1% formic acid); flow rate, 2 mL/min, t_R = 14.3 min)

XYZ Coordinates of Zr(DFO2K) optimized structure *

N	49.79700	-90.21100	0.67300
C	48.63600	-89.60800	0.32000
C	47.36800	-90.24200	0.95300
C	46.07400	-89.69800	0.33900
C	44.81500	-90.17400	1.06800
O	48.57500	-88.58600	-0.39000
N	47.45300	-91.70700	0.95800

C	51.11200	-89.87900	0.13100
C	51.72400	-91.08000	-0.59800
C	53.08100	-90.80800	-1.25700
C	54.23600	-90.53600	-0.28500
C	55.55200	-90.42200	-1.05200
N	56.69200	-90.03500	-0.22200
C	57.93000	-90.60200	-0.32400
C	59.09400	-89.80000	0.21200
C	60.43100	-90.49600	-0.00100

C	61.61300	-89.53700	0.07900
N	62.82500	-90.12200	-0.08300
C	64.06800	-89.36000	-0.19100
C	65.24900	-90.30500	-0.38500
C	66.57700	-89.57000	-0.58200
C	67.74800	-90.55000	-0.67100
O	56.64800	-88.68200	0.19400
O	58.07100	-91.72900	-0.85600
O	61.49100	-88.30700	0.26100
C	69.09200	-89.85900	-0.90100
N	70.20500	-90.78200	-0.68200
C	70.94600	-91.42300	-1.57300
C	70.91800	-91.15900	-3.05200
C	72.34900	-90.92300	-3.59500
C	72.96600	-89.67300	-2.98600
N	73.63500	-89.86300	-1.82200
C	74.01900	-88.77000	-0.92900
C	72.82500	-88.19500	-0.15200
C	73.25800	-87.24900	0.98800
C	72.59200	-87.51100	2.34800
C	73.09400	-88.73700	3.13400
N	72.51500	-90.03600	2.78200
C	71.55500	-90.67500	3.44100
C	70.86600	-90.05300	4.61800
O	70.42600	-91.08500	0.62700
O	71.79800	-92.28500	-1.11600
O	72.81500	-88.54600	-3.50800
O	71.21200	-91.85300	3.03600
O	73.09200	-90.69400	1.72800
N	50.72500	-95.89500	0.66700
C	51.43600	-97.15000	0.88900
C	52.89400	-97.07200	0.41600
C	53.72000	-95.99600	1.12900
C	55.16600	-95.91600	0.63200
C	55.93500	-94.77200	1.30000
N	57.30800	-94.64000	0.82000
C	58.37800	-95.24000	1.42800
C	59.67000	-95.27000	0.63300
C	60.86900	-95.71600	1.46700
C	61.99600	-96.23600	0.59000
N	63.24800	-95.81800	0.89500
C	64.41500	-96.29300	0.15200
C	65.71300	-95.61900	0.59300
C	66.86600	-96.07100	-0.31300
C	68.20200	-95.33500	-0.14000
O	57.41500	-94.32600	-0.55400
O	58.27100	-95.71800	2.57700
O	61.78300	-97.03600	-0.34800
C	69.02800	-95.75100	1.08500
N	70.35800	-95.12800	1.05800
C	71.41400	-95.50600	0.33500
C	71.55000	-96.90500	-0.20500
C	72.63200	-97.69300	0.56700
C	72.13600	-98.21700	1.90600
N	72.80700	-97.87800	3.03600
C	73.92200	-96.93800	3.20400
C	75.29900	-97.56700	2.97100
C	76.47100	-96.58300	3.12100
C	76.40200	-95.36800	2.16900
C	75.86400	-94.06800	2.81500
N	74.86800	-93.36400	1.99300
C	75.09200	-92.79600	0.81500
C	76.47600	-92.56000	0.29700
O	70.40100	-93.85100	1.56700
O	72.36700	-94.66700	0.17100
O	71.14200	-98.97800	1.95200

O	74.08500	-92.42600	0.09500	O	49.05900	-96.66300	-0.72100
O	73.56900	-93.49700	2.41100	O	47.65300	-91.93700	-1.30500
C	49.66000	-95.72400	-0.15800	Zr	72.07200	-92.54800	1.07300
C	49.26900	-94.27000	-0.36900	C	43.53300	-89.58800	0.46800
C	47.82400	-93.93900	0.04400	C	42.26300	-90.09300	1.14900
C	47.60300	-92.45200	-0.17200	N	41.05800	-89.51700	0.51800

* Density Functional Theory calculations performed by using Material Studio software via DMol^3/PBE.

Design, synthesis, and evaluation of DFO-Em: a highly soluble octadentate chelator for zirconium-89 radiochemistry
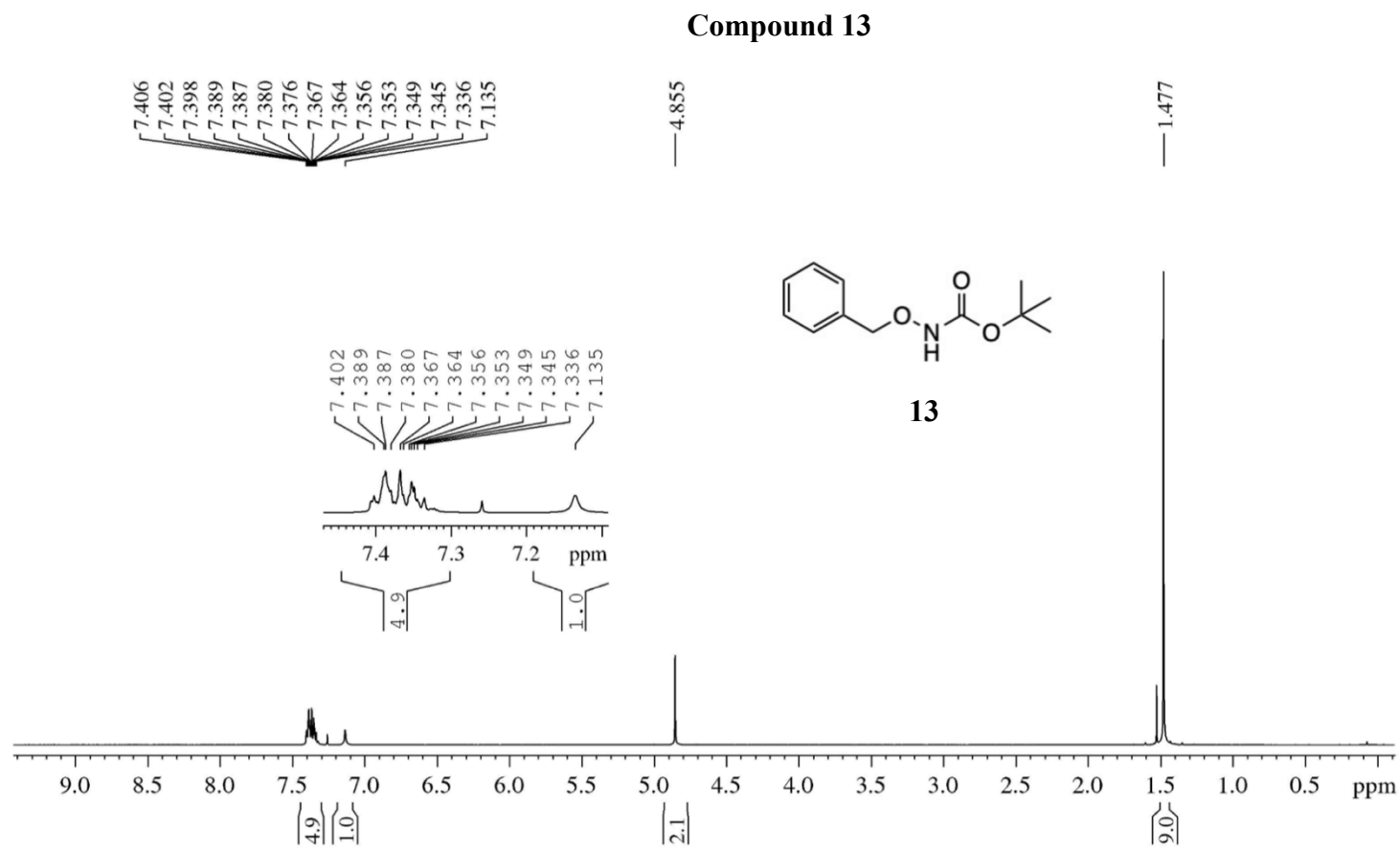
Compound 13

Figure S4-1. ^{1}H NMR spectrum of compound **13** in CDCl$_3$. The signal at 1.56 ppm is assigned to residual H$_2$O in the NMR sample.

Compound 13
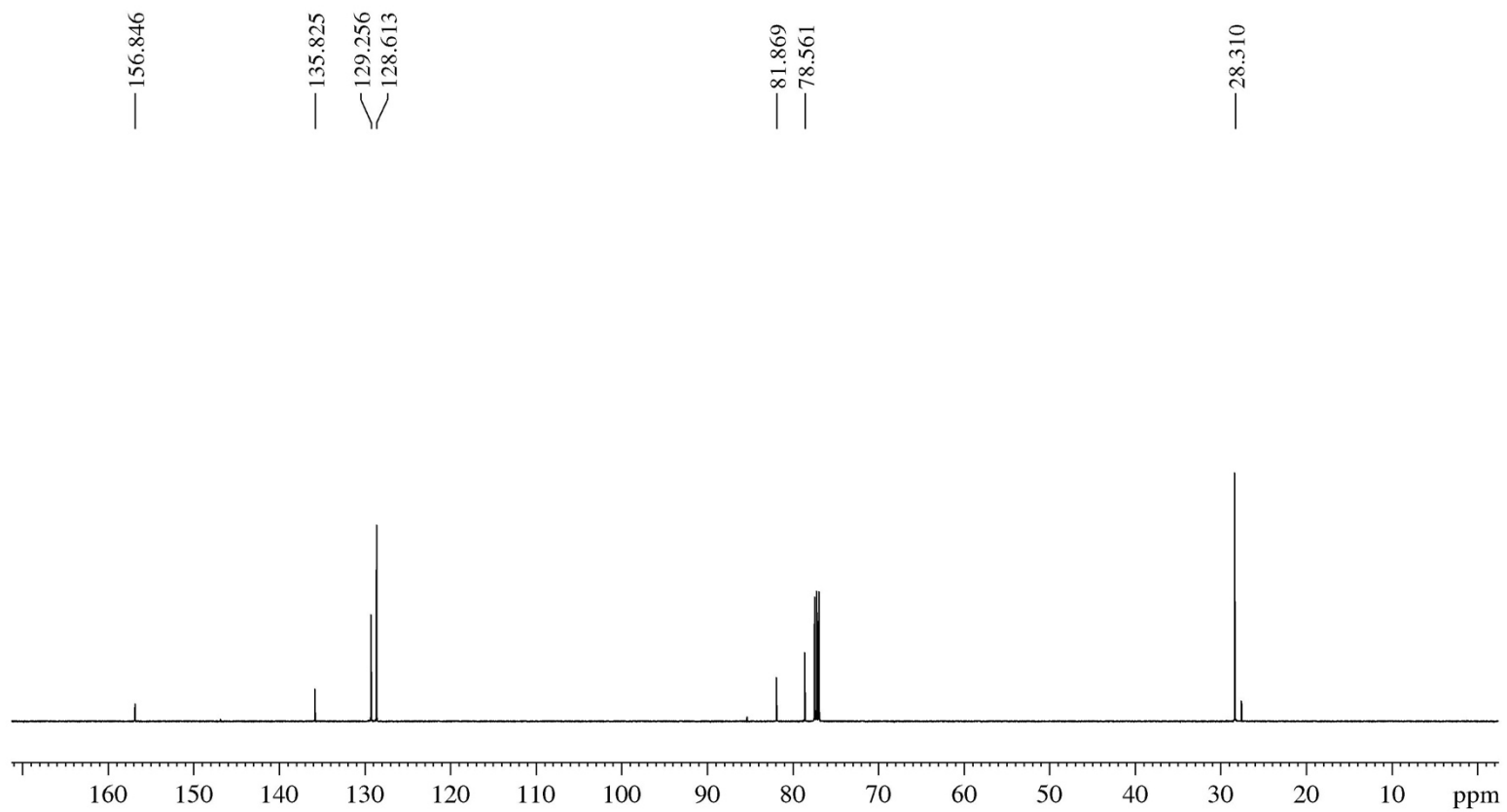
Figure S4-2. ^{13}C NMR spectrum of compound **13** in CDCl$_3$.

Compound 14
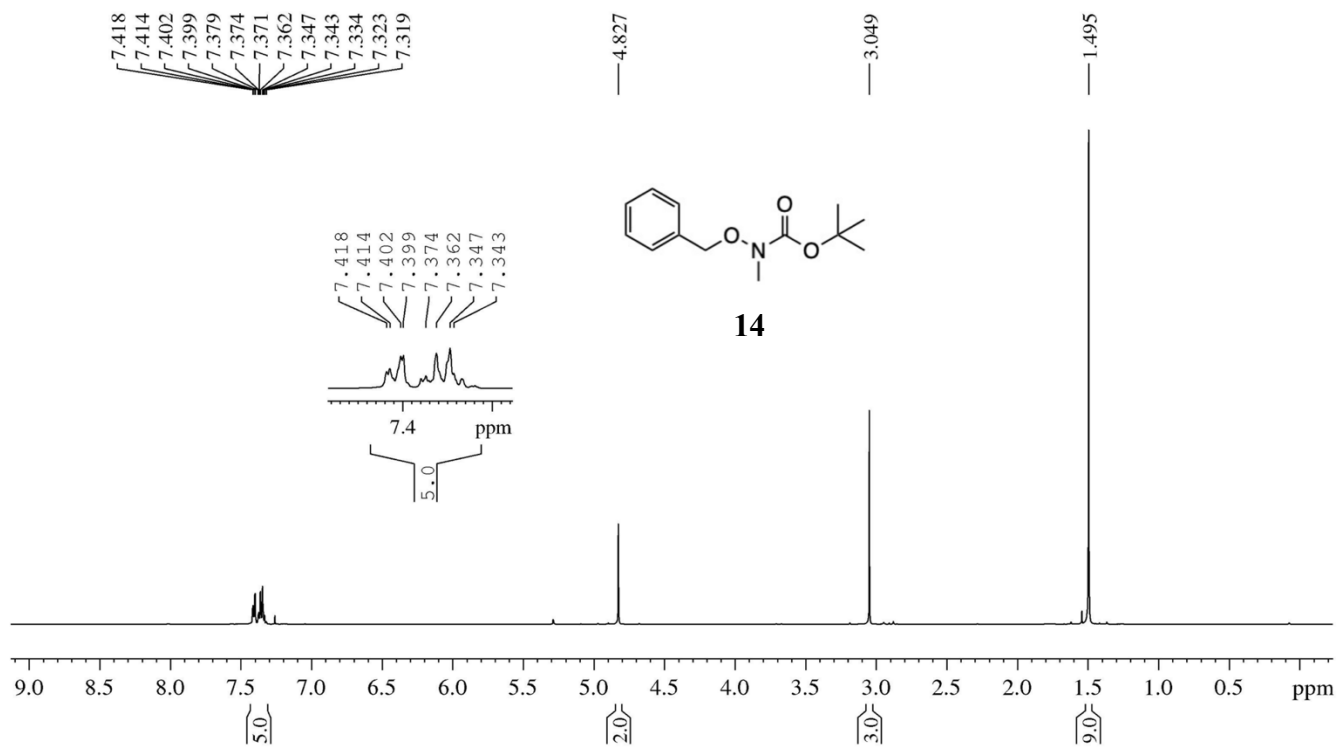
Figure S4-3. ^{1}H NMR spectrum of compound **14** in CDCl$_3$.

Compound 14
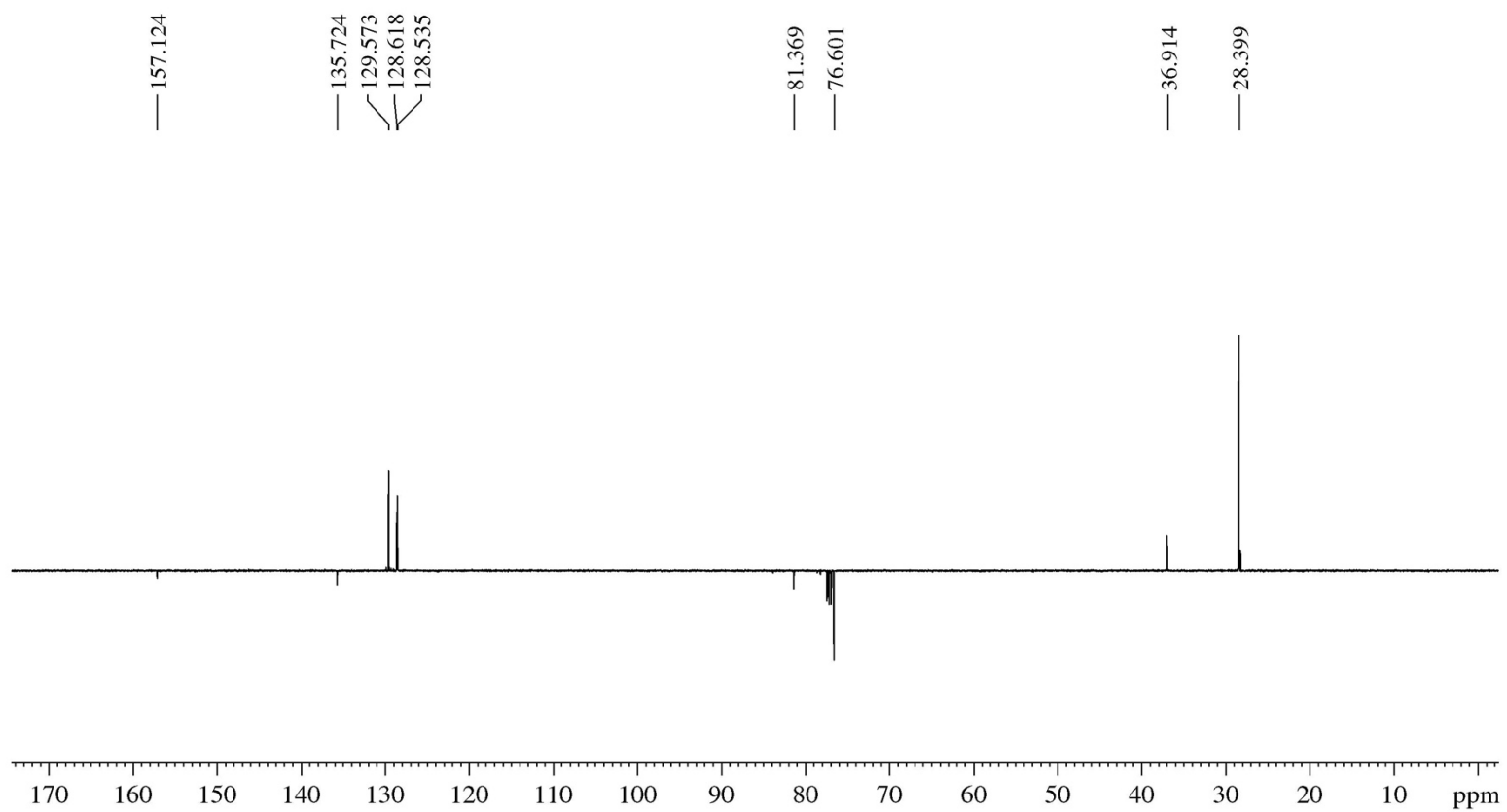
Figure S4-4. DEPT-135 NMR spectrum of compound **4** in CDCl₃.

Compund 15
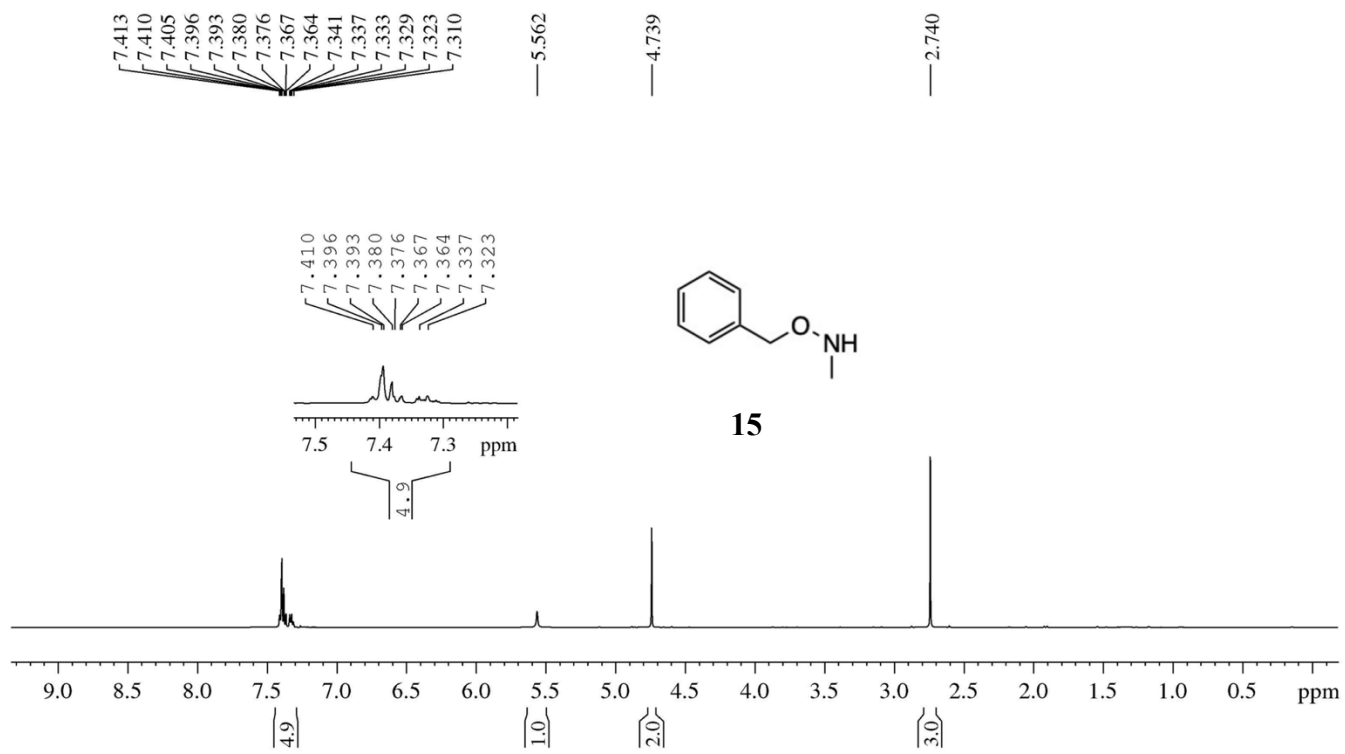
Figure S4-5. ^{1}H NMR spectrum of compound **15** in CDCl$_3$.

Compund 15
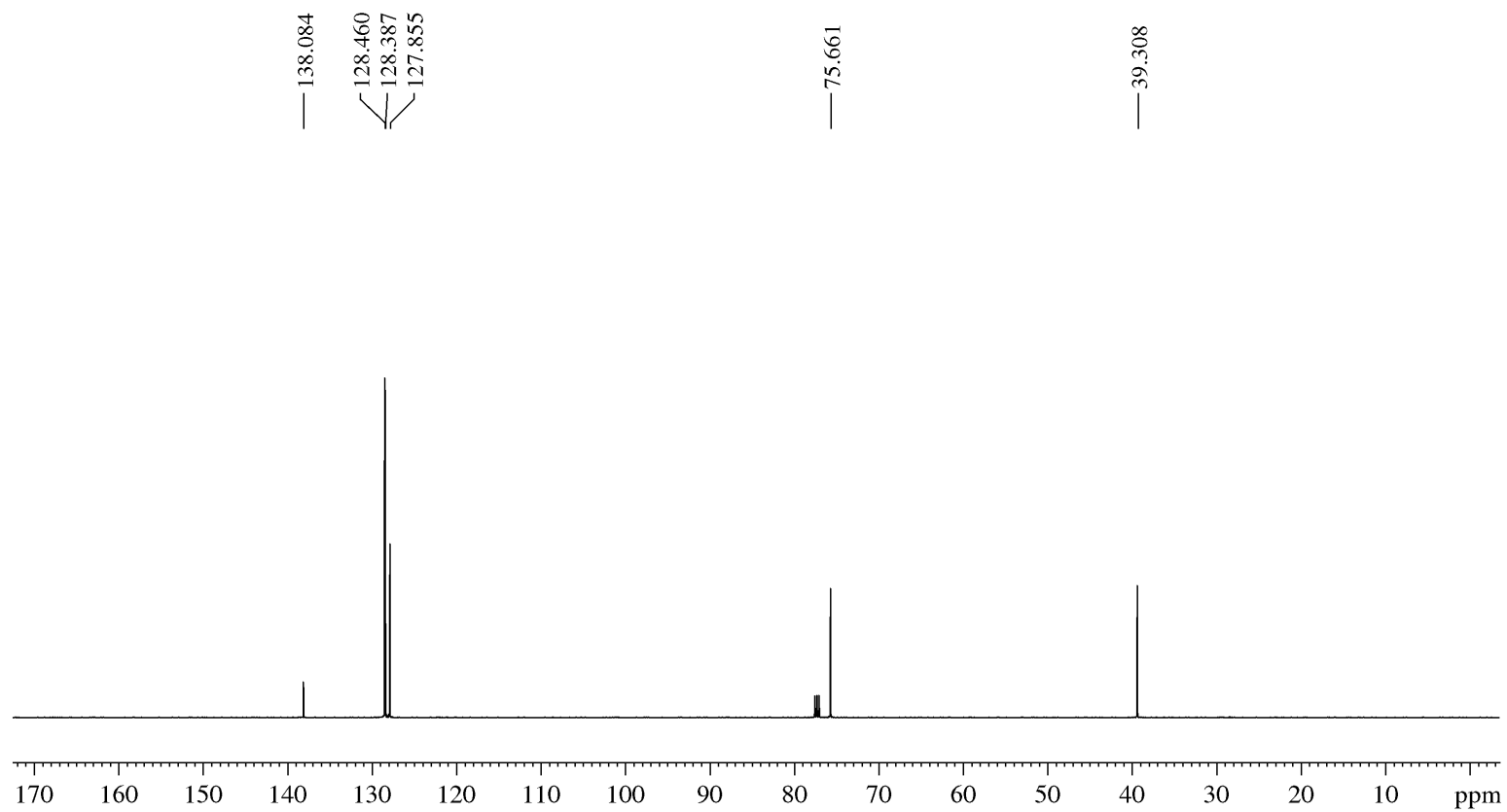
Figure S4-6. ^{13}C NMR spectrum of compound **15** in CDCl$_3$.

Compound 16
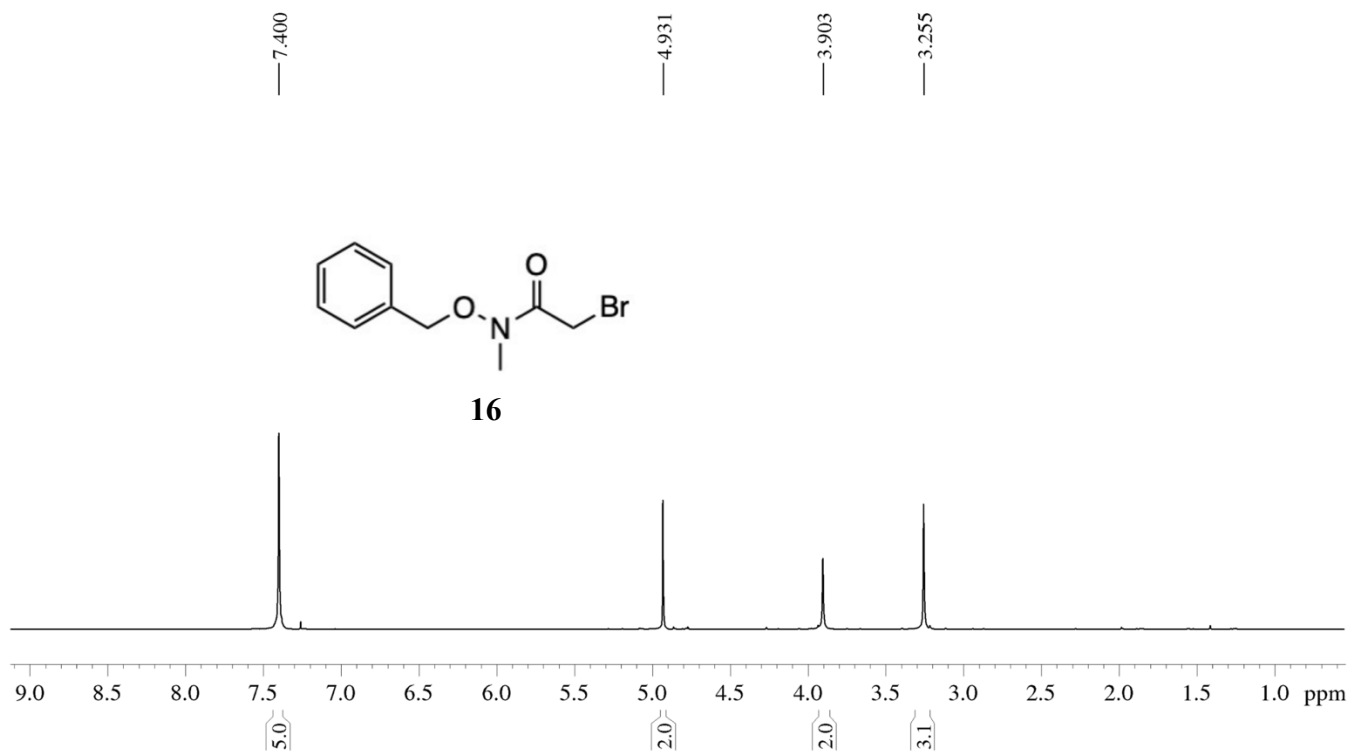
Figure S4-7. ^{1}H NMR spectrum of compound **16** in CDCl$_3$.

Compound 6
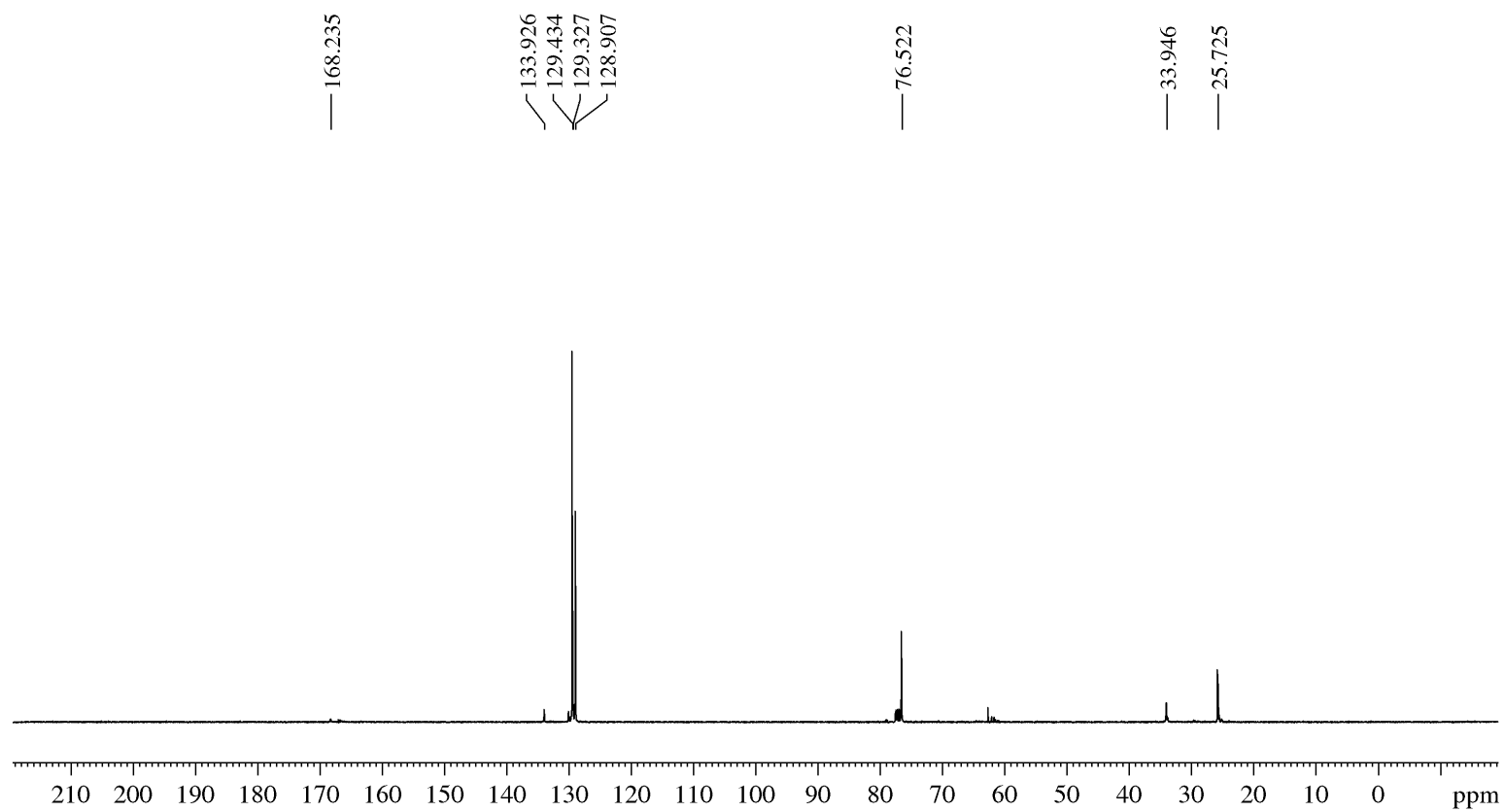
Figure S4-8. ^{13}C NMR spectrum of compound **16** in CDCl$_3$.

Compound 17
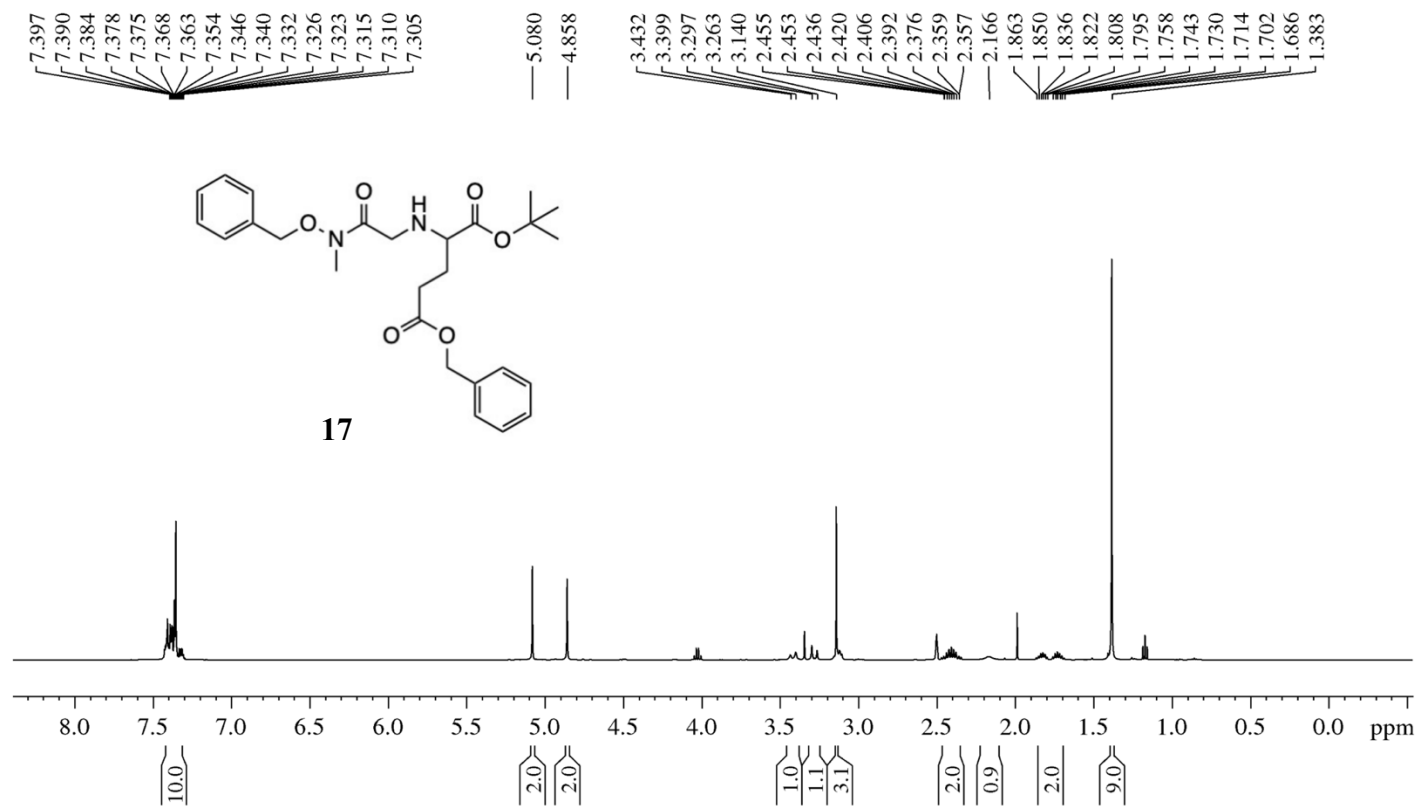
Figure S4-9. ^{1}H NMR spectrum of compound **17** in DMSO-D$_6$. The signals at 1.17, 1.99 and 4.03 ppm are assigned for residual ethyl acetate in the NMR sample.

Compound 17
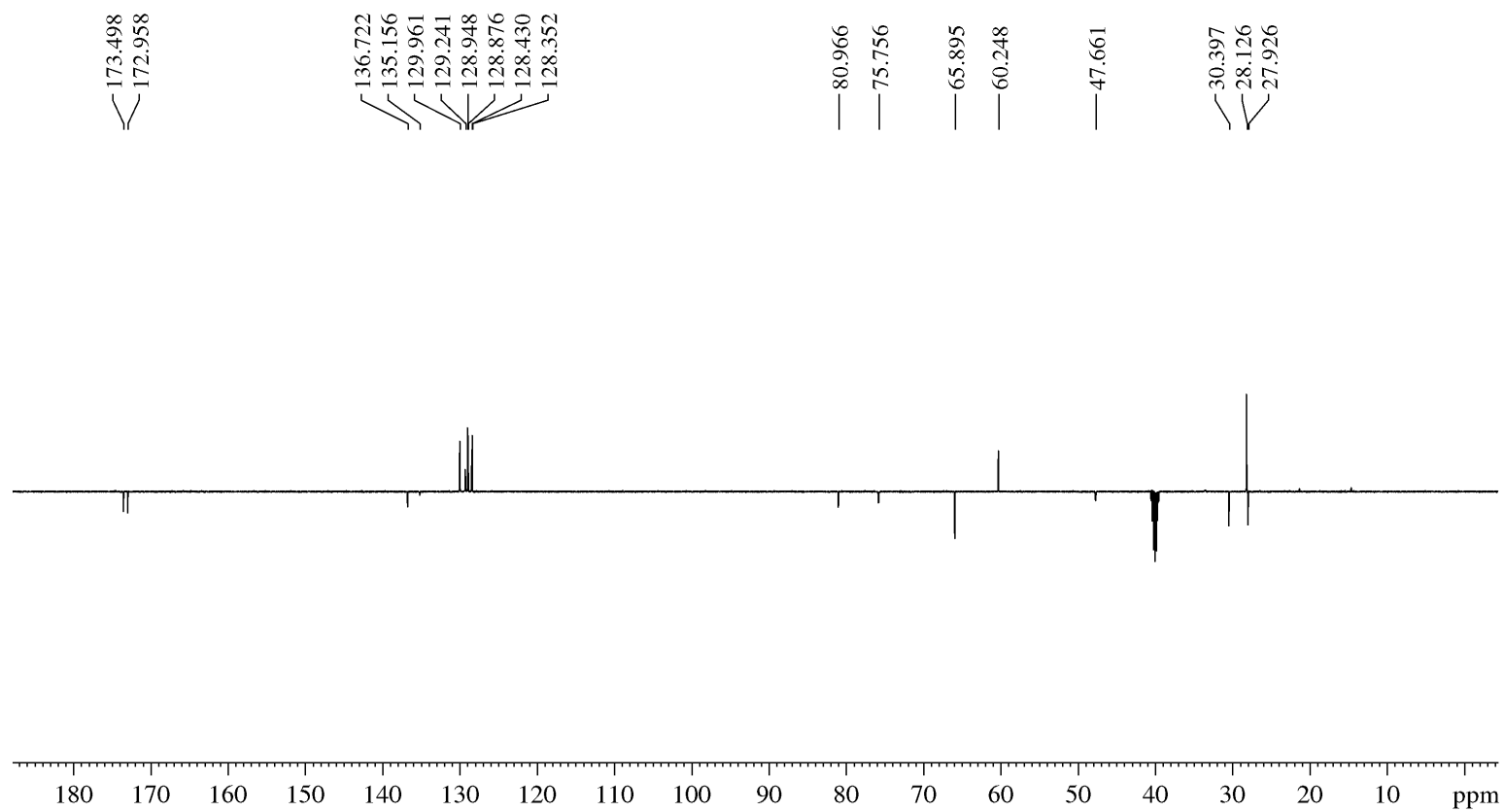
Figure S4-10. DEPT-135 NMR spectrum of compound **17** in DMSO-D$_6$.

Compound 18
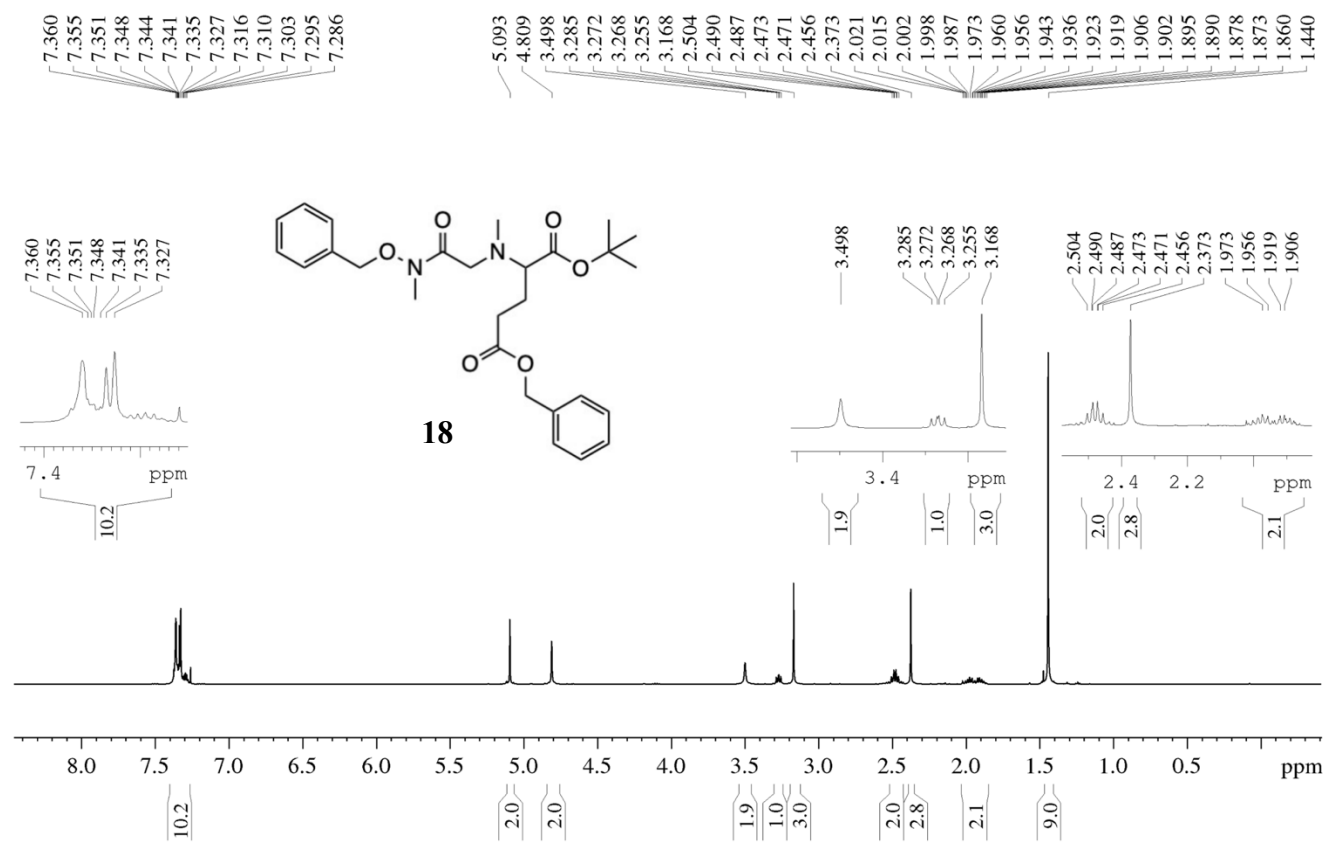
Figure S4-11. ^{1}H NMR spectrum of compound **18** in CDCl$_3$.

Compound 18
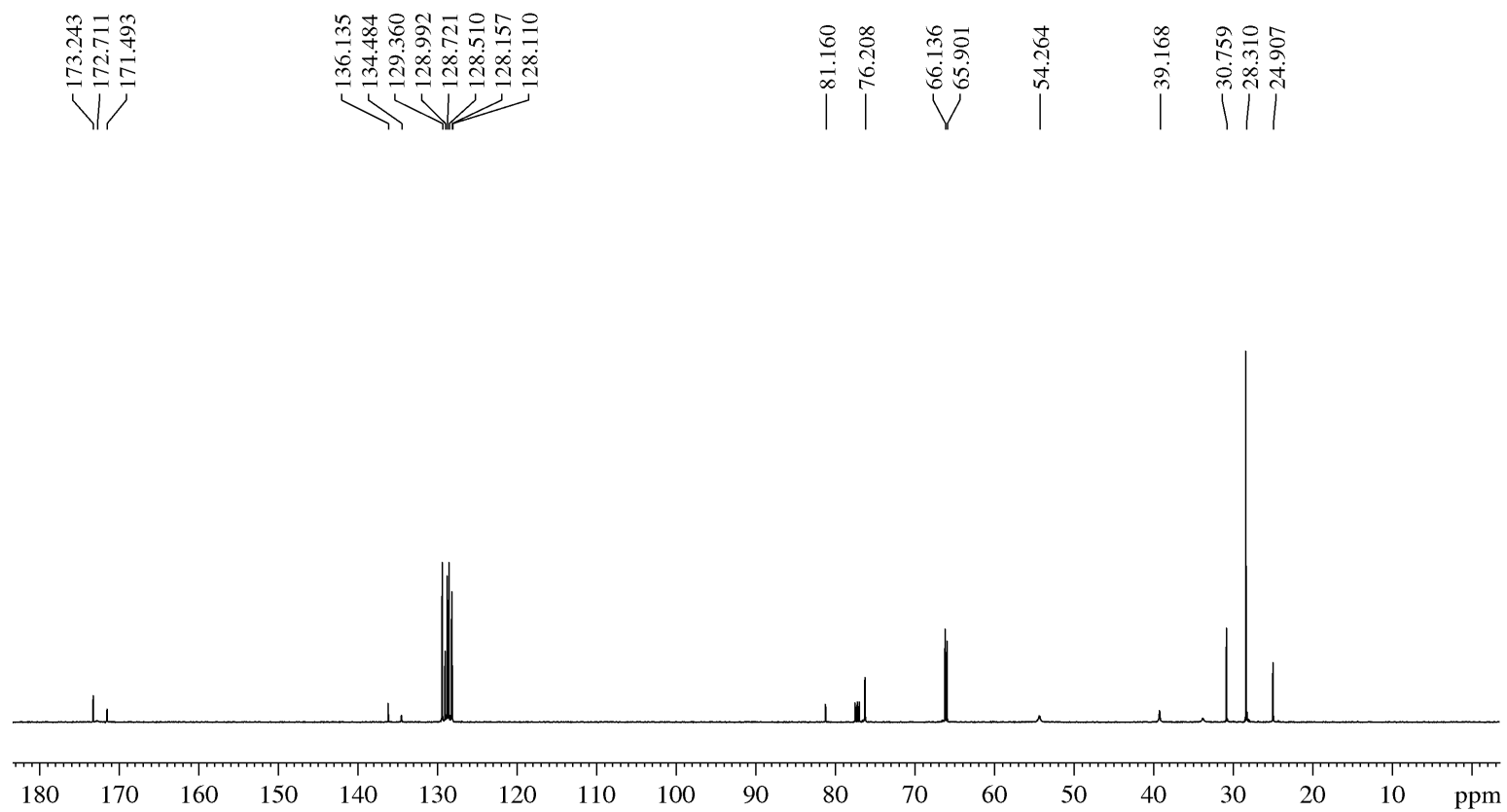
Figure S4-13. ^{13}C NMR spectrum of compound **18** in CDCl$_3$.
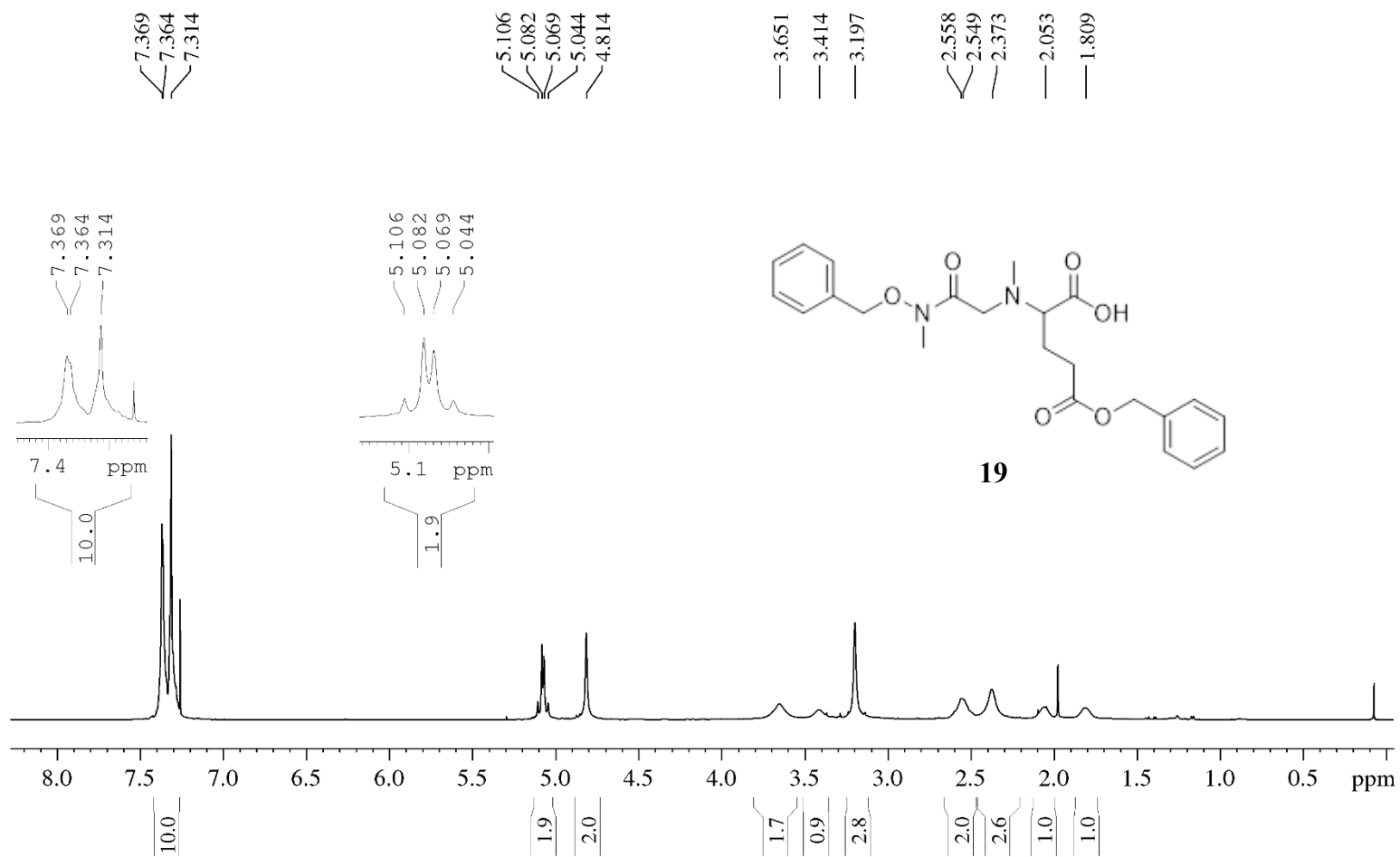
Compound 19

Figure S4-14. ^{1}H NMR spectrum of compound **19** in CDCl$_3$.
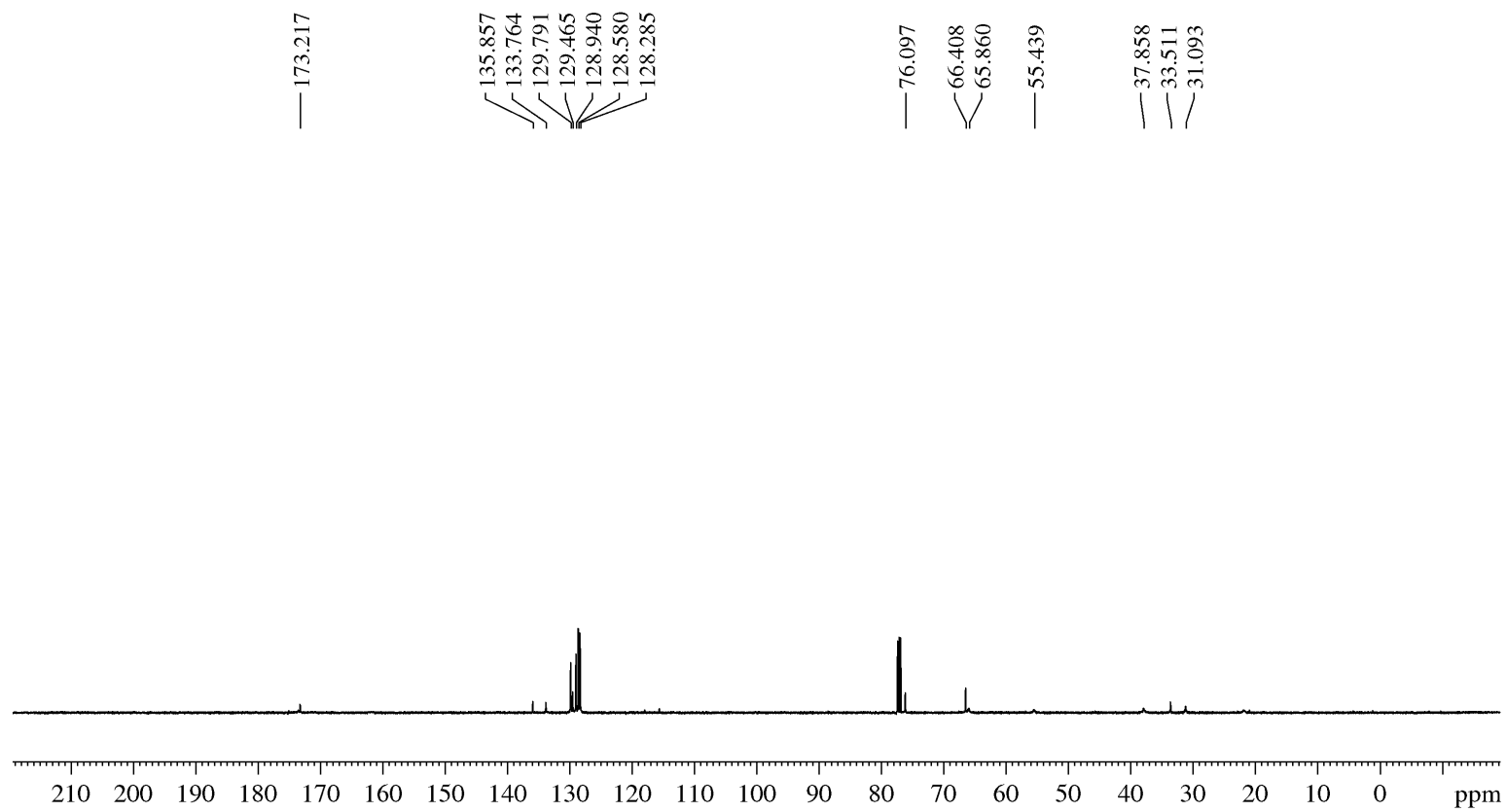
Compound 19

Figure S4-15. ^{13}C NMR spectrum of compound **19** in CDCl$_3$.

Compound 20
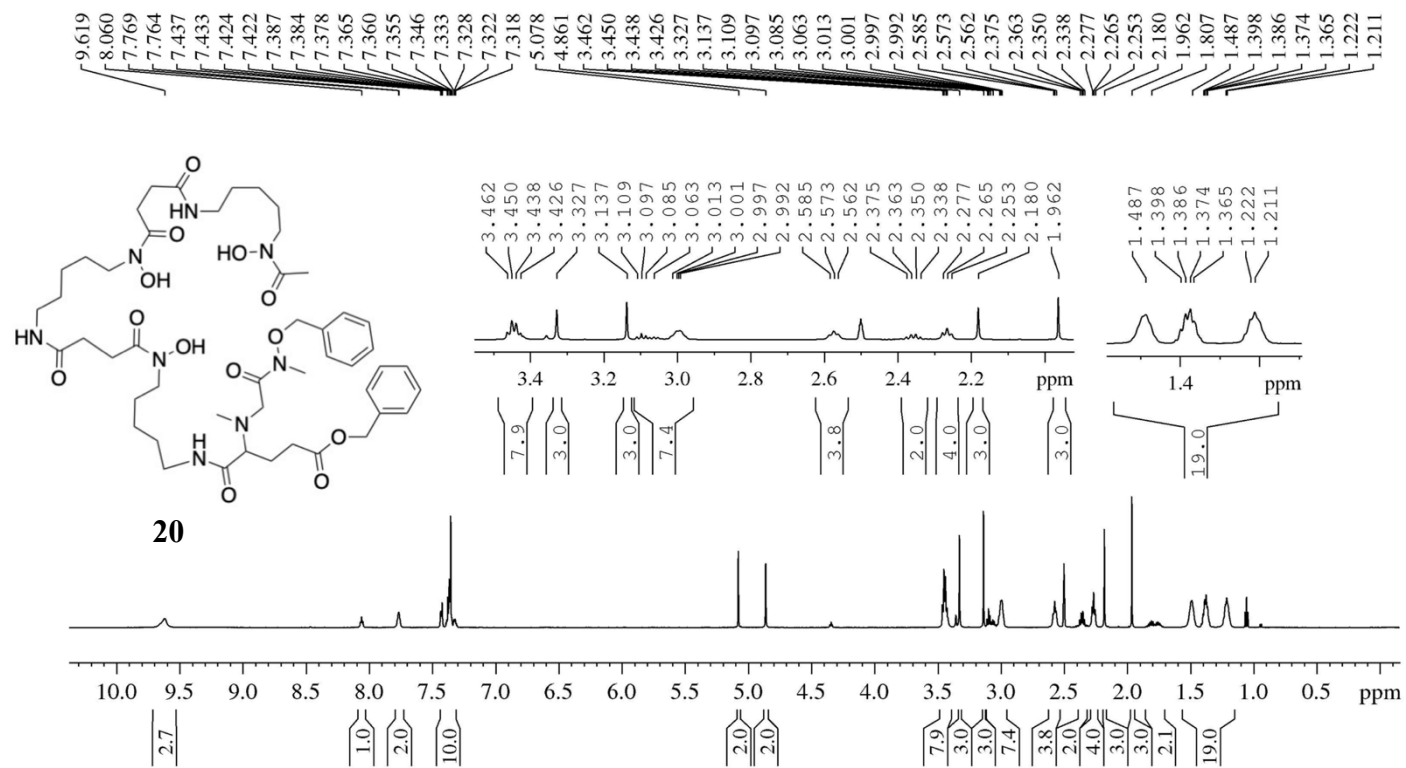
Figure S4-16. ^{1}H NMR spectrum of compound **20** in DMSO-D$_6$. The signals at 1.17, 1.99 and 4.03 ppm are assigned for residual ethyl acetate in the NMR sample.

Compound 20
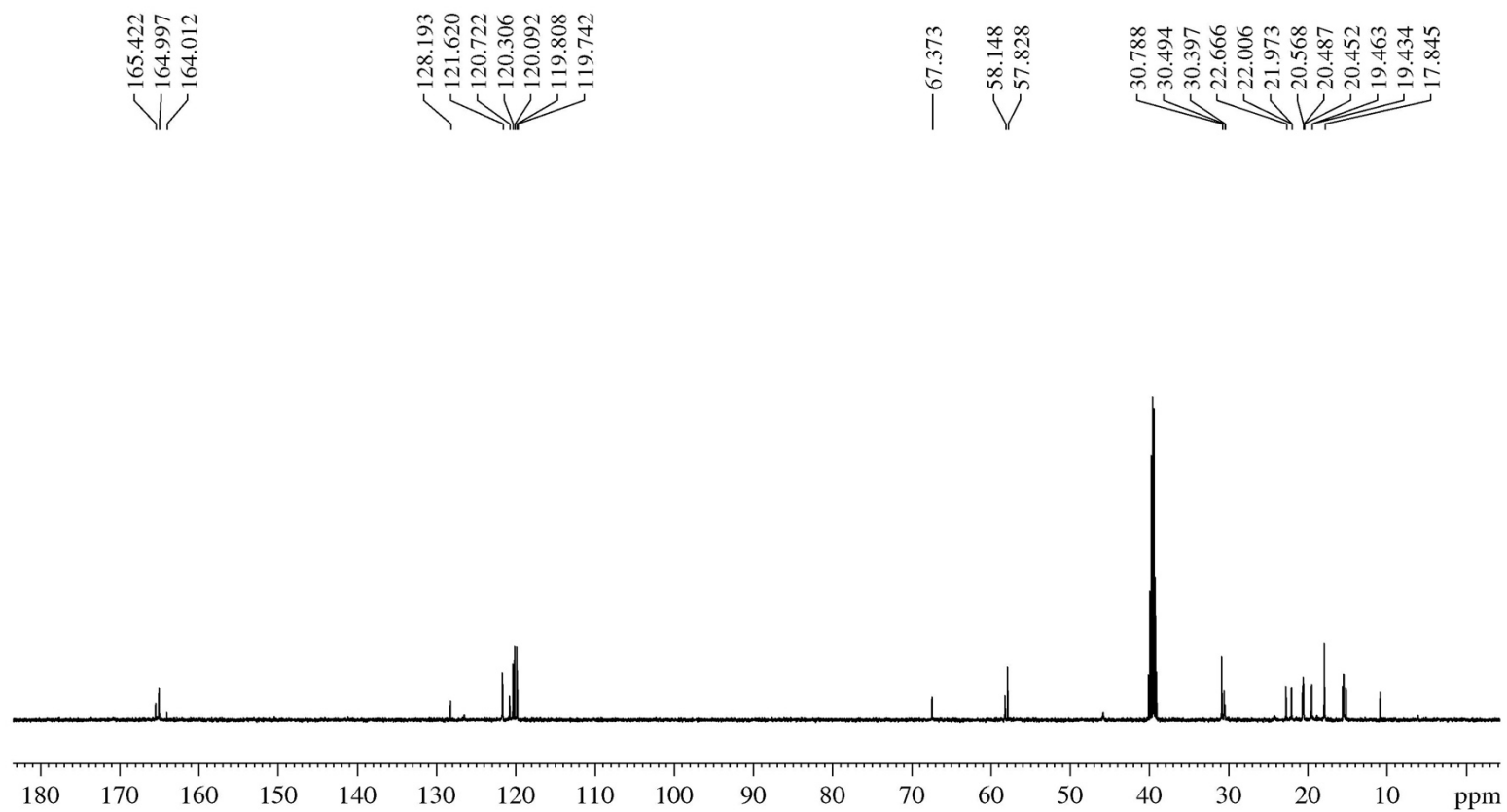
Figure S4-17. ^{13}C NMR spectrum of compound **20** in DMSO-D$_6$.

Compound 21
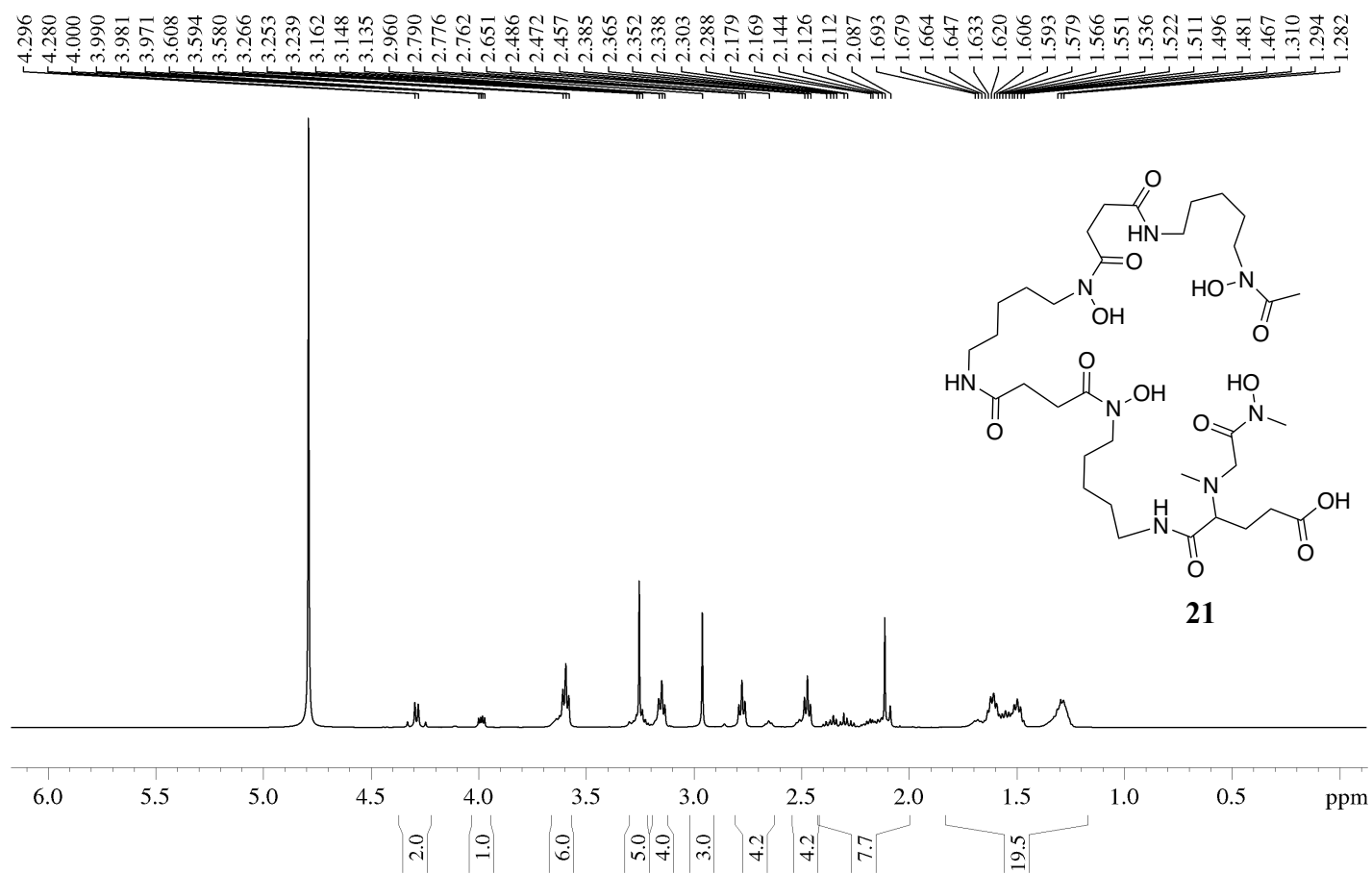
Figure S4-18. ^{1}H NMR spectrum of compound **21** in D$_2$O. The signal at 4.79 ppm is assigned for residual H$_2$O in the NMR sample.

Compound 21
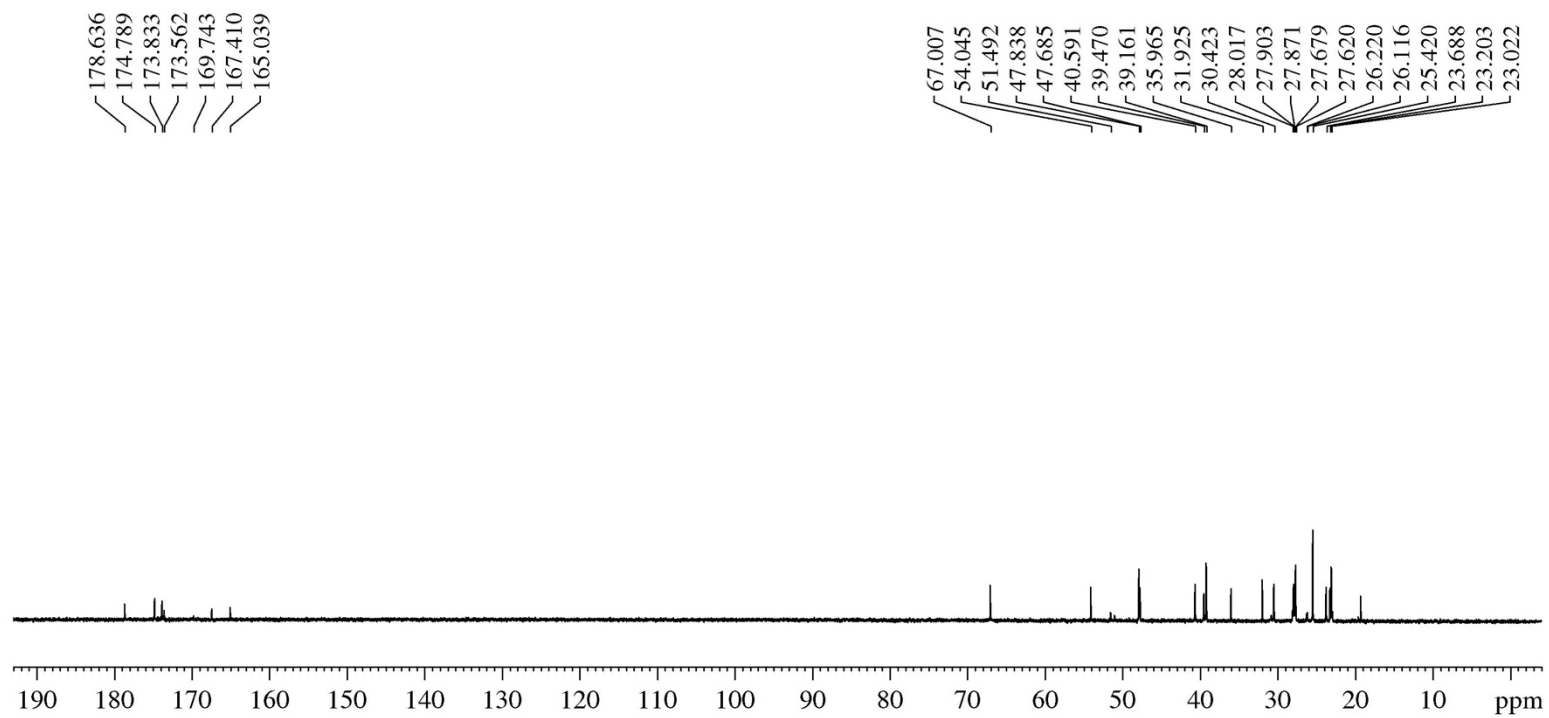
Figure S4-19. ^{1}H NMR spectrum of compound **21** in D$_2$O.
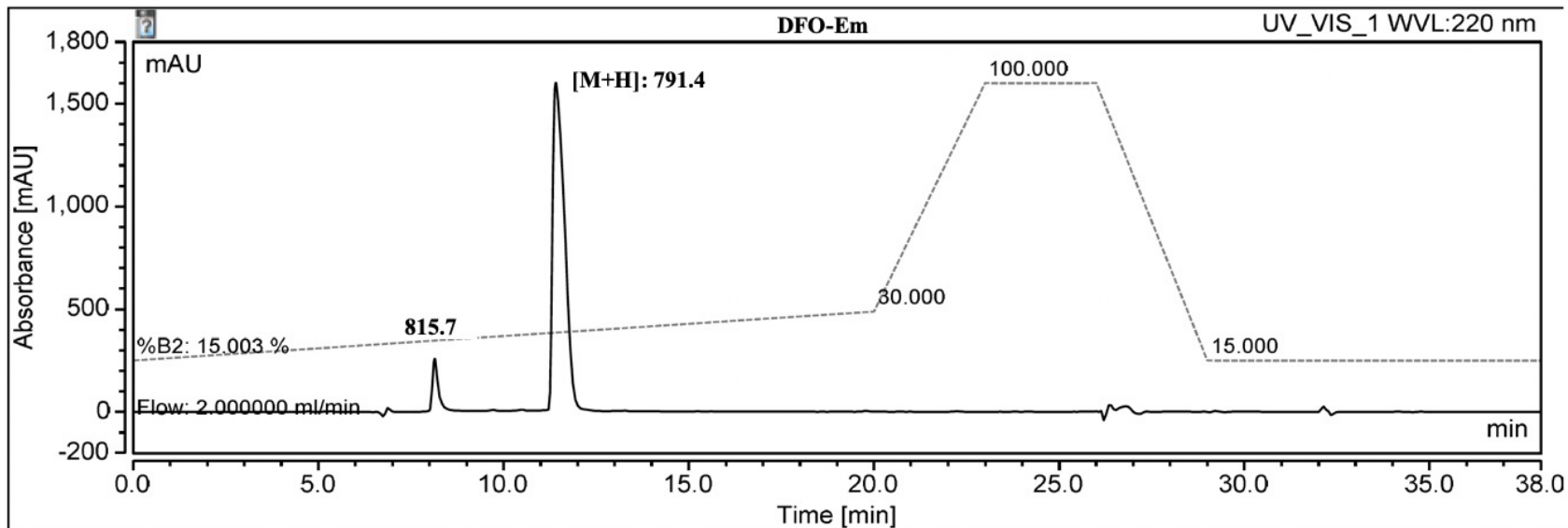
Figure S4-20. Analytical HPLC chromatogram of DFO-Em (**21**). HPLC conditions: C18 Inspire analytical DIKMA; 5 μm, 21.2 × 250 mm; (15 – 30% acetonitrile in water (0.1% formic acid); flow rate, 2 mL/min, t_R = 11.5 min).

Compound 22
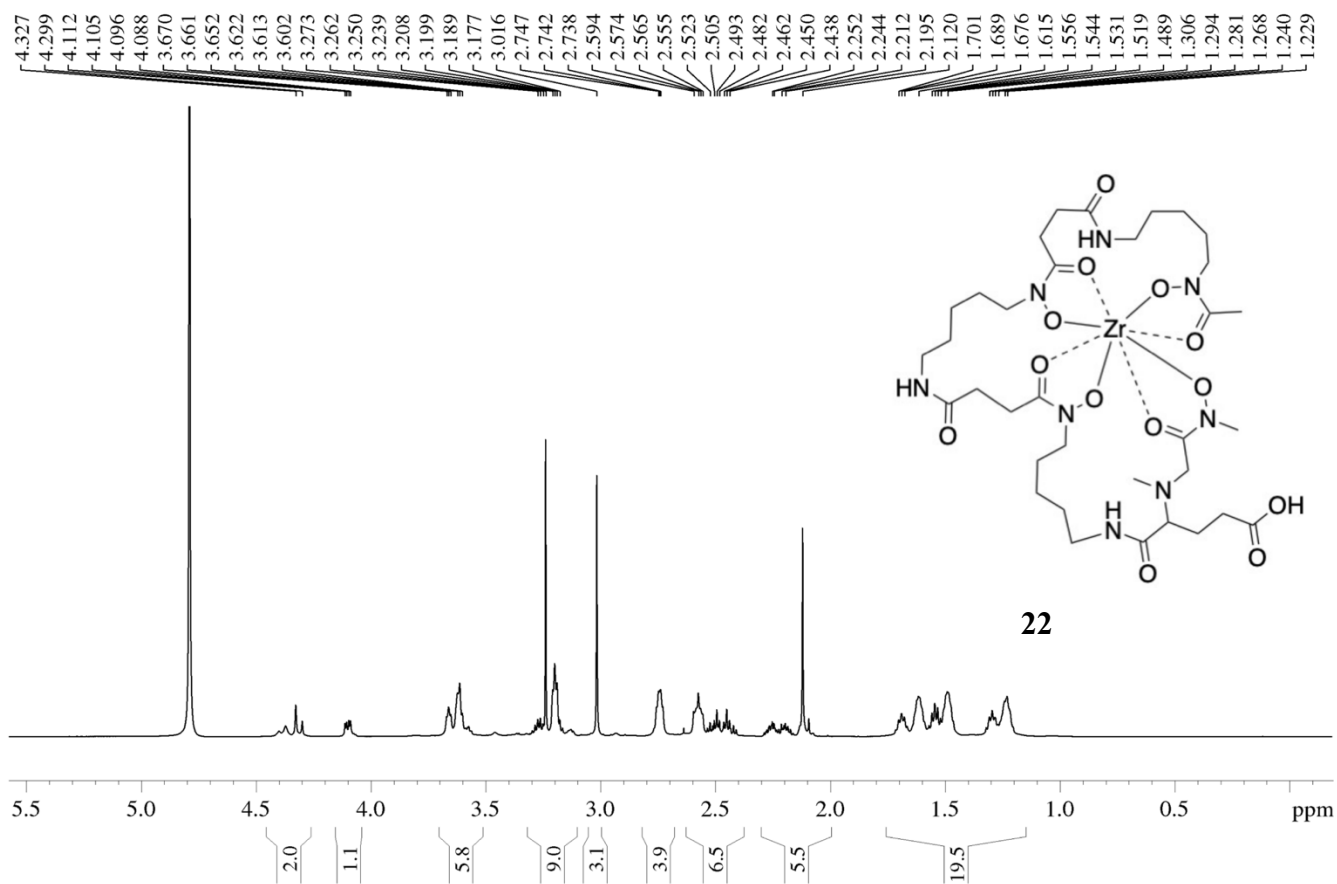
Figure S4-21. ^{1}H NMR spectrum of compound **22** in D$_2$O. The signal at 4.79 ppm is assigned for residual H$_2$O in the NMR sample.

Compound 22

174.204
174.019
166.572
164.901
164.426
164.269
164.138

66.529
54.264
51.085
50.538
50.236
40.838
39.553
38.440
38.388
36.013
30.886
30.691
29.412
27.748
27.216
27.150
26.314
26.115
25.177
25.090
23.115
22.407
22.117

180 170 160 150 140 130 120 110 100 90 80 70 60 50 40 30 20 10 ppm
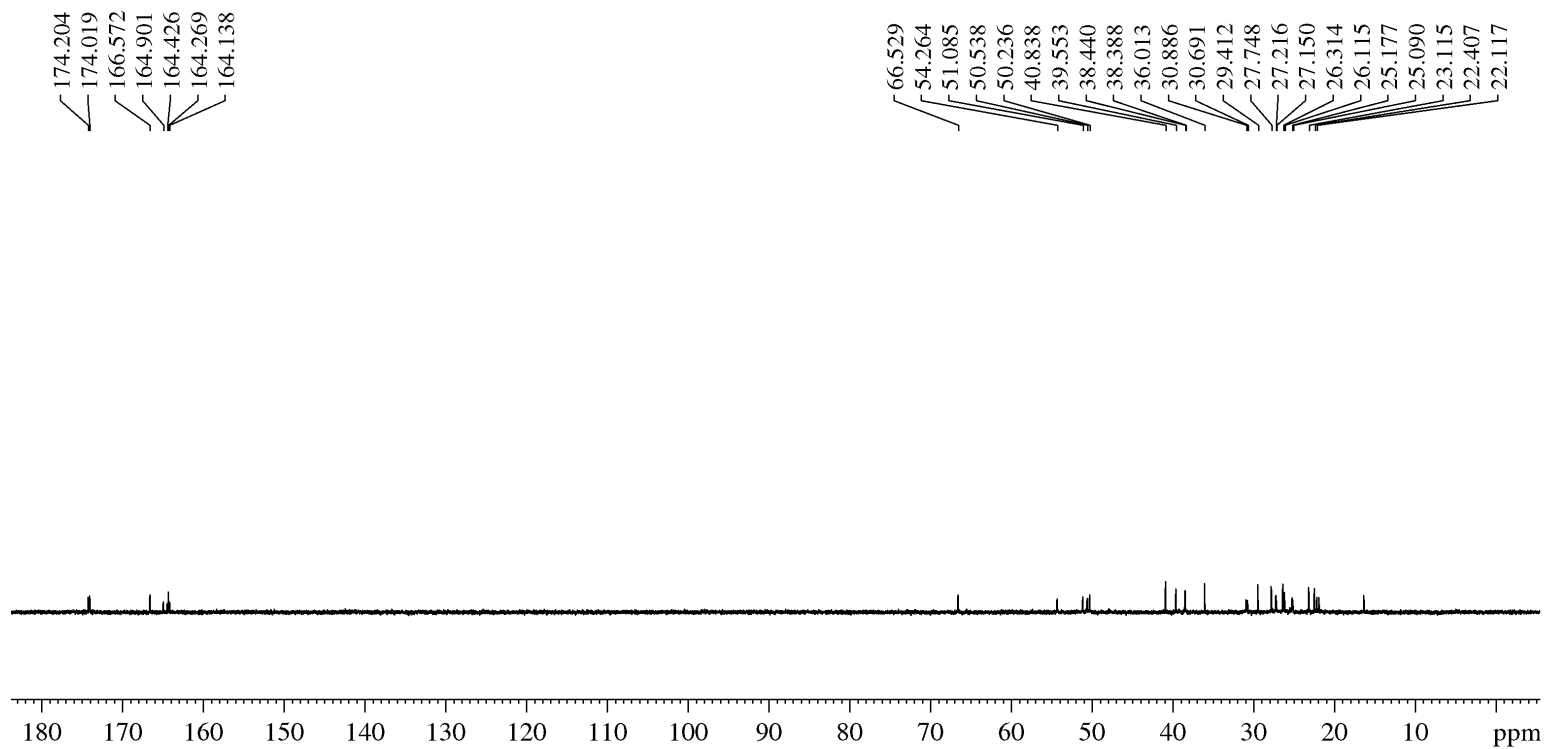
Figure S4-22. ^{13}C NMR spectrum of compound **10** in D_2O.

222

Table S4-1. Calculated Zr-O bond lengths of Zr(DFO-Em) isomers.*

Isomers	Avg. Z-O Bond Length (Å)
C-TTC**	2.240
C-CCC	2.239
C-TCT	2.239
C-CTC	2.252
C-CTT	2.242
C-CCT	2.245
C-TCC	2.235
C-TTT	2.239
N-CCC	2.247
N-CTC	2.242
N-CTT	2.240
N-CCT	2.248
N-TTT	2.236
N-TCC	2.238
N-TCT	2.235
N-TTC	2.234

* Density Functional Theory calculations performed by using Material Studio software via DMol^3/PBE.

** (*C*-) and (*N*-) refere to the either the Carbon or Nitrogen atom of the first HA group is in the back, and the subsequent HA are assigned as either cis (C) or trans (T) relative to the first HA.

XYZ Coordinates of the Zr(DFO-Em) isomers

Λ-*C*-TTT

114

C	-3.76400	-2.39500	1.10700
C	-2.53000	-3.01400	0.43300
O	-1.71700	-3.70900	1.07900
C	-4.69200	-3.54300	1.58500
C	-5.33400	-4.39600	0.49500
C	-6.46800	-3.72400	-0.23400
O	-6.84300	-4.42900	-1.33600
N	-3.48800	-1.53500	2.28600
C	-2.13500	-1.09900	2.64100
C	-1.32100	-0.21300	1.70100
N	-1.49400	1.09600	1.55800
O	-0.38000	-0.77300	1.01100
O	-0.73100	1.74800	0.64300
C	-2.31700	1.97900	2.36700
C	-0.30600	2.24500	-2.42000
C	-0.60500	3.48300	-3.23700
C	0.07700	4.73000	-2.65400
C	-0.48500	5.11400	-1.29000
O	0.69900	2.24500	-1.60700
N	-1.06200	1.15400	-2.49100
O	-1.71000	5.28800	-1.11500
N	0.42700	5.29400	-0.30400
C	0.05500	5.52900	1.09200
C	1.26500	5.94000	1.93700
C	2.34300	4.85800	2.11800
C	1.95600	3.73000	3.08200
C	2.92200	2.53600	3.06400
C	3.51300	1.87500	0.70100
C	4.82000	2.62000	0.63400

C	6.00100	1.76300	0.15600
N	2.80200	1.76700	1.82100
O	3.03500	1.31700	-0.35800
C	6.49400	0.76600	1.20000
O	6.33500	0.94700	2.42500
N	7.13800	-0.31400	0.69200
C	7.64400	-1.43200	1.49100
C	6.58000	-2.42300	1.98800
C	5.72100	-3.10900	0.91200
C	4.65900	-2.18700	0.30900
C	3.64400	-2.87900	-0.60100
N	2.65700	-1.90800	-1.06400
C	2.69300	-1.19300	-2.18800
O	1.91000	-0.18700	-2.29400
C	3.62000	-1.57900	-3.30500
O	1.77200	-1.49700	-0.09400
O	1.62400	1.08500	1.72100
O	-0.78000	0.12000	-1.64900
C	-2.19400	0.90200	-3.38400
C	-1.93000	-0.22000	-4.40100
C	-1.69300	-1.65400	-3.88900
C	-2.92100	-2.37700	-3.30200
C	-3.29200	-2.11500	-1.83500
N	-2.41600	-2.85400	-0.91100
Zr	0.90300	0.47300	-0.28800
H	-5.48600	-3.09100	2.19400
H	-4.09600	-4.18400	2.25000
H	-4.60300	-4.76100	-0.24500
H	-5.76000	-5.30900	0.94800
H	-2.22300	-0.60700	3.62200
H	-1.51200	-1.99300	2.77700
H	-1.65700	2.72700	2.82700
H	-2.83000	1.41800	3.15200

H	-3.05400	2.49000	1.73300
H	-1.69000	3.65600	-3.28000
H	-0.26200	3.33900	-4.27500
H	1.16400	4.58100	-2.60600
H	-0.11300	5.57300	-3.33500
H	1.37400	4.98000	-0.49400
H	-0.42000	4.61800	1.49400
H	-0.70000	6.32800	1.10900
H	0.89000	6.25200	2.92600
H	1.72100	6.83500	1.48000
H	3.26900	5.33600	2.47800
H	2.59900	4.42800	1.13500
H	0.95100	3.34700	2.84900
H	1.92400	4.12000	4.11300
H	3.96600	2.85000	3.18500
H	2.68800	1.83700	3.88000
H	5.07600	3.07200	1.59800
H	4.68300	3.44100	-0.08800
H	5.74700	1.24900	-0.78300
H	6.84200	2.43800	-0.07300
H	7.19900	-0.39300	-0.31900
H	8.18200	-1.02000	2.35800
H	8.37900	-1.95600	0.86200
H	5.92000	-1.91000	2.70700
H	7.12300	-3.19300	2.56200
H	5.21700	-3.97500	1.37500
H	6.36900	-3.51800	0.11600
H	5.13100	-1.38700	-0.27500
H	4.10200	-1.69000	1.11900
H	4.12600	-3.33000	-1.47800
H	3.09900	-3.67400	-0.07000
H	3.36200	-0.98000	-4.18600
H	3.53700	-2.64400	-3.55700

H	4.66900	-1.37300	-3.03900
H	-2.41000	1.83000	-3.92800
H	-3.06400	0.67900	-2.74800
H	-1.06400	0.08200	-5.01400
H	-2.80000	-0.22600	-5.08100
H	-0.86100	-1.65400	-3.17100
H	-1.36200	-2.24100	-4.76200
H	-2.78600	-3.46800	-3.41400
H	-3.80700	-2.12400	-3.90900
H	-3.25400	-1.04200	-1.59900
H	-4.32800	-2.45600	-1.69300
H	-1.59600	-3.30300	-1.31700
C	-4.52800	-0.52100	2.42600
H	-5.51700	-1.00000	2.37800
H	-4.50000	0.26200	1.64100
H	-4.44400	-0.04100	3.41100
H	-4.29800	-1.78900	0.35700
O	-7.03100	-2.68800	0.10400
H	-7.60400	-3.95400	-1.73800

Λ-*C*-TCT

114

C	-4.80900	-1.94100	0.29300
C	-5.01200	-1.30200	-1.10600
O	-5.51900	-0.16700	-1.19900
C	-4.57200	-3.46700	0.33700
C	-5.81000	-4.28100	-0.06700
C	-5.60400	-5.76100	0.13100
O	-6.03100	-6.49300	-0.93200
N	-3.81600	-1.13900	1.03200
C	-2.44900	-1.23900	0.54000
C	-1.57100	0.00900	0.49400
N	-1.95400	1.26800	0.66600

O	-0.33600	-0.20900	0.19400	O	1.86900	-0.22500	-1.10100
O	-0.97800	2.22700	0.53600	O	1.72000	3.39700	0.28100
C	-3.26600	1.81300	0.97800	O	-0.66700	1.18600	-2.15400
C	-0.86000	3.46400	-2.38000	C	-2.68800	1.95700	-3.19000
C	-1.49700	4.74600	-2.87200	C	-2.72900	0.87200	-4.27100
C	-0.86100	6.00500	-2.24600	C	-2.41600	-0.56600	-3.80000
C	-1.34600	6.29300	-0.82800	C	-3.40800	-1.61600	-4.31400
O	0.22800	3.51300	-1.70100	C	-4.75300	-1.60400	-3.57400
N	-1.36200	2.26100	-2.65100	N	-4.61800	-2.02900	-2.18000
O	-2.28400	7.10100	-0.62600	Zr	0.79800	1.60600	-0.58600
N	-0.71300	5.64900	0.18000	H	-4.22600	-2.95400	-2.02100
C	-1.20100	5.72700	1.56000	H	6.18100	0.04800	2.23000
C	-0.27300	5.06300	2.58100	H	-0.08300	4.87900	-0.06600
C	1.01600	5.83000	2.92700	H	-4.30800	-3.73700	1.37000
C	2.16300	5.79600	1.90200	H	-3.70600	-3.76100	-0.27800
C	3.02400	4.53100	1.90800	H	-6.11500	-4.09000	-1.10400
C	2.33300	2.10600	2.07900	H	-6.65900	-3.99200	0.57600
C	2.92300	1.88400	3.44400	H	-2.45800	-1.59800	-0.50200
C	4.35700	1.32000	3.42100	H	-1.84900	-1.98500	1.10100
N	2.31000	3.31300	1.51400	H	-3.99400	0.99400	0.96300
O	1.81800	1.13200	1.41800	H	-3.51400	2.56300	0.21600
C	4.42000	-0.19200	3.23400	H	-3.22500	2.30100	1.96300
O	3.55800	-0.95400	3.71800	H	-2.57900	4.73900	-2.67700
N	5.50300	-0.63900	2.55300	H	-1.38600	4.79800	-3.96700
C	5.84100	-2.05200	2.38000	H	-1.15000	6.87300	-2.85500
C	6.46100	-2.35800	1.01100	H	0.23500	5.91200	-2.28000
C	5.48600	-2.46900	-0.17000	H	-2.19400	5.24800	1.61400
C	4.70000	-1.19300	-0.47400	H	-1.34700	6.79000	1.81200
C	3.89200	-1.27900	-1.77300	H	-0.06000	4.03400	2.25600
N	2.99100	-0.13100	-1.88900	H	-0.86400	4.97100	3.50700
C	3.25600	1.06300	-2.41000	H	1.39900	5.45000	3.89100
O	2.44600	2.02300	-2.13300	H	0.74600	6.88400	3.10900
C	4.42300	1.29300	-3.32400	H	2.85900	6.62200	2.12400

H	1.78700	5.97600	0.88500
H	3.45200	4.36200	2.90400
H	3.86100	4.65400	1.20000
H	2.27800	1.15400	3.95400
H	2.90100	2.81000	4.03100
H	4.81800	1.52300	4.40100
H	4.97500	1.83500	2.67100
H	4.91600	-2.62600	2.53400
H	6.54900	-2.35300	3.17300
H	6.99700	-3.31600	1.10700
H	7.23400	-1.60100	0.78800
H	4.77900	-3.29500	0.02100
H	6.06700	-2.76100	-1.06300
H	5.39100	-0.33500	-0.54700
H	3.99800	-0.96900	0.34100
H	3.25500	-2.17500	-1.79100
H	4.54100	-1.31400	-2.65800
H	4.13400	1.09000	-4.36800
H	5.29000	0.66600	-3.08500
H	4.72000	2.34800	-3.25500
H	-3.09000	2.89300	-3.59900
H	-3.32600	1.65100	-2.34300
H	-2.07500	1.16000	-5.10900
H	-3.75700	0.91000	-4.66800
H	-2.40700	-0.59300	-2.70100
H	-1.39400	-0.83900	-4.10200
H	-2.96800	-2.62400	-4.22400
H	-3.61100	-1.46300	-5.38800
H	-5.46600	-2.27500	-4.07900
H	-5.19500	-0.60000	-3.55600
C	-3.90600	-1.26900	2.48500
H	-4.94500	-1.10800	2.80500
H	-3.28000	-0.49900	2.96100

H	-3.56800	-2.25500	2.86400
H	-5.76700	-1.75000	0.80300
O	-5.11300	-6.27700	1.13100
H	-5.87800	-7.43900	-0.71100

Λ-*C*-TCC
114
C	-4.36200	-1.50500	1.21500
C	-3.14400	-1.90500	0.35200
O	-2.25500	-2.63500	0.83300
C	-4.94900	-2.78200	1.83900
C	-5.39100	-3.82100	0.80600
C	-6.61800	-3.45600	0.01200
O	-6.81000	-4.31100	-1.03000
N	-3.90800	-0.50100	2.21400
C	-3.95400	0.86900	1.70500
C	-2.62500	1.41000	1.17800
N	-2.53800	2.69400	0.84100
O	-1.57900	0.68300	1.06600
O	-1.30200	3.16200	0.47900
C	-3.57800	3.70600	0.88700
C	-0.56600	3.23300	-2.57800
C	-0.63900	4.43900	-3.48400
C	0.27800	5.58300	-3.00900
C	-0.27300	6.36400	-1.81900
O	0.42600	3.10500	-1.76700
N	-1.47600	2.26700	-2.58100
O	-1.00900	7.36500	-1.99900
N	0.08100	5.94000	-0.58600
C	-0.48300	6.55200	0.62000
C	0.07400	5.96400	1.92000
C	1.50800	6.37400	2.29800
C	2.66600	5.74800	1.50200

C	3.08400	4.33100	1.90800
C	1.78500	2.25500	2.46700
C	2.39700	2.11400	3.83700
C	3.83700	1.56500	3.83400
N	2.06700	3.29500	1.68600
O	0.97400	1.36000	2.01500
C	3.92400	0.06100	3.60100
O	3.10300	-0.72900	4.10900
N	4.98500	-0.34400	2.85500
C	5.39400	-1.74000	2.70800
C	5.80600	-2.11000	1.28200
C	4.68100	-2.01200	0.23000
C	4.72600	-0.74700	-0.63300
C	3.62200	-0.68300	-1.69500
N	2.30800	-0.34000	-1.14400
C	1.30200	-1.13800	-0.81100
O	0.26000	-0.59500	-0.27700
C	1.30700	-2.61300	-1.06800
O	2.14000	0.99200	-0.87400
O	1.50700	3.30900	0.43800
O	-1.26300	1.22500	-1.71700
C	-2.66600	2.15200	-3.41900
C	-2.60500	1.00800	-4.44200
C	-2.61900	-0.44100	-3.92300
C	-3.90800	-0.88100	-3.20000
C	-3.99100	-0.61700	-1.68900
N	-3.08200	-1.49200	-0.94200
Zr	0.16600	1.62900	-0.08600
H	0.51500	5.01500	-0.48700
H	5.64000	0.36800	2.54100
H	-2.15500	-1.62800	-1.34800
H	1.75800	1.42400	4.40300
H	2.38400	3.08100	4.36000

H	-5.81200	-2.51800	2.46400
H	-4.19000	-3.24900	2.48100
H	-5.63900	-4.76500	1.32100
H	-4.58300	-4.08200	0.10600
H	-4.28000	1.53200	2.52000
H	-4.71900	0.97900	0.91000
H	-4.56000	3.24000	1.01200
H	-3.56000	4.26100	-0.06100
H	-3.39200	4.40500	1.71600
H	-1.67600	4.79700	-3.56600
H	-0.33300	4.14100	-4.50100
H	0.37800	6.30400	-3.83200
H	1.27400	5.17800	-2.78500
H	-1.57800	6.41700	0.60600
H	-0.29700	7.63800	0.58000
H	-0.03900	4.87100	1.88500
H	-0.59500	6.31800	2.72200
H	1.66300	6.14800	3.36800
H	1.58600	7.47100	2.20900
H	3.56900	6.36100	1.66200
H	2.46800	5.77800	0.42200
H	3.35300	4.31200	2.97100
H	3.97600	4.04300	1.32700
H	4.26700	1.73800	4.83400
H	4.47400	2.10900	3.12300
H	4.54200	-2.35100	3.03300
H	6.23200	-1.94500	3.39700
H	6.18000	-3.14600	1.33000
H	6.66700	-1.49300	0.97300
H	3.70500	-2.08000	0.74100
H	4.74000	-2.88600	-0.44000
H	5.69300	-0.70700	-1.16400
H	4.66900	0.15700	-0.00700

H	3.53900	-1.63500	-2.23700
H	3.84100	0.10100	-2.43200
H	2.30400	-3.03000	-1.24000
H	0.67900	-2.83100	-1.94700
H	0.84900	-3.11200	-0.20200
H	-2.78500	3.10300	-3.95300
H	-3.53000	2.04700	-2.74600
H	-1.70700	1.15900	-5.06400
H	-3.47100	1.14900	-5.11100
H	-1.73900	-0.61000	-3.28500
H	-2.48800	-1.09000	-4.80500
H	-4.05600	-1.96300	-3.35300
H	-4.77500	-0.38500	-3.67100
H	-5.02100	-0.81700	-1.36700
H	-3.76300	0.43500	-1.46300
C	-4.51900	-0.58800	3.54700
H	-4.33600	-1.57400	3.99200
H	-5.61100	-0.39400	3.55800
H	-4.03200	0.15600	4.19300
H	-5.15100	-1.05300	0.58800
O	-7.39100	-2.53400	0.25300
H	-7.64300	-4.04100	-1.47500

Λ-*C*-CCC

114

C	-3.95800	-2.90400	0.52700
C	-4.41700	-2.93700	-0.94800
O	-4.31900	-3.99000	-1.61500
C	-5.02800	-3.51000	1.45600
C	-6.28100	-2.64100	1.62000
C	-7.24600	-3.23100	2.62000
O	-8.53800	-3.13300	2.21100
N	-2.65400	-3.56900	0.73300

C	-1.57700	-3.01300	-0.08200
C	-0.92200	-1.68400	0.27500
N	-0.85900	-1.12800	1.47800
O	-0.27500	-1.12700	-0.69000
O	-0.12000	0.02100	1.60700
C	-1.39900	-1.60900	2.73900
C	0.24300	2.23900	-2.44300
C	0.30300	2.97400	-3.75300
C	1.33400	4.13400	-3.73300
C	0.87700	5.30700	-2.87700
O	1.22200	1.45800	-2.10300
N	-0.73900	2.39800	-1.56900
O	0.23100	6.26100	-3.35900
N	1.18500	5.20700	-1.55700
C	0.74100	6.13500	-0.51800
C	1.90100	6.72600	0.29400
C	2.79800	5.68300	0.98000
C	2.12000	4.88700	2.10200
C	2.89800	3.63300	2.52000
C	3.71200	2.21000	0.58600
C	5.05600	2.88100	0.45000
C	6.25100	1.92300	0.42800
N	2.82300	2.57600	1.50700
O	3.35900	1.29500	-0.24700
C	6.64500	1.40700	1.81100
O	6.30300	1.98300	2.86400
N	7.41900	0.29400	1.79500
C	7.83800	-0.44500	2.98800
C	6.72900	-1.24400	3.68800
C	5.98800	-2.29600	2.84300
C	5.01700	-1.68400	1.82800
C	4.01600	-2.66000	1.20900
N	3.08000	-1.92000	0.36100

C	3.12600	-1.77400	-0.95800		H	1.10700	4.56900	1.81000
O	2.34400	-0.91100	-1.50800		H	2.00100	5.52600	2.99200
C	4.04600	-2.61600	-1.79600		H	2.47200	3.20000	3.43700
O	2.19200	-1.13300	1.05200		H	3.95500	3.85100	2.71700
O	1.59200	1.97100	1.43800		H	5.21200	3.63400	1.22900
O	-0.62900	1.72000	-0.39500		H	5.03200	3.41200	-0.51600
C	-1.95900	3.20100	-1.71400		H	7.12100	2.46400	0.02000
C	-3.17100	2.42200	-2.23200		H	6.05900	1.08200	-0.25400
C	-3.57000	1.20600	-1.39200		H	7.62700	-0.11900	0.89100
C	-4.96600	0.68900	-1.74600		H	8.27200	0.26900	3.70500
C	-5.38600	-0.55300	-0.95400		H	8.64400	-1.12000	2.66500
N	-4.86600	-1.79400	-1.54000		H	5.99300	-0.54000	4.11000
Zr	1.21100	0.46000	-0.08900		H	7.20900	-1.74400	4.54700
H	-4.56800	-3.66300	2.44300		H	5.41700	-2.94000	3.53400
H	-5.32900	-4.49700	1.07400		H	6.71500	-2.95400	2.33400
H	-6.80400	-2.48200	0.66900		H	5.56700	-1.20900	1.00500
H	-6.00800	-1.64900	2.01800		H	4.43600	-0.88700	2.31700
H	-1.84900	-2.91100	-1.15100		H	3.41800	-3.17000	1.98000
H	-0.74800	-3.73900	-0.06600		H	4.51100	-3.42700	0.60000
H	-1.97100	-2.52700	2.55400		H	3.85600	-3.69000	-1.65600
H	-2.04400	-0.82900	3.17100		H	5.10000	-2.42400	-1.55000
H	-0.56400	-1.80300	3.42800		H	3.88100	-2.36000	-2.84900
H	-0.68100	3.35000	-4.06200		H	-1.74400	4.05100	-2.37400
H	0.62500	2.24800	-4.51400		H	-2.15800	3.60400	-0.71100
H	1.46200	4.50400	-4.75800		H	-2.99500	2.11800	-3.27800
H	2.30500	3.74600	-3.38700		H	-4.00600	3.14200	-2.25600
H	1.69500	4.37900	-1.26300		H	-3.55900	1.48400	-0.32400
H	0.03100	5.61100	0.14300		H	-2.82100	0.40700	-1.50500
H	0.18500	6.93300	-1.02600		H	-5.04100	0.47300	-2.82600
H	1.46800	7.40400	1.04900		H	-5.70400	1.48200	-1.54200
H	2.51900	7.34600	-0.37500		H	-6.48600	-0.61700	-0.92200
H	3.68900	6.18900	1.38700		H	-5.03800	-0.46600	0.08200
H	3.18300	4.99200	0.21100		H	-5.14900	-1.95200	-2.51000

C	-2.62700	-5.04000	0.68200
H	-3.40900	-5.45800	1.32700
H	-1.65800	-5.37300	1.08100
H	-2.75400	-5.45000	-0.33500
H	-3.80200	-1.85500	0.82500
O	-6.93300	-3.72900	3.69600
H	-9.09700	-3.50000	2.93200

Λ-*C*-CTC

114

C	-3.62000	-2.85300	0.82800
C	-3.36000	-2.46500	-0.62800
O	-2.71900	-3.21600	-1.39600
C	-4.76600	-3.90500	0.80600
C	-6.11600	-3.38300	0.29200
C	-7.18200	-4.44300	0.39900
O	-7.85000	-4.63200	-0.76900
N	-2.46600	-3.45100	1.53100
C	-1.09000	-3.19200	1.08700
C	-0.45500	-1.79300	1.06200
N	0.00600	-1.17700	2.14900
O	-0.23900	-1.22700	-0.07700
O	0.61800	0.03800	1.97500
C	0.06700	-1.66100	3.52100
C	-0.08200	1.85300	-2.26200
C	-0.43900	2.32700	-3.64600
C	0.77500	2.93700	-4.37200
C	1.02300	4.39100	-3.99100
O	0.66600	0.81100	-2.12400
N	-0.45900	2.49900	-1.16500
O	0.14300	5.08000	-3.42500
N	2.22300	4.94200	-4.30100
C	3.34800	4.40200	-5.06900

C	4.70100	4.81400	-4.46900
C	5.23800	3.91100	-3.34800
C	4.29900	3.70700	-2.15700
C	4.93900	2.83300	-1.06900
C	3.53300	2.35500	0.96800
C	4.26800	3.31700	1.87000
C	5.69000	2.90100	2.28400
N	3.92700	2.13300	-0.28000
O	2.49900	1.71400	1.38900
C	5.75600	1.65600	3.15900
O	4.89500	1.41000	4.02900
N	6.83900	0.86900	2.93600
C	7.22000	-0.28700	3.74700
C	7.67800	-1.48800	2.91000
C	6.56900	-2.37600	2.32400
C	5.60800	-1.67900	1.35700
C	4.58400	-2.65500	0.77100
N	3.49900	-1.95000	0.09200
C	3.18200	-1.95700	-1.19600
O	2.19600	-1.21900	-1.57800
C	3.92900	-2.80900	-2.18100
O	2.72800	-1.17900	0.92200
O	3.20100	1.22600	-1.00100
O	0.02000	2.00700	0.02100
C	-1.51700	3.51800	-1.04800
C	-2.91800	2.95400	-1.31500
C	-3.24300	1.66500	-0.55800
C	-4.57800	1.06200	-0.99800
C	-4.83100	-0.35000	-0.46900
N	-3.92200	-1.31900	-1.09400
Zr	1.44600	0.30500	-0.05600
H	-4.91400	-4.28300	1.82400
H	-4.42600	-4.74600	0.18500

H	-6.05600	-3.03100	-0.74500
H	-6.45400	-2.54000	0.91600
H	-1.00400	-3.53200	0.04900
H	-0.44600	-3.84000	1.70400
H	-0.10800	-2.73900	3.55100
H	-0.67200	-1.14700	4.15200
H	1.07800	-1.45200	3.89500
H	-1.25300	3.06000	-3.63400
H	-0.78100	1.44700	-4.21300
H	0.60000	2.90600	-5.46100
H	1.66900	2.32200	-4.19200
H	2.28600	5.93400	-4.06600
H	3.26300	3.30800	-5.11400
H	3.28000	4.77100	-6.10600
H	4.62800	5.85800	-4.11600
H	5.44000	4.82200	-5.28600
H	6.19700	4.33000	-2.99700
H	5.47400	2.92100	-3.77700
H	3.38400	3.19700	-2.48600
H	3.99400	4.67400	-1.72400
H	5.56700	3.42700	-0.39600
H	5.57300	2.05600	-1.52400
H	3.64900	3.42700	2.77000
H	4.32000	4.30500	1.38800
H	6.11600	3.72400	2.88100
H	6.34700	2.78500	1.41000
H	7.51000	1.18000	2.23800
H	6.35200	-0.54400	4.37100
H	8.03700	0.01400	4.42600
H	8.34300	-1.13300	2.10400
H	8.30700	-2.11700	3.56400
H	7.05100	-3.22700	1.81100
H	5.98500	-2.81000	3.15500

H	6.16800	-1.20100	0.53600
H	5.05200	-0.88500	1.87300
H	4.12100	-3.25100	1.57400
H	5.04800	-3.35100	0.06100
H	5.00300	-2.57200	-2.18800
H	3.52300	-2.61600	-3.18100
H	3.81900	-3.88100	-1.95900
H	-1.28400	4.34000	-1.73900
H	-1.42800	3.89400	-0.02100
H	-3.03200	2.76700	-2.39500
H	-3.64500	3.74500	-1.06400
H	-3.25400	1.85200	0.53000
H	-2.44200	0.92900	-0.73200
H	-4.62600	1.03300	-2.10100
H	-5.41600	1.69900	-0.67200
H	-5.87500	-0.63400	-0.68400
H	-4.70200	-0.37800	0.62100
H	-3.80800	-1.21200	-2.10400
C	-2.66100	-3.40400	2.98000
H	-3.60700	-3.89000	3.25300
H	-2.68100	-2.37500	3.39300
H	-1.85700	-3.96800	3.47300
H	-3.96800	-1.96600	1.38700
O	-7.44400	-5.07600	1.41800
H	-8.52800	-5.32600	-0.60300

Λ-*C*-CTT
114
C	-3.63700	-3.66000	0.07000
C	-4.08000	-3.48600	-1.39900
O	-3.90400	-4.40800	-2.22500
C	-4.63000	-4.55600	0.83700
C	-6.02000	-3.96200	1.05300

C	-6.08500	-2.84000	2.05700
O	-7.30900	-2.24600	2.06500
N	-2.25800	-4.18600	0.18400
C	-1.25300	-3.39500	-0.52200
C	-0.75300	-2.06600	0.02400
N	-0.76800	-1.69600	1.29700
O	-0.15600	-1.31200	-0.83900
O	-0.13100	-0.52800	1.63300
C	-1.23200	-2.45000	2.45000
C	-0.04200	1.76700	-2.27700
C	-0.17400	2.38600	-3.64000
C	0.86900	3.51100	-3.86700
C	0.48400	4.80900	-3.17100
O	0.94300	0.96400	-2.04700
N	-0.85900	2.07500	-1.27700
O	-0.07800	5.73700	-3.79400
N	0.76000	4.86400	-1.84200
C	0.34900	5.96100	-0.96700
C	1.49700	6.60300	-0.18100
C	2.28400	5.61600	0.70000
C	3.43100	4.91700	-0.04100
C	4.00300	3.71000	0.69200
C	2.88600	1.92500	2.02800
C	3.65100	2.25000	3.28600
C	5.14200	1.86400	3.27100
N	3.01600	2.64100	0.91900
O	2.06000	0.92500	2.00700
C	5.38400	0.36300	3.32500
O	4.74400	-0.37500	4.10100
N	6.37300	-0.09900	2.51700
C	6.85100	-1.47900	2.56800
C	6.28100	-2.41300	1.49300
C	6.84300	-2.22500	0.06900

C	6.13200	-1.23600	-0.87500
C	4.84500	-1.75800	-1.54300
N	3.61600	-1.52600	-0.78200
C	2.97800	-2.32600	0.06800
O	1.99600	-1.82500	0.72200
C	3.30400	-3.78200	0.20700
O	3.11400	-0.25000	-0.89500
O	2.25300	2.27000	-0.15200
O	-0.60800	1.49300	-0.06800
C	-2.09700	2.86500	-1.34900
C	-3.31100	2.09000	-1.86900
C	-3.60100	0.76600	-1.15700
C	-4.93900	0.16900	-1.60200
C	-5.23000	-1.22000	-1.02600
N	-4.59500	-2.29000	-1.80500
Zr	1.21900	0.25400	0.07300
H	-4.17900	-4.79400	1.81200
H	-4.75700	-5.50000	0.28900
H	-6.69500	-4.74900	1.43300
H	-6.48700	-3.62700	0.11400
H	-1.52700	-3.18800	-1.57600
H	-0.34300	-4.01500	-0.57900
H	-1.70300	-3.37600	2.10000
H	-1.94900	-1.83700	3.01300
H	-0.36500	-2.67400	3.08900
H	-1.18500	2.76500	-3.82900
H	0.01600	1.58600	-4.36900
H	0.92800	3.72200	-4.94300
H	1.85700	3.16000	-3.53100
H	1.16800	4.03900	-1.39900
H	-0.40300	5.57600	-0.25600
H	-0.14600	6.70400	-1.60600
H	1.04500	7.38400	0.45100

H	2.18400	7.11600	-0.87500
H	1.58300	4.86600	1.10700
H	2.70100	6.14500	1.57300
H	4.26300	5.62700	-0.17600
H	3.13100	4.61400	-1.05300
H	4.38900	4.01500	1.67200
H	4.83800	3.28000	0.11500
H	3.15400	1.70600	4.10100
H	3.56400	3.32300	3.50900
H	5.60400	2.28600	4.17900
H	5.66500	2.31500	2.41600
H	6.86400	0.56700	1.92700
H	6.56900	-1.86300	3.55900
H	7.95100	-1.45900	2.50700
H	5.18600	-2.32900	1.51000
H	6.51900	-3.43700	1.82600
H	6.86300	-3.20600	-0.43600
H	7.90200	-1.92300	0.15800
H	6.82900	-1.00400	-1.69800
H	5.91400	-0.27900	-0.37600
H	4.68700	-1.24800	-2.50300
H	4.92300	-2.83200	-1.75400
H	3.19300	-4.07100	1.26100
H	4.30900	-4.04800	-0.13700
H	2.57400	-4.36100	-0.38300
H	-1.91700	3.74900	-1.97400
H	-2.26600	3.22000	-0.32400
H	-3.19100	1.90100	-2.94900
H	-4.17800	2.76500	-1.76600
H	-3.62300	0.92300	-0.06500
H	-2.78100	0.05400	-1.34700
H	-4.98700	0.11300	-2.70400
H	-5.75600	0.84100	-1.29300

H	-6.31900	-1.39400	-1.02100
H	-4.88700	-1.27000	0.01400
H	-4.85500	-2.30100	-2.79400
C	-2.05200	-5.61500	-0.10000
H	-2.78900	-6.22500	0.43600
H	-1.05600	-5.89400	0.27700
H	-2.10900	-5.85900	-1.17600
H	-3.61700	-2.67600	0.56100
O	-5.17600	-2.49000	2.80200
H	-7.28600	-1.55000	2.75900

Λ-*C*-CCT

114

C	-3.58000	-2.94700	1.05100
C	-2.61600	-3.45400	-0.02400
O	-1.75000	-4.31900	0.23200
C	-4.65800	-4.05100	1.26400
C	-5.60500	-4.35100	0.10100
C	-6.68900	-3.32500	-0.11500
O	-7.45300	-3.62800	-1.19800
N	-2.96400	-2.69600	2.37900
C	-1.52000	-2.49300	2.54700
C	-0.89500	-1.12900	2.26400
N	-0.66000	-0.25800	3.24900
O	-0.49900	-0.82300	1.08600
O	-0.01900	0.91400	2.91400
C	-0.96600	-0.34500	4.66600
C	0.28000	2.57200	-1.55900
C	0.40400	3.14000	-2.94800
C	1.47100	4.24700	-3.06900
C	1.04600	5.56300	-2.43200
O	1.33400	2.21400	-0.91000

N	-0.89700	2.38500	-0.97300	N	-2.75900	-2.98300	-1.29200
O	0.69500	6.54800	-3.11500	Zr	1.02300	0.96300	0.99800
N	1.05500	5.56600	-1.07400	H	-5.26300	-3.77200	2.13800
C	0.70000	6.71100	-0.24100	H	-4.11600	-4.97100	1.52700
C	1.92500	7.37300	0.41000	H	-5.07800	-4.51300	-0.85200
C	2.82700	6.39900	1.18000	H	-6.12100	-5.30700	0.28800
C	2.17000	5.74700	2.40300	H	-1.00300	-3.20100	1.89000
C	2.92100	4.51100	2.89700	H	-1.28000	-2.77900	3.58200
C	3.62300	2.60800	1.40200	H	-1.23200	-1.36900	4.94200
C	5.04500	3.08600	1.23800	H	-1.79600	0.33000	4.92400
C	5.73000	2.42900	0.03300	H	-0.06800	-0.04500	5.22300
N	2.70800	3.34700	2.03200	H	-0.55900	3.49800	-3.33000
O	3.25600	1.48200	0.91900	H	0.71000	2.30400	-3.59900
C	6.26400	1.03300	0.32100	H	1.65700	4.44400	-4.13100
O	6.88300	0.78500	1.37800	H	2.41100	3.89400	-2.61800
N	6.10300	0.12200	-0.67100	H	1.37600	4.72000	-0.60800
C	6.71700	-1.20300	-0.63700	H	-0.01200	6.37000	0.52500
C	5.77700	-2.37500	-0.30600	H	0.17700	7.43100	-0.88400
C	5.00900	-2.99000	-1.49200	H	1.56300	8.16800	1.08400
C	3.71100	-2.32100	-1.97900	H	2.52000	7.86600	-0.37600
C	2.45900	-2.58900	-1.12600	H	3.74000	6.92700	1.49800
N	2.22500	-1.61700	-0.05700	H	3.16800	5.61500	0.48100
C	2.37500	-1.76200	1.25500	H	1.13500	5.44300	2.18800
O	2.07400	-0.77400	2.02300	H	2.11700	6.47100	3.23200
C	2.84100	-3.05000	1.86700	H	2.57600	4.21600	3.90100
O	1.76000	-0.40700	-0.51600	H	4.00100	4.69700	2.96100
O	1.44600	2.80800	2.10500	H	5.62400	2.84800	2.14700
O	-0.87800	1.74400	0.23900	H	5.06700	4.17800	1.12100
C	-2.23200	2.63600	-1.53200	H	6.61400	3.03500	-0.23000
C	-2.73400	1.49700	-2.42100	H	5.06400	2.43000	-0.84000
C	-2.96800	0.17700	-1.68300	H	5.54300	0.38700	-1.47500
C	-3.38400	-0.94700	-2.63400	H	7.50100	-1.14300	0.13000
C	-3.84200	-2.22100	-1.92300	H	7.20800	-1.37900	-1.60700

231

H	5.10000	-2.06300	0.50300
H	6.41500	-3.16900	0.11600
H	4.76400	-4.03700	-1.24100
H	5.70600	-3.05100	-2.34600
H	3.49000	-2.72100	-2.98200
H	3.82500	-1.23200	-2.10400
H	2.48600	-3.59400	-0.68600
H	1.56000	-2.53900	-1.75700
H	1.96800	-3.61200	2.23400
H	3.47200	-2.81600	2.73500
H	3.40400	-3.69400	1.18500
H	-2.20200	3.58200	-2.08700
H	-2.89000	2.78500	-0.66500
H	-2.02100	1.34800	-3.24900
H	-3.67900	1.83400	-2.88100
H	-3.76400	0.33000	-0.93300
H	-2.06800	-0.11300	-1.12000
H	-2.56200	-1.18500	-3.33100
H	-4.23100	-0.61000	-3.25600
H	-4.34000	-2.88400	-2.64900
H	-4.58800	-1.95800	-1.16400
H	-2.11200	-3.42800	-1.94500
C	-3.77100	-1.75500	3.15800
H	-4.82900	-2.04700	3.12800
H	-3.69700	-0.70800	2.79600
H	-3.45500	-1.78400	4.21000
H	-4.06300	-2.02100	0.69800
O	-6.90000	-2.33900	0.58500
H	-8.14600	-2.93500	-1.26700

Λ-*C*-TTC

114

| C | -3.99100 | -1.62700 | 0.51600 |

C	-4.46200	-1.70500	-0.94800
O	-5.48500	-2.34300	-1.27600
C	-4.26600	-2.93700	1.27300
C	-3.38000	-4.08600	0.75100
C	-3.61200	-5.38100	1.48700
O	-4.84800	-5.94400	1.35300
N	-4.58300	-0.41200	1.12600
C	-3.77500	0.12700	2.23400
C	-2.45700	0.66300	1.74300
N	-2.26200	1.93100	1.41300
O	-1.45500	-0.15200	1.61200
O	-1.02700	2.28200	0.97700
C	-3.21700	3.02900	1.44900
C	0.35600	2.25400	-1.95900
C	0.72800	3.34500	-2.93800
C	1.84600	4.25100	-2.42000
C	1.41100	5.10200	-1.23400
O	1.08400	2.03100	-0.92000
N	-0.71400	1.49000	-2.15300
O	0.27300	5.61400	-1.16600
N	2.35200	5.30600	-0.28500
C	2.10400	6.05800	0.94400
C	3.32200	6.02200	1.87000
C	3.71400	4.62300	2.37300
C	2.72100	4.01300	3.36600
C	2.93500	2.51400	3.60400
C	3.27600	1.06800	1.54300
C	4.78100	1.05100	1.63500
C	5.44500	1.22700	0.25300
N	2.53300	1.71400	2.44400
O	2.68200	0.48200	0.57100
C	5.79800	-0.09500	-0.41400
O	6.51300	-0.93700	0.17000

N	5.33800	-0.27100	-1.67400	H	3.23500	4.81300	-0.37600
C	5.57300	-1.48200	-2.46700	H	1.21400	5.63900	1.44100
C	4.90500	-2.74400	-1.90000	H	1.86300	7.10200	0.68500
C	3.40000	-2.60300	-1.66200	H	3.10500	6.67700	2.73100
C	2.82500	-3.79100	-0.88500	H	4.18000	6.47600	1.34400
C	1.36100	-3.62700	-0.46200	H	4.71000	4.67800	2.84200
N	1.10300	-2.41300	0.32200	H	3.82500	3.94400	1.51000
C	1.27800	-2.21800	1.62600	H	1.68700	4.14500	3.01500
O	1.00100	-1.06500	2.11600	H	2.79800	4.52700	4.33800
C	1.77600	-3.30800	2.52600	H	3.97800	2.28300	3.85400
O	0.59800	-1.35400	-0.40300	H	2.31300	2.16700	4.44300
O	1.18000	1.76600	2.20700	H	5.10300	0.09000	2.06700
O	-0.96000	0.50300	-1.23700	H	5.13700	1.83300	2.31400
C	-1.55400	1.48500	-3.34900	H	4.82000	1.85300	-0.40000
C	-1.20000	0.38100	-4.36400	H	6.40100	1.75300	0.39700
C	-1.52500	-1.07500	-3.99200	H	4.68900	0.42000	-2.03900
C	-2.98800	-1.51500	-4.16800	H	6.65900	-1.64500	-2.54300
C	-4.02600	-0.87000	-3.24100	H	5.19800	-1.26700	-3.47800
N	-3.69700	-1.01100	-1.82400	H	5.39900	-2.99900	-0.94900
Zr	0.38200	0.56400	0.59300	H	5.11200	-3.57200	-2.59900
H	-5.33000	-3.19700	1.16800	H	2.86800	-2.49100	-2.62400
H	-4.06100	-2.78100	2.34300	H	3.21000	-1.68200	-1.08800
H	-2.31700	-3.83000	0.86200	H	2.89000	-4.71500	-1.48500
H	-3.58200	-4.25400	-0.31900	H	3.44000	-3.96300	0.01600
H	-4.36600	0.91200	2.72000	H	0.70500	-3.54000	-1.33900
H	-3.54500	-0.62800	3.01300	H	1.02600	-4.49900	0.11500
H	-2.73600	3.87300	1.96000	H	2.73800	-2.99800	2.95800
H	-4.12200	2.73900	1.98900	H	1.91200	-4.27000	2.02300
H	-3.47900	3.32400	0.42300	H	1.06400	-3.43200	3.35500
H	-0.15400	3.96200	-3.16000	H	-1.43700	2.46300	-3.83200
H	1.04800	2.89100	-3.88900	H	-2.59400	1.42300	-3.00600
H	2.73700	3.66000	-2.17000	H	-0.12100	0.46500	-4.57600
H	2.13100	4.94300	-3.23200	H	-1.71400	0.64300	-5.30600

H	-1.18700	-1.28000	-2.96500
H	-0.91800	-1.72300	-4.64600
H	-3.04000	-2.60700	-4.02400
H	-3.31000	-1.31900	-5.20500
H	-4.16000	0.19800	-3.47400
H	-5.00300	-1.35000	-3.38500
C	-5.99400	-0.54200	1.50700
H	-6.16300	-1.19400	2.38500
H	-6.56600	-0.94400	0.66100
H	-6.38900	0.45700	1.74300
O	-2.78700	-5.94800	2.19200
H	-5.40000	-5.40400	0.74900
H	-2.86300	-0.52300	-1.47700
H	-2.90400	-1.46200	0.50700

Λ-*N*-CCC

114

C	-4.19400	-1.29700	1.08000
C	-4.94100	-0.94400	-0.22300
O	-6.15300	-0.64700	-0.23300
C	-4.94100	-2.40700	1.83500
C	-4.88200	-3.76300	1.09900
C	-5.41700	-4.85800	1.99100
O	-6.75100	-5.12700	1.91400
N	-3.92600	-0.15600	1.97900
C	-2.92800	0.80400	1.50200
C	-1.55400	0.28300	1.10000
N	-1.04200	-0.86800	1.54400
O	-0.89100	0.95800	0.25000
O	0.11900	-1.29400	0.93800
C	-1.37800	-1.60300	2.75100
C	0.01800	1.97300	-2.42800
C	-0.34200	3.27900	-3.10300

C	0.31000	4.49300	-2.43900
C	-0.27700	4.80400	-1.06700
O	0.99200	1.92800	-1.58300
N	-0.64300	0.85400	-2.70200
O	-1.46200	4.54400	-0.77400
N	0.56300	5.42800	-0.20500
C	0.18700	5.80800	1.15500
C	1.42200	6.09700	2.01000
C	2.39900	4.91900	2.14100
C	1.87600	3.74400	2.97400
C	2.78500	2.51300	2.92500
C	3.57700	1.78100	0.62900
C	4.80700	2.65500	0.59300
C	6.08700	1.94800	0.13900
N	2.71300	1.81200	1.64200
O	3.27600	1.04900	-0.38300
C	6.75000	1.13200	1.24600
O	6.55000	1.36100	2.45600
N	7.58900	0.15600	0.81600
C	8.22700	-0.82200	1.70100
C	7.28000	-1.86200	2.32100
C	6.48700	-2.74600	1.34100
C	5.30400	-2.02200	0.69300
C	4.41800	-2.90400	-0.18700
N	3.34600	-2.10400	-0.77700
C	3.30200	-1.55500	-1.98800
O	2.36700	-0.70700	-2.22800
C	4.29500	-1.93200	-3.04700
O	2.37700	-1.70900	0.11000
O	1.54200	1.11900	1.47000
O	-0.28400	-0.28700	-2.03600
C	-1.82500	0.76300	-3.56400
C	-1.86700	-0.50400	-4.42900

C	-2.48300	-1.75900	-3.79300
C	-4.01900	-1.80300	-3.68900
C	-4.69600	-0.84200	-2.70200
N	-4.18000	-1.00800	-1.34600
Zr	1.19300	0.05600	-0.39600
H	-5.99100	-2.11800	1.98500
H	-4.47100	-2.51500	2.82500
H	-3.83900	-4.01800	0.86500
H	-5.44600	-3.71900	0.15500
H	-3.26900	1.38900	0.62200
H	-2.78100	1.53900	2.31100
H	-1.52300	-2.66600	2.51100
H	-2.29900	-1.18700	3.17400
H	-0.54800	-1.50100	3.46500
H	-1.43200	3.42300	-3.08800
H	-0.03700	3.24000	-4.16100
H	1.40100	4.37200	-2.37300
H	0.12100	5.37400	-3.07600
H	1.50700	5.63500	-0.52000
H	-0.41200	4.98900	1.58100
H	-0.46200	6.69900	1.13300
H	1.07400	6.41300	3.00700
H	1.95600	6.96200	1.58000
H	3.34000	5.28100	2.58800
H	2.65700	4.56200	1.13200
H	0.87300	3.43500	2.64000
H	1.78200	4.05100	4.02800
H	3.83300	2.76900	3.12200
H	2.47700	1.77600	3.68300
H	4.98400	3.14100	1.55800
H	4.58300	3.45400	-0.13400
H	5.88900	1.31800	-0.74000
H	6.80900	2.71600	-0.18300

H	7.67600	0.01200	-0.18600
H	8.73700	-0.27800	2.51100
H	8.99900	-1.32800	1.10200
H	6.57600	-1.35100	2.99800
H	7.91300	-2.50500	2.95800
H	6.10600	-3.61900	1.89900
H	7.16400	-3.14600	0.56500
H	5.66000	-1.19400	0.06900
H	4.67400	-1.57300	1.47600
H	4.99500	-3.36600	-0.99800
H	3.94400	-3.70900	0.39400
H	3.89300	-1.61900	-4.01900
H	4.49400	-3.01100	-3.07000
H	5.25100	-1.40900	-2.88600
H	-1.81000	1.64300	-4.21700
H	-2.71400	0.84800	-2.92200
H	-0.83800	-0.72800	-4.74900
H	-2.43000	-0.25500	-5.34400
H	-2.01400	-1.92900	-2.81100
H	-2.18700	-2.62300	-4.40900
H	-4.31200	-2.82900	-3.41300
H	-4.45400	-1.60900	-4.68400
H	-4.59500	0.20700	-3.02600
H	-5.77400	-1.04900	-2.65800
C	-5.10800	0.54100	2.49600
H	-5.80800	-0.18200	2.93100
H	-5.64800	1.13100	1.73000
H	-4.78800	1.22600	3.29600
O	-4.74100	-5.47700	2.80400
H	-7.16500	-4.58100	1.21600
H	-3.18900	-1.21000	-1.24200
H	-3.20800	-1.70000	0.80100

Λ-*N*-CTC

114

C	-4.65300	-1.00900	1.54100
C	-4.30200	-2.50100	1.35300
O	-4.20700	-3.25700	2.34200
C	-6.16700	-0.76800	1.77400
C	-7.12600	-1.24000	0.66700
C	-7.51400	-2.69800	0.65800
O	-7.76300	-3.18700	1.90100
N	-3.81100	-0.47500	2.63200
C	-3.06500	0.73700	2.31800
C	-1.70700	0.55300	1.63600
N	-0.81000	-0.33800	2.05200
O	-1.39500	1.31900	0.66100
O	0.39100	-0.38200	1.38000
C	-0.88700	-1.22900	3.19700
C	-1.20900	2.21600	-2.15800
C	-2.08700	3.20600	-2.88400
C	-1.49300	4.61600	-2.90200
C	-1.62700	5.35000	-1.57500
O	-0.22300	2.62700	-1.44200
N	-1.42900	0.90600	-2.26100
O	-2.63400	5.21100	-0.84700
N	-0.62400	6.21400	-1.28400
C	-0.62500	7.10600	-0.12700
C	0.79000	7.40000	0.37800
C	1.58000	6.18200	0.87600
C	0.95700	5.49500	2.09200
C	1.79300	4.33800	2.64300
C	3.02700	2.70500	1.17800
C	4.40800	3.17400	1.55200
C	4.93400	2.59000	2.88500
N	1.92400	3.24300	1.68100

O	2.88000	1.73500	0.34600
C	4.81600	1.07400	2.96800
O	3.87300	0.52300	3.57300
N	5.79900	0.38100	2.34000
C	5.80900	-1.07500	2.19700
C	5.05800	-1.58800	0.96100
C	5.55800	-0.97200	-0.34900
C	5.14300	-1.72600	-1.61700
C	3.63700	-1.93300	-1.82900
N	2.79700	-0.73500	-1.67300
C	2.76300	0.33100	-2.46600
O	1.99500	1.31100	-2.15000
C	3.60700	0.39600	-3.70500
O	1.96900	-0.74100	-0.57400
O	0.74200	2.69200	1.27700
O	-0.56400	0.06300	-1.61800
C	-2.65400	0.28000	-2.76300
C	-2.40600	-1.03700	-3.51200
C	-2.26000	-2.31600	-2.65900
C	-3.58500	-3.03200	-2.35000
C	-4.45100	-2.46000	-1.21600
N	-4.02600	-2.96800	0.09800
Zr	0.76900	1.05200	-0.19900
H	0.14700	6.29000	-1.94300
H	6.51500	0.91000	1.85100
H	-6.77300	-0.97900	-0.33900
H	-8.07900	-0.69900	0.80700
H	-2.89000	1.29000	3.25700
H	-3.62200	1.43100	1.66100
H	-0.34200	-0.80500	4.05500
H	-0.43400	-2.18900	2.91500
H	-1.94300	-1.38600	3.43900
H	-3.07300	3.24000	-2.39400

H	-2.25200	2.86800	-3.91700
H	-2.05500	5.21100	-3.64200
H	-0.44500	4.59800	-3.23400
H	-1.24300	6.62900	0.64500
H	-1.11700	8.06000	-0.39000
H	0.70100	8.14300	1.18800
H	1.35900	7.89400	-0.42800
H	2.60300	6.51000	1.13000
H	1.68100	5.45300	0.05400
H	-0.04100	5.10500	1.84700
H	0.83100	6.22200	2.91200
H	1.32300	3.92400	3.55000
H	2.80200	4.67300	2.91300
H	5.06500	2.87000	0.72500
H	4.45200	4.27000	1.60800
H	4.36300	3.00100	3.72700
H	5.98400	2.90200	3.00500
H	5.36700	-1.50000	3.10900
H	6.86400	-1.38500	2.15300
H	3.98300	-1.38600	1.07500
H	5.18800	-2.68500	0.93700
H	6.66100	-0.92800	-0.34000
H	5.20200	0.07000	-0.41000
H	5.57300	-1.21400	-2.49200
H	5.58900	-2.73500	-1.61000
H	3.46100	-2.36300	-2.82800
H	3.23300	-2.64400	-1.09700
H	3.80700	-0.59100	-4.14300
H	4.57100	0.88000	-3.48700
H	3.08200	1.01400	-4.44500
H	-3.14000	1.00500	-3.42500
H	-3.32500	0.13100	-1.90200
H	-1.51400	-0.90000	-4.14200

H	-3.25000	-1.17300	-4.20900
H	-1.71300	-2.08100	-1.73500
H	-1.62700	-3.02200	-3.22100
H	-3.38800	-4.09300	-2.11400
H	-4.20400	-3.04500	-3.26200
H	-5.49900	-2.75100	-1.39000
H	-4.41700	-1.36400	-1.20700
C	-4.36200	-0.51700	3.98700
H	-4.77400	-1.51500	4.17900
H	-5.14600	0.24000	4.18300
H	-3.54900	-0.35400	4.71000
H	-6.30500	0.31800	1.89200
H	-6.47400	-1.23000	2.72000
O	-7.66600	-3.37600	-0.35600
H	-8.06200	-4.11600	1.79100
H	-4.36700	-0.46300	0.63000
H	-3.80900	-3.96700	0.10300

Λ-*N*-CTT
114

C	-4.90200	-0.35400	1.37300
C	-4.43000	-1.73300	0.86500
O	-4.33800	-2.69600	1.64900
C	-6.40900	-0.43900	1.70000
C	-7.31400	-0.66700	0.47900
C	-7.49800	-2.11200	0.06500
O	-7.74100	-2.33700	-1.26000
N	-4.05800	0.04300	2.52900
C	-3.01000	0.99700	2.17500
C	-1.78400	0.50800	1.41300
N	-1.20200	-0.66900	1.59500
O	-1.22800	1.33300	0.59500
O	-0.09400	-0.93500	0.83800

C	-1.48400	-1.67300	2.60600
C	-0.63900	2.17400	-2.45300
C	-1.32300	3.26800	-3.23200
C	-1.24200	4.62000	-2.51700
C	-2.05000	4.64200	-1.22600
O	0.19000	2.46100	-1.51400
N	-0.85100	0.89500	-2.73000
O	-3.26300	4.33900	-1.21800
N	-1.37600	5.05400	-0.12500
C	-1.95000	5.07000	1.22100
C	-1.05900	4.43200	2.29700
C	0.11300	5.29500	2.80400
C	1.39800	5.34500	1.95700
C	2.41900	4.22700	2.19200
C	2.21900	1.73800	2.45800
C	2.93400	1.71500	3.78600
C	4.46300	1.86400	3.69700
N	1.95900	2.88100	1.82800
O	1.82800	0.64700	1.89500
C	5.18200	0.60100	3.24500
O	4.85100	-0.52700	3.66500
N	6.23100	0.80000	2.40600
C	7.18700	-0.24300	2.03700
C	7.66100	-0.15300	0.58500
C	6.58300	-0.43300	-0.48000
C	5.92700	0.81500	-1.08200
C	4.84300	0.49400	-2.12100
N	3.56000	0.12900	-1.51200
C	3.06600	-1.07500	-1.25100
O	1.95100	-1.13500	-0.60600
C	3.72000	-2.34400	-1.69900
O	2.83000	1.19700	-1.05700
O	1.32600	2.79500	0.62300
O	-0.13500	-0.01200	-1.99400
C	-1.70400	0.41900	-3.84200
C	-1.65500	-1.08700	-4.08200
C	-2.39700	-1.98000	-3.07300
C	-3.88300	-1.60100	-2.87800
C	-4.18300	-0.89600	-1.55000
N	-4.17100	-1.88400	-0.46100
Zr	0.85200	0.78700	-0.17100
H	-0.36700	5.11700	-0.21200
H	6.47600	1.76000	2.17300
H	2.69800	0.75000	4.25300
H	2.53800	2.50300	4.44100
H	-6.71600	0.51000	2.15700
H	-6.59200	-1.24200	2.42800
H	-7.00200	-0.04700	-0.37400
H	-8.33200	-0.32400	0.73400
H	-2.62700	1.43900	3.11000
H	-3.38800	1.84500	1.56900
H	-0.67600	-1.66400	3.35300
H	-1.52000	-2.65600	2.11800
H	-2.45800	-1.45600	3.06100
H	-2.37500	3.00800	-3.41700
H	-0.83900	3.34700	-4.22000
H	-1.67900	5.38500	-3.17800
H	-0.19400	4.89200	-2.33700
H	-2.90000	4.52400	1.14900
H	-2.19100	6.11100	1.50700
H	-0.71000	3.45700	1.92900
H	-1.72200	4.23800	3.15600
H	0.38900	4.95500	3.81800
H	-0.25500	6.32700	2.93200
H	1.94300	6.27100	2.20300
H	1.18400	5.40800	0.88100

H	2.71000	4.20900	3.25000
H	3.32400	4.44300	1.59800
H	4.84000	2.07300	4.71100
H	4.74900	2.72400	3.07500
H	6.68900	-1.20600	2.21400
H	8.05900	-0.19500	2.71300
H	8.47100	-0.89100	0.48200
H	8.12500	0.83300	0.40700
H	5.81300	-1.08900	-0.04000
H	7.03900	-1.00600	-1.30400
H	6.69800	1.42600	-1.58000
H	5.47700	1.44600	-0.30000
H	5.16100	-0.31600	-2.79100
H	4.62900	1.37200	-2.74600
H	4.72700	-2.21400	-2.10200
H	3.09000	-2.81100	-2.46900
H	3.76500	-3.03600	-0.84800
H	-1.38200	0.93600	-4.75900
H	-2.73700	0.74200	-3.64100
H	-0.60600	-1.40800	-4.16500
H	-2.11200	-1.23700	-5.07500
H	-1.87200	-1.95300	-2.10600
H	-2.32500	-3.01500	-3.44300
H	-4.52400	-2.49500	-2.93800
H	-4.21700	-0.94400	-3.69700
H	-5.16700	-0.40800	-1.61100
H	-3.43400	-0.11200	-1.35600
C	-4.74100	0.45000	3.76100
H	-5.45800	-0.31900	4.07600
H	-5.27100	1.42200	3.68600
H	-3.98800	0.54100	4.55800
O	-7.50300	-3.06300	0.83200
H	-7.72600	-1.49000	-1.74900

H	-4.78900	0.40300	0.57700
H	-3.90200	-2.83300	-0.72000

Λ-*N*-CCT

114

C	-4.70500	-0.66500	0.95300
C	-5.15800	-0.23100	-0.45400
O	-6.23000	0.37400	-0.65100
C	-5.79400	-1.47800	1.67500
C	-5.92800	-2.89700	1.08200
C	-6.81800	-3.78600	1.91700
O	-8.15200	-3.50300	1.90800
N	-4.22700	0.45700	1.79500
C	-3.00500	1.10700	1.30900
C	-1.76700	0.26800	1.03500
N	-1.53700	-0.93400	1.56900
O	-0.91500	0.74700	0.21900
O	-0.41300	-1.59700	1.12700
C	-2.08400	-1.47900	2.80100
C	0.56500	1.44300	-2.28300
C	0.51800	2.72000	-3.09100
C	1.14100	3.91900	-2.36700
C	0.26200	4.42600	-1.23400
O	1.37200	1.31400	-1.27900
N	-0.19200	0.40800	-2.62100
O	-0.88000	4.88800	-1.44900
N	0.81700	4.37400	0.00000
C	0.11500	4.75500	1.22200
C	1.08600	5.24400	2.30200
C	2.09100	4.18800	2.78800
C	1.46000	3.03700	3.58000
C	2.33000	1.77800	3.63000
C	3.44000	0.93100	1.50500

C	4.81200	1.44100	1.87800	H	-2.93300	-0.86300	3.11900
C	5.64500	1.89300	0.66600	H	-1.29400	-1.46000	3.56600
N	2.40000	1.12100	2.32100	H	-0.51800	2.96500	-3.36200
O	3.23700	0.31200	0.39900	H	1.05500	2.55400	-4.04000
C	6.56700	0.80800	0.12900	H	2.15200	3.67100	-2.01600
O	7.31100	0.15300	0.89100	H	1.23200	4.74300	-3.09200
N	6.57000	0.64700	-1.21400	H	1.65700	3.80900	0.09100
C	7.39700	-0.33700	-1.91700	H	-0.48500	3.90300	1.58500
C	6.97500	-1.79400	-1.67800	H	-0.59000	5.55500	0.95500
C	5.49700	-2.08100	-1.95100	H	0.48700	5.60200	3.15500
C	5.11300	-3.51300	-1.57300	H	1.63400	6.11700	1.91100
C	3.60600	-3.78100	-1.52600	H	2.85900	4.68200	3.40600
N	2.87100	-2.90100	-0.60300	H	2.63900	3.78000	1.92000
C	2.83200	-2.94800	0.72600	H	0.49600	2.74100	3.14100
O	2.12000	-2.07300	1.33800	H	1.25700	3.35600	4.61400
C	3.56500	-4.00200	1.49600	H	3.34800	1.99900	3.97200
O	2.07900	-1.94500	-1.19900	H	1.90000	1.04300	4.32800
O	1.18100	0.67700	1.88100	H	5.36000	0.64400	2.40800
O	-0.06700	-0.73500	-1.89000	H	4.72100	2.27500	2.58400
C	-1.15100	0.43400	-3.74400	H	5.00100	2.29900	-0.12600
C	-1.47400	-0.93800	-4.34400	H	6.30800	2.70800	0.99700
C	-2.52500	-1.82000	-3.64900	H	5.88600	1.16700	-1.75500
C	-3.99600	-1.37400	-3.76500	H	8.44400	-0.20300	-1.60200
C	-4.47900	-0.23600	-2.85600	H	7.33800	-0.08500	-2.98500
N	-4.28200	-0.54500	-1.44300	H	7.20600	-2.05700	-0.63300
Zr	1.08500	-0.46200	0.04300	H	7.61500	-2.43200	-2.31300
H	-6.76100	-0.95500	1.62400	H	5.25900	-1.89500	-3.01400
H	-5.50200	-1.55000	2.73500	H	4.88400	-1.38000	-1.36200
H	-4.94400	-3.38400	1.04000	H	5.54700	-4.23300	-2.28700
H	-6.32900	-2.84900	0.05600	H	5.55100	-3.75800	-0.59100
H	-3.16900	1.66900	0.36600	H	3.14100	-3.60400	-2.50500
H	-2.71800	1.86300	2.06100	H	3.40900	-4.82800	-1.25200
H	-2.40400	-2.51900	2.64100	H	4.39700	-3.54500	2.05300

H	3.96100	-4.80900	0.87000
H	2.86900	-4.43300	2.23100
H	-0.69700	1.05100	-4.53000
H	-2.06000	0.95600	-3.41000
H	-0.53300	-1.50300	-4.42500
H	-1.80800	-0.74400	-5.37800
H	-2.23300	-1.98300	-2.60000
H	-2.46200	-2.81300	-4.12300
H	-4.63600	-2.24900	-3.56400
H	-4.20100	-1.07200	-4.80600
H	-3.98800	0.71800	-3.10000
H	-5.55600	-0.07600	-3.00100
C	-5.22900	1.48400	2.11000
H	-6.13800	1.01600	2.50400
H	-5.50500	2.10300	1.23600
H	-4.81600	2.14600	2.88500
O	-6.42000	-4.71900	2.60400
H	-8.33500	-2.76000	1.29800
H	-3.41700	-1.01000	-1.18000
H	-3.84000	-1.33400	0.82700

Λ-*N*-TTT

114

C	-4.18800	-3.15500	0.62000
C	-4.71700	-2.91700	-0.82100
O	-4.74300	-3.90900	-1.58500
C	-4.85300	-2.44400	1.81500
C	-6.37000	-2.63500	1.88000
C	-6.80400	-4.02800	2.26200
O	-8.14500	-4.19400	2.09700
N	-2.71200	-3.07500	0.55800
C	-2.15100	-1.73800	0.69500
C	-0.83000	-1.46200	-0.01300

N	-0.55300	-1.83800	-1.25500
O	0.02800	-0.72800	0.61200
O	0.64100	-1.41400	-1.78200
C	-1.32500	-2.67400	-2.15800
C	0.68200	2.18700	-2.83400
C	0.79100	3.13600	-3.99400
C	1.60900	4.40600	-3.63400
C	0.86300	5.31600	-2.66800
O	1.70600	1.45500	-2.52100
N	-0.38400	2.11300	-2.04900
O	0.06300	6.18500	-3.07200
N	1.09400	5.07000	-1.35000
C	0.35800	5.67900	-0.24400
C	1.27500	6.25100	0.84400
C	2.20800	5.22000	1.49700
C	1.50300	4.15400	2.34900
C	2.39300	2.95900	2.71500
C	3.67100	2.14400	0.69200
C	4.89800	2.99300	0.92600
C	6.21800	2.21300	0.89100
N	2.65600	2.10300	1.55500
O	3.56200	1.45500	-0.38800
C	6.53500	1.48900	2.20000
O	5.97400	1.77100	3.27800
N	7.49600	0.53900	2.09500
C	7.91900	-0.34400	3.18600
C	6.89900	-1.41100	3.61200
C	6.42500	-2.39600	2.53100
C	5.54200	-1.74200	1.46200
C	4.69400	-2.70900	0.63600
N	3.78600	-1.94400	-0.22200
C	3.98700	-1.60200	-1.49000
O	3.20300	-0.73000	-2.02500

C	5.09800	-2.22200	-2.28600
O	2.76700	-1.31900	0.45000
O	1.57900	1.33000	1.19700
O	-0.28800	1.28900	-0.96900
C	-1.62300	2.89400	-2.11200
C	-2.88300	2.12100	-2.51400
C	-3.35600	1.04100	-1.53000
C	-4.85700	0.75000	-1.64100
C	-5.34900	-0.38400	-0.73200
N	-5.05500	-1.69700	-1.32100
Zr	1.64500	0.19300	-0.67100
H	-4.63500	-1.36900	1.83200
H	-4.40500	-2.86100	2.73100
H	-6.80400	-1.95900	2.63600
H	-6.86800	-2.36600	0.93500
H	-1.96700	-1.45700	1.75100
H	-2.86200	-1.00000	0.29800
H	-0.68500	-3.50900	-2.47900
H	-1.61600	-2.08600	-3.04000
H	-2.19900	-3.06700	-1.63100
H	-0.19100	3.42000	-4.39100
H	1.32500	2.60500	-4.79500
H	1.78700	4.97500	-4.55700
H	2.58400	4.10300	-3.22400
H	1.73300	4.31200	-1.12900
H	-0.32300	4.92600	0.18800
H	-0.26600	6.47000	-0.67900
H	0.63400	6.71700	1.61000
H	1.88200	7.05800	0.40300
H	2.94600	5.75000	2.12200
H	2.80000	4.73400	0.70400
H	0.61400	3.76000	1.83200
H	1.14500	4.60900	3.28600
H	1.89200	2.32400	3.45900
H	3.35100	3.27700	3.14400
H	4.83500	3.54300	1.87000
H	4.92000	3.73500	0.11300
H	7.03900	2.92400	0.70400
H	6.22500	1.50300	0.05100
H	7.88000	0.36000	1.17100
H	8.16900	0.27700	4.06000
H	8.84900	-0.82400	2.84700
H	6.01900	-0.91000	4.04800
H	7.37500	-1.97800	4.43000
H	5.84600	-3.19100	3.03300
H	7.29200	-2.89300	2.06000
H	6.15400	-1.15500	0.76300
H	4.84900	-1.03600	1.94400
H	4.06700	-3.34800	1.27700
H	5.30900	-3.36100	0.00200
H	5.07500	-3.31900	-2.23800
H	6.08300	-1.88600	-1.92700
H	4.98700	-1.91200	-3.33100
H	-1.46800	3.72900	-2.80600
H	-1.75700	3.31900	-1.10500
H	-2.75300	1.69200	-3.52100
H	-3.67100	2.88800	-2.60500
H	-3.13800	1.36800	-0.50000
H	-2.77500	0.12100	-1.69200
H	-5.13100	0.51200	-2.68400
H	-5.42100	1.65900	-1.37600
H	-6.43900	-0.29500	-0.58300
H	-4.87900	-0.30100	0.25400
C	-2.02600	-4.04400	1.41700
H	-2.14200	-3.82700	2.49800
H	-0.95100	-4.03500	1.18400

H	-2.40800	-5.05300	1.21400
O	-6.07800	-4.91700	2.69300
H	-8.36000	-5.10600	2.39400
H	-4.40000	-4.22500	0.74600
H	-5.34400	-1.77500	-2.29900

Λ-*N*-TCC

114

C	-3.63400	-3.56300	0.56000
C	-3.99900	-3.44500	-0.93300
O	-3.78800	-4.40200	-1.70500
C	-4.62800	-4.49900	1.29000
C	-6.04700	-3.93600	1.44700
C	-6.97100	-4.14400	0.26600
O	-7.98800	-3.24100	0.13000
N	-2.22200	-3.98300	0.66900
C	-1.31100	-2.98400	1.19400
C	-0.56200	-2.03400	0.25500
N	-0.27700	-2.26400	-1.02000
O	-0.11600	-0.95600	0.80600
O	0.44200	-1.30000	-1.69000
C	-0.57400	-3.42700	-1.83700
C	0.35000	1.81800	-2.68600
C	0.25000	2.49000	-4.02800
C	1.22900	3.68700	-4.16200
C	0.74800	4.92400	-3.41800
O	1.38500	1.08900	-2.42700
N	-0.56100	1.99600	-1.73600
O	0.18600	5.86700	-4.01700
N	0.94100	4.91100	-2.07200
C	0.38600	5.91300	-1.16200
C	1.40500	6.50400	-0.18600

C	2.06500	5.46900	0.74400
C	3.35700	4.86500	0.18100
C	3.87300	3.66900	0.97600
C	2.65300	1.72200	1.96000
C	3.11700	1.99400	3.36900
C	4.61800	1.77200	3.64200
N	2.95600	2.51800	0.94500
O	1.91800	0.68000	1.71200
C	5.04700	0.31300	3.61100
O	4.48100	-0.54700	4.31700
N	6.10700	0.03300	2.80900
C	6.78600	-1.26200	2.81500
C	6.46800	-2.19300	1.63700
C	7.17400	-1.86700	0.30300
C	6.48100	-0.92400	-0.69900
C	5.38400	-1.56500	-1.57600
N	4.03400	-1.46300	-1.01800
C	3.36800	-2.31700	-0.24400
O	2.30000	-1.89500	0.32700
C	3.76900	-3.75200	-0.09200
O	3.48600	-0.20800	-1.14200
O	2.46000	2.18500	-0.28100
O	-0.35700	1.36800	-0.54300
C	-1.81800	2.75100	-1.82300
C	-3.03200	1.91200	-2.22300
C	-3.33000	0.72000	-1.30800
C	-4.75400	0.19100	-1.49600
C	-5.05700	-1.09600	-0.72300
N	-4.51500	-2.27700	-1.40800
Zr	1.47100	0.14300	-0.39200
H	-4.22900	-4.68900	2.29600
H	-4.68500	-5.46600	0.77000
H	-6.03100	-2.87700	1.74500

H	-6.54500	-4.46700	2.27800
H	-0.52000	-3.49300	1.77000
H	-1.80300	-2.30600	1.91600
H	-1.19300	-4.12000	-1.26100
H	0.37200	-3.89400	-2.15000
H	-1.12900	-3.10000	-2.72900
H	-0.77400	2.81000	-4.25700
H	0.52700	1.73600	-4.77900
H	1.30900	3.96200	-5.22100
H	2.22600	3.37700	-3.81100
H	1.34900	4.07400	-1.65600
H	-0.43400	5.44700	-0.58700
H	-0.05400	6.69700	-1.79200
H	0.86300	7.24900	0.41900
H	2.17700	7.05800	-0.74700
H	1.34000	4.66400	0.95900
H	2.29700	5.93800	1.71400
H	4.15700	5.62500	0.19100
H	3.23700	4.56400	-0.86800
H	4.02600	3.94700	2.02700
H	4.84000	3.33400	0.56600
H	2.53700	1.31900	4.01200
H	2.85400	3.02300	3.65800
H	4.82100	2.12500	4.66600
H	5.24200	2.37900	2.97200
H	6.52700	0.79900	2.29000
H	6.48800	-1.75200	3.75200
H	7.87100	-1.07400	2.85900
H	5.37700	-2.24400	1.51700
H	6.78900	-3.19900	1.95500
H	7.38000	-2.81500	-0.22500
H	8.16600	-1.44400	0.53900
H	7.25200	-0.55100	-1.39400

H	6.05900	-0.03600	-0.20200
H	5.33300	-1.05400	-2.54700
H	5.60800	-2.62000	-1.77600
H	3.80500	-4.00500	0.97700
H	4.72700	-4.00800	-0.55700
H	2.98300	-4.37400	-0.54900
H	-1.68400	3.58200	-2.52700
H	-1.96000	3.18800	-0.82500
H	-2.91000	1.56100	-3.26200
H	-3.89300	2.60200	-2.22700
H	-3.20000	1.02300	-0.25500
H	-2.59400	-0.07800	-1.48800
H	-4.97000	0.02000	-2.56600
H	-5.47000	0.96100	-1.16300
H	-6.15000	-1.20700	-0.62400
H	-4.63900	-1.03300	0.29000
C	-1.91800	-5.34900	1.09400
H	-2.55000	-6.06700	0.55700
H	-2.03300	-5.52000	2.18500
H	-0.87400	-5.57500	0.83000
O	-6.90700	-5.07400	-0.52500
H	-7.93100	-2.56300	0.83400
H	-3.71200	-2.57400	1.04100
H	-4.73700	-2.32400	-2.40500

Λ-*N*-TCT
114
C	-3.85900	-3.20800	0.91900
C	-4.49100	-2.80200	-0.44200
O	-4.64700	-3.71700	-1.28300
C	-4.34800	-2.54700	2.22300
C	-5.86500	-2.68000	2.43200
C	-6.29500	-4.09800	2.72000

O	-7.36500	-4.48200	1.97700
N	-2.39700	-3.26600	0.72800
C	-1.67400	-2.01100	0.85200
C	-0.45900	-1.78900	-0.04400
N	-0.31500	-2.24300	-1.28300
O	0.45000	-1.00100	0.42200
O	0.80000	-1.82500	-1.96300
C	-1.13200	-3.18900	-2.02400
C	0.55300	1.58400	-3.32000
C	0.38000	2.25700	-4.65700
C	1.48600	3.29200	-4.94400
C	1.17800	4.68100	-4.39900
O	1.50100	0.72300	-3.17000
N	-0.22200	1.84400	-2.27400
O	0.00300	5.04400	-4.15900
N	2.20900	5.53900	-4.19500
C	3.63300	5.42600	-4.53000
C	4.52000	6.06100	-3.44600
C	4.93600	5.13800	-2.28900
C	3.79500	4.42400	-1.55700
C	4.32900	3.53200	-0.42600
C	2.82500	2.03500	0.94300
C	2.98500	2.81700	2.22300
C	4.34200	2.63800	2.92900
N	3.45700	2.38400	-0.17200
O	2.07100	0.99200	0.90700
C	4.54400	1.26600	3.56200
O	3.61400	0.65500	4.12700
N	5.81500	0.79200	3.49800
C	6.29100	-0.40300	4.19600
C	7.28200	-1.24200	3.37600
C	6.66700	-2.20500	2.35200
C	5.92100	-1.52800	1.20300

C	5.30200	-2.53300	0.23000
N	4.32700	-1.87700	-0.64100
C	4.39900	-1.61500	-1.94000
O	3.42700	-0.95700	-2.47900
C	5.54400	-2.08700	-2.78600
O	3.22600	-1.42100	0.03000
O	3.29400	1.56600	-1.25600
O	0.06300	1.16200	-1.12100
C	-1.33300	2.79700	-2.16500
C	-2.73400	2.18300	-2.24000
C	-3.05800	1.11900	-1.18200
C	-4.56500	0.92000	-0.98600
C	-4.92200	-0.25400	-0.06700
N	-4.80500	-1.52700	-0.79200
Zr	1.86200	-0.09700	-1.08500
H	-4.07300	-1.48700	2.28800
H	-3.83600	-3.04900	3.05800
H	-6.43700	-2.28900	1.58000
H	-6.15900	-2.08700	3.31300
H	-1.29000	-1.83900	1.87700
H	-2.35000	-1.17000	0.64100
H	-2.00900	-3.45000	-1.42300
H	-0.53200	-4.09200	-2.21800
H	-1.42300	-2.73400	-2.98100
H	-0.60400	2.73200	-4.75900
H	0.44300	1.46300	-5.41700
H	1.60200	3.40100	-6.03500
H	2.45000	2.92000	-4.57000
H	1.90500	6.47000	-3.90700
H	3.89100	4.36900	-4.67600
H	3.80900	5.93500	-5.49300
H	4.00800	6.95700	-3.05600
H	5.43900	6.42700	-3.93200

H	5.52600	5.73300	-1.57100
H	5.62300	4.36900	-2.68500
H	3.25400	3.77600	-2.25900
H	3.06900	5.15000	-1.15500
H	4.45000	4.09600	0.50500
H	5.31300	3.12100	-0.70300
H	2.18600	2.48100	2.89700
H	2.82500	3.88900	2.03000
H	4.39100	3.36900	3.75500
H	5.17900	2.87500	2.25600
H	6.51700	1.38300	3.05900
H	5.40300	-0.99200	4.46200
H	6.77400	-0.09200	5.13800
H	8.00700	-0.57200	2.88100
H	7.86700	-1.83900	4.09500
H	7.47400	-2.83900	1.94400
H	5.97600	-2.88800	2.87800
H	6.60100	-0.86000	0.64800
H	5.10200	-0.90800	1.59200
H	4.75100	-3.31400	0.77900
H	6.05700	-3.03300	-0.38800
H	5.71000	-1.36300	-3.59400
H	5.29100	-3.05300	-3.24900
H	6.47800	-2.21100	-2.22800
H	-1.20100	3.56300	-2.94100
H	-1.18800	3.28900	-1.19200
H	-2.90600	1.77100	-3.24900
H	-3.43200	3.03100	-2.12700
H	-2.61200	1.41200	-0.21800
H	-2.58300	0.16600	-1.46400
H	-5.06800	0.77300	-1.95900
H	-5.00000	1.83600	-0.55200
H	-5.95400	-0.14200	0.30400

H	-4.26000	-0.25500	0.80400
C	-1.73400	-4.35600	1.44400
H	-2.25300	-5.30200	1.24200
H	-1.69100	-4.19900	2.54100
H	-0.70100	-4.45100	1.07700
O	-5.76100	-4.84100	3.53800
H	-7.58900	-5.40100	2.24600
H	-4.16200	-4.26400	0.97400
H	-5.19600	-1.49300	-1.73600

Λ-*N*-TTC

114

C	-4.01200	-2.69600	1.21500
C	-4.05600	-2.83200	-0.32400
O	-3.71800	-3.90800	-0.85800
C	-5.09400	-3.59900	1.83800
C	-6.53100	-3.15100	1.52500
C	-7.09600	-3.65800	0.22100
O	-7.95700	-2.76700	-0.34300
N	-2.64500	-2.98200	1.68700
C	-1.82800	-1.82300	1.98600
C	-0.76300	-1.33300	1.00000
N	-0.34100	-1.97400	-0.08200
O	-0.23100	-0.19500	1.28200
O	0.63700	-1.35800	-0.82200
C	-0.62000	-3.32800	-0.53300
C	0.77100	2.04500	-2.61100
C	1.01200	2.79400	-3.89200
C	1.84300	4.08300	-3.64100
C	1.03600	5.14500	-2.90600
O	1.72200	1.31400	-2.11900
N	-0.32900	2.18300	-1.88100

O	0.26700	5.91500	-3.51800	Zr	1.50100	0.48600	-0.03500
N	1.17300	5.15000	-1.55100	H	-4.95700	-3.58800	2.92800
C	0.30900	5.89900	-0.63600	H	-4.96500	-4.63500	1.49500
C	1.07900	6.66900	0.44100	H	-6.65200	-2.06000	1.58500
C	1.97400	5.79900	1.33400	H	-7.19600	-3.57500	2.29600
C	1.24700	4.86900	2.31800	H	-1.28400	-1.98600	2.93300
C	2.16300	3.77300	2.89000	H	-2.45600	-0.93100	2.16500
C	3.45500	2.67200	1.02800	H	-1.45100	-3.73500	0.05100
C	4.70900	3.50600	1.15900	H	0.29400	-3.93200	-0.42100
C	5.95200	2.77100	0.64200	H	-0.90100	-3.29300	-1.59400
N	2.45100	2.72500	1.90700	H	0.08000	3.04100	-4.41700
O	3.33100	1.85500	0.04900	H	1.59500	2.13400	-4.54900
C	6.36000	1.59000	1.51200	H	2.14000	4.50400	-4.61200
O	6.21100	1.61000	2.75200	H	2.75700	3.81600	-3.09100
N	6.93900	0.55400	0.85100	H	1.78500	4.44400	-1.15000
C	7.48400	-0.62400	1.52200	H	-0.40000	5.19700	-0.16700
C	6.65800	-1.90700	1.35600	H	-0.27600	6.58900	-1.25800
C	6.76700	-2.61600	-0.00800	H	0.33800	7.20600	1.05600
C	5.86600	-2.15800	-1.17000	H	1.70200	7.43200	-0.05000
C	4.40600	-2.63800	-1.11200	H	2.65600	6.45300	1.90300
N	3.52000	-1.77000	-0.33200	H	2.62700	5.19800	0.68100
C	3.08700	-1.92200	0.91600	H	0.38100	4.37700	1.84600
O	2.40200	-0.96100	1.44200	H	0.85300	5.45600	3.16400
C	3.30400	-3.17100	1.71100	H	1.68700	3.27200	3.74500
O	3.18200	-0.61300	-0.97800	H	3.11600	4.19500	3.23200
O	1.39300	1.87700	1.66900	H	4.86500	3.82000	2.19800
O	-0.31900	1.58400	-0.65900	H	4.59100	4.42400	0.56100
C	-1.54000	2.95700	-2.17200	H	6.79400	3.48200	0.64800
C	-2.77800	2.12400	-2.52000	H	5.80300	2.45600	-0.40000
C	-3.24100	1.13000	-1.44700	H	7.00900	0.61400	-0.16100
C	-4.66100	0.61300	-1.69500	H	7.54100	-0.36600	2.58800
C	-5.08400	-0.50200	-0.73600	H	8.51100	-0.79000	1.15900
N	-4.43600	-1.77100	-1.08700	H	5.61400	-1.68500	1.61900

H	7.02400	-2.60700	2.12500
H	6.57500	-3.69300	0.14300
H	7.81800	-2.55200	-0.33900
H	6.28900	-2.56900	-2.10200
H	5.86200	-1.06400	-1.29400
H	4.34400	-3.65900	-0.71400
H	3.97500	-2.65500	-2.12400
H	2.32300	-3.64300	1.88000
H	3.71300	-2.90500	2.69500
H	3.96400	-3.90200	1.23800
H	-1.31800	3.64700	-2.99400
H	-1.72800	3.56400	-1.27300
H	-2.61100	1.59700	-3.47400
H	-3.58300	2.85600	-2.70700
H	-3.20800	1.61500	-0.45700

H	-2.53600	0.28700	-1.39600
H	-4.76800	0.25000	-2.73300
H	-5.38000	1.44100	-1.58700
H	-6.17800	-0.63400	-0.77500
H	-4.81900	-0.22800	0.29400
H	-4.45800	-1.99700	-2.08400
C	-2.38500	-4.13800	2.54200
H	-2.92300	-5.02000	2.17500
H	-2.66000	-3.97700	3.60500
H	-1.31100	-4.37700	2.50500
H	-4.25200	-1.66000	1.50700
O	-6.87400	-4.75800	-0.27200
H	-8.32200	-3.19100	-1.15100

DFO-Km: A modular chelator with an amino-acid based linker and ideal properties for the construction of zirconium-89 based radiopharmaceuticals
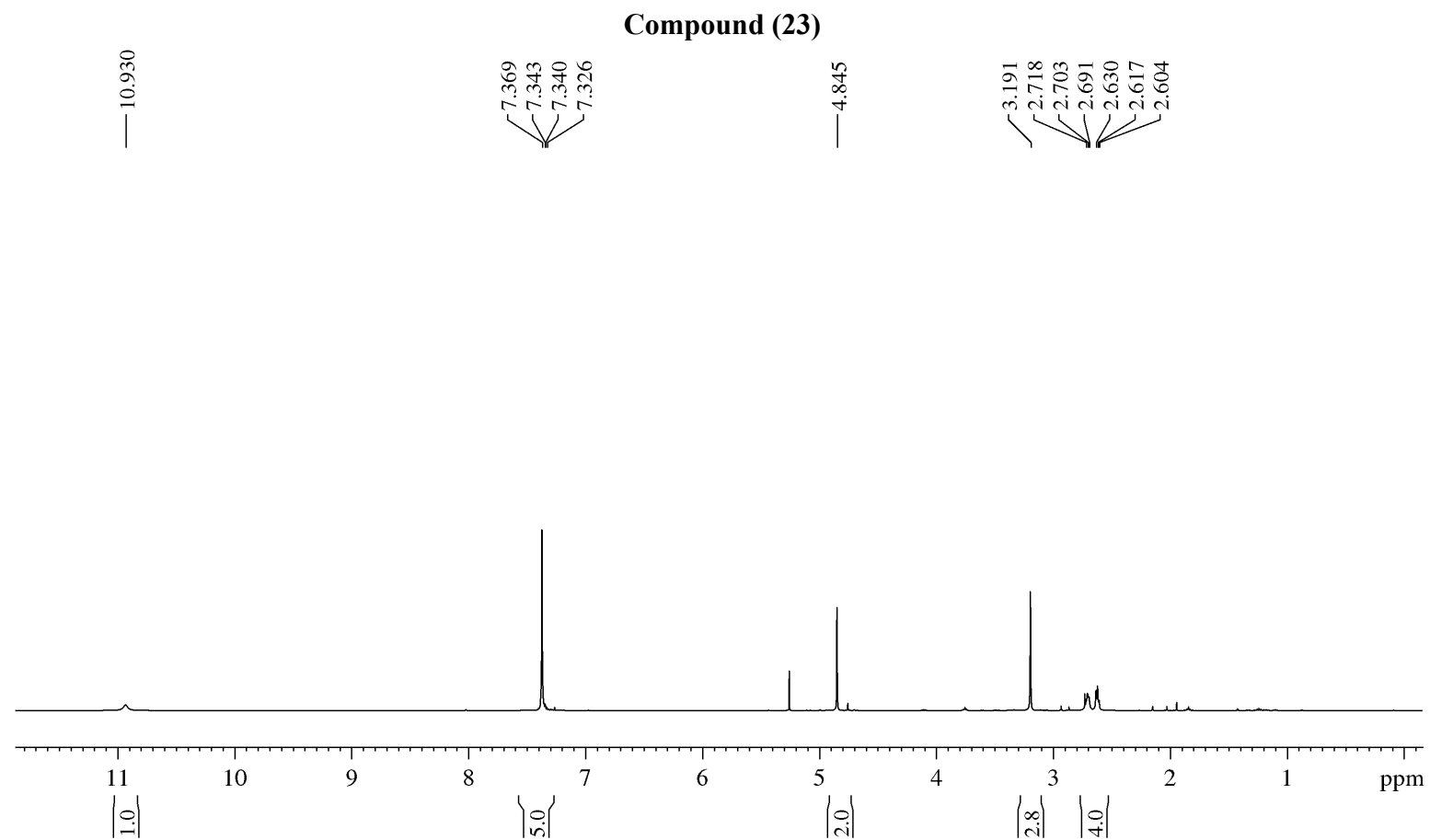
Compound (23)

Figure S5-1. ^{1}H NMR spectrum of compound **23** in CDCl$_3$. The signal at 5.30 ppm is assigned to residual dichloromethane in the NMR sample.

Compound (23)
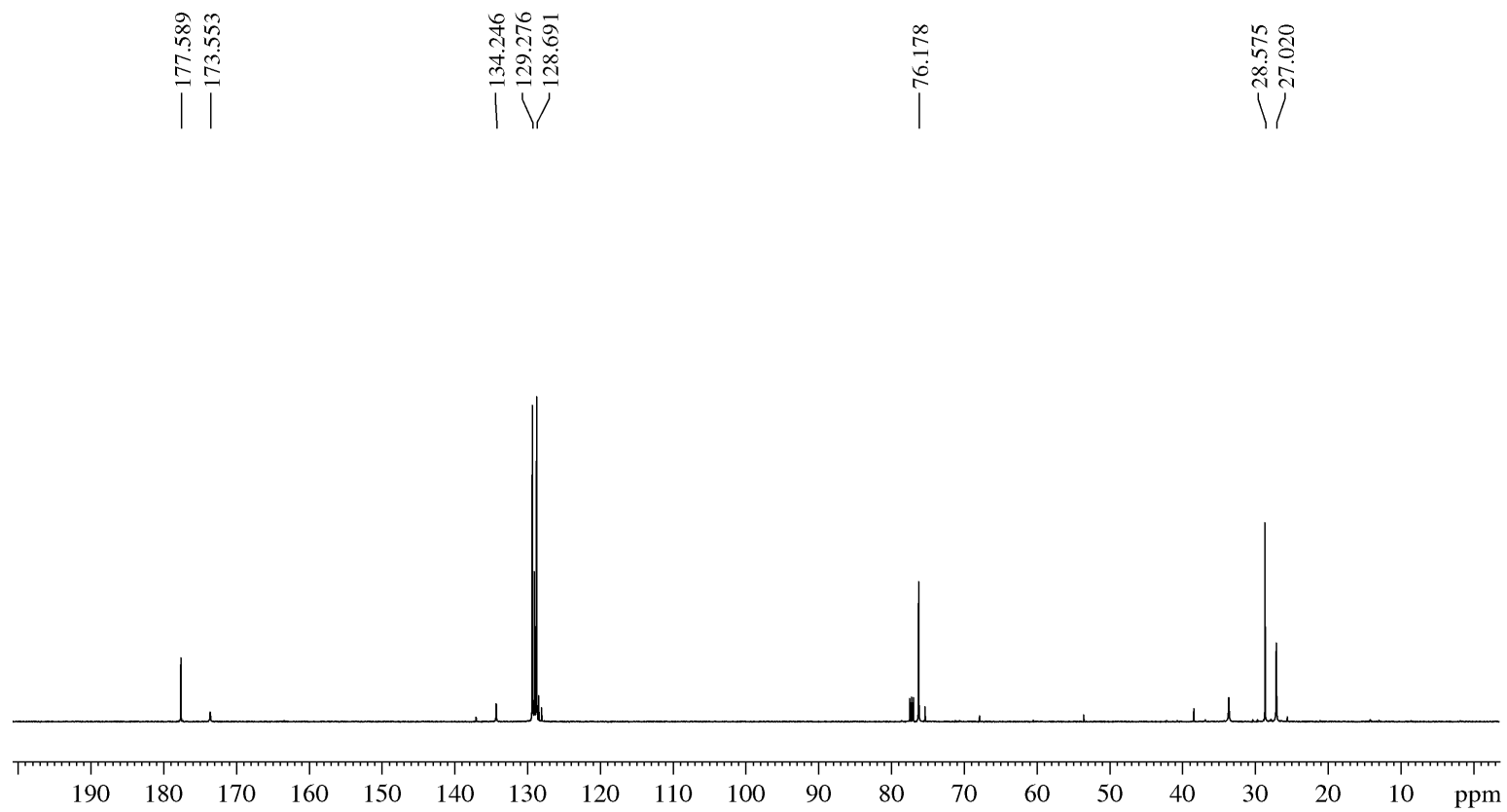
Figure S5-2. ^{13}C NMR spectrum of compound **23** in $CDCl_3$.

Compound (24)
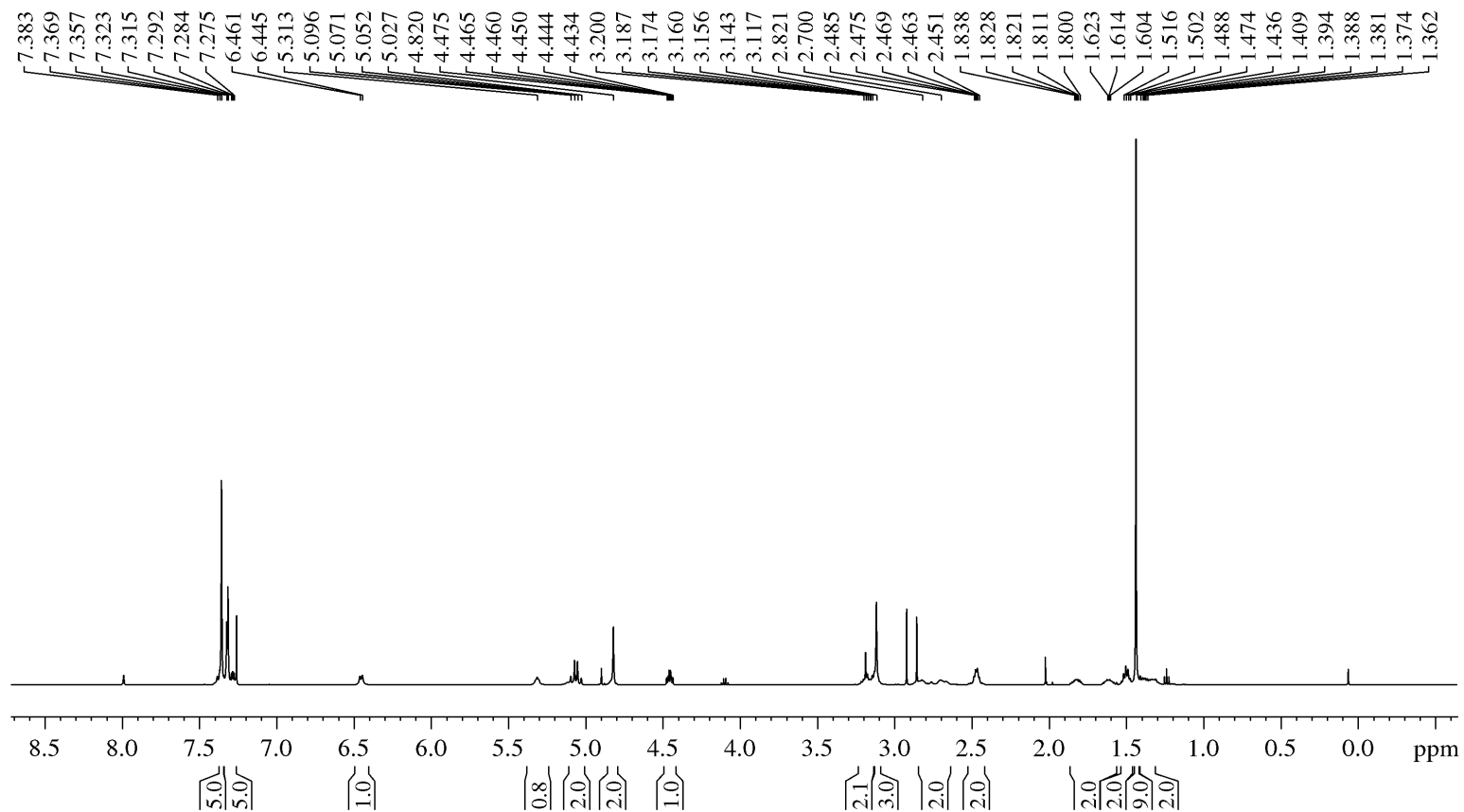
Figure S5-3. ^{1}H NMR spectrum of compound **24** in CDCl₃. The signal at 1.26, 2.05, 4.12 ppm are assigned to residual ethyl acetate in the NMR sample.

Compound (24)
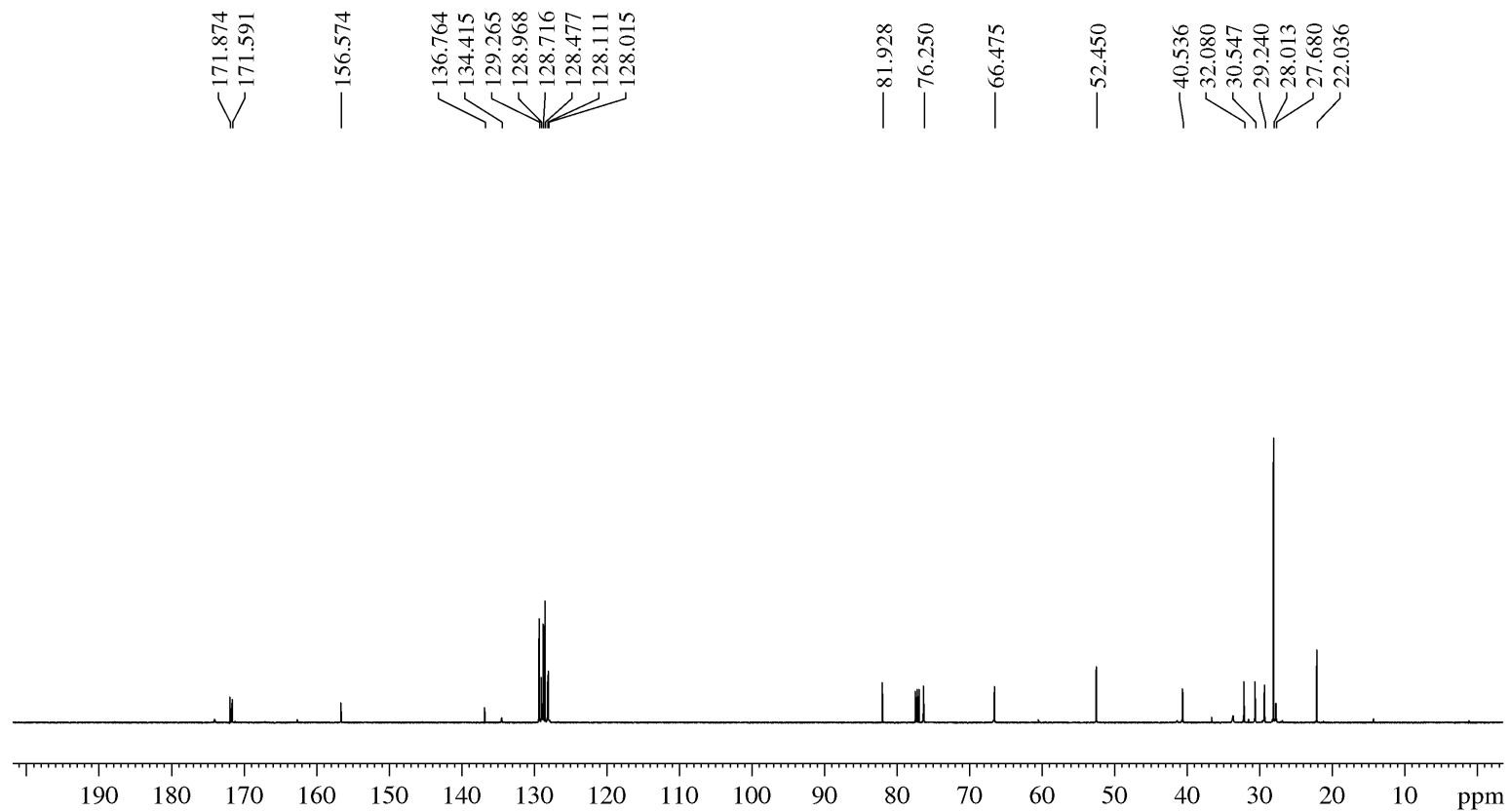
Figure S5-4. ^{13}C NMR spectrum of compound **24** in CDCl$_3$.

Compound (25)
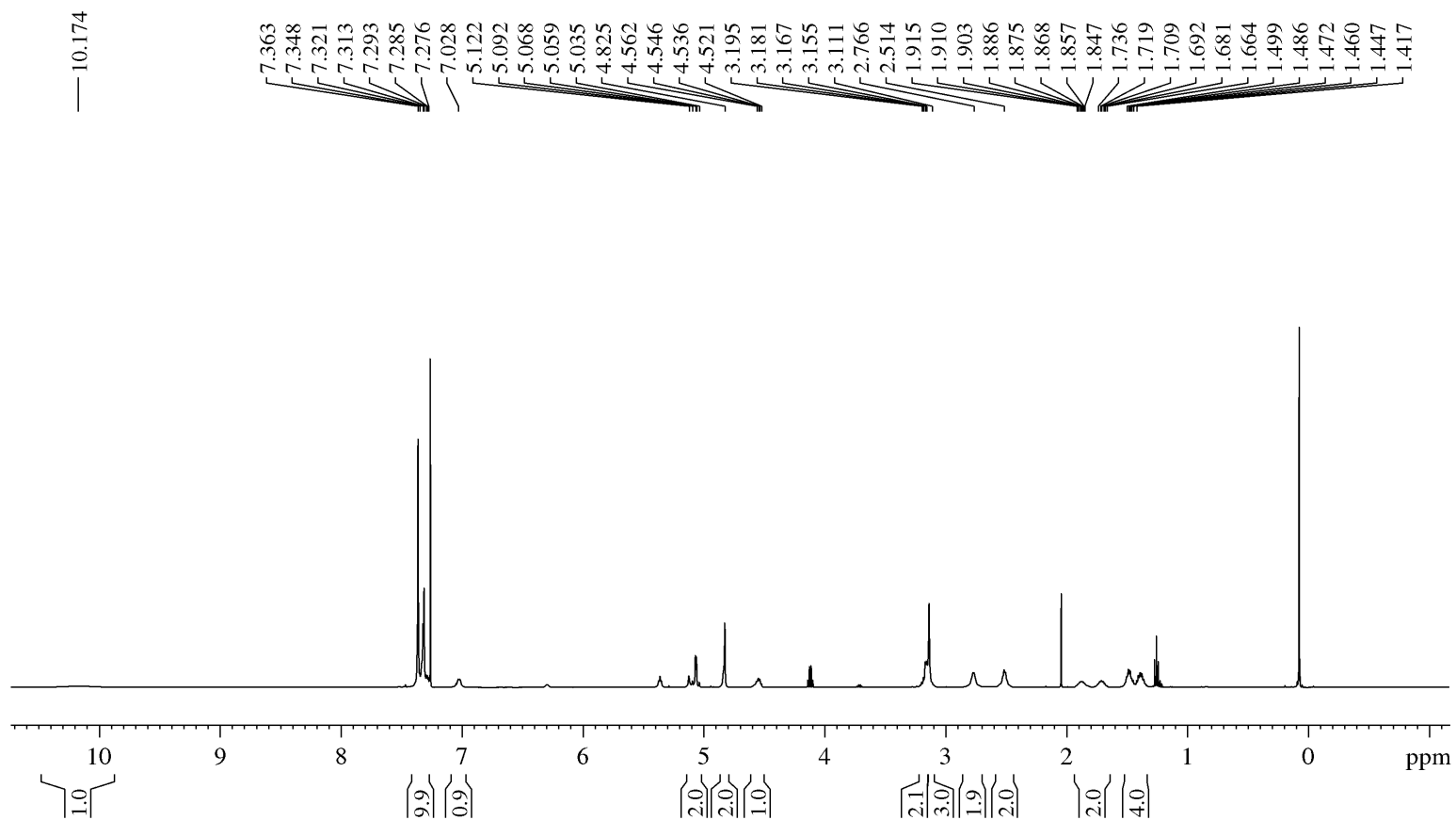
Figure S5-5. ^{1}H NMR spectrum of compound **25** in CDCl$_3$. The signal at 1.26, 2.05, 4.12 ppm are assigned to residual ethyl acetate in the NMR sample.

Compound (25)
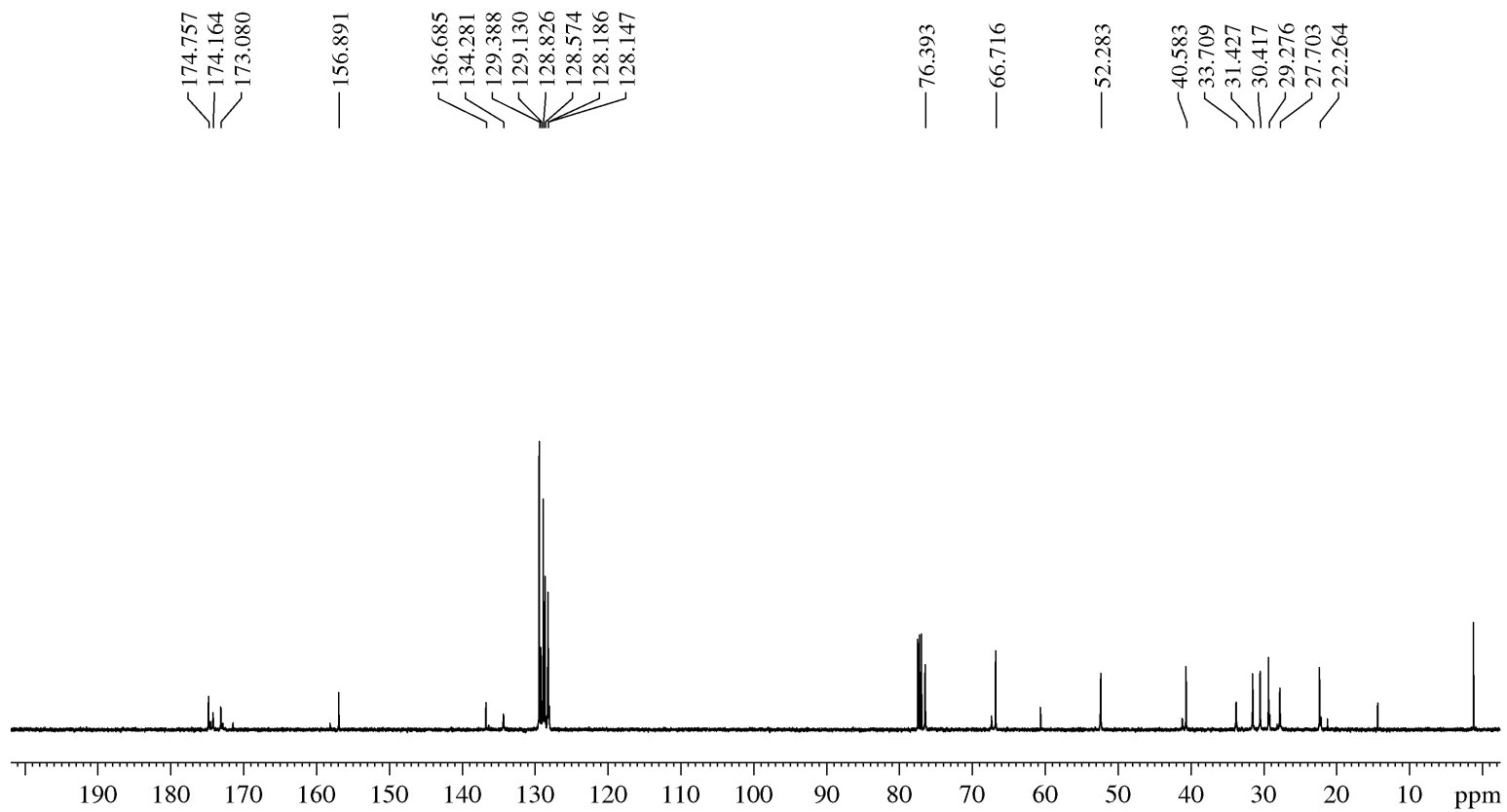
Figure S5-6. ^{13}C NMR spectrum of compound **25** in CDCl$_3$.

Compound (26)
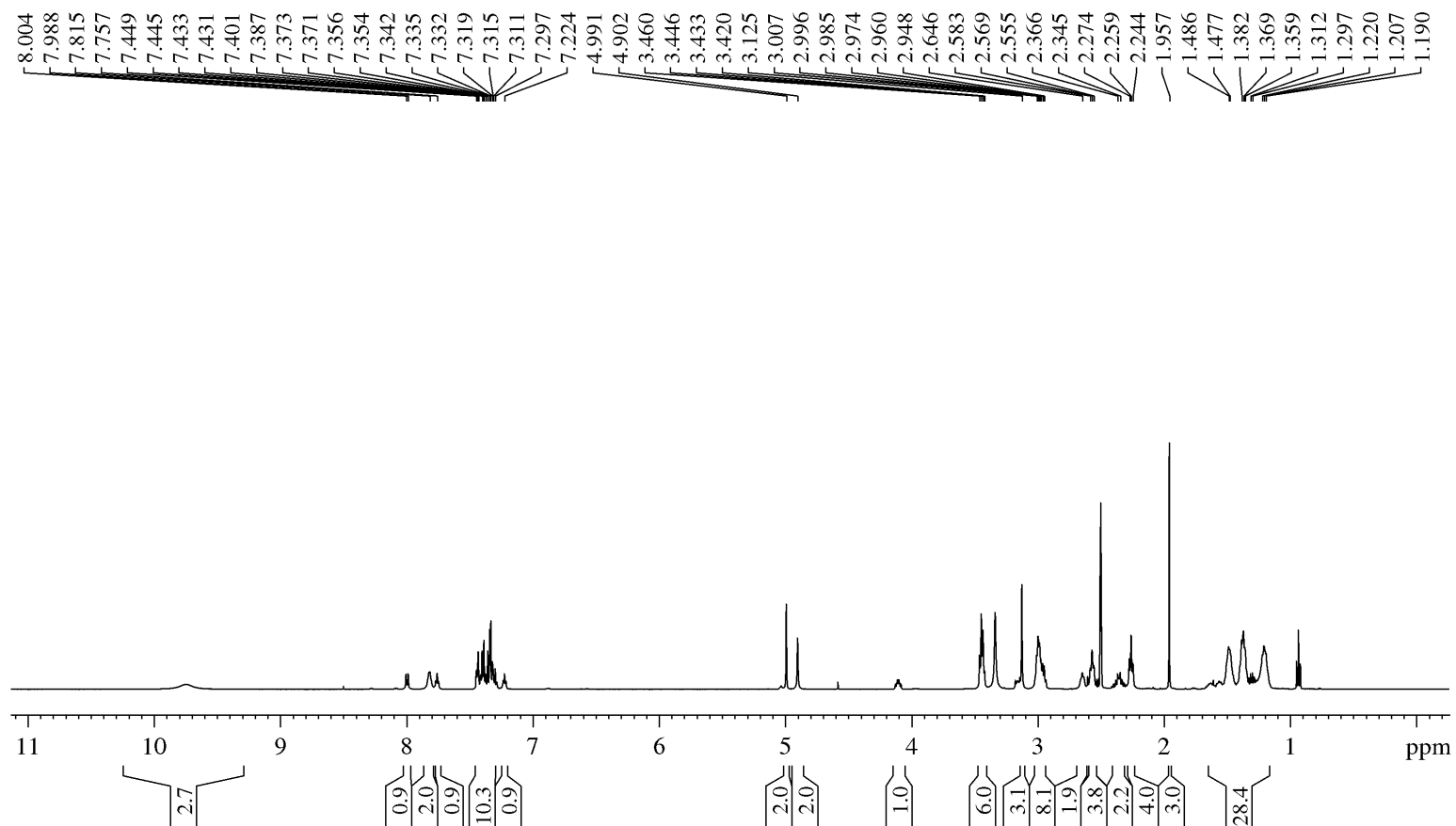
Figure S5-7. ^{1}H NMR spectrum of compound **26** in $(CD_3)_2SO$. The signal at 1.17, 199, 4.03 ppm are assigned to residual ethyl acetate in the NMR sample.
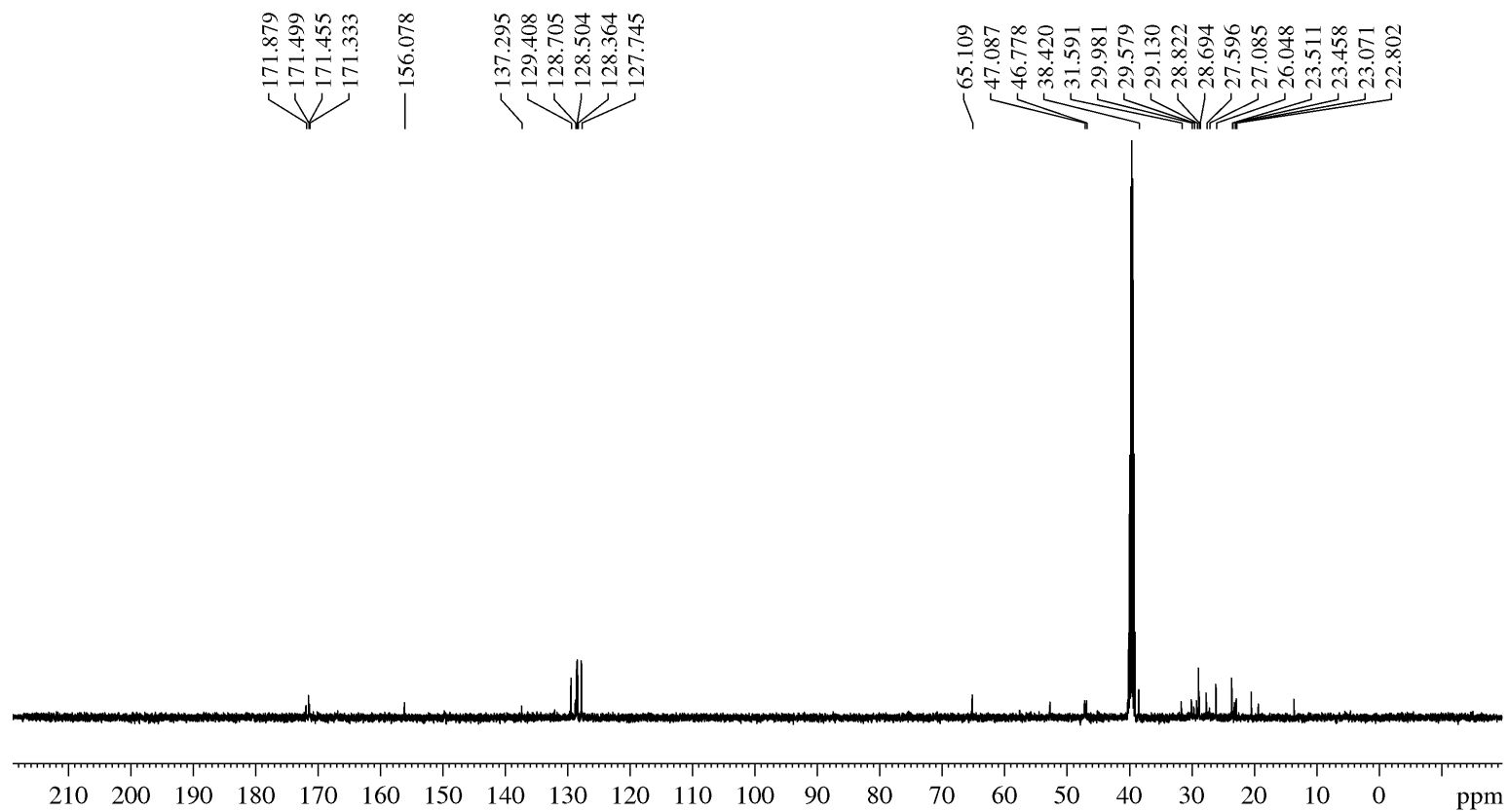
Figure S5-8. ^{13}C NMR spectrum of compound **26** in $(CD_3)_2SO$.

Compound (27) DFO-Km
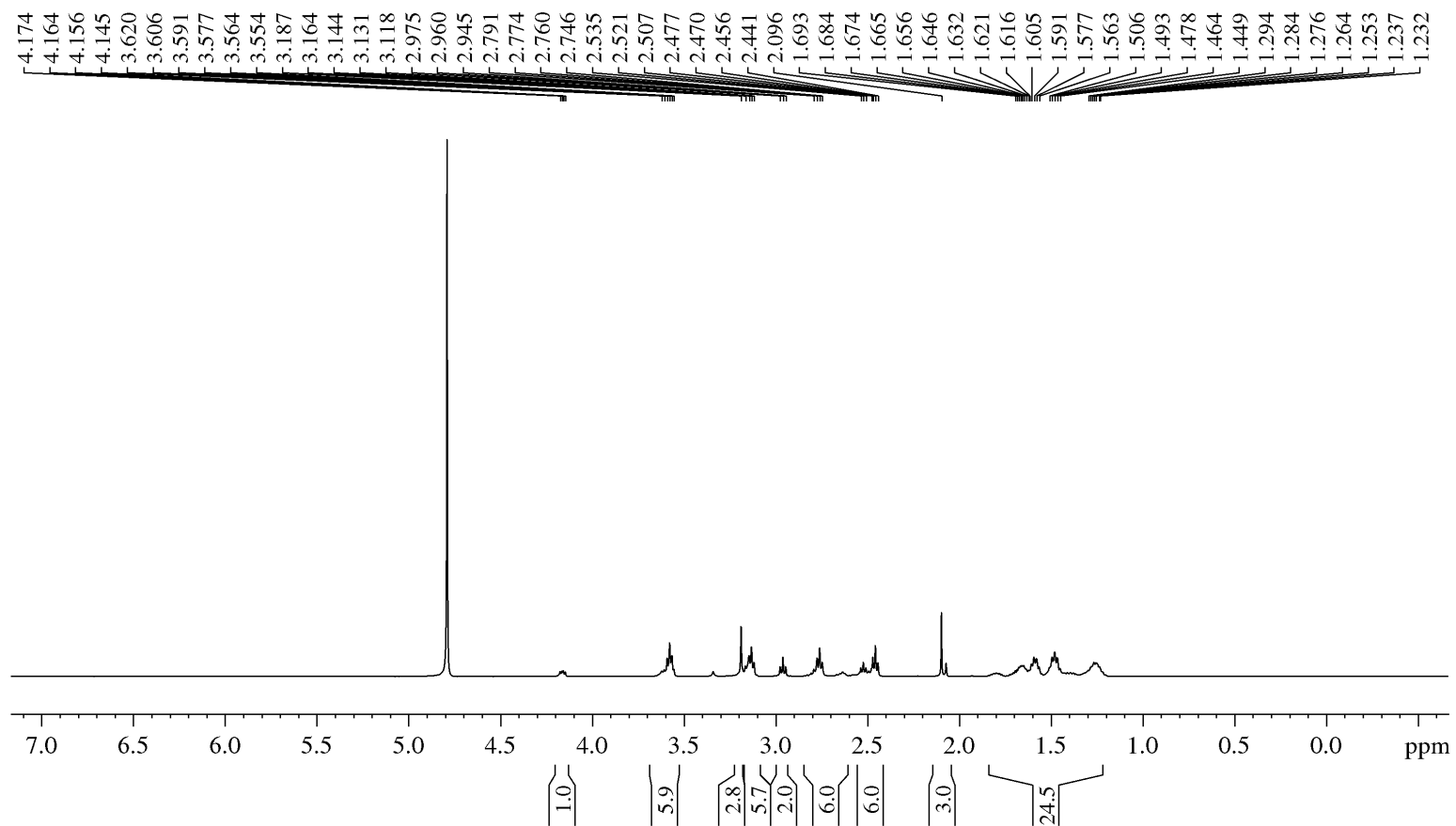
Figure S5-9. ^{1}H NMR spectrum of compound **27** in D$_2$O. The signal at 4.79 ppm is assigned to residual H$_2$O in the NMR sample.

Compound (27) DFO-Km
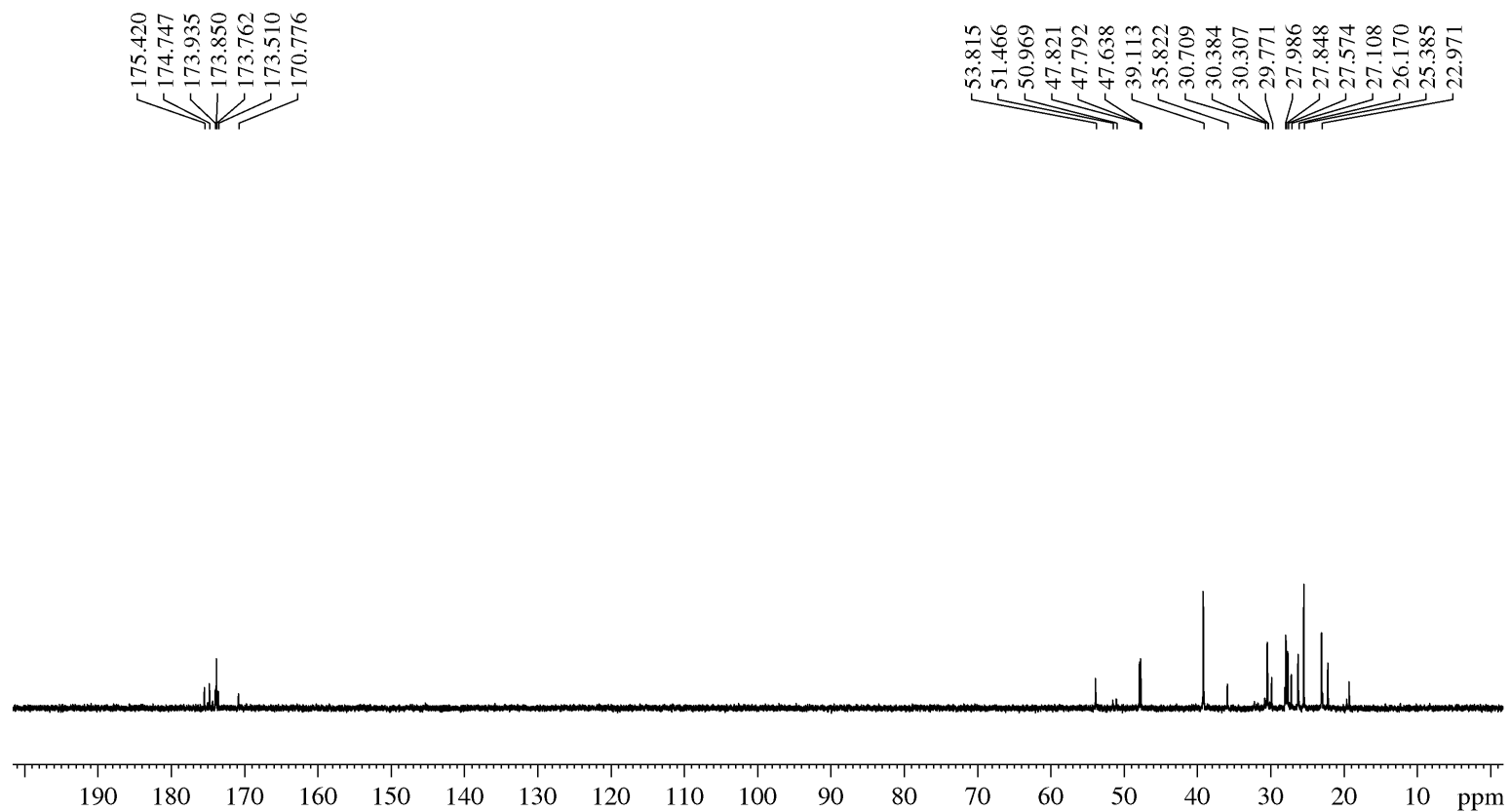
Figure S5-10. ^{13}C NMR spectrum of compound 27 in D$_2$O.

Compound (27) DFO-Km
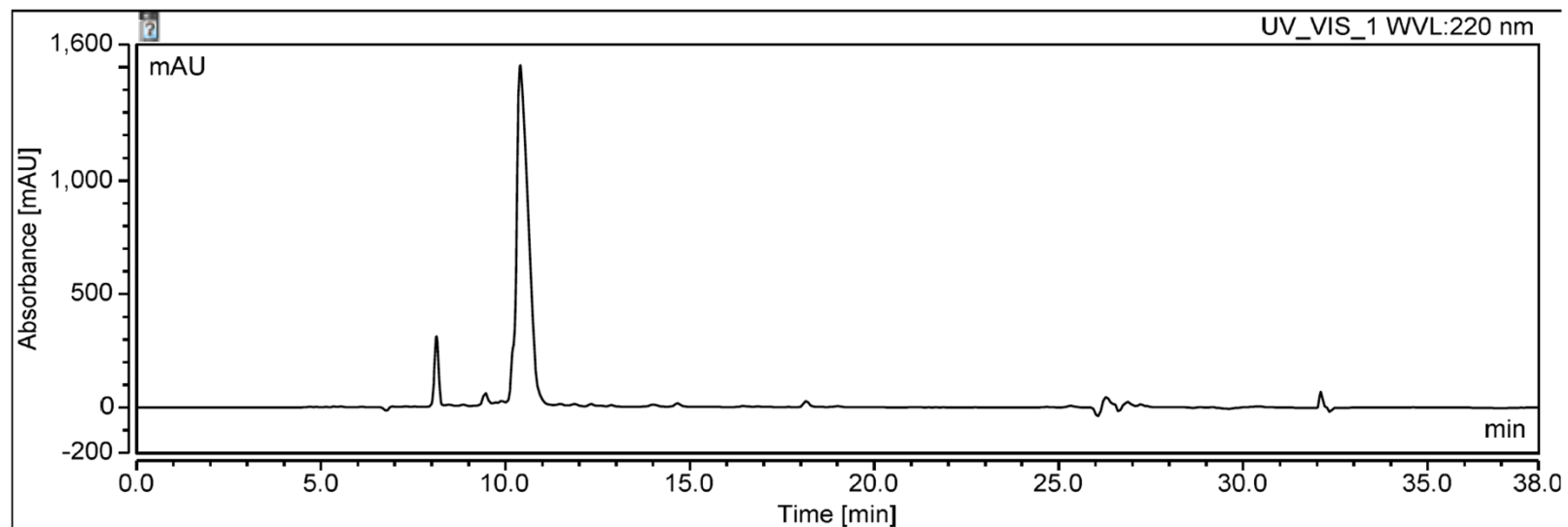
Figure S5-11. Analytical HPLC chromatogram for DFO-Km (**27**). HPLC conditions: C18 Inspire analytical DIKMA; 5 μm, 250 × 10.0 mm; (20 – 60% acetonitrile in water (0.1% formic acid); flow rate, 2 mL/min, t_R = 10.3 min). The peak eluted at t_R = 9.2 min was determined by LC-MS to be DFO-Km-Na.

Compound (28) ^{Nat}Zr-(DFO-Km)
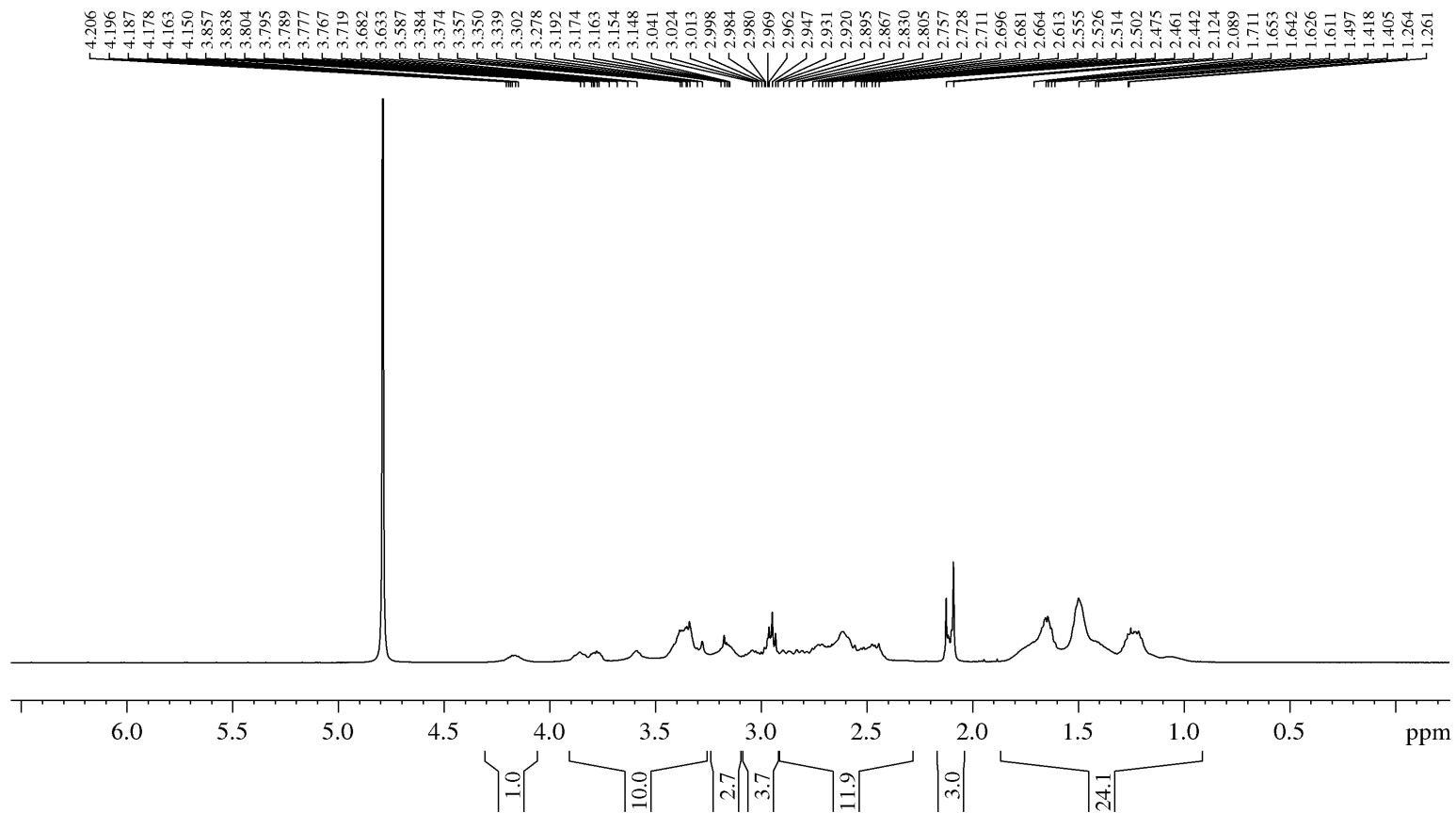
Figure S5-12. ^{1}H NMR spectrum of compound **28** in D$_2$O. The signal at 4.79 ppm is assigned to residual H$_2$O in the NMR sample.

Compound (29) *p*-SCN-Ph-DFO-Km
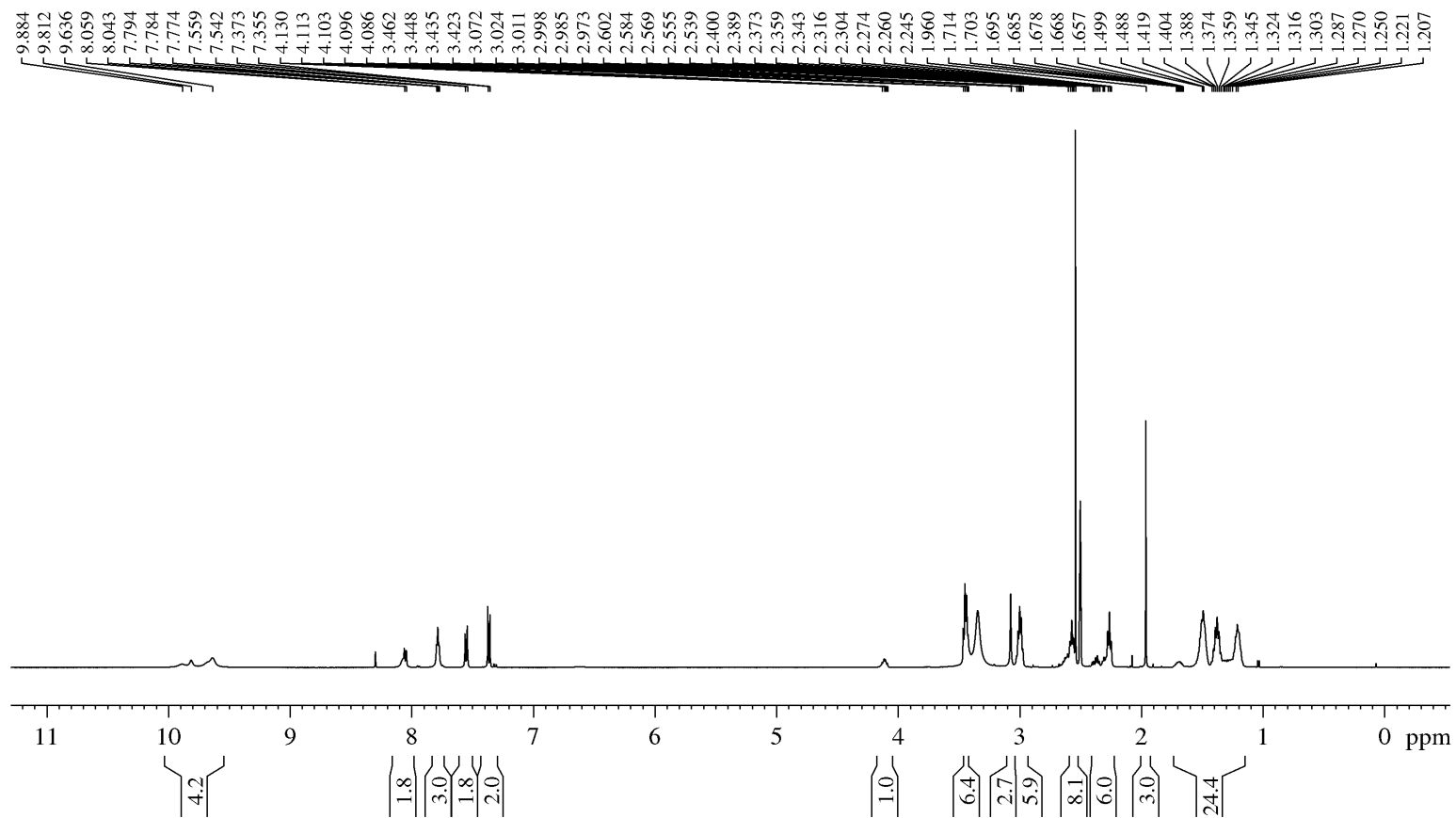
Figure S5-13. ^{1}H NMR spectrum of compound **29** in (CD$_3$)$_2$SO.

Compound (29) *p*-SCN-Ph-DFO-Km
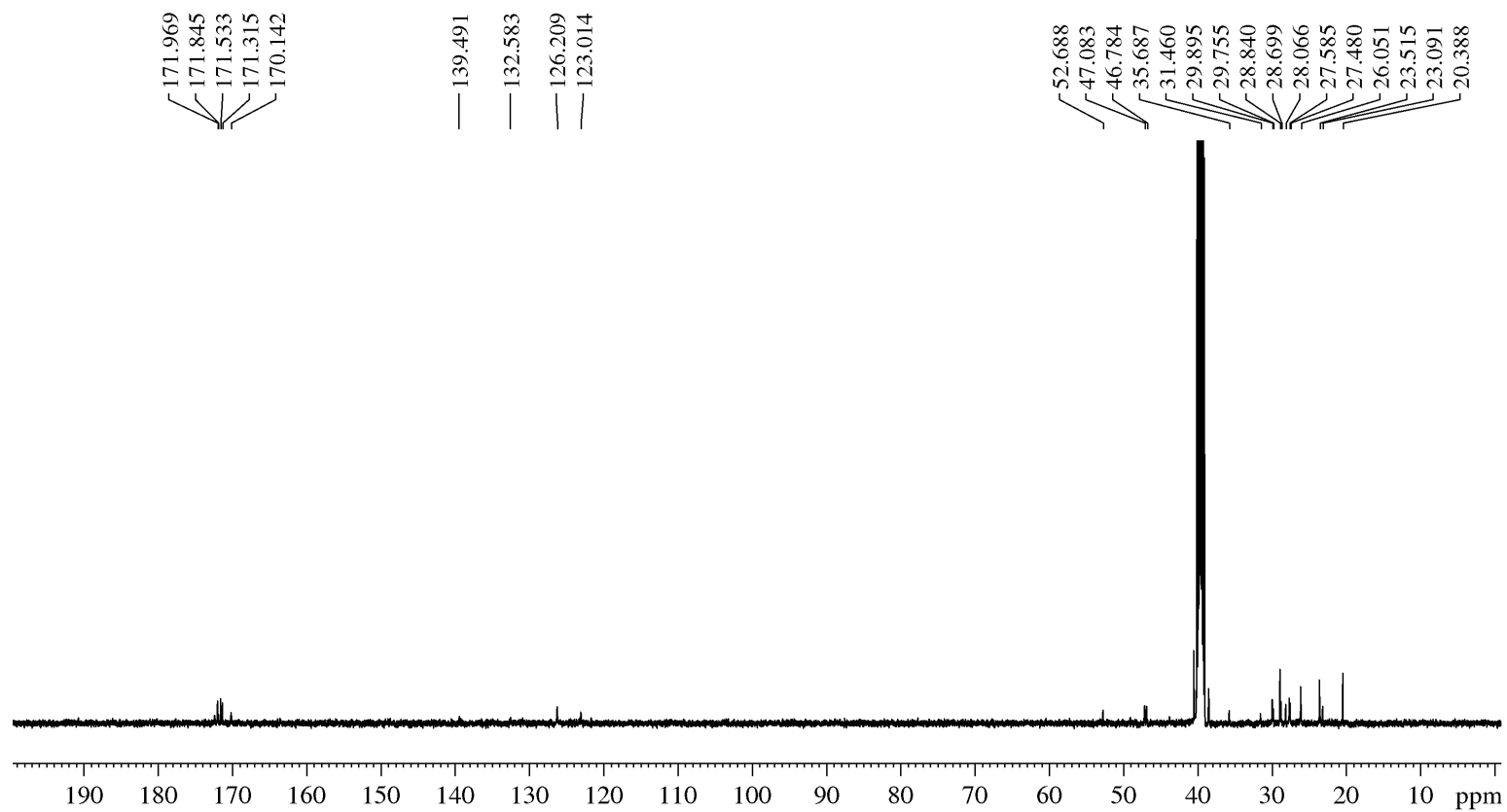
Figure S5-14. ^{13}C NMR spectrum of compound **29** in $(CD_3)_2SO$.

Compound (29) *p*-SCN-Ph-DFO-Km
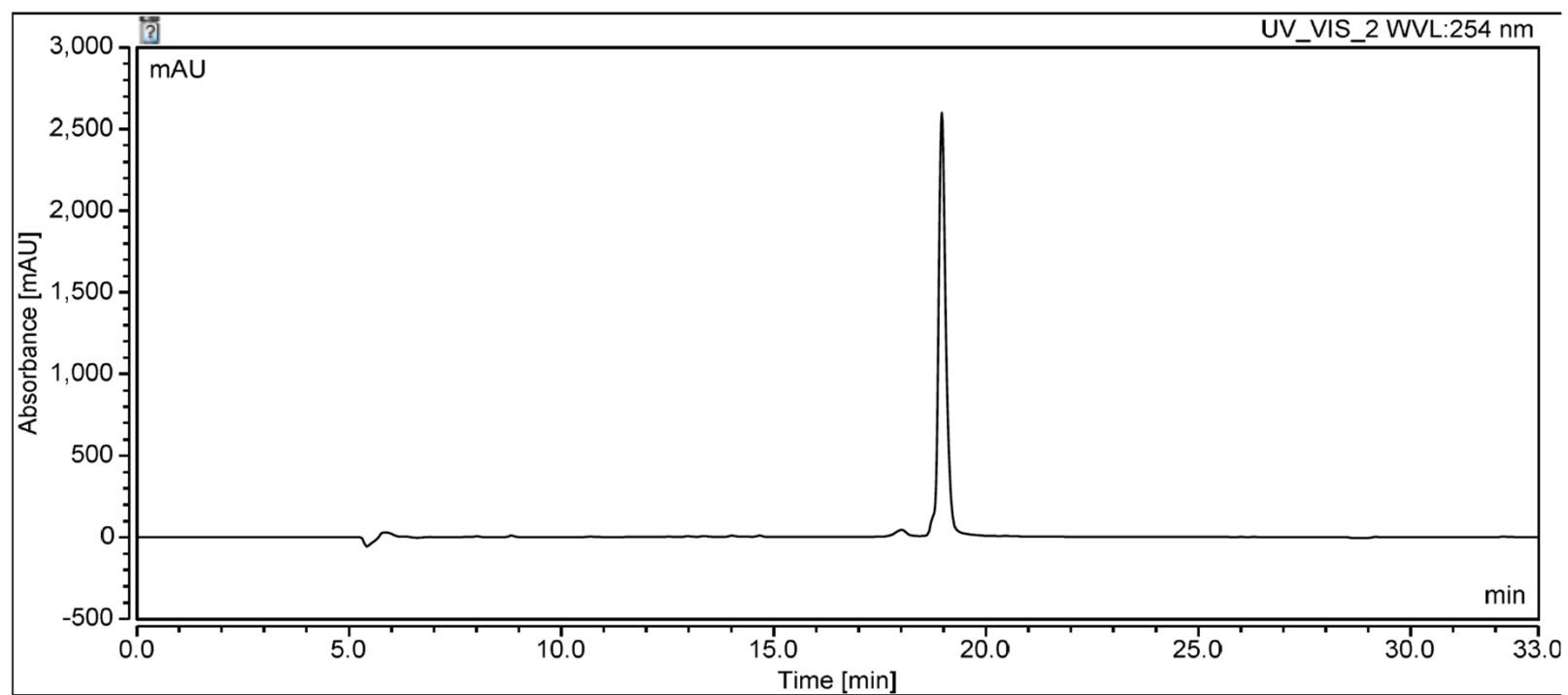
Figure S5-15. Analytical HPLC chromatogram for DFO-Km-NCS **(29)**. HPLC conditions: C18 Inspire analytical DIKMA; 5 μm, 250 × 10.0 mm; (20 – 60% acetonitrile in water (0.1% formic acid); flow rate, 2 mL/min, t_R = 18.9 min).

XYZ Coordinates of the Zr(DFO-Km) isomers

Λ-*C*-TTT

N	-3.64900	-2.41800	1.76700
C	-4.25500	-2.95500	0.55400
C	-3.16900	-3.72800	-0.20200
O	-2.41800	-4.50800	0.42600
C	-5.45500	-3.85900	0.91100
C	-6.27800	-4.35100	-0.28200
C	-7.49900	-5.16900	0.14900
C	-8.37100	-5.65500	-1.01800
N	-7.75500	-6.62400	-1.94300
C	-3.85600	-1.15100	2.20900
C	-3.18500	-0.79500	3.52900
O	-4.56600	-0.32900	1.59500
C	-1.64100	-0.75900	3.50900
C	-0.97500	-0.05200	2.35300
N	-1.21500	1.21200	2.04100
O	-0.11100	-0.69900	1.63500
O	-0.59700	1.72700	0.94600
C	-2.08200	2.13900	2.75100
C	-0.51500	1.98700	-2.03600
C	-0.94000	3.17000	-2.87600
C	-0.20900	4.46100	-2.48200
C	-0.60500	4.96300	-1.09900
O	0.61500	2.03300	-1.40500
N	-1.25700	0.88800	-1.93600
O	-1.80200	5.11600	-0.77500
N	0.42200	5.27700	-0.27300
C	0.23600	5.69500	1.11700
C	1.55400	6.15800	1.74300

C	2.63400	5.07400	1.89200
C	2.34000	4.02400	2.96900
C	3.30600	2.83100	2.95500
C	3.64200	1.96600	0.60500
C	4.90600	2.73200	0.30800
C	6.04700	1.84900	-0.21600
N	3.06000	1.95700	1.80200
O	3.06900	1.29200	-0.33300
C	6.70700	1.01700	0.88000
O	6.68300	1.35600	2.08100
N	7.33800	-0.10200	0.44500
C	7.95800	-1.09100	1.33000
C	6.97400	-1.99500	2.09200
C	6.02700	-2.85500	1.23700
C	4.89000	-2.05300	0.59600
C	3.81000	-2.88800	-0.09700
N	2.75200	-2.01300	-0.60400
C	2.68500	-1.42400	-1.80200
O	1.85500	-0.46400	-1.95800
C	3.54200	-1.90000	-2.94000
O	1.91800	-1.51600	0.37500
O	1.89700	1.24600	1.89700
O	-0.79400	-0.13300	-1.15900
C	-2.51000	0.61700	-2.64500
C	-2.32300	-0.16200	-3.95800
C	-1.98100	-1.66400	-3.86900
C	-3.19700	-2.60500	-3.81000
C	-3.89300	-2.77000	-2.45600
N	-3.05400	-3.55300	-1.53800
Zr	0.99300	0.41300	0.04700
H	-3.06200	-3.05400	2.30300
H	-4.61000	-2.09100	-0.02100

H	-6.10200	-3.27000	1.58200
H	-5.08300	-4.71700	1.49600
H	-5.64100	-4.96000	-0.94700
H	-6.62100	-3.48500	-0.87500
H	-8.12500	-4.55400	0.82100
H	-7.16900	-6.04200	0.74200
H	-9.28500	-6.11600	-0.61100
H	-8.69800	-4.78500	-1.61300
H	-7.42100	-7.42800	-1.40200
H	-6.91100	-6.21300	-2.35300
H	-3.49100	-1.52300	4.29800
H	-3.59600	0.17600	3.82600
H	-1.29800	-0.31400	4.45800
H	-1.23900	-1.78200	3.49200
H	-1.59200	3.11800	2.73000
H	-2.20800	1.82400	3.79300
H	-3.06300	2.20900	2.26000
H	-2.02400	3.33100	-2.79500
H	-0.73100	2.95600	-3.93800
H	0.87800	4.32600	-2.55800
H	-0.49900	5.24500	-3.20000
H	1.35200	4.98700	-0.56000
H	-0.20700	4.86200	1.68900
H	-0.49300	6.51800	1.13100
H	1.32300	6.58000	2.73500
H	1.95500	6.98800	1.13800
H	3.59500	5.56300	2.12200
H	2.78600	4.57100	0.92200
H	1.32100	3.62300	2.85500
H	2.39200	4.49300	3.96600
H	4.35600	3.15000	2.94400
H	3.15600	2.20600	3.84700
H	5.25800	3.28500	1.18400

H	4.65700	3.46900	-0.47300
H	5.69200	1.20500	-1.03400
H	6.82300	2.50200	-0.64900
H	7.29600	-0.31600	-0.54700
H	8.58900	-0.55700	2.05500
H	8.61900	-1.70400	0.69900
H	6.37900	-1.37400	2.78200
H	7.59300	-2.65600	2.72300
H	5.59100	-3.63400	1.88600
H	6.60600	-3.38600	0.46000
H	5.29100	-1.35300	-0.14900
H	4.39800	-1.43800	1.36600
H	4.21700	-3.46900	-0.93700
H	3.33600	-3.59300	0.60200
H	3.23200	-1.36800	-3.84700
H	3.44500	-2.98100	-3.10900
H	4.60300	-1.67800	-2.75700
H	-2.99000	1.57900	-2.86300
H	-3.14900	0.08600	-1.92600
H	-1.53400	0.35200	-4.53200
H	-3.25000	-0.03900	-4.54500
H	-1.30400	-1.84200	-3.01900
H	-1.41400	-1.92800	-4.77600
H	-2.89800	-3.61100	-4.15400
H	-3.95800	-2.26000	-4.53000
H	-4.11300	-1.79300	-2.00600
H	-4.85400	-3.28400	-2.61300
H	-2.35800	-4.15800	-1.97500

Λ-*C*-TCT

N	-4.51700	-2.42200	0.70300

C	-4.92800	-3.39500	-0.30700		N	2.64500	3.55500	1.24900
C	-5.19600	-2.62300	-1.61000		O	2.17600	1.39000	1.56900
O	-5.98300	-1.65500	-1.62100		C	5.03200	0.37900	3.15800
C	-6.17400	-4.17900	0.14300		O	4.26700	-0.34900	3.82300
C	-6.69300	-5.16200	-0.91200		N	6.03200	-0.10800	2.38200
C	-7.91900	-5.95200	-0.44300		C	6.41800	-1.51700	2.31900
C	-8.53500	-6.82700	-1.53500		C	6.86000	-1.95800	0.91800
N	-7.61700	-7.90300	-1.96500		C	5.74100	-2.25100	-0.09400
C	-3.27800	-2.36900	1.26200		C	4.84400	-1.05800	-0.43300
C	-3.11100	-1.25400	2.29200		C	3.84800	-1.37300	-1.55400
O	-2.38100	-3.19800	1.01400		N	2.86100	-0.30100	-1.69300
C	-1.64600	-0.90900	2.61700		C	2.98400	0.81600	-2.40500
C	-0.98900	0.14800	1.76100		O	2.18000	1.78300	-2.14000
N	-1.34000	1.42700	1.85900		C	4.02600	0.95300	-3.47300
O	-0.04100	-0.15800	0.94700		O	1.87700	-0.31500	-0.73200
O	-0.68600	2.33000	1.06900		O	1.88200	3.45200	0.11600
C	-2.34400	2.02100	2.72600		O	-0.85200	0.86500	-1.50300
C	-1.23500	3.09600	-1.89900		C	-3.07800	1.41900	-2.19400
C	-2.03600	4.28600	-2.37500		C	-3.28100	0.53600	-3.43000
C	-1.37500	5.63100	-2.00600		C	-2.58900	-0.83400	-3.38500
C	-1.57200	6.04600	-0.55100		C	-3.16400	-1.85100	-4.38000
O	-0.03500	3.26900	-1.46800		C	-4.54900	-2.39900	-4.00100
N	-1.70400	1.85100	-1.93300		N	-4.53400	-3.07000	-2.70100
O	-2.52800	6.79100	-0.22400		Zr	0.84200	1.54700	-0.28300
N	-0.66900	5.59600	0.35100		H	-4.08000	-4.08200	-0.43600
C	-0.85900	5.85200	1.78300		H	-5.15900	-1.65000	0.87600
C	0.29400	5.36200	2.66100		H	-3.90300	-3.86000	-2.58800
C	1.57800	6.21100	2.62500		H	6.64800	0.56300	1.92900
C	2.48300	6.07200	1.39000		H	-0.03900	4.83800	0.07100
C	3.37100	4.82500	1.35800		H	-6.96900	-3.46000	0.40000
C	2.76100	2.45400	1.99200		H	-5.91000	-4.71800	1.06900
C	3.50900	2.44600	3.29900		H	-5.87900	-5.85400	-1.19200
C	4.94600	1.90000	3.21500		H	-6.96200	-4.60600	-1.82700

H	-8.68900	-5.24400	-0.09300
H	-7.64600	-6.58500	0.41900
H	-8.85600	-6.17500	-2.37200
H	-9.44500	-7.30600	-1.14000
H	-6.84300	-7.49000	-2.49300
H	-8.10300	-8.49800	-2.64300
H	-3.59400	-1.62000	3.21300
H	-3.68800	-0.37200	1.97700
H	-1.04300	-1.82100	2.50300
H	-1.58200	-0.60000	3.67000
H	-2.71700	1.27700	3.43800
H	-3.17700	2.41100	2.12200
H	-1.87600	2.84800	3.27700
H	-3.06000	4.24500	-1.97400
H	-2.13400	4.22700	-3.47200
H	-1.84900	6.41300	-2.61400
H	-0.30700	5.59900	-2.25900
H	-1.79600	5.36700	2.10400
H	-1.00200	6.93700	1.91500
H	0.49900	4.30600	2.43000
H	-0.08600	5.37900	3.69600
H	2.18100	5.97600	3.52000
H	1.28900	7.27100	2.72700
H	3.18000	6.92600	1.36700
H	1.89700	6.12900	0.46200
H	4.00400	4.78000	2.25400
H	4.04000	4.87400	0.48200
H	2.93500	1.80500	3.98400
H	3.53200	3.45100	3.74000
H	5.47100	2.19700	4.13800
H	5.49600	2.36100	2.38100
H	5.55900	-2.10500	2.66900
H	7.24500	-1.69400	3.02800

H	7.45600	-2.87700	1.04500
H	7.55200	-1.20200	0.50500
H	5.11600	-3.07900	0.28600
H	6.21200	-2.62000	-1.02300
H	5.46600	-0.19900	-0.73700
H	4.27200	-0.74100	0.45000
H	3.28300	-2.29400	-1.34000
H	4.35900	-1.51100	-2.51600
H	4.20000	0.01200	-4.00900
H	4.98000	1.28600	-3.03700
H	3.69000	1.71900	-4.18400
H	-3.69400	2.32200	-2.28200
H	-3.40100	0.88100	-1.28800
H	-2.97300	1.08700	-4.33500
H	-4.37300	0.39700	-3.50300
H	-2.66000	-1.24700	-2.36400
H	-1.51400	-0.70500	-3.57800
H	-2.46800	-2.70100	-4.47500
H	-3.24400	-1.40200	-5.38400
H	-4.89100	-3.11200	-4.76800
H	-5.29800	-1.59800	-3.93200

Λ-*C*-TTC

N	-3.90900	-1.99300	1.73000
C	-4.33800	-2.82700	0.61100
C	-3.07900	-3.43400	-0.03300
O	-2.31200	-4.14800	0.64800
C	-5.32800	-3.91000	1.07100
C	-5.98700	-4.66500	-0.08700
C	-7.03900	-5.67500	0.38100
C	-7.73500	-6.42100	-0.76600
N	-6.88700	-7.31600	-1.57800

C	-4.16400	-0.66000	1.80300
C	-3.65200	0.04000	3.05300
O	-4.79900	-0.04200	0.92300
C	-2.11800	0.06300	3.22500
C	-1.27500	0.49600	2.04800
N	-1.31300	1.73400	1.57200
O	-0.44600	-0.33300	1.52200
O	-0.45800	2.04500	0.55200
C	-2.32000	2.74100	1.88400
C	-0.13900	2.13900	-2.19500
C	-0.51800	3.44800	-2.85000
C	0.24600	4.64300	-2.25100
C	-0.27100	5.07800	-0.88300
O	0.98500	2.04600	-1.56400
N	-0.91200	1.05900	-2.22200
O	-1.46900	5.38900	-0.71600
N	0.65300	5.18000	0.11000
C	0.27600	5.50700	1.48700
C	1.46900	5.83500	2.38700
C	2.44300	4.67400	2.64700
C	1.91600	3.51400	3.50400
C	2.87900	2.31100	3.55400
C	3.51800	2.03600	1.16300
C	4.83800	2.77200	1.22400
C	5.91100	2.13900	0.33000
N	2.90800	1.59200	2.27200
O	2.99000	1.75500	0.03600
C	6.59500	0.91400	0.93400
O	6.53500	0.63100	2.14800
N	7.30700	0.18400	0.04000
C	8.12300	-0.98400	0.37300
C	7.36500	-2.31900	0.45000
C	6.44800	-2.63100	-0.75200

C	5.01600	-2.14700	-0.50700
C	4.03400	-2.35300	-1.66500
N	2.72700	-1.80400	-1.28400
C	1.77000	-2.46900	-0.64100
O	0.92200	-1.78100	0.03500
C	1.67200	-3.96400	-0.70500
O	2.71800	-0.44500	-1.11900
O	1.79300	0.80700	2.06100
O	-0.46500	-0.03200	-1.52700
C	-2.17800	0.86700	-2.92600
C	-2.06500	-0.05400	-4.15300
C	-1.83500	-1.56200	-3.92200
C	-3.10200	-2.40300	-3.67800
C	-3.69300	-2.39800	-2.26600
N	-2.84100	-3.15300	-1.33400
Zr	1.03700	0.47100	0.01400
H	-3.34800	-2.43500	2.45500
H	-4.84500	-2.14300	-0.07900
H	-6.10400	-3.40700	1.67000
H	-4.80700	-4.61400	1.74100
H	-5.21100	-5.18200	-0.67900
H	-6.46800	-3.93800	-0.76500
H	-7.80800	-5.14700	0.97300
H	-6.57300	-6.41200	1.06000
H	-8.56000	-7.02600	-0.35500
H	-8.19600	-5.68800	-1.44900
H	-6.42700	-7.98700	-0.95400
H	-6.12200	-6.77200	-1.98900
H	-4.07500	-0.45900	3.93800
H	-4.06500	1.05400	3.02700
H	-1.88600	0.70900	4.08900
H	-1.75500	-0.94200	3.48300
H	-1.92300	3.70500	1.55800

H	-2.51000	2.76400	2.96400
H	-3.25600	2.54300	1.33900
H	-1.59900	3.62500	-2.75700
H	-0.30000	3.39500	-3.92900
H	1.32100	4.42800	-2.22500
H	0.09700	5.50500	-2.91900
H	1.53700	4.70200	-0.04200
H	-0.28900	4.66600	1.91700
H	-0.40800	6.36600	1.44800
H	1.06000	6.19700	3.34500
H	2.03100	6.67500	1.94800
H	3.35200	5.08000	3.12200
H	2.77100	4.28200	1.67500
H	0.94800	3.14800	3.12700
H	1.75100	3.85800	4.53900
H	3.90000	2.62500	3.81100
H	2.55400	1.58100	4.30600
H	5.20800	2.82900	2.25400
H	4.68000	3.80300	0.87600
H	5.48100	1.88200	-0.64900
H	6.69700	2.88900	0.14200
H	7.30800	0.49800	-0.92600
H	8.62200	-0.79500	1.33600
H	8.90300	-1.04700	-0.40000
H	6.76900	-2.34300	1.37600
H	8.13100	-3.10500	0.55700
H	6.44000	-3.71900	-0.93000
H	6.85500	-2.17000	-1.66900
H	5.01700	-1.07400	-0.27300
H	4.61700	-2.66400	0.38200
H	3.90000	-3.41500	-1.91000
H	4.36400	-1.83100	-2.57600
H	0.70300	-4.26100	-0.28800

H	2.46400	-4.44600	-0.11200
H	1.74800	-4.33600	-1.73600
H	-2.53000	1.85400	-3.25200
H	-2.89500	0.48600	-2.18400
H	-1.24400	0.34100	-4.77500
H	-2.98700	0.08300	-4.74400
H	-1.11000	-1.69900	-3.10500
H	-1.36000	-1.95900	-4.83400
H	-2.89700	-3.45400	-3.94900
H	-3.89600	-2.06600	-4.36500
H	-3.82400	-1.37100	-1.89800
H	-4.68800	-2.86600	-2.30500
H	-1.97100	-3.53700	-1.70000

Λ-*C*-TCC

N	-5.15200	-2.24600	2.80800
C	-5.46800	-2.27900	1.37500
C	-4.34700	-2.99500	0.58900
O	-3.77600	-3.98600	1.08700
C	-6.78500	-3.08300	1.23600
C	-7.32400	-3.28300	-0.18400
C	-8.58300	-4.15900	-0.19600
C	-9.18200	-4.36800	-1.58800
N	-8.27600	-5.13200	-2.47100
C	-4.50700	-1.37400	3.63500
C	-3.80000	-0.11500	3.14800
O	-4.48700	-1.61200	4.86300
C	-3.33600	-0.04300	1.68500
C	-2.12700	0.81900	1.42700
N	-2.22400	2.11900	1.18600
O	-0.96100	0.27600	1.36300

O	-1.07100	2.77600	0.86100
C	-3.40800	2.95900	1.21900
C	-0.70100	2.87400	-2.26200
C	-1.10100	4.05200	-3.11600
C	-0.36100	5.34400	-2.71900
C	-0.88200	6.00200	-1.44600
O	0.36800	2.94000	-1.54800
N	-1.41100	1.75400	-2.19900
O	-1.83400	6.81800	-1.49700
N	-0.26300	5.69000	-0.28400
C	-0.77500	6.19700	0.99300
C	-0.00500	5.68900	2.21500
C	1.37700	6.31600	2.46600
C	2.53200	5.89100	1.54500
C	3.20400	4.55400	1.87100
C	2.29100	2.30400	2.51600
C	3.03700	2.25000	3.82400
C	4.53600	1.92400	3.69100
N	2.34300	3.37400	1.72800
O	1.57600	1.30200	2.13000
C	4.83000	0.45600	3.40600
O	4.18100	-0.46100	3.95000
N	5.88200	0.23500	2.57500
C	6.48100	-1.07800	2.35600
C	6.79100	-1.37600	0.88800
C	5.55900	-1.44200	-0.03900
C	5.33000	-0.18200	-0.88200
C	4.13700	-0.29700	-1.83900
N	2.84300	-0.17000	-1.16200
C	2.04300	-1.11600	-0.68500
O	1.00500	-0.73600	-0.01600
C	2.27000	-2.57600	-0.91400
O	2.48300	1.12200	-0.88400

O	1.66100	3.31000	0.54400
O	-0.94100	0.78100	-1.35700
C	-2.61500	1.40500	-2.95000
C	-2.44000	0.16700	-3.85100
C	-2.68100	-1.21100	-3.21000
C	-4.16600	-1.51700	-2.89100
C	-4.56400	-1.40800	-1.41500
N	-4.03400	-2.55000	-0.65400
Zr	0.55200	1.45300	0.12900
H	-5.49600	-3.05400	3.32700
H	0.33800	4.86100	-0.25600
H	6.39600	1.04700	2.24000
H	-3.30400	-3.09900	-1.11000
H	-5.62700	-1.25800	1.01100
H	2.55500	1.47100	4.42800
H	2.92300	3.20100	4.36300
H	-7.54200	-2.57300	1.85200
H	-6.60900	-4.07100	1.69400
H	-6.54900	-3.75200	-0.81100
H	-7.56400	-2.30600	-0.63900
H	-9.35000	-3.69300	0.44700
H	-8.34800	-5.14200	0.24800
H	-9.46800	-3.38200	-2.00800
H	-10.11100	-4.95000	-1.48600
H	-7.48600	-4.53700	-2.73900
H	-8.76400	-5.32300	-3.35000
H	-4.46000	0.73500	3.39300
H	-2.93300	-0.02400	3.81900
H	-4.15600	0.28500	1.03600
H	-3.01400	-1.03800	1.35300
H	-4.28300	2.37500	1.52400
H	-3.57700	3.38900	0.22100
H	-3.25000	3.77300	1.94100

H	-2.18800	4.20600	-3.06000
H	-0.87400	3.82800	-4.17200
H	-0.51600	6.07700	-3.52200
H	0.71500	5.14200	-2.64100
H	-1.83400	5.90200	1.08500
H	-0.75500	7.29900	0.96300
H	0.05300	4.59200	2.16500
H	-0.63700	5.92500	3.08800
H	1.67000	6.10600	3.51000
H	1.27300	7.41400	2.40300
H	3.33900	6.63700	1.63200
H	2.22200	5.90300	0.49100
H	3.57800	4.56500	2.90200
H	4.06600	4.41200	1.20000
H	5.01800	2.14400	4.65900
H	5.02300	2.57100	2.94700
H	5.76800	-1.81400	2.75200
H	7.40700	-1.15700	2.95000
H	7.31600	-2.34400	0.87300
H	7.51400	-0.63400	0.50400
H	4.66400	-1.64800	0.57200
H	5.67000	-2.29700	-0.72600
H	6.22400	0.01200	-1.49800
H	5.18700	0.70000	-0.24000
H	4.16100	-1.25200	-2.38000
H	4.15400	0.51100	-2.58400
H	3.16400	-2.80100	-1.50400
H	1.39000	-2.98900	-1.43000
H	2.34800	-3.08600	0.05700
H	-2.87500	2.27400	-3.56500
H	-3.43200	1.26300	-2.22600
H	-1.42800	0.20100	-4.28600
H	-3.14000	0.28300	-4.69500

H	-2.05900	-1.30200	-2.30600
H	-2.31200	-1.96900	-3.92100
H	-4.42500	-2.53400	-3.23000
H	-4.81500	-0.83200	-3.46000
H	-5.65900	-1.38900	-1.33500
H	-4.18300	-0.46500	-0.99300

Λ-*C*-CCC

N	-4.97300	-2.98500	1.06500
C	-6.01400	-3.33200	0.08000
C	-5.43000	-3.13800	-1.34100
O	-5.05700	-4.10300	-2.03500
C	-6.64500	-4.71200	0.27200
C	-7.96600	-4.84900	-0.49400
C	-8.61500	-6.22400	-0.30400
C	-9.97600	-6.36900	-0.98400
N	-9.86500	-6.32300	-2.45700
C	-3.84300	-3.69600	1.34100
C	-2.77800	-2.91500	2.10500
O	-3.64300	-4.86300	0.96300
C	-1.63100	-2.66000	1.11100
C	-0.53100	-1.65000	1.34100
N	-0.29900	-0.95000	2.44600
O	0.22900	-1.43300	0.31900
O	0.68500	0.00300	2.39500
C	-0.91000	-1.03700	3.76500
C	0.14800	1.74500	-1.83300
C	-0.03800	2.39600	-3.17400
C	0.96700	3.55600	-3.39800
C	0.61300	4.78100	-2.57000

O	1.22200	1.05300	-1.61100		C	-5.87800	-0.62600	-1.24100
N	-0.70000	1.90100	-0.82800		N	-5.28900	-1.85800	-1.78000
O	-0.07900	5.71200	-3.03100		Zr	1.66200	0.28500	0.44700
N	1.05300	4.75300	-1.28300		H	-5.00100	-2.03400	1.42400
C	0.69000	5.73100	-0.25700		H	-6.80400	-2.58400	0.23600
C	1.88900	6.52700	0.27400		H	-6.82800	-4.85000	1.35000
C	3.01400	5.66200	0.86300		H	-5.93600	-5.48700	-0.04900
C	2.64600	4.90200	2.14500		H	-7.78100	-4.66800	-1.56600
C	3.59200	3.73500	2.45500		H	-8.67000	-4.06600	-0.15500
C	4.09600	2.25200	0.46200		H	-8.74600	-6.41200	0.77600
C	5.33200	3.00000	0.02100		H	-7.93500	-7.00700	-0.68500
C	6.56800	2.11900	-0.19100		H	-10.66100	-5.59600	-0.57800
N	3.39000	2.61600	1.53000		H	-10.40900	-7.34600	-0.71700
O	3.64900	1.27200	-0.23800		H	-9.61300	-5.37300	-2.74400
C	7.29200	1.76100	1.10600		H	-10.79400	-6.47700	-2.86000
O	7.11500	2.38600	2.17100		H	-3.19000	-1.97400	2.49500
N	8.16200	0.72700	0.99600		H	-2.44500	-3.53200	2.95100
C	8.89000	0.13500	2.12100		H	-2.07000	-2.32300	0.15700
C	8.02900	-0.65100	3.12300		H	-1.13900	-3.61700	0.87900
C	7.20200	-1.82100	2.56200		H	-1.42900	-1.98800	3.90000
C	6.00800	-1.37500	1.71200		H	-1.60300	-0.19800	3.92100
C	4.96300	-2.45800	1.44700		H	-0.09600	-0.97700	4.50000
N	3.81700	-1.87200	0.75000		H	-1.06200	2.76200	-3.31400
C	3.57500	-1.89400	-0.55600		H	0.14300	1.62700	-3.94000
O	2.62500	-1.15500	-1.01800		H	0.93600	3.85000	-4.45400
C	4.37600	-2.77000	-1.47500		H	1.98500	3.20500	-3.17200
O	3.03000	-1.05600	1.52300		H	1.58900	3.94000	-0.99300
O	2.20700	1.94700	1.73500		H	0.18200	5.19800	0.56200
O	-0.33400	1.35100	0.36500		H	-0.04200	6.40700	-0.71600
C	-1.93100	2.71600	-0.80900		H	1.51400	7.23200	1.03600
C	-3.14200	2.15800	-1.56200		H	2.29800	7.13400	-0.55000
C	-3.75800	0.85700	-1.03900		H	3.89200	6.29900	1.05700
C	-5.11800	0.61500	-1.70700		H	3.34000	4.95000	0.08700

H	1.62800	4.48900	2.08300
H	2.65400	5.58800	3.00700
H	3.40200	3.33400	3.46200
H	4.64700	4.03300	2.41400
H	5.57900	3.80900	0.71600
H	5.07500	3.46500	-0.94400
H	7.28100	2.66800	-0.82700
H	6.29900	1.20600	-0.74100
H	8.22000	0.25200	0.10000
H	9.41700	0.93800	2.65900
H	9.65400	-0.52300	1.68200
H	7.35300	0.05100	3.63700
H	8.72500	-1.03500	3.88800
H	6.82600	-2.40600	3.41900
H	7.85000	-2.50400	1.98400
H	6.34800	-0.99800	0.73800
H	5.49400	-0.54000	2.21400
H	4.58600	-2.89600	2.38500
H	5.36400	-3.27500	0.83200
H	4.35600	-3.82000	-1.15200
H	5.42800	-2.45100	-1.52300
H	3.94400	-2.69800	-2.48000
H	-1.68900	3.71600	-1.19900
H	-2.16200	2.83100	0.25700
H	-2.90200	2.04200	-2.63100
H	-3.90300	2.95700	-1.50900
H	-3.89700	0.92300	0.05400
H	-3.07900	0.00900	-1.22400
H	-4.99700	0.57300	-2.80500
H	-5.76700	1.48300	-1.51000
H	-6.93100	-0.54800	-1.56400
H	-5.87500	-0.66200	-0.14400
H	-4.92800	-1.79300	-2.73300

Λ-*C*-CTC

N	-3.08300	-3.15400	0.82100
C	-4.30800	-2.90800	0.06200
C	-3.89600	-2.31800	-1.28600
O	-2.98200	-2.87100	-1.93800
C	-5.11300	-4.21400	-0.15100
C	-6.48700	-4.00800	-0.79500
C	-7.27600	-5.31800	-0.91700
C	-8.68400	-5.15000	-1.48900
N	-8.66500	-4.71200	-2.90000
C	-3.07300	-3.18000	2.17500
C	-1.77600	-3.54800	2.88200
O	-4.09900	-2.95700	2.85400
C	-0.43700	-3.48300	2.12600
C	0.10200	-2.10600	1.80800
N	0.53200	-1.30300	2.77800
O	0.20700	-1.70200	0.58900
O	1.03100	-0.07800	2.42600
C	0.58500	-1.56700	4.20700
C	-0.18600	1.44500	-1.77700
C	-0.60700	1.93100	-3.13600
C	0.55400	2.55900	-3.92500
C	0.81200	4.01100	-3.54600
O	0.69600	0.50300	-1.69300
N	-0.66000	1.94800	-0.64600
O	0.03800	4.64200	-2.78900
N	1.90500	4.62400	-4.06500
C	2.92800	4.12700	-4.98900
C	4.34200	4.53700	-4.54900
C	5.00900	3.63500	-3.50000
C	4.20200	3.41700	-2.21800

C	4.97300	2.58200	-1.18800
C	3.64800	2.34300	0.94500
C	4.34700	3.44800	1.70300
C	5.81700	3.21000	2.09000
N	4.05200	1.93300	-0.25200
O	2.60600	1.77100	1.44700
C	6.05700	1.99200	2.97400
O	5.27500	1.67100	3.89000
N	7.20900	1.32500	2.70300
C	7.76100	0.23800	3.50900
C	8.24700	-0.95800	2.67600
C	7.17200	-1.97800	2.27800
C	6.08300	-1.44800	1.34400
C	5.06600	-2.54000	0.99800
N	3.86100	-1.98300	0.39100
C	3.39700	-2.13000	-0.84400
O	2.32300	-1.49600	-1.17200
C	4.08400	-3.00600	-1.84800
O	3.13600	-1.19100	1.24100
O	3.30800	0.94800	-0.83800
O	-0.13700	1.41800	0.50800
C	-1.65100	3.02500	-0.45000
C	-3.07400	2.73400	-0.94300
C	-3.67400	1.39000	-0.52500
C	-5.00200	1.12100	-1.24600
C	-5.50300	-0.32200	-1.13500
N	-4.56300	-1.24700	-1.77500
Zr	1.63100	0.07500	0.30800
H	-2.24000	-3.34600	0.28100
H	-4.91600	-2.21600	0.65800
H	-5.23600	-4.67700	0.84100
H	-4.50100	-4.89900	-0.76200
H	-6.36300	-3.55400	-1.79300

H	-7.07200	-3.29000	-0.19100
H	-7.36300	-5.77900	0.08300
H	-6.71500	-6.02800	-1.54900
H	-9.25800	-4.46400	-0.83300
H	-9.19900	-6.12300	-1.45500
H	-8.35900	-3.73600	-2.94600
H	-9.62700	-4.69900	-3.25100
H	-1.75000	-2.92600	3.78700
H	-1.92000	-4.58100	3.23800
H	-0.48800	-4.03000	1.17400
H	0.31300	-4.01900	2.73000
H	0.38500	-2.62300	4.41200
H	-0.15100	-0.94300	4.73500
H	1.59500	-1.31700	4.55700
H	-1.43000	2.64900	-3.07500
H	-0.96400	1.04900	-3.69000
H	0.32000	2.53000	-5.00100
H	1.46600	1.95600	-3.79600
H	1.98400	5.60700	-3.80200
H	2.84600	3.03400	-5.06400
H	2.72800	4.53600	-5.99400
H	4.30700	5.58000	-4.18600
H	4.98000	4.55200	-5.44600
H	5.99300	4.06700	-3.24900
H	5.21000	2.64900	-3.95600
H	3.27700	2.87100	-2.44700
H	3.91100	4.37900	-1.76800
H	5.69100	3.19300	-0.63100
H	5.53200	1.77300	-1.68300
H	3.75400	3.59800	2.61500
H	4.29100	4.38600	1.12900
H	6.15300	4.08700	2.67000
H	6.46700	3.16800	1.20600

H	7.80100	1.69300	1.96200
H	6.97800	-0.06800	4.21700
H	8.60400	0.63500	4.09900
H	8.77000	-0.58700	1.77800
H	9.00900	-1.48000	3.27600
H	7.66900	-2.84300	1.80300
H	6.69600	-2.36600	3.19600
H	6.52900	-1.05100	0.41700
H	5.53500	-0.62500	1.82200
H	4.73700	-3.05400	1.91600
H	5.48900	-3.28800	0.31800
H	4.87400	-2.44300	-2.37000
H	3.34300	-3.32100	-2.59400
H	4.53800	-3.90000	-1.40100
H	-1.26200	3.92800	-0.94100
H	-1.64400	3.19100	0.63500
H	-3.10900	2.80400	-2.04100
H	-3.70100	3.56400	-0.57400
H	-3.82100	1.35200	0.56800
H	-2.95900	0.58700	-0.77300
H	-4.88700	1.36400	-2.31700
H	-5.79100	1.78900	-0.86300
H	-6.48700	-0.41300	-1.62400
H	-5.63600	-0.60600	-0.08400
H	-4.25500	-0.97600	-2.71100

Λ-*C*-CTT

N	-3.87400	-4.25900	-0.19300
C	-5.13100	-3.52400	-0.30000
C	-5.39200	-3.13800	-1.76400
O	-5.26900	-3.99000	-2.66900
C	-6.26400	-4.43000	0.22600

C	-7.63400	-3.75700	0.34200
C	-8.70300	-4.71300	0.88600
C	-10.06900	-4.06100	1.10000
N	-10.68900	-3.64300	-0.17500
C	-2.70500	-3.84700	-0.74900
C	-1.52900	-4.77900	-0.49700
O	-2.61000	-2.80000	-1.41300
C	-0.16400	-4.13200	-0.75500
C	0.12200	-2.75200	-0.20800
N	-0.07900	-2.41800	1.06100
O	0.64800	-1.87500	-0.99500
O	0.24000	-1.14300	1.45800
C	-0.50700	-3.27600	2.15500
C	0.13400	1.37500	-2.27700
C	-0.04800	2.02400	-3.62100
C	0.94100	3.19600	-3.86000
C	0.49000	4.47600	-3.17300
O	1.18000	0.64800	-2.07400
N	-0.72900	1.53900	-1.28000
O	-0.06100	5.40000	-3.81100
N	0.68200	4.51500	-1.82800
C	0.17700	5.58500	-0.96800
C	1.25900	6.33900	-0.19000
C	2.10100	5.44200	0.73200
C	3.29000	4.78100	0.02300
C	3.90600	3.62200	0.79300
C	2.91000	1.73200	2.07700
C	3.59300	2.10700	3.37100
C	5.12800	1.97800	3.40200
N	2.99600	2.48200	0.98600
O	2.19000	0.65700	2.01500
C	5.65500	0.55200	3.34000
O	5.17700	-0.35900	4.04400

N	6.72700	0.36900	2.52500
C	7.51800	-0.86100	2.52700
C	7.09500	-1.92500	1.50500
C	7.52600	-1.67000	0.04700
C	6.61400	-0.82200	-0.86100
C	5.43400	-1.57400	-1.50900
N	4.17600	-1.50900	-0.76100
C	3.70000	-2.33400	0.16900
O	2.67400	-1.95100	0.83100
C	4.26400	-3.70300	0.39300
O	3.48200	-0.33200	-0.93500
O	2.31300	2.05200	-0.12000
O	-0.44200	0.88800	-0.11100
C	-1.92400	2.40300	-1.26100
C	-3.20800	1.85600	-1.89100
C	-3.86900	0.64600	-1.21900
C	-5.33900	0.53400	-1.65100
C	-6.08100	-0.72500	-1.18300
N	-5.82200	-1.88300	-2.04200
Zr	1.54200	-0.08400	0.02900
H	-3.87800	-5.11700	0.35100
H	-5.06700	-2.62800	0.33500
H	-5.95500	-4.79300	1.22100
H	-6.32800	-5.31000	-0.43600
H	-7.94400	-3.38200	-0.64700
H	-7.56200	-2.88000	1.00900
H	-8.36200	-5.12300	1.85300
H	-8.81900	-5.56900	0.19800
H	-9.95600	-3.22500	1.81900
H	-10.74400	-4.79500	1.56800
H	-10.16200	-2.85600	-0.56400
H	-11.61600	-3.25600	0.02200
H	-1.62800	-5.63900	-1.17900

H	-1.60400	-5.19700	0.51600
H	-0.00800	-4.03500	-1.83600
H	0.61900	-4.81900	-0.39200
H	-0.32300	-4.32700	1.91200
H	-1.57200	-3.12200	2.38700
H	0.09600	-3.00400	3.02900
H	-1.07900	2.36400	-3.78500
H	0.15700	1.24500	-4.36900
H	0.98700	3.40600	-4.93600
H	1.94700	2.89800	-3.52500
H	1.12700	3.71300	-1.37600
H	-0.54100	5.15000	-0.25100
H	-0.37800	6.27300	-1.61900
H	0.73900	7.10300	0.41000
H	1.91400	6.88100	-0.89400
H	1.44900	4.66700	1.17300
H	2.48200	6.03600	1.57900
H	4.09000	5.52400	-0.12300
H	3.01800	4.43800	-0.98300
H	4.22200	3.96200	1.78700
H	4.79300	3.25000	0.25700
H	3.16600	1.45300	4.14300
H	3.32600	3.14100	3.64000
H	5.46800	2.38500	4.36800
H	5.60500	2.59700	2.63100
H	7.08200	1.17100	2.01100
H	7.43600	-1.28600	3.53800
H	8.56800	-0.57600	2.36100
H	6.01000	-2.07200	1.59000
H	7.55900	-2.86900	1.83700
H	7.67600	-2.64400	-0.45100
H	8.52500	-1.20200	0.06900
H	7.23100	-0.44500	-1.69300

H	6.22600	0.06500	-0.33800
H	5.20300	-1.14100	-2.49300
H	5.68700	-2.63100	-1.67300
H	4.32700	-3.89100	1.47200
H	5.24400	-3.86500	-0.06400
H	3.56000	-4.43700	-0.03000
H	-1.65900	3.35000	-1.75000
H	-2.08400	2.62600	-0.19700
H	-3.04100	1.64200	-2.96000
H	-3.91300	2.70500	-1.86500
H	-3.82900	0.76700	-0.12200
H	-3.31800	-0.27800	-1.45600
H	-5.41700	0.59800	-2.75100
H	-5.88700	1.40700	-1.26000
H	-7.16600	-0.53200	-1.19000
H	-5.80700	-0.96700	-0.15000
H	-6.03700	-1.74700	-3.03100

Λ-*C*-CCT

N	-3.48000	-3.50400	1.31200
C	-4.43200	-3.45000	0.21100
C	-3.65700	-3.57500	-1.10800
O	-2.77700	-4.45800	-1.22100
C	-5.47900	-4.57500	0.35100
C	-6.62000	-4.52100	-0.66900
C	-7.65100	-5.63200	-0.44100
C	-8.86800	-5.55300	-1.36200
N	-8.50800	-5.78600	-2.77600
C	-3.36000	-2.53100	2.25500
C	-2.35100	-2.82400	3.35500
O	-4.03500	-1.48200	2.24000
C	-0.87000	-2.72800	2.92500

C	-0.34800	-1.36500	2.53300
N	-0.18300	-0.40700	3.44000
O	0.00300	-1.12300	1.32300
O	0.33300	0.79300	3.01300
C	-0.48800	-0.45500	4.86100
C	0.14500	2.12900	-1.53000
C	0.08400	2.68100	-2.92900
C	1.08600	3.82600	-3.19600
C	0.64000	5.14800	-2.58800
O	1.26700	1.71000	-1.04900
N	-0.93200	2.01400	-0.76500
O	0.15100	6.06300	-3.28300
N	0.77900	5.23200	-1.23900
C	0.42100	6.40100	-0.43900
C	1.64900	7.17000	0.07100
C	2.65100	6.30200	0.84600
C	2.11200	5.72200	2.15900
C	2.95400	4.56000	2.69700
C	3.75500	2.69800	1.19700
C	5.13100	3.29700	1.00900
C	5.96300	2.55100	-0.03500
N	2.81700	3.35000	1.88600
O	3.44200	1.56900	0.68700
C	6.56600	1.25100	0.47600
O	7.04900	1.16700	1.62500
N	6.62500	0.23700	-0.42300
C	7.36100	-1.00100	-0.17800
C	6.51600	-2.22300	0.21200
C	5.82000	-2.97000	-0.94100
C	4.48100	-2.43900	-1.48500
C	3.23100	-2.78200	-0.65000
N	2.82500	-1.74300	0.29900
C	3.00500	-1.68100	1.61600

O	2.58400	-0.63900	2.24300
C	3.64400	-2.78800	2.39800
O	2.18700	-0.68600	-0.30500
O	1.59300	2.73100	1.97500
O	-0.74900	1.40700	0.44800
C	-2.28700	2.53300	-1.02900
C	-3.13400	1.73600	-2.02200
C	-3.53100	0.32400	-1.58800
C	-4.42400	-0.33800	-2.64300
C	-4.98400	-1.70700	-2.25100
N	-3.94600	-2.73300	-2.12700
Zr	1.29200	0.78800	1.03300
H	-2.88900	-4.33000	1.37100
H	-4.92500	-2.47500	0.30300
H	-5.89400	-4.50100	1.36900
H	-4.95900	-5.54600	0.28500
H	-6.20800	-4.59800	-1.69000
H	-7.12600	-3.54100	-0.60300
H	-8.00400	-5.58200	0.60400
H	-7.16600	-6.61600	-0.56900
H	-9.37500	-4.58100	-1.20000
H	-9.58500	-6.33800	-1.07000
H	-7.96800	-4.98600	-3.12000
H	-9.36400	-5.78100	-3.33700
H	-2.57100	-2.13500	4.17900
H	-2.51900	-3.84700	3.72700
H	-0.68800	-3.38000	2.06100
H	-0.25500	-3.12000	3.75000
H	-0.52000	-1.49300	5.20600
H	-1.45100	0.03500	5.06800
H	0.31200	0.07400	5.39400
H	-0.93000	3.00200	-3.19500
H	0.33600	1.84500	-3.60400
H	1.16200	3.97800	-4.28000
H	2.07800	3.53700	-2.81900
H	1.22300	4.45100	-0.76500
H	-0.20800	6.06600	0.40000
H	-0.19500	7.04900	-1.07800
H	1.29200	7.99900	0.70600
H	2.16100	7.62800	-0.79200
H	3.55700	6.89600	1.05600
H	2.98100	5.48100	0.18700
H	1.08000	5.35800	2.04000
H	2.07800	6.50700	2.93200
H	2.64000	4.29700	3.72000
H	4.01800	4.82600	2.73300
H	5.66600	3.28300	1.97200
H	5.04000	4.35200	0.71400
H	6.82200	3.19000	-0.30100
H	5.38600	2.38900	-0.95600
H	6.18200	0.37500	-1.32700
H	8.06000	-0.77800	0.64000
H	7.95600	-1.23000	-1.07800
H	5.80200	-1.91900	0.99200
H	7.21100	-2.93200	0.69100
H	5.65600	-4.01600	-0.62800
H	6.53500	-3.02700	-1.78000
H	4.32600	-2.90000	-2.47400
H	4.50200	-1.35200	-1.65700
H	3.36600	-3.73000	-0.11300
H	2.36500	-2.90700	-1.31600
H	2.90000	-3.18500	3.10700
H	4.47400	-2.38000	2.99300
H	4.01800	-3.61500	1.78700
H	-2.18900	3.57400	-1.37000
H	-2.76900	2.55600	-0.04300

278

H	-2.62500	1.69000	-2.99900
H	-4.04800	2.33300	-2.18800
H	-4.06800	0.37200	-0.62400
H	-2.63000	-0.28700	-1.41500
H	-3.87300	-0.43000	-3.59500
H	-5.29000	0.31500	-2.84900
H	-5.70900	-2.03700	-3.01400
H	-5.53000	-1.63200	-1.30400
H	-3.40300	-2.91400	-2.97300

Λ-*N*-CCC

N	-4.59600	-1.25400	1.37100
C	-4.95300	-2.15400	0.28100
C	-3.70200	-2.94500	-0.13800
O	-3.01800	-3.52600	0.73100
C	-6.06200	-3.11800	0.75100
C	-6.56000	-4.09800	-0.31600
C	-7.62300	-5.05800	0.22700
C	-8.15600	-6.06300	-0.80600
N	-7.19100	-7.04500	-1.33300
C	-4.33300	0.07400	1.21900
C	-3.92300	0.78200	2.50300
O	-4.45900	0.67600	0.13600
C	-2.58300	1.54700	2.42200
C	-1.38700	0.86700	1.78600
N	-0.97700	-0.35100	2.14800
O	-0.73200	1.47900	0.87900
O	0.09800	-0.88100	1.47300
C	-1.36200	-1.14400	3.30000
C	-0.38300	2.00900	-2.07400
C	-0.80200	3.20000	-2.90500
C	-0.09200	4.49400	-2.48900
C	-0.55900	5.00100	-1.13200
O	0.72000	2.05100	-1.39900
N	-1.10300	0.89200	-2.04700
O	-1.76900	5.18300	-0.88000
N	0.42600	5.28600	-0.24700
C	0.18100	5.70600	1.13100
C	1.46800	6.21500	1.79000
C	2.57600	5.16300	1.95100
C	2.26700	4.07800	2.98800
C	3.22400	2.88200	2.92700
C	3.69800	1.96700	0.61200
C	4.98400	2.72500	0.39600
C	6.14800	1.86300	-0.10600
N	2.99100	2.06400	1.73600
O	3.21000	1.24100	-0.33100
C	6.77500	0.99000	0.97900
O	6.65000	1.23900	2.19500
N	7.49800	-0.05800	0.51400
C	8.13100	-1.06900	1.36600
C	7.17600	-2.07300	2.03200
C	6.26200	-2.88200	1.09700
C	5.07700	-2.07200	0.56900
C	4.04400	-2.88000	-0.21600
N	2.98300	-1.99300	-0.69000
C	2.87300	-1.40600	-1.88200
O	2.01100	-0.46900	-2.01600
C	3.72700	-1.84600	-3.03600
O	2.16300	-1.51900	0.30900
O	1.78500	1.41800	1.75000
O	-0.63500	-0.15400	-1.30500
C	-2.37400	0.64700	-2.73200

C	-2.24000	-0.15200	-4.03800		H	1.85100	7.06200	1.19700
C	-1.96900	-1.66400	-3.90700		H	3.51300	5.67200	2.23000
C	-3.22900	-2.54400	-3.86900		H	2.78100	4.68900	0.97600
C	-4.09900	-2.46100	-2.61400		H	1.24600	3.68900	2.85500
N	-3.38300	-3.00400	-1.45200		H	2.31900	4.50500	4.00200
Zr	1.09400	0.34100	-0.02900		H	4.27400	3.19500	2.93500
H	-4.36900	-1.69000	2.26100		H	3.06600	2.21900	3.79000
H	-5.31900	-1.52400	-0.53800		H	5.29500	3.25600	1.30000
H	-6.90100	-2.50300	1.11300		H	4.77000	3.48700	-0.37200
H	-5.67700	-3.68400	1.61600		H	5.82600	1.24500	-0.95700
H	-5.70800	-4.68100	-0.70600		H	6.93700	2.53400	-0.48500
H	-6.97900	-3.53600	-1.16900		H	7.52100	-0.20900	-0.49100
H	-8.47600	-4.47300	0.61600		H	8.70900	-0.55400	2.14800
H	-7.20900	-5.61700	1.08600		H	8.84900	-1.60500	0.72700
H	-8.98800	-6.62600	-0.35200		H	6.55600	-1.54300	2.77300
H	-8.58000	-5.51500	-1.66500		H	7.81700	-2.76600	2.60200
H	-6.75800	-7.53700	-0.54500		H	5.87800	-3.75000	1.66100
H	-6.41900	-6.55300	-1.79200		H	6.85000	-3.29400	0.25700
H	-3.92900	0.07700	3.34500		H	5.42700	-1.26600	-0.08900
H	-4.70700	1.52400	2.72100		H	4.56000	-1.58500	1.41100
H	-2.72100	2.45900	1.82900		H	4.49700	-3.37900	-1.08300
H	-2.31400	1.87100	3.44100		H	3.56900	-3.65200	0.41000
H	-1.71100	-2.13300	2.97000		H	3.27800	-1.46600	-3.96100
H	-2.14900	-0.64200	3.86700		H	3.81600	-2.93800	-3.10600
H	-0.48300	-1.26500	3.95200		H	4.74200	-1.42900	-2.95100
H	-1.88800	3.35500	-2.84100		H	-2.82900	1.62200	-2.94800
H	-0.57600	2.99500	-3.96500		H	-3.01000	0.14800	-1.98900
H	0.99700	4.35900	-2.51100		H	-1.44000	0.31600	-4.63400
H	-0.34600	5.27300	-3.22500		H	-3.17100	0.00300	-4.61200
H	1.35900	4.96000	-0.48300		H	-1.33400	-1.84400	-3.02600
H	-0.25100	4.86500	1.70100		H	-1.38100	-1.98600	-4.78100
H	-0.57300	6.50700	1.11700		H	-2.93900	-3.60000	-4.01300
H	1.20000	6.62000	2.78000		H	-3.87200	-2.28800	-4.72700

H	-4.39100	-1.42000	-2.41600
H	-5.02700	-3.03200	-2.78500
H	-2.57000	-3.58600	-1.65600

Λ-*N*-CTC

N	-5.27500	-0.98000	1.05800
C	-5.54600	-1.78100	-0.13100
C	-4.47900	-2.88300	-0.19000
O	-4.16900	-3.48300	0.86400
C	-6.96200	-2.39900	-0.04500
C	-7.38500	-3.23700	-1.25500
C	-8.79700	-3.81600	-1.08900
C	-9.28300	-4.62900	-2.28900
N	-8.48300	-5.85600	-2.48400
C	-5.19000	0.37500	1.07600
C	-4.96900	0.98300	2.45200
O	-5.31100	1.08100	0.05400
C	-3.80000	1.98300	2.53800
C	-2.39700	1.53500	2.17800
N	-1.87000	0.38800	2.60100
O	-1.66100	2.30000	1.45800
O	-0.58400	0.11700	2.20000
C	-2.36900	-0.53300	3.61100
C	-1.02600	2.98900	-1.46400
C	-1.59300	4.11300	-2.30000
C	-0.83800	5.43200	-2.14900
C	-1.11000	6.12400	-0.81900
O	-0.01500	3.16500	-0.68800
N	-1.54900	1.76700	-1.53500
O	-2.20600	6.02300	-0.23000
N	-0.09800	6.89200	-0.35100
C	-0.15500	7.63800	0.90500

C	1.25200	7.93900	1.42800
C	2.11000	6.70200	1.72900
C	1.65000	5.88400	2.93900
C	2.44600	4.58600	3.12800
C	2.90900	3.20800	1.07300
C	4.30600	3.76800	0.89900
C	5.05100	3.18500	-0.30300
N	2.14700	3.59400	2.09600
O	2.42900	2.36600	0.23500
C	5.74600	1.85400	-0.03400
O	6.17700	1.54000	1.09500
N	5.93100	1.07500	-1.13000
C	6.80300	-0.10200	-1.15200
C	6.14000	-1.45400	-0.85000
C	5.07500	-1.92400	-1.85700
C	3.66500	-1.34900	-1.63800
C	2.97600	-1.90700	-0.36900
N	2.35100	-0.87000	0.44400
C	2.66900	-0.45200	1.67000
O	1.98400	0.50500	2.17800
C	3.79100	-1.05100	2.46700
O	1.29000	-0.25100	-0.17700
O	0.86600	3.09400	2.16200
O	-0.93600	0.79500	-0.79300
C	-2.79000	1.36300	-2.19800
C	-2.65100	0.25800	-3.24900
C	-2.10600	-1.09000	-2.73800
C	-2.77600	-2.30800	-3.38700
C	-4.11100	-2.68400	-2.73000
N	-3.90700	-3.20600	-1.37400
Zr	0.39300	1.47800	0.80000
H	-5.12800	-1.50400	1.91800
H	-3.23200	-3.96900	-1.29400

H	0.76700	6.91900	-0.88400
H	5.56000	1.41100	-2.01400
H	-5.48900	-1.09500	-0.98400
H	-7.67000	-1.56700	0.09600
H	-7.00500	-3.01800	0.86600
H	-6.66600	-4.05900	-1.40400
H	-7.35300	-2.61700	-2.16800
H	-9.50500	-2.98600	-0.92100
H	-8.82800	-4.45300	-0.18800
H	-9.29600	-3.97300	-3.18300
H	-10.32600	-4.93800	-2.11000
H	-7.55300	-5.59700	-2.82500
H	-8.89700	-6.40100	-3.24600
H	-4.90100	0.19700	3.21300
H	-5.88500	1.54900	2.68400
H	-3.78500	2.40200	3.55900
H	-4.00100	2.82200	1.85900
H	-3.16100	-0.06100	4.20000
H	-1.53000	-0.76600	4.27900
H	-2.73100	-1.46400	3.15200
H	-2.64200	4.28000	-2.00900
H	-1.59700	3.81400	-3.35900
H	-1.18900	6.11700	-2.93900
H	0.24100	5.29300	-2.30100
H	-0.73200	7.03800	1.62200
H	-0.70400	8.58400	0.75800
H	1.14900	8.55500	2.33600
H	1.77500	8.56800	0.68700
H	3.15200	7.02600	1.89100
H	2.12200	6.05100	0.84000
H	0.58800	5.61200	2.84700
H	1.75200	6.48100	3.86000
H	2.19100	4.11900	4.09200

H	3.52800	4.77500	3.12300
H	4.89500	3.58200	1.81100
H	4.24100	4.86100	0.78700
H	5.85600	3.88700	-0.57800
H	4.39000	3.10500	-1.17700
H	7.60400	0.07300	-0.41800
H	7.26500	-0.13600	-2.15000
H	5.72800	-1.43200	0.17100
H	6.96100	-2.19000	-0.83000
H	5.01700	-3.02600	-1.82500
H	5.41000	-1.67200	-2.87900
H	3.04300	-1.56900	-2.51900
H	3.71600	-0.25500	-1.55400
H	3.69600	-2.43800	0.26200
H	2.18500	-2.62300	-0.63900
H	4.11000	-2.04300	2.13100
H	3.45900	-1.12400	3.51300
H	4.65800	-0.37300	2.43500
H	-3.22000	2.26100	-2.66100
H	-3.47800	1.04200	-1.40000
H	-2.04400	0.62100	-4.09400
H	-3.67000	0.11900	-3.64900
H	-2.23500	-1.14900	-1.64800
H	-1.01900	-1.12700	-2.89700
H	-2.10800	-3.18500	-3.34100
H	-2.96800	-2.12300	-4.45700
H	-4.62500	-3.44900	-3.33500
H	-4.77800	-1.81500	-2.68400

Λ-*N*-CTT

N	-5.44500	-0.39900	1.16400

C	-5.71300	-1.34200	0.08300
C	-4.56300	-2.35900	0.04500
O	-4.14900	-2.85500	1.11700
C	-7.05800	-2.05800	0.34900
C	-7.50100	-3.10200	-0.68500
C	-8.82900	-3.75300	-0.26800
C	-9.40300	-4.74800	-1.27500
N	-8.55000	-5.94700	-1.42800
C	-5.05800	0.89600	1.00000
C	-4.80200	1.63700	2.30500
O	-4.96100	1.44700	-0.11200
C	-3.47900	2.42700	2.36500
C	-2.18500	1.75300	1.95600
N	-1.87000	0.50100	2.26400
O	-1.34200	2.42300	1.25000
O	-0.72000	-0.00700	1.73200
C	-2.50800	-0.39900	3.20700
C	-1.00200	2.71500	-1.86400
C	-1.54400	3.86400	-2.68400
C	-0.84900	5.18700	-2.33800
C	-1.27100	5.72400	-0.97300
O	0.02600	2.89800	-1.11300
N	-1.54500	1.50300	-1.88100
O	-2.47200	5.72800	-0.62400
N	-0.27100	6.24400	-0.22000
C	-0.45900	6.80800	1.11500
C	0.09700	5.96400	2.28200
C	1.56200	6.24400	2.65600
C	2.63600	5.71500	1.68200
C	3.26500	4.37000	2.03700
C	2.43900	2.10300	2.69600
C	3.33100	2.03000	3.91200
C	4.82900	1.84000	3.61300

N	2.35100	3.22000	1.97400
O	1.70100	1.10700	2.35000
C	5.20100	0.40900	3.24200
O	4.68100	-0.57200	3.81100
N	6.17100	0.29600	2.29800
C	6.81100	-0.96600	1.93100
C	6.89900	-1.19300	0.42200
C	5.54500	-1.23300	-0.32200
C	5.22300	0.03100	-1.13100
C	3.95200	-0.08900	-1.97700
N	2.72300	-0.07200	-1.17800
C	2.03300	-1.09200	-0.68000
O	1.07400	-0.82400	0.14000
C	2.29900	-2.51900	-1.04100
O	2.33800	1.17500	-0.76100
O	1.50100	3.20400	0.90400
O	-0.95100	0.56400	-1.08000
C	-2.71600	1.04700	-2.62900
C	-2.40800	-0.01000	-3.70100
C	-2.07500	-1.44000	-3.20600
C	-3.18300	-2.47700	-3.44300
C	-4.40000	-2.36000	-2.51800
N	-4.01900	-2.70600	-1.14300
Zr	0.47000	1.32000	0.42300
H	-5.39200	-0.80000	2.09800
H	0.67500	6.13600	-0.57300
H	6.56500	1.15600	1.92400
H	-3.32000	-3.44600	-1.05900
H	-5.76200	-0.75200	-0.84000
H	2.98100	1.17700	4.50900
H	3.19700	2.93800	4.51900
H	-7.82800	-1.27400	0.43100
H	-6.98600	-2.54400	1.33800

H	-6.72500	-3.88000	-0.78800
H	-7.61500	-2.63000	-1.67700
H	-9.57700	-2.95800	-0.10400
H	-8.68800	-4.26400	0.70100
H	-9.58500	-4.22200	-2.23400
H	-10.38400	-5.09100	-0.91000
H	-7.71100	-5.69900	-1.96000
H	-9.04300	-6.62200	-2.02000
H	-4.90200	0.95000	3.15400
H	-5.61800	2.36900	2.41800
H	-3.36900	2.84000	3.38300
H	-3.54000	3.29400	1.69200
H	-3.23300	0.14000	3.82100
H	-1.72500	-0.79800	3.86400
H	-3.00200	-1.22700	2.67700
H	-2.62200	3.97900	-2.49000
H	-1.43300	3.64800	-3.75800
H	-1.15200	5.94000	-3.08500
H	0.24300	5.08400	-2.40300
H	-1.54400	6.92300	1.22800
H	-0.01200	7.81700	1.13200
H	-0.05100	4.89900	2.05100
H	-0.52300	6.20100	3.16300
H	1.75800	5.83200	3.66200
H	1.68600	7.33800	2.75300
H	3.48300	6.41900	1.64700
H	2.24600	5.65400	0.65800
H	3.68400	4.40600	3.05200
H	4.09100	4.17600	1.33400
H	5.39600	2.07000	4.53100
H	5.18500	2.54300	2.84800
H	6.22400	-1.75700	2.41300
H	7.82300	-0.99200	2.36900

H	7.42700	-2.15000	0.28500
H	7.55000	-0.42600	-0.02700
H	4.73400	-1.42000	0.40000
H	5.54800	-2.09200	-1.01300
H	6.05400	0.23700	-1.82500
H	5.13200	0.90500	-0.46700
H	3.97200	-1.00900	-2.57400
H	3.86900	0.76000	-2.67000
H	3.15600	-2.66100	-1.70700
H	1.39800	-2.93000	-1.52200
H	2.46300	-3.08600	-0.11400
H	-3.15100	1.93600	-3.10400
H	-3.44200	0.68200	-1.88500
H	-1.58100	0.36900	-4.32400
H	-3.29000	-0.04700	-4.36400
H	-1.81300	-1.40700	-2.13800
H	-1.16800	-1.78900	-3.72500
H	-2.77000	-3.49400	-3.32600
H	-3.54300	-2.41600	-4.48500
H	-5.19100	-3.04600	-2.86500
H	-4.81400	-1.34300	-2.54300

Λ-*N*-CCT

N	-5.27600	-1.00500	1.14400
C	-5.75000	-1.78900	0.00300
C	-4.66800	-2.83000	-0.32200
O	-4.19100	-3.51600	0.61000
C	-7.08000	-2.50400	0.33600
C	-7.60300	-3.42800	-0.77300
C	-8.90500	-4.14300	-0.38300
C	-9.45200	-5.08300	-1.46000
N	-8.56900	-6.24700	-1.68500

C	-4.96200	0.32100	1.10100		C	4.96400	-0.63700	-0.21900
C	-4.40700	0.89800	2.39900		C	3.90600	-1.14400	-1.20200
O	-5.16400	1.03500	0.09900		N	2.81800	-0.18500	-1.37100
C	-3.18100	1.82300	2.25400		C	2.60800	0.69500	-2.34800
C	-1.84400	1.38400	1.67500		O	1.66300	1.54700	-2.18800
N	-1.38500	0.13500	1.65200		C	3.43000	0.70400	-3.60000
O	-1.10300	2.30800	1.16800		O	1.99300	-0.09100	-0.27600
O	-0.19700	-0.09300	1.00200		O	2.16300	3.19900	0.04000
C	-1.87200	-1.04500	2.34800		O	-1.04700	1.06000	-1.34100
C	-1.18200	3.29900	-1.84800		C	-3.06900	1.75500	-2.40400
C	-1.83000	4.53500	-2.43300		C	-3.18700	0.62900	-3.43600
C	-1.11400	5.81600	-1.98600		C	-2.65900	-0.74900	-2.99700
C	-1.27200	6.07300	-0.49200		C	-3.40900	-1.92400	-3.64500
O	-0.07500	3.41700	-1.20700		C	-4.65200	-2.35300	-2.85400
N	-1.70900	2.08300	-1.97100		N	-4.26200	-3.00700	-1.60100
O	-2.39200	6.00400	0.05800		Zr	0.66300	1.61000	-0.09600
N	-0.14000	6.42100	0.16900		H	-5.90000	-1.07800	-0.81700
C	-0.07500	6.61700	1.61500		H	-5.00800	-1.54200	1.96600
C	0.98700	5.76100	2.32100		H	-3.57500	-3.75800	-1.69900
C	2.44000	6.26800	2.18700		H	6.87600	1.24400	2.27400
C	3.25000	5.81100	0.96200		H	0.73100	6.37700	-0.35000
C	3.89400	4.42800	1.10100		H	-7.82800	-1.72800	0.56600
C	2.64800	2.51500	2.17700		H	-6.92500	-3.09100	1.25800
C	3.40200	2.59400	3.48700		H	-6.83300	-4.18100	-1.00900
C	4.88700	2.19700	3.45700		H	-7.77100	-2.84700	-1.69700
N	2.93700	3.32400	1.15900		H	-9.67900	-3.39000	-0.15600
O	1.67900	1.68900	2.01400		H	-8.74100	-4.72300	0.54300
C	5.15300	0.71500	3.22600		H	-9.64000	-4.49900	-2.38500
O	4.38600	-0.17100	3.65300		H	-10.42700	-5.47300	-1.12700
N	6.30800	0.45100	2.56200		H	-7.72200	-5.94100	-2.17200
C	6.88400	-0.88000	2.38200		H	-9.02900	-6.88300	-2.34400
C	7.21200	-1.22800	0.92400		H	-4.25800	0.11200	3.14800
C	6.03600	-1.69400	0.05400		H	-5.21200	1.53600	2.80200

H	-2.97700	2.26300	3.24500		H	3.98000	-0.22700	-3.77300
H	-3.46800	2.66900	1.61200		H	4.15000	1.53600	-3.56400
H	-2.58700	-0.76700	3.12500		H	2.75900	0.88300	-4.45100
H	-1.00400	-1.51300	2.83100		H	-3.51000	2.67100	-2.81800
H	-2.32300	-1.76100	1.64600		H	-3.63200	1.48200	-1.49800
H	-2.88300	4.58700	-2.11800		H	-2.71300	0.93200	-4.38400
H	-1.82700	4.47800	-3.53300		H	-4.26900	0.55500	-3.64700
H	-1.57900	6.66800	-2.50800		H	-2.72900	-0.83600	-1.90200
H	-0.05500	5.79000	-2.27500		H	-1.58500	-0.81400	-3.22200
H	-1.07500	6.36800	1.99300		H	-2.74400	-2.80000	-3.73500
H	0.10800	7.68400	1.83900		H	-3.72100	-1.67000	-4.67200
H	0.88800	4.72100	1.97700		H	-5.26100	-3.05400	-3.44900
H	0.72300	5.76700	3.39100		H	-5.28400	-1.48500	-2.62800
H	3.00400	5.97600	3.09000					
H	2.41700	7.37000	2.20400		**Λ-*N*-TTT**			
H	4.08600	6.51100	0.80600					
H	2.65500	5.83300	0.03800		N	-4.37900	-2.66900	1.90100
H	4.50400	4.39900	2.01000		C	-5.26000	-2.65000	0.73600
H	4.55900	4.23500	0.24400		C	-4.45000	-2.45300	-0.55800
H	2.87100	1.93400	4.18400		O	-3.49900	-3.22000	-0.82300
H	3.32700	3.61600	3.89000		C	-6.02200	-3.99100	0.67200
H	5.31500	2.43400	4.44600		C	-6.71200	-4.31000	-0.66000
H	5.45700	2.79600	2.73300		C	-7.53600	-5.60200	-0.56100
H	6.16900	-1.59700	2.80800		C	-7.97100	-6.19200	-1.90400
H	7.80800	-0.93500	2.98000		N	-6.82800	-6.78400	-2.63400
H	7.96200	-2.03600	0.94700		C	-3.90700	-1.55900	2.53600
H	7.70800	-0.36200	0.45100		C	-2.97900	-1.84100	3.71200
H	5.56600	-2.57500	0.52800		O	-4.24400	-0.40400	2.21700
H	6.44500	-2.04500	-0.90900		C	-1.65600	-1.04800	3.71600
H	5.43000	0.27200	-0.63500		C	-0.75900	-0.98300	2.49400
H	4.45800	-0.34600	0.71200		N	-0.76300	-1.87900	1.50800
H	3.44800	-2.07600	-0.83500		O	0.00900	0.04500	2.37100
H	4.34700	-1.35400	-2.18400		O	-0.03500	-1.57200	0.39000

C	-1.10900	-3.29300	1.56400
C	-0.32400	1.85700	-1.80300
C	-0.54700	2.52000	-3.13300
C	0.42200	3.69600	-3.41100
C	0.09700	4.89700	-2.53600
O	0.63600	0.99500	-1.66200
N	-1.05800	2.13500	-0.73700
O	-0.87500	5.64200	-2.78000
N	0.89900	5.05100	-1.45100
C	0.68300	6.02100	-0.37900
C	2.00100	6.60100	0.14300
C	3.00300	5.56200	0.67100
C	2.57800	4.84800	1.96000
C	3.41300	3.60100	2.28400
C	3.70700	2.07900	0.28600
C	5.01200	2.67800	-0.18700
C	6.10000	1.64100	-0.49500
N	3.09400	2.47200	1.40400
O	3.13000	1.17900	-0.42100
C	6.92000	1.21700	0.72300
O	6.93900	1.87100	1.78600
N	7.64600	0.08700	0.53900
C	8.46100	-0.56700	1.56800
C	7.68400	-1.25300	2.70300
C	6.67500	-2.34700	2.30700
C	5.47800	-1.80600	1.51600
C	4.23400	-2.69300	1.50000
N	3.15900	-1.99500	0.78500
C	2.88100	-2.06900	-0.51500
O	2.07000	-1.21300	-1.03500
C	3.46000	-3.13800	-1.39100
O	2.60900	-0.96100	1.50200
O	1.87100	1.89300	1.66900
O	-0.74000	1.46000	0.40600
C	-2.15700	3.11300	-0.59800
C	-3.48300	2.71100	-1.24800
C	-4.01800	1.34100	-0.83900
C	-5.23100	0.93800	-1.67800
C	-5.82500	-0.41700	-1.28900
N	-4.83900	-1.49200	-1.42900
Zr	1.15200	0.26500	0.40300
H	-4.00200	-3.57200	2.17200
H	-5.96900	-1.82700	0.88100
H	-6.76100	-3.99100	1.49000
H	-5.30500	-4.80100	0.88500
H	-5.93900	-4.41500	-1.43900
H	-7.36500	-3.47700	-0.97300
H	-8.43300	-5.41000	0.05300
H	-6.94300	-6.36800	-0.03100
H	-8.50700	-5.42100	-2.49200
H	-8.68900	-7.00500	-1.71500
H	-6.22900	-6.03500	-2.99300
H	-7.18400	-7.25500	-3.47100
H	-2.81600	-2.92000	3.83200
H	-3.53100	-1.52600	4.61200
H	-1.05400	-1.38900	4.57300
H	-1.88800	0.00700	3.91800
H	-1.48400	-3.55900	2.55300
H	-0.18500	-3.86200	1.38400
H	-1.85000	-3.52800	0.78900
H	-1.58000	2.87500	-3.23800
H	-0.38500	1.74900	-3.89800
H	0.29000	4.00300	-4.45900
H	1.46500	3.37000	-3.28200
H	1.64000	4.36900	-1.32500
H	0.12000	5.53900	0.43900

H	0.04400	6.81600	-0.78500
H	1.75500	7.31900	0.94300
H	2.47600	7.17700	-0.66800
H	3.97200	6.06100	0.83700
H	3.20200	4.82000	-0.12000
H	1.52100	4.54100	1.91900
H	2.66900	5.54400	2.81000
H	3.21500	3.25800	3.30900
H	4.48800	3.80400	2.20400
H	5.40700	3.41300	0.52200
H	4.78600	3.21600	-1.12100
H	6.80300	2.07500	-1.22500
H	5.65800	0.75800	-0.98000
H	7.54100	-0.39600	-0.34800
H	9.13400	0.18600	2.00800
H	9.08500	-1.30300	1.04200
H	7.16100	-0.48300	3.29300
H	8.44400	-1.69300	3.37100
H	6.31200	-2.81400	3.23900
H	7.18100	-3.14500	1.73700
H	5.76400	-1.62400	0.47100
H	5.17200	-0.83500	1.93500
H	3.86400	-2.89300	2.51700
H	4.41400	-3.66100	1.01800
H	2.74700	-3.97200	-1.48500
H	4.41500	-3.53800	-1.03400
H	3.60900	-2.71100	-2.39100
H	-1.82500	4.08100	-0.99500
H	-2.27600	3.21800	0.48800
H	-3.38900	2.75500	-2.34500
H	-4.20600	3.50000	-0.97800
H	-4.27700	1.33300	0.23100
H	-3.22400	0.58600	-0.95500

H	-4.95200	0.92200	-2.74700
H	-6.03100	1.69100	-1.58000
H	-6.70400	-0.63800	-1.91900
H	-6.16200	-0.37900	-0.24700
H	-4.29900	-1.48800	-2.29700

Λ-*N*-TCC

N	-3.94000	-3.92700	1.13700
C	-5.17300	-3.42500	0.54100
C	-4.89100	-3.09300	-0.93200
O	-4.39700	-3.96900	-1.67600
C	-6.30100	-4.46600	0.65400
C	-7.65300	-3.96500	0.13700
C	-8.75800	-5.01900	0.26600
C	-10.14200	-4.52500	-0.15900
N	-10.19300	-4.19400	-1.59800
C	-3.14300	-3.18800	1.95900
C	-1.88600	-3.90500	2.42400
O	-3.43600	-2.04100	2.34200
C	-0.65200	-2.99800	2.54500
C	-0.21000	-2.11300	1.39700
N	-0.09500	-2.52200	0.13800
O	0.14200	-0.90400	1.67600
O	0.34100	-1.60600	-0.79100
C	-0.27500	-3.85600	-0.40900
C	-0.04700	1.55500	-2.13800
C	-0.28300	2.16700	-3.49100
C	0.76100	3.26200	-3.83400
C	0.43900	4.59900	-3.18300

O	0.96700	0.77000	-1.98300	C	-5.81600	-0.71100	-0.73500
N	-0.80900	1.82700	-1.08400	N	-5.18200	-1.85600	-1.39700
O	-0.11000	5.52000	-3.82500	Zr	1.43000	0.09000	0.09800
N	0.73900	4.69300	-1.86100	H	-3.58400	-4.81200	0.78300
C	0.36800	5.83200	-1.02200	H	-5.43900	-2.53000	1.11400
C	1.54500	6.51300	-0.31500	H	-6.38800	-4.74800	1.71500
C	2.36900	5.57100	0.57900	H	-6.00100	-5.37100	0.10000
C	3.48200	4.83400	-0.17400	H	-7.55200	-3.66400	-0.92000
C	4.08000	3.65700	0.58700	H	-7.94700	-3.06000	0.69700
C	3.03400	1.88200	1.99700	H	-8.81700	-5.35300	1.31600
C	3.82400	2.24700	3.23100	H	-8.49200	-5.90500	-0.33700
C	5.34900	2.03600	3.16100	H	-10.43500	-3.67500	0.49000
N	3.11700	2.57800	0.86900	H	-10.87500	-5.32800	0.02000
O	2.22600	0.86800	2.02100	H	-9.65300	-3.34000	-1.76700
C	5.79700	0.58200	3.13700	H	-11.15500	-3.94100	-1.84100
O	5.30100	-0.27800	3.89100	H	-1.70000	-4.79200	1.80500
N	6.81800	0.31100	2.28200	H	-2.09800	-4.29000	3.43600
C	7.54300	-0.96000	2.29600	H	0.20700	-3.62600	2.83600
C	6.94500	-2.07300	1.42200	H	-0.80900	-2.29900	3.37700
C	7.23600	-1.99100	-0.08900	H	-0.35200	-4.59700	0.39100
C	6.38500	-1.04500	-0.96000	H	0.60700	-4.08700	-1.02200
C	5.12700	-1.67200	-1.59800	H	-1.17100	-3.89000	-1.04700
N	3.90500	-1.51900	-0.80700	H	-1.29900	2.56600	-3.60300
C	3.45600	-2.26800	0.19900	H	-0.17700	1.35200	-4.22300
O	2.52200	-1.78400	0.93100	H	0.76200	3.42500	-4.91900
C	3.94400	-3.66200	0.44100	H	1.76100	2.91100	-3.54000
O	3.29000	-0.29900	-0.97000	H	1.15900	3.88300	-1.39900
O	2.33900	2.16600	-0.17700	H	-0.35200	5.48300	-0.26100
O	-0.46900	1.22900	0.09700	H	-0.15400	6.54500	-1.67300
C	-1.97300	2.73200	-1.03700	H	1.11400	7.32300	0.29600
C	-3.29300	2.16300	-1.55700	H	2.19800	6.99500	-1.06100
C	-3.82600	0.92500	-0.83400	H	1.69100	4.84100	1.05500
C	-5.25800	0.60400	-1.27700	H	2.82300	6.14500	1.40300

H	4.31200	5.53000	-0.37700
H	3.13900	4.48400	-1.15600
H	4.47500	4.00100	1.54900
H	4.91000	3.22200	0.00800
H	3.42000	1.63200	4.04600
H	3.63300	3.29900	3.49500
H	5.78100	2.46700	4.07900
H	5.79900	2.58900	2.32700
H	7.20100	1.07800	1.73600
H	7.56400	-1.30300	3.34100
H	8.57900	-0.74700	1.99100
H	5.86700	-2.12100	1.62500
H	7.37500	-3.01800	1.79500
H	7.15700	-3.00700	-0.51400
H	8.29600	-1.71000	-0.21200
H	7.00700	-0.69700	-1.79900
H	6.09000	-0.14200	-0.40500
H	4.90500	-1.18200	-2.55600
H	5.28200	-2.73800	-1.81200
H	4.37800	-3.73900	1.44800
H	4.67900	-4.00900	-0.29400
H	3.07000	-4.33100	0.41400
H	-1.71900	3.64200	-1.59500
H	-2.06400	3.01400	0.02000
H	-3.21200	1.95000	-2.63600
H	-4.02800	2.98300	-1.46500
H	-3.81300	1.09400	0.25600
H	-3.16400	0.06600	-1.02500
H	-5.31500	0.58300	-2.38000
H	-5.93100	1.41500	-0.95400
H	-6.90700	-0.74600	-0.89900
H	-5.64000	-0.77200	0.34700
H	-5.01700	-1.74700	-2.39900

Λ-*N*-TTC

N	-4.19000	-2.83300	1.96300
C	-5.06900	-2.93200	0.80000
C	-4.22500	-2.92200	-0.48500
O	-3.32400	-3.77800	-0.64300
C	-5.88400	-4.23600	0.88700
C	-6.74800	-4.53600	-0.34200
C	-7.56000	-5.82600	-0.17100
C	-8.34500	-6.24500	-1.41400
N	-7.44900	-6.66600	-2.51200
C	-3.74500	-1.65500	2.48300
C	-2.77600	-1.79800	3.65000
O	-4.13300	-0.54500	2.07500
C	-1.57000	-0.84700	3.60500
C	-0.69400	-0.69900	2.37700
N	-0.50400	-1.62800	1.44600
O	-0.08900	0.42800	2.22700
O	0.26400	-1.27200	0.36700
C	-0.74200	-3.06200	1.51300
C	0.18500	2.09000	-2.05700
C	0.18800	2.78700	-3.38900
C	1.06100	4.06500	-3.38900
C	0.44400	5.17400	-2.54600
O	1.20400	1.37900	-1.68600
N	-0.81200	2.22300	-1.19600
O	-0.55100	5.81800	-2.94100
N	1.02400	5.37400	-1.33600
C	0.52700	6.29100	-0.31200
C	1.66300	7.00000	0.43100
C	2.65600	6.06400	1.13900

C	2.08000	5.29300	2.33400
C	2.93600	4.09000	2.75300
C	3.71100	2.62100	0.84900
C	5.07900	3.25800	0.73300
C	6.05400	2.41400	-0.08700
N	2.84400	2.99000	1.79300
O	3.34200	1.70700	0.03600
C	6.57600	1.19400	0.66100
O	6.67600	1.17300	1.90500
N	6.98500	0.16700	-0.12700
C	7.67000	-1.01400	0.39400
C	6.77100	-2.21700	0.71300
C	6.29500	-3.04900	-0.49100
C	5.09400	-2.54900	-1.31800
C	3.69900	-2.83400	-0.72700
N	3.12300	-1.74200	0.06500
C	3.09200	-1.59600	1.38600
O	2.57100	-0.52200	1.87900
C	3.58800	-2.64600	2.33200
O	2.58000	-0.74400	-0.70200
O	1.61900	2.36100	1.77200
O	-0.67300	1.58200	-0.00000
C	-2.06200	2.98300	-1.36900
C	-3.18100	2.23100	-2.09000
C	-3.69800	0.97800	-1.38000
C	-4.86400	0.33900	-2.13900
C	-5.45700	-0.89800	-1.45900
N	-4.49400	-2.00300	-1.44000
Zr	1.30500	0.65700	0.44100
H	-3.74900	-3.69400	2.27500
H	-5.74500	-2.07100	0.83800
H	-6.51600	-4.17400	1.78800
H	-5.18000	-5.07100	1.03800

H	-6.09300	-4.62200	-1.22500
H	-7.43600	-3.69500	-0.53800
H	-8.26800	-5.69700	0.66600
H	-6.88000	-6.65000	0.10900
H	-9.03000	-5.42300	-1.70500
H	-8.97600	-7.11100	-1.15700
H	-6.97800	-5.84400	-2.90000
H	-8.01900	-7.02500	-3.28400
H	-2.47600	-2.84500	3.78900
H	-3.34600	-1.53400	4.55600
H	-0.91000	-1.08300	4.45600
H	-1.92900	0.17600	3.78200
H	-1.10400	-3.34700	2.50200
H	0.22400	-3.55800	1.34700
H	-1.45600	-3.37300	0.73800
H	-0.82900	3.03700	-3.71500
H	0.60200	2.08100	-4.12400
H	1.13100	4.43500	-4.42200
H	2.07800	3.81800	-3.05100
H	1.79900	4.76500	-1.08800
H	-0.11300	5.73500	0.39400
H	-0.11200	7.02500	-0.82000
H	1.20600	7.68000	1.16900
H	2.21300	7.63000	-0.28600
H	3.52200	6.65700	1.47700
H	3.06600	5.35300	0.40200
H	1.06900	4.91600	2.11700
H	1.98700	5.96600	3.20100
H	2.60100	3.69400	3.72300
H	3.99300	4.37000	2.85200
H	5.50100	3.43800	1.73000
H	4.97300	4.24200	0.25000
H	6.93300	3.03600	-0.32600

H	5.60100	2.11600	-1.04300		C	-5.33100	-4.34800	0.84600
H	6.87800	0.26600	-1.13300		C	-6.47800	-4.34800	-0.17000
H	8.17900	-0.69900	1.31600		C	-7.09500	-5.74200	-0.33000
H	8.44300	-1.30400	-0.33600		C	-8.21000	-5.82100	-1.37200
H	5.92800	-1.86900	1.32400		N	-7.69900	-5.59900	-2.74100
H	7.36900	-2.87900	1.36300		C	-2.98100	-2.14400	2.68600
H	6.05600	-4.06800	-0.14000		C	-1.76900	-2.53400	3.51600
H	7.15300	-3.17200	-1.17500		O	-3.45600	-0.99300	2.70200
H	5.12500	-3.07200	-2.28800		C	-0.54200	-1.62200	3.30700
H	5.17100	-1.47600	-1.54700		C	-0.10900	-1.20100	1.91800
H	3.71200	-3.74700	-0.11900		N	-0.16500	-1.97900	0.84200
H	2.97900	-2.99900	-1.54000		O	0.34500	-0.00400	1.76700
H	2.73600	-2.99400	2.93800		O	0.18000	-1.41400	-0.35700
H	4.31400	-2.19800	3.02600		C	-0.32300	-3.42100	0.75800
H	4.05100	-3.51100	1.84800		C	-0.26600	1.87600	-2.36200
H	-1.83000	3.91700	-1.89800		C	-0.62700	2.40900	-3.72300
H	-2.36500	3.25000	-0.34700		C	0.52900	3.17400	-4.39500
H	-2.85100	1.96900	-3.11000		C	0.60600	4.63900	-3.98600
H	-4.00600	2.95300	-2.21100		O	0.54000	0.86900	-2.26300
H	-4.01900	1.23300	-0.35700		N	-0.72400	2.42100	-1.24100
H	-2.87800	0.25100	-1.26300		O	-0.36000	5.22500	-3.44500
H	-4.54700	0.07100	-3.16300		N	1.75200	5.31900	-4.24600
H	-5.68100	1.07300	-2.25500		C	2.94500	4.91900	-4.99800
H	-6.37200	-1.20900	-1.99000		C	4.23600	5.46400	-4.36600
H	-5.73100	-0.64600	-0.42800		C	4.84600	4.59700	-3.25500
H	-3.92700	-2.11500	-2.28300		C	3.92800	4.31800	-2.06300
					C	4.57300	3.35800	-1.05700
					C	3.33900	2.49600	0.96800
Λ-*N*-TCT					C	4.20400	3.25700	1.94500
					C	5.64400	2.72500	2.11600
N	-3.51200	-3.15200	1.94500		N	3.56200	2.58100	-0.33900
C	-4.62400	-2.99500	1.00800		O	2.35800	1.75700	1.36400
C	-4.07400	-2.51800	-0.35000		C	5.78900	1.58200	3.11700
O	-3.33000	-3.27200	-1.01600					

O	5.10200	1.52300	4.15800
N	6.75500	0.68000	2.80700
C	7.17100	-0.42400	3.67400
C	7.51400	-1.71100	2.91100
C	6.32600	-2.53800	2.39500
C	5.52900	-1.87200	1.27100
C	4.31000	-2.68800	0.83100
N	3.39100	-1.85900	0.05000
C	3.16900	-1.84500	-1.26100
O	2.44100	-0.89700	-1.74200
C	3.74100	-2.88800	-2.17500
O	2.85700	-0.83100	0.77900
O	2.74100	1.86100	-1.15900
O	-0.28500	1.86800	-0.06800
C	-1.79000	3.42600	-1.09900
C	-3.20000	2.86500	-1.31300
C	-3.55500	1.64700	-0.46000
C	-4.95600	1.10700	-0.77800
C	-5.25300	-0.25800	-0.15800
N	-4.42000	-1.29000	-0.79400
Zr	1.37300	0.42600	-0.21700
H	-3.02500	-4.04400	1.92600
H	-5.31200	-2.25600	1.43600
H	-5.70400	-4.65700	1.83600
H	-4.57600	-5.08800	0.53200
H	-6.09300	-4.00000	-1.14300
H	-7.25800	-3.63100	0.14200
H	-7.49800	-6.07300	0.64300
H	-6.30100	-6.45900	-0.60800
H	-9.01700	-5.11400	-1.09000
H	-8.65100	-6.83000	-1.34600
H	-7.44700	-4.61300	-2.85200
H	-8.46300	-5.74900	-3.40600
H	-1.51600	-3.59100	3.36900
H	-2.06000	-2.43600	4.57400
H	0.32300	-2.08200	3.81500
H	-0.71400	-0.66900	3.82200
H	-0.43000	-3.85900	1.75300
H	0.58500	-3.82900	0.29200
H	-1.19700	-3.65800	0.13500
H	-1.51200	3.05500	-3.68600
H	-0.87300	1.53500	-4.34400
H	0.38300	3.15500	-5.48800
H	1.48200	2.65900	-4.20800
H	1.69600	6.31000	-4.00600
H	2.98300	3.82300	-5.06200
H	2.85500	5.29900	-6.03000
H	4.04700	6.48600	-3.99400
H	4.98300	5.56600	-5.17000
H	5.77800	5.07400	-2.90600
H	5.14600	3.63000	-3.69700
H	3.00300	3.84200	-2.41200
H	3.64100	5.25500	-1.55900
H	5.19500	3.89000	-0.32900
H	5.21200	2.62900	-1.58300
H	3.69200	3.22600	2.91600
H	4.25200	4.31100	1.63600
H	6.26400	3.55000	2.50500
H	6.08900	2.44200	1.15200
H	7.29600	0.83800	1.96000
H	6.35200	-0.59400	4.38600
H	8.05300	-0.10800	4.25900
H	8.19900	-1.47000	2.07900
H	8.09700	-2.33700	3.60500
H	6.71000	-3.51300	2.04900
H	5.65000	-2.75700	3.24000

H	6.18200	-1.69100	0.40100
H	5.15600	-0.89700	1.60700
H	3.74200	-3.03200	1.71000
H	4.59200	-3.56800	0.24100
H	4.69600	-2.54300	-2.59800
H	3.03800	-3.04000	-3.00500
H	3.90900	-3.84900	-1.67600
H	-1.58200	4.24200	-1.80400
H	-1.67100	3.81500	-0.08000
H	-3.33200	2.60700	-2.37700
H	-3.90500	3.69000	-1.11000
H	-3.49300	1.90200	0.61100
H	-2.80600	0.85700	-0.62800
H	-5.08500	1.03400	-1.87300
H	-5.72400	1.81500	-0.42700
H	-6.32000	-0.50300	-0.29200
H	-5.03000	-0.24100	0.91800
H	-4.05200	-1.06800	-1.72000

SUPPLEMENTARY I: Supporting Information

DFO2: A High-Denticity Chelator Based on Desferrioxamine for Enhanced Coordination of Zirconium-89

Elaheh Khozeimei Sarbisheh[⊥,1], Akam K. Salih[⊥,1], Shvan J. Raheem[1], Jason S. Lewis[2,3,4,5], Eric W. Price*,[1]

[1] Department of Chemistry, University of Saskatchewan, Saskatoon, SK, Canada

[2] Department of Radiology, Memorial Sloan Kettering Cancer Center, NY, USA

[3] Radiochemistry and Molecular Imaging Probes Core, Memorial Sloan Kettering Cancer Center, New York, NY, USA

[4] Department of Pharmacology, Weill Cornell Medical College, New York, NY, USA

[5] Molecular Pharmacology Program, Memorial Sloan Kettering Cancer Center, New York, NY, USA

[6] Department of Radiology, Weill Cornell Medical College, New York, NY, USA

*Corresponding author

Eric W. Price, Department of Chemistry, 110 Science Place, University of Saskatchewan, SK, S7N-5C9, Canada, Email: eric.price@usask.ca, Phone: +1.306.966.4788, Fax: +1.306.966.4666

These authors contributed equally to this work

Key words: [89]Zr, zirconium-89, DFO, desferrioxamine, antibody, chelator conjugation, radiometals, PET, immuno-PET, radioimmunotherapy, dosimetry
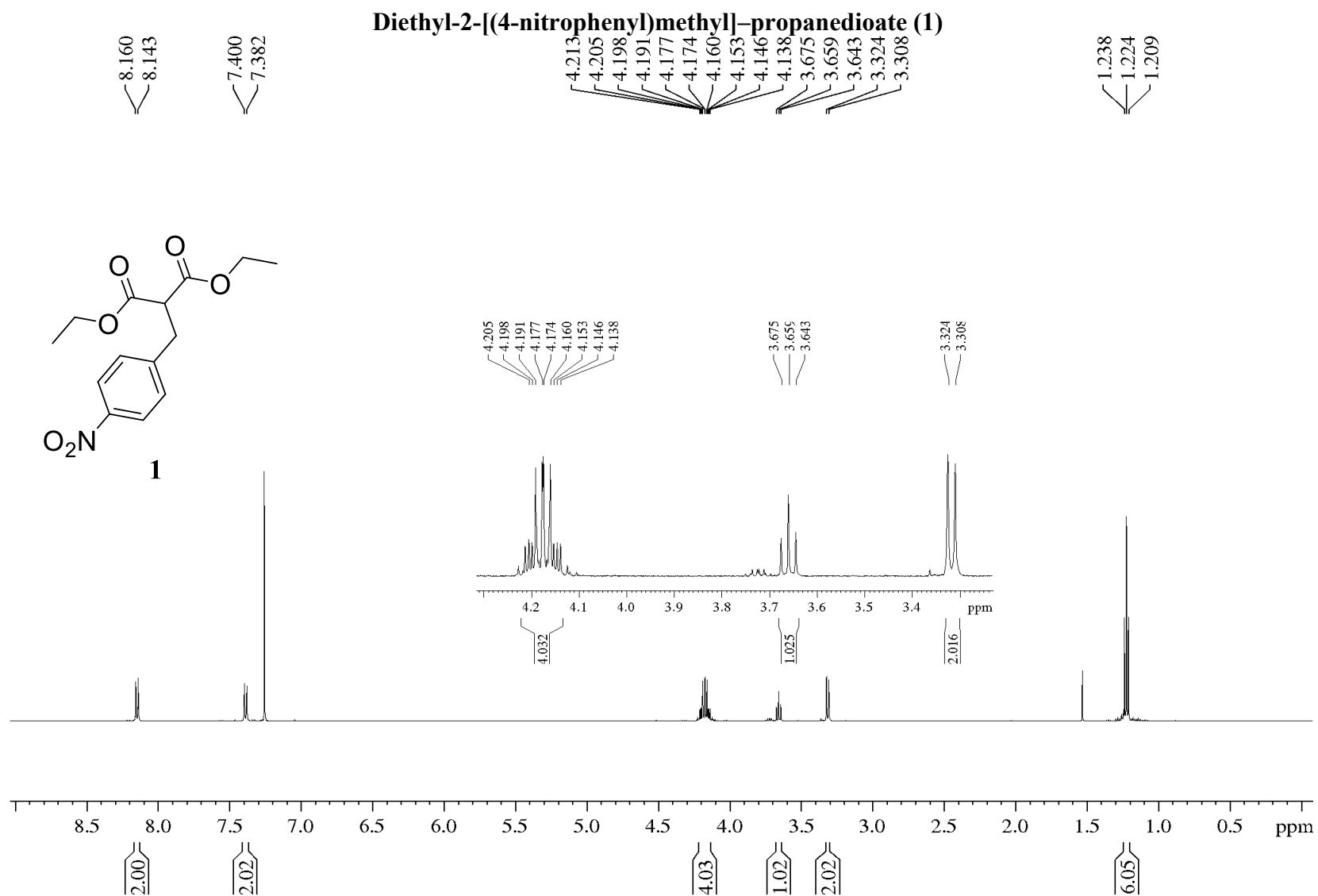
Disclosures: None.

Diethyl-2-[(4-nitrophenyl)methyl]–propanedioate (1)

Figure S 1. ^{1}H NMR spectrum of compound **1** in CDCl$_3$.
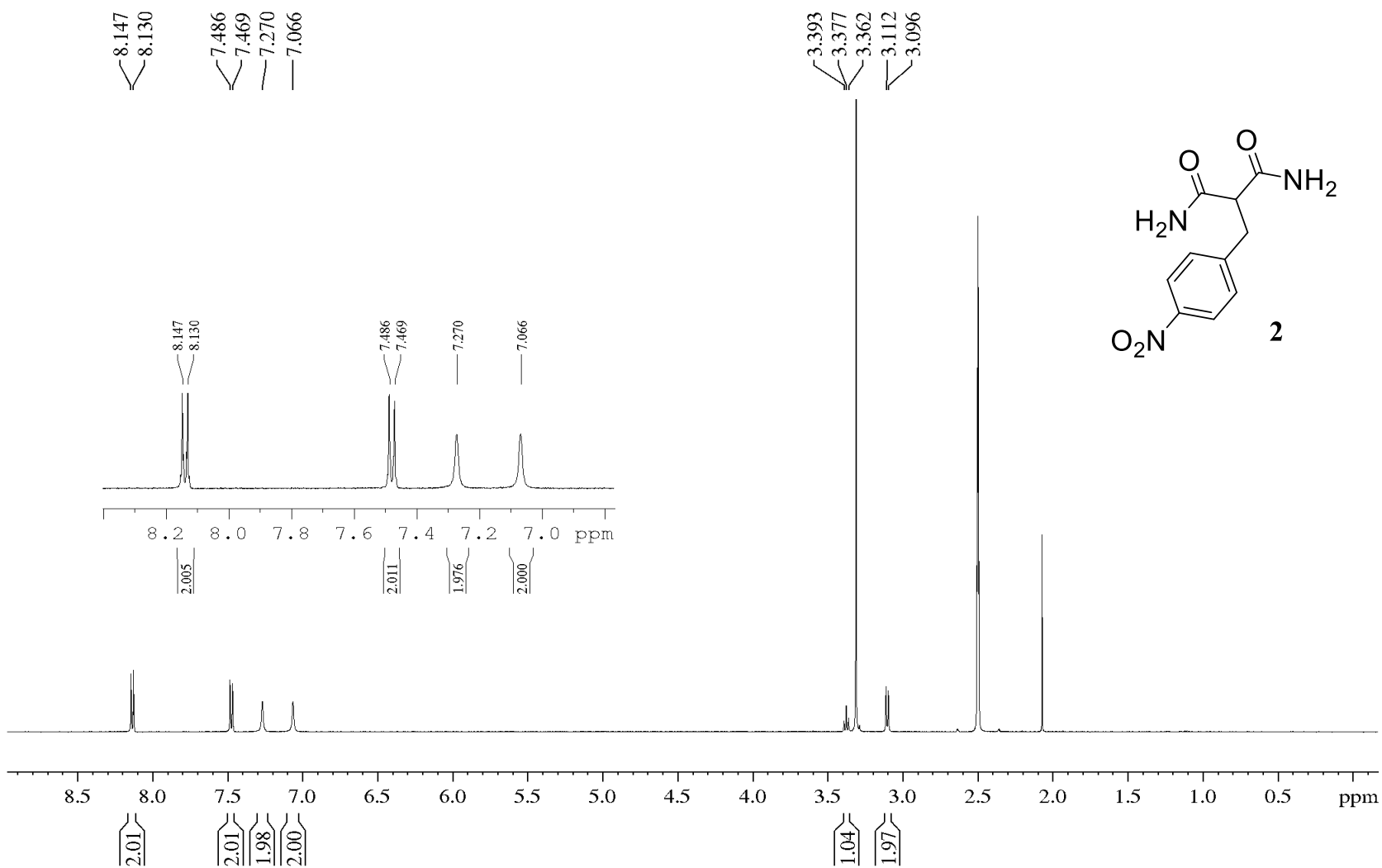
2-(4-nitrobenzyl) malonamide (2)

Figure S2. ^{1}H NMR spectrum of compound **2** in $(CD_3)_2SO$. Signals at 3.31, 250 and 2.07 ppm are assigned for residual H_2O, DMSO and acetonitrile respectively in the NMR sample.

(2-(p-nitrobenzyl)-1,3-propylenediamine (3)
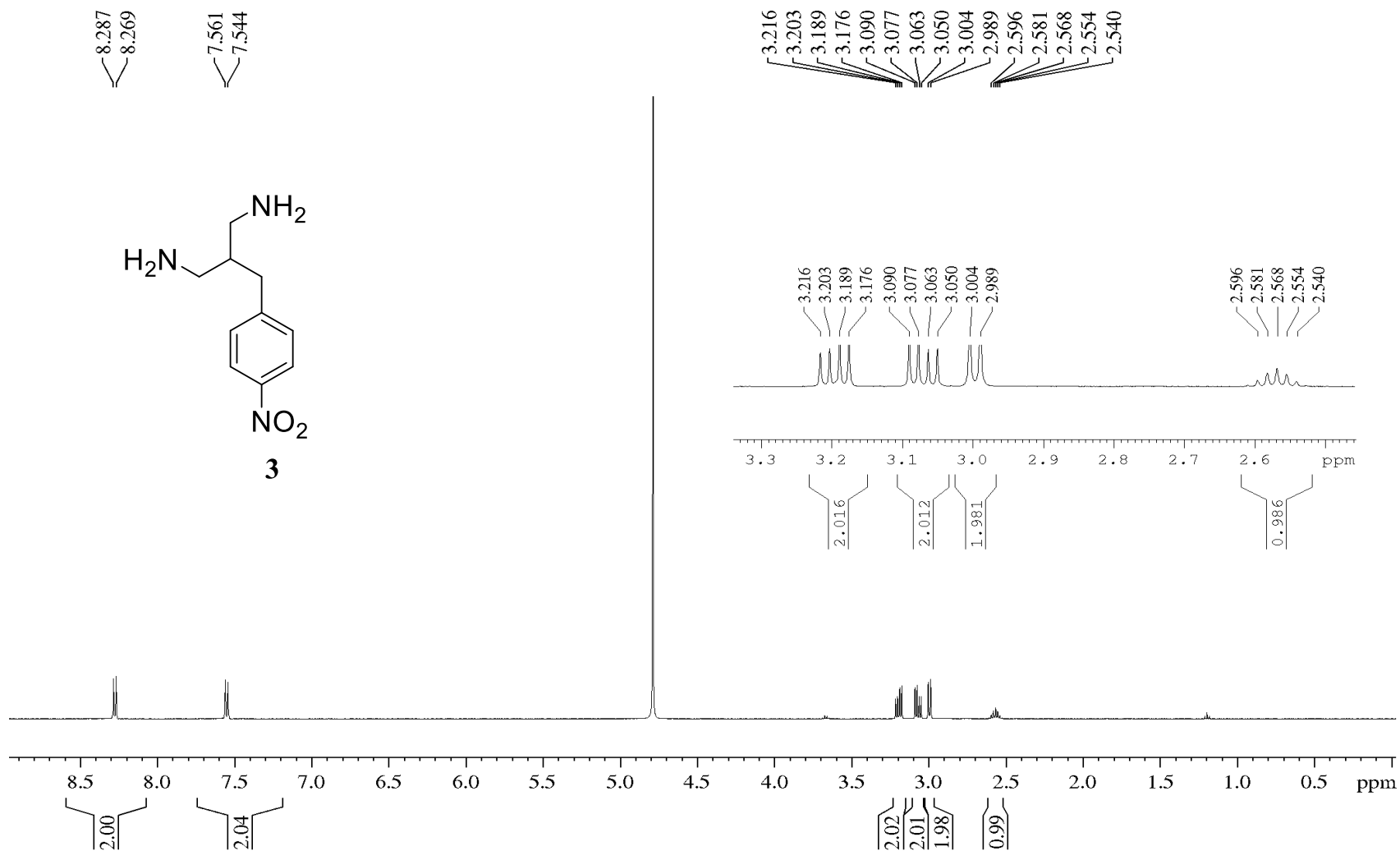

Figure S3. ^{1}H NMR spectrum of compound **3** in D_2O. Signals at 3.56 and 1.17 ppm are assigned for residual diethyl ether in the NMR sample.

DFO-COOH
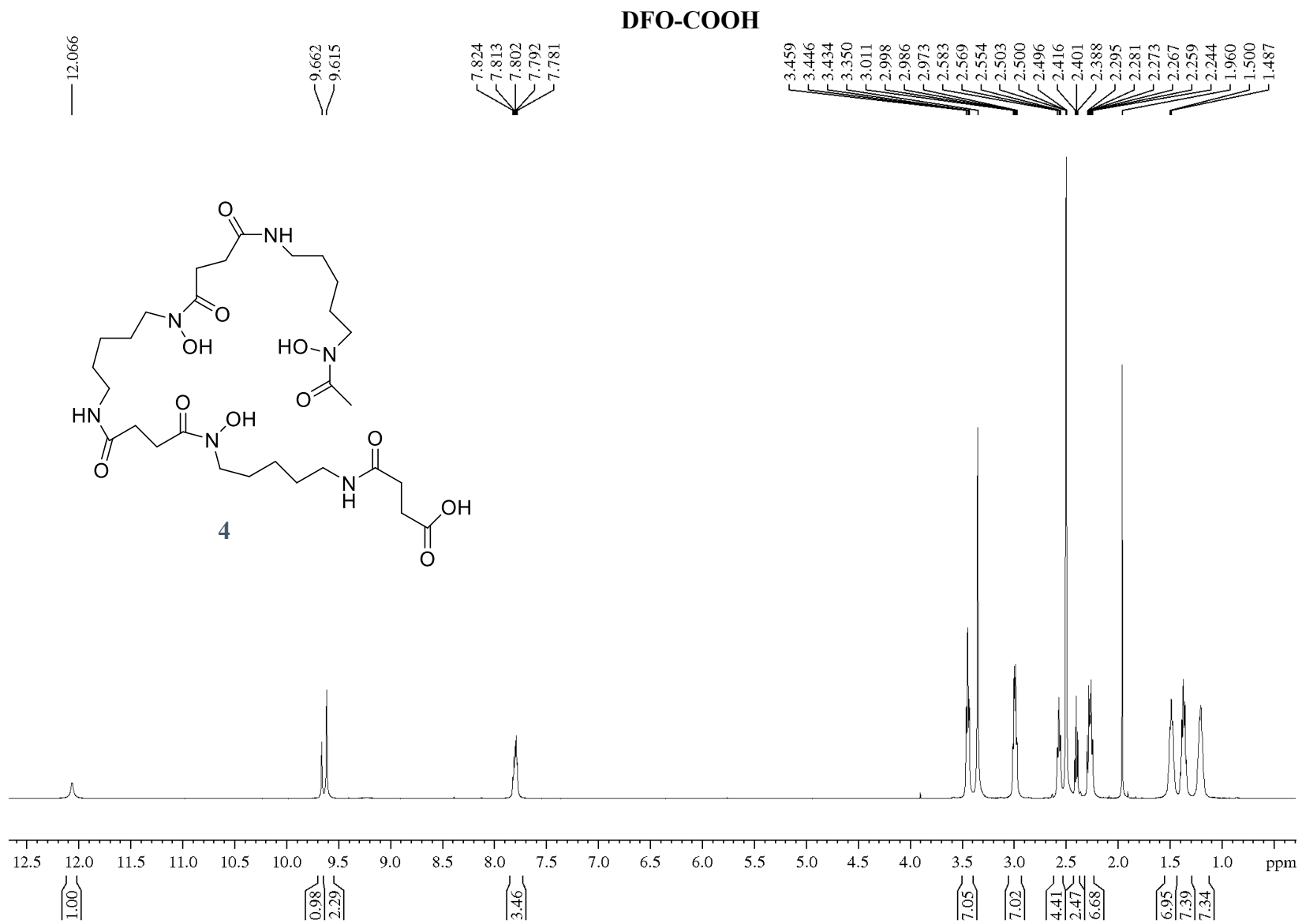
Figure S4. ^{1}H NMR spectrum of compound **4** in $(CD_3)_2SO$.
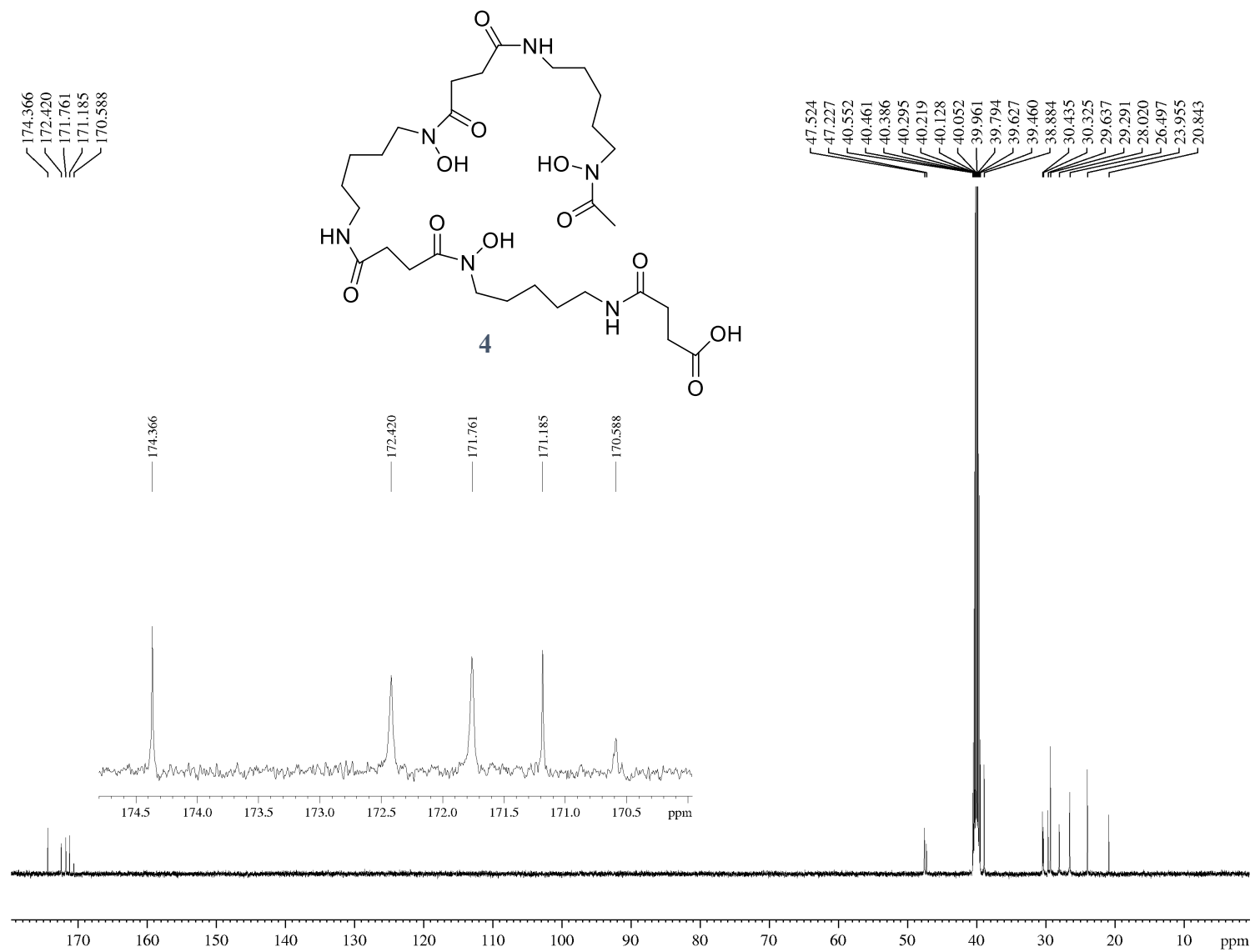
Figure S5. UDEFT-^{13}C{1H} NMR spectrum of compound **4** in (CD$_3$)$_2$SO.

Figure S6. ^{1}H NMR spectrum of **DFO2** (**5**) in $(CD_3)_2SO$.
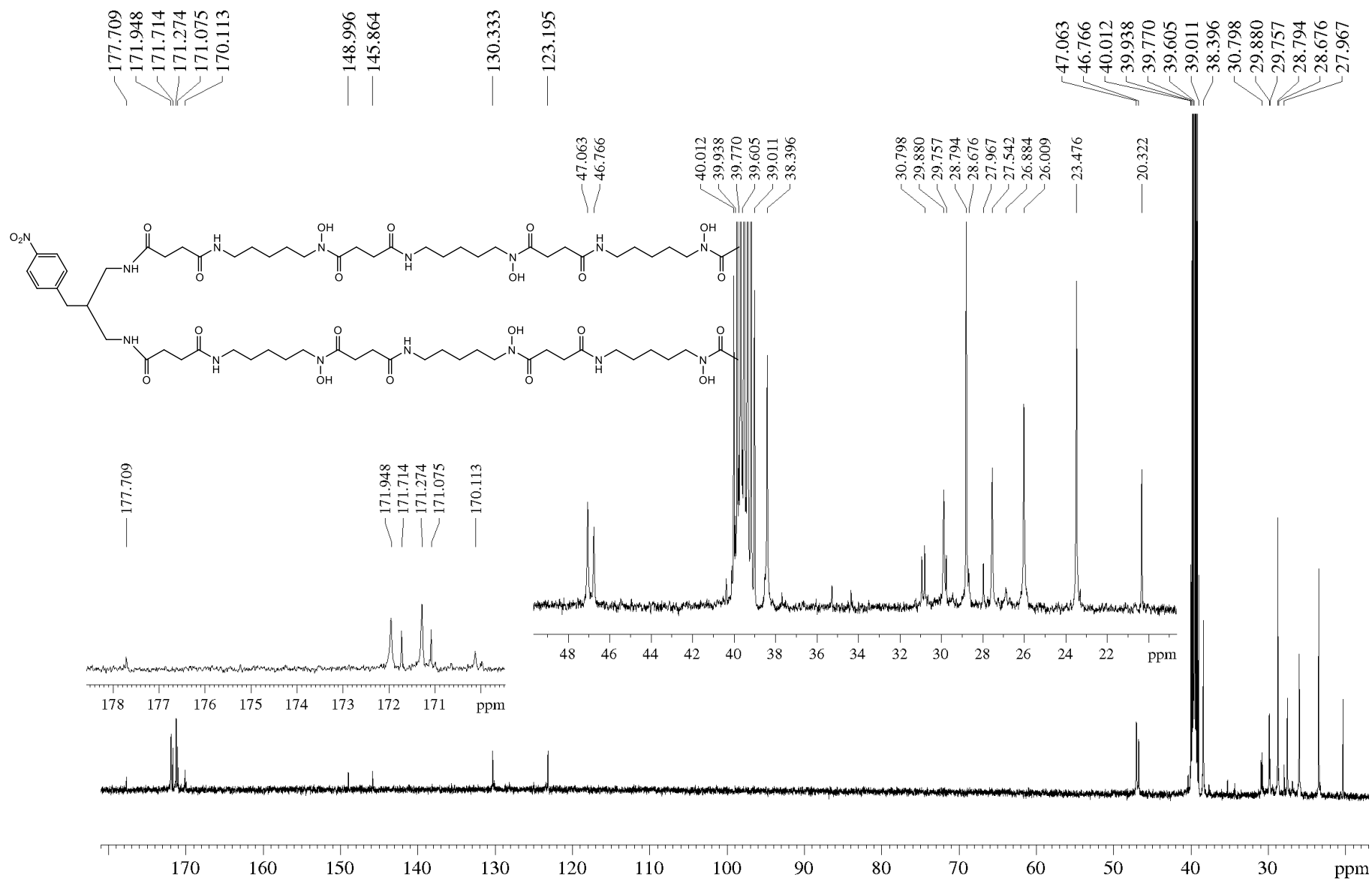
Figure S7. UDEFT-^{13}C{1H} NMR spectrum of **DFO2** (**5**) in $(CD_3)_2SO$.
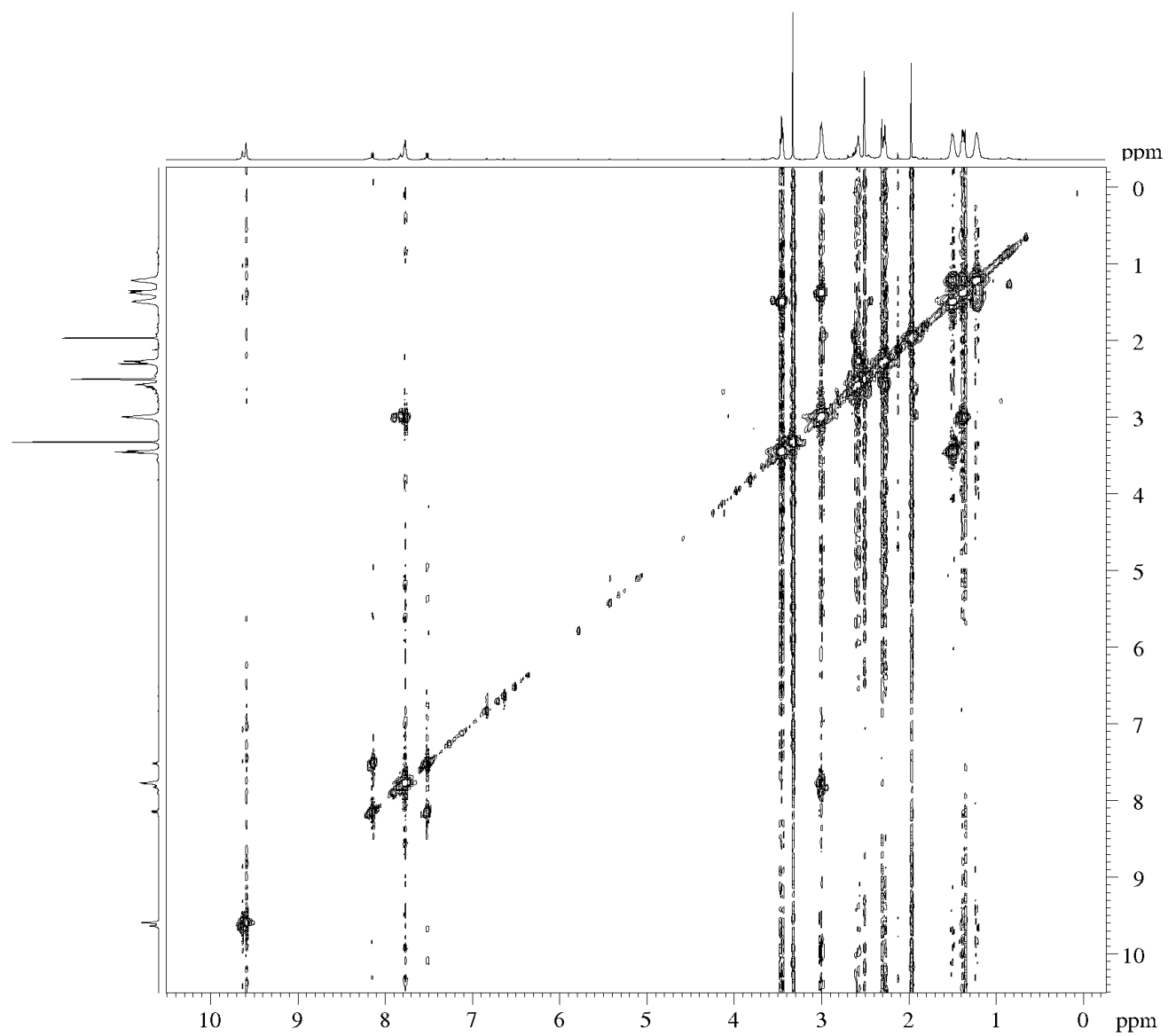
Figure S8. Cosy-NMR spectrum of **DFO2** (5) in $(CD_3)_2SO$.

Zr(DFO2)
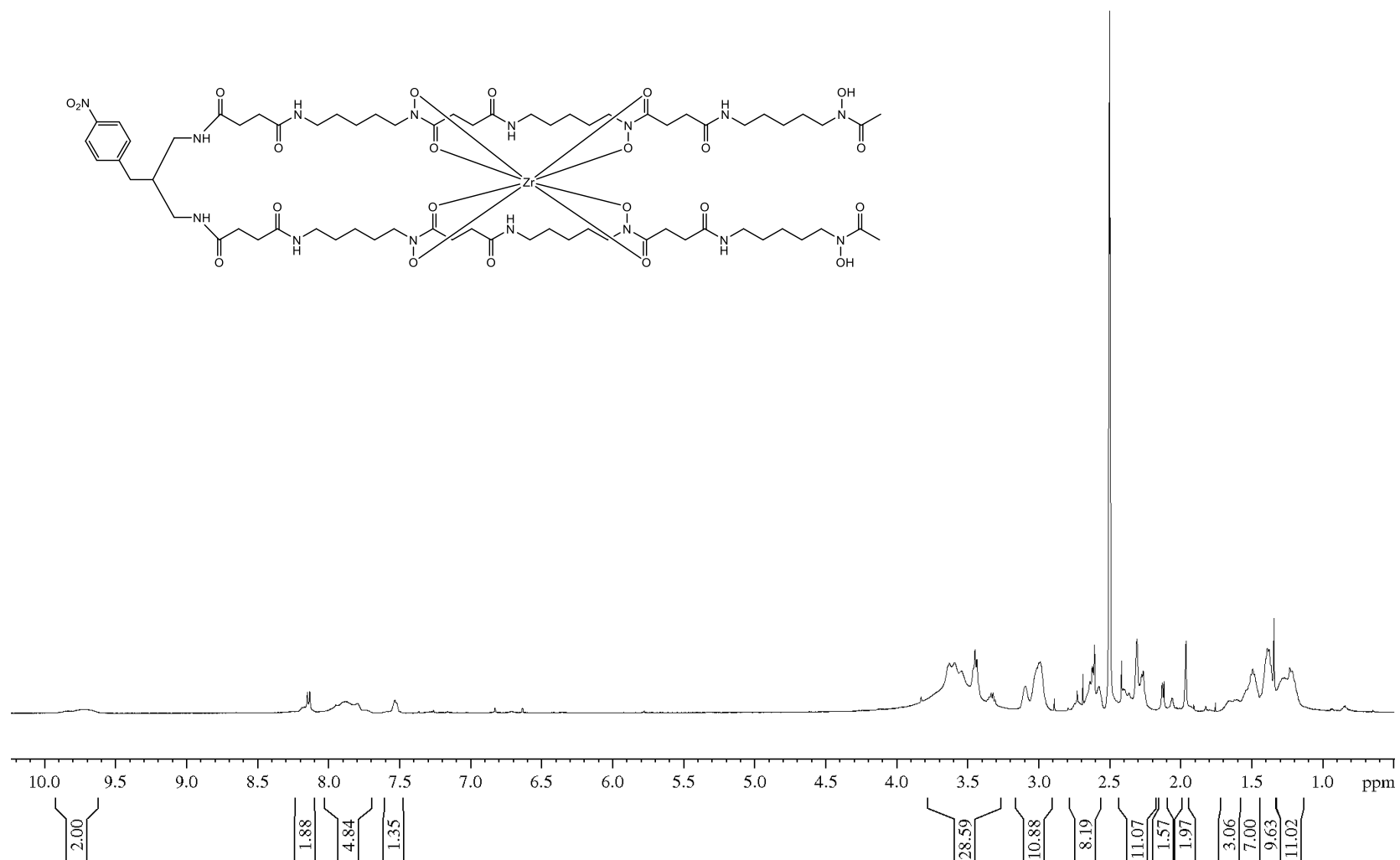
Figure S9. ^{1}H NMR spectrum of **Zr(DFO2)** (**6**) in $(CD_3)_2SO$
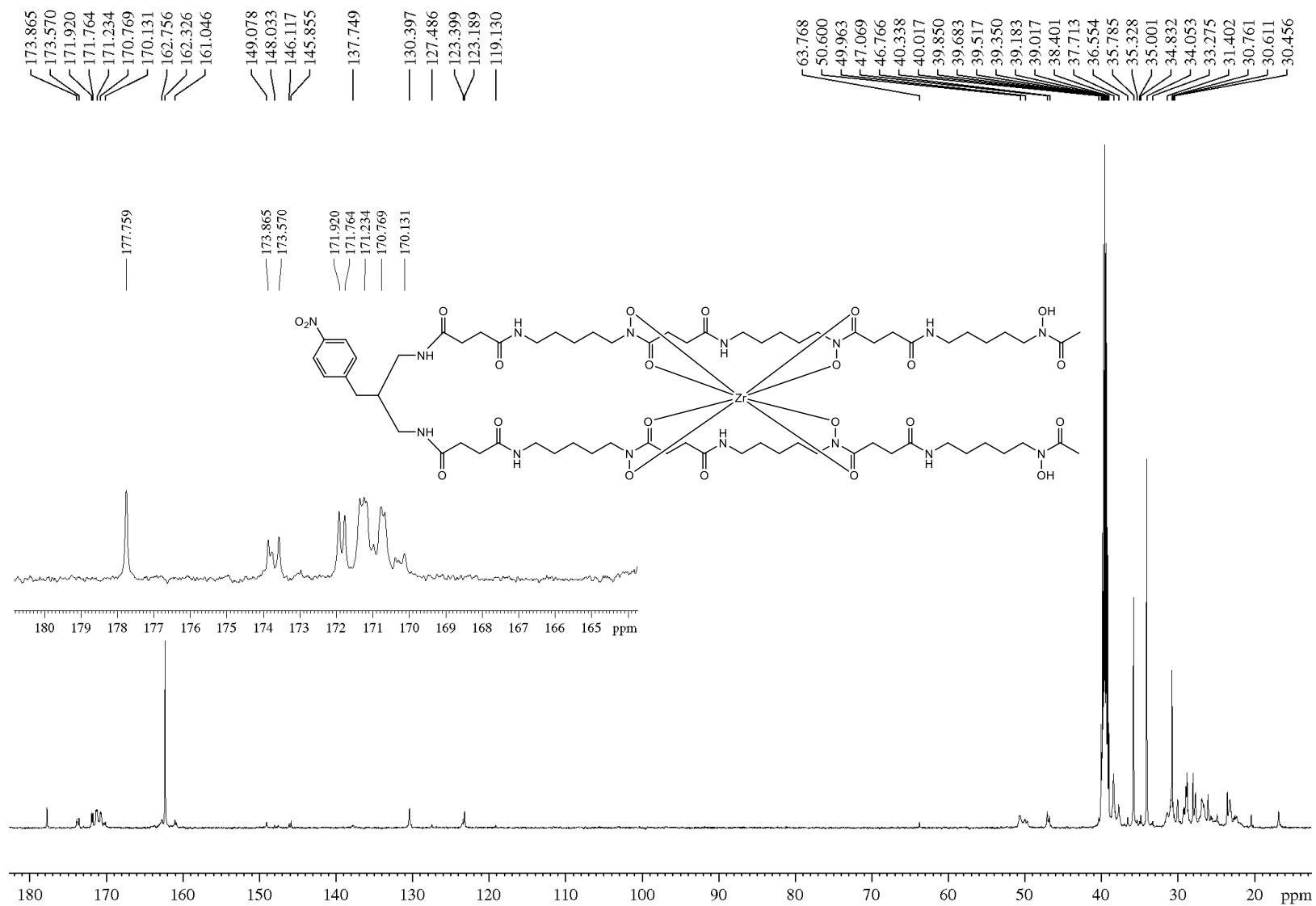
Figure S10. UDEFT-^{13}C{^{1}H} NMR spectrum of **Zr(DFO2)** (6) in $(CD_3)_2SO$. Signals at 30.8, 35.8, and 162.3 ppm are assigned for residual DMF in the NMR sample.
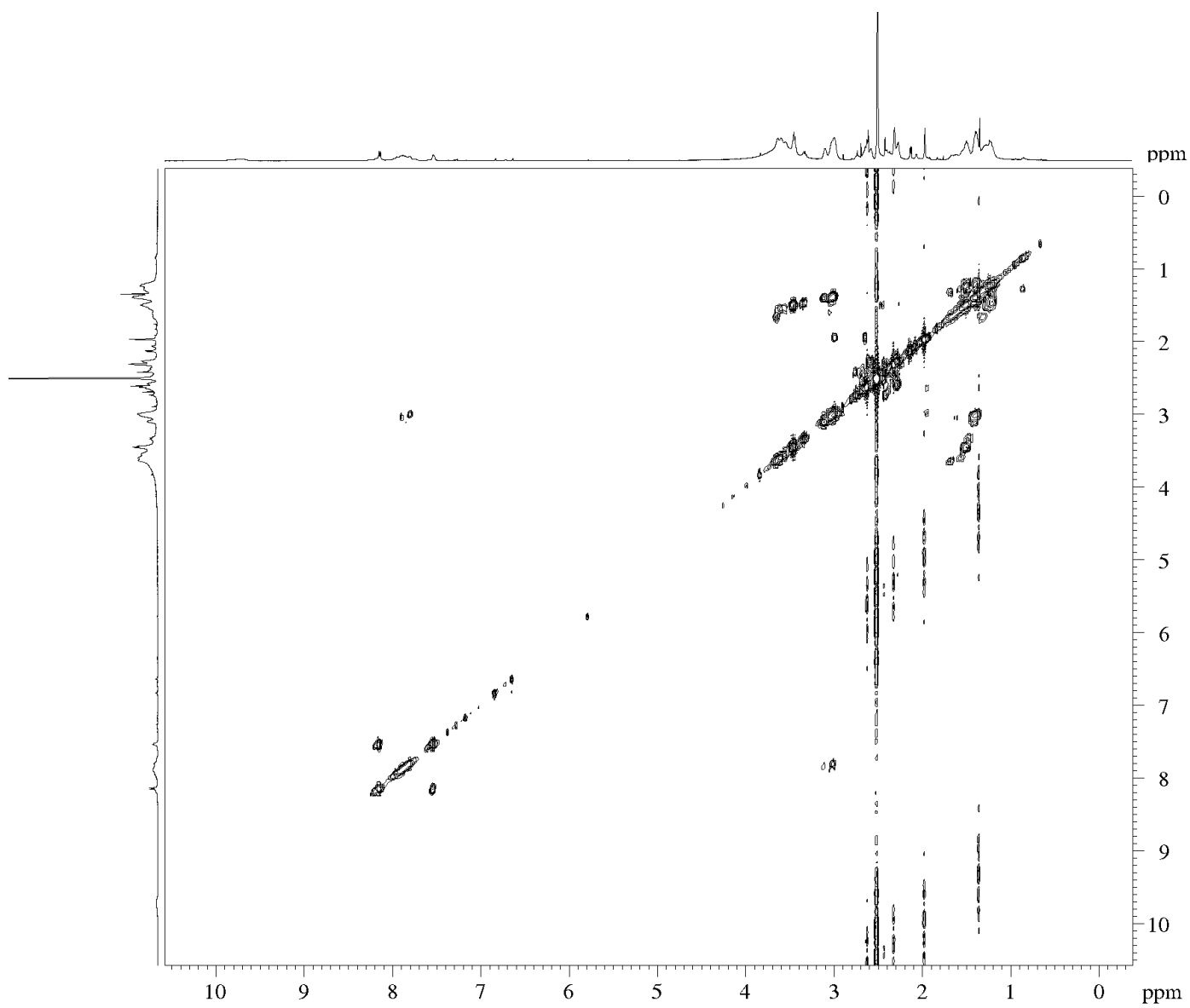
Figure S11. Cosy-NMR spectrum of **Zr(DFO2)** (6) in $(CD_3)_2SO$.
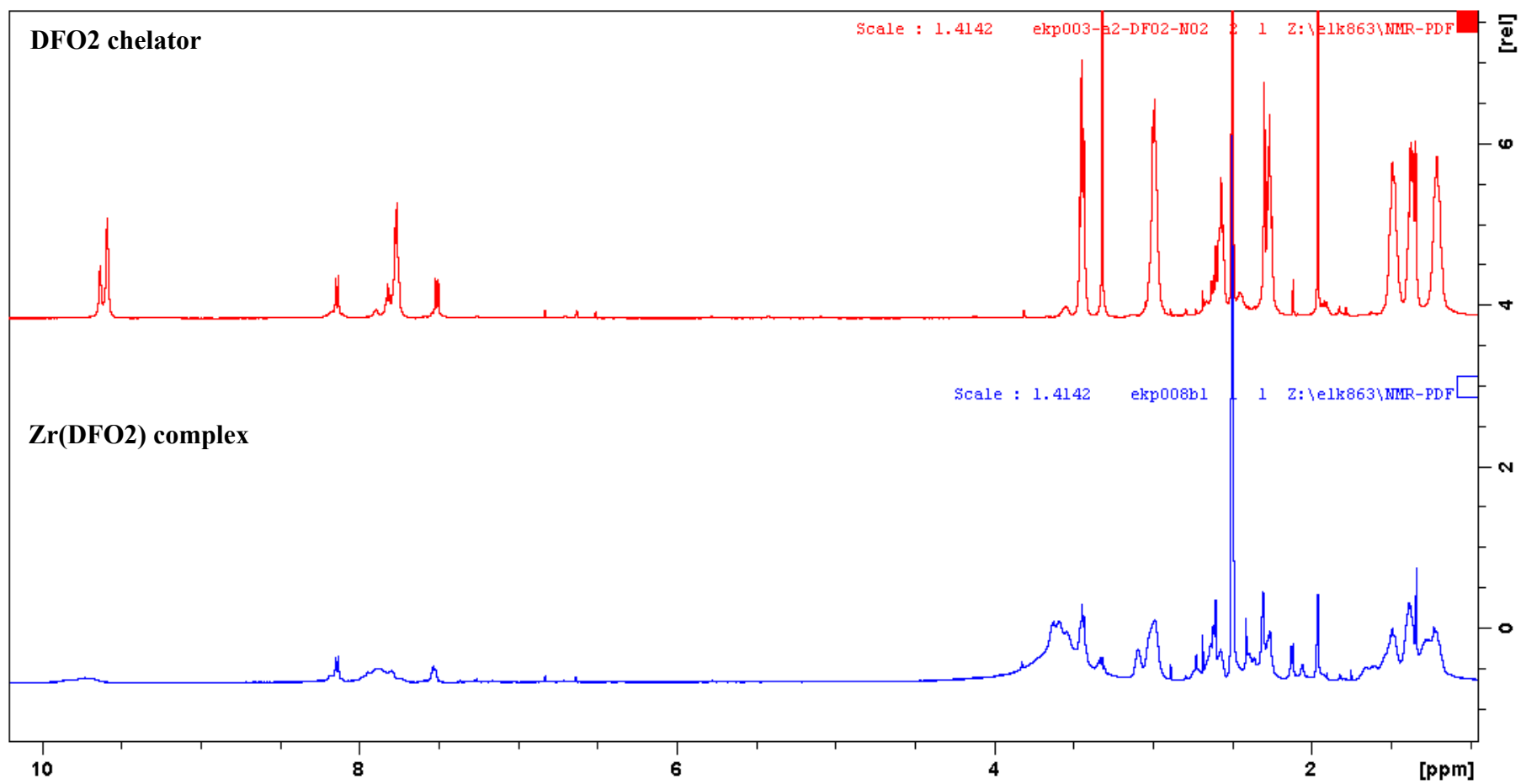
Figure S12. Comparison of ^{1}H NMR spectra of **DFO2** (**5**) and **Zr(DFO2)** (**6**) in $(CD_3)_2SO$.
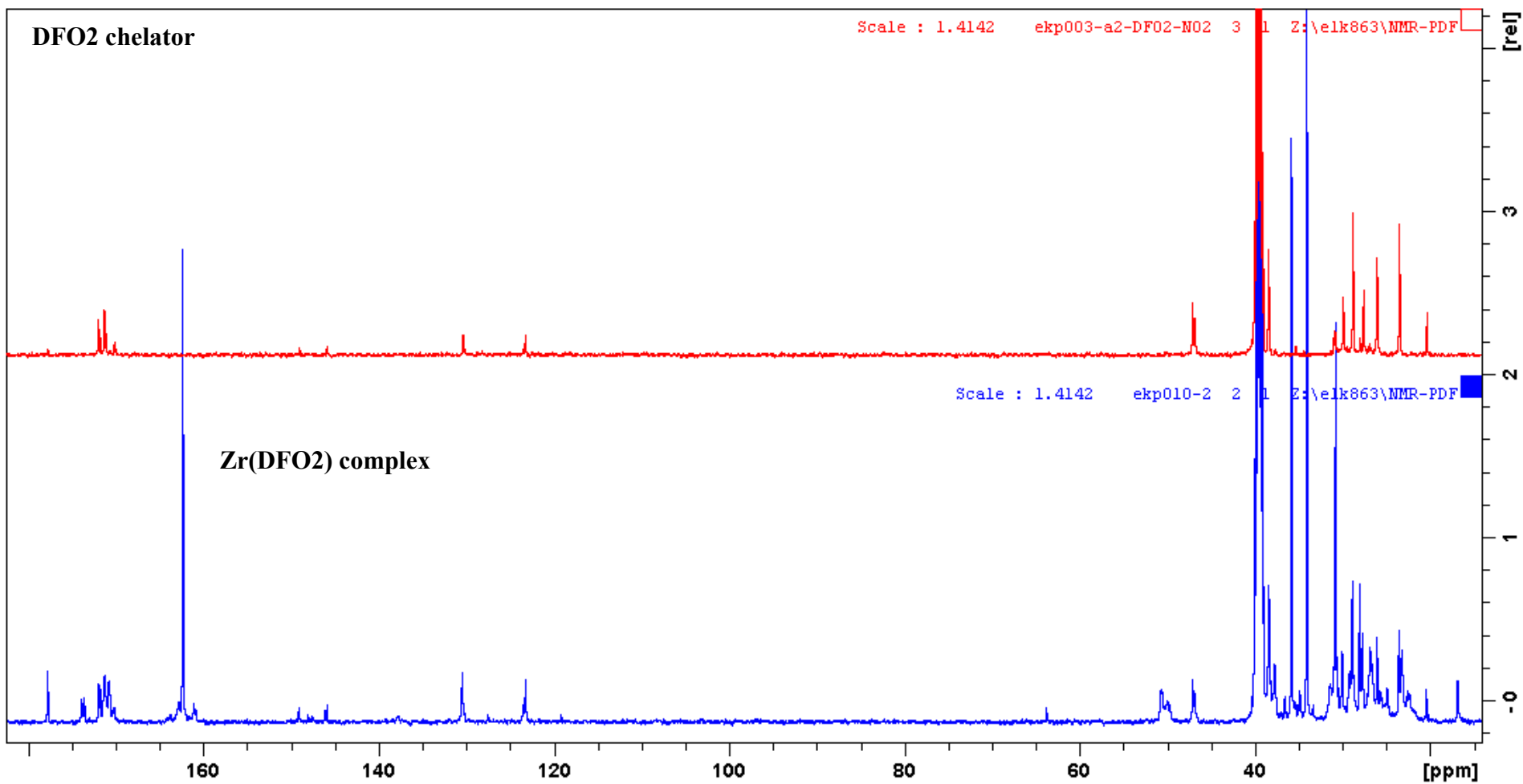
Figure S13. Comparison of UDEFT-^{13}C{^{1}H} NMR spectra of **DFO2** (**5**) and **Zr(DFO2)** (**6**) in $(CD_3)_2SO$.

Density Functional Theory (DFT) Calculations

DFT geometry optimizations were carried out using DMol^3 and Biovia Materials Studio, version 2017 R2,(1, 2) using the generalized gradient approximation (GGA) employing the Perdew-Burke-Ernzerhof (PBE)(3) functional both for the potential during the self-consistent field (SCF) procedure and for the energy.(4) DMol^3 double numerical plus d-function (DND) basis set using 4.4 basis file included polarization functions for all atoms with all-electron core treatments. Quantum simulation of solvated molecules were modeled using the conductor-like screening model (COSMO) solvation model(5, 6) in DMol^3, with a dielectric value representing water (ε = 78.54).

Due to the complicated structure of Zr(DFO2) complex, the structure first partially optimized via calculating of its energy with VAMP calculations. The neglect of diatomic differential overlap (NDDO) Hamiltonian formalism at PM6 level was used. The XYZ coordinate from this calculation was then incorporated in a geometry optimization calculation with DMol^3, as described above.
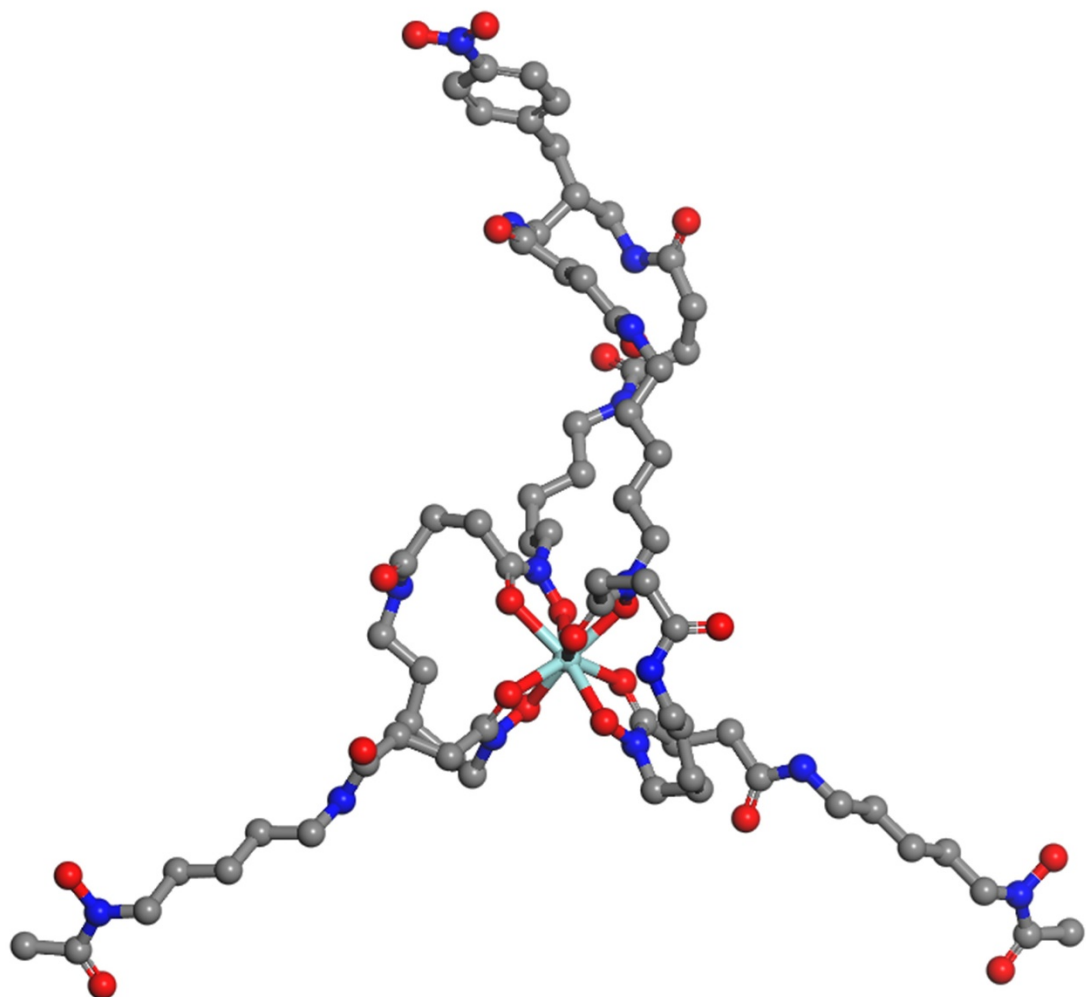
Figure S14. Calculated structure of **Zr(DFO2)** complex.

Table S1. Calculated Zr-O bond lengths of Zr(DFO2) complex.*

Zr(DFO2)*		
Bond Type	**Bond Length (Å) DFT***	**Avg. Bond Length (Å)**
N…O-Zr	2.223	
N…O-Zr	2.201	
N…O-Zr	2.228	2.217
N…O-Zr	2.217	
C…O-Zr	2.263	
C…O-Zr	2.254	
C…O-Zr	2.290	2.270
C…O-Zr	2.273	
Avg. of all 8 (O-Zr) bond lengths		**2.244**
O=C...Zr	3.107	
O=C...Zr	3.079	
O=C...Zr	3.084	3.086
O=C...Zr	3.075	
O-N…Zr	3.094	
O-N…Zr	3.101	
O-N…Zr	3.08	3.086
O-N…Zr	3.07	

*Density Functional Theory calculated using Material Studio software via DMol^3/PBE.

Zr(DFO2) (**6**)
XYZ Coordinates
 217

C	3.156334	5.722321	-1.90515
N	2.656399	6.960369	-1.31647

C	2.9083	4.500256	-1.0128
C	3.544283	3.219588	-1.56081
C	3.202803	1.998646	-0.70517
C	3.897063	0.72307	-1.19232
N	3.402374	-0.45775	-0.48862
C	3.92352	-1.07265	0.566328
C	5.3003	-0.74845	1.112974
O	3.198037	-1.95792	1.163116
O	2.132284	-0.81294	-0.8408
C	6.530967	-0.97555	0.204987
C	6.587497	-2.28407	-0.57742
N	6.18015	-3.39288	0.08744
O	7.025365	-2.31488	-1.74784
C	5.947192	-4.68417	-0.56231
C	4.608516	-4.70526	-1.30952
C	4.164835	-6.10776	-1.72493
C	2.821967	-6.15531	-2.47026
C	1.535496	-5.96648	-1.63974
N	1.153038	-4.59331	-1.29431
C	0.273471	-3.81685	-1.92175
O	1.736388	-4.07264	-0.17353
C	-0.48464	-4.25625	-3.1479
O	0.06129	-2.63658	-1.44223
C	0.274661	-4.09787	-4.48389
C	0.64077	-5.42853	-5.14844
N	1.642226	-5.34644	-6.05898
O	0.040205	-6.49177	-4.8912
C	2.0242	-6.44422	-6.94258
C	1.242627	-6.45008	-8.26131
C	1.652596	-7.60216	-9.1833
C	0.885837	-7.59403	-10.51

C	1.286548	-8.76081	-11.4152
N	0.616632	-8.73402	-12.7104
O	1.124651	-7.77367	-13.6158
C	-0.19041	-9.72061	-13.2055
O	-0.5518	-10.6713	-12.4786
C	-0.62231	-9.57583	-14.6456
C	1.381746	7.414032	-1.4578
C	1.068067	8.640677	-0.60469
O	0.551609	6.880273	-2.22248
C	-0.37926	9.104215	-0.72052
C	-0.7793	10.05864	0.399359
O	-0.06742	10.24549	1.409543
O	-1.01593	10.66753	-4.61719
C	-1.83892	9.746422	-4.41009
C	-1.49437	8.321827	-4.83014
O	-4.26469	7.387102	-3.19818
C	-2.61682	7.273511	-4.97903
C	-3.24876	6.816209	-3.67214
C	-4.5097	-9.36934	15.16119
O	-3.99468	-10.5757	13.11803
C	-3.74388	-9.6202	13.88448
O	-2.42362	-7.74465	14.54487
N	-2.75571	-8.72617	13.58375
C	-1.81202	-8.84424	12.47971
C	-1.93232	-7.70744	11.46167
C	-0.91702	-7.85124	10.32425
C	-1.05454	-6.75056	9.270309
C	-0.07599	-6.93572	8.107733
O	1.762991	-4.93228	7.124925
N	-0.29201	-5.95893	7.046535
C	0.624348	-5.05243	6.622492

C	0.188178	-4.20959	5.43185
O	1.326636	-3.23163	2.489621
C	0.645299	-4.87821	4.114609
O	-0.84523	-3.21929	1.1421
C	0.395029	-4.02356	2.896795
N	-0.75279	-4.039	2.226886
C	-1.90995	-4.91024	2.455549
C	-3.26225	-4.19069	2.524423
C	-3.44581	-3.17403	3.661673
C	-2.82263	-1.80576	3.374176
C	-3.09389	-0.75756	4.45736
O	-0.59274	0.421337	5.248254
N	-2.55089	0.540138	4.058673
C	-1.29613	0.961784	4.371578
C	-0.78754	2.147531	3.560014
O	-0.47714	-0.55065	0.015786
O	0.976115	-0.50105	2.131544
C	0.485067	1.786273	2.761927
C	0.36333	0.592515	1.838601
N	-0.37802	0.61083	0.732382
C	-0.96682	1.788173	0.10063
C	-2.49699	1.766912	-0.00194
C	-3.06274	3.167312	-0.28722
C	-2.63676	3.765583	-1.63405
N	-2.65201	5.768408	-3.06515
C	-3.05099	5.231783	-1.766
N	-3.0249	9.956317	-3.78661
C	-3.40402	11.2612	-3.25471
C	-2.63744	11.65453	-1.97285
C	-2.91727	10.64075	-0.8438
N	-1.98087	10.68791	0.276383

C	-3.00522	13.10853	-1.59299
C	-2.11854	13.73534	-0.54639
C	-0.76636	14.01709	-0.83567
C	0.074046	14.59275	0.114306
C	-0.44369	14.89192	1.382947
C	-1.78165	14.63497	1.702669
C	-2.60814	14.06071	0.734182
N	0.428645	15.49981	2.386471
O	1.615075	15.72265	2.080691
O	-0.04906	15.7574	3.507469
H	4.237969	5.850765	-2.08885
H	2.663666	5.588636	-2.88211
H	3.238907	7.405219	-0.6032
H	1.815555	4.361503	-0.90466
H	3.309768	4.705106	-0.00213
H	4.643515	3.349044	-1.61033
H	3.202231	3.045845	-2.59958
H	2.113284	1.826503	-0.72174
H	3.486666	2.183316	0.347922
H	4.984897	0.789605	-1.0583
H	3.698432	0.55684	-2.26676
H	5.390962	-1.35586	2.028257
H	5.315264	0.30506	1.45196
H	7.427392	-0.92404	0.852118
H	6.64595	-0.16989	-0.53458
H	5.73472	-3.26213	0.997776
H	5.958473	-5.45069	0.23332
H	6.791592	-4.88894	-1.24093
H	4.686898	-4.05711	-2.2033
H	3.840582	-4.25667	-0.66103
H	4.104376	-6.76016	-0.83079

H	4.932881	-6.55973	-2.38233
H	2.718757	-7.15305	-2.93683
H	2.828749	-5.43095	-3.30491
H	1.612079	-6.50462	-0.67858
H	0.692937	-6.40053	-2.19866
H	-1.39102	-3.63157	-3.16271
H	-0.81551	-5.30439	-3.05674
H	1.17246	-3.46584	-4.37023
H	-0.37341	-3.5703	-5.20803
H	2.04202	-4.42475	-6.24844
H	1.856361	-7.38499	-6.39245
H	3.107336	-6.35659	-7.13818
H	1.402782	-5.48505	-8.7793
H	0.161883	-6.518	-8.03529
H	1.483836	-8.56661	-8.66476
H	2.740188	-7.54374	-9.38657
H	1.073467	-6.63791	-11.0346
H	-0.20223	-7.64677	-10.3166
H	1.017701	-9.72344	-10.9539
H	2.3767	-8.75623	-11.6001
H	0.55734	-6.97534	-13.4801
H	-1.1752	-8.63371	-14.8029
H	-1.2698	-10.4279	-14.8985
H	0.248861	-9.55855	-15.3212
H	1.756752	9.456562	-0.89292
H	1.303368	8.407254	0.448517
H	-1.05503	8.23002	-0.69032
H	-0.55045	9.578615	-1.69973
H	-0.73482	7.958089	-4.11078
H	-0.97677	8.414132	-5.80097
H	-2.18256	6.400123	-5.49741

H	-3.42601	7.66549	-5.61811
H	-5.24782	-10.1749	15.28319
H	-5.02882	-8.39713	15.12387
H	-3.8377	-9.34675	16.03456
H	-2.88828	-6.92734	14.23882
H	-2.0157	-9.81697	12.00546
H	-0.79367	-8.87609	12.91101
H	-1.78106	-6.73652	11.97026
H	-2.95871	-7.70358	11.04711
H	-1.05177	-8.83789	9.839294
H	0.109861	-7.8429	10.74124
H	-0.88998	-5.75841	9.731058
H	-2.08859	-6.75248	8.871991
H	-0.18545	-7.95187	7.683217
H	0.966287	-6.81955	8.443676
H	-1.19682	-5.9812	6.571526
H	0.661247	-3.21795	5.526938
H	-0.90495	-4.0622	5.427679
H	0.178962	-5.87116	4.009088
H	1.736126	-5.036	4.156394
H	-1.73565	-5.46553	3.389334
H	-1.93272	-5.64286	1.626478
H	-4.00867	-4.99959	2.63285
H	-3.4628	-3.70558	1.552991
H	-3.04451	-3.59098	4.606607
H	-4.53244	-3.03738	3.830788
H	-3.22476	-1.43168	2.413263
H	-1.73235	-1.884	3.237125
H	-2.61729	-1.03746	5.409929
H	-4.1782	-0.64224	4.636858
H	-3.0153	0.998947	3.272956

H	-0.52398	2.956887	4.26423
H	-1.57017	2.544301	2.892445
H	1.288717	1.529683	3.46982
H	0.820089	2.679051	2.206124
H	-0.50714	1.867131	-0.89983
H	-0.64563	2.66553	0.681169
H	-2.91799	1.40271	0.952224
H	-2.8155	1.05059	-0.78085
H	-4.16706	3.12263	-0.24315
H	-2.74682	3.847687	0.528185
H	-3.07873	3.179277	-2.46203
H	-1.53886	3.70533	-1.75046
H	-1.74775	5.461518	-3.43242
H	-2.58522	5.828146	-0.9576
H	-4.14405	5.346209	-1.67859
H	-3.64971	9.151425	-3.6184
H	-4.48981	11.23607	-3.05993
H	-3.21912	12.02639	-4.02741
H	-1.56147	11.62073	-2.21699
H	-2.91787	9.620093	-1.25921
H	-3.92853	10.81164	-0.43379
H	-2.19189	11.33072	1.044363
H	-4.05958	13.143	-1.26272
H	-2.9356	13.72406	-2.51055
H	-0.36559	13.79066	-1.83036
H	1.11892	14.81331	-0.11911
H	-2.16656	14.8784	2.696377
H	-3.65743	13.86287	0.982283
Zr	1.000633	-2.126	0.542142

References:

1.   Delley B. An all-electron numerical method for solving the local density functional for polyatomic molecules. J Chem Phys. 1990;92(1):508-17.
2.   Delley B. From molecules to solids with the DMol3 approach. J Chem Phys. 2000;113(18):7756-64.
3.   Perdew JP, Burke K, Ernzerhof M. Generalized Gradient Approximation Made Simple. Physical Review Letter. 1996;77(18):3865-8.
4.   Peverati R, Truhlar DG. M11-L: A Local Density Functional That Provides Improved Accuracy for Electronic Structure Calculations in Chemistry and Physics. The Journal of Physical Chemistry Letters. 2011;3(1):117-24.
5.   Klamt A, Schuurmann G. COSMO: A New Approach to Dielectric Screening in Solvents with Explicit Expressions for the Screening Energy and its Gradient. J Chem Soc Perkin Trans. 1993;2:799-805.
6.   Andzelm J, Ko¨lmel C, Klamt A. Incorporation of solvent effects into density functional calculations of molecular energies and geometries. J Chem Phys. 1995;103(21):9312-20.